Large Space Antenna Systems Technology - 1982

Proceedings of a conference held in
Hampton, Virginia
November 30 - December 3, 1982

25

25th Anniversary
1958-1983

NASA

TECH LIBRARY KAFB, NM

0078705

Large Space Antenna Systems Technology - 1982

NASA

National Aeronautics
and Space Administration

Scientific and Technical
Information Branch

1983

PREFACE

This publication is a compilation of the unclassified papers presented at the NASA Conference on Large Space Antenna Systems Technology held at the Langley Research Center, Hampton, Virginia, November 30 – December 3, 1982. The conference was sponsored jointly by the NASA Office of Aeronautics and Space Technology (OAST) and the NASA Langley Research Center. The conference was organized into five sessions: Systems, Structures Technology, Control Technology, Electromagnetics, and Space Flight Test and Evaluation. All speakers and topics were selected by the session cochairmen and included representation from industry, universities, and government. The program was organized to provide a comprehensive review of space missions requiring large antenna systems and of the status of key technologies required to enable these missions.

In addition to the formal sessions, three forums were conducted on topics of current special interest. Forum topics were Systems Studies, Limitations of Ground Testing, and Structure and Control Interaction. Proceedings of the forums are not included in this publication.

The general cochairmen for the conference were Dell P. Williams, Director, Space Systems Division, NASA Office of Aeronautics and Space Technology, and Paul F. Holloway, Director for Space, Langley Research Center. The program chairman was Dr. Earle K. Huckins III, Head, Large Space Antenna Systems Technology Office, Langley Research Center. The conference committee wishes to express its appreciation to the session chairmen, authors, and conference administrative assistants for their outstanding contributions to the meeting.

This publication was expedited and enhanced through the efforts of the staff of the Research Information and Applications Division, Langley Research Center.

E. Burton Lightner
Langley Research Center

CONTENTS

PART 1

SYSTEMS

Communications

Space Science

Military (Classified)

Earth Observations

Systems Analysis

STRUCTURES TECHNOLOGY

Structures and Materials Technology

Large Space Antenna Structural Systems

PART 2[*]

CONTROL TECHNOLOGY

---

[*]Part 2 is presented under a separate cover.

ELECTROMAGNETICS

SPACE FLIGHT TEST AND EVALUATION

ATTENDEES

NASA Headquarters
Washington, DC

J. B. Dahlgren
J. D. DiBattista
Dr. D. A. Gilman
L. Holcomb
F. D. Kochendorfer
J. E. Miller
S. L. Venneri
D. P. Williams

NASA Langley Research Center
Hampton, VA

Dr. D. P. Hearth
R. H. Petersen
P. F. Holloway
R. C. Goetz
H. T. Wright
Dr. M. F. Card
Dr. G. D. Walberg
I. Abbasy (GWU)
H. M. Adelman
E. L. Ahl, Jr.
F. O. Allamby
F. Allario
J. L. Allen, Jr.
M. J. Anderson
W. W. Anderson
E. S. Armstrong
G. C. Ashby, Jr.
Dr. M. C. Bailey
J. G. Batterson
M. E. Beatty III
F. B. Beck
W. K. Belvin
K. S. Bey
H. J. C. Blume
D. E. Bowles
L. Bowman
W. J. Boyer
O. H. Bradley
J. D. Buckley
H. G. Bush
D. H. Butler
T. G. Campbell
J. J. Catherines
H. K. Clark
Dr. C. R. Cockrell
M. Cooper (GWU)
R. H. Couch

NASA Langley Research Center
Hampton, VA   (Continued)

E. A. Crossley, Jr.
K. A. Crumbly
L. J. DeRyder, Jr.
L. A. Dillion-Townes
Dr. S. C. Dixon
J. A. Dodgen
J. T. Dorsey (GWU)
R. S. Dunning
J. R. Elliott
R. W. Faison
J. C. Fedors
M. J. Ferebee, Jr.
Dr. W. B. Fichter
W. Fitzgerald
A. Fontana
R. E. Fulton
Dr. L. B. Garrett
M. C. Gilreath
J. W. Goslee
W. L. Grantham
W. H. Greene
J. Hagaman
H. A. Hamer
B. R. Hanks
P. W. Hanson
Dr. R. F. Harrington
J. E. Harris
W. L. Heard, Jr.
C. L. Herstrom
W. F. Hinson
R. Hodges
S. E. Holloway III
W. R. Hook
Dr. G. C. Horner
L. G. Horta
Dr. J. M. Housner
Dr. E. K. Huckins III
J. W. Johnson
W. R. Jones
J. N. Juang
L. S. Keafer, Jr.
C. R. Keckler
B. M. Kendall
V. Klein (GWU)
P. Klich
F. Kopriver III
W. Lee
E. B. Lightner
S. A. T. Long

NASA Langley Research Center
Hampton, VA (Continued)

U. M. Lovelace
J. B. Lovell
M. H. Lucy
J. Mahaney (ODU)
J. A. Martin
H. G. McComb, Jr.
P. McGowan
M. McMillin
Dr. M. M. Mikulas, Jr.
R. Miserentino
Dr. R. C. Montgomery
J. C. Moorman
V. Mukhopadhyay (GWU)
J. R. Newsom
A. K. Noor (GWU)
G. C. Olsen
R. S. Pappa
Dr. L. D. Pinson
W. H. Reed III
M. D. Rhodes
D. K. Robertson
J. C. Robinson
R. A. Russell
A. A. Schy
K. N. Shivakumar
Dr. J. J. Singh
F. M. Smith
J. Sobieski
L. D. Staton
J. S. Sutila
G. Sykes
J. B. Talbot
L. W. Taylor, Jr.
Dr. D. R. Tenney
Dr. E. A. Thornton (ODU)
J. D. Timmons
R. H. Tolson
Dr. S. S. Tompkins
L. F. Vosteen
W. W. Wagner, Jr.
J. E. Walz
J. C. Ward, Jr.
N. D. Watson
A. P. Wiehing
J. L. Williams
J. P. Williams
R. T. Wingate
R. L. Wright
J. W. Young

NASA Ames Research Center
Moffett Field, CA

M. K. Kiya
R. B. Pittman
B. L. Swenson

NASA Goddard Space Flight Center
Greenbelt, MD

H. Montgomery
W. T. Walton
J. P. Young

Jet Propulsion Laboratory
Pasadena, CA

K. C. Coon
W. A. Edmiston
R. E. Freeland
W. A. Imbriale
V. Jamejad
Dr. R. Levy
F. Naderi
Y. Rahmat-Samii
Dr. D. G. Rea
G. Rodriguez
Dr. P. N. Swanson
S. N. Swanson
S. Szirmay
A. F. Tolivar
K. E. Woo

NASA L. B. Johnson Space Center
Houston, TX

R. F. Baillie

NASA Lewis Research Center
Cleveland, OH

B. E. LeRoy
J. E. Maloy
R. Sharp

NASA Marshall Space Flight Center
Huntsville, AL

H. J. Buchanan
M. R. Carruth
E. C. Hamilton
R. W. Schock
W. E. Thompson

Advanced Technology Center
Huntsville, AL

B. Sallo

Aerojet Liquid Rocket Co.
Sacramento, CA

L. H. Luehr

Aerospace Corp.
Los Angeles, CA

E. Jacobs
G. Smit

AFOSR
Bolling Air Force Base, DC

A. K. Amos
R. Sierakowski

AFWAL
Wright Patterson Air Force Base, OH

H. C. Croop
G. R. Holderby
W. Johnston
J. Pearson
Lt. D. B. Ridgely
V. B. Venkayya

Astro Research Corp.
Carpinteria, CA

B. Cambell
Dr. J. M. Hedgepeth

Battelle Columbus Lab
Columbus, OH

S. A. Kingsley

The BDM Corp.
Albuquerque, NM

R. K. Hoppe
K. F. Probst

Bendix Field Engineering Corp.
Greenbelt, MD

M. J. Aucremanne
G. T. Foote

Boeing Aerospace Co.
Seattle, WA

T. H. Chase
R. M. Gates
C. T. Golden
W. W. Smith
E. E. Spear

Brunswick Corporation
Costa Mesa, CA

C. B. Kurz

C. S. Draper Laboratory
Cambridge, MA

F. N. R. Ayer
K. Daly
Dr. E. Fogel
S. D. Ginter
J. G. Lin
C. M. Satter
Dr. K. Soosaar
R. R. Strunce, Jr.
J. D. Turner

College of William and Mary
Williamsburg, VA

Dr. E. Kamaratos

Communications Research Center
Ontario, Canada

D. G. Zimcik

COMSAT Laboratories
Clarksburg, MD

P. M. Caughran
Y. S. Lee
H. Gerson
R. M. Sorbello
A. I. Zaghloul

Edighoffer
Hampton, VA

H. Edighoffer

Essex Corp.
Huntsville, AL

N. Shields, Jr.

European Space Agency
The Netherlands

A. Saitto
H. A. Superfine

Fairchild Space & Electronics Co.
Germantown, MD

L. DiBiasi
R. E. Kramer

Foldes Inc.
Wayne, PA

P. Foldes

Ford Aerospace & Communications Corp.
Palo Alto, CA

E. Nygren

General Dynamics Convair
San Diego, CA

N. L. Cohen
M. P. Dudeck
J. A. Fager
H. B. Henderson
S. Kulick
A. R. Robertson
J. R. Sesak
G. R. Stone
J. D. Weber

General Electric Company
Philadelphia, PA

D. J. Cuthbert
M. Garnek
J. D. Keising
E. J. Kuhar, Jr.
V. Navon
C. V. Stahle
R. B. Wiley

General Research Corporation
Santa Barbara, CA

R. F. Crawford
D. J. Mihora

Georgia Institute of Technology
Atlanta, GA

S. N. Atluri

Goodyear Aerospace Company
Washington, DC

R. W. Morris

Grumman Aerospace Corporation
Bethpage, NY

J. T. Diglio
R. Gran
R. R. Price
J. L. Schultz
W. E. Simpson
S. Wong

Harris Corporation
Melbourne, FL

B. B. Allen
H. J. Andrews
W. F. Croswell
J. W. Shipley
M. R. Sullivan

Honeywell, Incorporated
Minneapolis, MN

R. P. Singh

Howard University
Washington, DC

Dr. P. M. Bainum
R. Krishna
M. G. Manoharan
C. McKissack
A. S. S. R. Reddy

Hughes Aircraft Co.
Los Angeles, CA

V. E. Cascia
M. F. Caulfield
B. M. Flynn
S. O. Lane
T. M. Paige

Hydraulic Research TEXTRON
Irvine, CA

R. Quartararo

Itek Corp.
Lexington, MA

J. J. Cleary

Johns Hopkins University
Laurel, MD

T. B. Coughlin

Kentron International
Hampton, VA

C. L. Blackburn
E. P. Brien
R. E. Calleson

Kentron International
Hampton, VA   (Continued)

R. A. Dacosta
J. K. Jensen
R. W. LeMessurier
J. E. Phelps
J. E. Price
R. E. Wallsom

Lawrence Livermore National Lab
Livermore, CA

S. R. Arnold
H. S. Cabayan
W. E. Larimore
A. J. Spero

L'Garde, Inc.
Newport Beach, CA

G. J. Friese
M. Thomas

Lockheed Missiles and Space Company
Sunnyvale, CA

E. L. Becker
N. F. Garcia
R. R. Johnson
G. Turner
A. A. Woods, Jr.

Lockheed Palo Alto Research Laboratory
Palo Alto, CA

J. N. Aubrun

Martin Marietta Corporation
Denver, CO

J. V. Coyner, Jr.
Dr. R. C. Engels
T. C. Fenner
J. J. Herbert
W. H. Huang
M. W. Kuethe
F. K. Mattson
W. A. Schartel
F. R. Schwartzberg

Massachusetts Institute of Technology
Cambridge, MA

J. H. Lang
J. W. Mar

McDonnell Douglas Technical Services
Huntsville, AL

Dr. W. R. Mahaffey
T. P. Poole

MIT Lincoln Lab
Lexington, MA

S. E. Forman

MRJ Inc.
Fairfax, VA

W. L. Poesch
Dr. R. Shieh

National Bureau of Standards
Boulder, CO

A. C. Newell

Naval Electronics Systems Command
Arlington, VA

R. L. DuPuy
S. A. Nichols

Naval Research Laboratory
Washington, DC

K. T. Alfrend
R. E. Lindberg, Jr.
V. E. Noble

North Carolina State University
Raleigh, NC

J. C. Brand
C. Christodoulou
Dr. J. F. Kauffman

OCSE – Rome Air Development Center
Rome, NY

R. W. Carman
R. Schneible

Old Dominion University
Norfolk, VA

Dr. P. Dechaumpai
Dr. E. A. Thornton

ORI, Inc.
Silver Springs, MD

W. C. Hayes
L. R. Patterson
R. Whitman

RADC/EEC
Hanscom AFB, MA

D. J. Jacavaco

RCA Astro Electronics
Princeton, NJ

E. R. Ganssle
W. P. Manger
Dr. S. Parekh
H. H. Soule

Riverside Research Institute
Arlington, VA

A. L. DeVillers

Rockwell International
Downey, CA

H. S. Greenberg
D. Hays
J. Wokurka

SPAR Aerospace Limited
Ontario, Canada

F. Charron
R. T. Cooper
Dr. J. S.-C. Yuan

TRW
Redondo Beach, CA

W. Akle
Dr. J. S. Archer
J. T. Bennett
R. L. Hammel
M. Horstein
L. R. Mortaloni
R. H. Van Vooren

UCLA
Los Angeles, CA

L. A. Schmit

University of Kentucky
Lexington, KY

T. R. Tauchert

University of Virginia
Charlottesville, VA

J. K. Haviland
M. F. Mallette

U.S. Government
Washington, DC

R. Jeans
P. Schmid

Virginia Associated Research Campus (VARC)
  of the College of William and Mary
Newport News, VA

A. Kyser

VPI&SU
Blacksburg, VA

R. T. Haftka
W. L. Hallauer, Jr.

Vought Corporation
Dallas, TX

R. L. Cox
J. J. Pacey

LARGE SPACEBORNE ANTENNA TECHNOLOGY:

A SYSTEM PERSPECTIVE

F. Naderi
Jet Propulsion Laboratory
Pasadena, California

APPLICATIONS AND USERS OF LARGE SPACEBORNE ANTENNAS

Large space antennas are being proposed for a number of applications, some of which are listed below. In Very Long Baseline Interferometry (VLBI) a large Earth orbiting antenna and several Earth based antennas are employed to, in effect, synthesize a very large aperture. In such systems the signal-to-noise ratio is proportional to the product of the antenna apertures. Since the radio signals received from very distant sources are weak, large antenna apertures are required to provide adequate signal-to-noise ratio.

Soil moisture mapping, which is essential for global crop forcasting, can be conducted from space by using passive microwave radiometry. In order to achieve high spatial resolution, large antenna systems are used.

Next generation of communication satellites will enable the users to directly access the spacecraft. To allow for this, large satellite antennas must be employed to overcome low gain of user antenna.

This presentation focuses on this last application. Furthermore, within the class of communication satellites, a land mobile satellite is used to illustrate the typical requirements that the system imposes on these large antennas.

- Applications
    - VLBI
    - Radiometry
    - Communications
    - Deep Space Relay
    - etc.

- Users
    - Government (Technology Development)
    - Industry (Commercial Use)
    - DoD

> Today's Presentation Focuses on One Application of Large Antennas, i.e. Satellite Communications. Furthermore, Within This Class of Satellites, Land Mobile Satellite is Used to Illustrate System Needs and Requirements.

2

LAND MOBILE SATELLITE SYSTEM

Land Mobile Satellite System (LMSS) is a communication system which provides radio communication to a large group of users within a vast geographical area (e.g. communications to and from mobile vehicles anywhere within the U.S.). Such radio communication may be in the form of radio telephone, paging, dispatch, or data transmission. The intended applications of LMSS range from emergency medical to disaster relief, from law enforcement to truck dispatch. By providing service to vast rural areas, LMSS compliments the current terrestrial service in the metropolitan areas and hence provides for a nationally ubiquitous coverage.

- ● <u>What is it ?</u>

    Land Mobile Satellite System (LMSS) Provides Radio

    Communications (Such as Radio Telephone, Paging, Dispatch,

    Data) to a Group of Users Which Roam Around Within a Vast

    Coverage Area (e.g. Communications to and from Mobile Vehicles)

LAND MOBILE SATELLITE OPERATION

The major element in the LMSS is a communication satellite at the geosynchronous orbit employing a large multiple beam antenna. This antenna provides a number of spot beams (possibly 90) to completely blanket the coverage area. Three such beams are shown in the figure below.

A typical call may originate from a home telephone connected to the wireline net-work. This call is routed via the wireline network to a base station where it is transmitted to the satellite over the backhaul link. (The system presented here uses S-band for the backhaul link; however, other bands such as the C, K_u or K_a may also be used depending on their availability.) The satellite translates the back-haul frequency to UHF and relays the call over the backhaul link, and the base station forwards the call through the wireline network to the originating phone. Additionally, calls may also originate from the mobile phone and be routed to a fixed phone or another mobile phone. The base stations serve as the interface between the LMSS and the wireline network and, in general, control the operation of the LMSS by providing such functions as paging a mobile user, making channel assignments, call-routing, etc.

BEAM No. 1

BEAM No. 2

BEAM No. N

— — — WIRELINE NETWORK (TERRESTRIAL OR SATELLITE) INTERCONNECTION
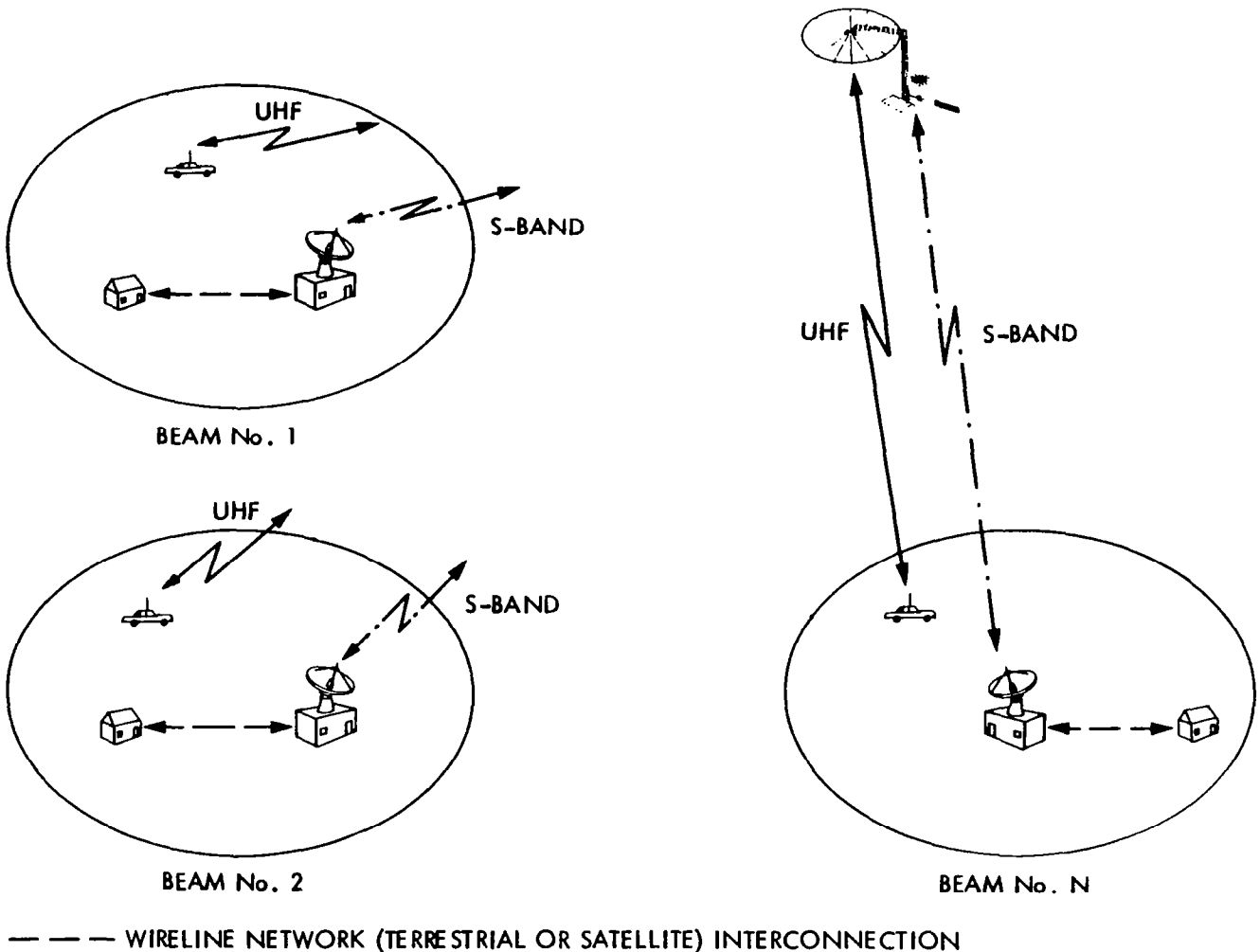
WHY DOES LMSS NEED A LARGE SATELLITE ANTENNA?

There are basically two reasons why LMSS requires a large antenna. The reasons are briefly described below and are further discussed through illustrations on the next three pages.

1 - To Enable Inexpensive Small User Equipment

- Hundreds of Thousands of Users Will Access the Satellite Directly. The Economy of Scale Dictates Complexity Inversion; i.e., Small Inexpensive User Equipment at a Cost of Complex Satellite Antenna.

2 - To Enable Frequency Reuse

- Scarce Allocation Neccessitates Judicious Use of Frequency Spectrum. Large Antennas Producing Multiple Spot Beams Allow Reuse of the Frequency Through Spatial Diversity.

TRUNKED SATELLITE SYSTEMS

In present day communications satellite systems, signals from geographically dispersed users are routed via land lines to a few powerful ground stations. At these stations the signals are multiplexed and are transmitted to the satellite using powerful ground transmitters and antennas. Such ground stations enable communications with satellites that have relatively small antennas. The illustration below is roughly to scale and underscores the above points.

SATELLITE ANTENNA

GROUND ANTENNA
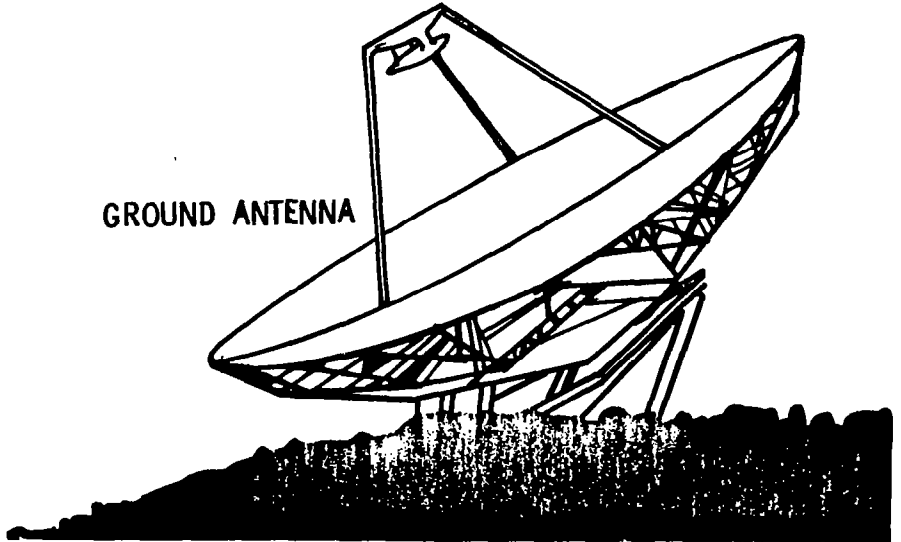
DIRECT-TO-USER SATELLITE SYSTEM

In contrast to the trunked satellite system, LMSS users use small inexpensive antennas mounted on their vehicle to communicate with the satellite directly. The user constantly moves about, therefore the vehicle antenna needs to be omnidirectional so as to "see" the satellite from all possible vehicle orientations. Because of this, the vehicle antenna does not have much gain, and thus a large antenna is needed at the other end (i.e., the satellite).

SATELLITE ANTENNA

GROUND ANTENNA.
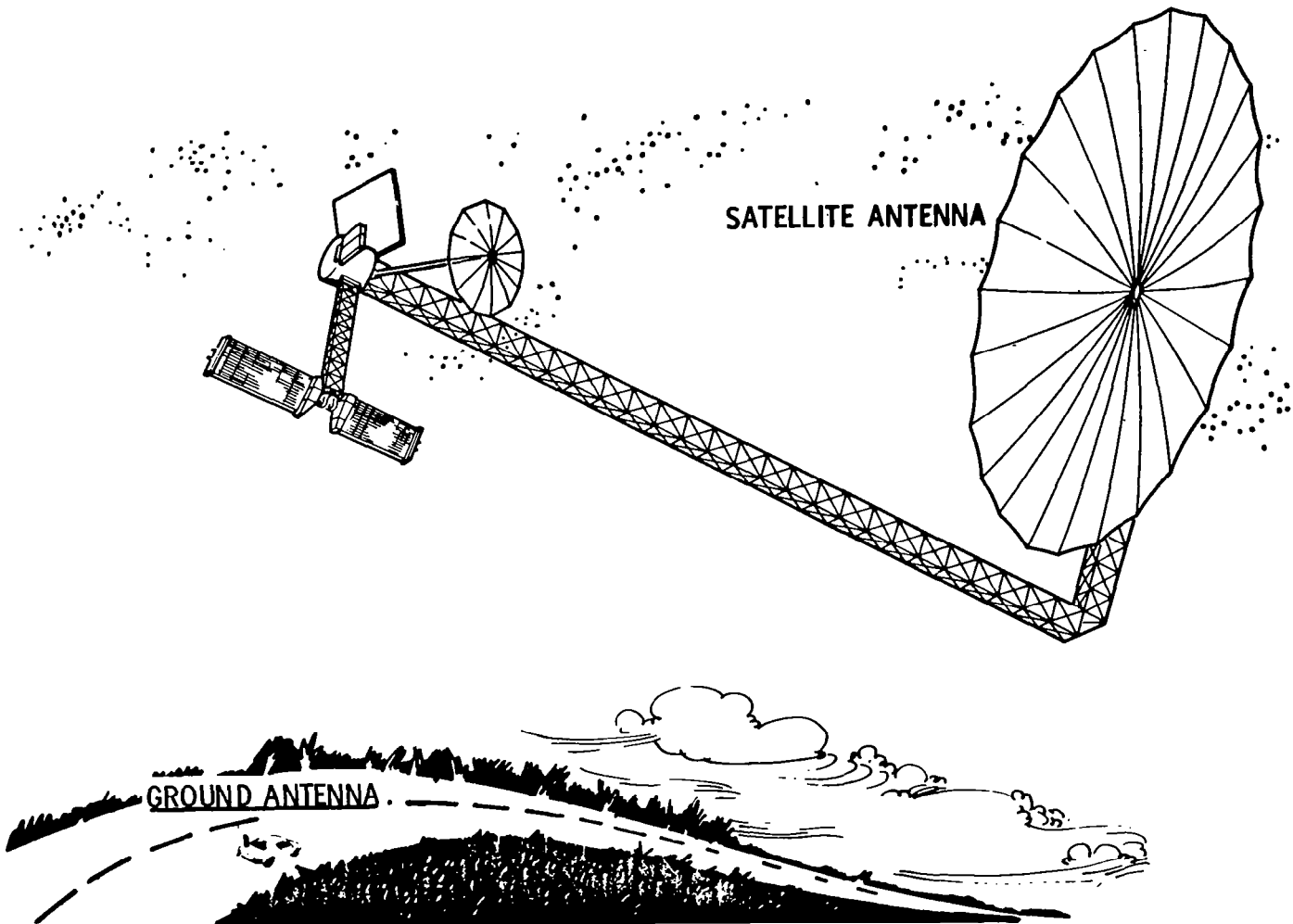
INCREASED CAPACITY AND FREQUENCY REUSE

Due to electromagnetic spectrum scarcity, the frequency allocation to such services as LMSS is very limited. It is therefore essential to use whatever bandwidth is available as efficiently as possible. Large antennas producing multiple spot beams allow reuse of the frequency through spatial diversity. (The concept of frequency reuse is illustrated on the following page.) The number of spot beams that can be packed within a given coverage area is dependent on the size of antenna which is being used. This relationship is shown below. Note that producing 90 to 100 beams to cover CONUS requires a 50 to 60 meter antenna.

- FREQUENCY = 871 MHz
- BEAMS CONTIGUOUS AT -3 dB FOOTPRINT
- SATELLITE AT 110° WEST LONGITUDE

NUMBER OF BEAMS

ANTENNA DIA (meter)
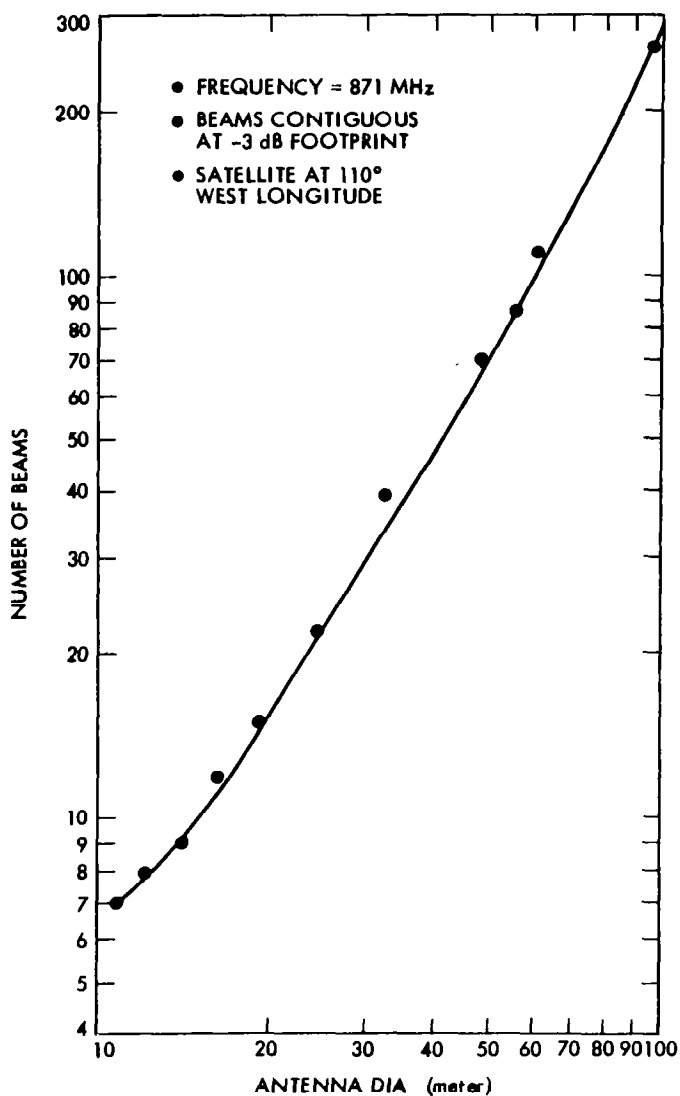
FREQUENCY REUSE AND SIDELOBE CONTROL

It was mentioned on the previous page that large multiple beam antennas enable frequency reuse through spatial diversity. This, however, requires an antenna feed design which adequately suppresses sidelobes to prevent unwanted spillover. The concept is illustrated below. The "dotted" spot beam shares the same frequency band with the thirteen "co-channel" beams which have been darkened in color in the figure below. In other words, the same frequency band has been "reused" in the fourteen beams. Also shown is the antenna radiation pattern that produces the dotted beam. Note that while the main lobe of this radiation pattern produces the dotted beam, there are some unavoidable sidelobes that spill energy to other co-channel beams and hence interfere with their operation. Thus, successful design of a multiple beam antenna is predicated on producing and maintaining low sidelobes to enable frequency reuse.
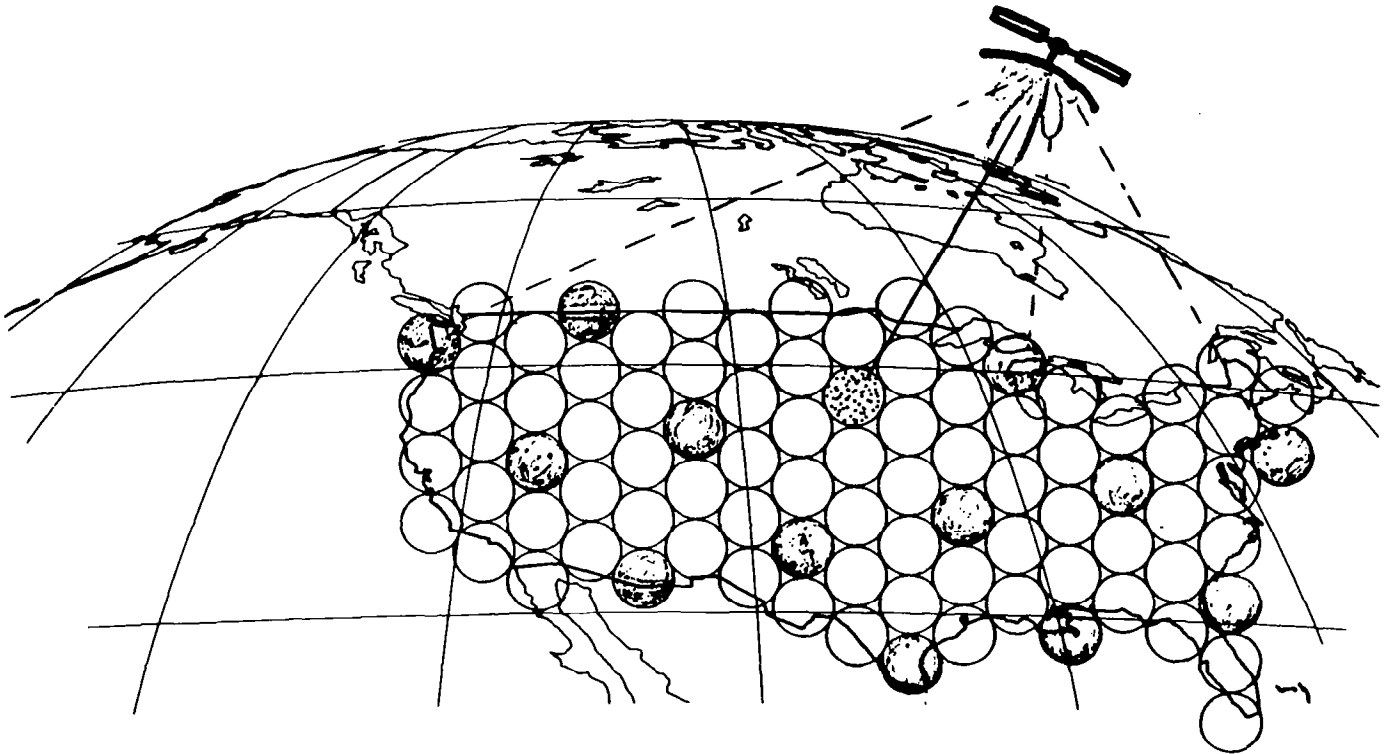
It may be suggested that the reason for the requirement of a large antenna on the LMSS spacecraft stems from the fact that the operating frequency is at UHF ($\approx$900 MHz) and that in fact the selection of a higher frequency enables one to reduce the antenna size. There is some flaw with this argument. Consider the relationship below, where the received power (by the user) is shown as a function of the satellite transmitter power P_T, the free space loss L, and the transmitting and receiving antenna gains G_T and G_R. If we fix the total power on the spacecraft (i.e., fix P_T) one can see that as long as the receiving antenna is isotropic, then by raising the operating frequency, any advantage gained by the transmitting antenna gain is exactly offset by the free space loss, leaving the design in no better shape.

- **DOES THE REQUIREMENT FOR A LARGE ANTENNA STEM FROM THE FACT THAT THE OPERATING FREQUENCY IS AT UHF?**

$$P_R = \frac{P_T \cdot G_T}{L} \cdot G_R$$

with $G_T = \left(\frac{\pi D}{\lambda}\right)^2$, $L = \left(\frac{\lambda}{4\pi R}\right)^2$, G_R ISOTROPIC

RECEIVED POWER

CONCEPTUAL DESIGN OF THE LMSS SPACECRAFT

The figure below is the drawing of a conceptual design of the LMSS spacecraft. The configuration as shown includes a 55-meter UHF antenna. The reflector is attached to the bus by means of an L-shaped mast with the upper section and lower section of the mast being 34 and 83 meters in length. The large panel in the upper left is a planar UHF feed array which enables the antenna to produce 87 spot beams on CONUS. This feed panel is broken into five segments for the purpose of stowage in the Shuttle cargo bay. The spacecraft also has an S-band reflector which provides the communication between the spacecraft and the base stations. The UHF transmitters, which are distributed and packed between the layers of the UHF feed panel, radiate 2 kW of RF power. Even at an optimistic fifty percent efficiency, these transmitters will dissipate 2 kW of waste heat. Heat pipes carry the wasted heat from the transmitters to the edges of the UHF feed panel where thermal radiators will dissipate the heat. The beginning-of-life power capability of the spacecraft is 10 kW.

11
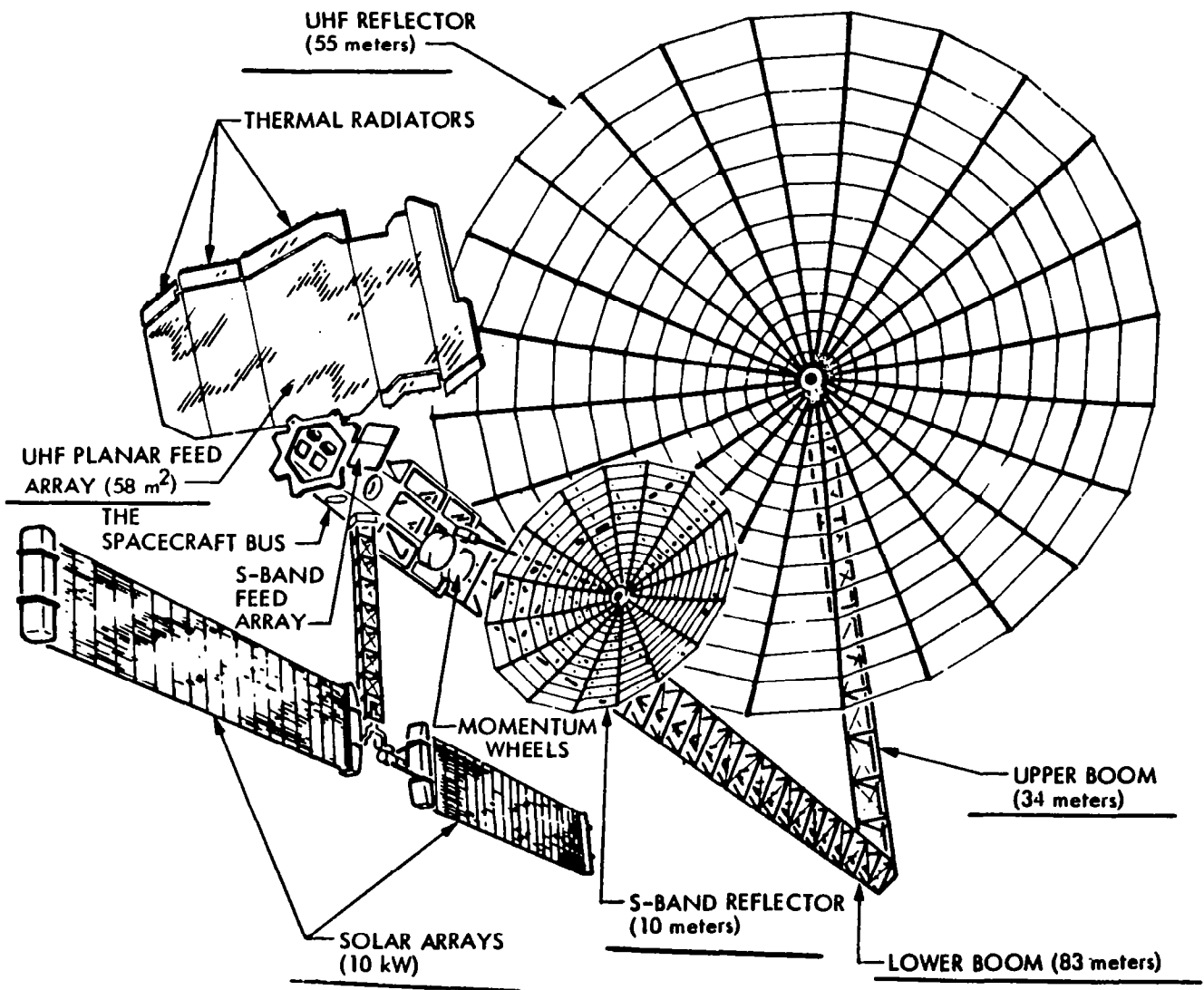
SIZE OF LMSS SPACECRAFT

The stowage of LMSS spacecraft inside the Shuttle is a considerable challenge. To put this in the proper perspective, the figure below shows a conceptual drawing of the LMSS spacecraft drawn to the same scale as the Shuttle orbiter and the ATS-6 with its 9-m antenna, which to date is the largest deployable satellite antenna flown in a nonclassified mission.

SCALED DRAWING OF MSAT, ATS-6, STS SHUTTLE

ATS-6

THE SHUTTLE

LAND MOBILE SATELLITE
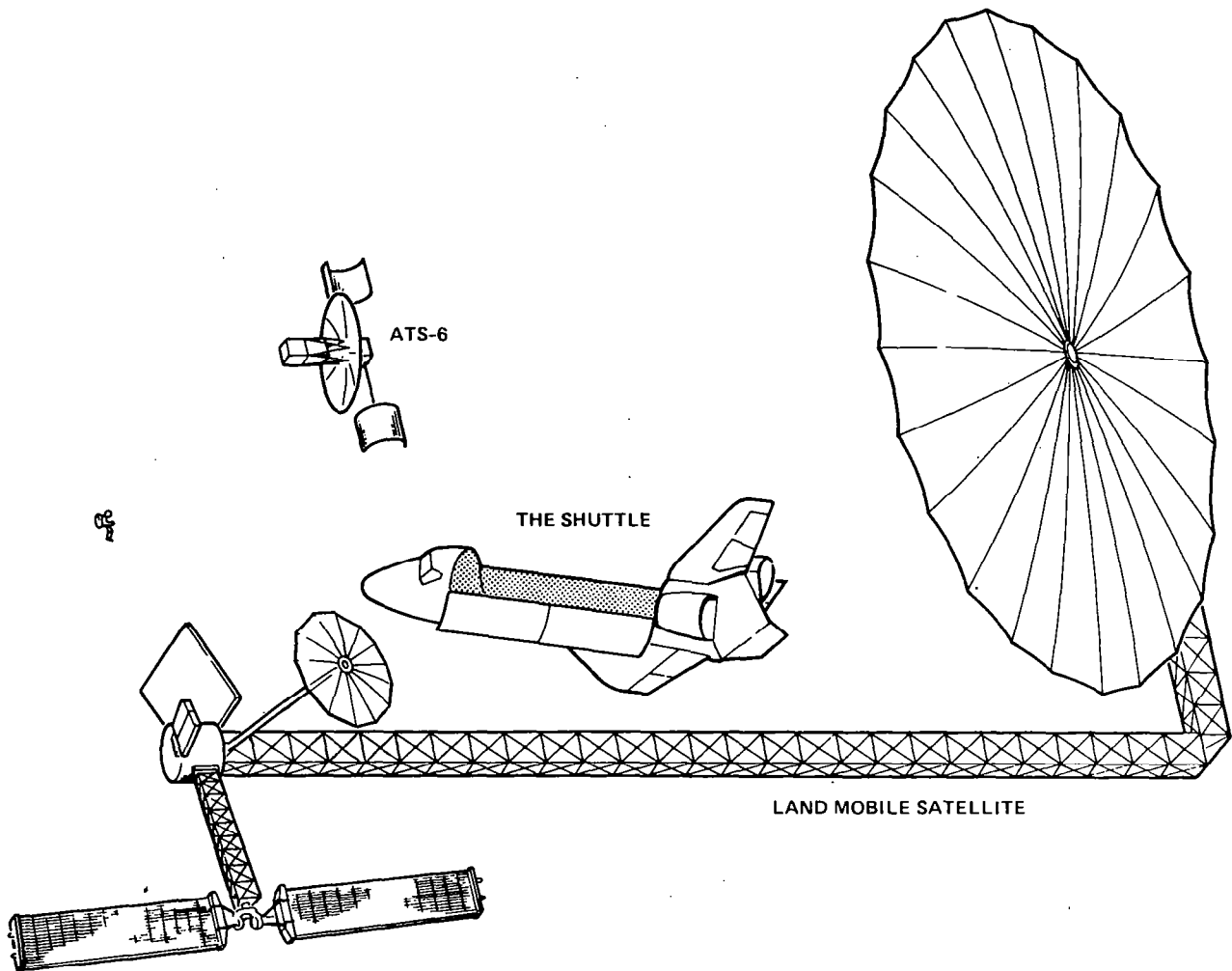
ANTENNA OUTPUT UNDER IDEAL CONDITIONS

A large antenna can be viewed as a means for management of electromagnetic energy. This management may be in the form of collecting or receiving energy, or focusing energy radiation in a particular direction. In fact, if we view the antenna as a device, then the radiation pattern can be viewed as its output. Under ideal (but not achievable) conditions (i.e., having a reflector surface which is perfectly parabolic, a mast that is rigid and maintains perfect alignment of the feed and the reflector, and a perfect feed), the output radiation pattern is well behaved, having low sidelobes, high gain and well pointed boresight. However, as is pointed out on the next page, such an ideal antenna does not exist.

REFLECTOR:

IDEAL PARABOLIC
SURFACE

- PERFECT RADIATION:

    - LOW SIDELOBES
    - HIGH GAIN
    - WELL POINTED BORESIGHT
    - ETC.
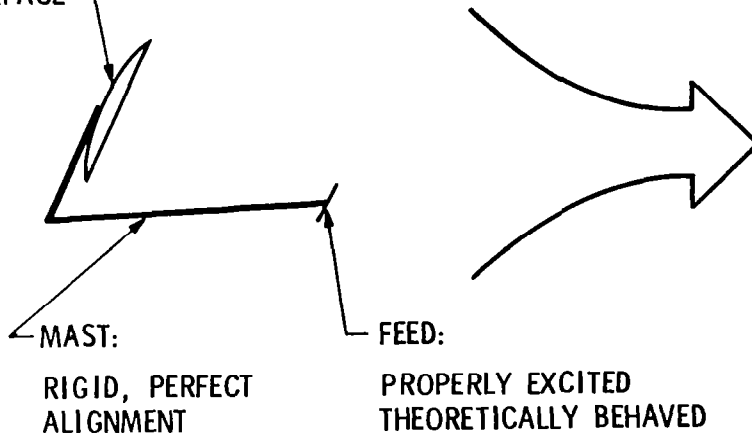
MAST:
RIGID, PERFECT
ALIGNMENT

FEED:
PROPERLY EXCITED
THEORETICALLY BEHAVED

13

WHAT CAN GO WRONG?

In practice, large antennas differ from the idealized antenna in several aspects. First, the reflector surface is distorted away from the desired smooth parabolic surface. This distortion is the result of manufacturing or thermally induced errors, or is simply caused by dynamic disturbances in the spacecraft attitude control system. Furthermore, because of weight considerations the structure of these antennas (both the reflector and the supporting mast) is flexible and is easily excited, resulting in unavoidable system disturbances. The misalignment of the feed and the reflector, which results from the flexible antenna structure, compounds the reflector distortion problem and tends to degrade the antenna output, namely, the radiation pattern. Feed induced errors only tend to exacerbate this degradation.

- ● REFLECTOR SURFACE DISTORTION

  - ● RANDOM

  - ● DETERMINISTIC

- ● FEED INDUCED ERRORS

  - ● FEED EXCITATION

  - ● FEED ARRAY SURFACE DISTORTION

- ● RELATIVE FEED REFLECTOR MOVEMENT

WHICH WAY TO A SUCCESSFUL ANTENNA DESIGN?

Confronted with the problems which were highlighted on the previous page, an antenna system designer is faced with a dilemma of how to design a workable antenna which meets the system requirements (in the case of LMSS, sidelobe levels on the order of -35 dB and pointing requirements of 0.5 degrees with a stability of 0.05 degrees). He has the option of going with a lightweight structure and putting the burden of control and alignment on the control subsystem, necessitating a fairly complex and advanced control technology. Another option is to decide on a fairly rigid structure (sacrificing weight) but relaxing the demand on the control subsystem. A third choice is to opt for sophisticated feed technology not only to produce very low sidelobes but also to compensate for some structural deformity and distortion.

Exercising any of these options, i.e., independent optimization of the RF, structure, and control subsystems, will more than likely lead to either an extravagant or an inadequate design. The key to a successful antenna design is to develop integrated multi-disciplinary design tools which allow tradeoffs and sensitivity analysis across the three disciplines.

Advanced Control Technology

Sophisticated Feed

Rigid Structures

The Key is an Integrated Multi-Disciplinary Technology Development
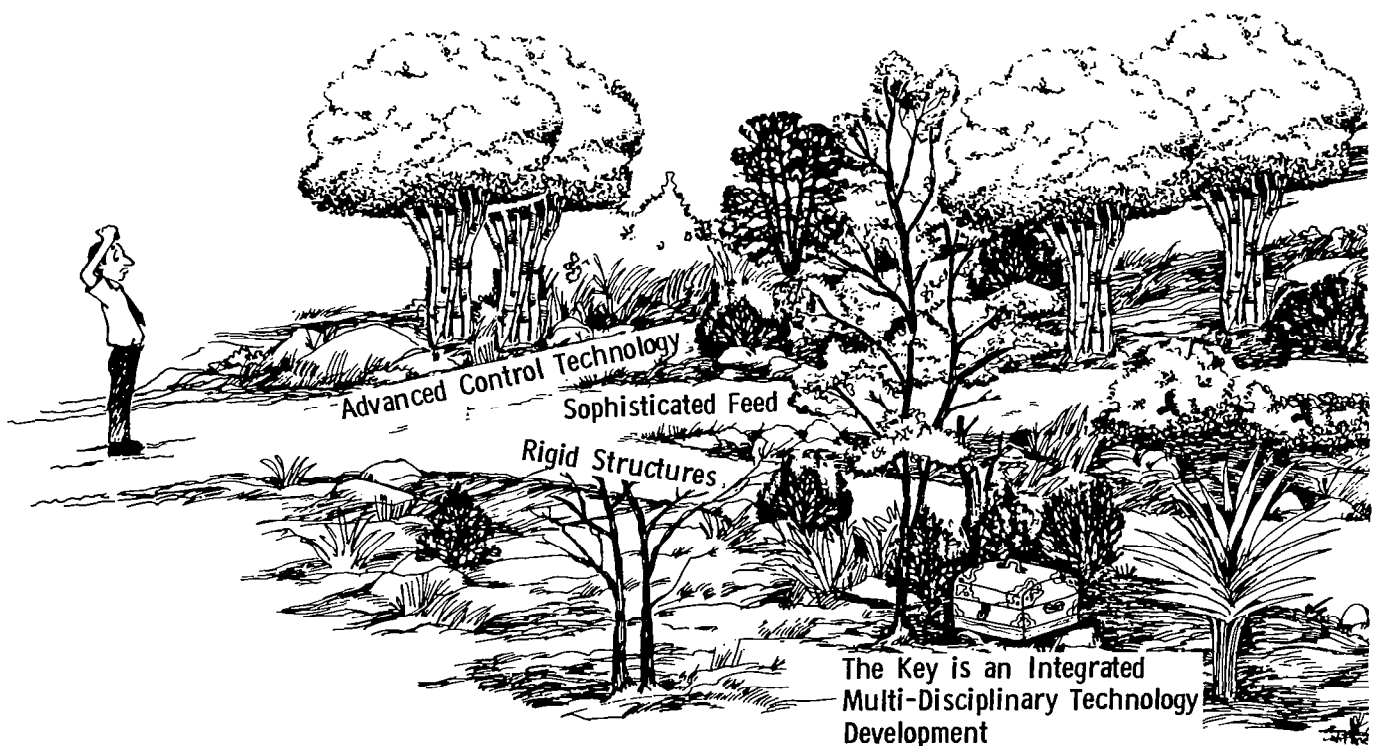
LARGE ANTENNA DESIGN PHILOSOPHY

Summarizing the discussion from the last page, it is important to recognize that the design of large antennas requires close coordination and integration of the RF, structure and control disciplines. This enables the designer to spread the burden of the stringent system design requirements in some optimum fashion among the three subsystems.

- Large Antennas are Systems Whose Successful Designs are Predicated on Close Coordination and Integration of the Following Three Disciplines

  1 - RF

  2 - Control

  3 - Structures

- The Burden of Stringent Design Requirements (e.g. Sidelobe Levels and Pointing) Must be Shared in an Optimum Fashion Among the Three Disciplines

- Independent and Isolated Technology Development in Each Discipline Leads Either to Failure or Extravagant Designs

LAND MOBILE SATELLITE SYSTEM REQUIREMENTS

John D. Kiesling
General Electric Space Systems Division
Philadelphia, Pennsylvania

LAND MOBILE SATELLITE SYSTEM OPERATION

A Land Mobile Satellite System (LMSS) provides voice, data and related communications services to moving vehicles and persons. Communications between the mobiles and satellite are in the 806-890 MHz band. The satellite translates these signals to a "fixed services band" such as 14/12 GHz band (Ku-band), and communicates in this band with fixed terminals called gateways. The gateways are located at convenient places such as telephone switches (which provide entry into the national telephone system), dispatcher headquarters, computer centers, etc. Communications are therefore principally mobile to fixed. A third communications link, also at Ku-band, is needed between the satellite and a single fixed ground station. This link provides satellite command, telemetry and ranging and also provides a network control function. The latter, through a common signalling system, receives requests and assigns channel slots, and otherwise controls, monitors and polices the network and collects billing information.

UHF
(MOBILES)

Ku-BAND
(GATEWAYS)

- NETWORK OPERATIONS CENTER
- SATELLITE OPERATIONS CENTER

- TELCO
- DISPATCHER
- COMPUTER
- CONTROL CENTER
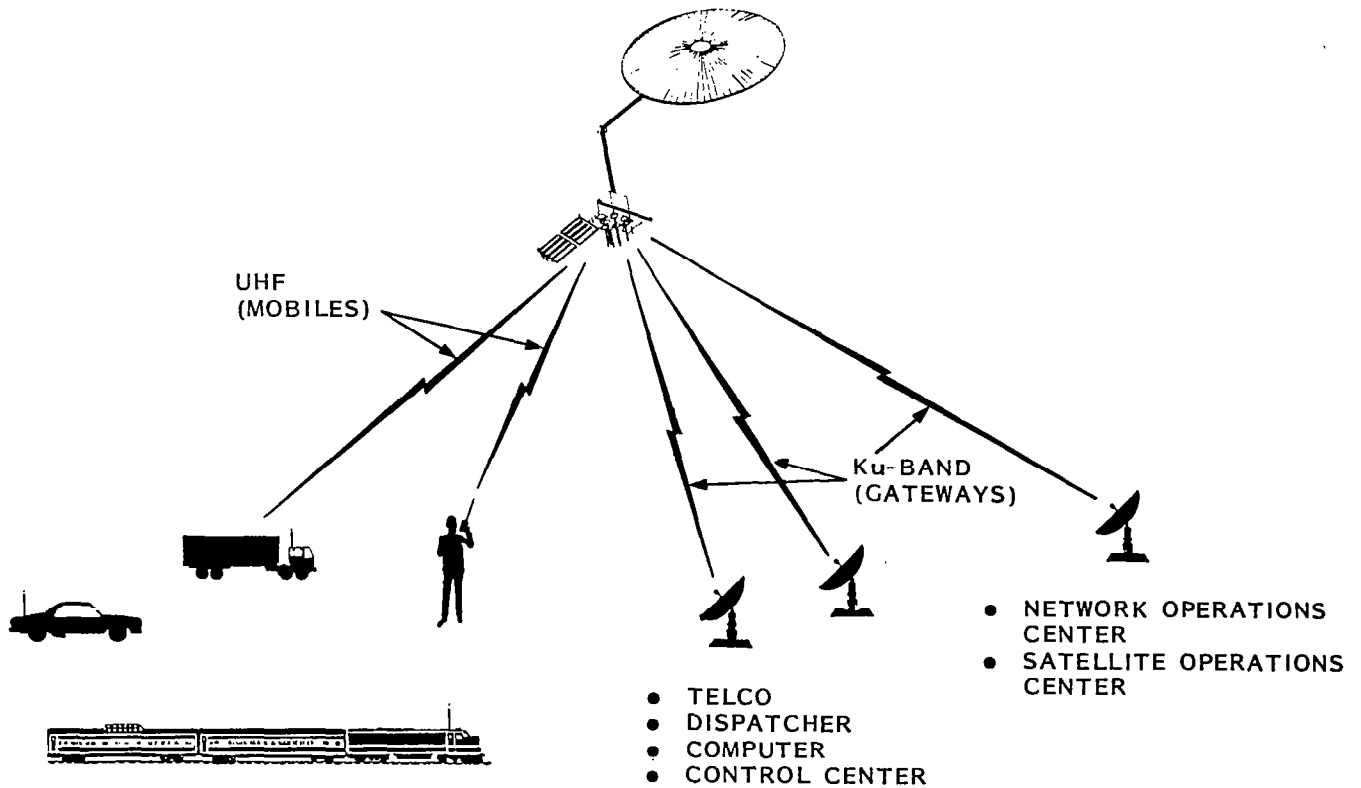
Land Mobile Satellite System Operating Concept

LAND MOBILE SATELLITE CHARACTERISTICS

Vehicle radio equipment including antenna must be low cost and conveniently packaged – consistent with a moving vehicle or person. As a result the mobile radio exhibits relatively low performance in terms of radiated power and sensitivity and therefore the satellite is burdened to provide the additional sensitivity and radiated power so that good communications performance is achieved. Land mobile satellites radiate considerably higher power per voice channel than do fixed services satellites at C-band or Ku-band.

Spectrum also is scarce in the lower frequency radio bandwidth favorable to LMSS, and particularly scarce in the 806-890 MHz band allocated by the ITU to land mobile communications in the Americas. It is estimated that only approximately 10 MHz may be available for a land mobile satellite, (as contrasted to 500 MHz available to fixed satellites in C-band or Ku-band). Ten megahertz is not sufficient bandwidth to provide the needed capacity, consequently multiple spot beams are envisioned, with frequency reuse to generate sufficient bandwidth and hence capacity. This is accomplished by assigning only a fraction, say a fourth, of the total available bandwidth to each beam and then arranging the beams so that co-frequency beams are separated by at least a beamwidth to minimize interference. The resulting UHF antenna is very large, perhaps in the range of 30 to 100 meters. Offset fed configurations are favored for good side lobe performance but this consideration coupled with the large feed system results in an asymmetrical, unbalanced, inconvenient spacecraft configuration.

An example configuration is shown.

COLLAPSIBLE TRUSS REFLECTOR DEPLOYMENT BOOM

AFT MODULE WITH REACTION CONTROL

SOUTH

COLLAPSIBLE TRUSS BUS/FEED DEPLOYMENT BOOM

105 FT DIA. APERTURE "FLEX-RIB" UHF REFLECTOR (DEPLOYED)

1.8 KW SOLAR ARRAY

NORTH

EARTH

17'x17' UHF FEED ASSEMBLY (DEPLOYED)

6' DIA APERTURE KU BAND ANTENNA

EAST (ORBIT)

SPACECRAFT BUS WITH REACTION CONTROL AND ATTITUDE CONTROL SUBSYSTEMS
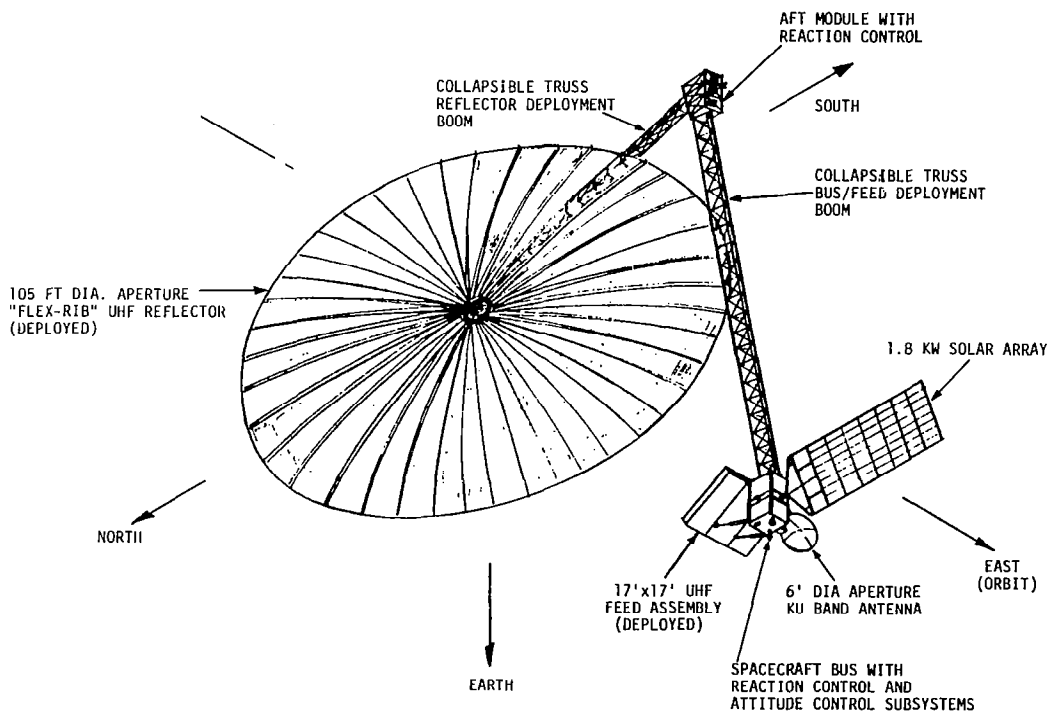
Example Offset, Direct Fed, Parabolic Reflector Configuration

LAND MOBILE SATELLITE SYSTEM SERVICES

Land mobile satellite system users require two generic kinds of services. One is radio telephone, a public network in which the mobile is connected via the satellite and gateway to the national telephone network, thus enabling him to communicate with anyone having a telephone. The second service is special mobile radio or SMR service, in which the mobile is connected via the satellite and a dedicated gateway to the mobile's base station. The base station can be a "dispatcher" for controlling the routing of buses, trucks, trains, etc, a central computer for processing data, such as oil well logging data (data sent by mobiles at oil wells) or some other command and control purpose. An SMR can be either an industry or government network. The table tabulates a projection of the market for LMSS to the year 2000. The prediction is based on an analysis of current trends in terrestrial radio telephone and SMR, which identifies a portion of the market suitable for LMSS by virtue of requirements for extended range including national coverage and better performance. In addition, a new market is identified, consisting typically of long haul trucking and oil and gas well logging, not now effectively served by terrestrial systems. The demand is described in terms of erlangs of traffic intensity, which is numerically equal to the approximate number of telephone circuits required for service during the busy hours.

	1990	1995	2000	SERVICE BANDWIDTH KHz
NEW SERVICES (0.01 ERLANGS PER TRUCK)				
TRUCK TRACTORS (1)	869	959	1059	4
OIL & GAS	430	498	584	
	1299	1457	1643	
COMMERCIAL & PUBLIC RADIO (0.01 ERLANGS PER MOBILE)				
CONSERVATIVE	1113	1562	2190	4
LIKELY	4404	7093	11423	4
OPTIMISTIC	9760	15718	25314	4
RADIO TELEPHONE (0.03 ERLANGS PER MOBILE)				
CONSERVATIVE	1548	1975	2521	15
LIKELY	6507	9126	1280	15
OPTIMISTIC	8634	13906	19503	15
CONSERVATIVE ⎫ (2)	5805	7406	9454	4
LIKELY ⎬	24401	34223	48000	4
OPTIMISTIC ⎭	32378	52148	73136	4
TOTAL				
CONSERVATIVE	8217	10425	13287	4
LIKELY	30104	42773	61066	4
OPTIMISTIC	43437	69323	100093	4

(1) INTERACTIVE DATA DEMAND FOR TRUCK TRAILERS IS NEGLIGIBLE COMPARED TO VOICE TRAFFIC

(2) CONVERTED TO 4 KHz CHANNELS BY RATIO OF 15/4 = 3.75

Total Service Demand, Erlangs

LAND MOBILE SATELLITE SYSTEM CAPACITY

The market projection versus time can be converted into capacity demand versus time for the "conservative," "likely" and "optimistic" cases. Capacity demand is measured in terms of 4 kHz equivalent trunks. That is, some services, voice, data, etc. may use a 4 kHz bandwidth, but others may use 15 kHz, 30 kHz or more. However, all are measured in terms of 4 kHz. The number of satellite antenna beams is depicted at the right in terms of specific satellite concepts A, B, C, D. The "likely" traffic projection in the last decade of this century requires a satellite with 53 antenna beams, or an aperture of 45 meters. Two such satellites are required to provide the service. The "optimistic" market projection for the last decade requires an 88 beam, 58 meter aperture.
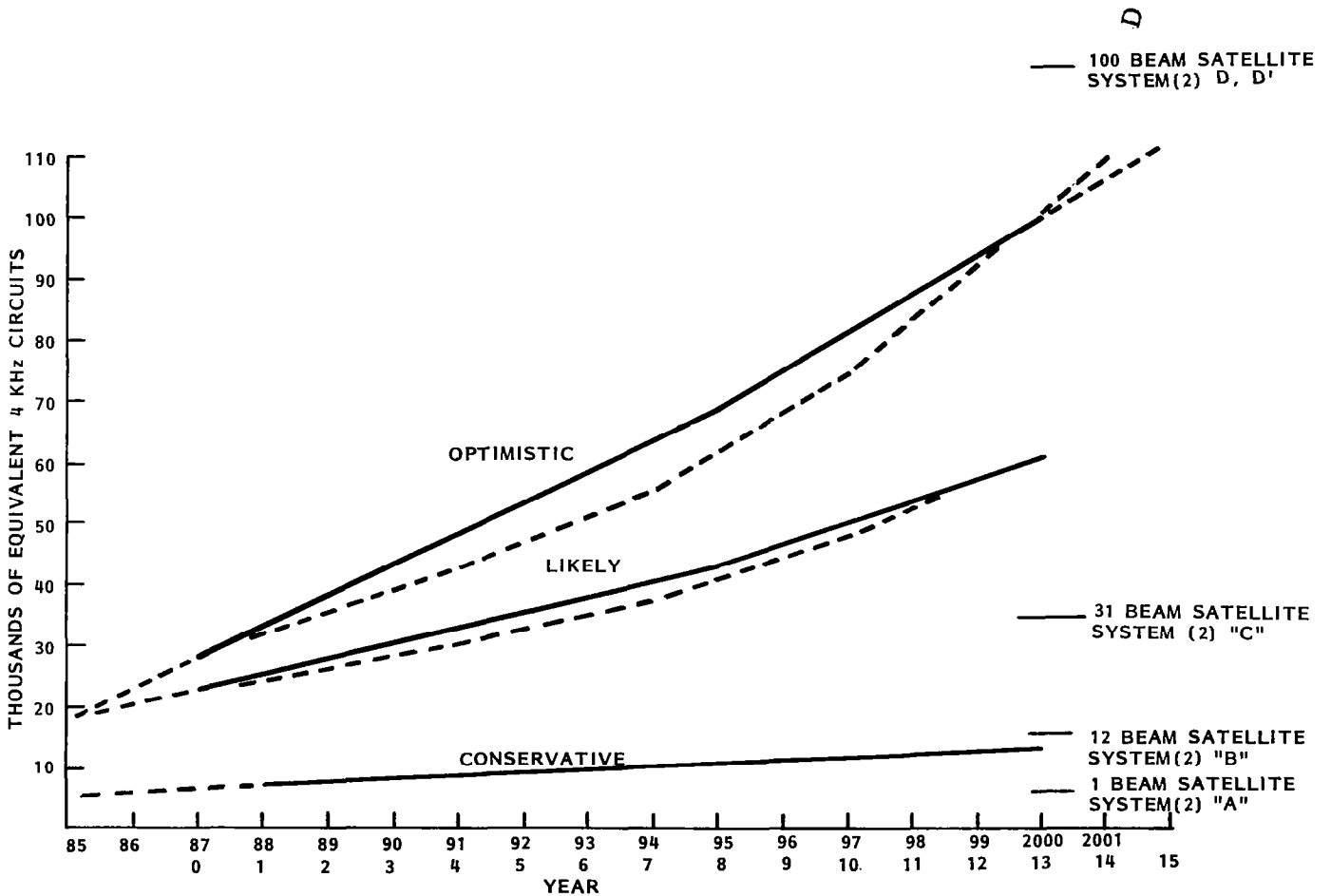
Total Market Projection

LAND MOBILE SATELLITE COMMUNICATIONS CONCEPT

Each beam of a multiple beam antenna contains a receiver and a transmitter. With a 4:1 frequency segmentation plan as previously described, each beam uses only 2.5 MHz of the available 10 MHz. For receiving, the receiver outputs of four such beams can be added together, and such groups translated in frequency to form a continuous spectrum at S-band, which is then amplified in a single amplifier and transmitted to the gateways via a single CONUS antenna beam. The converse occurs in the S-band to UHF link. The transponder arrangement is complicated further by reliability considerations which require M/N redundancy and therefore complex, heavy arrays of "ring" switches. In addition, the assumed allocated UHF and S-bands have their respective transmit and receive bands close together so that complex, heavy filters are required in each beam to diplex receivers and transmitters. Also, it turns out that for numbers of beams greater than 31, a single S-band beam no longer suffices because of an inadequate allocation (only 190 MHz is available). For higher capacity, multiple S-band beams are required which increases the routing problem within the satellite, possibly requiring on-board switching. Alternatively, Ku-band with 500 MHz allocation can be used for fixed link. A single Ku-band beam is sufficient; however, the high capacity and extra rain margins needed increase the Ku-band power significantly.

While repetitive from beam to beam these transponder arrangements still represent a substantial engineering challenge to achieve the performance, reliability and low weight characteristic of satellite systems.
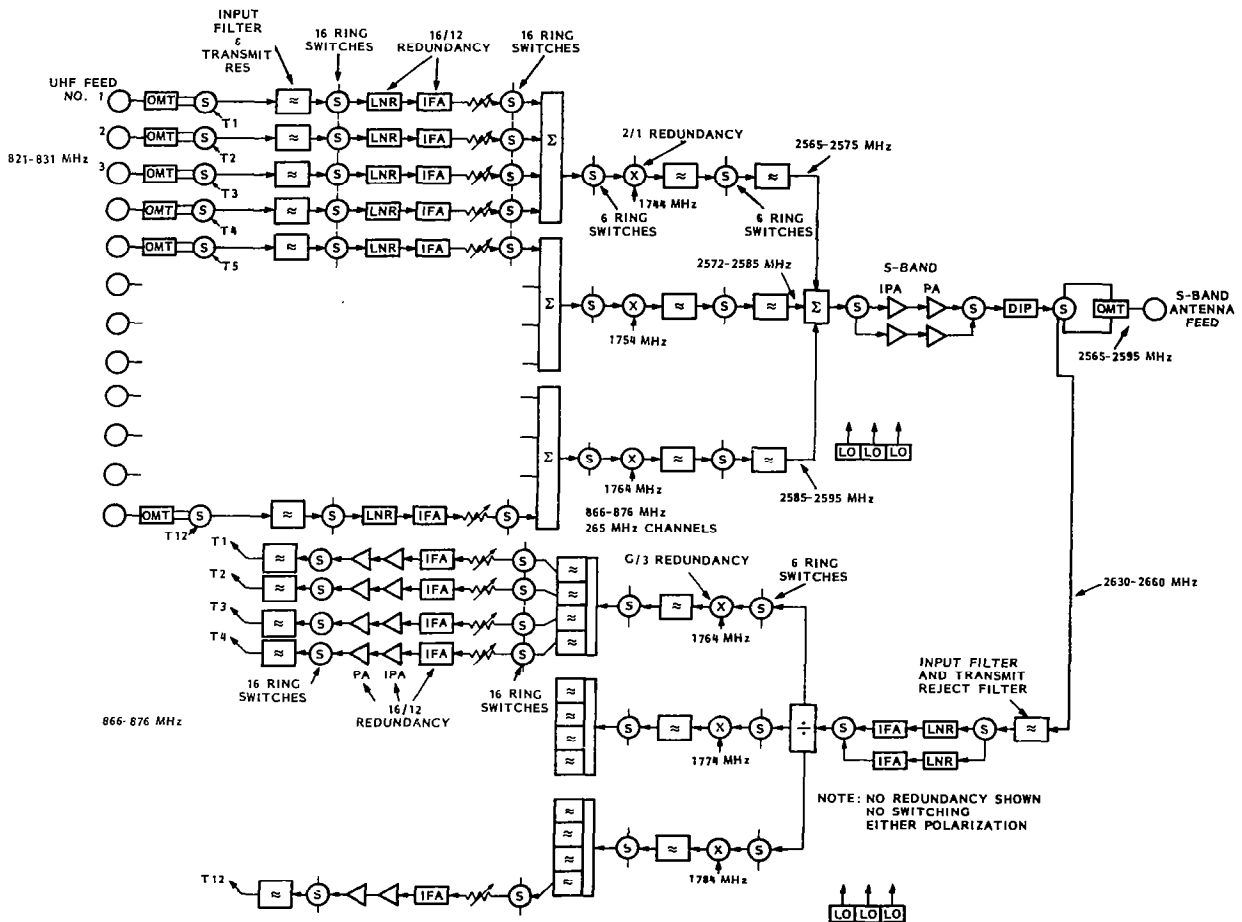
Multiple Beam Transponder Configuration

LAND MOBILE SATELLITE MASS AND POWER

The mass and power of various LMSS satellite configurations can be estimated subsystem by subsystem. Five specific concepts were examined, each for three different UHF power levels over a 10 dB range. Concepts A, B and C use single beam S-band fixed links. Concept D uses a 15 beam S-band fixed link with on-board SS-FDMA routing and switching. An alternative, Concept D', uses a single Ku-band beam.

Concept A spacecraft power is high relative to its capacity because of the lower gain of its single beam antenna. Concept D mass and power are both high due to the complex routing and switching system. Concept D' power is high because of the Ku-band link.

It is apparent that the satellite mass and power are large for the multiple beam configurations. This is characteristic of any LMSS with a reasonable capacity.

CONCEPT	NO. OF UHF BEAMS	NO. OF FS BEAMS	TOTAL BANDWIDTH* MHz	UHF TRANSMIT POWER PER BEAM WATTS	FS TRANSMIT POWER PER BEAM WATTS	ROUTING CONCEPT	SPACECRAFT WEIGHT LBS	SPACECRAFT POWER WATTS
A	1	1	10	174	3.5	FDMA	593	767
A1	1	1	10	550	3.5	FDMA	1,012	1,948
A2	1	1	10	1,738	3.5	FDMA	2,053	5,682
B	12	1	30	3.5	8.3	FDMA	1,798	540
B1	12	1	30	11.2	8.3	FDMA	1,913	844
B2	12	1	20	35.5	8.3	FDMA	2,051	1,059
C	31	1	77.5	1.2	21.4	FDMA	3,422	687
C1	31	1	77.5	3.9	21.4	FDMA	3,524	961
C2	31	1	77.5	12.4	21.4	FDMA	3,809	1,789
D	100	15	250	0.26	0.44	SS-FDMA	16,647	9,033
D1	100	15	250	0.84	0.44	SS-FDMA	16,738	9,221
D2	100	15	250	2.6	0.44	SS-FDMA	17,011	9,775
D'	100	1	250	0.26	954	FDMA	12,316	2,624
D'1	100	1	250	0.84	954	FDMA	12,360	2,802
D'2	100	1	250	2.6	954	FDMA	12,531	3,367

* PER SATELLITE

Summary of Concept Characteristics

LAND MOBILE SATELLITE SYSTEM INVESTMENT AND MASS CHARACTERISTICS

Satellite costs can be estimated using the methods described in the SAMSO* model. Design cost, cost of three satellites, two launch vehicles, insurance, launching services, and control centers define the LMSS space investment (excluding gateways, mobiles, expenses, etc) for the 5 concepts studied. Investments versus spacecraft mass for the five concepts are located in the figure, and a dashed line representing investment versus mass is indicated, as if these relationships were a continuous function. Investment is proportional to mass (it is obvious the mass has an exponent nearly equal to one). UHF power over the 10 dB range has no substantial effect on space system investment; only the single beam concept investment is affected by UHF power. The investment trends versus mass seem reasonable by present experience; however, it is apparent that very large investments will be required for the multiple beam configurations, approximately $500 M for the 12 beam Concept A and approximately $2000 M for the 100 beam Concepts D and D'.

---

* Unmanned Spacecraft Cost Model, Fifth Edition, DOD Space Division, SAMSO, SD-PR-81-45, June 1981.
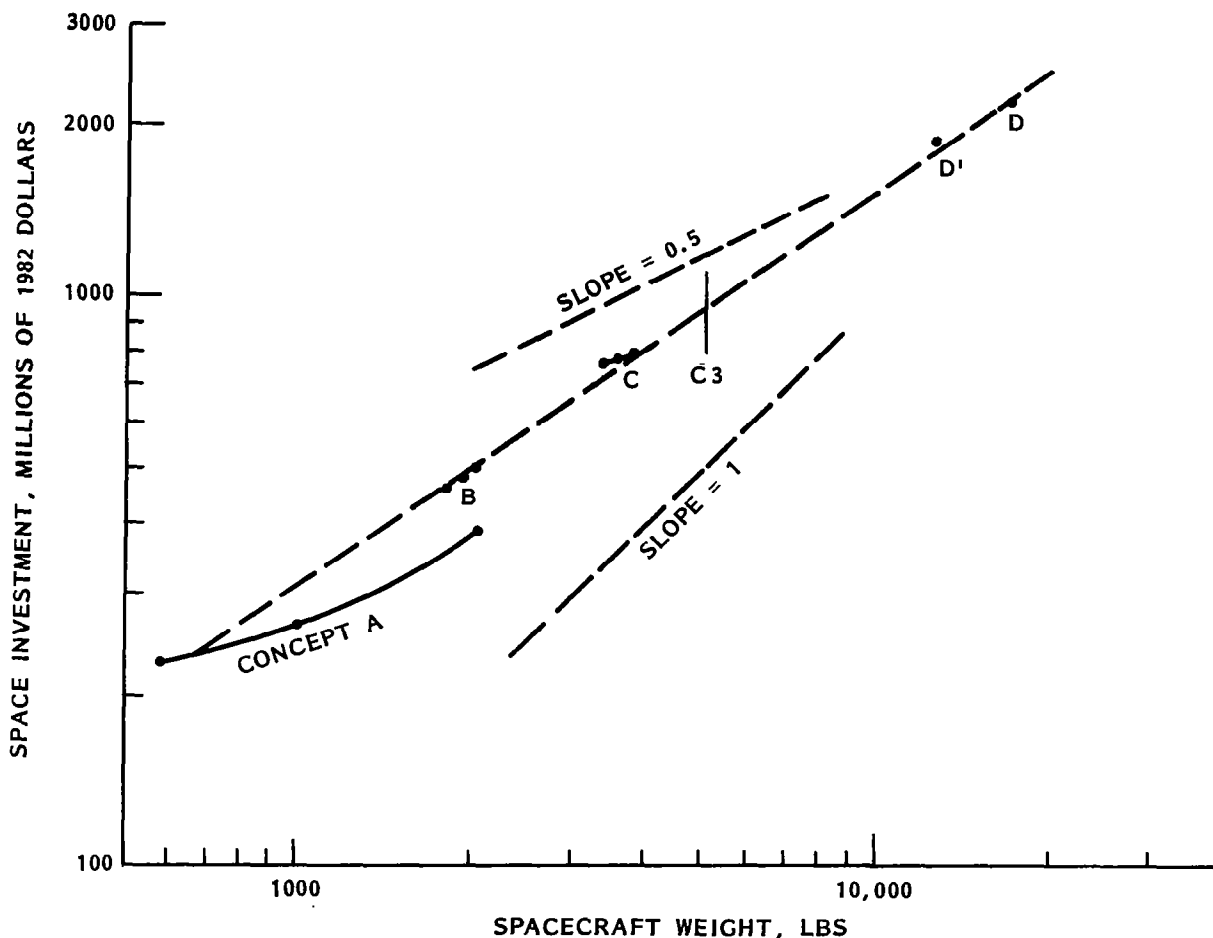
Space Investment vs Spacecraft Weight

LAND MOBILE SATELLITE INVESTMENT VERSUS CAPACITY

Space segment investment versus capacity in equivalent 4 kHz circuits shows two interesting trends. From Concept A to B costs versus capacity escalates rapidly. This is due to the change from a single beam configuration with 10 MHz bandwidth to a 12 beam configuration with only 2.5 MHz per beam, e.g., 12 beams increases capacity only by a factor of 3.

Investment versus capacity also increases dramatically in the region past Concept C for the reasons described previously. The on-board SS-FDMA weight and power for Concept D is substantial. The Ku-band power for Concept D' is substantial. Since the slope is nearly one there is little economy of scale in this region; e.g., the investment per equivalent circuit is nearly constant.
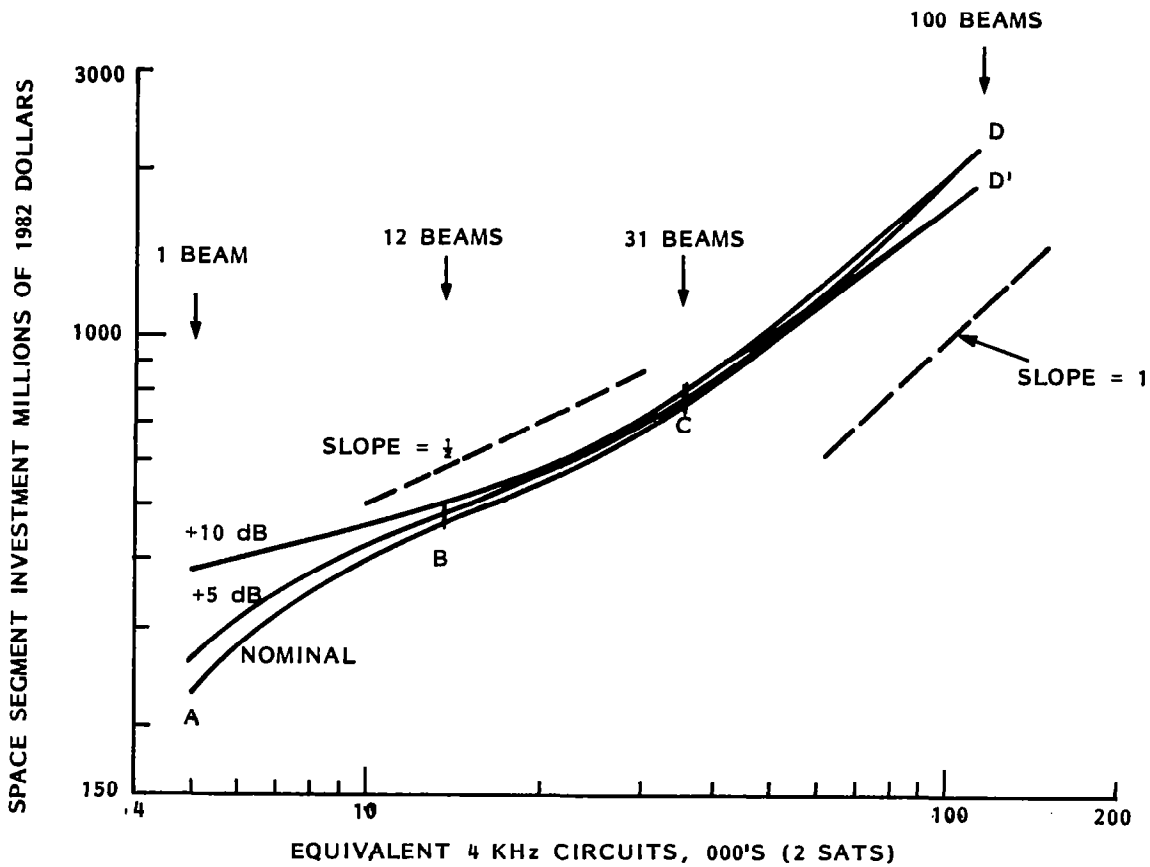
Space Investment vs Equivalent 4 KHz Circuits

LAND MOBILE SATELLITE ON ORBIT CONFIGURATION

A satellite configuration based on a 105' UHF antenna has a modest capacity with regard to the potential market described herein, yet is a substantial technical undertaking, considerably beyond present experience in a number of areas:

- Deployment of a large, offset (non symmetrical) 105' antenna reflector

- Location of the heavy communications module, containing feeds, low noise amplifiers, power amplifiers, etc. at the offset focus

- Deployment of solar arrays and fixed services antenna

- Attitude and orbital control of large, extended, flexible structure with inconvenient center of gravity and time varying (in orbit) center of pressure

- Thermal control of extended structure containing various active modules.
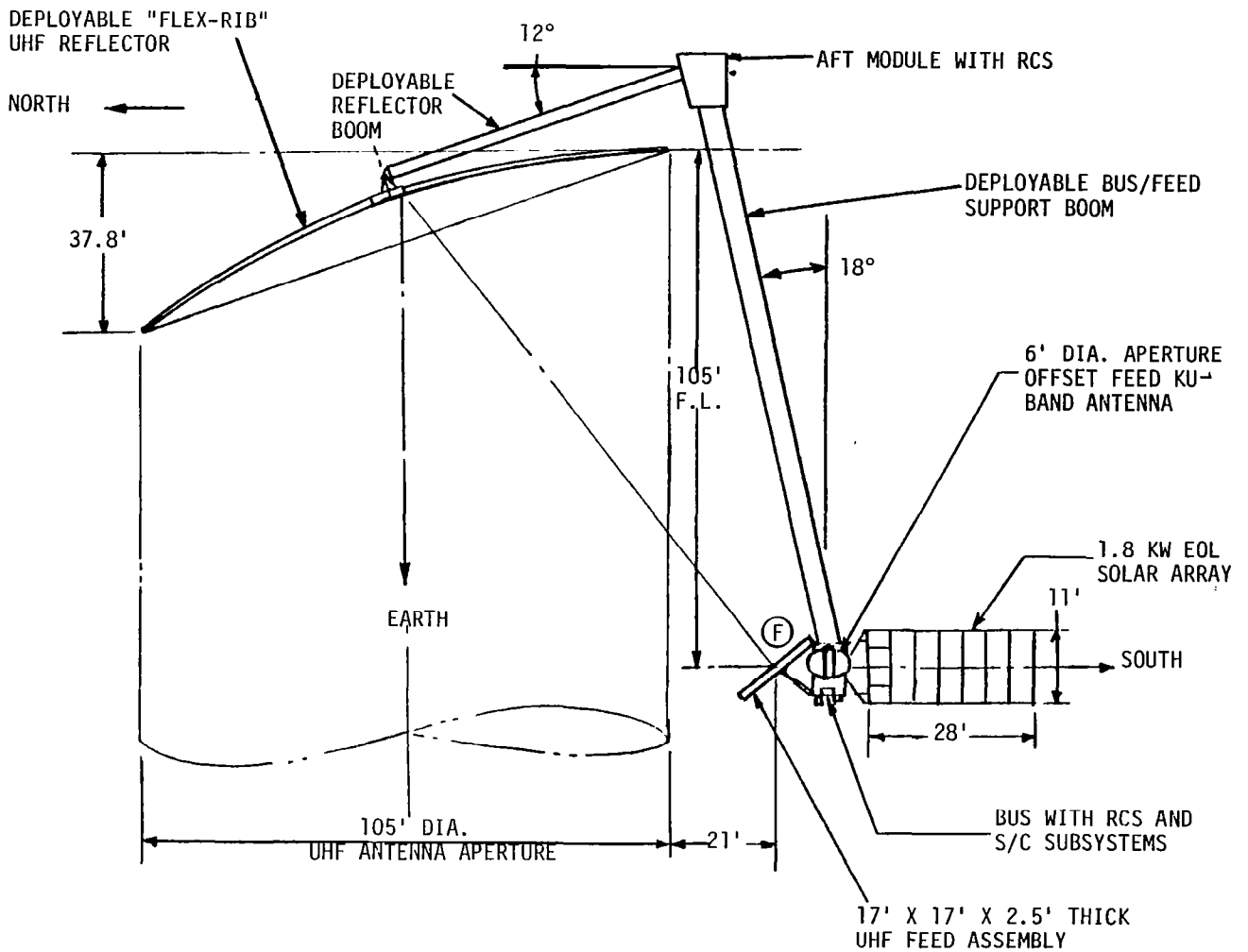
On-orbit Spacecraft Configuration

LAND MOBILE SATELLITE LAUNCH CONFIGURATION

The satellite is shown in its launch configuration. Stowage of the deployable UHF antenna, extendable booms which form the spacecraft structure and modules containing communications, solar array, propulsion, attitude control and fixed services antenna is a substantial technical challenge. Ground test of deployment is probably not feasible, and an in-orbit test risks a vast sum of money.

VIEW LOOKING AFT

Launch Configuration
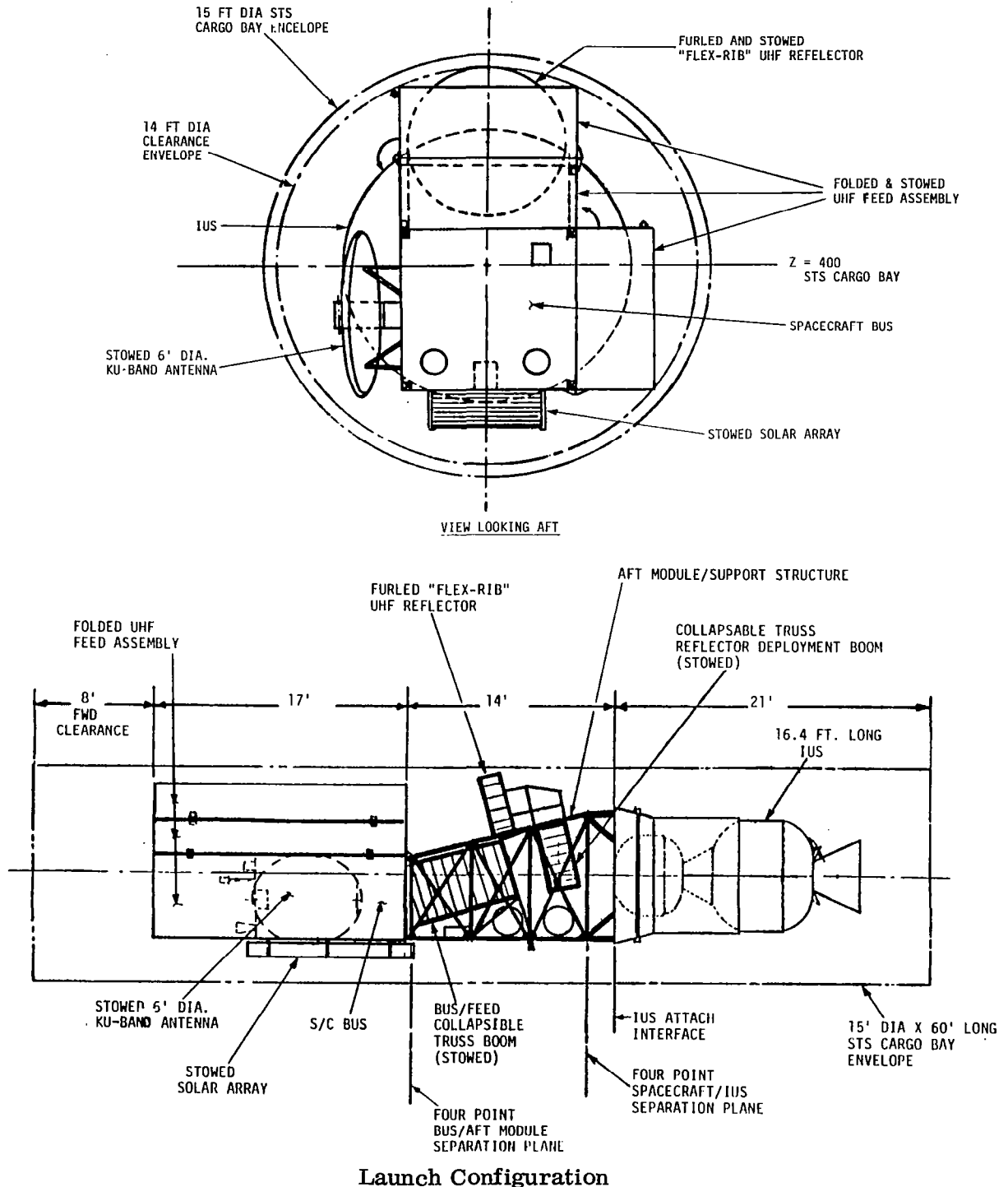
LAND MOBILE SATELLITE SYSTEM TECHNOLOGY

The table is a compendium of problems to be resolved prior to deployment of experimental or operational land mobile satellites. Particularly disturbing issues relate to antenna deployment and to the peculiarities of controlling such a large flexible spacecraft with distributed elements. Thermal control, attitude control and orbit control techniques will surely be different than those employed in present day compact, rigid satellites. The right hand column is GE's recommendations to NASA on how these problems might be solved in an ongoing developmental program leading to the deployment of an experimental/developmental land mobile satellite.

In addition to detailed design studies, technology development involving "proof of concept" or POC is needed for the satellite antenna and the satellite UHF power amplifiers.

ITEM	CHARACTERISTICS	ISSUES	PROGRAM
DEPLOYABLE MULTIPLE BEAM UHF ANTENNA	$\approx$ 34 FEEDS, (INCLUDING OFF-SHORE), 28 METERS, OFFSET FED, UHF RECEIVE TRANSMIT	DEPLOYMENT IN GEOSYNCHRONOUS OR STS ORBIT (WITH RETRACTION CAPABILITY?); EVA SUPPORT (?); MECHANICAL PROPERTIES FOR ATTITUDE CONTROL AND SECONDARY PROPULSION; LOCATION OF LNA'S, HPA's	REQUIREMENTS DEFINITION STUDY, ONGOING LARGE APERTURE DEVELOPMENT, PHASE "C" DESIGN STUDY; FEED POC
SPACECRAFT BUS	$\sim$ 3950 LBS, 1800 WATTS, STS LAUNCHED	ANTENNA STOWAGE AND DEPLOYMENT; FEED STOWAGE AND DEPLOYMENT; CONVENIENT CG SYSTEM; RF AND DC POWER LINE LENGTHS; MECHANICAL RESONANCE, STIFFNESS, MOMENTS	REQUIREMENTS DEFINITION STUDY; PHASE "C" DESIGN STUDY
FILTERS/DIPLEXERS	FREQUENCY TRANSLATION, DIPLEXING	SELF INTERFERENCE FROM SPURIOUS; ACTIVE/PASSIVE INTERMODULATION INTERFERENCE WITH SATELLITE RECEIVER; SATELLITE USEFUL BANDWIDTH, RERADIATION OF OUT OF BAND INTERFERENCE, RECEIVER INTERMODS CAUSED BY OUT OF BAND INTERFERENCE; EFFICIENT RECEIVE/TRANSMIT DIPLEXING; GAIN STABILITY. LIGHTWEIGHT FILTERS, DIPLEXERS, CONVERTERS	REQUIREMENTS DEFINITION STUDY, PHASE "C" DESIGN STUDY
LAUNCH VEHICLE	IUS OR IUS DERIVATIVE OR ALTERNATIVE	COST	REQUIREMENTS DEFINITION STUDY, PHASE "C" DESIGN STUDIES
FIXED LINK	SINGLE BEAM FOR CONUS (PLUS OFFSHORE SPOTS) $\sim$ 5'; TWTA POWER	SSPA ALTERNATIVE; TWTA REDUNDANCY SCHEME	REQUIREMENTS DEFINITION STUDY, PHASE "C" DESIGN STUDY
LINEARIZED UHF AMPLIFIERS	12 WATT MODULES, EFFICIENCY GREATER THAN 35%	EFFICIENCY; INTERMODULATION LEVELS; REDUNDANCY ARRANGEMENTS	LINEAR AMPLIFIER POC
ACS	POINTING CAPABILITY $\approx$ 0.2°	STABILITY; ON ORBIT ASSESSMENT, ADJUSTMENT OF PARAMETERS; EFFECT OF FLEXIBLE STRUCTURE; EFFECT OF CG	REQUIREMENTS DEFINITION STUDY, PHASE "C" DESIGN STUDY
SECONDARY PROPULSION	STATIONKEEPING ± 0.1°	EFFECT OF CG; LOCATION OF THRUSTERS; THERMAL CONTROL; REDUNDANCY	REQUIREMENTS DEFINITION STUDY, PHASE "C" DESIGN STUDY
POWER	1800 WATTS, SUBSTANTIAL ECLIPSE CAPABILITY	NONE (LIGHTWEIGHT MODERN ARRAY, NICKEL HYDROGEN BATTERIES)	REQUIREMENTS DEFINITION STUDY, PHASE "C" DESIGN STUDY
THERMAL	ANTENNA SHADOWING, DISPERSED ACTIVE COMPONENTS, ECLIPSE TEMPERATURE-PASSIVE SYSTEM	NONE	REQUIREMENTS DEFINITION STUDY, PHASE "C" DESIGN STUDY
TT&C	CONVENTIONAL SYSTEM	NONE	REQUIREMENTS DEFINITION STUDY, PHASE "C" DESIGN STUDY

Space Segment Technology Assessment

SATELLITE SYSTEMS REQUIREMENTS
FOR LAND MOBILE COMMUNICATIONS

M. Horstein
TRW Space & Technology Group
Redondo Beach, California

SYSTEM REQUIREMENTS

The system design objective is to provide a satellite link through a gateway station, connecting mobile users in areas not served by a terrestrial cellular system to the switched telephone network (STN). The proposed frequency allocation comprises a pair of 10-MHz bands in the 806-890 MHz range specified by the 1979 World Administrative Radio Conference (WARC) for land-mobile satellite service (LMSS). The satellite design is constrained by projected STS capability with an upper stage of the wide-body Centaur or Integral Propulsion System (IPS) type. For the latter (a TRW design), the payload is limited to approximately 10,400 lb. The design is to be based on 1990's technology, with initial operating capability scheduled for 1995. The satellite should be designed for a 7-year life. Mobile-unit compatibility with cellular system specifications is desirable, if consistent with other system requirements.

GATEWAY
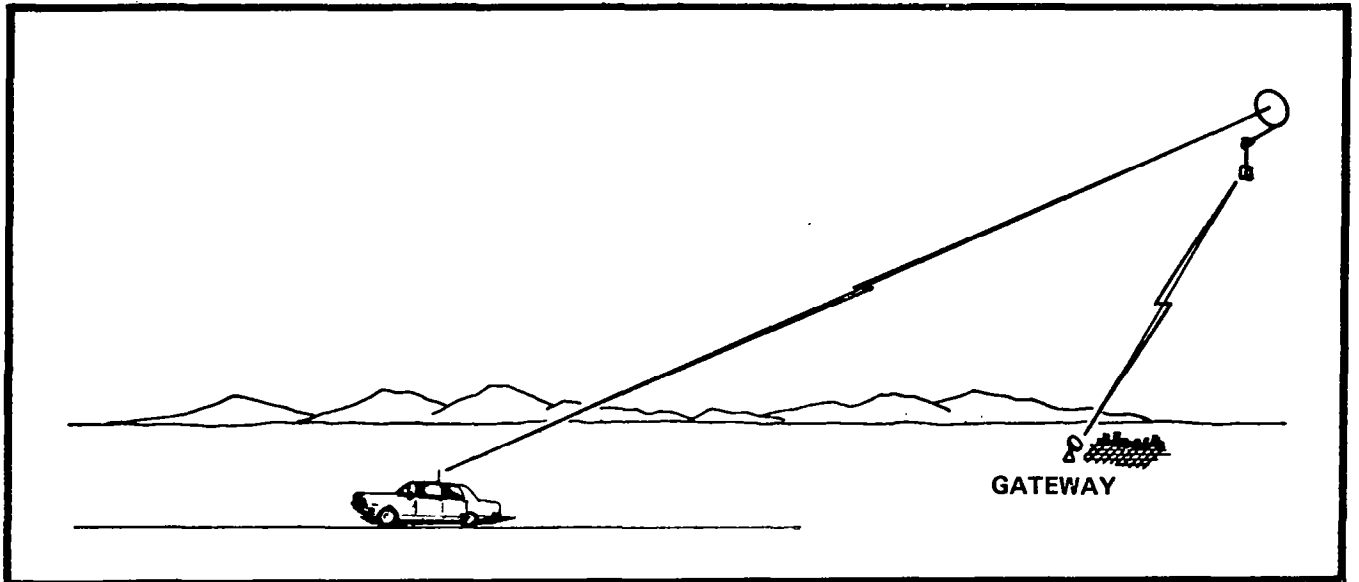
CELLULAR–SYSTEM COMPATIBILITY ISSUES

A separate mobile–unit antenna is required for satellite communications, where elevation angles range from 10° to 60°. By contrast, cellular system transmission is confined to directions close to the horizon. Mobile units and base stations in cellular systems are typically designed with receiver noise figures of 9 dB. Much smaller mobile–unit noise figures are required for satellite operation to minimize satellite power requirements. Cellular system call–setup procedures must be modified because of the relatively long round–trip satellite propagation delay of 0.5 second. A random–access protocol of the ALOHA type is suitable in the satellite case. Finally, to be compatible with cellular–system transmission, narrowband FM with 2:1 compounding and a peak deviation of 12 kHz is required. The carrier noise bandwidth is 27 kHz and the associated carrier spacing is 30 kHz.

- **SEPARATE MOBILE ANTENNA REQUIRED FOR SATELLITE OPERATIONS**

- **LOWER-NOISE-FIGURE RECEIVER REQUIRED FOR SATELLITE OPERATIONS**

- **RANDOM-ACCESS PROTOCOL FOR CALL SETUP REQUIRED IN SATELLITE SYSTEM**

- **NARROWBAND FM, WITH 30-kHz CHANNEL SPACING, USED IN CELLULAR SYSTEM**

MULTIPLE-BEAM CONUS COVERAGE

A multiple-beam satellite antenna structure, which permits frequency reuse, provides the necessary system capacity. A typical CONUS-coverage beam pattern as seen from geosynchronous orbit is shown in the figure. Beam crossovers occur at the half-power point. To avoid excessive cochannel interference, a certain minimum distance must be maintained between beams using the same frequencies. Depending on the feed/reflector geometry (i.e., whether offset-fed or center-fed), the set of available carrier frequencies is divided into either four or seven subsets, with one subset assigned to each beam. Accordingly, the frequency reuse factor is either 1/4 or 1/7 times the number of beams generated. The channel capacity for the system is given by the product of the frequency reuse factor and the number of channels per beam.

A separate gateway station is typically provided for each 7-beam UHF cluster. Any of the fixed-satellite frequency bands could be used for the satellite/gateway links. Ku-band (14/12 GHz) is preferred because of its ample allocation and relatively modest rain attenuation. (C-band was deemed too crowded for consideration).

0.48-DEG HPBW

GATEWAY
BEAM CLUSTER
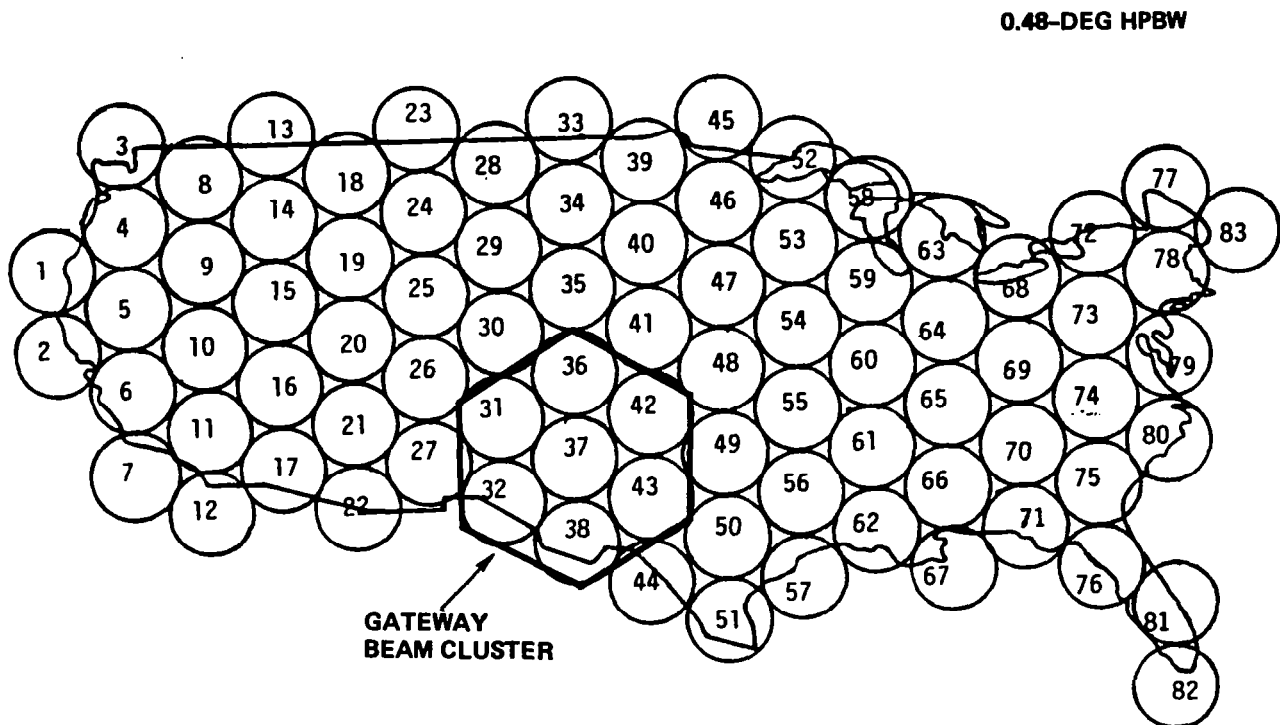
FREQUENCY REUSE

It is desirable to divide the full complement of carrier frequencies into as few subsets as possible to minimize the number of beams and, therefore, the reflector diameter needed to accommodate the projected system traffic. Cochannel interference analysis indicates that 4 frequency sets suffice with an offset-fed reflector, but that 7 frequency sets are required with a center-fed reflector. In the former case, the minimum distance between cochannel beams (i.e., between beam centers) is 2 HPBW. In the latter case, the minimum separation is 2.65 HPBW. The added separation for the center-fed reflector is needed to avoid high-level comalobes (the first in-board sidelobe) resulting from the feed blockage.

4 FREQUENCY SETS
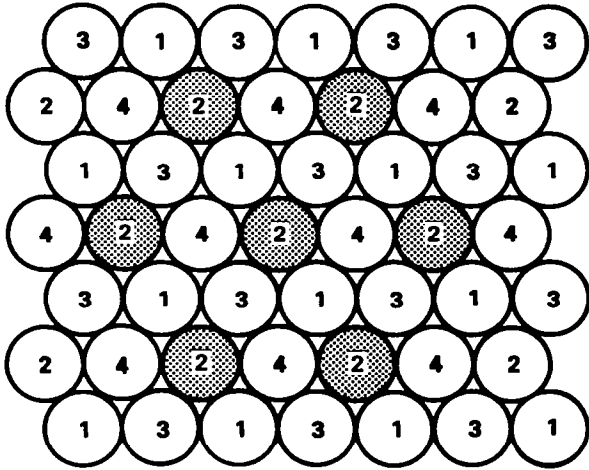
7 FREQUENCY SETS
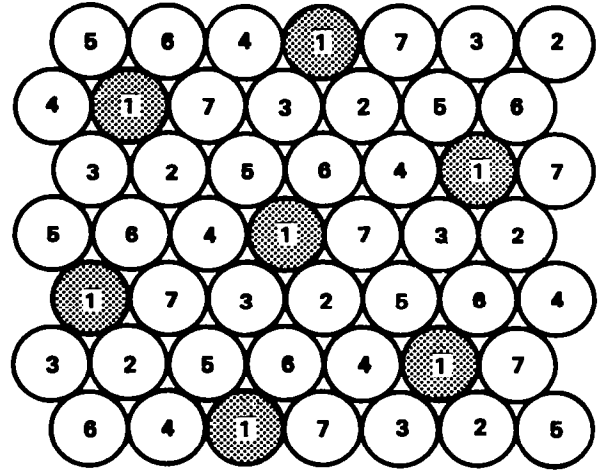
SUBSCRIBER SCENARIO

The baseline satellite designs accommodate roughly 350,000 subscribers at the end of seven years of system operation. Traffic is limited to radio-telephone service. (Dispatch or data traffic, which would also be served by a satellite system, is not considered). On the average, a subscriber is assumed to contribute 0.026 erlang to the busy-hour traffic load. Thus, the system is designed for a capacity of about 9,000 erlangs.

The satellite design, and the reflector diameter in particular, is determined by the end-of-life traffic load. On the other hand, the rate of traffic build-up determines the revenue profile over the life of the system and therefore strongly influences the subscriber charge associated with a particular satellite design.

GEOGRAPHIC SUBSCRIBER DISTRIBUTION

The required system capacity (i.e., the number of beams) depends on the per-beam subscriber statistics. The number of subscribers in a given beam can be computed as the product of two factors: 1) the average number of subscribers per square mile, and 2) the beam area in square miles. The first factor is illustrated by the map below (derived from data in Reference 1) on a state-by-state basis. The second factor depends on satellite longitude and beam location. Beam areas corresponding to a given solid angle are generally larger in the northern regions and therefore tend to include a greater number of subscribers. Thus, the second factor tends to reinforce the effect of the first factor in the heavily populated northeast part of CONUS.

The net effect of the nonuniform subscriber distribution is to require about twice the number of beams as would be needed for a uniform distribution, if the subscribers in all beams are to be provided a reasonable grade of service.

x10^{-9} **SUBSCRIBERS/SQ.MI.**
TOTAL SUBSCRIBERS

- 0–100
- 101–200
- 201–300
- 301–400
- 401–550
- 551–667

BASELINE SYSTEM CHARACTERISTICS

To accommodate the subscriber population and geographic distribution described, extreme bandwidth efficiency is required. This led to the choice of a non-cellular-compatible form of modulation: FM with 5-kHz peak deviation and 12-kHz channel spacing, as compared with 12-kHz and 30-kHz, respectively, for the cellular system. The former peak deviation is characteristic of terrestrial noncellular mobile radio systems.

Additionally, it was found necessary to use two satellites, each providing CONUS coverage, for STS compatibility. Each satellite generates only half the number of beams that would be required with a single satellite; consequently, the satellite antenna can be made smaller by a factor of $\sqrt{2}$ than that needed with a single satellite.

The user must be able to discriminate between cochannel transmissions from different satellites. The necessary discrimination is provided by a mechanically steerable antenna, about 2 ft. long, which consists of a linear array of microstrip patches.

Two baseline satellite designs were developed. One is based on an offset-fed reflector and the other utilizes a center-fed configuration. Four frequency sets suffice for the former, but seven are required for the latter.

- **NON-CELLULAR-COMPATIBLE FM**

  − **5-kHz PEAK DEVIATION**

  − **12-kHz CARRIER SPACING**

- **TWO-SATELLITE SYSTEM**

  − **33-DEG LONGITUDINAL SPACING**

  − **EACH SATELLITE PROVIDES COMPLETE CONUS COVERAGE**

- **MECHANICALLY STEERABLE USER ANTENNA**

- **FEED/REFLECTOR GEOMETRY**

  − **OFFSET-FED, 4 FREQUENCY SETS**

  − **CENTER-FED, 7 FREQUENCY SETS**

USER ANTENNA CONCEPT

The prime requirement placed on the user antenna is to reject cochannel signals from the unwanted satellite, while providing reasonable gain in the direction of the desired satellite. The required directivity is provided by a linear array of four microstrip patches spaced by one-half wavelength. The antenna length is slightly over 2 feet.

After the antenna boresight is rotated to the azimuth of the desired satellite, it is held in that direction, despite any user vehicle motion, by a monopulse tracking system. The gain toward the desired satellite is maintained close to the boresight value by a suitable (semi-permanent) tilt of the plane of the antenna. For a typical tilt angle of 45°, a minimum gain of about 9 db can be realized from any point in CONUS.

Rejection of cochannel signals is aided by employing one sense of circular polarization with one satellite, and the opposite sense with the other. The user antenna would be switchable between the two polarization senses.

TILT
ANGLE

FEED
POINT

PRINTED
MICROSTRIP
CIRCUIT
ELEMENTS

ROTATOR

180° HYBRID
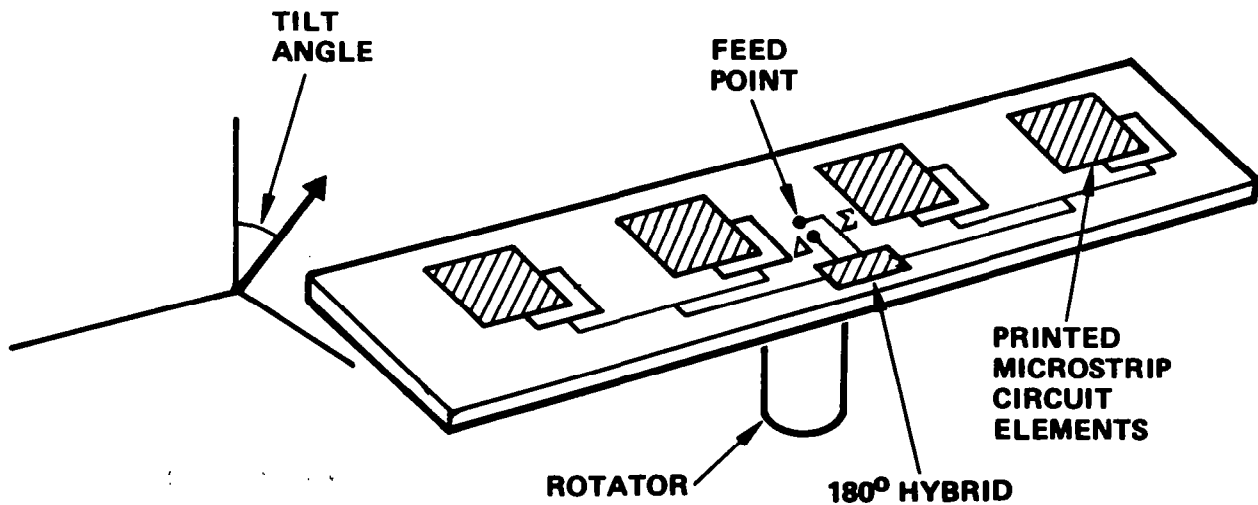
OFFSET-FED SATELLITE CONFIGURATION

A 46-m reflector is required in the offset-fed configuration, which employs 4 frequency sets. A total of 61 beams is generated, with a HPBW of 0.57°. Each beam can support as many as 208 voice channels, a small number of which must be reserved for signaling purposes.

A wrap-rib design is employed for the reflector. A total of 36 ribs is required to ensure surface accuracy compatible with good sidelobe performance. The reflector is supported from the rear, at its center, by an L-shaped mast. The main mast is 69 m long, a length made necessary by sidelobe considerations. This mast length provides an f/D of 1.5 with respect to the reflector diameter, or 0.67 with respect to the parent parabola. The flexibility of this structure (<1 Hz response frequency) necessitates advanced attitude control concepts.

Power considerations on transmission, and signal quality considerations on reception, demand that the UHF power amplifiers and receivers be located on the feed assembly. Thermal hardware for heat dissipation must also be collocated with the feeds.

A 3-m Ku-band antenna provides a multibeam structure for satellite/gateway transmission with beamwidths comparable to those at UHF.
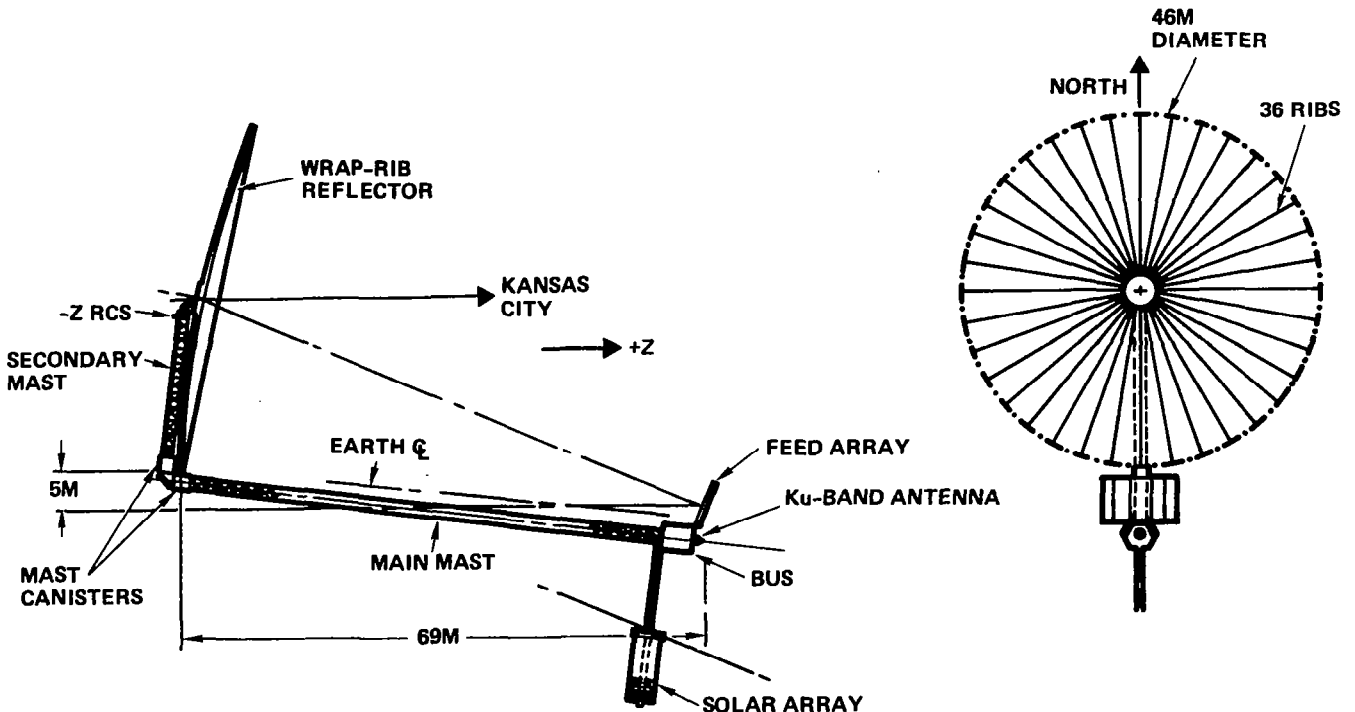
CENTER–FED SATELLITE CONFIGURATION

A 62-m reflector is required in the center-fed design, because of the 7 frequency subsets. A total of 101 beams is generated, with a HPBW of 0.42°. Each beam can support up to 119 voice channels.

In this case, 40 ribs are needed for the desired reflector surface accuracy. A 46.5-m mast results in an f/D of 0.75. This structure is much more rigid than the offset-fed design; consequently, attitude control is much less of a problem. However, the effect on RF performance of the mast, together with the cabling that runs from the solar array to the bus, is a factor to be considered.

The solar array is positioned behind and extends beyond the reflector to avoid shadowing. The gravity-gradient effect of the single solar panel, rather than a symmetric pair of panels, biases the antenna boresight toward the desired pointing direction.
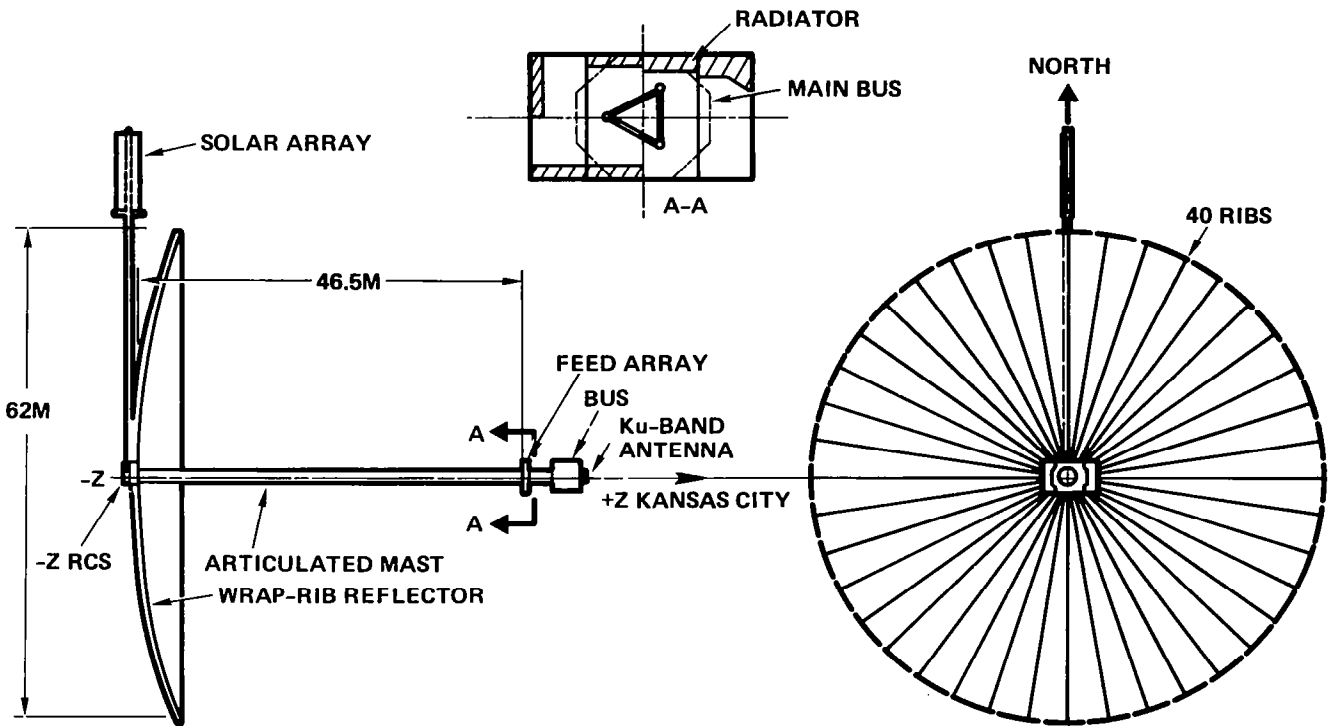
FEED CLUSTER APPROACH TO BEAM FORMATION

The feed spacing is determined by the requirement to generate a pattern of contiguous beams with 3-dB crossovers. On the other hand, good sidelobe control implies a highly tapered reflector illumination, which in turn mandates a certain minimum area per feed. The two requirements are in conflict for both baseline configurations, in any one-to-one association between feeds and beams (i.e., a single-feed-per-beam approach).

The effective feed area is increased by generating each beam from a cluster of feed elements. A 7-feed cluster is required for a center-fed reflector. The center element receives by far the greatest portion of the excitation, with the remainder divided equally among the six outer elements. A 4-feed cluster suffices for the offset-fed design. The desired reflector illumination is achieved by suitable adjustment of the amplitude and phase of the excitation to each feed.

To complete the clusters for beams on the periphery of the coverage area, the number of feeds must be greater than the number of beams. For the center-fed design, 152 feeds are needed to generate 101 beams. In the offset-fed case, 61 beams providing CONUS coverage can be generated from 84 feeds, if the clusters are oriented as shown in the figure.

● **CENTER-FED DESIGN**

    — **OVERLAPPING 7-FEED CLUSTERS PROVIDE REQUIRED DIRECTIVITY**

    — **152 FEEDS REQUIRED TO FORM 101 BEAMS**
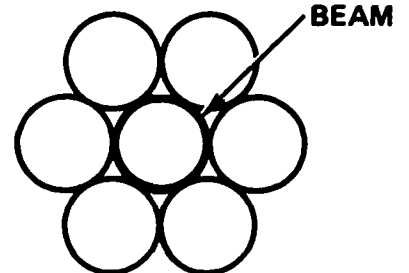
● **OFFSET-FED DESIGN**

    — **OVERLAPPING 4-FEED CLUSTERS PROVIDE REQUIRED DIRECTIVITY**

    — **WITH CLUSTER IN ORIENTATION SHOWN, 84 FEEDS REQUIRED TO FORM 61 BEAMS**
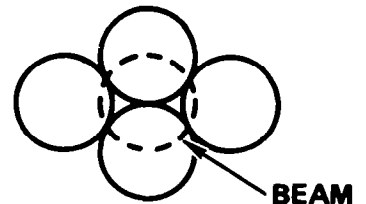
OVERLAPPING FEED CLUSTERS FOR ADJACENT BEAMS

Feed clusters for adjacent beams have one or more elements in common. Adjacent 7-feed clusters (used with a center-fed reflector) have four common elements. The center element in one cluster can be an outer element for as many as six other clusters. Each of these seven clusters (i.e., beams) is assigned a different frequency subset, so that the element in question transmits only one carrier on any given frequency. (In other words, clusters corresponding to cochannel beams are nonoverlapping). Each element transmits carriers at two different power levels: a high level for the carrier subset associated with the cluster for which the element is at the center, and a much lower level for the other subsets.

Adjacent 4-feed clusters (used with an offset-fed reflector) have either one or two common elements. Conversely, each element can belong to as many as four clusters. Since each of these clusters is assigned a different frequency subset, it is again true that each element transmits only one carrier on a given frequency.

7-FEED CLUSTER   **4-FEED CLUSTER**

4-FEED CLUSTER
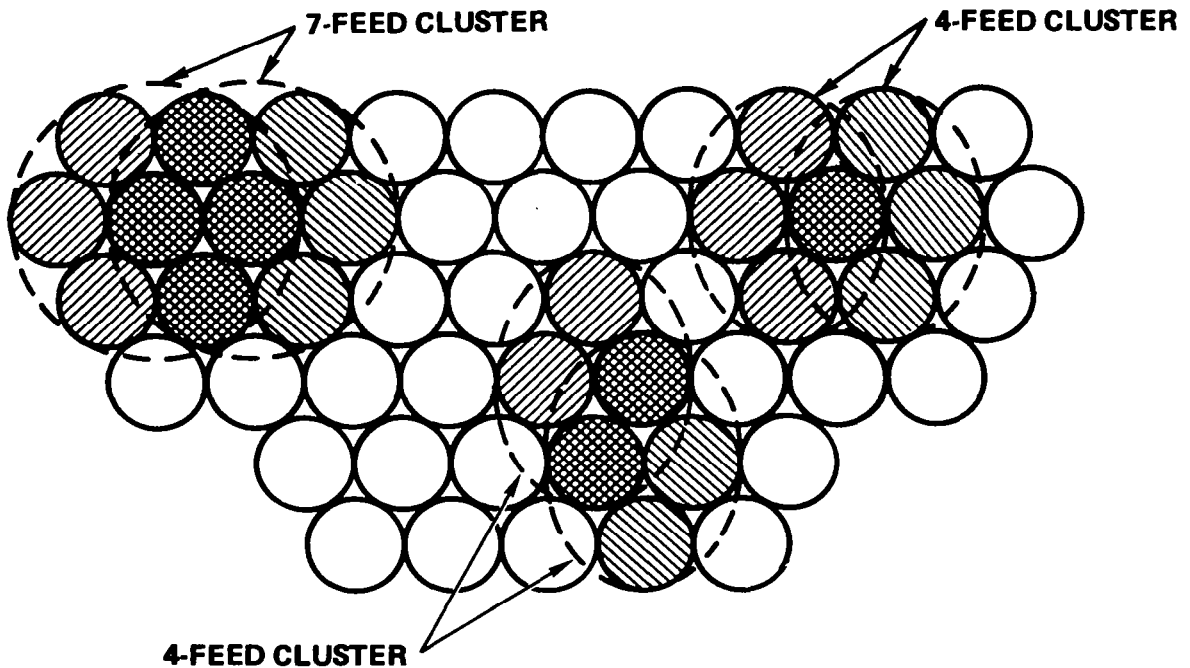
UHF RADIATING ELEMENTS

Each feed element in the center-fed design consists of a single micro-strip patch, plus ground plane. (Four such patches, fed in phase, constitute a single feed element in the JPL offset-fed design described in Reference 2). Thus, a feed cluster comprises seven microstrip-patch elements.

The short-backfire element has been chosen for the offset-fed design because it is particularly effective in providing the needed gain in a 4-feed cluster arrangement. The short backfire is essentially a dipole placed within a resonant cup. To provide additional gain, a passive director element can be added.

CENTER FED

(MICROSTRIP–JPL DIAGRAM)
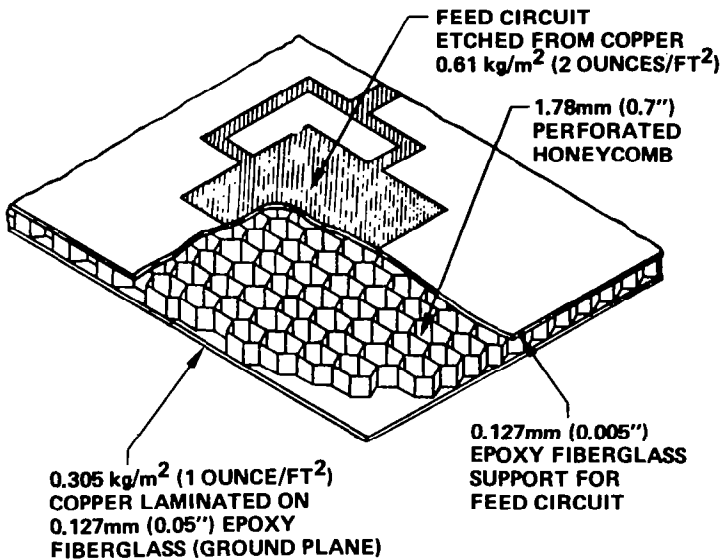
OFFSET FED

(SHORT BACKFIRE)

FEED CIRCUIT ETCHED FROM COPPER 0.61 kg/m^2 (2 OUNCES/FT^2)

1.78mm (0.7") PERFORATED HONEYCOMB

0.127mm (0.005") EPOXY FIBERGLASS SUPPORT FOR FEED CIRCUIT

0.305 kg/m^2 (1 OUNCE/FT^2) COPPER LAMINATED ON 0.127mm (0.05") EPOXY FIBERGLASS (GROUND PLANE)

6"

6.8"

(0.001" THICK ALUM. ALLOY)

3.5" (0.005" THICK ALUM. ALLOY)

27"
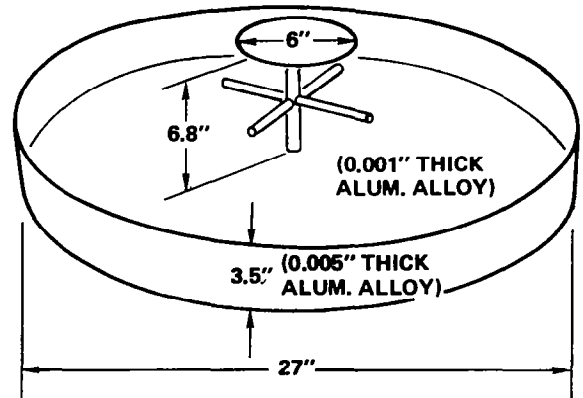
0.46 LB/ELEMENT

1.5 LB/ELEMENT

TRANSMIT BEAMFORMER SCHEMATIC FOR 4-FEED CLUSTER

Because of losses incurred in the beamformer network, it must precede the final power amplifiers. It is collocated with the power amplifiers on the feed assembly.

Each UHF upconverter contains the voice carriers intended for a common beam. The signal representing an individual voice carrier is divided into a pair of high-level signals and a pair of low-level signals. These are fed to the appropriate feed elements, through summing devices, as indicated in the figure. Thus, the more closely spaced pair of elements in a cluster is fed at a higher level, and the more widely spaced elements at a lower level. There is also a phase shift between the two pairs of elements.

Conversely, each feed radiates signals for four different beams. Two sets of carriers will be at the higher level and two at the lower level, according to the role played by the feed element in each cluster.

The reader is referred to Reference 2 for a description of the beamformer network for a 7-feed cluster.

43
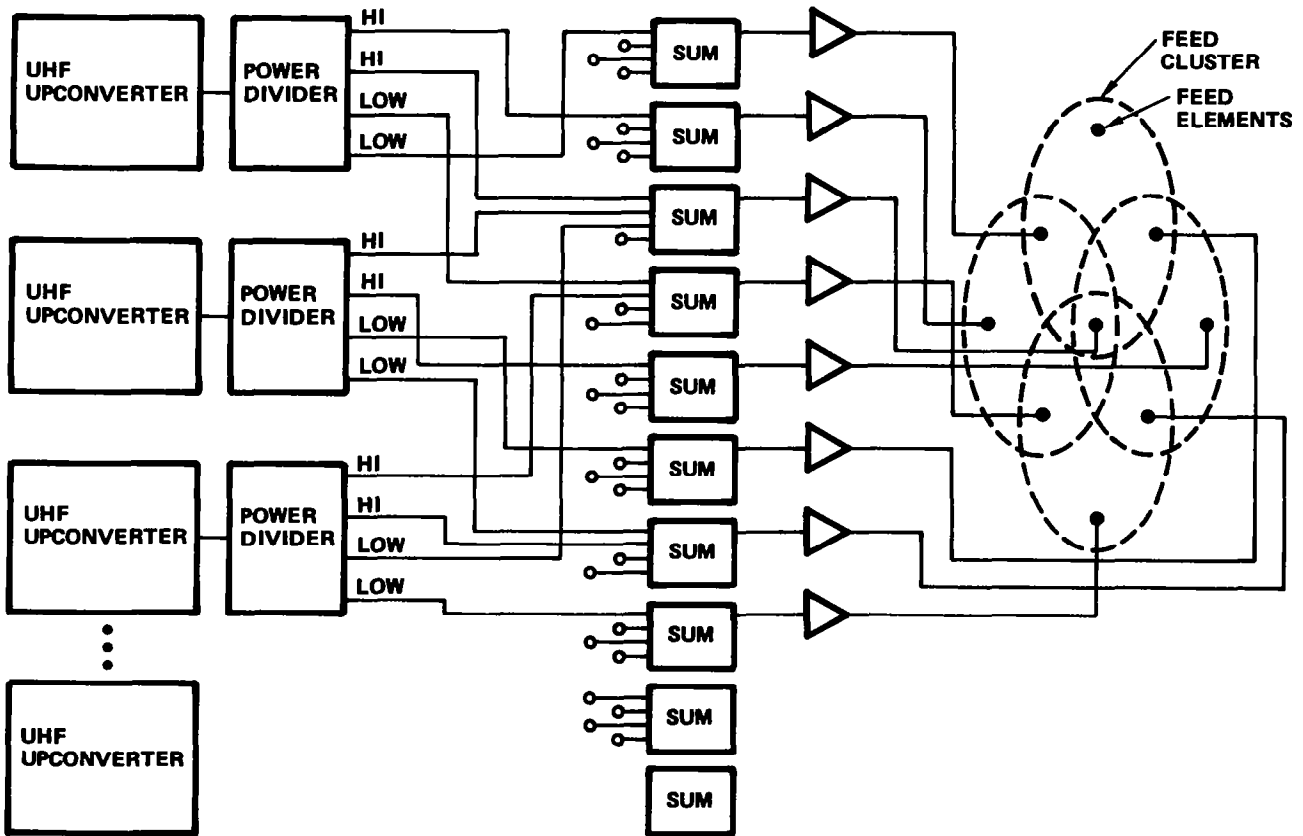
SATELLITE WEIGHT SUMMARY

Both the center-fed and offset-fed designs are well within the projected STS/IPS capability of 10,400 lb. The center-fed design is estimated to weigh about 10% less than the offset-fed design. This is not the result of any single factor, but instead is the net effect of differences in a number of subsystem weights. The weight of the reflector/mast combination is essentially the same for both designs, the shorter mast for the center-fed reflector being offset by the added weight of the larger reflector.

The contingency factor of 20% is the amount by which the initial weight estimate will typically grow as the design matures. Beyond this factor, there is ample room for growth, as evidenced by the 24% and 13% margins in the two cases.

ITEM	WEIGHT (LB)			
	CENTER-FED		OFFSET-FED	
REFLECTOR		1050		800
MASTS		260		510
COMM & DATA (INCL. Ku-BAND)		360		360
FEED ASSEMBLY		1630		2115
RADIATING ELEMENTS	70		125	
ELECTRONICS	560		455	
BEAM-FORMING NETWORK	150		335	
RF & DC CABLING	350		250	
THERMAL CONTROL	270		440	
STRUCTURE	230		510	
ATTITUDE CONTROL		430		830
REACTION CONTROL		1400		1160
DRY	310		255	
PROPELLANT	1090		905	
THERMAL CONTROL (BODY)		100		100
ELECTRICAL POWER		540		530
DC CABLING		540		480
STRUCTURE & INTEGRATION		690		760
TOTAL		7000		7645
CONTINGENCY (20%)		1400		1530
BOOSTER CAPABILITY (IPS)		10400		10400
MARGIN		2000 (24%)		1225 (13%)

REFERENCES

1. Anderson, R. E.: Satellite-Aided Mobile Radio Concepts Study: Concept Definition of a Satellite-Aided Mobile and Personal Radio Communication System. NASA CR-166646, 1979.

2. Naderi, F., Editor: Land Mobile Satellite Service (LMSS). JPL Publication 82-19, Jet Propulsion Laboratory, Pasadena, CA, February 15, 1982.

AUDIO DIRECT BROADCAST SATELLITES

J. E. Miller
NASA Headquarters
Washington, DC

SATELLITE SOUND BROADCASTING

Satellite sound broadcasting is, as the name implies, the use of satellite techniques and technology to broadcast directly from space to low-cost, consumer-quality receivers the types of sound programs commonly received in the AM and FM broadcast bands. It would be a ubiquitous service available to the general public in the home, in the car, and out in the open.

Interest in satellite sound broadcasting to serve the general public is not new. Several feasibility studies of the concept were conducted in the late 1960's [1, 2]. These studies examined the technical characteristics of systems operating in the HF, VHF and UHF bands. The studies showed that the satellite system would be large, heavy and require high prime power—requirements that, at the time, were incompatible with the state of the art of satellite technology and launch vehicle capability. Interest in satellite sound broadcasting waned until the mid to late 1970's, at which time the technical characteristics of systems operating in the HF band were reexamined [3] and an inquiry into the technical characteristics of systems operating in the 500 MHz to 2000 MHz band was initiated [4].
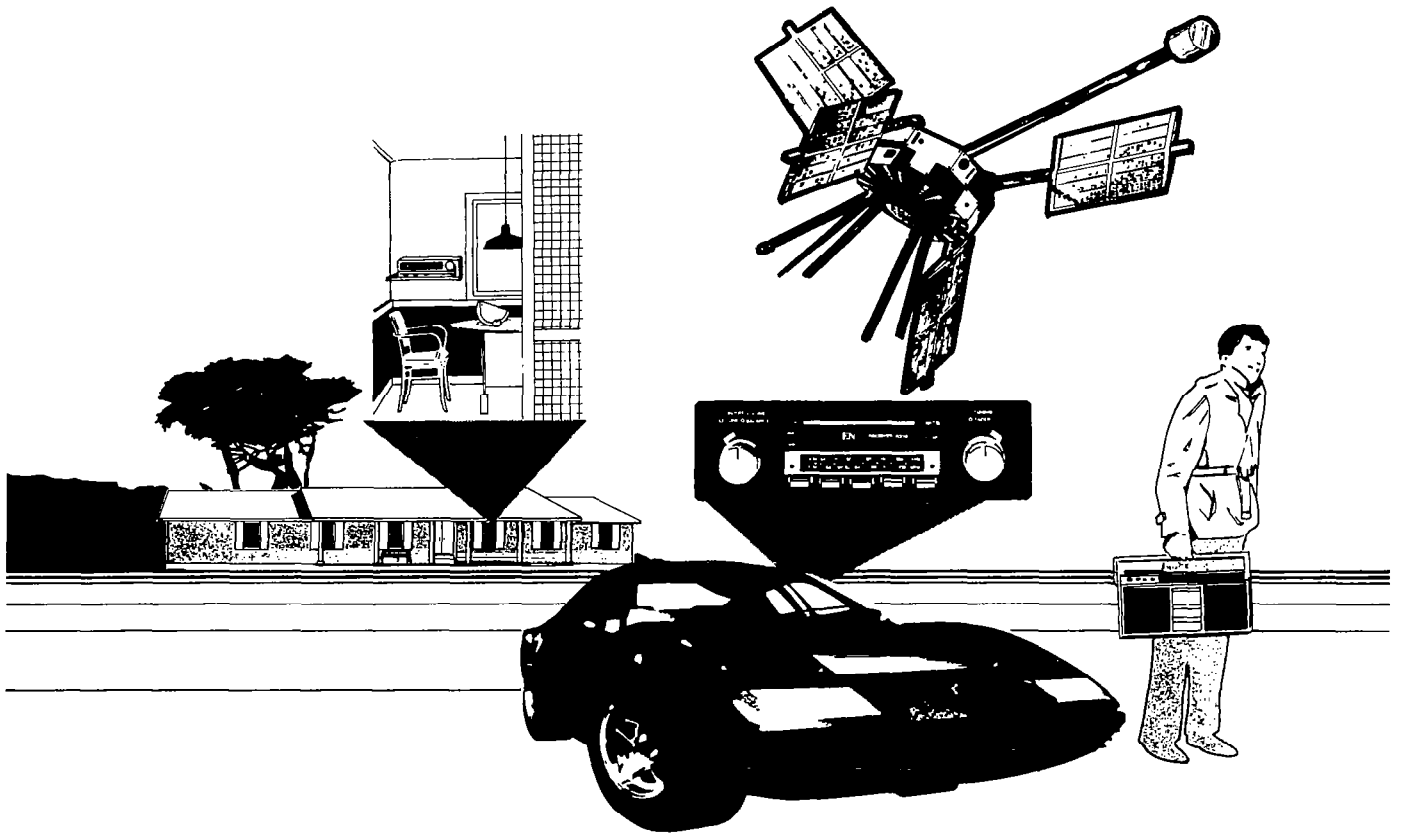
TECHNICAL CHARACTERISTICS

A range of possible technical requirements is shown in the figure. In the HF band, the rather large field strength requirement derives from the large amount of natural and man-made noise to be overcome, particularly in an urban environment, and from the absorption and reflection characteristics of the ionosphere, buildings and homes.

Ambient noise and the ionosphere play an almost insignificant role in dictating the field strength in the 500 MHz to 2000 Mhz band. In this band, the reduction of the effective area of the non-directional receiving antenna (40 dB less at 2000 MHz compared to 20 MHz) is the predominant reason for the large field strength requirement. However, building penetration and multipath losses also play a significant role in this band [4].

The on-axis EIRP and transmitter power are computed on the assumption of a geostationary satellite orbit. However, it should not be implied that other orbits would not be appropriate. In fact, an inclined, elliptical orbit might prove to be a cost-effective means to provide reliable service in the HF band at latitudes where the angle of incidence at the ionosphere from a geostationary satellite would otherwise be too small to permit reliable, if any, penetration.

Multiple beams with multiple channels per beam is a likely requirement for a geostationary satellite. These beams should be steerable over the Earth's disk to permit broadcasting at different hours into different service areas. The 3-dB beamwidth of 0.6 degrees to 3 degrees derives from a similar requirement established for television broadcasting satellites [5].

The antenna aperture diameter ranges from the currently feasible to a significant technological challenge. Operating in the 15 Mhz to 26 MHz band from geostationary altitude will require an aperture up to some 1400 meters in diameter if a 0.6 degree beamwidth is required. This should be viewed as a possible long-range requirement since early systems will be weight limited, and, as shown in the next figure, the weight of the antenna can quickly dominate the weight of the communication subsystem and thus the weight of the entire spacecraft.

FIELD STRENGTH (EDGE OF BEAM)	100 μV/m – 1 mV/m	
EIRP (ON-AXIS)	60 dBW – 80 dBW	
COVERAGE AREA	EARTH DISK	
NUMBER OF BEAMS	MULTIPLE, STEERABLE	
3 dB BEAMWIDTH	0.6 deg – 3 deg	
SHAPE	ELLIPTICAL, CIRCULAR	
NUMBER OF CHANNELS/BEAM	MULTIPLE	
TRANSMITTER POWER/CHANNEL	12 WATTS – 28 kW*	
OPERATING FREQUENCY	26 mHz	1.5 GHz
MODULATION	AM, SSB	FM
APERTURE DIAMETER	270 m – 1400 m	4.7 m – 23.5 m

*DOES NOT INCLUDE POWER REQUIRED FOR AMPLITUDE MODULATOR

SPACECRAFT WEIGHT AND PRIME POWER ESTIMATE

The figure presents an estimate of the weight of a single channel geostationary satellite sound broadcasting spacecraft which produces a field strength of approximately 100 μV/m at 26 Mhz at the edge of the service area. As can be seen, the spacecraft weight is strongly determined by the antenna weight.

REQUIRED EIRP = 62.8 dBW
OPERATING FREQUENCY = 26 mHz

RF POWER (dBW)	37	36	33	30
PER CHANNEL (kW)	5	4	2	1
S/C ANTENNA GAIN (dBi)	26.8	27.8	30.8	33.8
3 dB BEAMWIDTH (degrees)	7.8	6.9	4.9	3.5
ANTENNA DIAMETER (m)	103	117	164	230
ANTENNA WEIGHT (kg)	454	567	893	1433
TRANSPONDER WEIGHT (kg)	136	134	129	127
TOTAL COMM. SUBSYSTEM WEIGHT (kg)	590	701	1023	1560
BOL DC POWER (kW)	13.7	11	5.6	3
TOTAL S/C BOL WEIGHT (kg)	1667	1769	2201	3138

S/C LIFETIME = 5 YEARS
ECLIPSE COVERAGE = 50%
SOLAR ARRAY WEIGHT FACTOR = 66 W/kg
BATTERY WEIGHT FACTOR = 65 W-hr./1 kg
POWER AMPLIFIER EFFICIENCY = 60%
PROPELLANT I_{sp} = 300 sec
PITCH AXIS POINTING ACCURACY = 0.1 degree

SUMMARY OF POSSIBLE REQUIREMENTS

Following are some possible requirements of this system.

- **ANTENNA**
  - **DIAMETER UP TO:**
    - **— 1400 METERS AT HF**
    - **— 72 METERS AT 500 mHz**
    - **— 18 METERS AT 2000 mHz**
  - **SIDELOBES: 30 TO 40 dB**

- **TRANSMITTER POWER UP TO 28 kw/CHANNEL**

- **THERMAL CONTROL: UP TO SEVERAL HUNDREDS OF kw**

- **POWER: UP TO SEVERAL HUNDREDS OF kw**

- **ORBITS**
  - **GEOSTATIONARY**
  - **ELLIPTICAL/INCLINED**

- **LIFETIME: 10 YEARS**

REFERENCES

1. Voice Broadcast Mission Study. RCA Report, No. AED-R-3187, May 1967.

2. Voice Broadcast Mission Study. GE Report, No. 67SD4330, July 14, 1967.

3. Phillips, G.J. and Knight, P.: Use of the 26 MHz Band for Satellite Broadcasting. EBU Review, Technical Part, No. 170, August 1978, pp 173-178.

4. Satellite Sound Broadcasting with Portable Receivers and Receivers in Automobiles: CCIR Report 955, XV Plenary Assembly, Geneva 1982.

5. Provisions for All Services and Associated Plan for the Broadcasting - Satellite Service in Frequency Bands 11.7-12.2 GHz (in Regions 2 and 3) and 11.7-12.5 GHz (in Region 1): Appendix 30, International Radio Regulations, International Telecommunications Union, Geneva, 1979.

52

LARGE DEPLOYABLE REFLECTOR:
AN INFRARED AND SUBMILLIMETER ORBITING OBSERVATORY

Paul N. Swanson
Jet Propulsion Laboratory
Pasadena, California

and

M. K. Kiya
NASA Ames Research Center
Moffett Field, California

LARGE DEPLOYABLE REFLECTOR

The Large Deployable Reflector (LDR) is to be a dedicated astronomical observatory in space. It will operate in the 1-mm to 30-μm wavelength region where the Earth's atmospheric opacity makes ground-based observations nearly impossible. The primary mirror will be 20 m in diameter, made up of 37 individual segments. The reflector will be actively controlled to provide an overall surface accuracy of ≼2 μm. The LDR will be placed in orbit by the Space Shuttle and revisited at approximately 2-year intervals during its 10-year lifetime.

LDR, a joint effort between the Jet Propulsion Laboratory and the Ames Research Center, had its beginnings in 1977. Since that time, continuing studies by the two centers, industry, and universities have resulted in a recommendation by the National Academy of Sciences that LDR be one of the two major space efforts in astronomy for the 1980's.

A workshop was held at Asilomar, Calif., in June 1982 at which approximately 100 scientists and engineers defined the scientific objectives of LDR and discussed its technical feasibility. The present conceptual design represents a consensus of the Asilomar workshop and is a balance between technical feasibility in the 1980's and scientific capability.
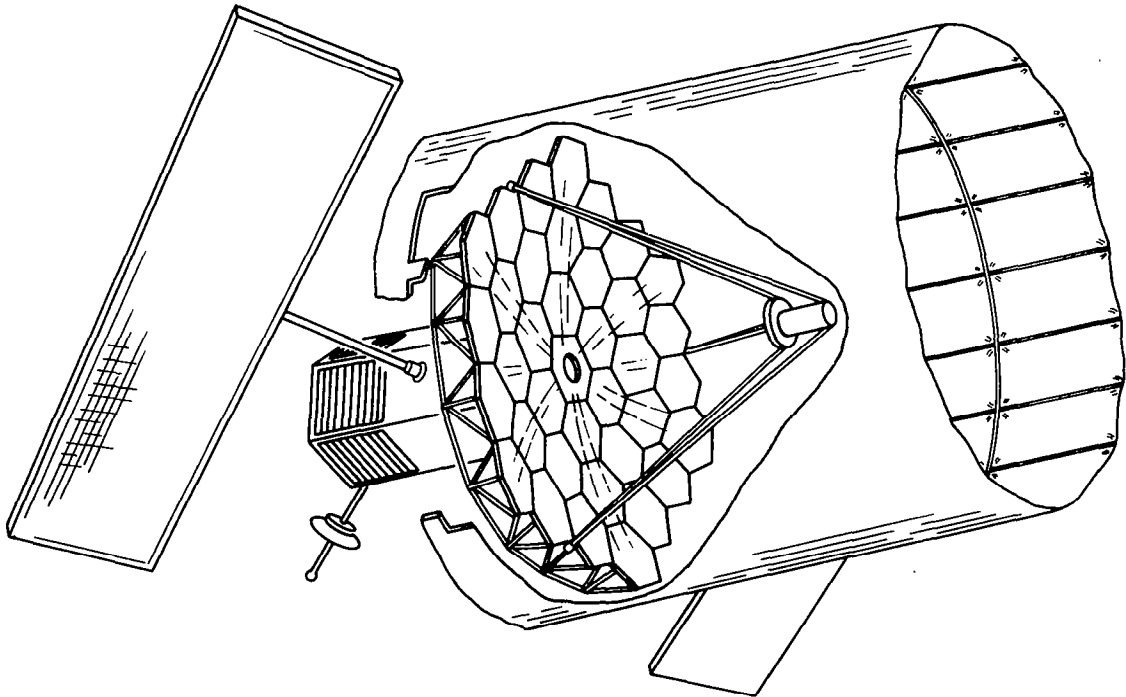
Figure 1

LDR Requirements

Observational Requirement ——▶	Functional Requirement ——▶	Telescope Requirement
1. Observe throughout region obscured by Earth's atmosphere.	• 30 μm <λ<1-mm diffraction limited (50μm acceptable)	• rms surface error <2 μm • rms slope <1.5 μrad
2. Far-IR Studies of: • Galaxies at cosmological distances. • Spiral structure in distant galaxies. • Giant molecular clouds in nearby galaxies. • Protostars in our galaxy.	• Spatial resolution comparable to ground based telescopes. • ≲1 arc sec in far infrared ——▶ D/λ >2 x 10^5 • Absolute pointing to HPBW/5 • Pointing jitter to HPBW/10	• D >6.5 m @ 30 μm • D >20 m @ 100 μm • ≲0.06 arc sec absolute • ≲0.03 arc sec jitter
3. Observe faint objects at large distances.	• Sensitivity ∝ D^2 number of sources ∝ D^3 ——▶ D as large as possible • Spatial chopping to eliminate sky background to 1 part in 10^6 • Stray light at detectors below telescope emission • Minimize telescope background emission	• D ≳20 m • 2 Hz, 1 arc min spatial chopping • Limits view angle to Sun and Earth • Primary temp ≈150 K • Secondary temp <150 K • Emissivity <.05 @ 100 μm <.01 @ 1 mm
4. Mapping extended sources planets, molecular clouds, H II regions.	• 1° x 1° raster-scan • ≳3 arc min IFOV	• Scan mirror • Array detectors • Long focal length
5. Near-IR studies of high red shifted galaxies (Z ≳3).	• Spatial resolution ≲2 arc sec in 1 - 30-μm range. • ε <0.1 in 1 — 10-μm range.	• "Light bucket" operation at λ <30 μm • Micro roughness <λ/40 = 0.2 μm @ λ = 10 μm = 0.02 μm @ λ = 1 μm
6. Observe extrasolar planets.	• Sidelobes <-40 dB at θ >10 arc sec @ λ = 30 μm	• Uniform illumination ——▶ -39 dB @ 10 arc sec, low scatter
7. Cosmic background.	• Detector noise limited at λ = 1 mm (background NEP <10^{-16} W-$Hz^{-1/2}$)	• ε <.01 ——▶ roughness <7μm
8. Mission-related requirements.	• Single Shuttle launch • 10-year lifetime • Maximize viewing time • Revisit capability	• Deployable structure • Segments <4-m diameter • Mass <27,000 kg • >750-km orbit • ≳20°/min slew
9. Maximum detector sensitivity throughout spectral range.	• Background limited noncoherent detectors. • High resolution spectroscopy $\Delta\lambda/\lambda$ < 10^{-6}, 50-1000 μm	• NEP ≲10^{-16} W-$Hz^{-1/2}$ @ 10-100 μm • NEP ≲10^{-17} W-$Hz^{-1/2}$ @ 100-1000 μm • Coherent receivers with T_{sys} ≲1000 K • Cryogenic systems, 0.1 K to 50 K

Figure 2

The figure shows the minimum operating wavelength versus diameter for a number of well-known telescopes. The minimum operating wavelength is defined here as the diffraction-limited wavelength with the rms surface errors, ε, equal to $\lambda/13$. The numbered circles on the right side of the figure near the solid line represent a sampling of the world's best radio telescopes. The solid line is an approximate upper limit to D/λ for these lightweight structures. This D/λ limit of $\lessapprox 7700$ may be somewhat exceeded by some of the planned new radio telescopes indicated by the numbered squares. At the left of the figure are the Space Telescope (12) and the Hale 200-inch telescope (13). These "monolithic" telescopes have $D/\lambda > 10^6$ but are exceedingly heavy. The LDR is shown as a shaded region near the middle of the figure. LDR requires a $D/\lambda \approx 6 \times 10^5$ but with a weight per unit area comparable to the radio telescopes. This can be accomplished by making the primary reflector from a number of lightweight segments, each segment having a D/λ and an areal density comparable to the advanced radio telescopes. The individual segments can be mosaicked together and actively controlled to produce the 20-m LDR aperture.

DIAMETER VS. OPERATING WAVELENGTH COMPARISON FOR THREE CLASSES OF TELESCOPES

1	U. TEXAS	9	IRAM 15m
2	OVRO 10m		SRC 15m
2A	OVRO, ULTIMATE DESIGN GOAL	10	MPIFR/IRAM 30m
3	NRAO 11m	11	SIRTF
3A	NRAO 11m, NEW SURFACE	12	SPACE TELESCOPE
4	CRIMEA	13	HALE 200"
5	NRAO VLA	14	U. OF TEXAS 300"
6	OVRO 40m	15	UCB 10m SEGMENTED
7	BONN 100m	16	NEW TECHNOLOGY TELESCOPE
8	NASA DSN 64m		

Figure 3

56
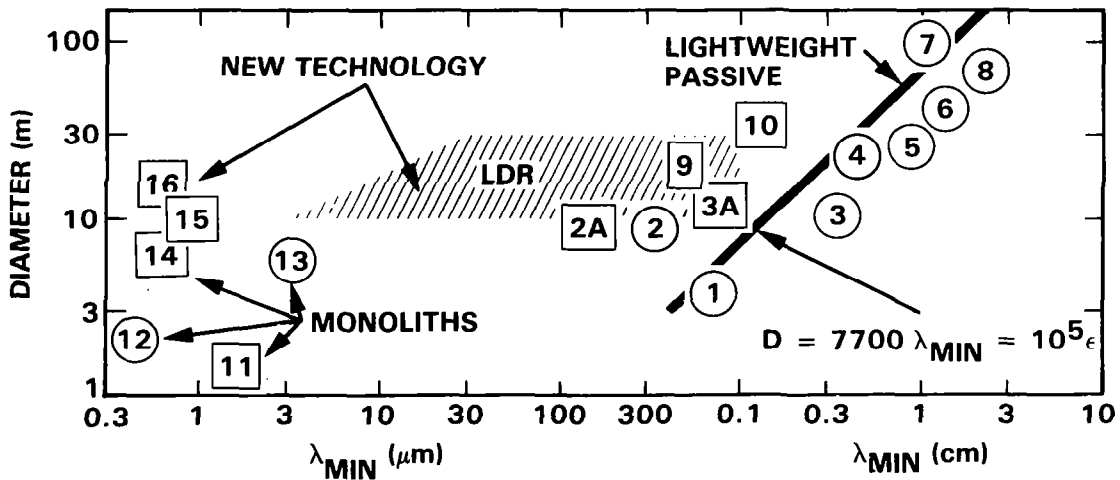
TECHNOLOGY

The LDR is a new class of telescope that challenges the present state of the art in many areas. Weight must be kept to a minimum to meet the requirement of a single Shuttle launch. In addition, a polar orbit, which minimizes thermal problems and simplifies observing, can be accomplished if the total weight is kept below 12,000 kg. The main technology drivers are the reflector segment construction and material. The areal density should ideally be below 15 kg/m^2 (about the same as a U. S. dime) and the surface figure below 2 μm rms. The reflector backup structure and focal plane support require lower tolerances than the actively controlled reflector surface. However, the structure must be capable of being deployed from a folded configuration in the Shuttle bay. In addition, the structure must be stiff enough so that natural vibrations do not exceed the capability of the surface control system to remove their effect. The figure measurement system must be able to measure the position of each optical element within $\lesssim 1$ μm. The control system will calculate the optical errors and reposition the secondary mirror and each reflector segment to reduce these errors to $\lesssim 2$ μm rms. Several optical techniques exist for surface measurement to much less than 1 μm, and position actuators with submicron accuracy are available. The controls problem also includes active vibration control, slewing of the telescope up to 20°/min without inducing large vibrational perturbations, and absolute pointing of ≈ 0.06 arc seconds.

- SYSTEMS (WEIGHT, COST, POWER, DEVELOPMENT, LIFETIME)

- OPTICAL CONFIGURATION (TYPE, F/NO, FOV, PRIMARY SHAPE)

- REFLECTOR SEGMENTS (MATERIAL, FIGURE, WEIGHT, MANUFACTURING)

- STRUCTURES (BACKUP, DEPLOYMENT)

- CONTROLS (FIGURE, VIBRATION, POINTING, SLEWING)

- FIGURE MEASUREMENT

- SCIENCE INSTRUMENTS (DETECTORS, SPECTROMETERS, CRYOGENICS)

- SPACECRAFT (POWER, TELEMETRY, PROPULSION)

- MISSION (LAUNCH, VEHICLE, WEIGHT, ORBITS, REVISIT)

Figure 4

SYSTEM WEIGHT

The figure shows total system weight versus reflector diameter for a number of reflector construction techniques. The maximum Shuttle capacity is presently about 25,000 kg for a 28° inclination orbit and about 12,000 kg for a 98° polar orbit. It has been estimated that approximately 8,000 kg will be used for the LDR spacecraft, science instruments, and propulsion system to boost it up to a 700-km orbit. The remaining payload can be used for the reflector. By assuming a certain reflector areal density, adding 20% for backup structure and the 8,000-kg overhead, the curves shown can be generated. Fusion-welded glass, the Space Telescope technique, allows only an 11-m diameter reflector before reaching the 25,000-kg limit. For the 20-m nominal LDR reflector, the maximum areal density is 47 kg/m^2 for a low inclination orbit and approximately 12 kg/m^2 for a polar orbit. It can be seen that the only present candidate techniques are the projected performances of cored glass and honeycomb sandwich constructions.

The present Shuttle payload capability will undoubtedly be increased by about 5,000 kg. On the other hand, the 8,000-kg estimates for the LDR spacecraft, instruments, and propulsion system are thought, by some, to be too low, possibly by a factor of two. In addition, at this early stage of conceptual design it would be wise to leave ample margin for error in the weight estimates. For this reason the goal for panel areal density is approximately 15 kg/m^2.
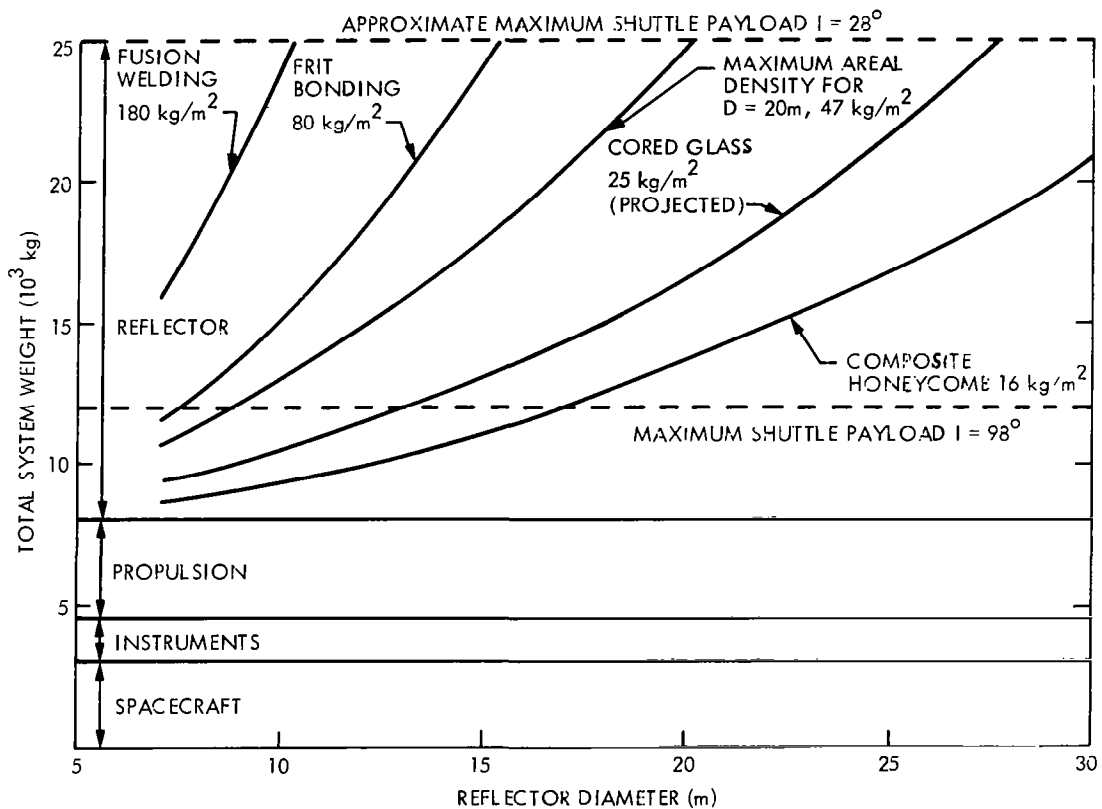
Figure 5

The reflector segments must be capable of passively maintaining a surface figure of ≼2 μm from manufacture through launch and orbital cooldown to ≈ 200 K. The segment size is nominally 2 m with a 4-m maximum, limited by the Shuttle bay. The areal density must be less than 50 kg/m^2 for a 20-m LDR in a low inclination orbit, while a polar orbit requires ≈ 12 kg/m^2.

Referring to the figure, the simplest approach would be to make a solid reflector segment from low-expansion glass. However, a solid glass mirror of 12 kg/m^2 would be only 4 mm thick. Manufacturing, polishing, handling, and deployment would be very difficult, not to mention the low resonant frequencies that would exist. It is better from a structural point of view to expand the same amount of material into a deeper structure as shown in the top left figure. Both frit-bonded glass and cored glass approach 50 kg/m^2 in 2-m sizes. Projections indicate that cored glass can be made as light as 25 kg/m^2. Foam core glass made from ULE or Zerodur is an attractive approach. However, only very small samples have ever been produced. Honeycomb sandwich construction, as shown at the bottom right, has been used to make radio telescopes with less than 10 μm surfaces and a demonstrated areal density of less than 15 kg/m^2. In addition, composite honeycomb sandwich segments have been replicated with less than 4 μm rms surfaces in 2-m sizes. The light weight and low cost of this technique make it very attractive for LDR if the surface requirements can be achieved.

POSSIBLE MIRROR CONSTRUCTION TECHNIQUES

FRIT-BONDED EGG CRATE
ULE
FUSED QUARTZ

SOLID BLANK
ALUMINUM
ZERODUR
ULE
CERAMIC

FOAM CORE
ULE
ZERODUR

HONEYCOMB SANDWICH
ALUMINUM
COMPOSITE
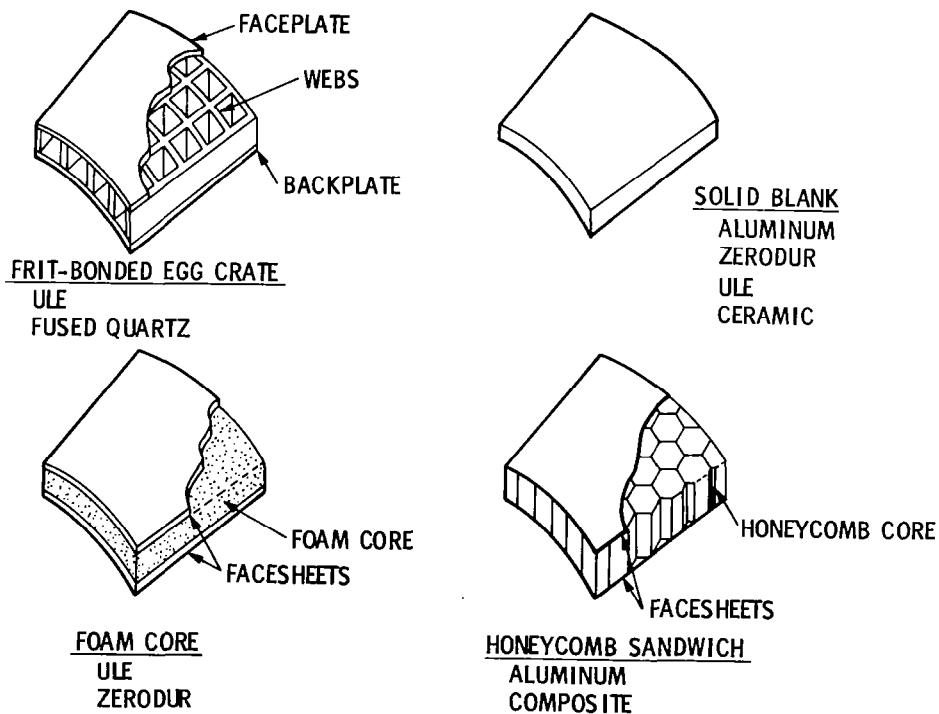
Figure 6

The reflector segments are the most crucial development area since many of the other subsystem technologies depend upon the segment characteristics. For example, if the segments have a certain areal density, then reflector diameter and total weight can be traded off to meet Shuttle payload and orbital constraints. The best surface figure that can be maintained on the segments will determine the shortest wavelength for LDR operation, which, in turn, impacts the science instruments, figure measurement and control systems, and pointing system.

The deployment of the truss backup structure and up to 37 individual reflector segments is probably the next most challenging problem. Concepts for deployment exist but details have yet to be worked out.

There are concepts for the surface measurement system, and certainly laser interferometers are capable of the accuracy required, but a complete measurement system has not been built or even completely designed.

The controls problem is, in general, an extension of existing structural control technology, but the micron surface accuracy and sub-arc-second pointing requirements are more severe than normally encountered. The ratio of maximum dimension to maximum error of $\approx 10^7$ is over an order of magnitude greater than that found in most conventional structures.

In the area of scientific instruments, there has been a lack of development of astronomical receivers in the submillimeter region since they have not, in the past, been useful from the ground. Coherent receivers capable of high spectral resolution in the wavelength region between 100 μm and 600 μm are the highest priority for new development.

LDR REQUIRED TECHNOLOGY DEVELOPMENT SUMMARY

- REFLECTOR PANEL, MATERIALS AND CONSTRUCTION

- SURFACE FIGURE MEASUREMENT SYSTEM

- CONTROL LAWS FOR ADAPTIVE OPTICS, POINTING, SLEWING AND VIBRATION

- CONTROL SYSTEM FOR ADAPTIVE OPTICS, ATTITUDE CONTROL, POINTING, VIBRATION CONTROL

- REFLECTOR SUPPORT STRUCTURE AND DEPLOYMENT SCHEME

- SUBMILLIMETER COHERENT RECEIVERS

- LONG LIFE CRYOGENIC SYSTEMS

Figure 7

ANTENNA TECHNOLOGY FOR ORBITAL
VERY LONG BASELINE INTERFEROMETRY (VLBI)

E. C. Hamilton
NASA Marshall Space Flight Center
Huntsville, Alabama

61

VERY LONG BASELINE INTERFEROMETER TECHNIQUES

Since it is not economically feasible to construct steerable antennas much larger than 100 meters on Earth (400 meters for fixed telescopes), radio interferometry became a very useful technique for high resolution astronomy observations of quasars, galactic nuclei, and interstellar hydroxyl (OH) and water vapor (H_2O) masers.

The radio interferometer in figure 1a could achieve a baseline of 120 km. It was limited by the line of sight between the local oscillator and IF transmitter and receiver. However, a thousands of kilometers baseline was realized using video recording techniques shown in figure 1b. These techniques began in 1967 (ref. 1). These techniques have resulted in an intercontinental baseline and greatly improved resolution in the tenths of milli-arc-seconds. The size of the Earth has become a practical limitation, and future effort should be toward placing one element on an orbiting platform. The goal for the last decade of this century might very well be to have free-flying observatories in high elliptical Earth orbits. In a few years these observatories, in concert with an intercontinental array of ground antennas, could survey the entire celestial sphere. To provide the initial planning for this thrust into orbital VLBI, the Office of Space Sciences and Applications appointed and funded a technical working group chaired by Dr. Bernard F. Burke of MIT and supported by Marshall Space Flight Center and the Jet Propulsion Laboratory. For the most part, the data in this paper is a result of this group effort.

(a) TWO-ELEMENT RADIO INTERFEROMETER   (b) INDEPENDENT ATOMIC OSC INTERFEROMETER

Figure 1

A SPACE VLBI PROGRAM

To achieve the ultimate goal of large Orbiting Very Long Baseline Interferometers (OVLBI) requires advances in several areas of space technologies. While this paper will be confined to the initial step of a Shuttle experiment, the technology developed and demonstrated here would apply across the entire range of activities. Figure 2 illustrates the three parts that logically lead to the ultimate goal. The first part in mid-1980 would demonstrate antenna technology and provide a clear indication of the initial science results. While the 7-day mission (approximately 3 days of VLBI observations) would provide only a limited amount of observations, it would provide an opportunity for international participation in an exciting new innovation. The Soviets are quite interested in OVLBI and are planning an experiment in this same time frame.

Once the technology and techniques of OVLBI are well understood, the next logical step would be to have much longer periods of observations. A platform might afford this step 2 in the evolution. The ultimate step of a long life, high altitude observatory that may be serviced by Orbiter or become a part of a space station could be possible in the late 1990's.

SHUTTLE EXPERIMENT	PLATFORM CONFIGURATION	FREE FLYER
• Antenna Test Program	• Improved Resolution	• Highest Resolution
• Demonstrated Technologies	• Full Sky Survey	• Full Sky Coverage
• Initial Science Results	• Temporal Studies	• Long Duration Temporal Studies

1985   1990   1995   2000

Figure 2

50-METER DEPLOYABLE ANTENNA ATTACHED TO THE SHUTTLE

The initial concept of a space VLBI experiment was to augment a 50-meter mesh deployable antenna with the necessary equipment for it to perform some basic VLBI observations at the conclusion of the 7-day Shuttle mission. The artist's concept of how such a configuration might appear is shown in figure 3. The antenna depicted in this sketch is a hybrid between the hoop/column that LaRC has been contracting with Harris Corporation and the wire wheel being developed by Grumman for MSFC and DARPA/RADC. The central mast is a "supermast" being developed by Astro for MSFC. At the conclusion of antenna tests, the Shuttle would be used to point at various radio sources, and in conjunction with several ground-based terminals, an interferometer would be formed as shown in Figure 1b.
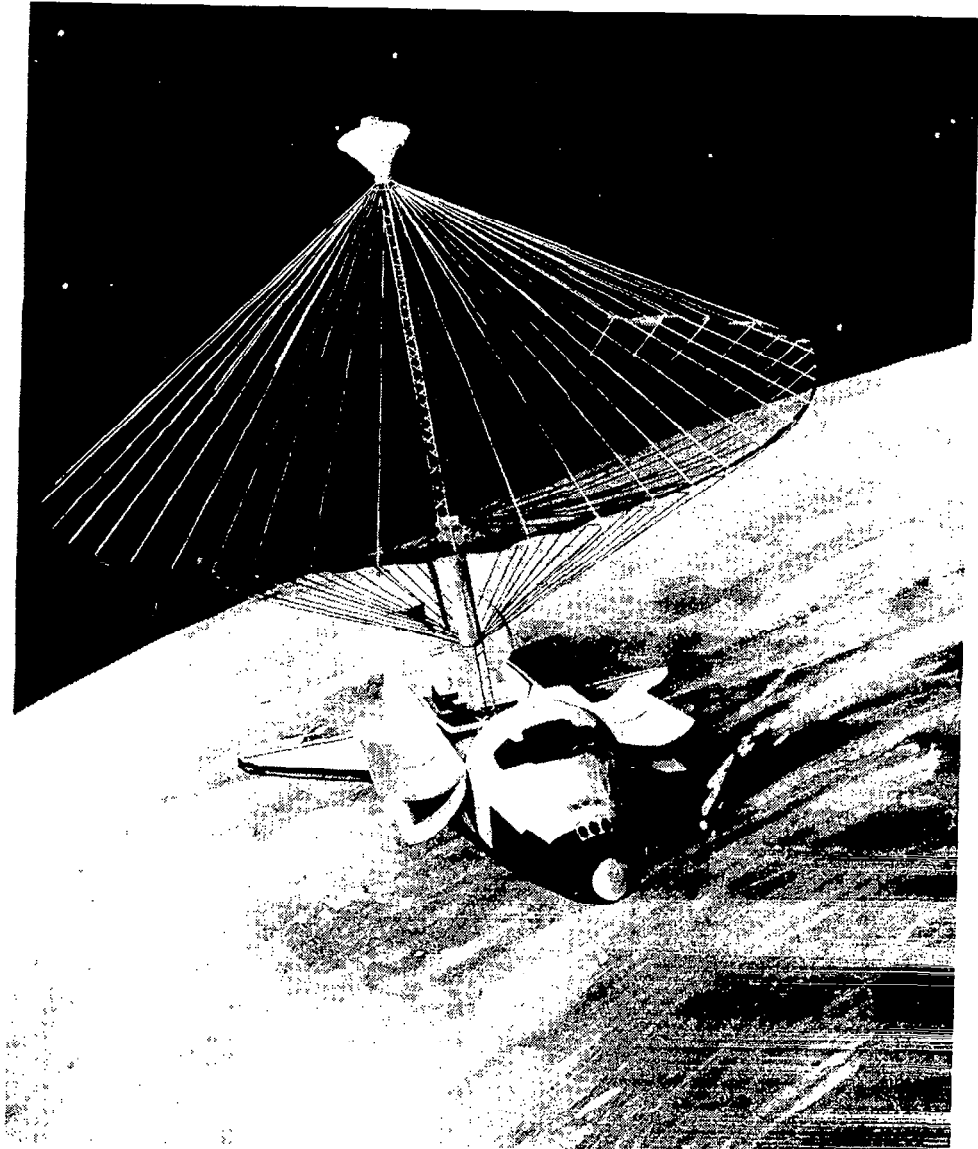
Figure 3

SPACE VLBI SYSTEM

In figure 4 the dotted lines indicate the equipment necessary for a space VLBI experiment. The configuration shown is a cassegrain system with the subreflector sized to the 3-meter limit of the cargo bay. The preamps are located as close to the feed as possible for a low system noise temperature. The local oscillator and mixer are also located at the feed so that only intermediate frequency (IF) must be sent down the 50-meter mast over a coaxial cable. The atomic oscillator/clock is located at the base of the antenna because the volume exceeds that available in the crew compartments. The recorders and other electronics are located in the cabin so that mission/payload specialists can operate the experiment with minimum interface to the Shuttle. It is anticipated that several videotape cassette changes may be necessary during the experiment. It should be clear that there is no difference in the concept for the space elements of the VLBI experiment and the ground. The question of technology is purely our ability to develop components and subsystems that can perform in space as well as they do on the ground., • the exception is the crucial subsystems comprised of the antenna and its pointing system.
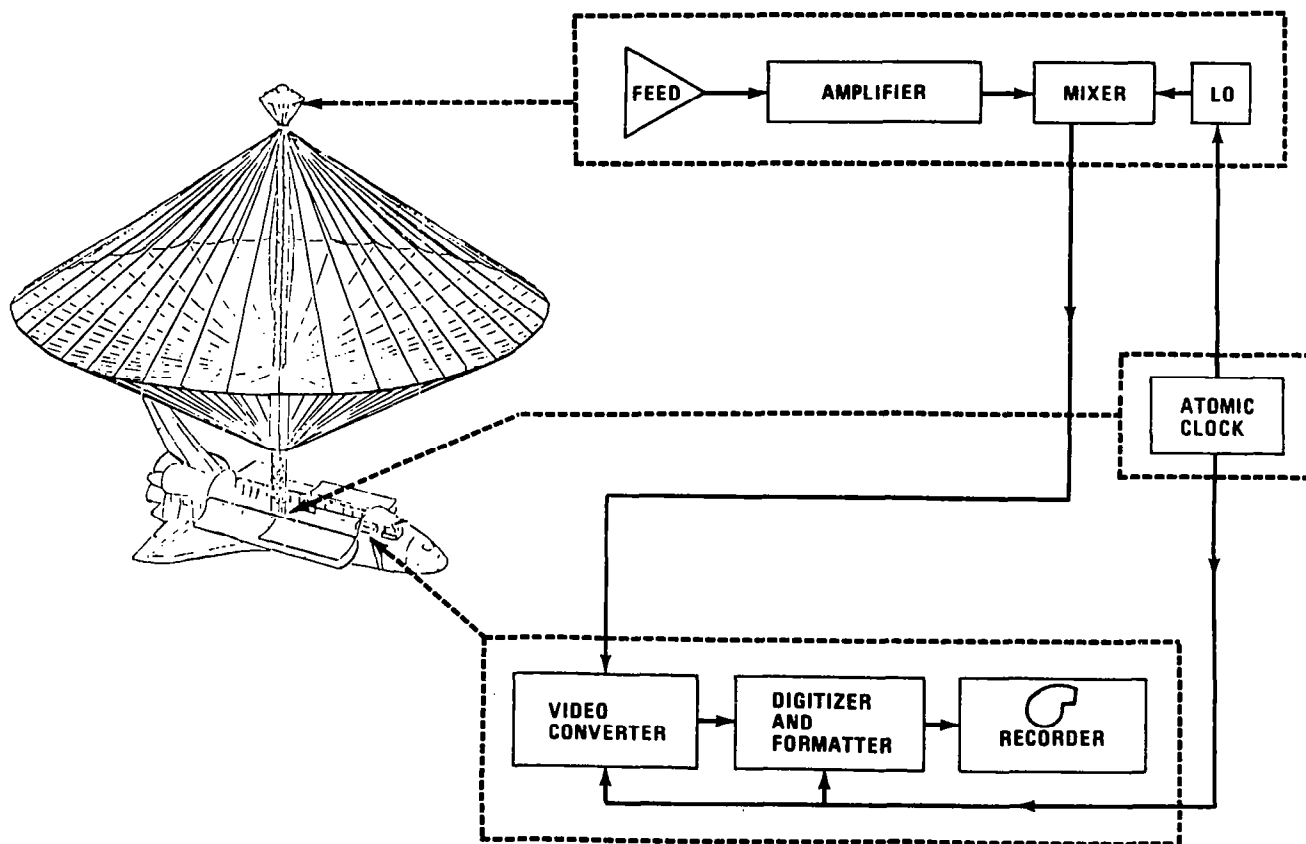
Figure 4

VLBI DEMONSTRATION EXPERIMENT PARAMETERS

The working group established some basic requirements and system parameters for guidance in determining the feasibility of a space VLBI mission. Combined with antenna flight experiments ,these parameters are summarized in figure 5. The data presented is from NASA TM 82491 and is a compilation of the working group's activity over the past two years (ref. 2). The key technology areas indicated by this table can be summarized but not prioritized into four areas, shown in figure 6.

	SURFACE ACCURACY	FREQ. (GHz)	BEAM TYPE	POLARIZATION	RECEIVER BANDWIDTH	SYSTEM NOISE TEMPERATURE
ANTENNA SYSTEM	$> \dfrac{\lambda}{30}$ @ 1.4 GHz	1.66 2.3 8.4	SINGLE	ONE SENSE – CIRC. POL. TO BE DETECTED	100 MHz	160°K @ AMBIENT

	ELECTRICAL AXIS	ANT. TRACKING/ POINTING SUBSYS.	KNOWLEDGE OF POINTING	SLEW RATE	INTEG. TIME
POINTING REQUIRE–MENTS OF ANTENNA SYSTEM*	POINTED TO WITHIN 1/2 BEAMWIDTH OF TARGET ---------------- 1.66 GHZ – 0.25° 2.3 – 0.18° 8.4 – 0.05°	± 0.025°	±0.01°	3°/MIN	60 SEC (REQUIRED TO TRACK SOURCE FOR 60 SEC WITHOUT VRCS FIRING)

	ALTITUDE	INCLINATION	POSITION KNOWLEDGE	VELOCITY KNOWLEDGE
ORBIT REQUIRE–MENTS	MINIMUM: 360 km	$40° < i < 57°$	± 10km	± 1 m/SEC

* ANTENNA SYSTEM POINTING INCLUDES: ORBITER, ANTENNA STRUCTURE, MOVABLE FEED/SUBREFLECTOR AND BEAM STEERING TO REACH REQUIRED ACCURACIES.

Figure 5

66

The fact that data must either be recorded onboard or transmitted to the ground probably precludes simultaneous observation at three frequencies. In fact, it appears that a two-frequency feed system may be the baseline for the time being. However, a design that does not require a switch in the RF path was highly desirable to prevent insertion losses. In addition, it was highly desirable to have a monopulse tracking feed to provide an error signal for some type of pointing subsystem. A tilting subreflector appears to be most promising, but other types of pointing have not been ruled out. Probably one of the most basic requirements is that of a low-noise amplifier (LNA). It certainly will not require a cryogenically cooled maser like the ones in the DSN. It will be obvious later that the diameter of the antenna is the most important of all these parameters.

- MULTIFREQUENCY FEEDS

- LOW SYSTEM NOISE

- TILTING SUBREFLECTOR

- LARGE ACCURATE APERTURE

Figure 6

MULTIFREQUENCY FEED CONCEPTS

The multihorn concept has the basic drawback in the fact that the low frequency horns are not at the focal point of the system. Also, the monopulse feed occupies a lot of space needed for the prime signal reception (fig. 7a). The combination of helices provides an acceptable coverage from 1.6 GHz to 8.4 GHz but does not provide a pointing error signal (fig. 7b). The coaxial corregated horn with the four supplemental horns covers S-band and X-band requirements (fig. 7c). The small horns are used to determine when energy is not focused in the primary receiving horn. It remains to be determined if these small horns can provide sufficient power when observing extremely weak sources for tracking purposes. The bandwidth could be an order of magnitude less than the 100 MHz for VLBI. An optical detector such as a star tracker may provide a better tracking signal for pointing the antenna. It is apparent that this area requires effort to fabricate a few interesting concepts and to test them on a terrestrial telescope prior to design of a flight system.

(a)
**MULTIHORN
MONOPULSE
FEED**

(b)
**NESTED
HELIX**

(c)
**DUAL-FREQUENCY
CONICAL HORN**
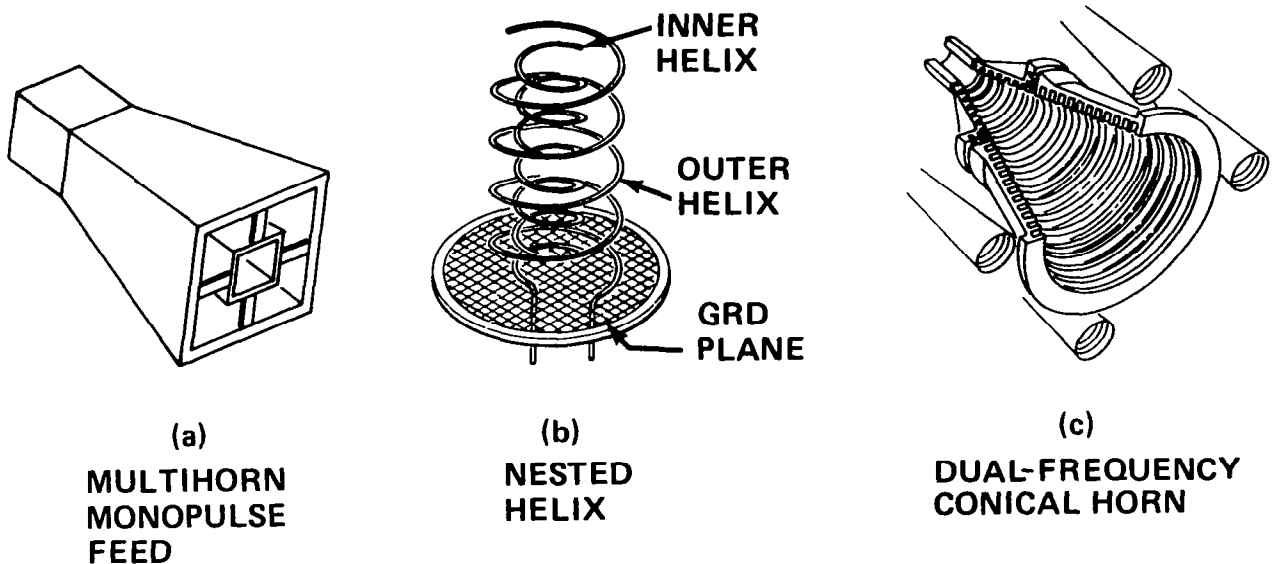
Figure 7

LOW-NOISE RECEIVER

In the past, ultra-low-noise receivers have used cryogenically cooled parametric amplifiers and masers as preamplifiers. The cost and complexity of these devices and the extreme sensitivity to pump output power and frequency preclude their consideration for flight experiments. The GaAs FET has proven to be an excellent replacement for the expensive parametric amplifiers in ground-based communication satellite terminals. The FET amplifiers have been coupled to Peltier coolers to provide receivers with a noise figure of less than 2 dB (160 K). A typical design using cascaded low-noise FETS is shown in figure 8. The ultra-low-noise preamplifier consists of two NE 13783 FETS. The postamplifier is made up of several FETS cascaded together. A circulator is used to isolate the two stages. The preamplifier is cooled to improve the noise figure and gain while the postamplifier is heated to stabilize the performance (ref. 3).

At room temperature the operating noise temperature for the combined preamplifier and post-amplifier can be determined by the equation:

$$T_e = T_A (L - 1) + L \left(T_{e1} + \frac{Te2}{G_1} + \frac{Te3}{G_1 G_2} \right)$$

where

T_A = 293 K

L = loss due to cable and coupler ($\approx$ 1/4 dB)

T_{e1}, T_{e2} = effective noise temperature of the FET devices at room temperature ($\approx$ 102 K) in the first two stages

T_{e3} = effective noise temperature of the postamplifier (290 K)

G_1 = G_2 = gain of the first and second stages (7 dB)

Thus T_e = 293 (1.06 – 1) + 1.06 [102 + 102/5 + 290/25] = 160 K.

At room temperature, thermal noise sources dominate the performance of GaAs MESFETS in microwave amplifiers. With cooling, a significant noise reduction has been observed (ref. 4). This reduction in effective noise is due to the mobility of the majority carriers. A frequently used relationship for noise reduction as a function of device temperature is:

$$T_{e'} = T_e \left(\frac{T_d}{T_a} \right)^{3/2}$$

where it is assumed that the transconductance is approximately proportional to $T^{-\frac{1}{2}}$ from 70 K to 300 K (ref. 4). When T_e = total amplifier noise temperature at ambient temperature (160 K) then T_d = cooled device temperature and T_a = ambient temperature (293 K).

ULTRA-LOW-NOISE ANTENNA
MOUNTED PREAMPLIFIER
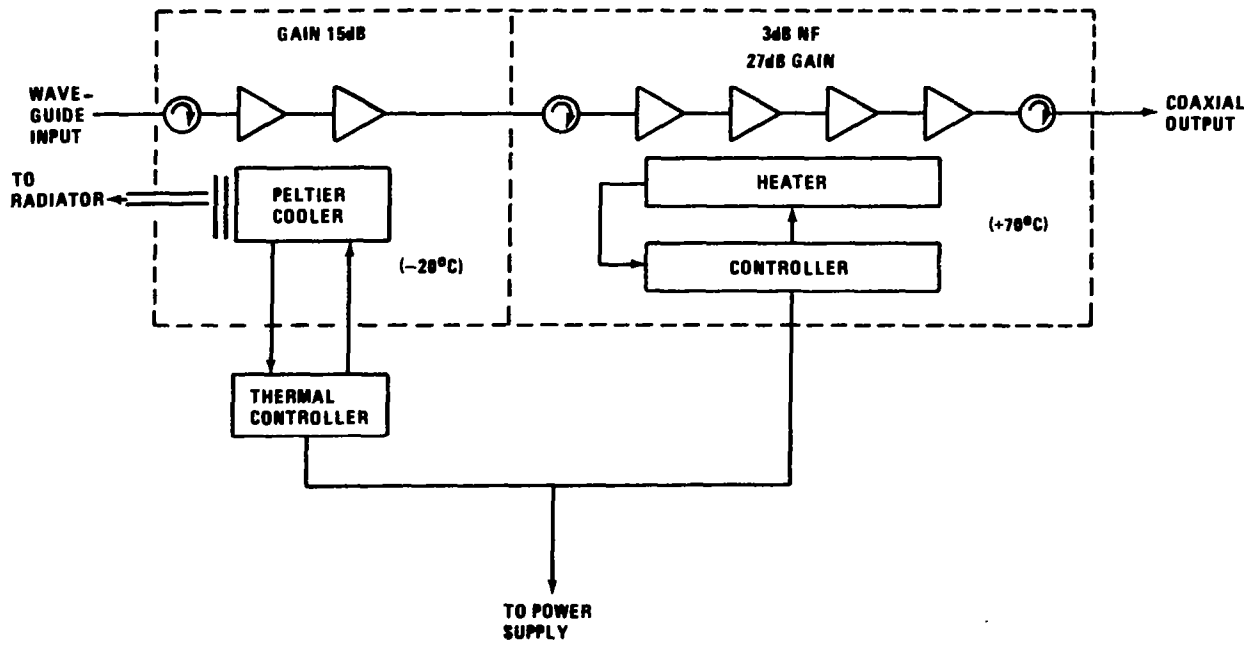
Figure 8 (From ref. 3).

EFFECT OF COOLING THE FET AMPLIFIER

A plot of the amplifier effective noise temperature (T_e) as a function of cooled device temperature (T_d) is shown in figure 9a. If it were possible to specify the vehicle orientation for all observations such that the preamplifier package would always view space, it might be possible to operate the FET devices around 180 K. However, this would be too restrictive from the astronomers point of view, so a thermal electric heat pump was proposed to transfer heat from the amplifier to a radiator. The radiator is designed such that one section has a view of space and can be switched into the cooling loop using variable conductance heat pipes. A cross section of a typical preamplifier thermoelectric pump (PTEP) used in ground communication satellite antennas is shown in figure 9b (ref. 5). In spaceborne applications the pins-on-plate heat exchanger would be replaced by a fluid loop or heat pipe exchanger, and a means of flowing the heat from the PTEP to the radiator would be provided. The insulation shown in figure 9b would probably be replaced by a superinsulation covering over the entire package or some other type that would be appropriate for operation in a vacuum environment. To reduce the time required for cooldown during the orbital experiment, prelaunch cooling may be required.

LOW-NOISE AMPLIFIER PERFORMANCE

$$T_e' = T_e \left[\frac{T_d}{293} \right]^{3/2}$$
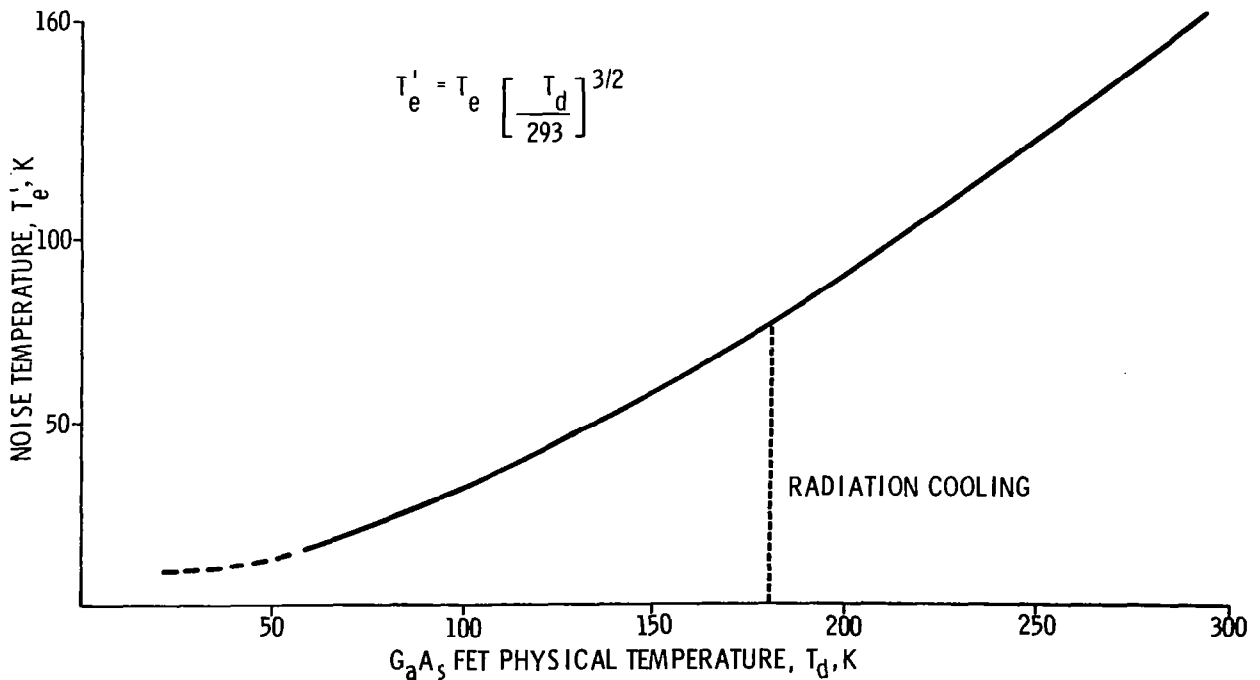
(a)

Figure 9

CROSS-SECTIONAL DIAGRAM OF A PTEP

HERMETIC WINDOWS (2)

PACKAGE COVER

WAVEGUIDE

HEATSHIELDS

PREAMPLIFIER

INSULATION FILLED INTERMEDIATE VOLUME

THERMOELECTRIC HEAT PUMP

AIRFLOW

PINS—ON—PLATE HEAT EXCHANGER

AXIAL FLOW FAN

(b)
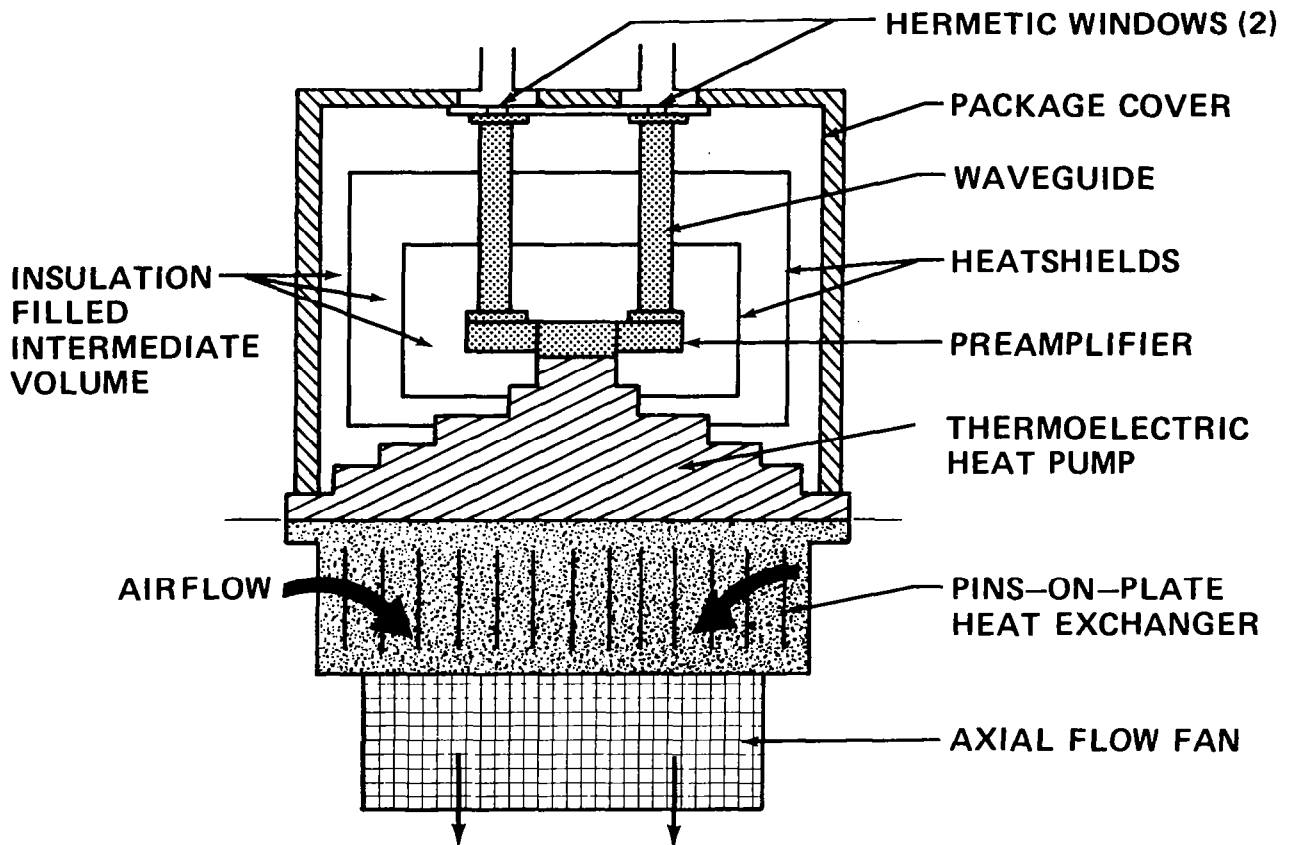
Figure 9

Aside from a large deployable reflecting surface, the second most difficult technology will be acquiring and maintaining the source within the 3 dB beamwidth of the antenna (0.05° at 8.4 GHz). It may not be possible to deploy the reflector and perform boresighting tests and feed alignment prior to flight. This means that the feeds or subreflector or both must be capable of adjustment on orbit to provide satisfactory performance. In figure 10 we see that three parameters can influence the proper location of the subreflector. These parameters are local surface deviations, the departure from a parabolic surface (Δz), and a change in focal length and rotation or bending in the feed mast (Δf). To compensate for these structural errors requires the feed to translate from A to A'. The distance has been greatly exaggerated in figure 10 to make the point clear. The technology problem is not how to design a movable subreflector and feed but rather how to determine where A' is with respect to A in an automated system. In addition to this "initial alignment" (termed initial alignment since the structure will be stable enough that this should not be required but once during the experiment), we see in figure 11 bending at the base of the antenna due to Shuttle thruster firings which the pointing system must compensate for.

ANTENNA SURFACE SYSTEM CHARACTERISTICS

$$F \overset{\Delta}{=} \text{CHANGE IN FOCAL LENGTH OF BEST FIT SURFACE}$$
$$Z \overset{\Delta}{=} \text{TRANSLATION OF BEST FIT SURFACE}$$
$$\sim\!\!\curvearrowleft \overset{\Delta}{=} \text{ACTUAL SURFACE POSITION}$$
$$\theta_x \overset{\Delta}{=} \text{ROTATION ABOUT X-AXIS}$$
$$\phi_y = \text{ROTATION ABOUT Y-AXIS}$$
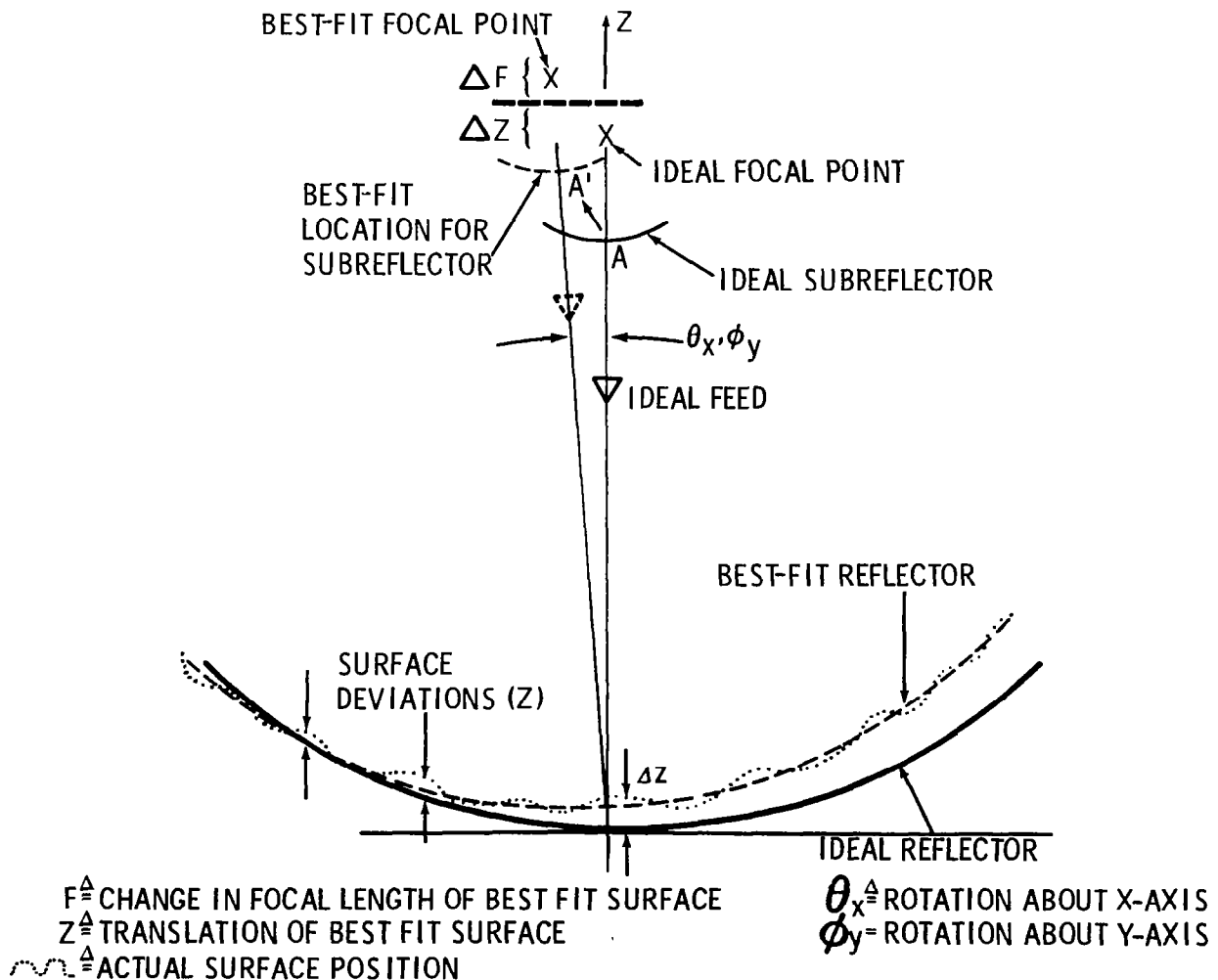
Figure 10

It is necessary to compensate for altitude disturbances during flight by firing the Shuttle vernier thrusters. In these simulations conducted by C. S. Draper Laboratory, the displacement was less than 0.1 degree peak-to-peak (ref. 6). This could, however, require as much as 0.5° tilt of the subreflector, depending on the beam deviation factor of the antenna. The simulation indicated that there would be almost 100-second intervals between firings, so observation must be coordinated with thruster firings to avoid interference. This agrees with the requirement in figure 5.

FLEX SIMULATION GRAPHICS REPRESENTATION OF ANTENNA AND ORBITER
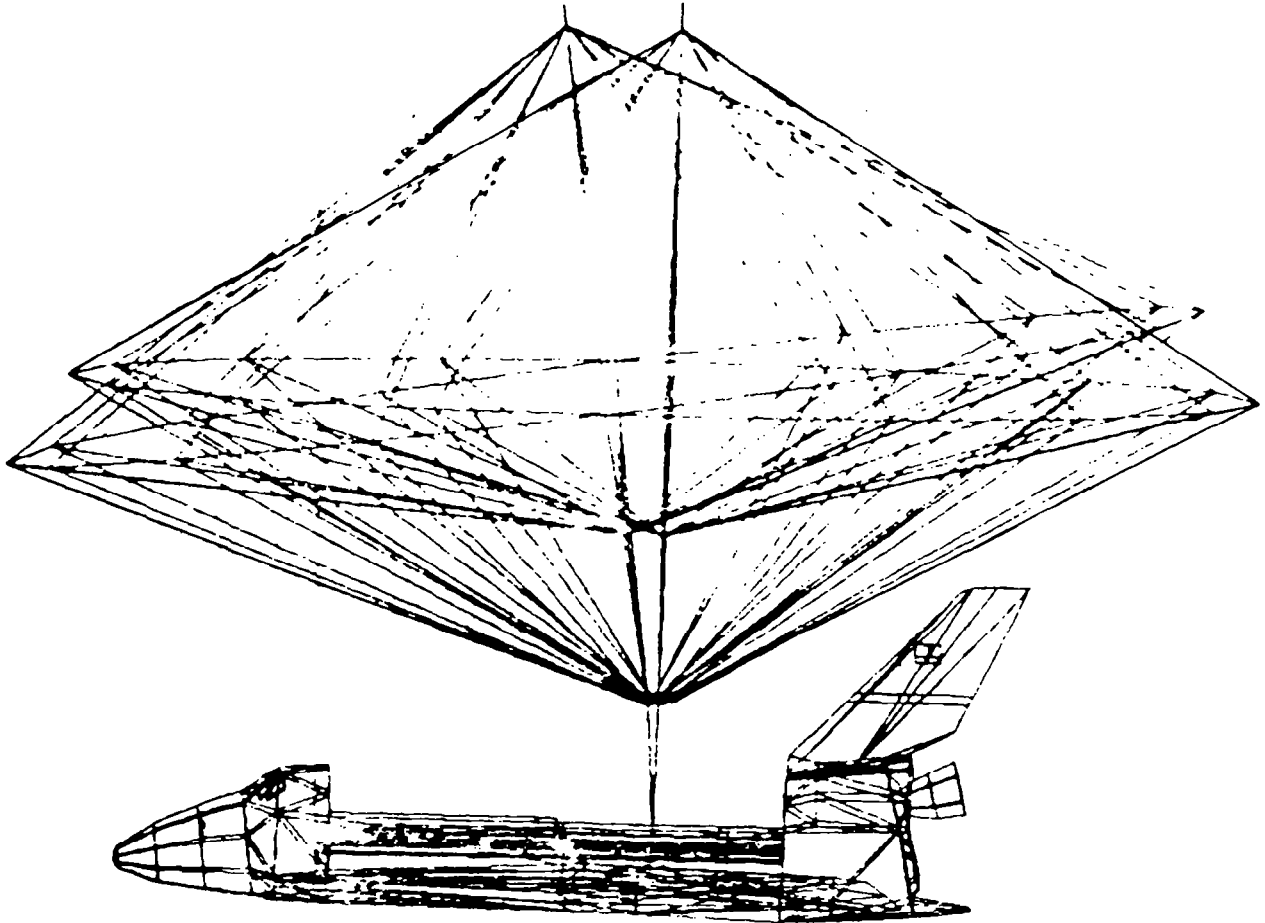
NOTE: ANTENNA MOTION IS GREATLY EXAGGERATED

Figure 11

LARGE ACCURATE APERTURE

The final technology area that requires discussion is that of the collecting area. It should be pointed out that the sensitivity of a space VLBI depends on both the ground antennas and the space-borne antennas as indicated in figure 12.

This equation indicates also that all of the parameters we have discussed thus far are under the square root radical. Even though the aperture efficiency enters the equation as a square root it is quite important in the case of the space antenna. Aperture efficiency is composed of blockage due to sub-reflector and support struts, spillover, illumination, scattering due to surface roughness, and leakage through the mesh reflecting surface.

Even though the term aperture efficiency enters the equation under the square root radical it is quite important. In ground-based systems illumination and spillover, efficiencies of 80 to 90% have been achieved by shaping both the primary and the secondary for uniform illumination (ref. 7). This may approach 98% for dual-reflector systems with diffraction shaping.

The space-deployed mesh reflector does not appear to lend itself to shaping of the primary surface. In fact, the primary only approaches the parabolic shape by segmenting the reflector. It may, however, be possible to achieve near uniform illumination by shaping the subreflector and then experimentally determining the correct focal point that results in the correction of the quadratic phase errors introduced by shaping of the subreflector. This procedure has been demonstrated on the ground in experiments (ref. 8). The technology challenge is how to do it in space with an antenna that is too large and flexible for deployment and measurements in one g prior to flight.

The spillover of the subreflector (forward spillover) is a function of the feed and subreflector sizes. As the diameter of these components is increased, a point is reached where the loss due to aperture blockages offsets any gain from decreased spillover. The spillover loss of the main reflector (rear spillover) may be somewhat limited by the subreflector diameter, which was constrained to the 3-meter diameter of the Shuttle cargo bay. Hopefully, 1% spillover loss can be achieved.

The projected area of subreflectors onto the main reflector represents a blockage region and a loss. If the illumination is uniform, the blockage efficiency can be expressed as

$$N_b = \left[1 - \left(\frac{ds}{dm} \right)^2 \right]^2$$

However, if the subreflector is shaped such that all the energy is reflected onto that part of the main reflector not blocked by the subreflector, a more optimistic expression is

$$\frac{N_{Br}}{N_o} = 1 - \left(\frac{ds}{dm} \right)^2$$

Since the maximum diameter of the subreflector is 3 meters and that of the main reflector is 50 meters, the blockage efficiency would be on the order of 99.6% ($N_{BL} = 0.996$).

The losses through the mesh should be small with proper opening size and tension on the mesh. The TDRSS antenna mesh is made up of gold plated molybdenum wire about 1 mil in diameter. The weave results in 10 openings/inch. The efficiency will range from 99.8% at the lower frequency to 96.8% at the upper frequency.

INTERFEROMETER SENSITIVITY

$$SNR = 1.8 \times 10^{-4} \ S_c \ D_1 \ D_2 \sqrt{\frac{e_1 e_2 \ g_1 \ g_2 \ B\tau}{T_1 T_2}}$$

WHERE

S_c = CORRELATED FLUX IN JANSKYS

e_1, e_2 = ILLUMINATION EFFICIENCY

D_1, D_2 = DIAMETER OF APERTURE, METERS

T_1, T_2 = EFFECTIVE SYSTEM TEMPERATURE, K

B = BANDWIDTH, Hz

τ = INTEGRATION TIME, SECONDS

g_1, g_2 = MISPOINTING COEFFICIENT

Figure 12

SURFACE ERROR EFFECTS

The remaining factor influencing the efficiency, surface roughness, is probably the most significant for space antenna and the most discussed. In 1966 a Ruze paper worked out a model for reasonable surface tolerance losses (ref. 9):

$$\eta = e - \left(\frac{4\pi \, \epsilon}{\lambda} \right)^2$$

where ϵ is the rms surface error, in the same units as the wavelength (λ). The value of ϵ is a function of thermal distortion due to space thermal vacuum, surface approximations due to gores, and manufacturing tolerance. Some of these parameters vary as a function in diameter. In figure 13 are some interesting estimates of what the technology may be capable of producing. The lower curves indicate what may be possible with today's technology. The middle curve is what may be possible with more stable materials such as metal matrix and better measuring instruments for manufacturing. The third curve assumes the growth in the second curve plus a closed loop sensing and adjusting on orbit. It is interesting to note that several studies and hardware programs (refs. 10-13) verify the shape of the first curve. If we find during development that we can reach the 2×10^4 predicted in the lower curve, the efficiency would still be quite low at 8.4 GHz (46%), but at 2.4 GHz it is 94%. This results in about 78% aperture efficiency at 2.3 GHz but only 42% for the 8.4 GHz. This points out just how important surface tolerances are to the efficiency. However, it should also be pointed out that in the 8.4 GHz case the power gain of 69 dB and at 2.3 GHz the gain of 62 dB are both quite respectable.
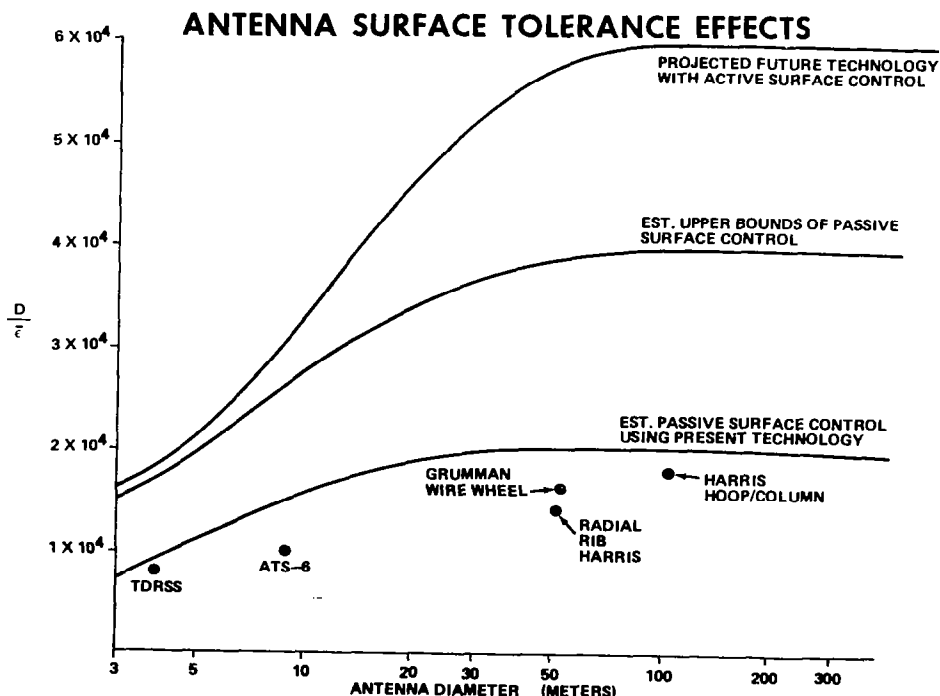
Figure 13

VLBI FEED ASSEMBLY

A conceptual design of the tilting cassegrain subreflector, dual corrugated horn and RF electronics has been under study. A key change has been the replacement of the hydrogen maser with a rubidium cell and quartz oscillator. This was to reduce complexity and cost. A hydrogen maser was used on the Redshift Experiment and was baselined for the flight, but the cost of $3 to $5.2M caused us to look at less costly devices. The frequency standard phase variation should not exceed one radian at the highest signal frequency during one sampling interval. The case of 8.4 GHz for 100 seconds results in a requirement of 4 parts in 10^{13}. The cesium and rubidium atomic frequency standards developed for the GPS approach this but may mean that integration time may have to be reduced slightly. It may be possible to compensate for this by lowering the temperature of LNA. Also, phase locking a high quality crystal oscillator to a rubidium oscillator can provide coherence time of one minute at $\lambda = 3$ cm.

The subreflector actuators provide for necessary tilting to null any error signal in a monopulse feed system. The simulation indicates that the fast response is not necessary, so that electric motor drives may be used as actuators. In addition to subreflector tilt, the whole subassembly may require adjustment for initial alignment (fig. 14).

The thermal radiators must be covered with RF absorbant material and yet have good thermal characteristics. A prototype of this subassembly should be built and tested on a ground-based antenna to insure the proper function prior to incorporation into the deployable antenna.

VLBI COMPONENTS LOCATION
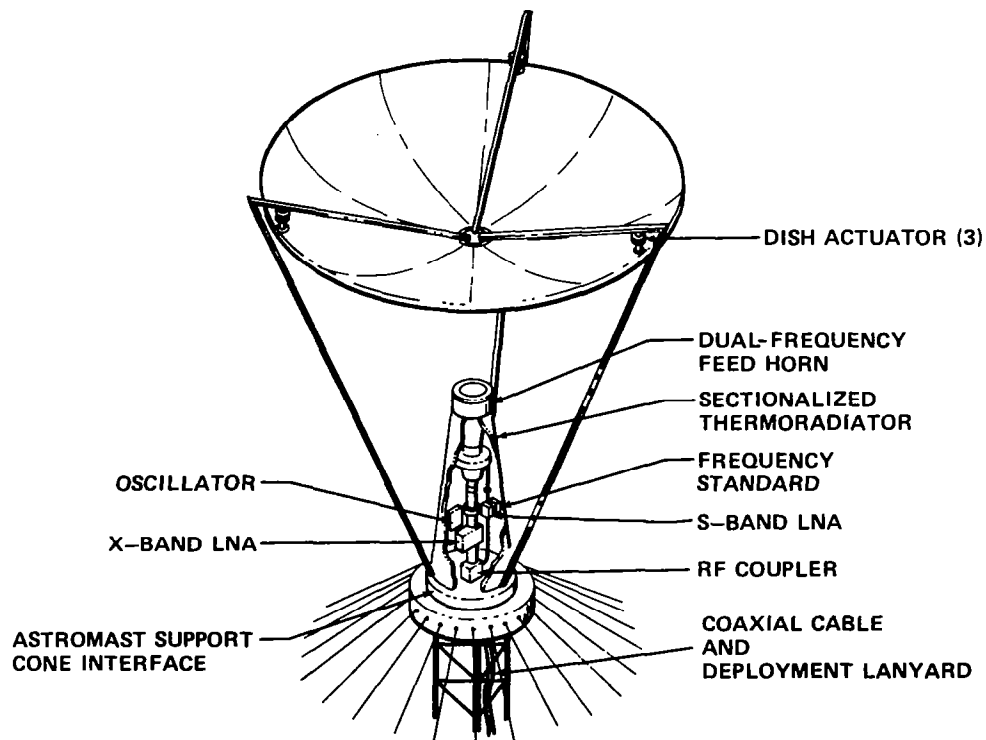
Figure 14

SUMMARY

The subsystems necessary to do the space VLBI experiment appear to be available but require space qualifications. There appear to be several 50-meter antenna concepts that could be used. Certainly there are problems to be solved. Feed positioning with respect to reflector, pointing such a large structure to accuracy indicated, and integration into the Shuttle control system are all significant engineering challenges. However, there do not appear to be any problems that would be insurmountable in the latter part of this decade.

REFERENCES

1. Cohen, Marshall H.: Introduction to Very Long Baseline Interferometry. IEEE Proc., Vol. 61, No. 9, September 1973.

2. Morgan, Samuel H.; and Roberts, David H.: Shuttle VLBI Experiment Technical Working Group Summary Report. NASA TM-82491, 1982.

3. Askew, R. E.; and Wolkstein, H. J.: A Low Noise Peltier-Cooled FET Amplifier. RCA Review, Vol. 42, No. 4, December 1981.

4. Pierro, John: Cryogenically Cooled GaAs FET Amplifier with a Noise Temperature Under 70K at 5 GHz. IEEE Transaction on Microwave and Techniques, December 1976.

5. Hung, H. L.; and Hyman, N. L.: Thermoelectrically Cooled MESFET Low-Noise Amplifier for Earth Stations. COMSAT Technical Review, Vol. 10, No. 2, Fall 1980.

6. Burke, Bernard F.: Radio Telescopes Bigger Than the Earth. Astronautics and Aeronautics, Oct. 1982.

7. Bathker, D. P.: Microwave Performance Characterization of Large Space Antennas. JPL Publication 77-21, May 15, 1977.

8. Collins, C. W.: Shaping of Subreflectors in Cassegrain Antennas for Maximum Aperture Efficiency. IEEE Trans. on Antennas and Propagation, Vol. AP-21, No. 3, May 1973.

9. Ruze, John: Antenna Tolerance Theory — A Review. Proc. IEEE, Vol. 54, No. 4, April 1966, pp. 633-640.

10. Deployable Antenna Flight Experiment Definition Study. Vol. II. Grumman Aerospace Corp., 1982.

11. Deployable Antenna Flight Experiment. Third Quarterly Review. Harris Corp., Government Systems Group, June 1981.

12. Sullivan, Mark R.: Maypole (Hoop/Column) Concept Development Program. Large Space Systems Technology - 1981, NASA CP-2215, Part 2, 1982, pp. 503-550.

13. Freeland, R. E.: Industrial Capability for Large Space Antenna Structures. JPL Report No. 710-12, May 1978.

PUSHBROOM RADIOMETRY AND ITS POTENTIAL
USING LARGE SPACE ANTENNAS

Richard F. Harrington and Lloyd S. Keafer, Jr.
NASA Langley Research Center
Hampton, Virginia

Electromagnetic radiation is emitted by matter which has been heated to a temperature above absolute zero. The amount of blackbody radiation in the microwave frequency region of interest ($10^8 < f < 10^{10}$ Hz) emitted by matter can be determined from the Rayleigh-Jeans approximation to Planck's Radiation Law. The amount of electromagnetic radiation from matter which is not a blackbody is a function of the emissivity of the material. The emissivity e is a factor less than unity and is a function of several parameters including chemical composition, temperature, frequency, surface characteristics, and viewing angle.

A radiometer is an instrument which detects and provides a measure of the electromagnetic radiation being emitted by a material or surface area within the radiometer's antenna beamwidth. Microwave radiometers provide the capability for remote measurements from Earth orbits of geophysical parameters such as those given in Figure 1. These measurements will require the use of a microwave imaging radiometer using a large aperture deployable antenna with multiple beams in a pushbroom mode to achieve high spatial resolution and large swath width.

MICROWAVE RADIOMETER APPLICATIONS

LAND

- **SOIL MOISTURE**

OCEAN

- **SEA SURFACE TEMPERATURE**
- **WIND SPEED**
- **SALINITY**

ICE

- **EDGE LOCATION**
- **CONCENTRATION**
- **AGE (FIRST YEAR/MULTI-YEAR)**

ATMOSPHERIC

- **WATER VAPOR**
- **NON-PRECIPITATING LIQUID WATER(CLOUDS)**
- **PRECIPITATING LIQUID WATER (RAIN)**

Figure 1

CRITICAL RADIOMETER PARAMETERS

The design of a pushbroom radiometer for a large space antenna system is a complex compromise between several conflicting critical parameters. These critical radiometer design parameters are listed in Figure 2. The choice of frequency is a function of several parameters and will be discussed in Figure 3. The amount of received electromagnetic radiation is a function of both the incidence angle and polarization. A non-zero, constant angle of incidence with the surface is desirable in some geophysical applications. Both horizontal and vertical linear polarization are desirable to aid in the mathematical inversion from brightness temperature to geophysical parameters. The required measurement accuracy is a function of the geophysical parameter being measured and affects the choice of radiometer bandwidth and integration time. Frequency allocation and selection influence the available bandwidth, while increasing the integration time to improve accuracy degrades spatial resolution. The mission objectives, orbital selection, and radiometer design (such as aperture size and number of beams) determine the spatial resolution, swath width, and temporal repeats.

FREQUENCY

INCIDENCE ANGLE

POLARIZATION

ACCURACY

RESOLUTION (SPATIAL)

SWATH WIDTH

TEMPORAL REPEATS

Figure 2

FREQUENCY SELECTION CRITERIA

The criterion for selection of the optimum frequency for the pushbroom
radiometer is a function of the four factors listed in Figure 3. A fundamental
criterion is to choose a frequency at which the amount of electromagnetic radia-
tion is sensitive to the change in the geophysical parameter to be measured.
The upper frequency limitation is determined by the losses due to absorption by
oxygen and water vapor in the atmosphere. The lower frequency limitation is due
to excessive background noise from the galaxy.

Radio frequency interference (RFI) is a problem in passive remote sensing.
The change in the power spectral density received by a radiometer operating at
5 GHz measuring a change in the sea surface temperature from 10°C to 11°C is
5.5×10^{-24} W/Hz of bandwidth. An electromagnetic radiation source, such as
a radio or radar transmitter, must not transmit a signal that is 0.1 times
this level or an error in the measurement will result. For example, an isotropic
radiator on the Earth's surface transmitting 0.0003 W and received through the -30
dB sidelobes of a 180-m diameter radiometer antenna would just be detectable.
Therefore, for successful operation of a passive microwave pushbroom radiometer,
a frequency must be selected which is a WARC (World Administrative Radio Conference)
frequency allocation for spaceborne passive remote sensing.

○ # SENSITIVITY OF ELECTROMAGNETIC RADIATION TO CHANGE IN THE GEOPHYSICAL PARAMETER

○ # ATMOSPHERIC LOSSES

○ # GALACTIC AND COSMIC NOISE

○ # RADIO FREQUENCY INTERFERENCE - WARC FREQUENCY ALLOCATIONS

Figure 3

FREQUENCY ALLOCATIONS FOR MICROWAVE REMOTE SENSING

Those frequencies which have been allocated by the World Administrative Radio Conference for passive radiometric measurements from space in the frequency range from 1 GHz to 16 GHz are listed in Figure 4. As can be seen, the selection of frequency and available bandwidth for remote sensing in the microwave portion of the spectrum has been severely restricted by the WARC frequency allocations. Selection of frequencies and bandwidths outside of these allocations is possible; however, protection from radio frequency interference becomes more difficult.

FREQUENCY (GHZ)	MEASURAND
1.37-1.43	SALINITY-SOIL MOISTURE
2.64-2.69	
4.2-4.4	SEA SURFACE TEMPERATURE
6.4-7.2	
10.6-10.7	WIND RAIN ICE
15.2-15.4	

Figure 4

RADIOMETER EXPERIENCE IN THE ANTENNA AND MICROWAVE
RESEARCH BRANCH AT NASA LANGLEY

Related radiometric experience during the past several years in the Antenna and Microwave Research Branch at NASA Langley is illustrated in Figures 5, 6, and 7. Figure 5 shows a single beam UHF radiometer that was designed, developed, and fabricated at Langley. This instrument operates at 611 MHz and is used to measure salinity and soil moisture. Flight tests will be conducted during the spring of 1983. Figure 6 shows the results of a flight test across the western boundary of the Gulf Stream to evaluate the performance of the Stepped Frequency Microwave Radiometer (SFMR) using the first known digital signal processing in a microwave radiometer. The precision single beam L-band (1.413 GHz) radiometer provided a comparison data set during these tests. Figure 7 illustrates the Pushbroom Microwave Radiometer (PBMR) hardware development. This three/four beam 1.413 GHz radiometer will be test flown in the spring of 1983 on the NASA P-3 along with the UHF radiometer and SFMR.
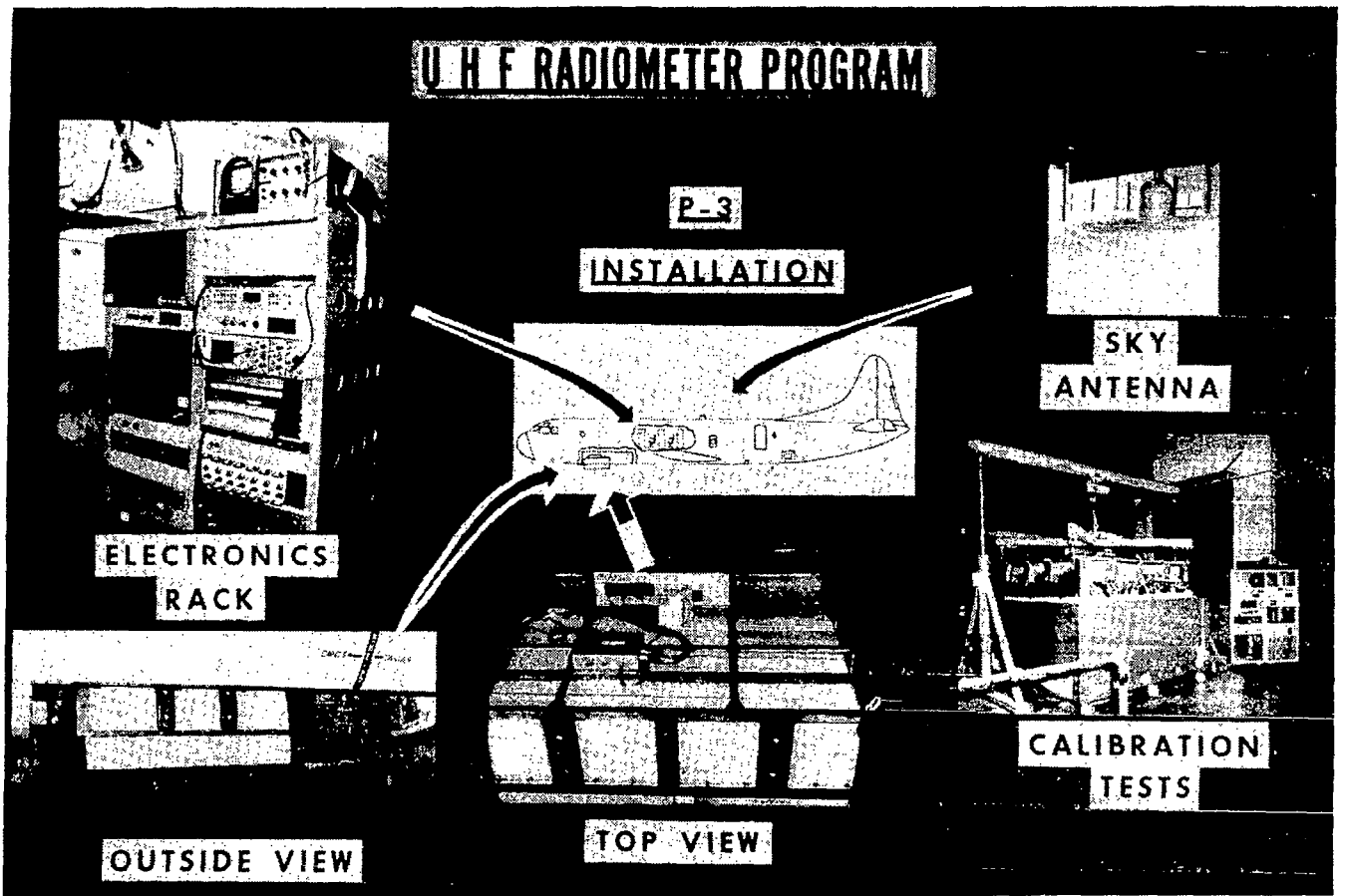
Figure 5

FLIGHT TEST EVALUATION OF A NOISE INJECTION DICKE MICROWAVE RADIOMETER EMPLOYING DIGITAL SIGNAL PROCESSING

NASA AIRCRAFT

C-BAND DIGITAL PROCESSING RADIOMETER

L-BAND RADIOMETER

DATA PROCESSING

FLIGHT DATA

TEST RESULTS
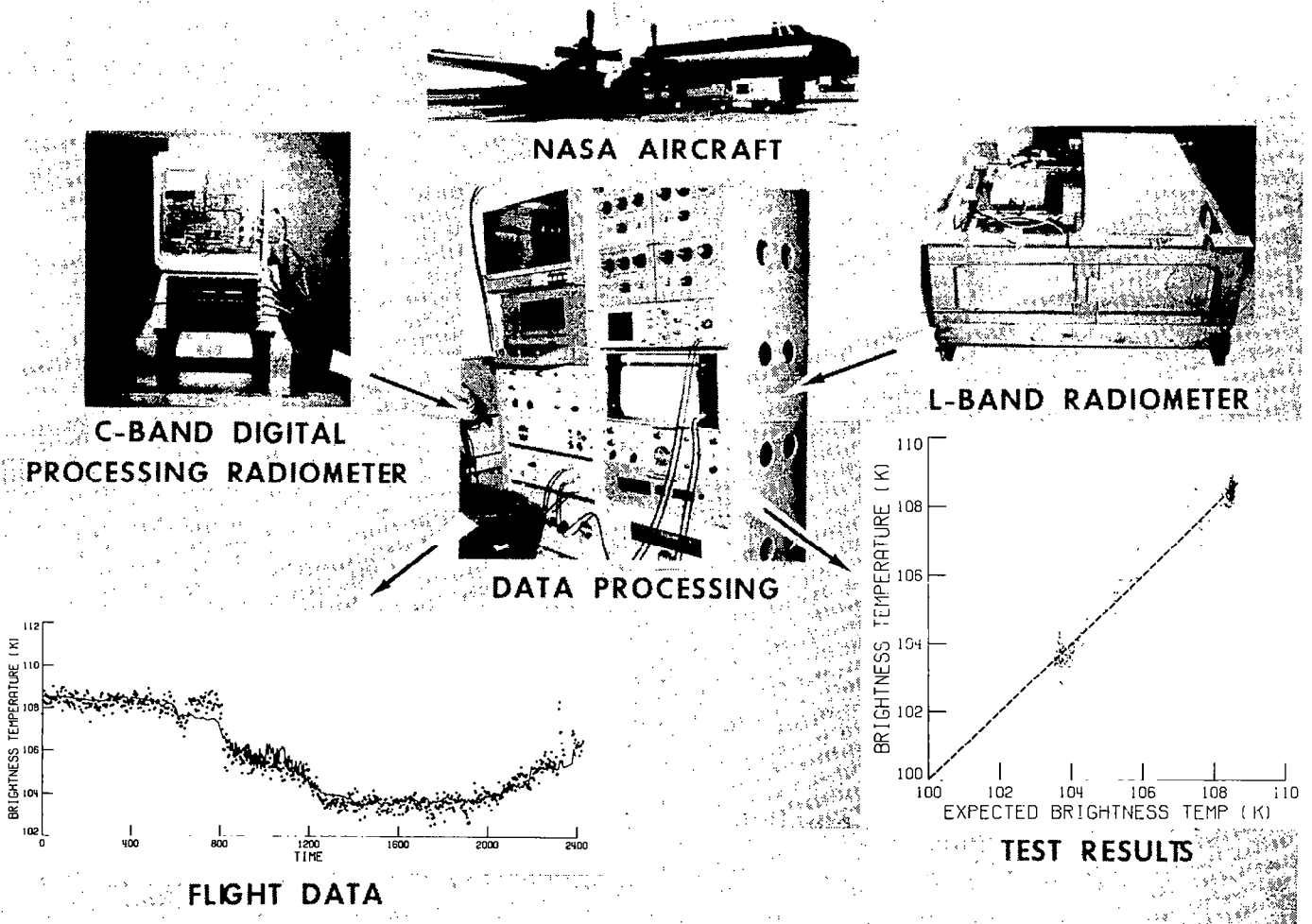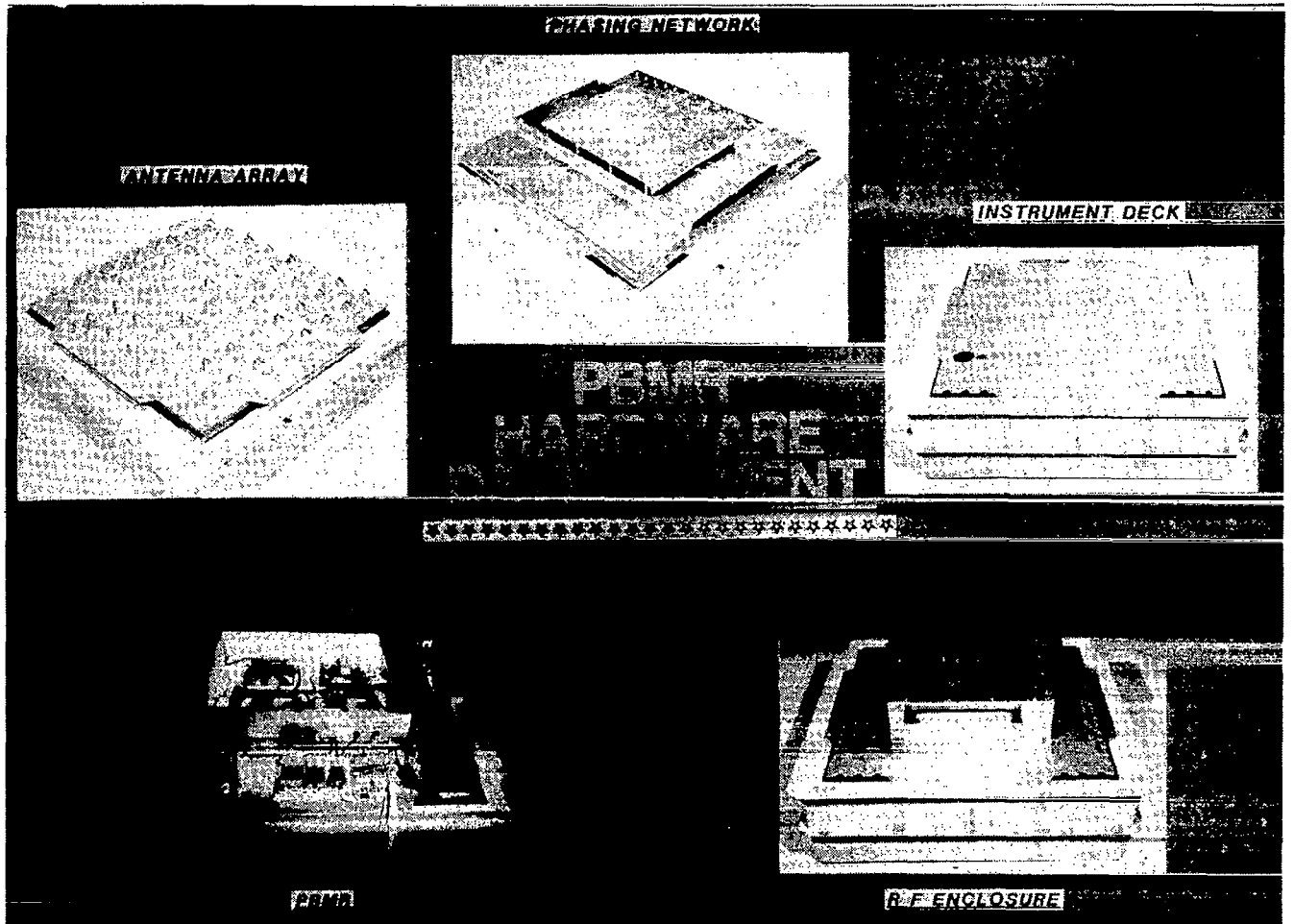
Figure 6

Figure 7

The power required by a microwave radiometer due to the electromagnetic radiation from the land surface is a function of several variables which are listed in Figure 8. If soil moisture is the principal geophysical parameter to be measured by the microwave radiometer, then the physical surface temperature, soil type, biomass cover, and surface roughness must be known or measured by independent methods. Also the frequency, incidence angle, and polarization of the microwave radiometer must be selected to increase its sensitivity to the electromagnetic radiation due to soil moisture while decreasing, if possible, the sensitivity to other parameters, such as surface roughness.

The correlation of the electromagnetic radiation, T_B, to volumetric soil moisture content as a function of frequency is shown in Figure 9. It can be seen from these data that biomass cover limits the useful frequency range to frequencies below 2 GHz for soil moisture measurements of any soil other than bare soil.

ELECTROMAGNETIC RADIATION (T_B)

FUNCTION OF :

- **SOIL MOISTURE**

- **PHYSICAL SURFACE TEMPERATURE**

- **SOIL TYPE**

- **BIOMASS COVER**

- **SURFACE ROUGHNESS**

- **POLARIZATION**

- **INCIDENCE ANGLE**

- **FREQUENCY**

Figure 8

SOIL MOISTURE
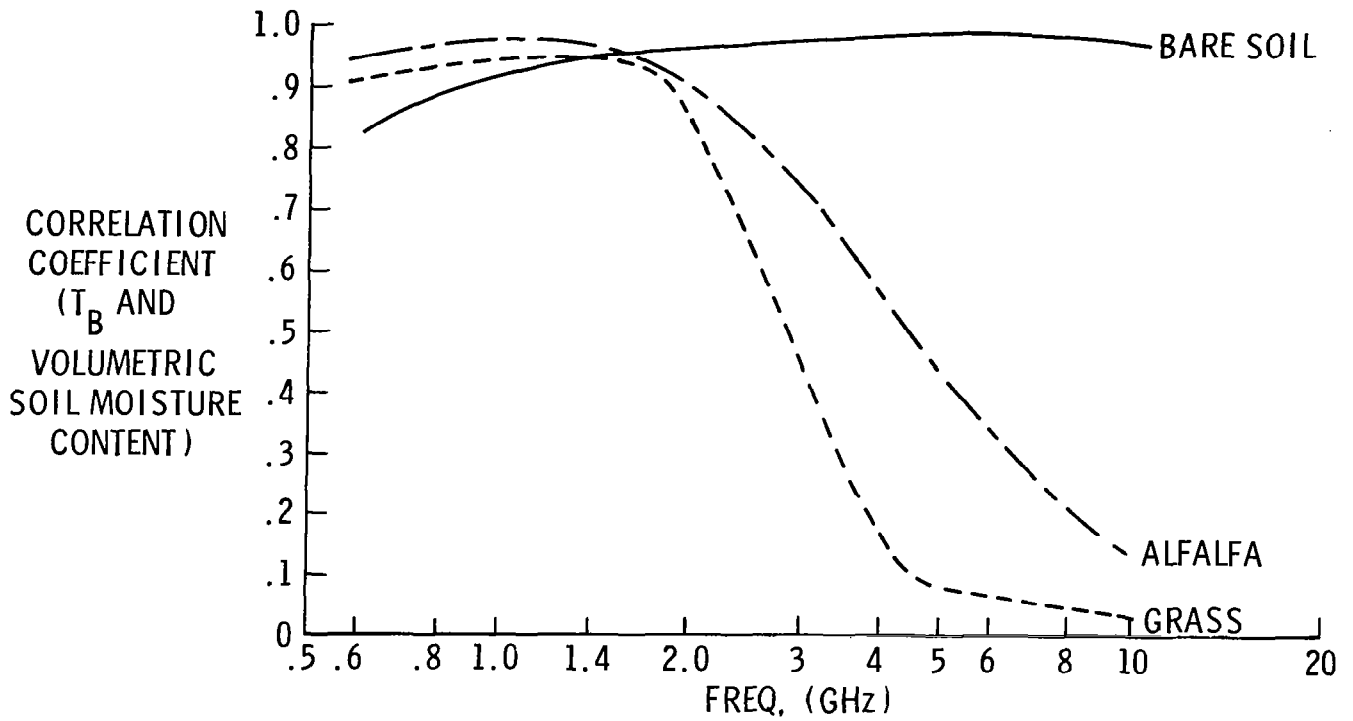
Figure 9

The power received by a microwave radiometer due to the electromagnetic radiation from the ocean surface is a function of several variables which are listed in Figure 10. Microwave radiometers operating at multiple frequencies and polarizations have been used to measure several of these parameters simultaneously. However, measurement of wind speed by measuring the change in electromagnetic radiation due to surface roughness and surface coverage is a complex task. This is the result of the fact that the surface roughness and surface coverage are functions of wind velocity and direction, current velocity and direction, fetch, and duration of both wind and current. The frequency, incidence angle, and polarization of the microwave radiometer must be selected to increase its sensitivity to the electromagnetic radiation due to the desired geophysical parameter while decreasing, if possible, the sensitivity to other geophysical parameters.

ELECTROMAGNETIC RADIATION (T_B) FUNCTION OF:

- **PHYSICAL SURFACE TEMPERATURE**

- **SALINITY**

- **SURFACE ROUGHNESS**
  WINDS (VELOCITY AND DIRECTION)
  CURRENTS (VELOCITY AND DIRECTION)
  FETCH
- **SURFACE COVERAGE**
  FOAM AND STREAKS
  WHITECAPS
  POLLUTION
  FREQUENCY

- **INCIDENCE ANGLE**

- **POLARIZATION**

Figure 10

SEA SURFACE TEMPERATURE SENSITIVITY

The sensitivity of the electromagnetic radiation, T_B, to a change in sea surface temperature as a function of frequency for incidence angles of 0° and 53° using vertical polarization is shown in Figure 11. The two extreme values of sea surface temperature (SST), 0^oC and 30^oC, are plotted for both 0° and 53° incidence. Other values of SST and incidence angles lie between these curves. The curve has been plotted for open ocean with a value of salinity equal to 36 parts per thousand being used in the calculation. If a reasonable sensitivity of 0.25 K per ^oC was chosen as a design criterion, then the 0° incidence angle (nadir) would be the maximum allowable frequency range for the radiometer design. For a 53° incidence angle and vertical polarization, the frequency range would be limited to 2.6 GHz to 8.3 GHz. The choice of a larger sensitivity factor would reduce the operating frequency range, while a lower sensitivity factor would increase the radiometric accuracy required for a given geophysical parameter accuracy. The sensitivity for horizontal polarization is less than for vertical polarization.

Figure 11

92
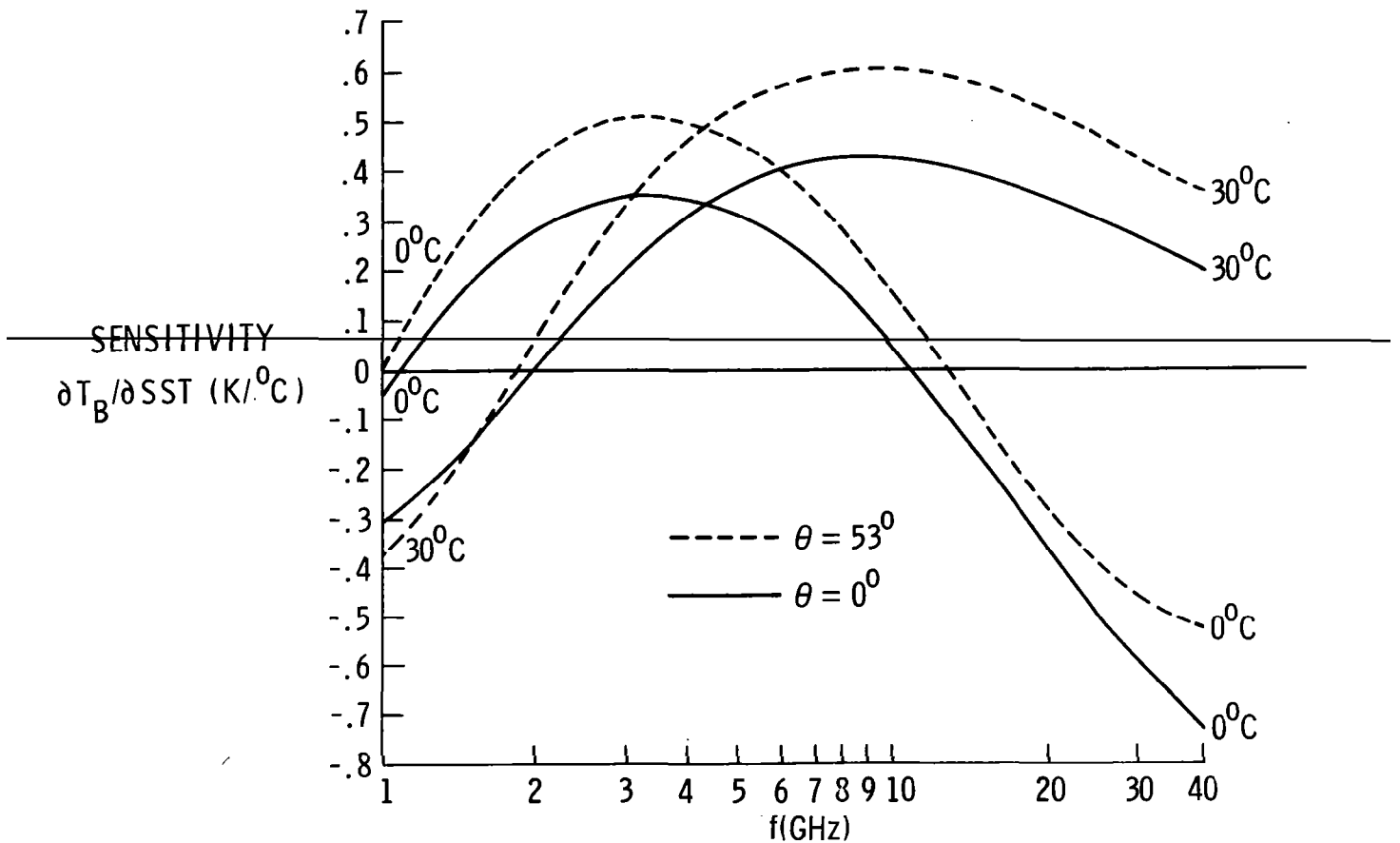
SALINITY SENSITIVITY

The sensitivity of the electromagnetic radiation, T_B, to a change in salinity as a function of frequency for incidence angles of 0° and 53° using vertical polarization is shown in Figure 12. Two values of salinity, 10 parts per thousand and 36 parts per thousand, are shown. These values represent typical values for estuaries and open ocean, respectively. Figure 12 was computed assuming a sea surface temperature of $20^\circ C$ as a typical value. These curves vary as a function of sea surface temperature. The measurement of salinity with a reasonable sensitivity of 0.25 K per part per thousand of salinity for open oceans at $20^\circ C$ would require a frequency less than 2.2 GHz for a 0° incidence angle and less than 2.8 GHz for a 53° incidence angle. Referring both to Figures 11 and 12, it can be seen that a frequency near 1.4 GHz could be selected such that the sensitivity of T_B to sea surface temperature approaches zero while the sensitivity to salinity is better than -0.5 K per part per thousand and represents an optimum frequency selection for salinity measurements.
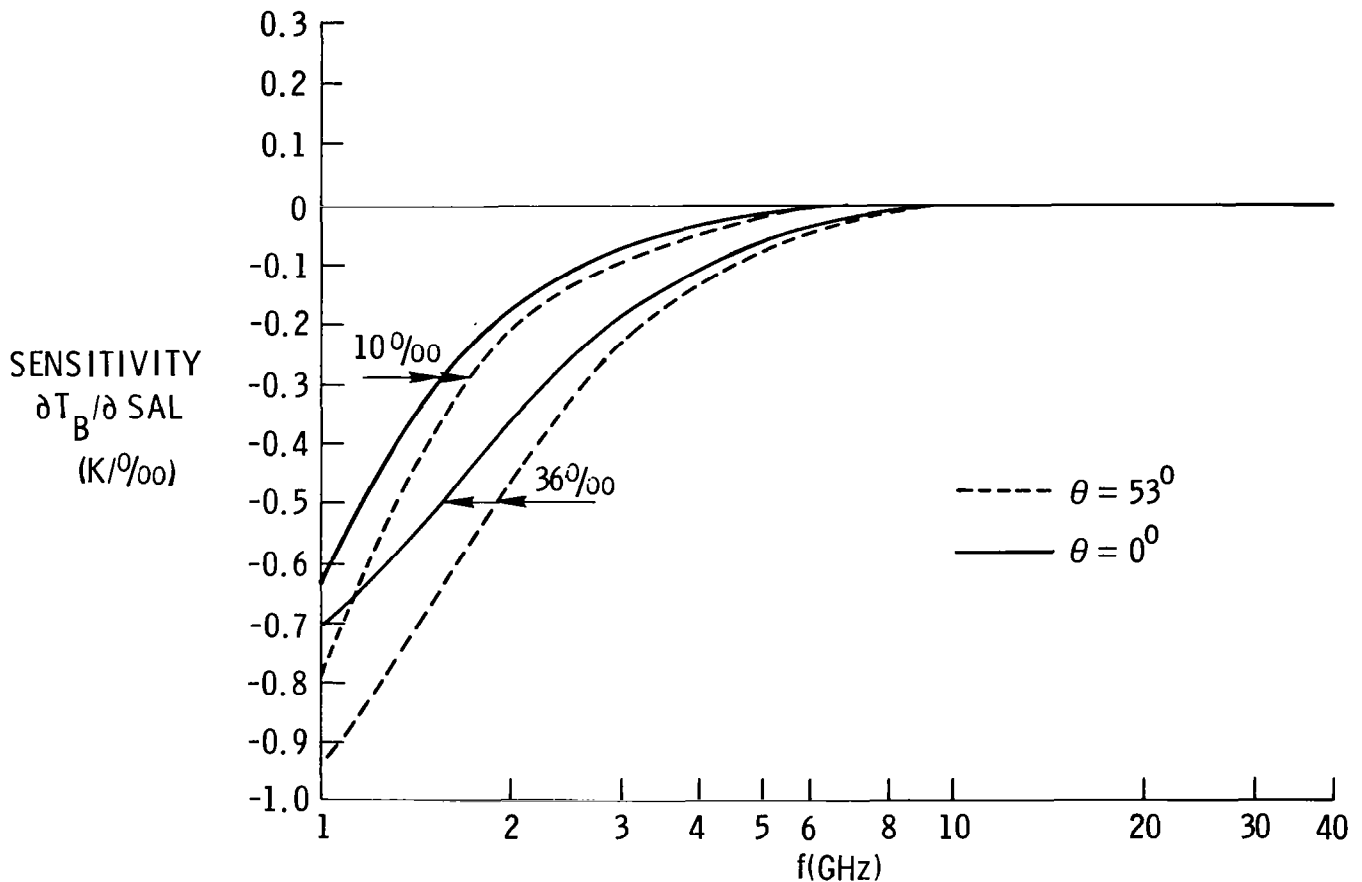
Figure 12

The sensitivity of the electromagnetic radiation, T_B, to a change in wind speed as a function of frequency is shown in Figure 13. Curves are shown for 0° incidence angle (nadir) and both vertical and horizontal polarization. Data were obtained during microwave radiometric measurements over the Bering Sea from the NASA CV 990 during the joint US/USSR Bering Sea Experiment of February–March 1973. Off–nadir measurements are at an incidence angle of 38°. Inferred values at nadir were computed from 38° vertical and horizontal data. The sensitivity to wind speed increases with frequency and is a function of polarization and incidence angle. However, there are incidence angles at which the sensitivity to surface roughness due to wind speed for vertical polarization is minimized. However, the effect of foam coverage is still present. At 6 GHz, wind speed sensitivities vary between 0.4 to 0.7 K per meter per second of wind velocity. Assuming a 0.25 K per ^{o}C SST sensitivity, this would translate to a SST wind speed error sensitivity of 1.6^oC per meter per second to 2.8^oC per meter per second, which is highly significant for an accuracy requirement of $\pm 1^o$C. Present capability of remote sensing of wind speed is 1.3 m/sec (1σ) for the SEASAT SASS scatterometer and 2 to 3 m/sec for the SEASAT SMMR microwave radiometer. The resulting error would be between $\pm 2^o$C (1σ) and $\pm 8^o$C (1σ).
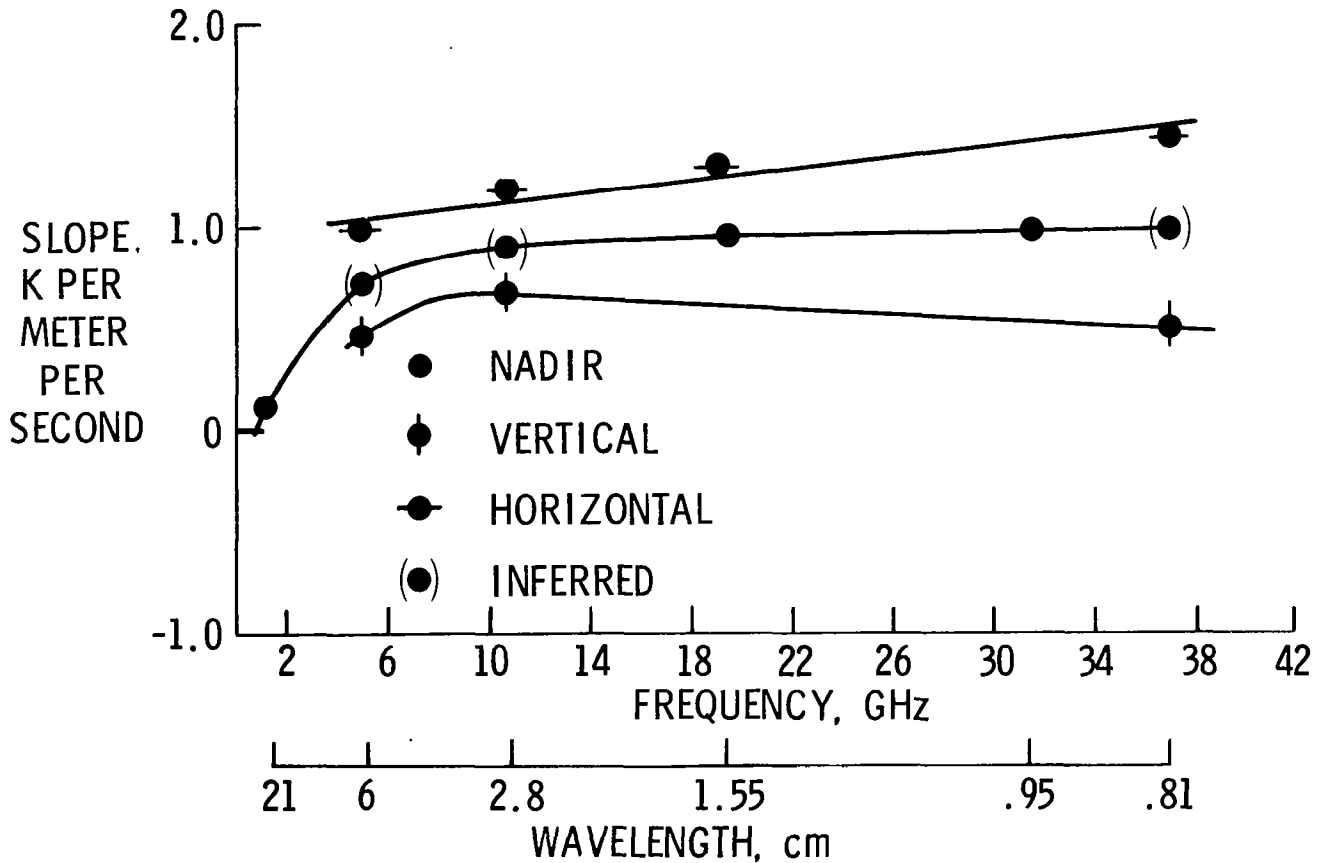
Figure 13

REQUIRED APERTURE VS WAVELENGTH

The required antenna diameter as a function of wavelength for a 600-km orbit is shown in Figure 14. Spatial resolutions of 1 km and 10 km for both an optimistic criterion and a conservative criterion are plotted. The optimistic criterion represents an angular resolution equal to the half-power beamwidth of a perfect aperture (1.22 λ/D) where D is the diameter and λ is the wavelength. The conservative criterion represents an angular resolution equal to 2 times the main beamwidth (6.00 λ/D). For the mandatory 10-km spatial resolution, a 200-m aperture is not required for a single beam, but for 1-km spatial resolution, the 50-m aperture is adequate only at the upper end of the frequency range. Also, the effect of finite integration time required for the proper operation of a microwave radiometer has not been included.

Minimum Required Antenna Diameter at 600 km Orbital Altitude
for Various Spatial Resolution Requirements
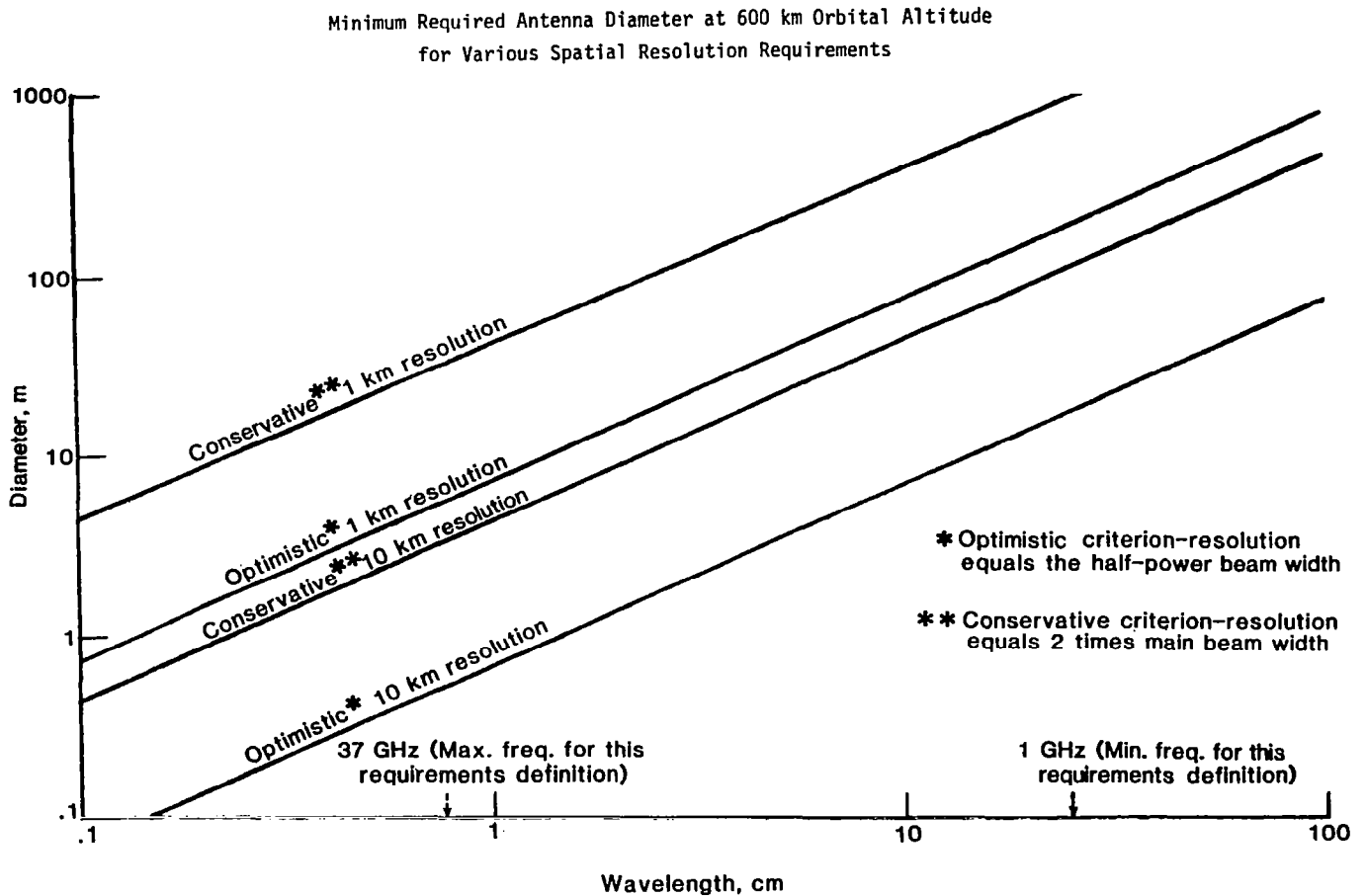
Figure 14

ANTENNA REQUIREMENTS

The design requirements for an antenna to be employed in a microwave radiometer system are listed in Figure 15. The requirement for high beam efficiency (better than 90%) and low sidelobes (15 dB below the isotropic level) will be discussed in later figures. The antenna input has a power reflection coefficient which reflects the 300 K electromagnetic radiation being emitted by the input of a microwave radiometer back into the radiometer. This reflected signal can be removed as a bias if it remains stable to within ±0.0001 during a measurement period. Any absorptive losses within the field of view of the microwave radiometer radiate electromagnetic energy into the radiometer equal to the product of the absorption and the physical temperature of the absorption. Therefore, the surface absorption of the antenna and its physical temperature must be known to an accuracy better than ±0.1 K (1σ) so they can be removed as a bias. The conflicting requirements of high spatial resolution (small spot size) and wide swaths for geophysical coverage require the use of either a single beam being scanned, scanning multiple beams (whiskbroom), or non-scanning multiple beams (pushbroom).

- **BEAM EFFICIENCY**

- **SIDELOBE LEVEL**

- **STABILITY OF VSWR**

- **SURFACE ABSORPTION (LOSSES)**

- **MEASUREMENT OF PHYSICAL TEMPERATURE**

- **ANTENNA SCANNING TECHNIQUES**

Figure 15

96

ANTENNA SIDELOBE REQUIREMENT

The response of a microwave radiometer during the crossing of a land-sea boundary as a function of sidelobe level is presented in Figure 16. A computer model was developed to determine the error due to sidelobe level as a function of beamwidth, frequency, and sidelobe level. A computer run for a 1.4 GHz, 0.5°, 3 dB beamwidth and sidelobe levels of +5 dB, 0 dB (isotropic), -5 dB and no sidelobes has been shown. A substantial error exists for many resolution cells on either side of the boundary (located at 0° angle). The horizontal axis represents the angle between the spacecraft and the land-sea boundary in degrees. Therefore, four resolution cells exist between -1.0° and $+1.0^{\circ}$. A value of 250 K was assumed for the land value and 90 K was assumed for the sea value.

RESPONSE OF MICROWAVE RADIOMETER ANTENNA AT LAND-SEA BOUNDARY DUE TO SIDELOBE LEVEL
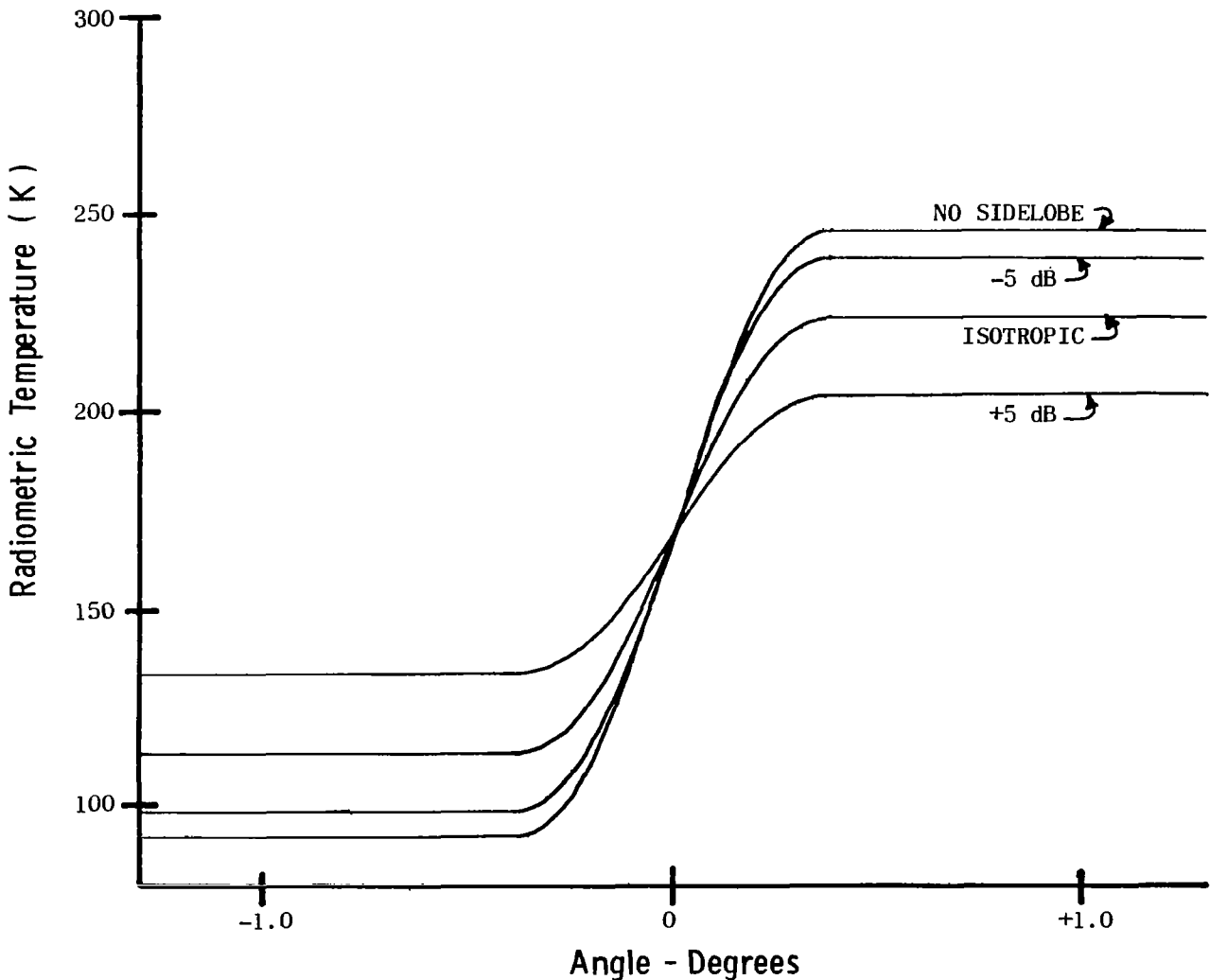
Figure 16

The error at the first resolution cell adjacent to the land-sea boundary and the antenna beam efficiency as a function of sidelobe level in dB below the maximum on-axis gain are shown in Figure 17. These data were obtained from the computer model discussed in the previous figure. For an error requirement of 0.1 K to 0.5 K, the sidelobe level would have to be at least 75 dB below the main lobe with beam efficiencies greater than 99%. However, antenna pattern correction algorithms can be used which are capable of correcting for known side-lobe levels. This should be able to account for about 15 dB to 20 dB of sidelobe correction. Therefore, a realistic specification using antenna pattern correction algorithms would be to have a sidelobe level below isotropic (0 dB) and a beam efficiency better than 90% (assuming non-uniform sidelobes).

ERROR AT LAND / SEA BOUNDARY AND BEAM
EFFICIENCY AS A FUNCTION OF SIDELOBE LEVEL

Freq. = 1.4 GHz

G_{max} = 52.38 dB

θ_{3dB} = 0.5°

Figure 17

98
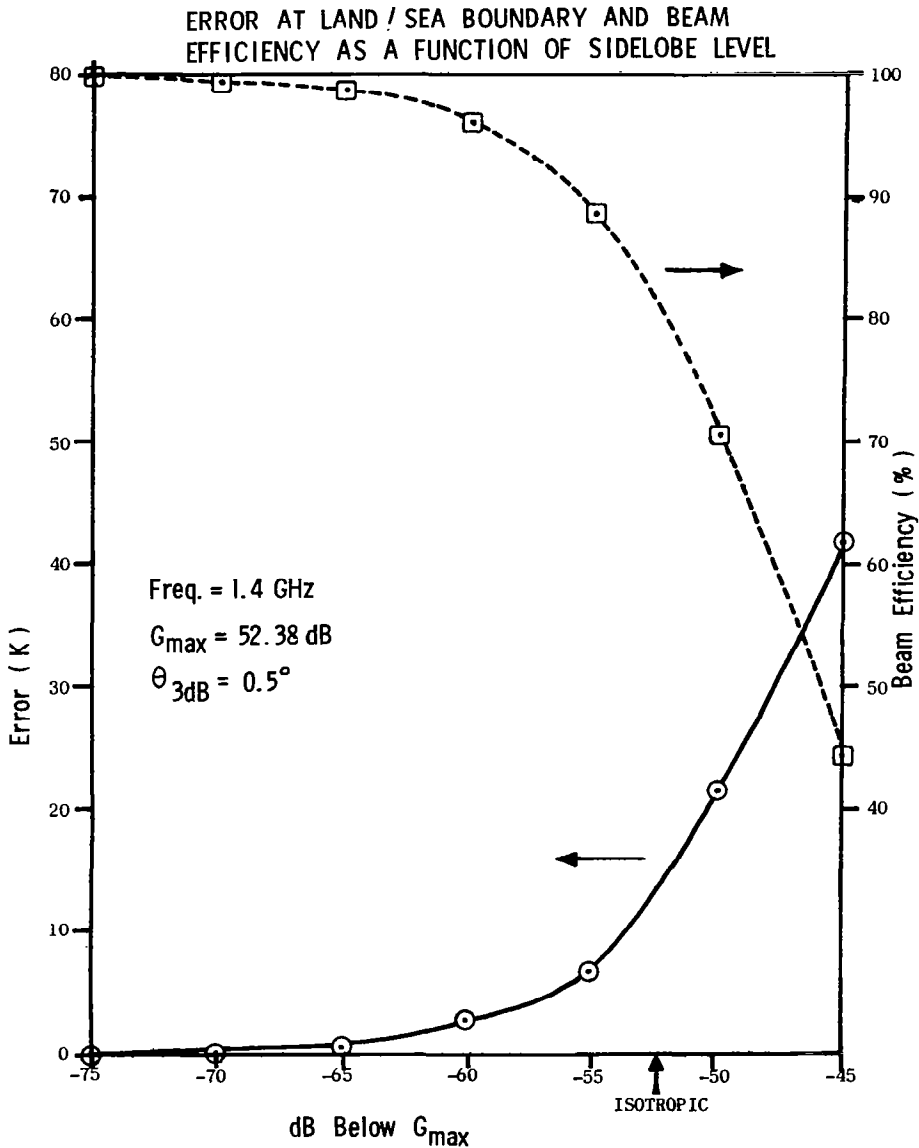
ANTENNA SCANNING TECHNIQUES

The options for achieving large swath width with antennas having high spatial resolutions (narrow angular beamwidths) are presented in Figure 18. Single beam systems are limited by the required integration time to achieve the necessary radiometric resolution in the microwave radiometer. This will be illustrated in the next figure. Multiple beam systems can be designed using a whiskbroom technique or a pushbroom technique. For smaller apertures that can be mechanically scanned, the whiskbroom offers an advantage that the number of radiometers is reduced along with off angle scan requirements. However, fixed incidence angle with beam position would not be possible. Pushbroom provides for fixed incidence angle and eliminates mechanical scanning of the spacecraft, but requires a larger number of radiometers.

SINGLE BEAM

- **MECHANICAL SCANNING**

- **ELECTRONIC SCANNING**

MULTIPLE BEAM

○ **WHISKBROOM - MULTIPLE BEAMS POSITIONED ALONG GROUND TRACK AND SCANNED ACROSS GROUND TRACK**

○ **PUSHBROOM- MULTIPLE BEAMS POSITIONED ACROSS GROUND TRACK - NOT SCANNED**

Figure 18

SINGLE BEAM RADIOMETER SENSITIVITY REQUIREMENT

   The minimum detectable change in the electromagnetic radiation received by a microwave radiometer is defined as the radiometer sensitivity, ΔT. Sensitivity or measurement resolution requirements are 0.5 K for soil moisture and 0.1 K for sea surface temperature. The radiometric sensitivity is a function of the type of radiometer, system noise temperature, bandwidth, and integration time. The available integration time is a function of swath width, orbital altitude, and spatial resolution requirements. Assuming a Dicke switched radiometer with a 200-MHz bandwidth and 400 K system noise temperature, the radiometer sensitivity for a single beam scanning microwave radiometer system is shown in Figure 19. It is easily seen that a multiple beam system would be required for any reasonable swath width requirement.
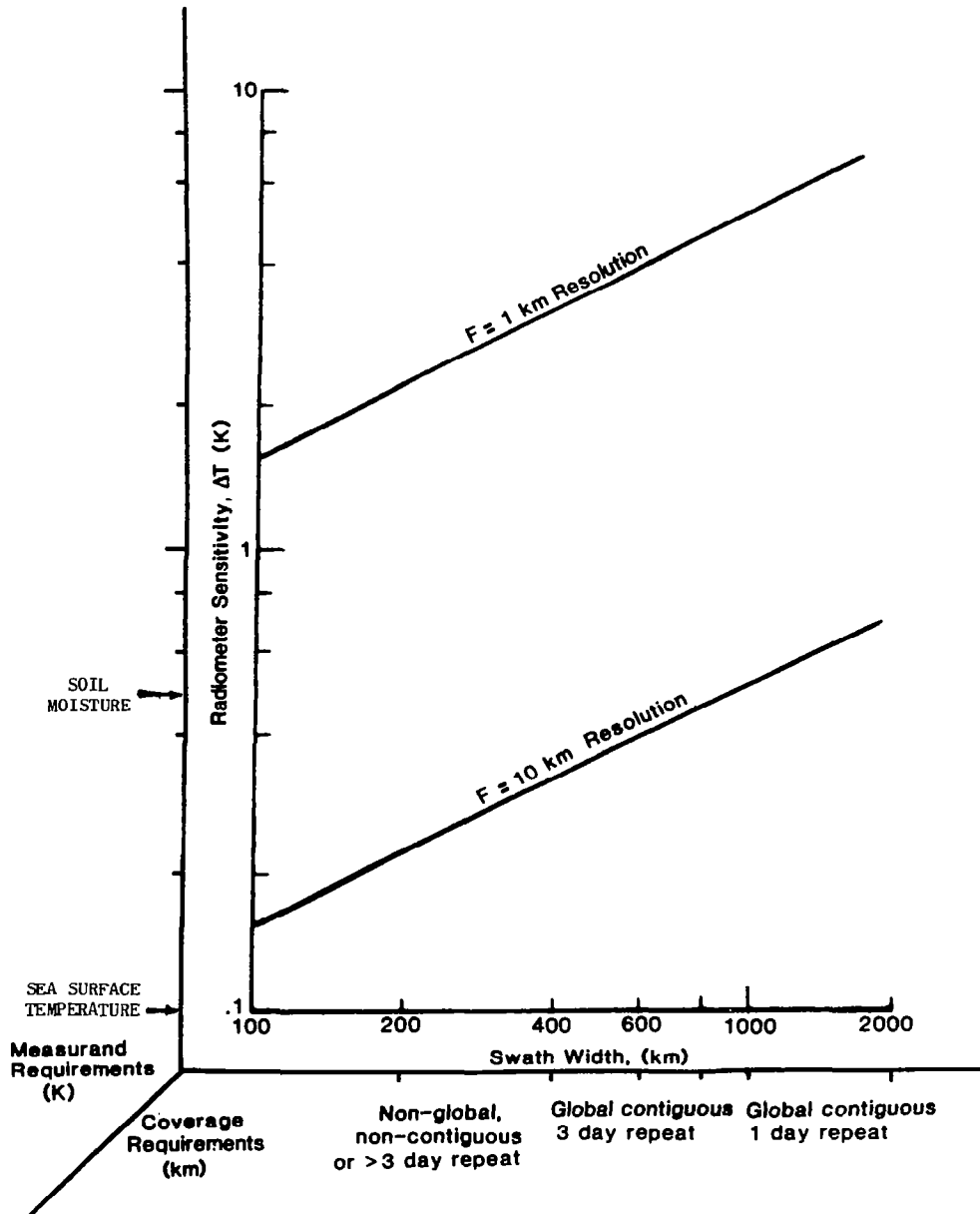
Figure 19

DEVELOPMENT OF PUSHBROOM RADIOMETRY FOR
LARGE SCALE ANTENNA

The development of pushbroom radiometry for large space antenna systems through an evolutionary technology development concept is shown in Figure 20. This begins with the first pushbroom microwave radiometer (PBMR) presently undergoing testing in the Antenna and Microwave Research Branch at NASA Langley Research Center. The PBMR operates at 1.4 GHz for soil moisture and salinity measurements, has either 3 or 4 beams, and is capable of 100-m resolution for 300-m altitudes. The next step would be to use the 15-m hoop column model antenna for a pushbroom microwave radiometer. With this concept 40 beams could be obtained at 1.4 GHz with 11-km resolution from a 500-km altitude. This naturally leads to a 100-m hoop column antenna which can be launched in a single Shuttle mission and would provide 200 beams in a pushbroom configuration. A 2-km resolution could be obtained from 500-km altitude.

This evolutionary technology development would provide the knowledge necessary to erect the ultimate remote sensing system in orbit as shown in Figure 21.
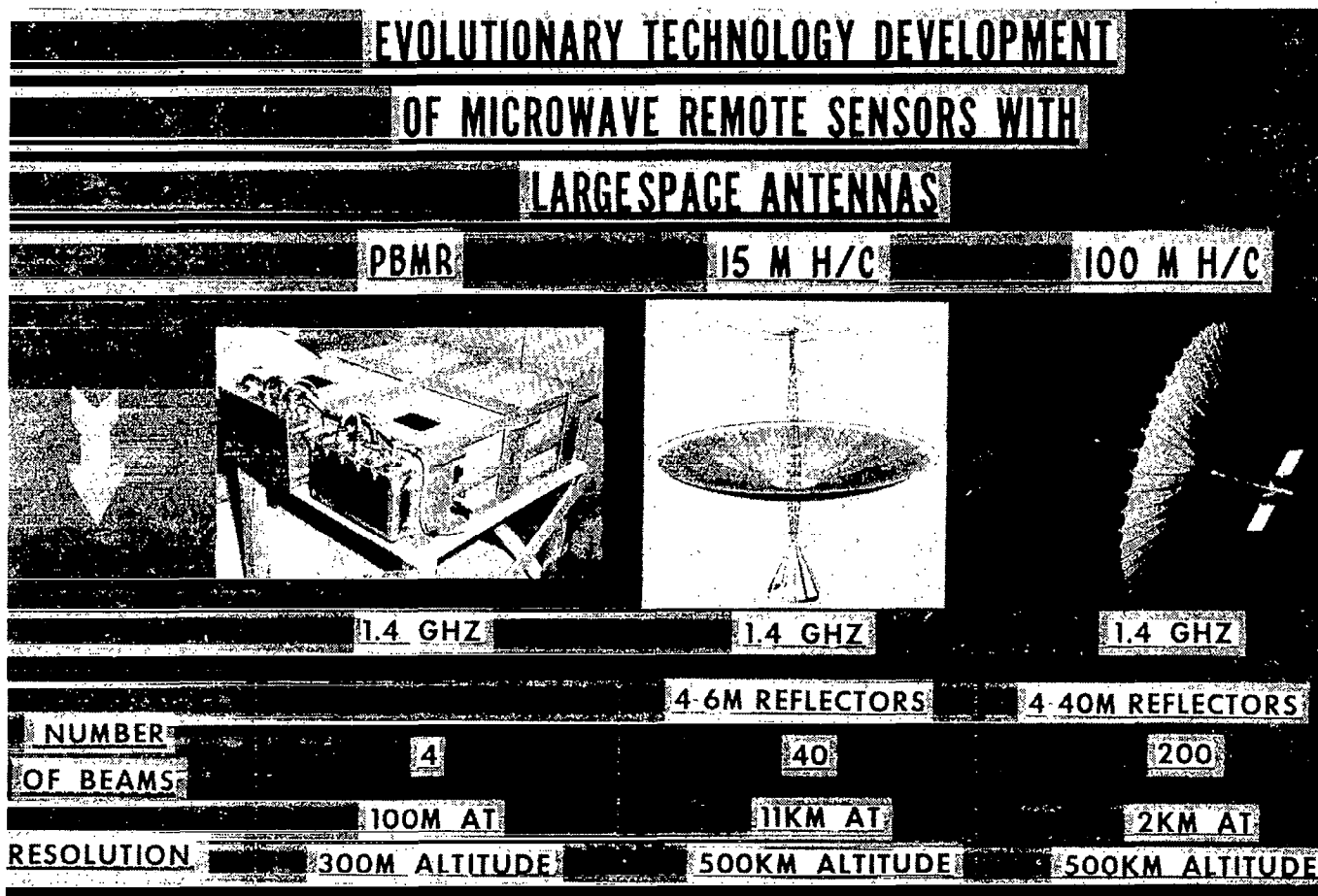
Figure 20

MICROWAVE RADIOMETER SPACECRAFT CONCEPT
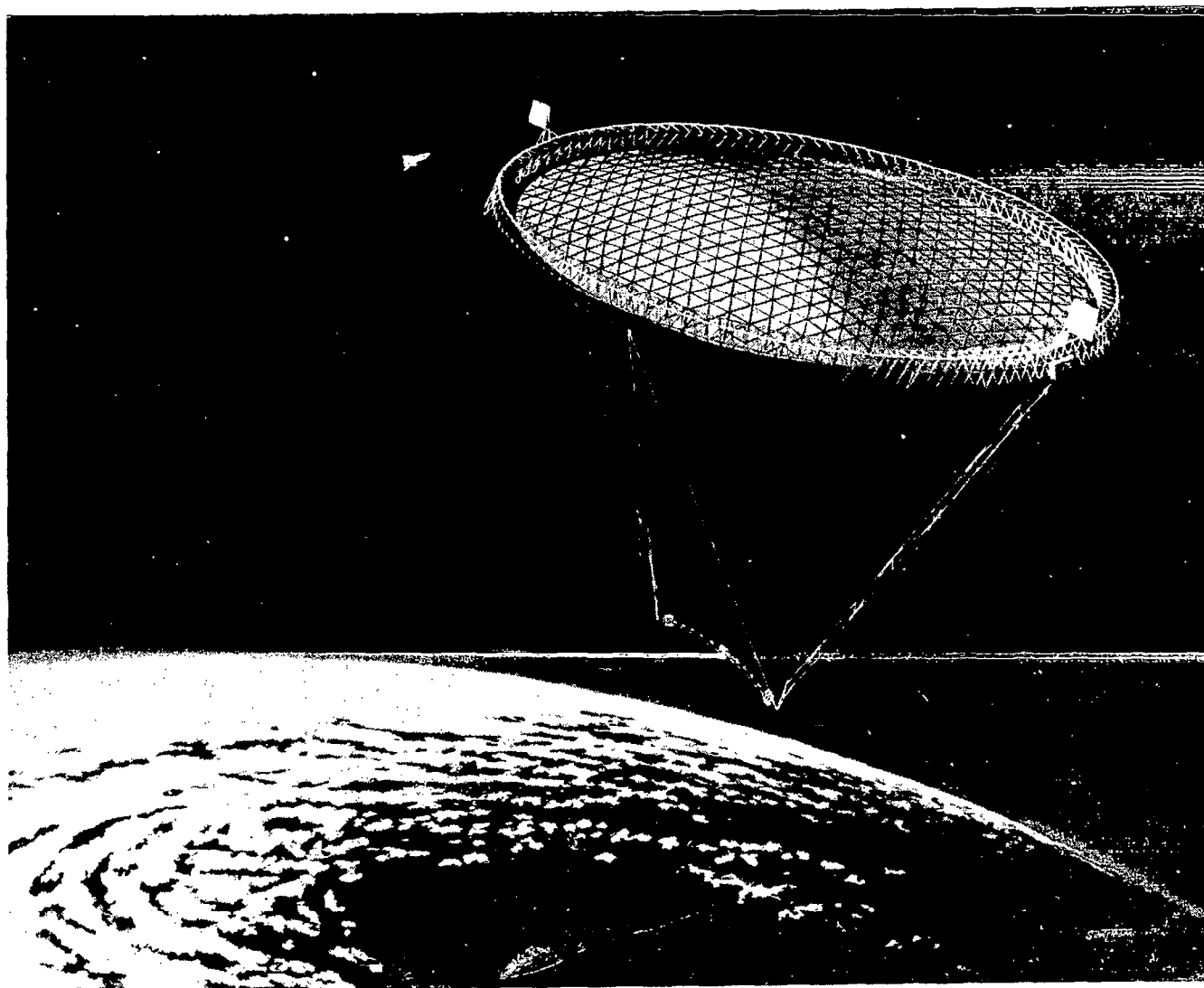
Figure 21

SUMMARY

The key measurands for a microwave pushbroom radiometer using large space antennas would be soil moisture and sea surface temperature. The key requirements for the radiometer system are listed in Figure 22.

NASA RP-1101 (ref. 1) provides more detail on pushbroom radiometry for large space antennas.

KEY MEASURANDS

- ## SOIL MOISTURE

- ## SEA SURFACE TEMPERATURE

REQUIREMENTS

- ## MULTIPLE FREQUENCIES

- ## MULTIPLE BEAMS (PUSHBROOM)

- ## DUAL POLARIZATION

- ## LARGE DIAMETER (50 TO 200 M)

- ## RADIOMETRIC PRECISION AND RESOLUTION (0.1K)

- ## HIGH BEAM EFFICIENCY (> 90%)

Figure 22

REFERENCE

1. Keafer, Lloyd S., Jr.; and Harrington, Richard F.: Radiometer Requirements for Earth Observation Systems Using Large Space Antennas. NASA RP-1101, 1983.

EARTH OBSERVATION SYSTEM:
SPACECRAFT DESIGN

J. J. Herbert and Will A. Schartel
Martin Marietta Corporation, Denver Aerospace
Denver, Colorado

EARTH OBSERVATION SATELLITE

The Earth Observation Satellite (EOS) was a study funded by NASA Langley Research Center. The study was a system investigation of the total spacecraft integration with its major subsystems and sensors. Mission optimization and ranking using various sensors was also an objective of the contract. Integrating the spacecraft and major subsystems with the large microwave radiometer was done, essentially making the radiometer a free-flyer without an external spacecraft. Another program objective was to provide design and analysis data on microwave radiometer satellites augmented with additional Earth, ocean, and atmospheric sensors.

A top-down systems approach resulted in a detailed design integrating subsystems and sensors into the microwave support structure. An important objective of the program was to identify technology needs for Earth observation satellites. The definition and understanding of these design drivers are critical in order to set priorities for future EOS work.

106
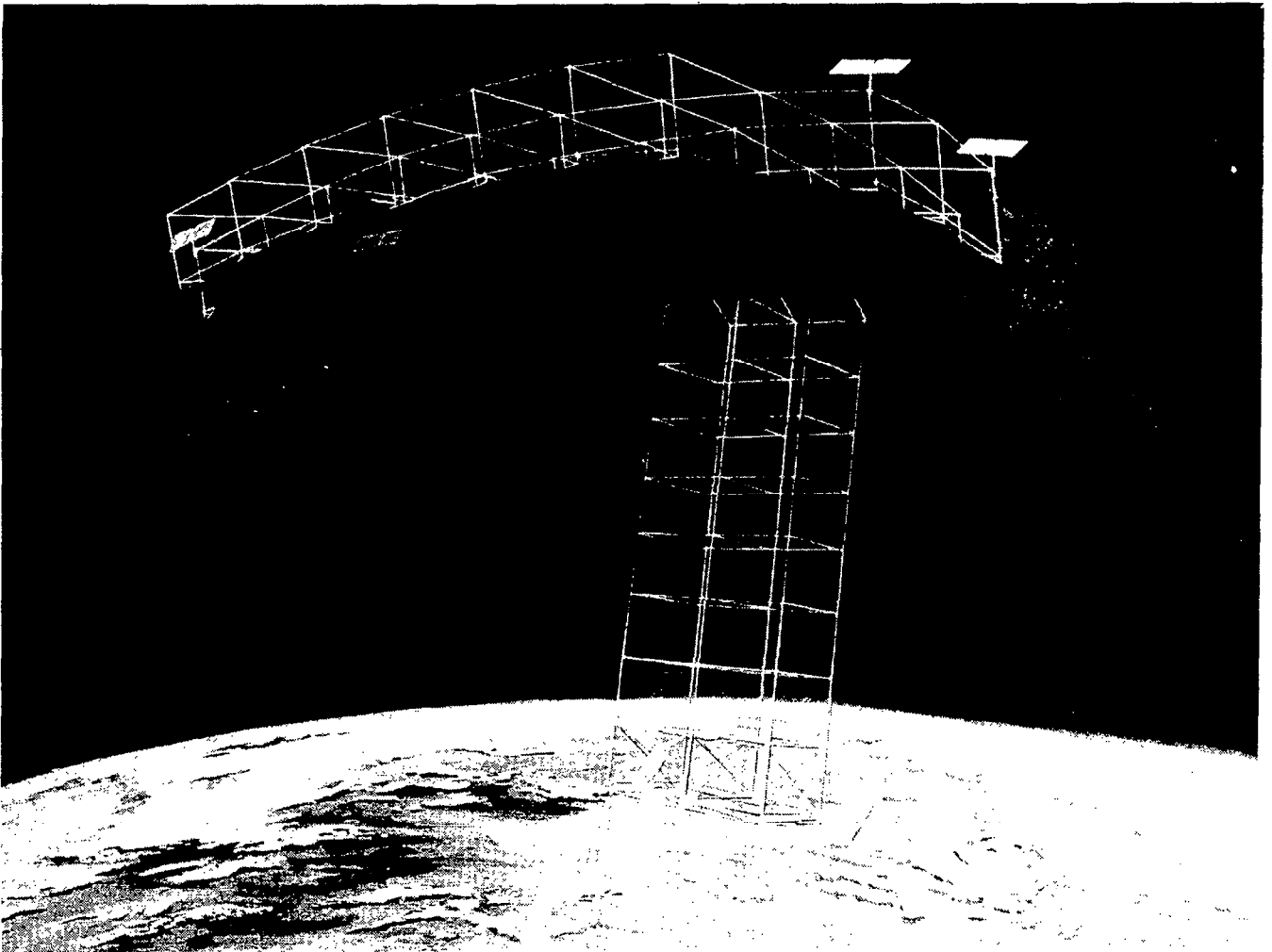
DEPLOYED EOS STRUCTURE

The deployed EOS structure with all the subsystem and overall dimensional data is shown in the figure. The structure is composed of box-truss elements. Each box element is approximately 15 m square. The structural system is composed of an 8 X 4 (120 m X 60 m) configuration of boxes in antenna support structure and an 8-bay double feed mast. The RF mesh was attached 2 m above the antenna support structure on extensions of the vertical members. Data management, control function, and communication are located at the top of the feed mast, perpendicular to the 30-m feed boom. Most of the science instruments are centrally located in a beam extended from the antenna support structure.
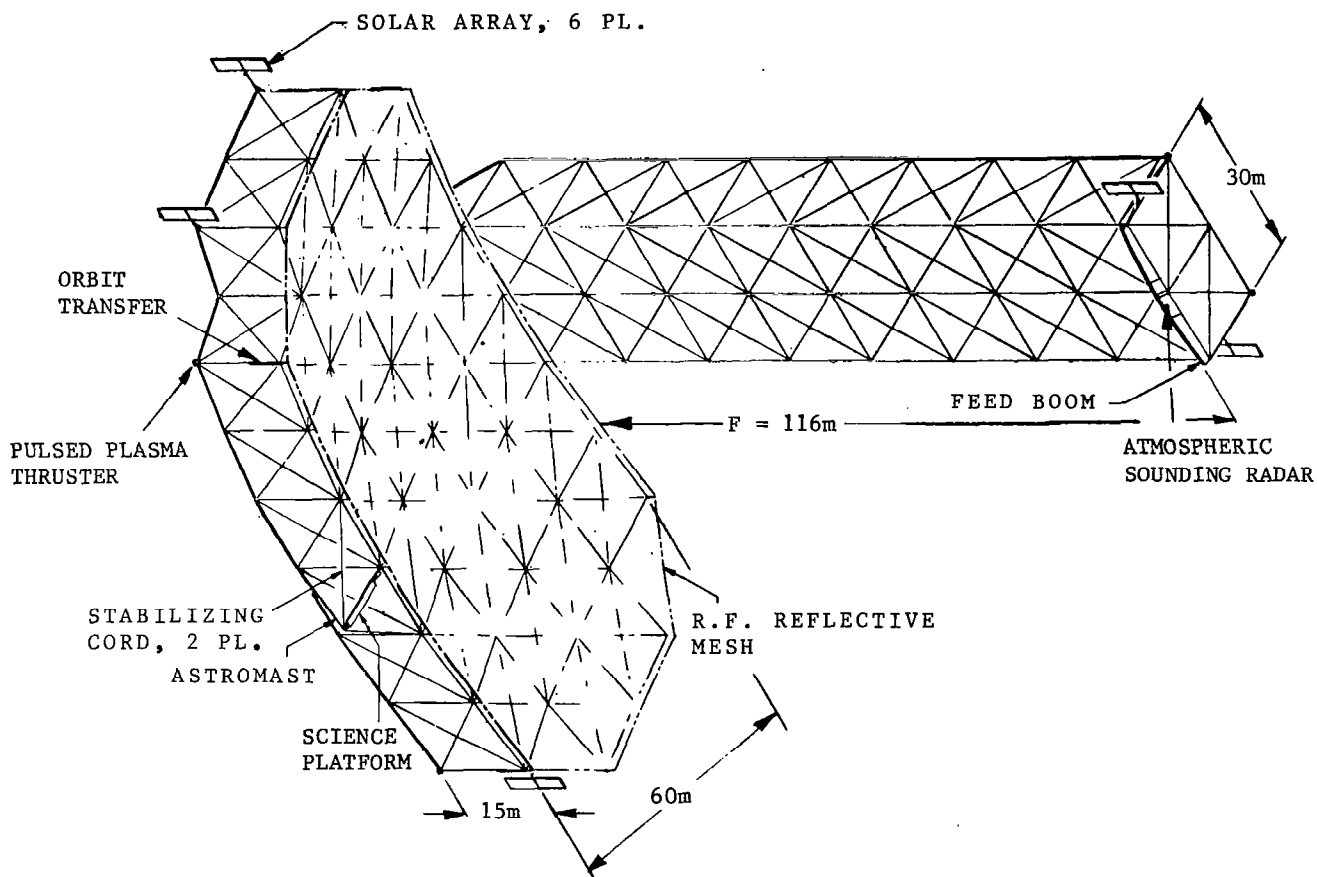
EOS STOWED CONFIGURATION

These two figures show how the stowed EOS configuration fits in the STS cargo bay. The feed horns actually fill the largest portion of the volume in the Shuttle, in contrast to the portion of the volume they comprise in the deployed system. Most of the subsystem is located on the periphery of the stowed box-truss structure.

In the stowed condition, the cube corner fittings butt against each other, forming a plane at the top and bottom surfaces. The plane formed by the cube corner fittings provides a load path for loads incurred during launch, with inplane sharing loads handled by interlocking pins between the fittings.
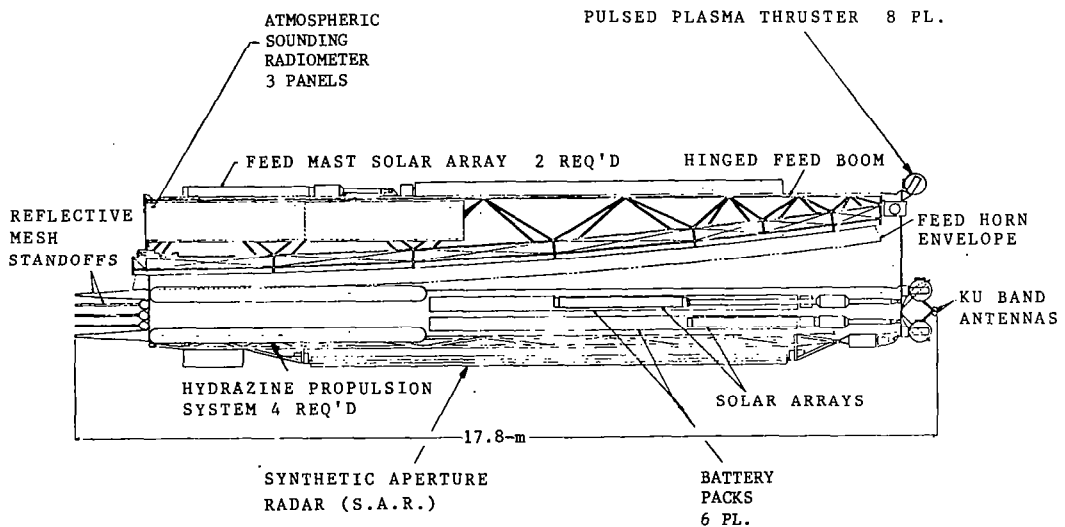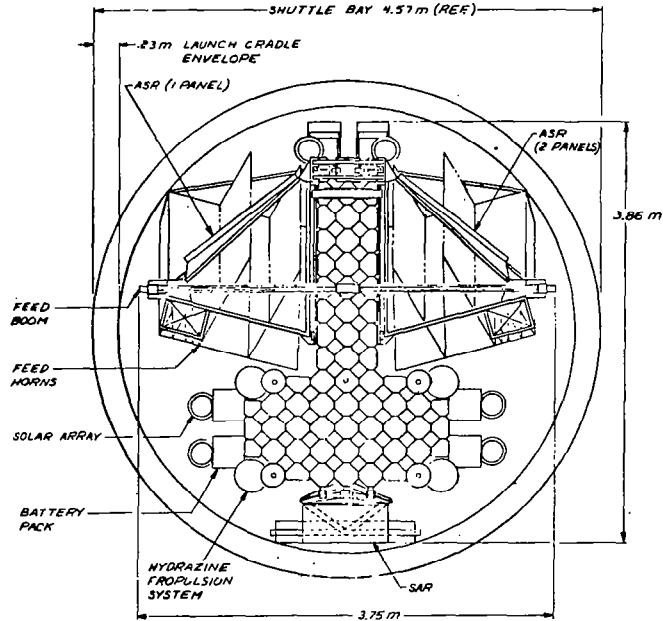
FEED BOOM/STRUCTURE DEPLOYMENT

The first step in feed boom/structure deployment is the linear deployment of the 1.5-m box truss supporting the feed boom.

The second step is the linear deployment of the outermost 15 m X 15 m box truss cube of the support mast. This will allow the feed boom to clear subsystems mounted to the stowed mesh support cubes during its deployment.

The third step is to deploy the feed boom. A drive motor rotates and latches the feed halves together.

The feed cubes and two innermost rows of mesh support cubes are deployed laterally for the fourth step. This anchors the ends of the feed boom in place.

The entire feed mast is rotated 90° relative to the mesh support cubes for the fifth step.

The next step is to deploy the feed mast, one row of cubes at a time, and then the mesh support cubes, one row at a time. The final structure will measure 120 m long by 60 m wide by 120 m high.

LINEAR
BEARING

HINGED
FITTING

LINEAR
BEARING

3

PENTAHEDRAL
STRUCTURE

MAIN
SPAR

2

FEED
HORNS

CORNER
FITTINGS

HINGED
FITTING

SCREW
DRIVE

LINEAR
BEARING

STOWED

LINEAR
BEARING

HINGED
FITTING

1
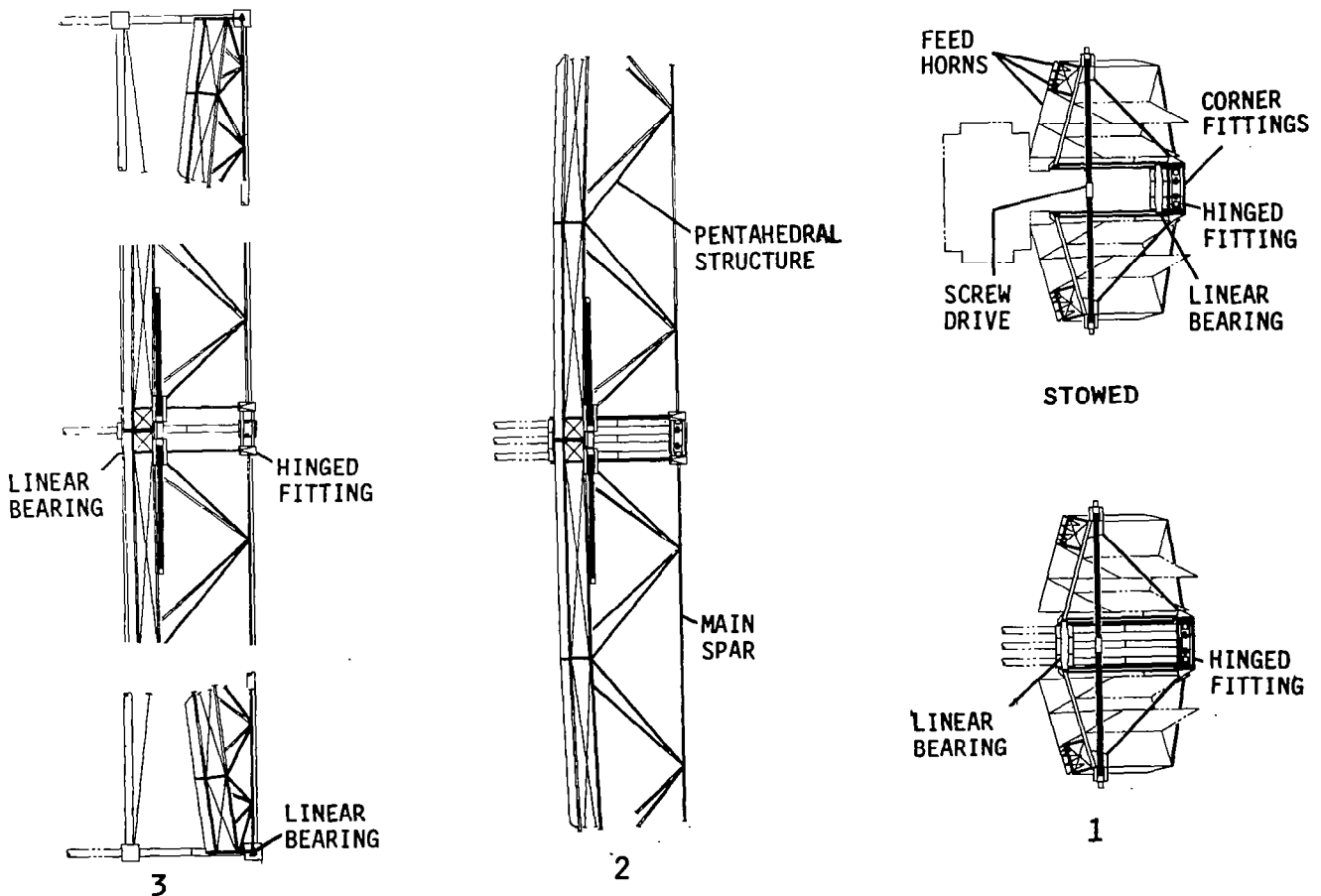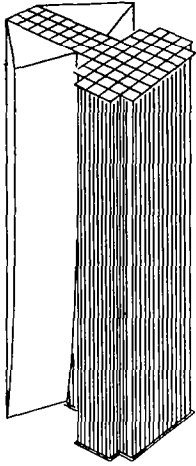
STOWED

1 & 2

3

4

STRUCTURE DEPLOYMENT

5

120m

60m

15m

120m
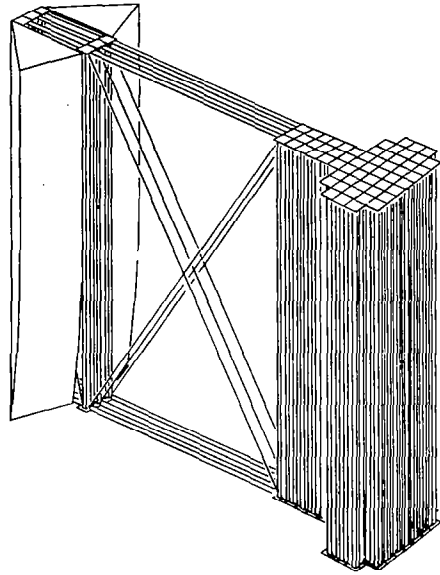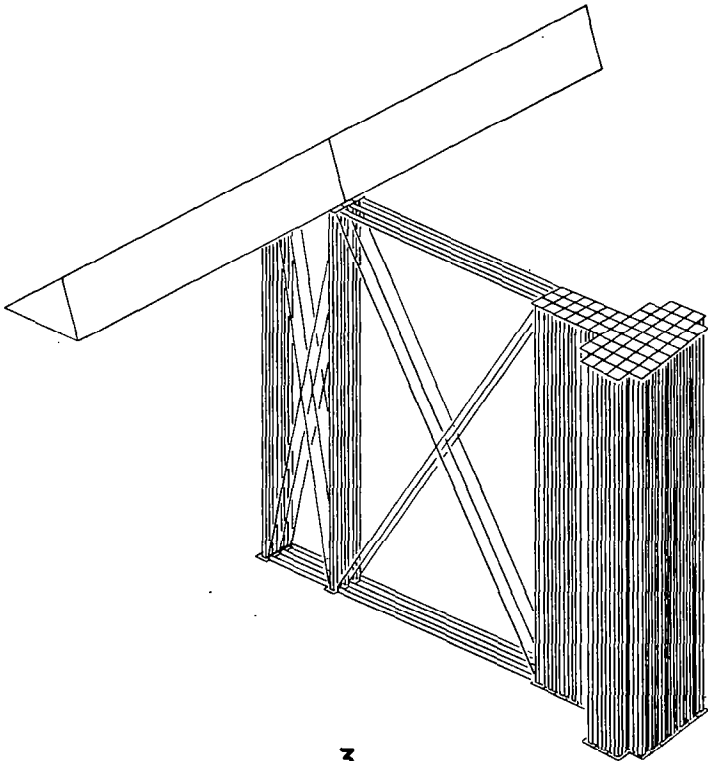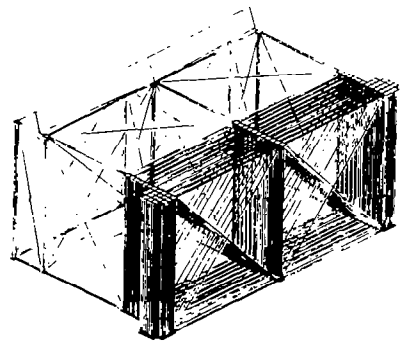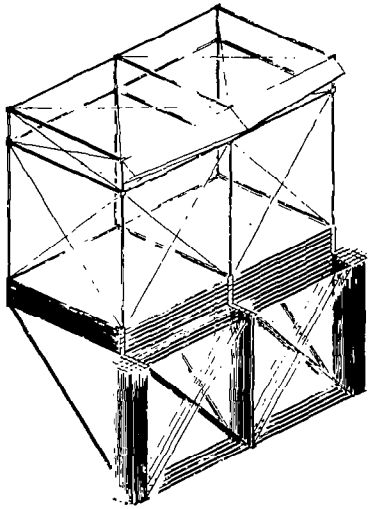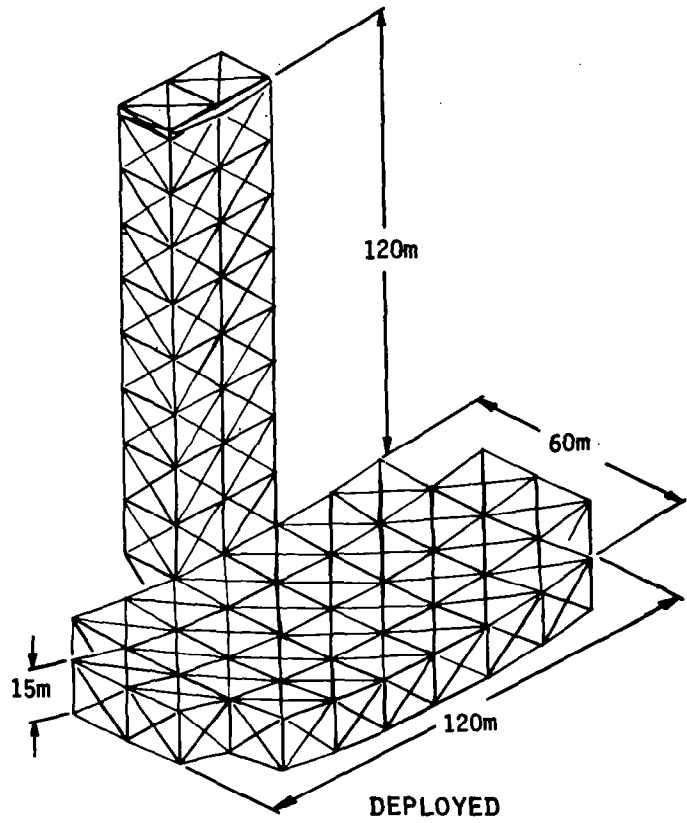
DEPLOYED

BOX TRUSS STRUCTURAL ELEMENT

The EOS structure is designed using the deployable box-truss structure to form the parabolic dish and feed mast. This truss comprises a deployable frame consisting of two equal-length structural members ("verticals"), two structural members hinged in the middle ("surface tubes") that connect the ends of the verticals and fold inward to stow between the adjoining verticals, and telescoping diagonal braces that lie in, and control the shape of, the deployed frame. Prototype hardware has been fabricated with all-composite tubes and fittings, and low-cost manufacturing processes are being developed for all repetitive components.

The shape of a box-truss reflector and feed mast is controlled by the diagonal tension braces in each frame face. The diagonals are multiple-ply graphite-epoxy tapes that telescope for stowage and deployment. Both diagonal tapes in each frame face lie flat in the plane of the frame, thereby equalizing solar input to the two tapes and minimizing thermal distortions.

CUBE CORNER FITTING ASSEMBLY

Depicted is a typical cube corner fitting assembly. The vertical and surface members are made of a graphite-epoxy layup. The surface member is 3.28 inches in diameter with a 0.025-inch wall thickness. The vertical member is a square-finned tube made up of a 1-inch square with 2-inch 45° fins. All thicknesses in the vertical members are 0.050 of an inch. The pretensioned diagonal members are manufactured of Teflon[R]-coated graphite cords. Notice how compact the surface member nests in the finned vertical member with the interior diagonal packaged in between them.

The parabolic box-truss design is an accurate truss with all the force lines of action going through a coincident point. The cube-corner fitting attachment point for the surface tube is adjusted so the surface tube line of action goes through a point coincident with all the other surface tubes and diagonal members of that particular cube corner fitting. Moving the attachment points to eliminate end moments on the vertical members dramatically increases the fundamental mode of the entire structure. Along with movement of attachment of the surface tube, specific surface member lengths must be kept identical in any row or column of the structure. This design feature ensures the structure remains orthogonal during sequential deployment in either direction. Identical member lengths are made possible by the geometric property that any cutting plane through the surface and parallel to the vertex axis will show an identical parabola through the intersection points.

SURFACE TUBE MEMBER

EXTERNAL DIAGONAL MEMBER

FINNED VERTICAL MEMBER

INTERIOR DIAGONAL MEMBER

COINCIDENT LOAD PATH

10.16 cm

SURFACE TUBE MEMBER

21.59 cm

SURFACE TUBE MEMBER

CORD FITTING

FINNED VERTICAL MEMBER

STOWED TUBES
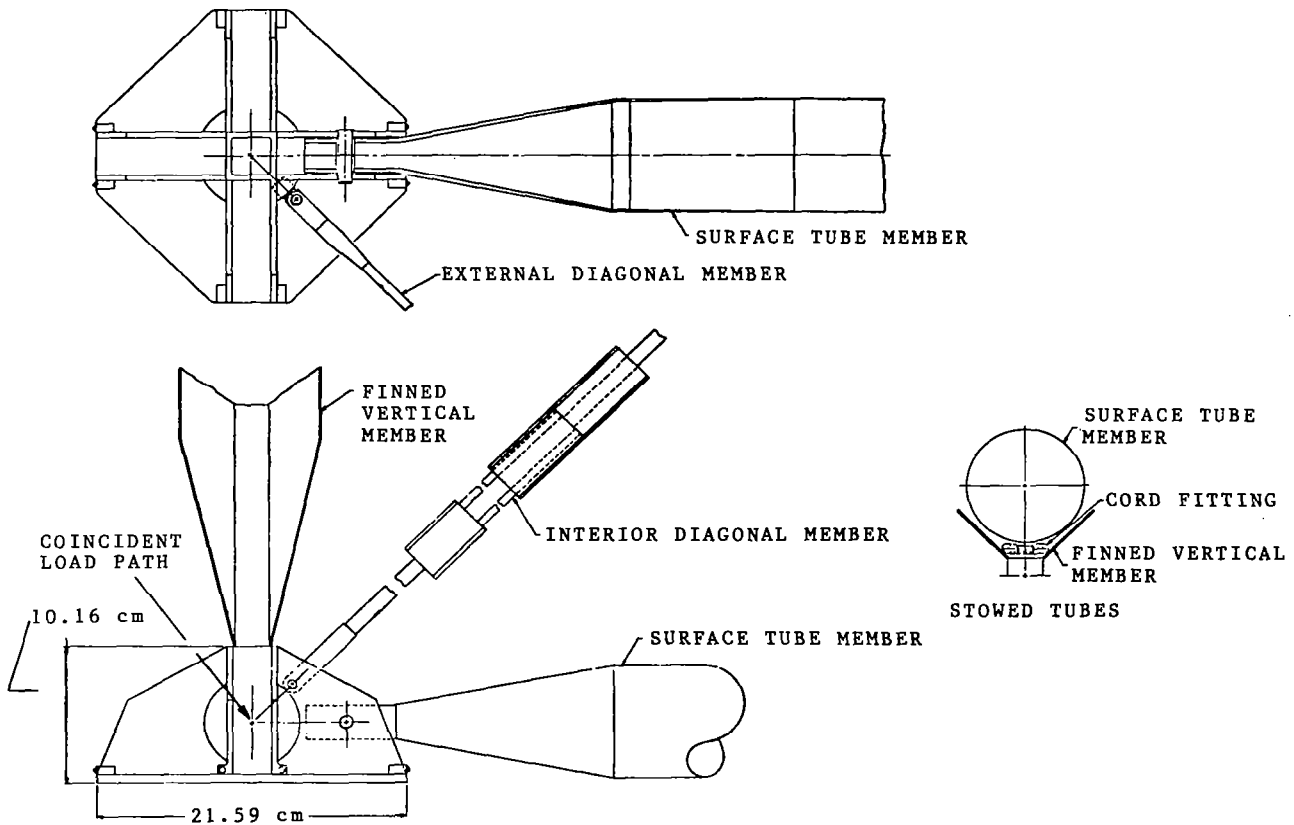
EOS SUPER JOINT

The connection point between the feed mast and the antenna support structure is a unique design. Fourteen different members' lines of force must converge through a coincident point. The fitting assembly is a 3-dimensional joint with feed box trusses rotating out and up during deployment. The brace structural members fold up inside the interlocking vertical channels during stowage. The channels are of different thickness in the flanges and web so their centroidal planes intersect at deployment, maintaining a true truss configuration. The end fitting for the surface tubes in the feed mast is bonded to the back of the feed mast vertical channel. This complex fitting is fabricated from several smaller graphite-epoxy laminates that are bonded and mechanically fastened into a single, unique, hinged cube-corner fitting. The advantages of a box-truss feed mast are longer focal lengths and larger feeds because of higher system fundamental modes resulting from the integrated design.
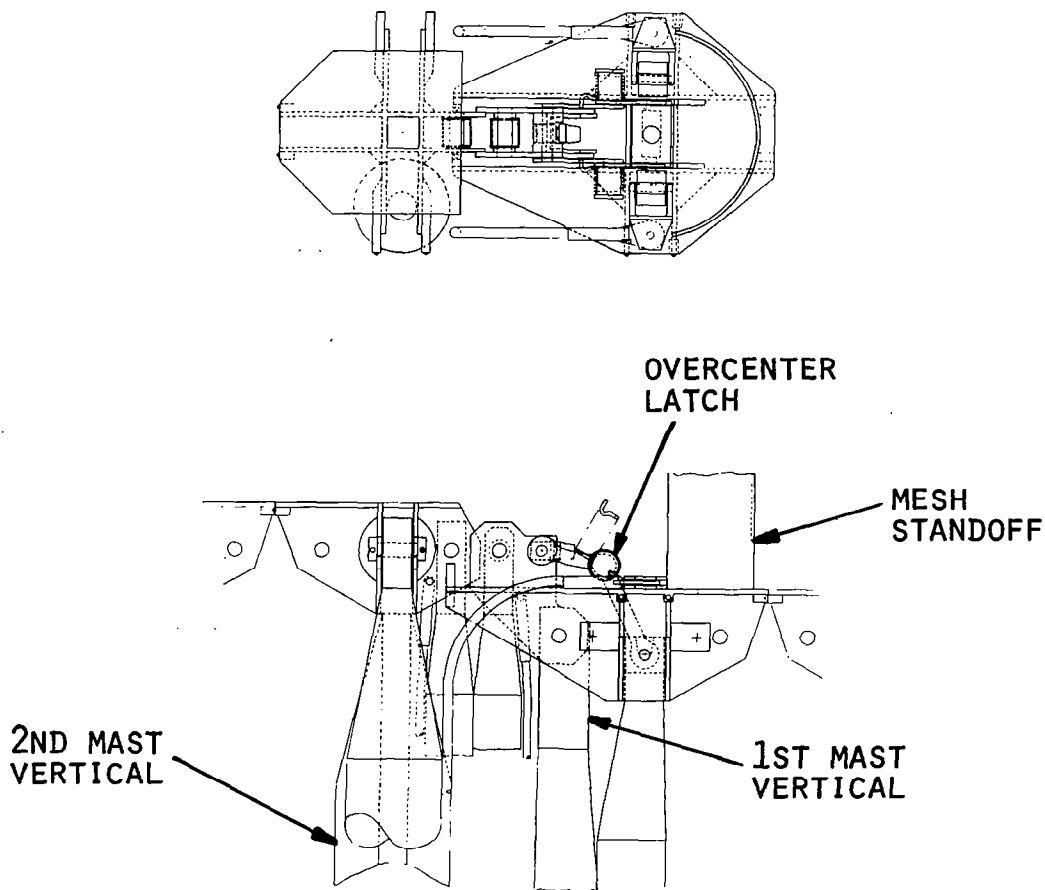
DYNAMIC ANALYSIS

The dynamic analyses of the EOS structure with subsystems revealed a fundamental frequency of 1.08 Hz. If the EOS system is configured with 1300 kg of slewing fuel, the fundamental frequency drops to 0.9 Hz. The structure is extremely stiff due to a unique deployable offset feed mast. The novel feature of this design is that it uses an extension of the reflector truss structure rather than adding appendages. The design features efficient stowage, simple integration to the reflector structure, excellent thermal stability, light weight, and very high stiffness and dynamic stability. These features are achieved by using the efficiency and features of a deep truss structure. Previous offset feed masts were appendages added to the reflector structure and had less efficient packaging, more difficult integration, and substantially lower dynamic stability. Because of the high strength and stiffness, this mast can easily accommodate the more complicated and massive advanced feeds (e.g., line feeds, array feeds, and multifrequency multibeam feeds).

FREQUENCY 1.08 HERTZ

ANTENNA CONFIGURATION PARAMETERS

The geometry and physical dimensions for the EOS radiometer are a compromise between conflicting requirements. User needs require large antennas, while the Shuttle restricts ultimate size. The multifeed array boom is folded in half during stowage. Each half is 15 m long, and is the longest length that can be packaged in the STS cargo bay. This limitation drives the size of other components such as the reflector.

The sensitivity of microwave emission to the geophysical parameters determined the operating frequencies. The primary mission for the radiometer is to measure soil moisture at 1.42 GHz.
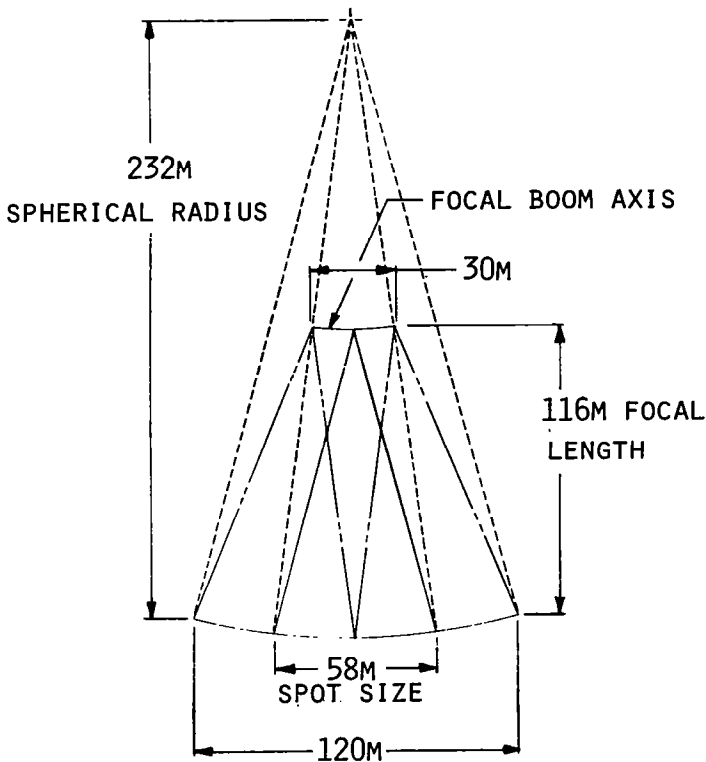
o 30 METER FEED BOOM
  DESIGN DRIVER DUE TO
  PACKAGE LENGTH

o 58 METER SPOT SIZE
  - KEEP PHASE ERRORS
    TO $\lambda/8$

o PLANAR FEED ARRAY WITH
  SHARED ELEMENTS

FREQ GHZ	1.42	5.5	10.68
WAVELENGTH	21.0	5.5	2.8
RESOLUTION KM			
OPTIMISTIC	2.8	0.9	0.4
CONSERVATIVE	14	4	1

- SWATH WIDTH   200 KM
- FIELD OF VIEW   15 DEG
- ALTITUDE   700 KM

RIGHT HAND FEED BOOM ASSEMBLY

The feed boom structure is formed from pentahedral substructures. A main spar runs the length of the feed connecting together the tops of each pentahedron. The linear bearing shaft running the full length of the feed boom also is mounted to this spar. The legs and base members of each pentahedron, as well as the top spar, are graphite-epoxy tubes; there are no base members crossing the width of the structure except at the ends. A honeycomb core panel running the length of the feed forms the base for each pentahedral truss. This panel attaches to the truss base members that run lengthwise. Cutouts in the honeycomb core are used to mount the 1.5-GHz horns. These are made up of a series of planar arrays with shared elements.

A series of box-truss structures along the front edge of the feed structure are mounted to the bottom face of the honeycomb panel. The structural members are epoxy-graphite tubes and cords. The base is a honeycomb core panel. The 5.5-GHz horns and the 10.5-GHz horns are mounted through cutouts in this panel. The focus of the parabola is located along the 10.5-GHz horns.

HORN PANEL CUTOUTS

HONEYCOMB PANEL

GRAPHITE/EPOXY SUPPORT STRUCTURE

15 m
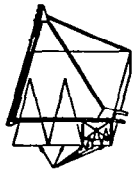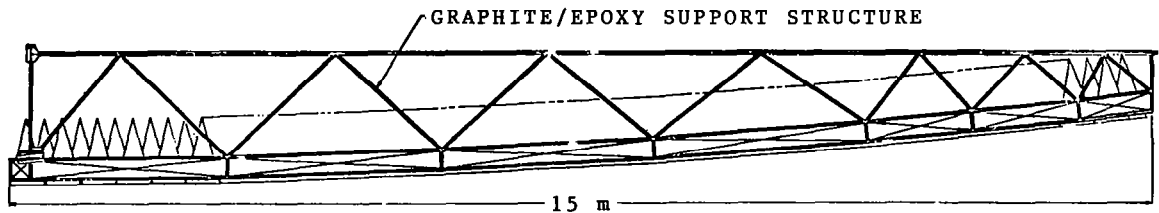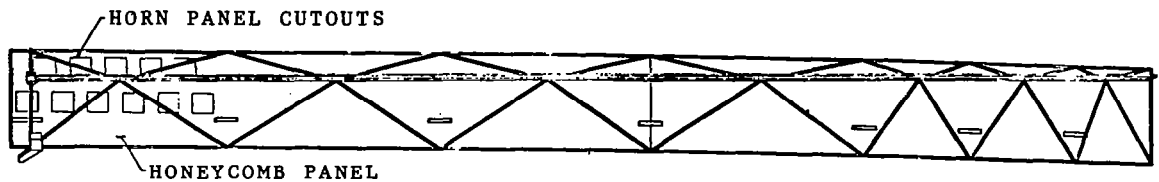
FEED HORNS
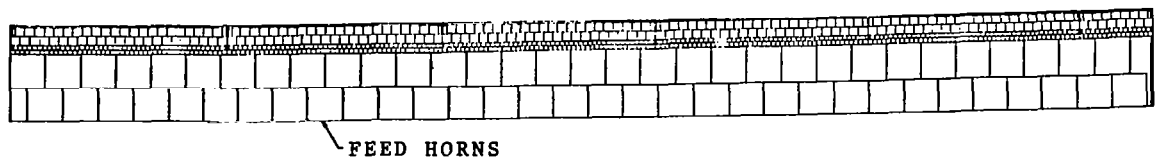
FEED HORNS

Another aspect of EOS is to investigate the benefit of combining multidisciplinary ancillary sensors to the radiometer and assessing the cross discipline utility and synergistic benefit. The proposed complement would cover a broad spectral bandwidth covering the visible, thermal IR, and microwave regions to maximize information yields and usefulness. In addition, the sensors have been selected to be compatible with the operational constraints imposed by the orbit.

The ultimate goal is to assemble an ensemble of sensors that resemble current Landsat or NOSS payloads but also effectively combine and complement the LMR.

Four observational missions have been proposed: baseline, land, ocean, and atmospheric.

o   FOUR POSSIBLE MISSIONS

            MISSION   I - BASELINE ONLY

            MISSION II - BASELINE + LAND OBSERVATION

            MISSION III - BASELINE + OCEAN

            MISSION IV - ANY OF ABOVE + ATMOSPHERIC

o   SENSORS SELECTED FOR COMPATABILITY AND MAXIMUM DATA CORRELATION

o   INSTRUMENTATION MOUNTED ON INTEGRATED SCIENCE PALLET

o   COVER BROAD SPECTRAL BANDWIDTH

            - USUAL, THERMAL IR, MICROWAVE

            - MAXIMIZE SYNERGISTIC BENEFIT

MEASUREMENT POSSIBILITIES

The measurement possibilities, information, correlation, and synergistic benefits are exemplified for the land mission. The sensors with descriptive information are:

ASR	18, 21, 37 GHz	
SAR	X-band radar, 25 m resolution	
MLA	0.45 - 0.09 µm	4 bands
MIRI	10 - 12 µm	3 bands
MRS	0.45 - 0.09 µm	command pointing capability

This complement of sensors, as shown in the left-hand column below, can provide a wide variety of observations. The complete monitoring of these observables requires multispectral sensing. For example, the radiometric signature of snow at 5 GHz is influenced by its wetness, while dry snow is most effectively mapped with the ASR. The degree of snow metamorphism can be inferred with the SAR, and finally, the full extent of the snow cover is photographed with the MLA in the visible spectrum.

OBSERVABLE	LMR*	ASR*	SAR*	MLA*	MIRI*	MRS*
SOIL MOISTURE	3					
SEA SURFACE TEMP	3					
GEOLOGY MINERAL ID			2		3	
LAND SURFACING IMAGING			2	3	2	1
LMR MODEL INPUTS		3				
AGRICULTURE						
CROP STRESS					3	2
CLASSIFICATION			1	3	2	2
ICE/SNOWPACK	2	2	3	1		

SENSOR USE
   3 - PRIME SENSOR
   2 - COMPLEMENTARY
   1 - HELPFUL CONTRIBUTION

*LMR - LARGE MICROWAVE RADIOMETER
 ASR - ATMOSPHERIC SOUNDING RADIOMETER
 SAR - SYNTHETIC APERTURE RADAR
 MLA - MULTISPECTRAL LINEAR ARRAY
 MIRI - MID IR IMAGER
 MRS - MULTI-RESOURCE SCANNER

The sensors were selected to support a particular mission. For example, the Mid-Infrared Imager (MIRI) included in the land mission is primarily intended to be used for geology and mineral identification studies.

The selection of a sensor for a particular mission does not preclude obtaining information in other disciplines. The cross-discipline utility of the sensors for the land mission is illustrated. The primary observation of the MIRI is in geology, but the thermal IR bands of this instrument can also be used to obtain ocean surface temperatures.

The SAR has wide application in ice/snowpack monitoring, ocean studies, and crop identification.

ATMOSPHERIC SOUNDING RADIOMETER		LARGE MICROWAVE RADIOMETER

ATMOSPHERIC   LAND MISSION   OCEAN

SYNTHETIC APERTURE RADAR		MID IR IMAGER

ICE, OCEAN, CROP IDENT   OCEAN TEMP
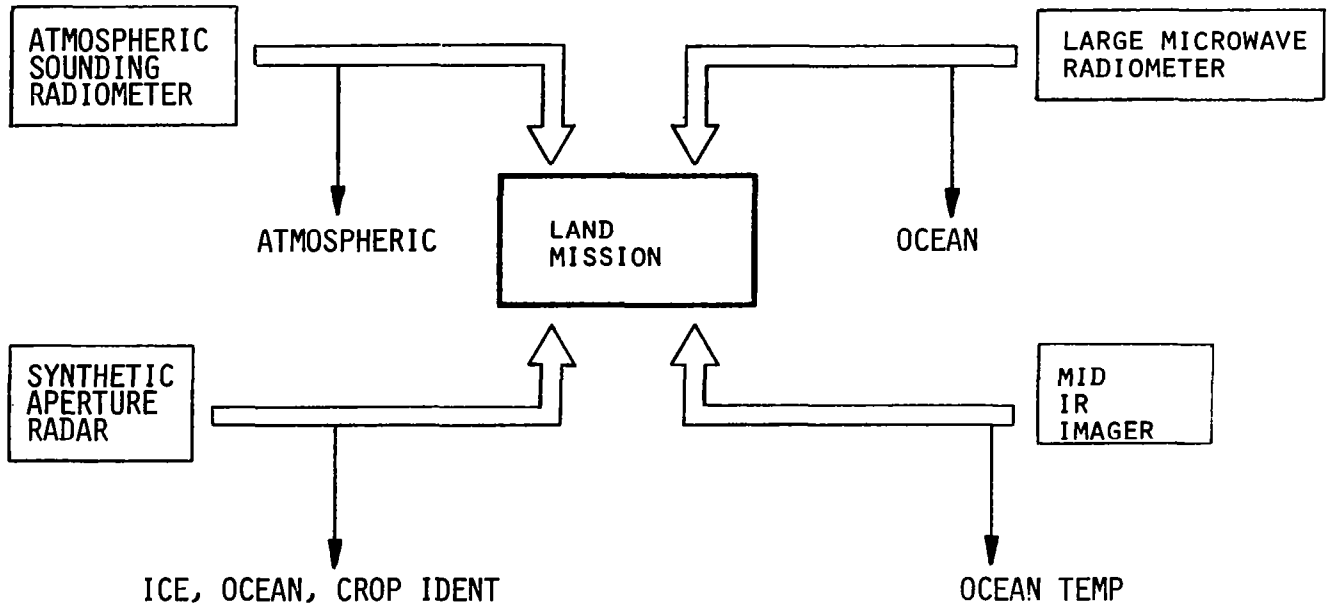
INTEGRATED SCIENCE PALLET

The integrated science pallet provides the structural support for the sensors and a convenient means of interfacing them to the main radiometer structure.

Large space antennas are deployable structures, making subsystem and sensor integration difficult. The pallet concept applied to LSA offers many advantages over the alternative of distributing sensors in available places. The pallet provides for single sensor location, central data processing, and multiplexing.

High-resolution sensors require arcsecond stability that may be unattainable when structural dynamics are considered. Individual sensors or the entire pallet can be isolated from the structure with an isolation control system.

o PERMITS SENSORS TO BE INTEGRATED ON ONE BEAM

- EASES PACKAGING

- SINGLE SENSOR LOCATION

o CENTRAL DATA PROCESSING AND MULTIPLEX

- LESSENS CABLING

- EASES SENSOR/DATA MANAGEMENT SUBSYSTEM INTERFACE

o COMMAND POINTING CAPABILITY

- 20 DEG CAPABILITY

o CAN INCLUDE ISOLATED CONTROL SYSTEM IF REQUIRED

- ENTIRE PALLET

- INDIVIDUAL SENSORS

INTEGRATED SCIENCE PALLET

A possible configuration for the ISP is shown with the sensors configured for an ocean mission. This illustration is intended to demonstrate the concept, sensor placement, and truss design of the pallet.

This particular pallet is approximately 15 m long and 1.2 m wide. The sensors depicted on this illustration are to scale.
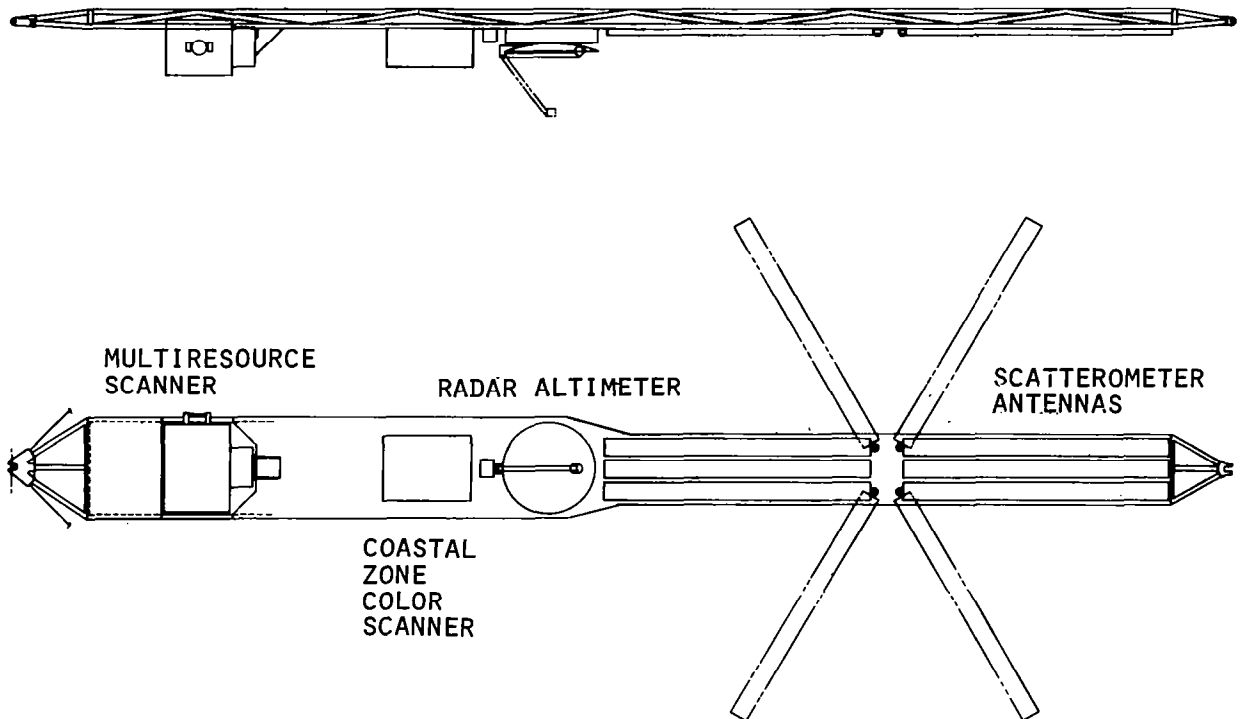
SOLAR ARRAY PACKAGING AND STRUCTURAL ATTACHMENT

The integration of subsystem components is generally restricted on LSS due to the closeness of structural members while stowed. The vertical tube member of the box truss has been utilized as an attachment interface for the Solar Array and its associated Electric Power Module. This mounting solution requires that subsystem components be configured to be long (up to 15 m) and narrow (approximately 0.30 m).

The subsystem itself consists of a solar array, power processing and conditioning, and 50 A-hr batteries composed of 24 nickel-hydrogen cells. These were selected in lieu of nickel cadmium because of the longer lifetime and greater depth of discharge possible.
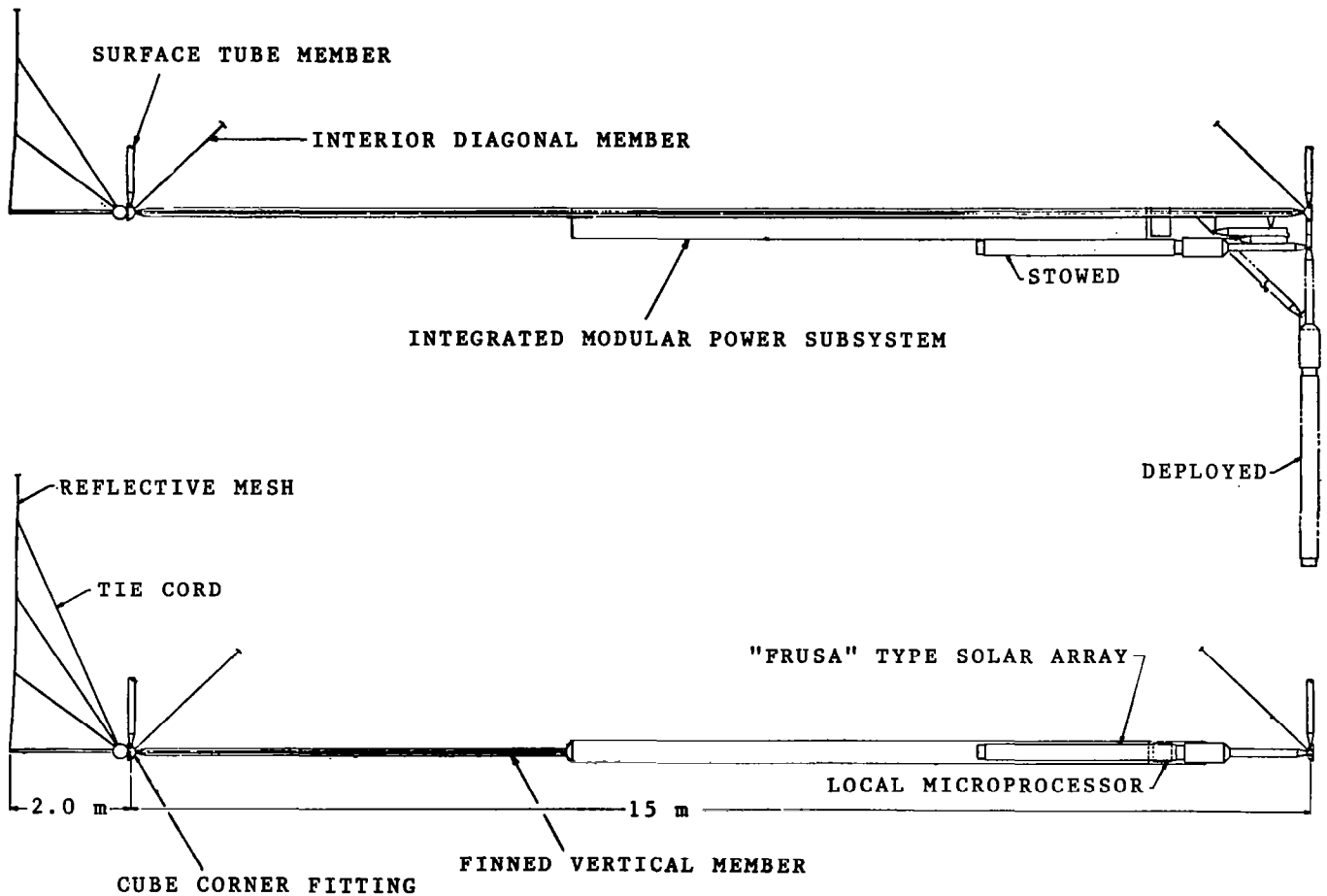
BLOWDOWN N_2H_4 SYSTEM PACKAGING AND STRUCTURAL ATTACHMENT

The mounting of the orbit transfer propulsion is another example of using vertical members to integrate subsystem components to the structure. The ability to incorporate the orbital transfer propulsion eliminates the need for a separate transfer vehicle and permits a greater percentage of the Shuttle bay to be occupied with spacecraft.

The hydrazine system selected is simple and reliable. It is used to boost the spacecraft from the Shuttle limit of approximately 250 km to the operating altitude of 705 km. The system is designed to provide:

v	= 275 m/s	change in velocity
	0.01 m/s^2	acceleration limit
	70 N	thrust
	7400 kg	spacecraft mass

A hydrazine system has also been selected for the out-of-plane propulsion subsystem, and enables the spacecraft to slew a maximum of 15° off of nadir. The addition of 1200 kg of fuel permits 340 maneuvers. The inclusion of slewing capability requires additional fuel tanks and exhaust nozzles, but these can be easily integrated into the structure.

The primary advantage of the slewing capability is increased mission flexibility and performance. To be most effective, orbits must be selected which provide adjacent ground swaths (ground coverage) that are displaced by approximately 200-300 km on successive days (such as those of the Landsat missions). With slewing capability, the EOS spacecraft could be slewed to reimage objects seen on previous days and considerably shorten the revisit time.
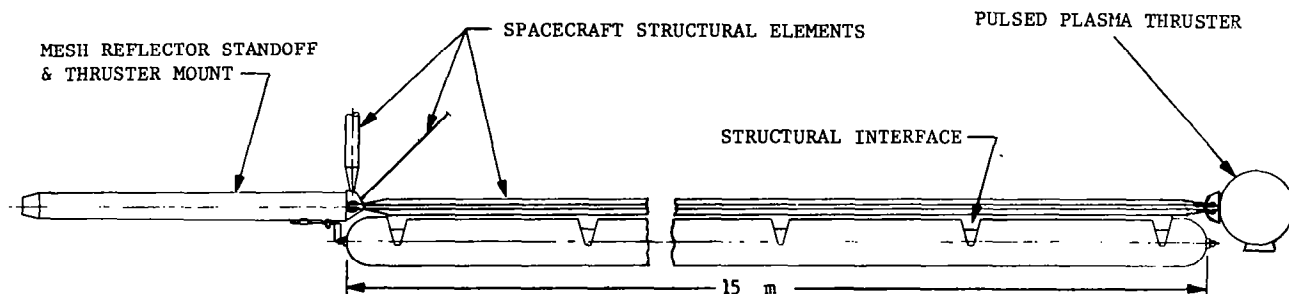
N_2H_4 ORBIT TRANSFER THRUSTER/TANK ASSEMBLY

RF REFLECTIVE MESH DESIGN

The reflective mesh is tricot-knitted 0.003-cm-diameter gold-plated molybdenum monofilament wire. The weave size is 5.5 ends/cm to ensure adequate RF reflectivity. The reflective mesh is suspended above the box-truss structure by a series of 2-meter standoffs and tie cords. The mesh is shaped into the parabolic shape by the direct tie-back system. The maximum rms surface distortion of 0.018 cm occurs during a full-shadow condition with a temperature of -90°C. This analysis was performed using a nonlinear, stress-stiffened finite element technique.

- SURFACE CORD
- TIE BACK CORD
- STANDOFF
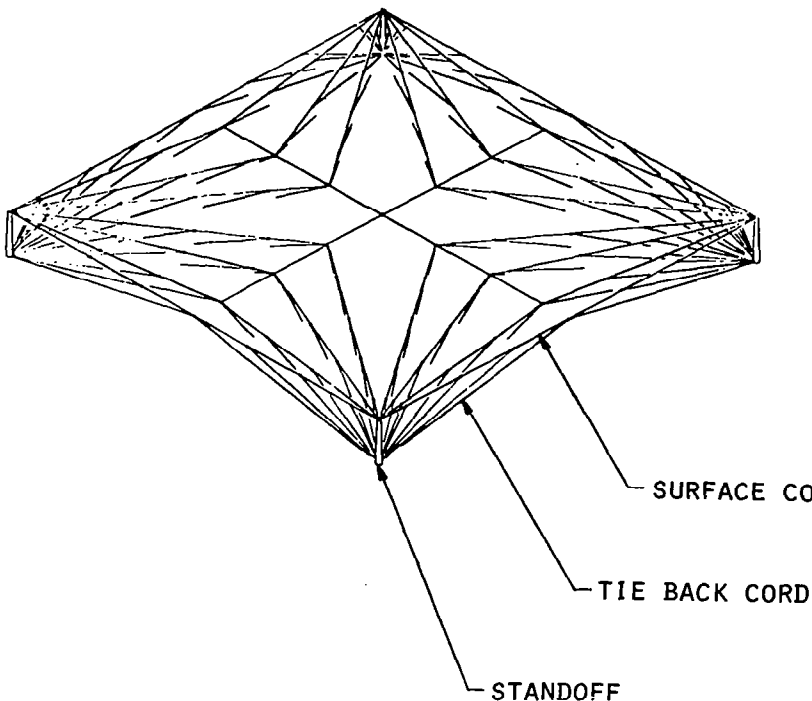
O TYPICAL TIE SYSTEM FOR ONE 15-METER BOX TRUSS SECTION

O TIE CORDS ARE MADE OF LOW MODULUS CONTINUOUS FILAMENT GRAPHITE

O COEFFICIENT OF THERMAL EXPANSION FOR THE CORD IS ON THE ORDER OF -0.1CM/CM/C° TO GIVE THE SURFACE GOOD THERMAL STABILITY

O MAXIMUM RMS SURFACE DISTORTION OF 0.018CM DUE TO THE THERMAL ENVIRONMENT OCURRING AT FULL SHADOW

O TIE SPACING IS 1 METER MAXIMUM TO ENSURE SURFACE ACCURACY WHEN GEOMETRIC SADDLING EFFECTS ARE TAKEN INTO ACCOUNT

REFLECTOR ERROR - EOS

The performance and usefulness of the radiometer are dependent on many factors, one of which is the quality of the reflector surface. Besides diffraction, deviations from a perfect surface will scatter energy out of the main beam, and its magnitude is determined by the size and distribution of the errors. A measure of antenna performance is beam efficiency, which must be very high because the contribution due to side-lobes must be minimized. A beam efficiency of greater than 90% must be achieved, and requires surface errors to be 1/55 of the wavelength (λ).

This table indicates the technology improvements required. Existing mesh technology with passive surface control can achieve 3.75mm error. It is anticipated that a 2.5x advance in surface technology is possible. The associated improvement in beam efficiency is shown in the table. An order of magnitude improvement is possible with active surface control.

O EXISTING TECHNOLOGY - 3.75-MM ERROR FOR 58-M SPOT

O PUSHING TECHNOLOGY - 2.5X RESULTS IN 1.5-MM ERROR

| FREQUENCY, GHz | PASSIVE SURFACE CONTROL | | | | ACTIVE SURFACE CONTROL | |
| | EXISTING | | 2.5X ADVANCE | | | |
	ERROR	BEAM EFFICIENCY	PROJECTED ERROR	BEAM EFFICIENCY	PROBABLE ERROR	BEAM EFFICIENCY
	λ/07	0.05	λ/17	0.60	λ/68	0.96
	λ/13	.40	λ/33	.86	λ/132	.99
	λ/50	.94	λ/125	.98	λ/500	1.00

O FOR BEAM EFFICIENCY OF >90% A SURFACE ACCURACY OF BETTER THAN λ/55 IS NEEDED

EOS SUBSYSTEM SUMMARY

Multidiscipline/multisensor Earth observation platforms have the potential of generating vast quantities of data. The design drivers for the data management/ handling subsystem were based on the capability of TDRSS and the ground processing facility. A realistic assessment of instrument duty cycles and operating protocols were established for the sensors and the anticipated data rates were calculated. For a land observation mission the data rates were divided into a nearly continuous rate of approximately 500 kbs with high data spurts of 100 Mbs for up to 30 seconds.

DATA MANAGEMENT/HANDLING

GOAL WAS TO DEVELOP AN EFFICIENT END-TO-END SYSTEM (S/C TO USER)
- CONSIDERED BOTH TDRSS AND GROUND PROCESSING CAPABILITY

DATA RATES
- NEAR CONTINUOUS AT 500 KBS
- SPURTS APPROACHING 100 MBS

OPERATIONALLY EMPLOYS
- DATA COMPRESSION
- PREPROCESSING
- DIRECT DATA TRANSMISSION
- TAPE RECORDING AND HIGH SPEED PLAYBACK THROUGH TDRSS

MANAGEABLE PROBLEM
- NEED TO CONSIDER BOTH INSTRUMENT DUTY CYCLES AND PROTOCOLS

The principal technology driver for LSS is the long system lifetimes of ten to fifteen years. This must be achieved by employing high-reliability components, redundancy, and operating alternatives in the event of a particular failure.

A suggested alternative is to design with resupply in mind, although this capability requires a teleoperator, and this may not be possible.

The electric power subsystem requires the development of various components to ensure long system lifetime. The use of nickel hydrogen cells permits greater depth of discharge and an operating life of seven years. The event of power system failure requires improved power system monitoring and diagnostic ability which will improve the degraded system management.

The development of high-voltage power components is necessary due to the higher operating bus voltages needed to reduce power loss to acceptable levels during long transmission distances.

o GUIDANCE, NAVIGATION, AND CONTROL

- AUTOMATION
  -- REQUIRED FOR THE COMMAND POINTING CAPABILITY OF SENSORS
  -- SIGNIFICANT REDUCTION IN MISSION SUPPORT COSTS
  -- ENABLES REAL-TIME DATA MANAGEMENT

- USE FAULT-TOLERANT COMPUTERS

o RF RADIOMETER

- SURFACE ACCURACY REQUIREMENTS

- FEED DESIGN AND IN-ORBIT CALIBRATION

- RECEIVER COMPLEXITY

EOS TECHNICAL ISSUES

It is anticipated that the guidance and control of future spacecraft will be highly automated in operation. This is desirable from both an operational and practical standpoint. Automation is required for the command pointing capability of sensors and enables real-time data management of the scientific data. Automation of spacecraft functions will reduce the need for continuous ground interaction and will significantly reduce mission support costs. Spacecraft autonomy requires more complex onboard computers, which increases the probability of malfunction. The continued development of fault-tolerant computers is required.

The microwave radiometer has a variety of technical issues to be solved before large-scale radiometers of the type considered in this paper become a reality. Techniques for in-orbit calibration and temperature stability of the receiver electronics have not been fully addressed.

o RELIABILITY, LIFETIME - MAJOR TECHNOLOGY DRIVER

- 10-15 YEAR LIFTIME OF MISSION

- EMPLOY REDUNDANCY AND OPERATING ALTERNATIVES

o RESUPPLY/REFURBISH/MAINTENANCE

- 3-YR RESUPPLY IS SUGGESTED ALTHOUGH THIS CAPABILITY REQUIRES TELEOPERATOR

- INTERFACE REQUIREMENTS IMPOSED UPON S/C SUBSYSTEMS

- DOCKING/GRAPPLING REQUIREMENTS AND CONSTRAINTS

o ELECTRIC POWER

- USE NICKEL-HYDROGEN CELLS VS NiCd

- IMPROVED POWER SYSTEM MONITORING
    -- DEGRADED SYSTEM MANAGEMENT

- DEVELOP HIGH-VOLTAGE (150-400V) POWER COMPONENTS

15-METER DEPLOYABLE
APERTURE MICROWAVE RADIOMETER

J. V. Coyner, Jr.
Martin Marietta Corporation
Denver Aerospace
Denver, Colorado

Figure 1 summarizes the historical background for the study. The Large Antenna Multifrequency Microwave Radiometer (LAMMR) was a 4-meter-diameter mechanically scanned (at 1 rps) antenna operating at frequencies from 4.3 to 36 GHz. This LAMMR system was scheduled to fly on the National Oceanic Satellite System (NOSS) in 1986 to measure sea surface temperature and wind speed along with several other atmospheric and sea ice parameters. The LAMMR was limited to a 4-meter solid reflector to stay within the Shuttle/NOSS launch volume and to operate with radiometric precision up to 36.5 GHz. Under the 4-meter aperture constraint, LAMMR could not meet the user resolution requirement for sea surface temperature (25 km minimum, 50 km goal) in an RFI free band, i.e., 4.3 GHz. This study explores the feasibility of meeting this requirement goal with a 15-meter mechanically scanned deployable reflector.

Two other research objectives can also be studied by adding one active (approximately 5 GHz) and two additional passive (1.4 and 6.4 GHz) channels to investigate soil moisture and precipitation profiles over land. These two objectives are closely related because the precipitation is the source of the soil moisture in unirrigated regions, and the soil moisture changes between samples (2/day) could indicate that precipitation may have occurred while the sensor was not in view. The 5-GHz active channel will measure the surface radar cross section, σ , which appears to correlate with solid moisture according to some field measurements. The active channel will also be range gated to measure precipitation profiles in the conically scanned column.

o LARGE ANTENNA MULTIFREQUENCY MICROWAVE RADIOMETER (LAMMR WAS A 4-METER-DIAMETER SOLID ANTENNA)

    - MECHANICALLY SCANNED AT 1 RPS
    - OPERATING AT FREQUENCIES FROM 4.3 TO 36 GHZ
    - WAS TO FLY ON NOSS IN 1986
    - MEASURED SEA SURFACE TEMPERATURE, WIND SPEED, AND SEVERAL OTHER ATMOSPHERIC AND SEA ICE PARAMETERS

o LAMMR COULD NOT MEET USER RESOLUTION REQUIREMENT FOR SEA SURFACE TEMPERATURE (25 KM MINIMUM; 5 KM GOAL)

o 15-METER-DIAMETER MECHANICALLY SCANNED DEPLOYABLE ANTENNA (MSDA) DOES MEET USER REQUIREMENT RESOLUTIONS (5 KM X 6 KM)

    - 5.1 GHZ ADDED ACTIVE CHANNEL (SURFACE RADAR CROSS/SECTION (σ) AND RANGE GATED TO MEASURE PRECIPITATION PROFILES)

    - 1.414 AND 6.4 GHZ ADDED PASSIVE CHANNELS (SOIL MOSTURE AND PRECIPITATION PROFILES OVER LAND)

Figure 1

Figure 2 summarizes the contract number, agency, period of performance, and contract dollar value.

15-METER DIAMETER MECHANICALLY SCANNED DEPLOYABLE ANTENNA

CONTRACT NUMBER: NAS5 - 26496

AGENCY: NASA GODDARD SPACE FLIGHT CENTER

PERIOD OF PERFORMANCE: 1 APRIL 1981 TO 1 MARCH 1982

CONTRACT VALUE: $34.2 K

Figure 2

MSDA DESIGN REQUIREMENTS AND SPECIFICATIONS

The objectives of this study were to provide a preliminary design with structural model data and thermal-performance estimates of a 15-meter mechanically scanned deployable antenna (MSDA) that could be launched onboard a Shuttle orbiter to provide radiometric brightness temperature maps of the Earth and oceans in selected bands over a frequency range from 1.4 to 11 GHz. This study assumed that this antenna would be attached to a spinning platform (360 deg, 6 rpm, 35-deg conical scan axis) on a free-flyer spacecraft in a 700-km altitude, 12-hour Sun-synchronous orbit. Figure 3 summarizes the design requirements and specifications that were involved in this study.

o DEPLOYABLE 15-METER-DIAMETER EFFECTIVE CIRCULAR APERTURE, OFFSET-FED PARABOLIC REFLECTOR AND FEED STRUCTURE

o DYNAMICALLY BALANCED, CONICALLY SCANNED (35-deg NADIR ANGLE, 6 rpm) SYSTEM

o 90% EFFICIENCY ON ALL BEAMS, WHICH ARE:

	CHANNEL, GHz			
	1.414	4.3	5.1	11.0
BEAMWIDTH, deg	1.07	0.35	0.3	0.35
BEAMS IN TRACK	3.0	10.0	12.0	10.0
RF BANDWIDTH	28.0	200.0	100.0	100.0

o MOUNT ON SPINNING PLATFORM ON A GENERIC FREE-FLYER SPACECRAFT

o OPERATIONAL ORBIT*: 700-km ALTITUDE, 12:00 SUN-SYNCHRONOUS

o LAUNCH IN SHUTTLE ORBITER.

o ANTENNA/FEED ASSEMBLY STOWS IN A VOLUME NOT TO EXCEED A 4-METER-DIAMETER CYLINDER 7 METERS LONG

o STOWED SYSTEM STRUCTURAL RESONANT FREQUENCY MUST BE ≥ 25 Hz

o SCANNING (DEPLOYED, ROTATING) SYSTEM RESONANT FREQUENCY SHOULD BE ≥ 12 Hz

*99% Inclination, 99-minute period, orbital plane precesses to remain aligned with subsolar point

Figure 3

DESIGN DRIVERS

The primary mechanical design challenge was to develop a 15-meter-diameter reflector and feed mast that would achieve the desired 12-Hz structural frequency within the package constraints and desired low structural mass. Two other critical issues were the ability to provide a rigid stable attachment to the spacecraft and to provide mounting points where spin balance ballast masses could be added. There were also design challenges related to the achievement of the antenna RF performance requirements (90 percent beam efficiency and beamwidth). Figure 4 summarizes the design drivers of this study.

1. DEPLOYED STIFFNESS

2. SURFACE ACCURACY

3. STOWED DIAMETER

4. STOWED FREQUENCY

5. SPIN ADAPTER STRUCTURE

Figure 4

DESIGN OPTIONS CONSIDERED

Four reflector designs were considered for the reflector structure. A truss-
type radial rib concept had the advantage of the relative simplicity of the reflector
structure but had difficult offset feed mast structure integration and an inability
to achieve the 12-Hz requirements. The hoop/column had the most efficient packaging
but also had the difficult offset feed mast integration and inability to achieve the
12-Hz requirement. Both the tetrahedral and box truss met the 12-Hz requirement.
The box truss was selected because of the orthogonal, sequential deployment and the
integrated offset feed mast. Figure 5 summarizes the design options considered.

REFLECTOR:

-   RADIAL RIB

-   HOOP/COLUMN

-   TETRAHEDRAL TRUSS

-   BOX TRUSS

FEED MAST:

-   ASTROMAST

-   BOX TRUSS INTEGRATED FEED MAST

Figure 5

BOX TRUSS BUILDING BLOCK

The 15-meter-dia mechanically scanned deployable antenna (MSDA) is designed using the deployable box truss structure (figure 6) to form the parabolic dish and feed mast. This truss comprises a deployable frame consisting of two equal-length structural members ("verticals"), two structural members hinged in the middle ("surface tubes") which connect the ends of the verticals and fold inward to stow between the adjoining verticals, and telescoping diagonal braces that lie in and control the shape of the deployed frame. Prototype hardware has been fabricated with all composite tubes and fittings, and low-cost manufacturing processes are being developed for all repetitive components.

The shape of a box truss reflector and feed mast is controlled by the diagonal tension braces in each frame face. The diagonals are multiple-ply graphite-epoxy tapes that telescope for stowage and deployment.

A key feature of the truss is the hinge and latch in the middle of each folding surface tube. All moving parts are in the hinge and latch interior. This eliminates protuberances that could interfere with the diagonal braces or an antenna surface during deployment. Redundant coil springs in the hinge are sized to produce the desired deployment rate. The spring-driven overcenter latch increases in mechanical advantage when the deploying tube is approximately 10 deg from full deployment. The latch spring is sized to meet diagonal brace and antenna surface tensioning requirements. A redundant mechanical latch functions in parallel with the overcenter latch.
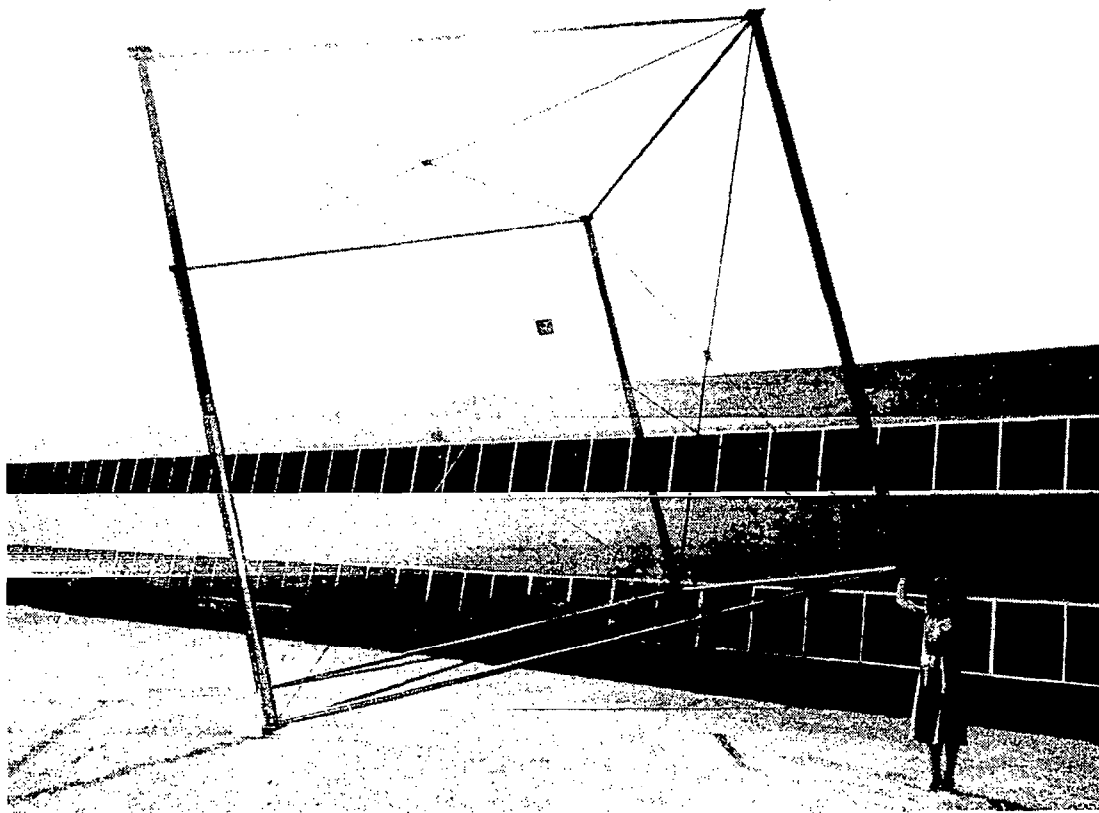
Figure 6

STOWED 4.57-METER BOX TRUSS CUBE

Figure 7 shows the single 4.57-meter graphite-epoxy cube in the stowed configuration. A single 4.57-meter cube stows in a 25-cm X 25-cm X 4.57-meter package. The cube weighs 27 kg, but a flight-optimized cube would weigh below 20 kg per cube.

Figure 7

138
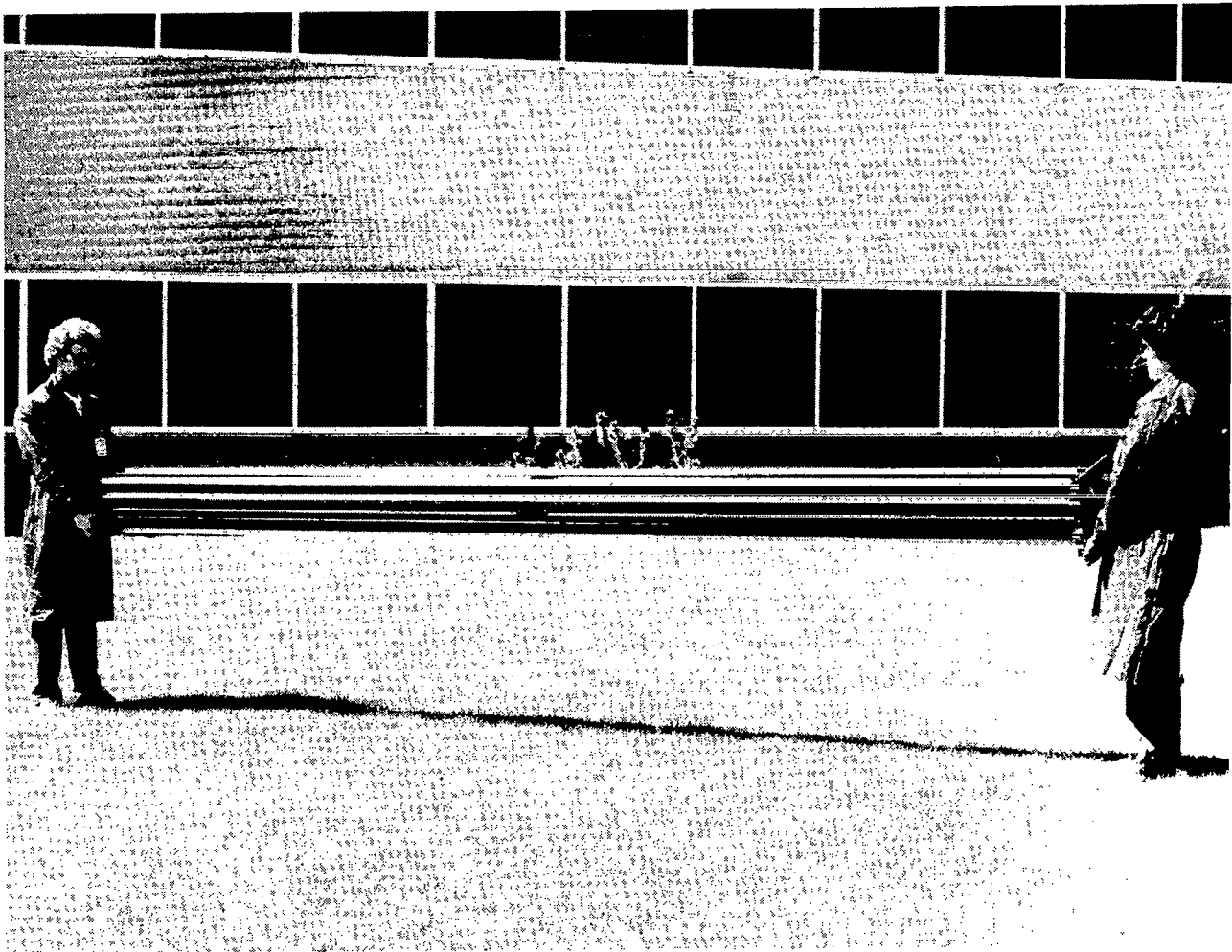
OFFSET FED PARABOLIC ANTENNA

The 5-bay by 5-bay graphite epoxy antenna support structure (figure 8) has an extremely high stiffness-to-weight ratio and excellent thermal stability. Because of the box truss configuration, the structure easily stows within the allotted envelope. This 5 X 5 offset feed box truss design exceeds all requirements with the exception of the 25-Hz stowed requirement. The structural members in the strongback region have increased cross-sectional area to provide local stiffness. The increased cross-sectional areas were determined in an iterative process using the strain distribution in the structural modes obtained from the finite element dynamic computer runs. This process optimized member sizes by defining high-stiffness members in areas of high-strain energy and low-stiffness (weight) members in areas of low strain energy. The heart of the strongback section is the nondeployable "superbox". The 2- x 2- x 4-m superbox is extremely stiff and provides the interface points between the spacecraft and the antenna via the spin-adapter structure. The superbox allows the structure to meet the 12-Hz fundamental frequency requirement through its rigidity at the interface point.

A unique deployable feed mast has been developed for the offset feed space deployable antenna. The novel feature of this design is that it uses an extension of the reflector truss structure rather than adding appendages. The design features efficient stowage, simple integration to the reflector structure, excellent thermal stability, light weight, and very high stiffness and dynamic stability. Previous offset feed masts were appendages added to the reflector structure and had less efficient packaging, more difficult integration, and substantially lower dynamic stability. Because of the high strength and stiffness, this mast can easily accommodate the more complicated and massive advanced feeds.
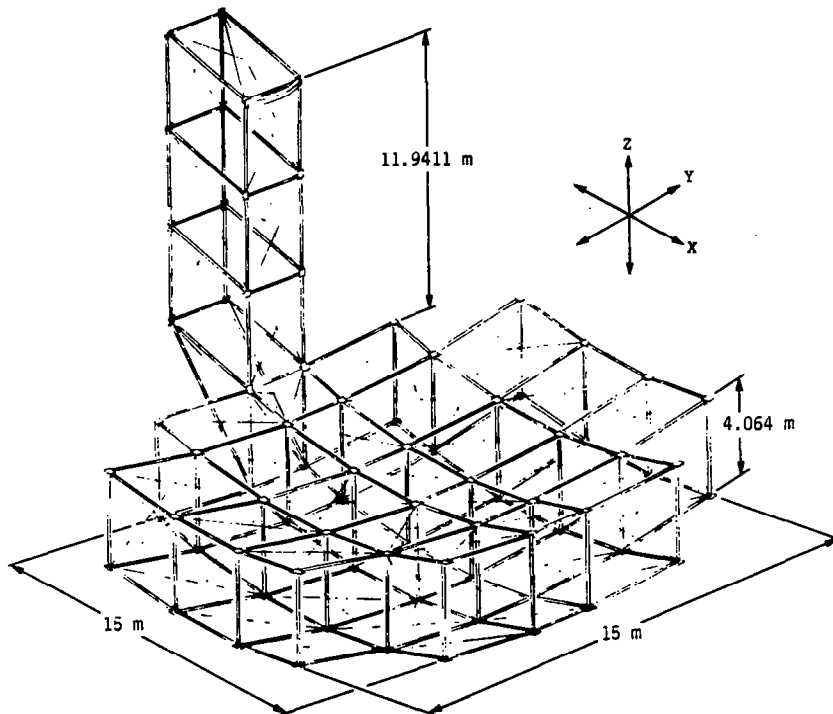
Figure 8

ANTENNA PERFORMANCE SUMMARY (11.941-m FOCAL LENGTH)

The 15-meter-diameter antenna (11.941-meter focal length) met all the mechanical, structural, and surface accuracy requirements as shown in figure 9. The stowed structural frequency was below 25 Hz; however, by providing a tip restraint, this could be raised from 17.2 Hz to 25 Hz if required. The deployed frequency of 12.35 Hz was achieved without driving the antenna mass up drastically. The antenna (minus ballast mass) weighs 400 kg. It is essential to minimize the mass of the system to reduce the angular momentum of the spinning antenna.

● REFLECTOR DIAMETER, M	15.0
● FOCAL LENGTH, M	11.941
● REFLECTOR AND FEED SUPPORT MAST, KG	400.07
● FEED MASS ALLOCATION, KG	27.14
● BALLAST MASS, KG	22.68
● DEPLOYED FREQUENCY, HZ	
MODE 1	12.35
MODE 2	12.75
MODE 3	13.19
● STOWED ENVELOPE, M	3.84 DIA X 4.47
● STOWED FREQUENCY, HZ	17.2
● SURFACE ACCURACY (RMS) WORST CASE, CM	0.097
● FEED LOCATION ACCURACY (AXIAL), CM	0.024
(CENTRIFUGAL CORRECTED) (LATERAL), CM	0.051

Figure 9

ANTENNA PERFORMANCE SUMMARY (18-m FOCAL LENGTH)

A second configuration was evaluated which had an 18-meter focal length. This additional configuration was analyzed based on the RF analysis results that showed an improved radiometer performance at the longer focal lengths. The structure was not reoptimized to achieve the 12 Hz. However, this could be done with a resulting weight impact. Figure 10 summarizes the performance parameters for the 18-meter focal length system. The only significant changes were a reduction in the structural frequency to 7.07 Hz and a weight increase to 485 kg.

● REFLECTOR DIAMETER, M	15.0
● FOCAL LENGTH, M	18.0
● REFLECTOR AND FEED SUPPORT MAST, KG	484.99
● FEED MASS ALLOCATION, KG	27.14
● BALLAST MASS, KG	22.68
● DEPLOYED FREQUENCY, HZ	
MODE 1	7.07
MODE 2	8.17
MODE 3	13.05
● STOWED ENVELOPE, M	4.04 X 4.47
● STOWED FREQUENCY, HZ	17.2
● SURFACE ACCURACY (RMS) WORST CASE, CM	0.097
● FEED LOCATION ACCURACY (AXIAL), CM	0.024
(CENTRIFUGAL CORRECTED) (LATERAL), CM	0.051

Figure 10

MSDA STOWED CONFIGURATION

The MSDA stowed configuration is shown in figure 11. All of the structural members compactly stow around the superbox, thus allowing the antenna to easily meet the stowage requirement. In the stowed condition, the cube-corner fittings butt against each other and form a plane at the top and bottom surfaces. The plane formed by the cube-corner fittings provides a load path for loads incurred during launch with in-plane shearing loads handled by interlocking pins between the fittings.

The dynamic characteristics of the MSDA in the stowed configuration were analyzed with the NASA Structural Analysis (NASTRAN) Finite Element Program. The model was conservative in the sense that it only contained the superbox stiffness with the rest of the masses lumped at the model's eight nodes. The first fundamental frequency obtained was 17.2 Hz, but this number is extremely conservative considering that the model did not take into account the stiffness added by the members being pinned and supported together during stowage. An additional restraint ring would readily permit attainment of the 25-Hz requirement.

Figure 11

142

MSDA DEPLOYMENT SEQUENCE

The structure is deployed in a controlled sequence of steps. Feed beams are deployed one cube at a time, and trusses are deployed one row of cubes at a time. In the latter case, the steps are accomplished in a preselected sequence in the two orthogonal deployment directions. This type of deployment is compatible with flat, cylindrical, and parabolic trusses, and virtually any beam shape.

As shown in figures 12 and 13, the feed mast flips up first, after which the boxes on either side of the superbox deploy outward. The bays on either side of the middle deployed three are then deployed. Following this sequence, an entire row of five bays is deployed outward away from the feed mast. This is followed by each row deploying outward until the antenna support structure is fully self-deployed. The feed mast will then deploy its three boxes upward for the completion of the entire sequence. The deployment is controlled by latches between the cube-corner fittings. These latches release by remote control in proper sequence, initiating deployment of each section of the antenna support structure. The sequential nature of the deployment process dissipates the deployment energy in an incremental manner, thereby reducing the possibility of producing structural failure in the deploying truss.

Figure 12

143
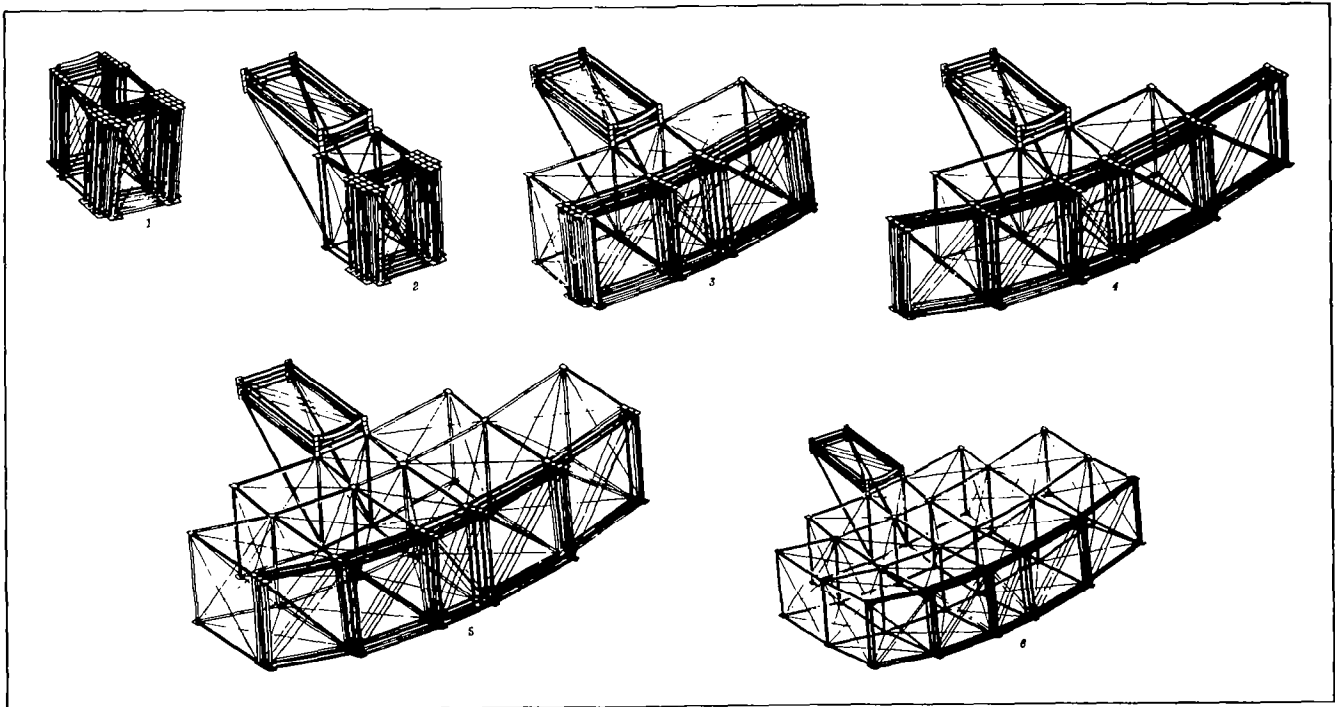
Figure 13 shows the completion of the reflector deployment and the full feed mast deployment. Total deployment of the reflector and feed mast (10 steps) takes approximately 5 minutes.
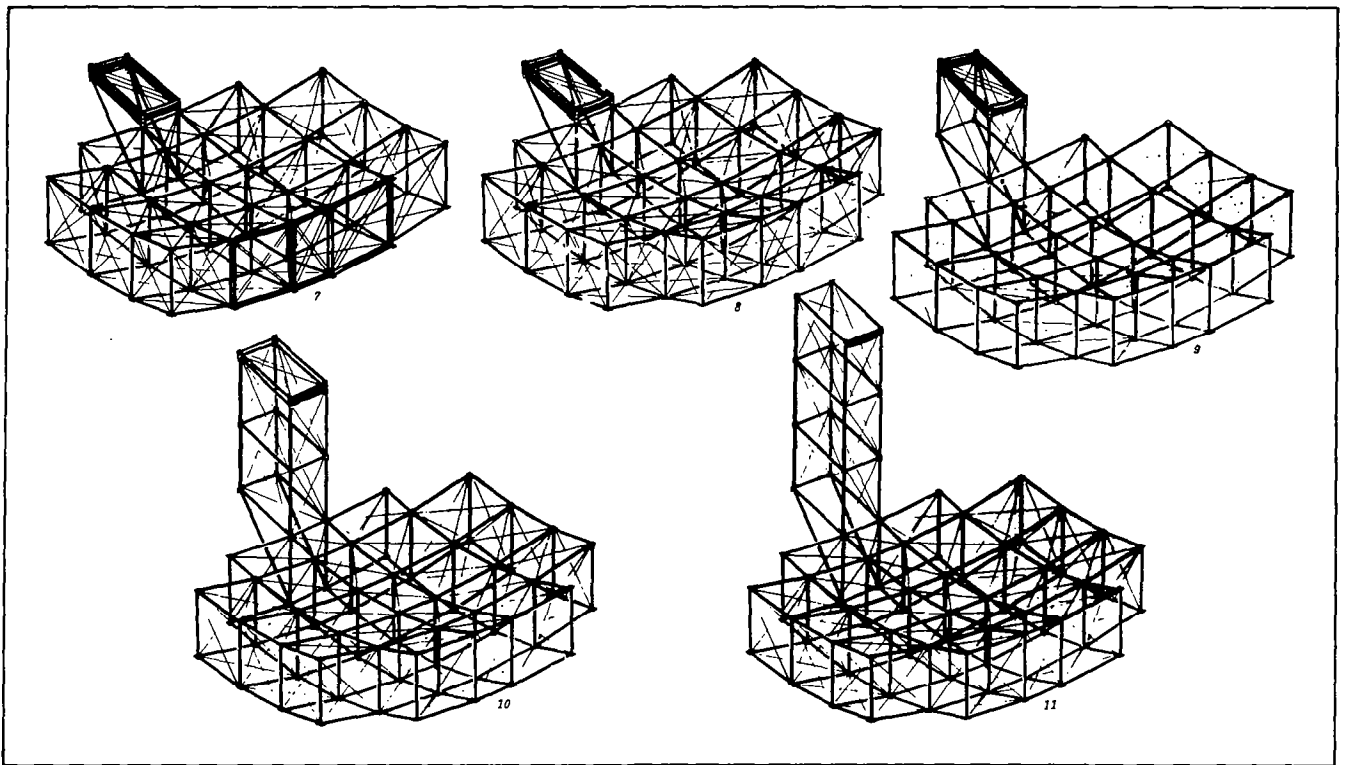
Figure 13

SPIN ADAPTOR STRUCTURE

The spin adaptor structure shown in figure 14 was developed to provide the inter-
face between the antenna superbox and the spin bearing ring that attached to the
spacecraft. This structure had a severe stiffness requirement to provide no signifi-
cant base flexibility that would degrade the fundamental frequency of the spinning
antenna. Since the spin adaptor structure was nondeployable, the desired stiffness
was easily achieved through the use of robust graphite truss members and an efficient
truss design.

Reflector Interface
(4 places)

2.0

2.0

Graphite-Epoxy
Members

Bearing Ring
(0.75 dia)

(All Dimensions in Meters)
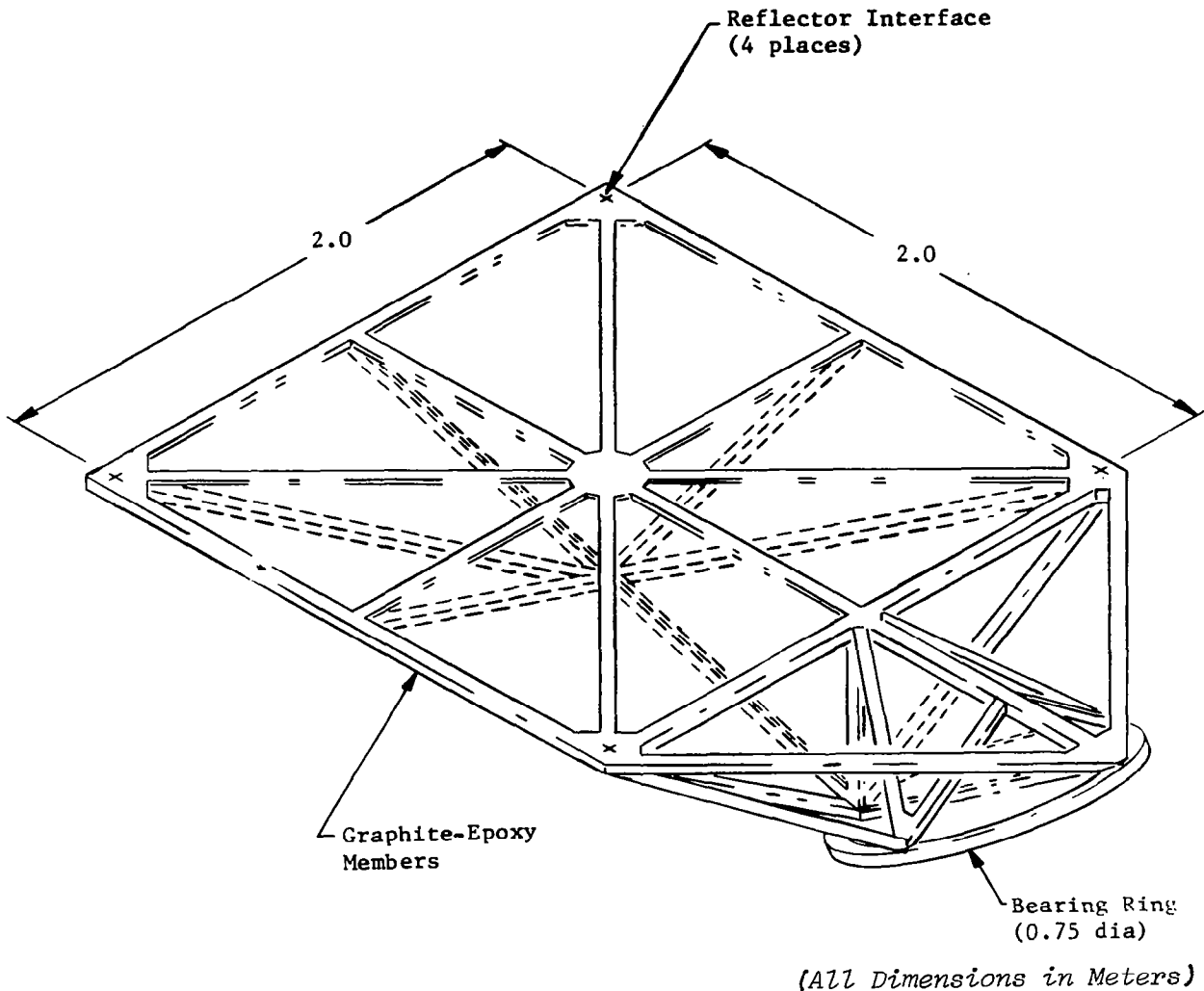
Figure 14

OPTIMIZATION PROCESS FOR DEPLOYED DYNAMICS

The MSDA dynamic analysis was performed using beams and rods to model the antenna support structure and the feed mast. The model contained 78 active nodes that connected 386 structural members. The surface and vertical members were modeled with beam elements, while the interior and exterior diagonals were represented by rod elements. Because the surface members are pinned at either end, this degree of freedom is released in the rotational direction along the axis of those pins in the model. A lumped mass was placed at all the node points to simulate the mass of the cube-corner fitting and the integral end fittings in the tubes. A lumped mass was placed on appropriate nodes to simulate standoff and mesh mass. The midlink hinge mass and the crossover fitting mass were distributed along the length of their respective members because no node existed at that point. The feed and ballast were modeled with a 27.12-kg lumped mass divided between nodes at the top and front of the feed mast (Figure 15).

The dynamic computer model was run several times in an iterative process to satisfy the 12-Hz requirements. The original 4- X 4-bay structure was abandoned in favor of a 5- X 5-bay structure that gives the system a much better interface between the antenna structure and the spacecraft. The Astromast feed was also discarded in favor of the offset box truss integral feed mast that has the higher stiffness needed to meet the 12 Hz-requirement. By increasing the stiffness in those members carrying the highest strain energies, the first fundamental frequency of the structure was increased to 12.55 Hz.
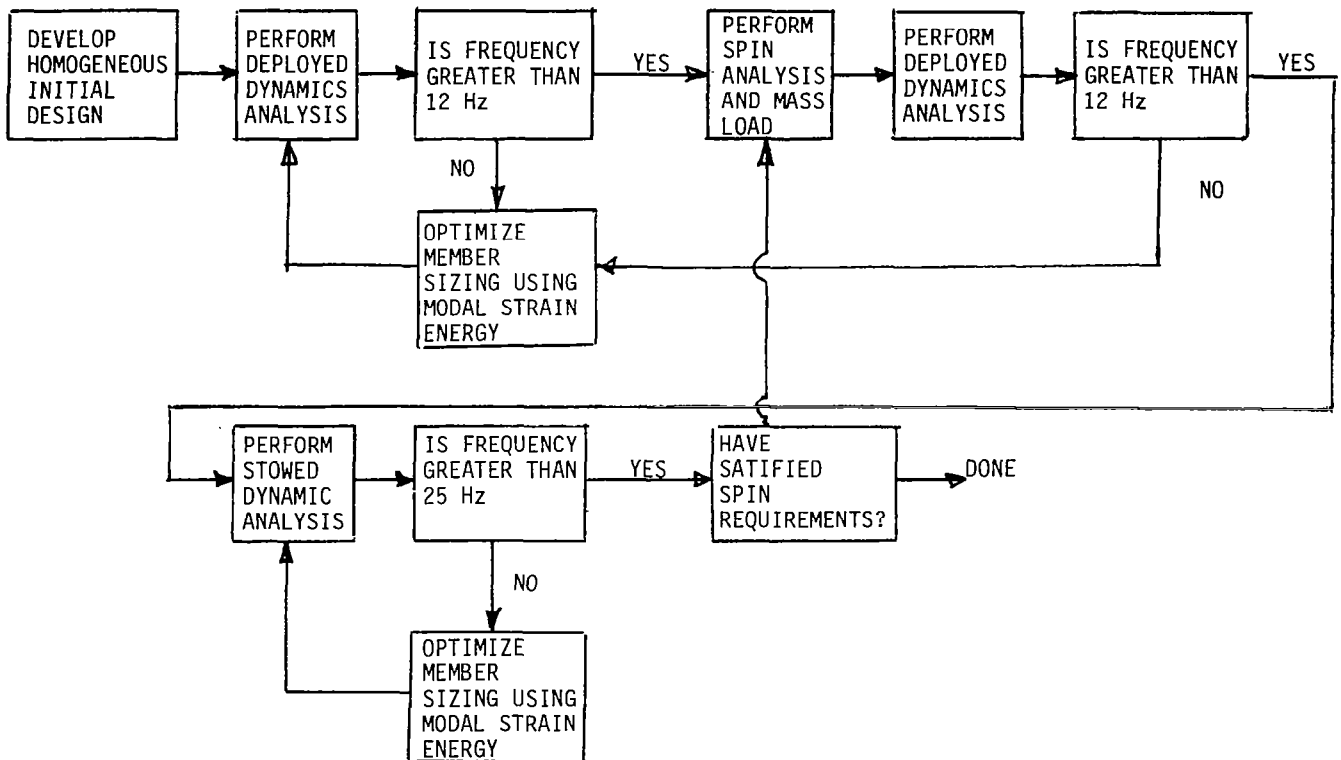
Figure 15

MODAL CHARACTERISTICS SUMMARY

The first mode is a bending mode about the y-axis with its root at the base of the superbox. The second fundamental frequency of 12.75 Hz is a twisting mode on the superbox base about the x-axis and z-axis where the feed mast and antenna structure are twisting in phase. The third mode is very similar to the second mode with a frequency of 13.19 Hz. Figure 16 summarizes the dynamic data.

MODE	FREQ, Hz	DESCRIPTION
1	12.55	ANTENNA SUPPORT STRUCTURE BENDING ABOUT Y-AXIS
2	12.75	TORSIONAL MODE ABOUT X-AXIS AND Z-AXIS
3	13.19	TORSIONAL MODE ABOUT X-AXIS AND Z-AXIS

Figure 16

Figure 17 shows a computer-generated exaggerated deflection plot of the fundamental mode of the antenna system. This mode is primarily a bending mode about the base attachment with the superbox and local members around the superbox doing most of the deflecting. This is the reason that the section properties of the members are varied from large in the local region around the attachment to minimum at the periphery of the structure.
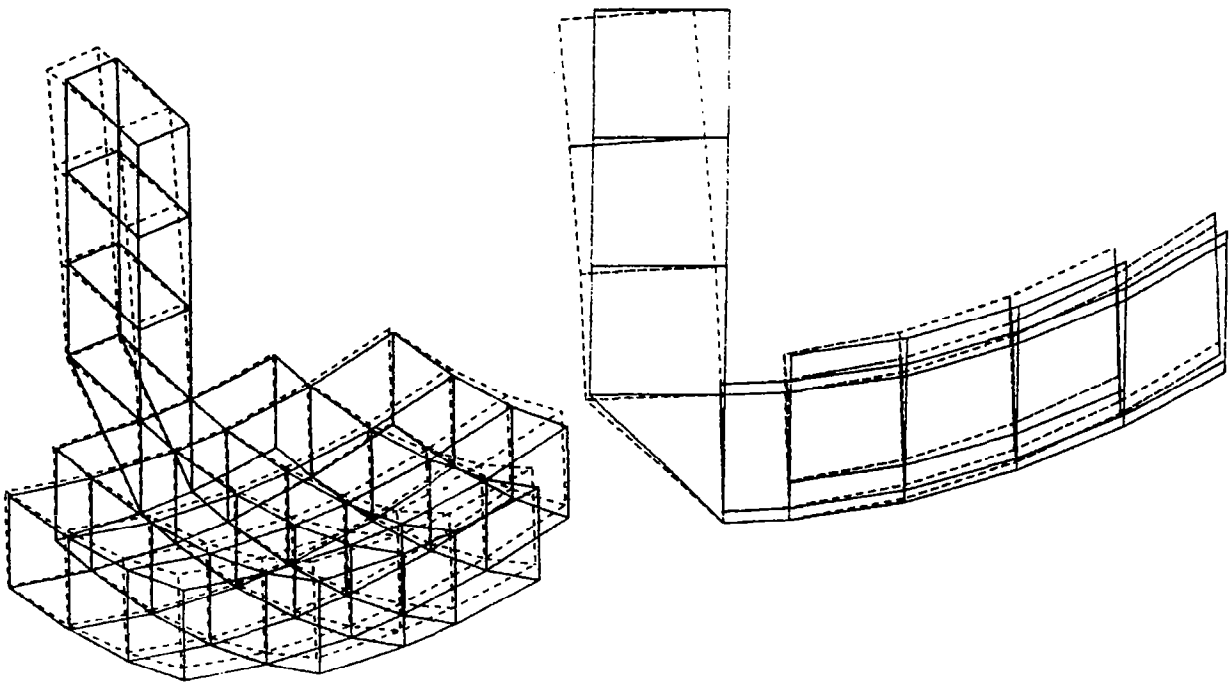
Figure 17

BALLAST AND SPACECRAFT LOCATION AND INERTIAL PROPERTIES

The dynamic balancing of the MSDA antenna involved attaching ballast at various points in the structure. The objective was to align the spin axis with one of the principal inertial axes as seen in figure 18. Early in the project, the antenna configuration had the spin axis 35 deg to the other side of the z-axis, but it was found that a much smaller amount of ballast had to be added in its present configuration. The ballast mass and location were determined by a Martin Marietta computer program written using the weight generator from the NASTRAN finite model. The balancing computer program recalculated the principal inertias including ballast of the structure, so an iterative process was used to determine the optimum ballast location and minimum mass.

Feed 11.34 kg

Feed Allocation 27.14 kg

Ballast 15.8 kg

Mass = 449.9 kg
I_1 = 1.182 E4 kg m^2
I_2 = 1.84 E4 kg m^2
I_3 = 1.368 E4 kg m^2

3.09

35°

Spin Axis

I_1

.88

I_3

2.0

Spin Adaptor Structure

Spacecraft

Ballast 22.68 kg

3.0   2.0
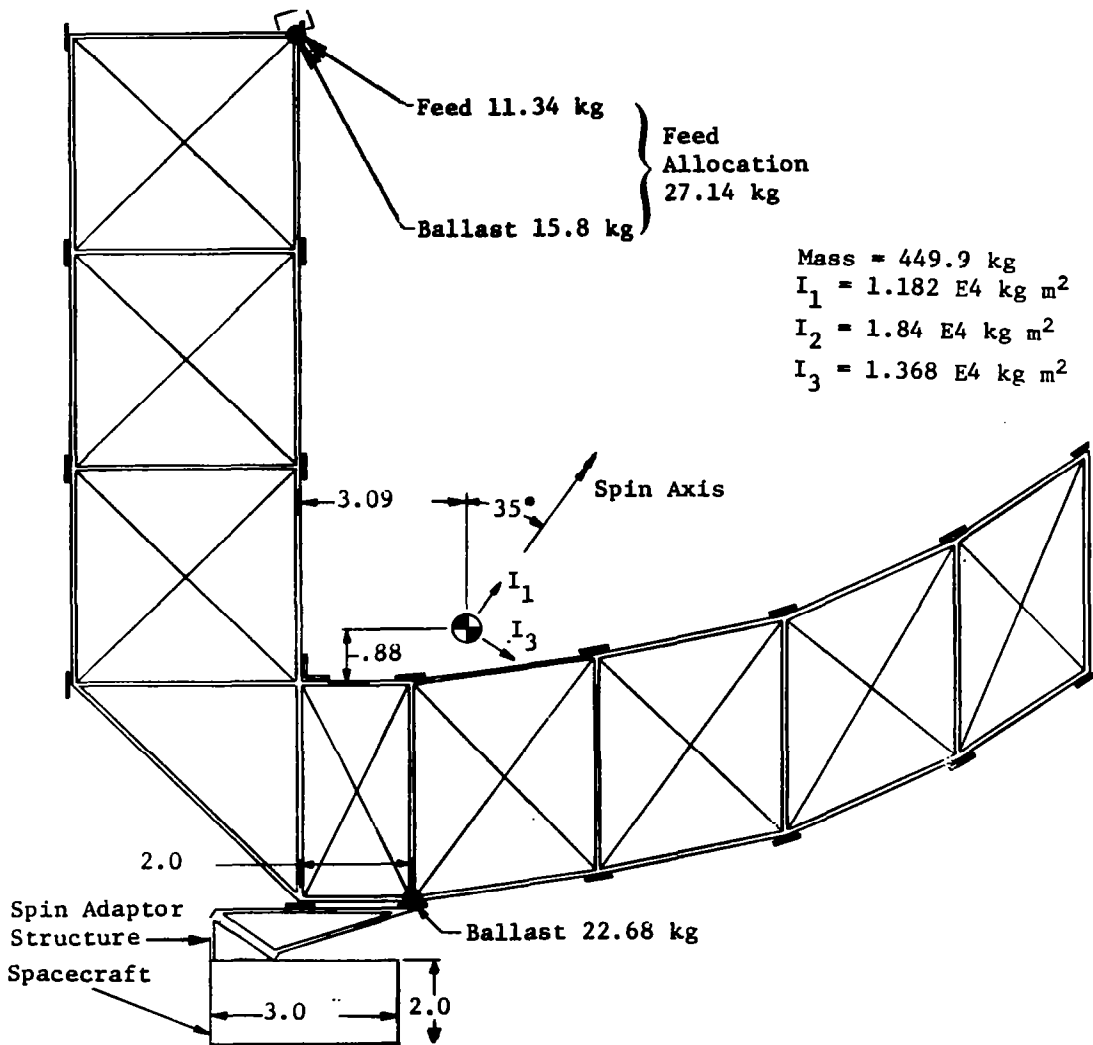
Figure 18

SPIN BALANCE SUMMARY

Figure 19 summarizes the results of the spin balance analysis. The locations and magnitudes for the four ballast masses are two 11.34-kg masses at the base of the superbox and two 7.9-kg masses, one located on either side of the feed. The feed location has the advantage of allowing extra feed mass allocation for a total of 27.14 kg to be used instead of ballast. The ballast location at the bottom of the superbox has the advantage of allowing the use of heavier members in that area without any penalty of lowering the fundamental frequency. These ballast locations are illustrated in figure 18. Spin balance was easily achieved with minimal added mass to the structure.

- BALLAST MASS AND LOCATION DETERMINED USING MMDA PROGRAM AND MASS GENERATOR IN NASTRAN FINITE ELEMENT PROGRAM

- BALLAST LOCATION SELECTED TO MINIMIZE IMPACT ON STRUCTURAL DYNAMICS AND MINIMIZE BALLAST MASSES REQUIRED.

- FEED AND SUPERBOX LOCATIONS SATISFIED ABOVE REQUIREMENTS.

- FEED LOCATION ALSO HAS ADVANTAGE OF PROVIDING EXTRA FEED MASS ALLOCATION (11.34-KG TO 27.14-KG FEED MASS ALLOCATION).

Figure 19

150

MESH DESIGN

The mesh surface design is summarized in figure 20. The radio-frequency (RF) reflective surface is formed by suspending a tricot-knitted, 0.003-cm-dia, gold-plated, molybdenum monofilament wire mesh. This design has the desirable properties of high RF reflectivity, corrosion resistance, low weight, wrinkle resistance, low spring rate, puncture resistance, and radiation resistance.

The mesh tie system design is a double-catenary cord system. This cord system is made up of three types of graphite-epoxy cords: upper surface cords, drop cords, and rear cords. The upper surface cords, which are continuous cords across the total mesh surface, rest on the mesh surface and are spaced evenly between the box truss standoffs. The point at which two surface cords cross is then pulled down into shape by drop cords that then attach to a rear cord catenary. The rear cord catenary system spans individual box truss cube standoffs. The total mesh surface is formed by individually tensioning mesh panels (sized for compatibility with truss cube) and then sewing them together. The mesh is then attached to the deployed truss standoffs. The mesh attachment points were located and marked while the mesh panels were on the mesh stretching table. The surface cords with attachment beads and drop cords are then strung across the surface of the mesh. The rear cords are then strung, and the drop cords are loosely fastened to the rear attachment beads. At this point, mesh setting is started. During the setting process, a constant force is maintained in the front surface cords. Each upper surface attachment point will be adjusted to match the parabolic shape required.

- GOLD-PLATED MOLYBDENUM MONOFILAMENT WIRE MESH

    - 5.5 OPENINGS/CM
    - 0.003-CM TRICOT-KNITTED

- ORTHOGONAL GRAPHITE-EPOXY SURFACE CORDS

- DOUBLE CATENARY GRAPHITE-EPOXY REAR CORD SYSTEM

- 42.8-CM DROP CORD SPACING

Figure 20

MESH TEST MODEL

An IR&D activity was initiated to design and understand a parabolic mesh reflector. This activity included fabrication of mesh models and surface distortion measurements. The shape of the reflector surface using the double-catenary cord system is defined by several factors: mesh tension and compliance, upper surface cord pattern (spacing), tension and stiffness, drop-cord stiffness and length, rear-cord stiffness and length, and local radius of curvature. Further, geometric saddling effects (pillowing) due to biaxially tensioned mesh and the upper surface cord pattern cause local deformations. Figure 21 shows a scale test model of a reflector surface. Measurements were made to determine pillow shape versus mesh tension and cord tension. When the panel's shape is duplicated and scaled to a mesh surface on a 15-meter reflector with an 11.94-meter focal length and average drop-cord spacing of 42.8 cm, the rms surface errors (best-fit mesh saddles relative to the ideal parabola) are 0.020 cm, and the worst-case deflections (drop-cord attachment points) are 0.067 cm behind the ideal parabola. Assuming 1/40 of a wavelength can be assigned to rms mesh distortions, the mesh surface design proposed would be appropriate for frequencies of 11 GHz.
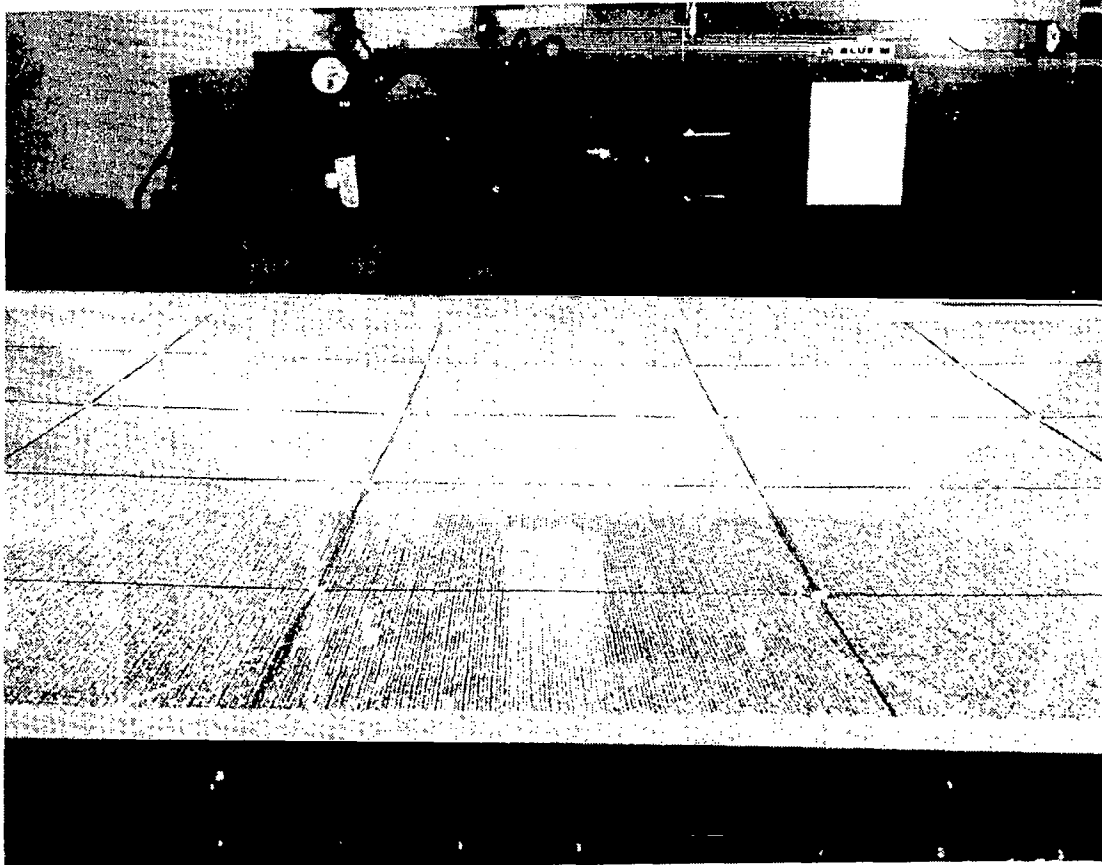
Figure 21

THERMAL-THERMOELASTIC SUMMARY

A thermal analysis of the MSDA structure (summarized in figure 22) was performed to provide temperature data as input to a thermal deformation analysis. The thermal-thermoelastic model that was used for this analysis included the total box truss structure for the feed mast and reflector, the complete mesh as a shadower of the truss structure, and a 2-meter-tall by 3-meter-dia spacecraft as a shadower. This provided a rigorous definition of temperatures and thermal deflections of the truss structure that supports the mesh surface under the varying thermal environments. The mesh model, however, was a simplified single box mesh and tie system. Although this did not provide a total thermal distortion profile over the total reflector, it did provide a conservative thermal distortion rms error. This rms error included the effects of the mesh tie distortion relative to the truss, plus the distortion of the truss relative to its nominal shape.

To perform analyses, math models were built to use our standard thermal analysis computer programs: Thermal Radiation Analysis System (TRASYS) and Martin Marietta Interactive Thermal Analysis System (MITAS). Because MSDA has such a large number of members (more than 450), it was expedient to create utility programs that would use the MSDA NASTRAN data base to create both the TRASYS surface data description inputs and the MITAS thermal node description inputs. This technique used the same node identification number for all three analysis programs, as well as ensuring that all three programs used the same physical and spatial description of the MSDA members.

- TRASYS (THERMAL RADIATION ANALYSIS SYSTEM) AND MITAS (MARTIN MARIETTA INTERACTIVE THERMAL ANALYSIS SYSTEM) USED FOR ANALYSIS

- FULL-TRUSS STRUCTURE MODELLED WITH MESH AND S/C BLOCKAGE

- MESH TRANSPARENCY VS SUN ANGLE INCLUDED

- REPRESENTATIVE MESH TIE SYSTEM SELECTED FOR ANALYSIS, RESULTS EXTRAPOLATED TO OTHER PANELS

- 10 DIFFERENT POSITIONS IN THE ORBIT ANALYZED
    - NORTH AND SOUTH POLE POSITIONS
    - SUBSOLAR AND ANTISOLAR POSITIONS
    - 45° AND 135° POSITIONS
    - BEFORE AND AFTER ENTERING EARTH SHADOW
    - BEFORE AND AFTER LEAVING EARTH SHADOW

- SPIN EFFECT ACHIEVED BY AVERAGING TEMPERATURES AT 0°, 90°, 180°, 270° AND 360° ABOUT SPIN AXIS

- THERMAL MASSES INCLUDED IN TRANSIENT CASE

Figure 22

REFLECTOR SURFACE AND FEED LOCATION DISTORTION

Both the reflector surface and the feed have operational accuracies (see figure 23) that provide satisfactory RF performance of the antenna at the operating frequencies. At the lower operating frequency of 1.414 GHz, the surface accuracy is $\lambda/220$ and at the higher operating frequency of 11.0 GHz the surface accuracy is $\lambda/34$. The feed movement is a 0.020-cm defocus and a -0.088-cm lateral beam shift. Both numbers produced an insignificant degradation in the antenna performance.

o REFLECTOR SURFACE (PILLOWING + MANUFACTURING + THERMAL + SPIN)

SADDLE DISTORTIONS = 0.020 CM RMS

SPIN + THERMAL DISTORTION = 0.013 CM RMS

MANUFACTURING = 0.064 CM RMS

WORST-CASE TOTAL RMS = 0.097 CM RMS

o FEED DISTORTION (MANUFACTURING + THERMAL + SPIN)

DEFLECTION AT FEED, CM

X	Y	Z
-0.088	0.002	0.020

Figure 23

RF SUMMARY

Two antenna parameters were selected based on trade-offs between conflicting requirements for the RF analysis summarized in figure 24. These are (1) reflector illumination taper and (2) reflector focal length. Two performance considerations enter into the trade-off: (1) A tapered illumination is needed to meet the beam efficiency requirement and to hold down the side-lobe levels, but if the taper is excessive, the 0.3-deg beamwidth requirement will not be met. (2) A long focal length also helps to meet the beam efficiency requirement by reducing the coma distortion for off-axis beams. It also reduces main-beam broadening of the off-axis beams. But if the focal length is excessive, it causes structural, packaging, and weight problems in the design of the feed support tower. An initial design was made of the feed system. This was not fully optimized but is adequate to give approximate values for beam efficiency and to show the degradation of the off-axis beams.

- ANTENNA PARAMETERS BASED ON TRADE-OFF BETWEEN CONFLICTING REQUIREMENTS

- TAPERED ILLUMINATION REQUIRED TO MEET BEAM EFFICIENCY

- EXCESSIVE TAPER VIOLATES 0.3-deg BEAMWIDTH

- LONG FOCAL LENGTH GOOD FOR RF, BAD FOR DYNAMICS

- RF PARAMETERS
    - 16-dB ILLUMINATION TAPER
    - FEEDS POINTED 33° AWAY FROM PARABOLIC AXIS
    - STAGGERED HORN ARRANGEMENT
    - 5.1-GHz HORN USED FOR ANALYSIS (9.7 cm x 15.9 cm x 36.5 cm)

- CONCLUSIONS
    - BEAM EFFICIENCIES 99.69% AND 99.95% (ON-AXIS AND OFF-AXIS)
    - 3-dB BEAM WIDTHS 0.29° x 0.31° AND 0.62° x 0.38° (ON-AXIS AND OFF-AXIS)
    - LONGER HORN TO REDUCE PHASE ERROR AND GIVE DEEPER NULLS
    - SLIGHTLY LARGER E-PLANE HORN APERTURE FOR LOWER EDGE TAPER
    - INCREASE 33° TILT TO GIVE DESIRED 2.9 dB-EDGE DIFFERENTIAL
    - REDUCE TAPER IN RANGE OF 12-15 dB
    - INCREASE FOCAL LENGTH

Figure 24

SYSTEMS DESIGN AND COMPARATIVE
ANALYSIS OF LARGE ANTENNA CONCEPTS

L. Bernard Garrett and Melvin J. Ferebee, Jr.
NASA Langley Research Center
Hampton, Virginia

IDEAS CAPABILITIES

Conceptual designs are evaluated and comparative analyses conducted for several large antenna spacecraft for Land Mobile Satellite System (LMSS) communications missions. Structural configurations include trusses, hoop and column and radial rib. The study was conducted using the Interactive Design and Evaluation of Advanced Spacecraft (IDEAS) system. The current capabilities, development status, and near-term plans for the IDEAS system are reviewed. Overall capabilities are highlighted in figure 1.

IDEAS is an integrated system of computer-aided design and analysis software used to rapidly evaluate system concepts and technology needs for future advanced spacecraft such as large antennas, platforms, and space stations. The system was developed at Langley to meet a need for rapid, cost-effective, labor-saving approaches to the design and analysis of numerous missions and total spacecraft system options under consideration.

IDEAS consists of about 40 technical modules (refs. 1-6), efficient executive, data-base (ref. 7) and file management software, and interactive graphics display capabilities. The software modules reside on both mainframe and super minicomputer systems. A single analyst at the interactive terminal can rapidly model the structure and design and analyze the total spacecraft and mission. The coupling of on-orbit environmental computational algorithms with analysis and design modules permits rapid evaluation of competing spacecraft. Parametric studies and technology-level trade-offs are easily accomplished using IDEAS. Data and graphical summary information are presented to the analyst on graphics display terminals for immediate assessment and interactive modification of the spacecraft or mission design, as appropriate. Spacecraft concepts evaluated using IDEAS include microwave radiometer satellites, communication satellite systems, solar-powered lasers, power platforms, and orbiting space stations.

Figure 1

158
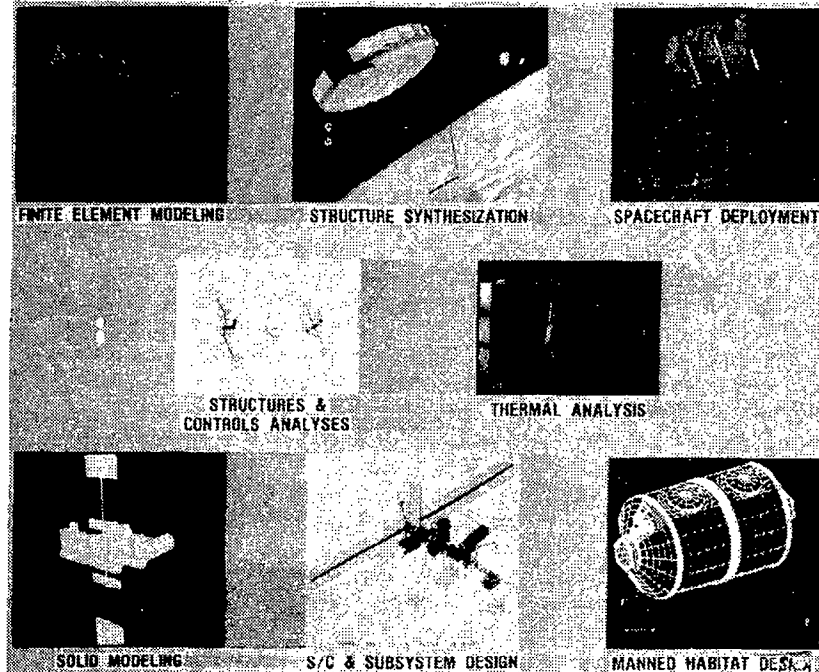
IDEAS SOFTWARE

The IDEAS technical programs are shown in figure 2. The IDEAS software currently includes all technical modules from the following design and analysis programs:

(1) Large Advanced Space Systems (LASS) computer program (refs. 1-3) which emphasizes structural, thermal and controls analysis/design, and costs for large structures (11 software modules)

(2) Spacecraft Design and Cost Module (SDCM) (ref. 4) which performs subsystem design and cost analyses through data base searches and iteration (6 modules)

(3) Advanced Space Systems Analysis (ASSA) software (ref. 5) which emphasizes structural synthesizers, environmental modeling, orbital transfer and simplified RF analyses (8 modules)

(4) Space Station Conceptual Design Model (SSCDM) program (ref. 6) which sizes habitable modules and laboratory space, designs life support and related spacecraft subsystems, and computes logistic requirements (15 modules)

(5) Earth Observation Spacecraft (EOS) programs are currently under development with the emphasis on structural deployment analysis and expanded RF and orbital environmental analysis capabilities (five new and five upgraded modules)

Additional IDEAS capabilities include antenna packaging algorithms, plate and shell modules for space station, rigid body control system expansions, and extensive improvements to output graphics displays, including color. Programs are being developed to analyze the kinematics and kinetics of large structures during deployment and to accomplish space station design and operations analyses.
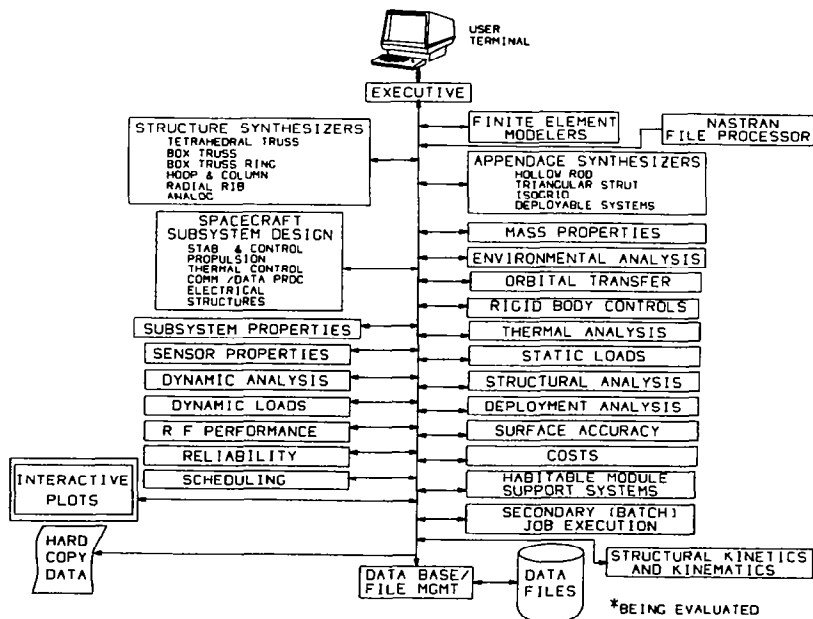
Figure 2

FINITE ELEMENT MODELING OF ANTENNA STRUCTURAL CONCEPTS

IDEAS has an automated finite-element modeling capability using mathematical synthesization to rapidly generate dishes of any size, shape, and structural density for several classes of repeating structures. The structural classes include tetrahedral and box trusses, hoop-and-column, radial-rib, and box-ring trusses as shown in figure 3. From single user inputs, which include dish diameter, number of bays, ribs or cable/mesh segments, focal length over diameter, dish structural depth, material and section properties, and hinge and mesh masses, the synthesizers rapidly create the mass and inertia properties and the finite-element model in formats compatible with subsequent design and analysis programs in the IDEAS system. IDEAS also has stand-alone finite-element modeling software for off-line model generation and digitizing hardware and software. Post-processor software can read input NASTRAN formatted files and can convert these data to IDEAS program compatible files.

Figure 3

160
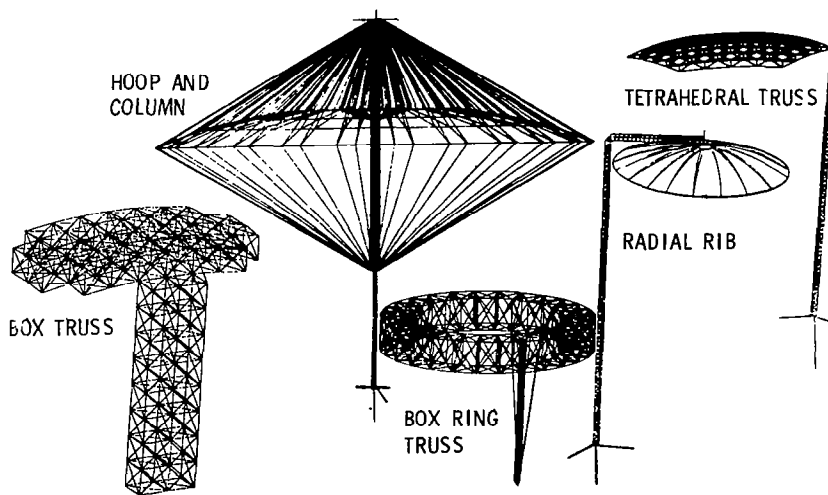
APPENDAGE SYNTHESIZERS

This program allows the user to design and add structural appendages to the dish or platform and to locate spacecraft subsystems on the structure. This process results in an updated finite-element model and mass/inertia properties for the entire spacecraft. Standard structural members include the hollow rod, a mass-efficient isogrid, a relatively stiff triangular strut, and tension cables as shown in figure 4. These members are automatically designed to user specified Euler buckling loads (or tensile loads for the pretensioned cables).

STANDARD ELEMENTS

HOLLOW TUBE   TRIANGULAR TRUSS

ISOGRID   TENSION CABLE
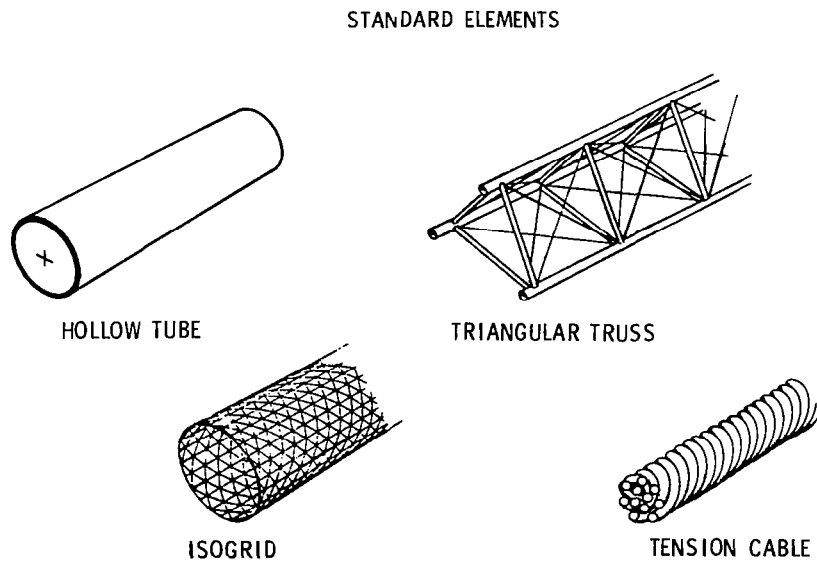
Figure 4

MODELING OF DEPLOYABLE MASTS

   Three classes of deployable structural appendages are modeled in this program as shown in figure 5. They are elastically deformable longeron masts (usually limited to about 1 m diameter), two types of triangular masts (usually limited to less than 3 m diameter based on Shuttle orbiter packaging volume constraints) and box-truss masts (which are repeating elements of the box truss dish, and can range up to 15 to 20 m in width). The triangular masts provide moderate stiffness to the overall spacecraft. The box-truss mast, which compactly folds into the Shuttle orbiter, offers a high stiffness, low flexibility potential for future space applications.
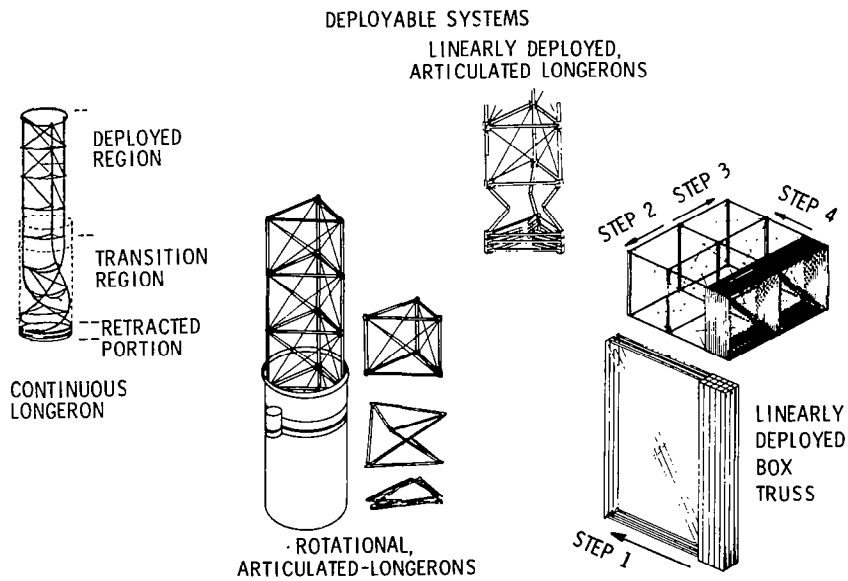
Figure 5

Limited research effort has been devoted to the important areas of deployment, kinematic, and kinetic analyses of large antenna. The spacecraft undergo large changes in center of gravity and inertia that may influence spacecraft stability and rigid body control system design. Figure 6 shows the large changes in inertia about the z-axis (along the column centerline) associated with deployment of a hoop and column antenna. Deployment times can range from less than a minute up to approximately 1 hour for the various antenna concepts. For the fast deploying structures it is critical that the kinetic behavior be fully understood. The high stress buildup in the structural members at latch-up can be the major structural design driver. Deployment-induced vibrations may also lead to undesirable dynamic behavior of the spacecraft. Futher efforts are required in these areas. Near-term plans include the extension of IDEAS capabilities to calculate inertia changes and center-of-gravity shifts for all the structural concepts and the initiation of preliminary studies in the design and characterization of the kinetic behavior of the structures and mechanisms.

MASS-2900 kg

MAST FULLY DEPLOYED HOOP STOWED
$I_x = 1.6 \times 10^6$ kg-m^2
$I_z = 3 \times 10^3$ kg-m^2

HOOP 50% DEPLOYED
$I_x = 1.7 \times 10^6$ kg-m^2
$I_z = 2.1 \times 10^5$ kg-m^2

HOOP FULLY DEPLOYED
$I_x = 2.0 \times 10^6$ kg-m^2
$I_z = 8.3 \times 10^5$ kg-m^2
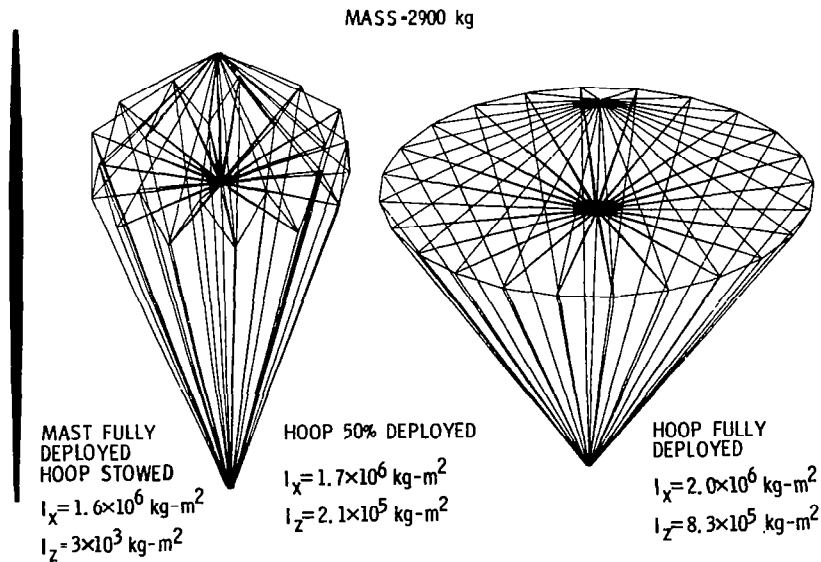
Figure 6

LAND MOBILE SATELLITE SYSTEM STUDY

The IDEAS capabilities are applied to the comparative analysis and evaluation of several large antenna concepts proposed for future Earth observation and communications missions. The spacecraft concepts can generally be classified within one of three generic structural categories: lattice truss, tension stabilized, or cantilevered beam systems. Each structure has unique characteristics that both enhance and limit its utility for missions requiring large antenna aperture. Studies (ref. 8-10) have been conducted for each separate concept; however, no one has set forth and applied a consistent set of guidelines for evaluating the designs. Even for identical missions the structural design criteria and subsystem performance requirements differ from concept to concept. Thus, it is a formidable task to rigorously compare and rank each of the competing designs without the capabilities of programs such as IDEAS.

Spacecraft designs evaluated are: hoop-and-column (tensioned-stabilized), wrapped-radial-rib (cantilevered), and tetrahedral-truss structures. A box-truss concept is introduced as an alternative concept. Finite element models of these designs are shown in figure 3. Antenna sizes range from 55 to 122 m in diameter. All are Shuttle orbiter deployed. The spacecraft concepts are analyzed and ranked using more than 20 attributes. The mission focus in this study is the land mobile satellite system communications mission.

Mass and structural analyses were conducted on each of these structural concepts (tetrahedral-truss, hoop-and-column, and radial-rib) for several design load conditions. The tetrahedral truss and radial rib are 55-m-diameter offset-fed antenna. The hoop column is a 122-m-diameter quad aperture center-fed system.

Design Load Conditions

Primary design load cases of 100 N and 20 kN on the reflector structure and the feed mast were considered. These design loads represent the maximum compressive loading that each element will support before undergoing Euler buckling (as a pinned-pinned column) and were used to size the structural elements. The 100-N case corresponds to a spacecraft designed for on-orbit operational loads only (no consideration of ground handling, launch or deployment loads). The 20-kN case represents the spacecraft in an inverted ground testing condition (1 g statically loaded), which is probably the worst orientation to which the spacecraft would be subjected. This load was determined by detaching the feed mast from the structure, inverting the feed mast and spacecraft bus and then calculating the compressive load the feed mast experiences. As a first estimation, the total mass of the UHF feed, spacecraft bus, and solar arrays were slightly less than 2000 kg with a resultant equivalent force of 20 kN. For the radial-rib concept, the reflector strongback consisted of 24 ribs with each rib divided into 6 segments and tapered by varying the design loads. For the operational loading condition, the ribs were tapered using a tip design load of 100 N and graduating linearly to a root load of 600 N. For the 1-g case, the tip load was 5000 N and the root load was 30 kN. Since the hoop-column concept is essentially a tension-compression structure, only the compression elements (the hoop and feed-mast structure) were sized by the above design loads. Tension members in the hoop column were sized so the maximum stress allowed in the member was 1.25 times the maximum tensile load any tensile element would experience.

In addition to the above design loads, industry baseline design loads for both the radial rib (ref. 8) and a hoop-column design, revised to increase torsional stability (see ref. 9 for earlier design data on the hoop column), were executed in the IDEAS program and compared with the current results.

Mass Properties

The individual dish synthesizer modules and the appendage synthesizer module of the IDEAS program are exercised interactively for each design loading case to produce a mass properties report for each case. A summary of system masses for each design load of each concept is shown in figure 7. The first number above each bar is the dish design load. The second number is the mast design load. The total mass consists of a lumped subsystem mass and the masses of the spacecraft structure, propulsion system, and UHF feed system.

The lumped subsystem and UHF feed system masses, developed in the system study of reference 10, are used in the present study. To maintain similarity

between the offset feed concepts, the masses of the radial-rib subsystems and UHF feed system are used for the tetrahedral-truss concept.

The mass of the tetrahedral-truss spacecraft was 3357 kg for the 100-N loading condition. Strengthening the feed mast for the 20-kN loading produced only a 3 percent mass increase. However, designing the reflector to the 20-kN loading condition resulted in a structural mass of 4612 kg for the tetrahedral truss, an increase of 30 percent. The mass increases are due to the increase in minimum wall thickness of the tapered tubular elements necessary to carry this compressive load before Euler buckling occurs. Truss dish packaging considerations led to the ultimate selection of 4-cm-diameter, 0.1-cm-thick tubes that are designed to carry 1000-N compressive loads. The triangular-strut mast was designed for a 60-kN column buckling load which is consistent with the load carrying capability of the radial-rib long mast.

In the radial-rib concept, the loading was varied linearly along the tapered length of the ribs. The tip-to-root loading varied from 100 N to 600 N for the low-loading condition and 5 kN to 30 kN for the high-loading conditions. Since the mass of the element is proportioned to the cube root of the loading, the rib mass increased by a factor of 3.7 for the 50-fold loading increase.

The hoop-column concept is basically a tension-stabilized system and consequently undergoes only a 33 percent increase in structural (tension cable) weight for the 20-kN loading condition.

Propellant masses required for attitude control of each concept are also noted in figure 7. (Station-keeping propellant requirements are not considered in this analysis but are estimated to be approximately 36 percent of the spacecraft total mass.) The propellant required for maintaining the spacecraft attitude is considerably less for the hoop-column concept (~75 kg) than for the other concepts because the hoop column is more nearly gravity-gradient stabilized.

Figure 7

166
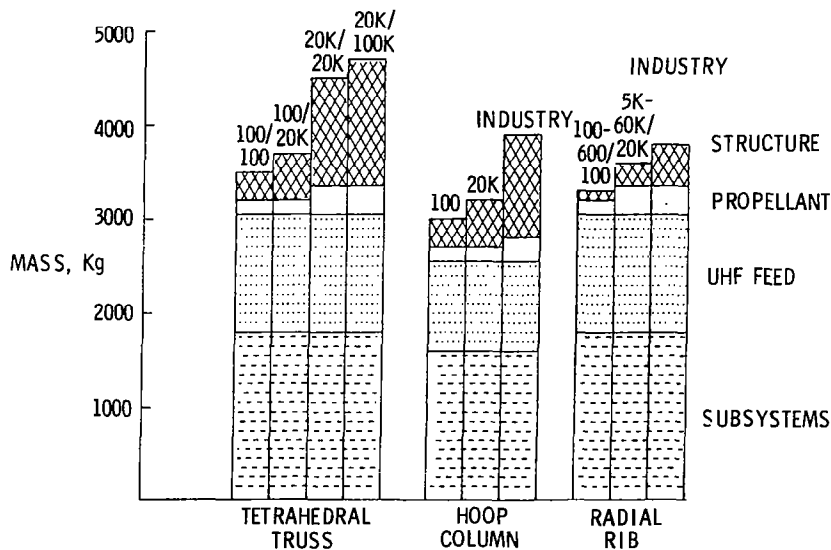
PACKAGING STUDY FOR THE TETRAHEDRAL TRUSS ANTENNA DISH

Packaging study results for the radial rib and the hoop-column antennas are in reference 10. Tetrahedral truss dish packaging data were generated in IDEAS for a wide range of structural member sizes and thickness. Packaging diameters for both inward- and outward-folding surface struts and structural mass data are shown in figure 8 for a range of design loads and structural member sizes/thickness. For the 5-m diameter 8-bay truss dish with a 2.4-m truss depth the packaging lengths are 5.4 m and 14.1 m for inward- and outward-folding struts, respectively. Noncylindrically shaped packaged spacecraft probably will be restricted to about 4.2- and 4.3-m widths in the Shuttle orbiter cargo bay as noted in the figure. Further, in order to accommodate an upper stage orbital transfer vehicle, it is estimated that the structural mass (which typically ranges from 10 to 30 percent of the total spacecraft mass) will be constrained to a range of 3000 to 5000 kg (maximum) for geosynchronous Earth orbital spacecraft. Based on these constraints, an outward-folding structure was tentatively selected with 4-cm-diameter, 0.1-cm-thick structural members designed to 1000-N compressive loads. Thinner structural members lead to large diameter tubes with large packaging volume requirements whereas the thicker tubes violate the structural mass constraints. Additional study is warranted on the tetrahedral-truss strut designs to quantify deployment loads and on packaging of the structure with mesh attached.
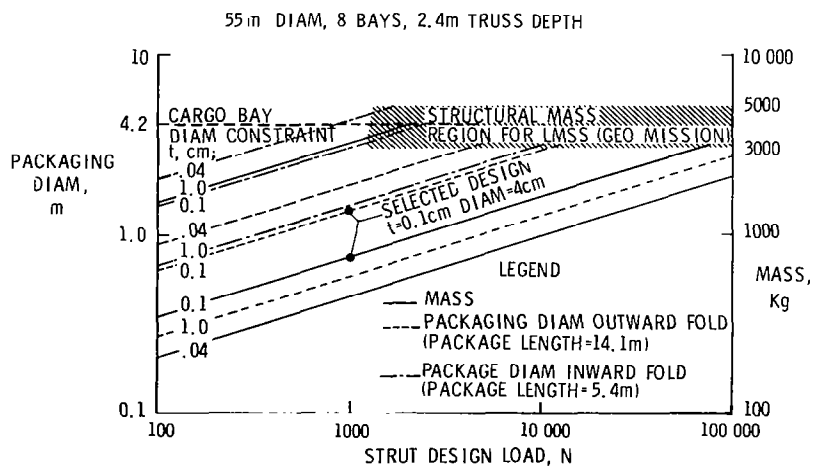
Figure 8

Summary data for each structural concept are shown in figure 9. Industry designs were used for the hoop-column and radial-rib concepts. The IDEAS generated design data were used for the tetrahedral truss antenna. The radial-rib concept is far superior to the tetrahedral truss and the hoop column in terms of structural mass and piece parts. However, the total spacecraft masses for the three concepts are reasonably close, ranging from 4100 kg for the 55-m-diameter radial rib to 4500 kg for the 122-m hoop column. Structural member types and dimensions for the main dish elements and masts are shown in the figure. The stowed configuration dimensions are noted at the top of the figure. The hoop column, even with its large diameter, stows most compactly. Radial-rib and hoop-column packaging data were from reference 10. The tetrahedral truss stowed dimensions were generated in the IDEAS program.
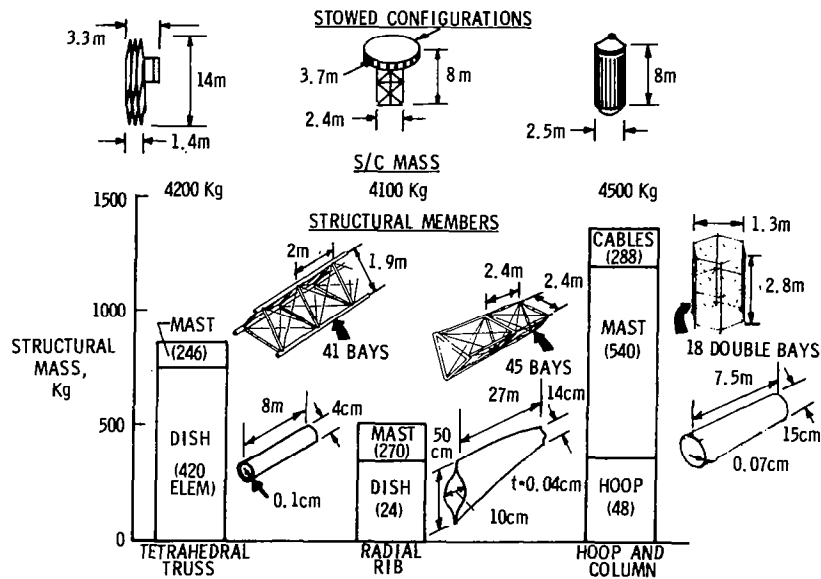
Figure 9

LMSS DYNAMICS COMPARISONS

Modal analysis data generated from several independent analyses are shown in figure 10. The first four flexible body frequencies are shown for both the dish alone and for the total spacecraft (dish, structural appendages, and subsystems) concepts. For the dish only the frequency ranges are: 0.2 to 0.3 Hz for the JPL radial-rib analysis (ref. 11), 1-3 Hz for the tetrahedral truss, and 7-15 Hz for a stiff-box truss dish. The additions of the feed beam support masts and subsystems reduce the first flexible body modes by factors of 2 or 3 for the radial rib (based on ref. 12) and for the box truss with a stiff-box truss mast. The first frequency of the tetrahedral truss with the triangular strut mast decreases by an order of magnitude below the dish-only frequency. Also noted in the figure are the frequencies for the revised (torsionally stabilized) hoop-column antenna spacecraft. The first flexible body frequencies for the hoop-column, radial-rib, and tetrahedral-truss spacecraft are all on the order of 0.1 Hz.

Low flexible body frequencies are of concern to the spacecraft designers and analysts. However, no significant on-orbit disturbances have been identified for the large antenna spacecraft under study for NASA applications (including the LMSS) that will excite the flexible body modes. There are no significant spacecraft maneuver or slew requirements for these missions. Yet, most of the masts have been designed to maximize their stiffness within the Shuttle orbiter packaging volume constraints. So, if flexible body control turns out to be a problem for the moderate frequency triangular masts, then development of a large stiff-box truss mast may be a viable alternative to the implementation of complex flexible body control system sensors and actuators. This entire area requires a more quantitative assessment of the on-orbit disturbances and their effects on the flexible body dynamics.
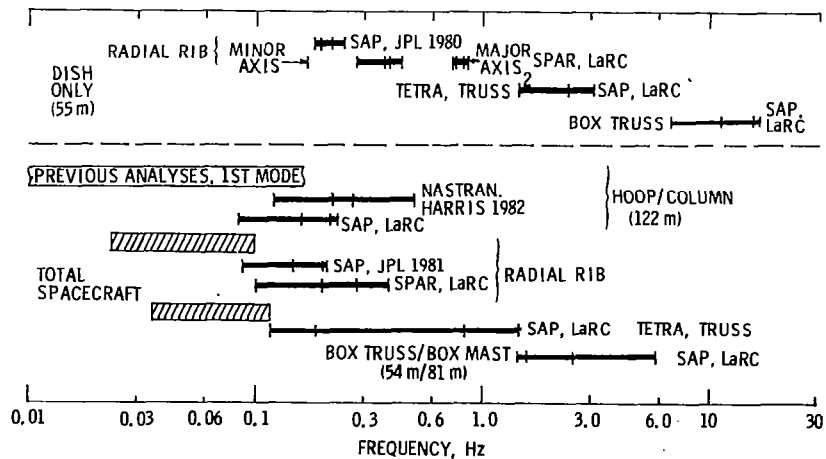

Figure 10

LMSS STATIC LOADING ANALYSES

Static structural analyses were conducted on the tetrahedral-truss, the hoop-column, and the radial-rib concepts to determine changes in surface accuracy due to the on-orbit environment or spacecraft induced (pretensioned cables) loads. These loads included gravity-gradient, thermal, and, in the case of the hoop column, pretension effects of the cables that support the hoop and form the reflector surface.

Gravity-gradient forces were calculated for each element in the model and were input into the model as nodal loads. A thermal analysis was performed at an orbital point 1.426 radians from the vernal equinox. At this point, the Sun's incident radiation is nearly parallel with the plane of the dish. Edge-heating of the reflector dish was assumed to represent a worst-case heating as well as a worst-case distortion of the reflector surface. Should this distortion be severe, considerable degradation in antenna performance would be evident.

The contour distortion plot for a 100-N design load tetrahedral truss dish is shown in figure 11. The rms surface accuracy was 0.0023 cm, well within the 1.2-cm accuracy requirements for the LMSS. The other concepts also fell within the submillimeter surface accuracy ranges from environment loading sources (see ref. 13). The hoop-column antenna surfaces are sensitive to cable pretension which, unless accurately set, can influence the surface distortions. It appears that thermal effects do not contribute to any significant distortions in the major structural members for the low CTE materials. However, no detailed thermal analyses were conducted in-house on the mesh systems which consist of 100's or 1000's of cord and cable elements in the radial-rib and hoop-column design.
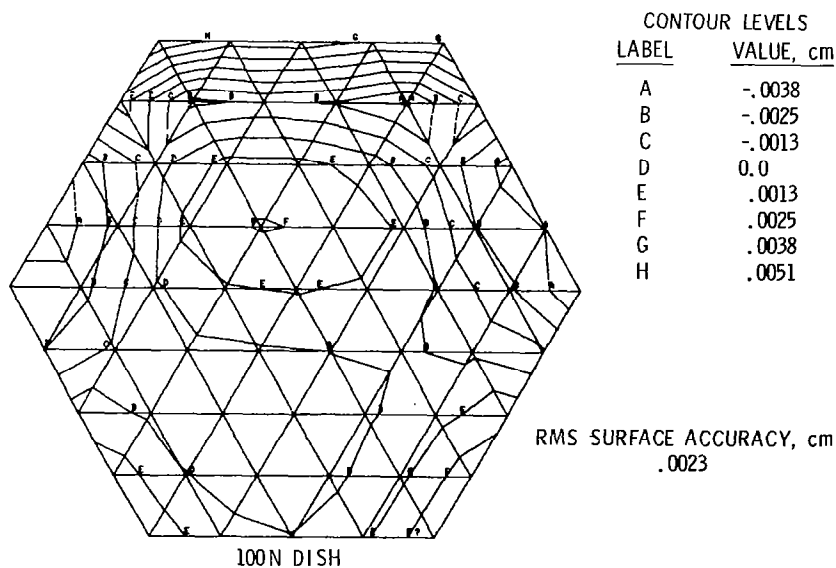
CONTOUR LEVELS

LABEL	VALUE, cm
A	-.0038
B	-.0025
C	-.0013
D	0.0
E	.0013
F	.0025
G	.0038
H	.0051

RMS SURFACE ACCURACY, cm
.0023

100N DISH

Figure 11

LMSS CONCEPTS COMPARISON

Approximately 20 attributes were used to compare the tetrahedral-truss, hoop-column, and radial-rib concepts as shown in figure 12. The list is not exhaustive and no attempt was made to weigh any of the attributes in terms of importance to mission success and reliability. However, the list should provide a mechanism for more detailed evaluation of the various concepts and hopefully will contribute to identification of critical technology development, design, and test needs. Rationales for the scores are given below.

Structural Strength: All concepts were overdesigned for on-orbit loads (typically 100 N) and when stowed in cradles for a 5-g launch. Hoop-column upper support cable tension elements retained a satisfactory factor of safety (1.25) under a 1-g deployed condition. The thin-ply, lenticular radial ribs could only support 0.5- to 0.6-g loads in a fully deployed state and thus have to be supported by overhead cables in the 1-g environment.

Structural Stiffness: The tetrahedral truss dish is considerably stiffer than the radial rib or the hoop column as shown in figure 10. The addition of the feed masts and subsystems reduces the frequencies for the concepts. If flexible-body dynamics are a problem, then the radial rib, with its first elastic mode being one of short mast twist (see ref. 12 and 13), is particularily susceptible to thruster firing disturbances that may lead to unacceptable boresight offset for a communications mission.

Subsystem Mounting Locations: Any spider joint on the tetrahedral truss strongback is a potential subsystem mounting location. Truss dish extremities provide long lever arms for thruster placements. The hoop periphery, column, and hub locations limit subsystem placement options for the hoop column. The hub and mast are the only acceptable locations for the radial rib.

ATTRIBUTE	TETRAHEDRAL TRUSS		HOOP COLUMN		RADIAL RIB	
STRUCTURAL STRENGTH						
ON ORBIT	2 }		2 }		2 }	
1-G LOAD	2 }	2	1 }	2	0 }	1
LAUNCH (STOWED)	2 }		2 }		2 }	
STRUCTURAL STIFFNESS						
DISH	2		1		1	
FEED MAST	1		1		0	
SUBSYSTEM MOUNTING LOCATIONS	2		1		0	
TENSION/COMPRESSION vs. BENDING						
STRUCTURE	2		2·		1	
UNIVERSAL APPLICABILITY OF						
STRUCTURE	2		0		0	
MULTIPURPOSE APPLICATIONS	2		0		0	
CONFIDENCE IN ANALYSIS						
STATIC	1		1		1	
DYNAMIC	1		0		0	
STABILITY/RIGIDITY OF FIGURE						
CONTROL SYSTEM	2		1		1	
PART COUNT COMPLEXITY	1		1		2	
PACKAGING VOLUME						
DISH	1		2		2	
FEED MAST	1		2		1	
FEED INTEGRATION	2		1		0	
SUCCEPTIBILITY TO MFG. TOLERANCES						
LENGTH	1		2		2	
MEMBER ROTATION	2		2		1	
DEPLOYMENT EASE	0		2		2	
IMPACT OF SINGLE MEMBER FAILURE	2		0		0	
FIGURE RESHAPING ON ORBIT	0		0		0	
TECHNOLOGICAL MATURITY	1		1		1	

LEGEND: 0- MARGINALLY MEETS REQUIREMENTS
1- MEETS REQUIREMENTS 2- EXCEEDS REQUIREMENTS

Figure 12

Compact tension/compression truss structures are inherently stronger and stiffer than cantilevered bending structures.

Universal Applicability of Structure: If antenna size requirements exceed Shuttle orbiter capabilities it is possible to assemble modular tetrahedral trusses. This modular approval does not appear feasible for hoop-column or radial-rib antenna. Further, ground test and flight experience gained from one size truss structure can be transferred more directly to other sizes for the truss than the other concepts.

Confidence in Analysis: Static analyses of the main structure can be accomplished with a reasonable level of confidence for all concepts. Dynamic modeling and analysis of the mesh type of structures (hoop-column and radial-rib) are extremely difficult because of the influence of the secondary mesh cables and cords on the overall structural dynamics.

Part Count Complexity: The radial rib has significantly fewer piece parts than the hoop column or tetrahedral truss (see fig. 9).

Packaging Volume: The hoop-column structure stows most compactly. The tetrahedral-truss dish is least attractive and requires outward-folding surface elements (which create mesh management problems) to achieve an adequate packaging in the Shuttle orbiter cargo bay (see fig. 9).

Feed Integration: Only one feed support mast is needed in the tetrahedral truss, whereas the radial rib requires both a short mast (~30 m) to attach to the hub and to clear the dish, then another long mast, about the same size and length (~85 m) as the tetrahedral-truss mast. The radial-rib masts leave only a small volume for integration of the feed. The hoop column is restricted to center-fed systems so each feed can illuminate only a portion of the full-dish aperture.

Susceptibility to Manufacturing Tolerences: High stress buildup can occur in the truss concept if dish structural member lengths are not within about 1 mm tolerence. Rotation errors in the curved lenticular ribs will distort the antenna surface of the radial-rib concept.

Deployment Ease: The motor-driven deployment systems for the radial-rib and hoop-column concepts provide more predictable, controllable deployment than the tetrahedral truss.

Impact of Single Member Failure: The tetrahedral truss has nine structural members at each node point (spider connector). Many of these members are redundant so the loss of several members is not catastrophic for the truss.

Figure Reshaping in Orbit: No figure reshaping in orbit is expected for any concept.

Technological Maturity: Each concept has about the same level of technological maturity and is judged sufficient to meet the requirements if no active flexible body control systems are required. Extended design, development, and testing will be required to flight qualify any of the concepts for the LMSS mission.

REFERENCES

1. Garrett, L. Bernard: Interactive Design and Analysis of Future Large Spacecraft Concepts. NASA TP-1937, 1981.

2. Leondis, A. F.: Large Advanced Space System (LASS) Computer Program. AIAA Paper 79-0904, May 1979.

3. Leondis, Alex: Large Advanced Space Systems Computer-Aided Design and Analysis Program. NASA CR-159191, 1980.

4. Campbell, B. H.: Spacecraft Design and Cost Model Development Final Report, Aerospace Corp. Report ATM-76(8191)-3, June 30, 1976. (See also Campbell, B. H.: Systems Cost/Performance Analysis. Aerospace Corp. Reports ATM-75(7363)-3 Vol. I-III, March 1975).

5. Farrell, C. E.; and Zimbelman, H. F.: Advanced Space Systems Analysis Software--Technical, User and Programmer Guide. NASA CR-165798, Sept. 1981.

6. Darby, H. R.; Coomer, T. N.; and Collins, F. M.: Manual for the Space Station Conceptual Design Model. General Dynamics Corp., Fort Worth, Report MR-0-243, April 1969.

7. Wilhite, A. W.; and Rehder, J. J.: AVID: A Design System for Technology Studies of Advanced Transportation Concepts. AIAA Paper 79-0872, May 1979.

8. Naderi, Firouz, (Ed.): Land Mobile Satellite Service (LMSS): A Conceptual System Design and Identification of the Critical Technologies Parts I and II. JPL Publication 82-19, Feb. 18, 1982.

9. Sullivan, Marvin R.: LSST (Hoop/Column) Maypole Antenna Development Program, Phase 1 Final Report. NASA CR-3558, Parts 1 and 2, 1982.

10. Golden, C. T.; Lackey, J. A.; and Spear, E. E.: Configuration Development of the Land Mobile Satellite System (LMSS) Spacecraft. Large Space System Technology-1981, William J. Boyer, compiler, NASA CP-2215, Part 2, 1982, pp. 711-760.

11. El-Raheb, M.: Analytical Performance Prediction for Large Antennas. Large Space System Technology-1980, Frank Kipriver III, compiler, NASA CP-2168, Vol. I, 1980, p. 334.

12. El-Raheb, M.: Analytical Performance Prediction for Large Antennas. Large Space Systems Technology-1981, William J. Boyer, compiler, NASA CP-2215, Part 2, pp. 471-478.

13. Ferebee, M. J., Jr.; Garrett, L. B.; and Farmer, J. T.: Interactive Systems Analysis of a Land Mobile Satellite System. AIAA Paper 83-0219, January 1983.

LARGE SPACE SYSTEMS AUXILIARY PROPULSION REQUIREMENTS

Joseph E. Maloy
Lewis Research Center
Cleveland, Ohio

and

William W. Smith
Boeing Aerospace Company
Seattle, Washington

INTRODUCTION

To meet the needs of a variety of civilian and military missions objectives large space systems (LSS) will become a greater percentage of our orbiting hardware. These LSS's will be transported to low Earth orbit (LEO) by the space transportation system (STS Shuttle). Concurrently, for LSS missions to orbit higher than LEO, the predominant mission scenario is that the LSS will be deployed or assembled in LEO and then transferred to a higher orbit.

In support of the LSS concepts, the Office of Aeronautics and Space Technology (OAST) has sponsored studies to determine LSS mission propulsion requirements. Since the fall of 1979, the Boeing Aerospace Company, under contract to NASA and Lewis Research Center, has been studying the disturbance forces and torques that will be experienced by LSS, and they have identified some of the associated auxiliary propulsion systems (APS) requirements. This presentation provides an insight into the results of some of the APS studies, focusing primarily on the APS requirements of single Shuttle launchable LSS's.

Several parameters were considered in determining LSS auxiliary propulsion requirements. These parameters include the following:

(1) Generic configuration
(2) Size and openness
(3) Orbit
(4) Angle of orientation
(5) Correction frequency
(6) Duty cycle
(7) Number and location of thrusters and direction of thrusters
(8) APS/LSS interactions

The following are the criteria used to determine thruster(s) location(s):

(1) Use maximum moment arm
(2) North/South and East/West stationkeeping capability
(3) Zero ΔV imparted during stationkeeping
(4) Zero torque imparted during stationkeeping
(5) Minimal heat flux and contamination from plume
(6) No thruster mounting on solar array surface or at the ends of solar arrays
(7) Minimize the number of thrusters used

The APS characteristics which are being generated for each LSS class include the following:

(1) Number and distribution of thrusters
(2) Thruster modulation
(3) Thrust level
(4) Mission energy requirements
(5) Total APS mass component breakdown
(6) State-of-the-art (SOA) adequacy/deficiency

176

CONFIGURATIONS

In an effort to determine the scope of APS requirements for LSS, a set of generic LSS's was defined. The environmental disturbance forces and torques that acted on the LSS's in LEO and GEO orbits were then determined. Specific structural configurations were defined that were representative of those most likely to serve the needs of the late 1980's and 1990's. The specific configurations are as follows:

Configuration	Example mission
Large aperture phased array antenna	Personal communications, educational television, electronic mail
Land mobile satellite system with wrap rib	Mobile communications, space-based radar, jamming satellite
Land mobile satellite system with hoop column	Mobile communications, personal communications
Geostationary platform	Science experiments
Science and applications space platform (SASP)	Platform with up to 25-kW power supply for science experiments
Space operations center (SOC)	Manned operations center which provides a location for construction, flight support, servicing, research, and testing

Each of the configurations selected fits the study ground rule of a single Shuttle launch with the exception of the SOC, which was considered to be representative of a multiple Shuttle launch LSS of the 1980's. A sketch and configuration description of each specific structural configuration studied are given in figures 1 to 6.

The antenna is a series of three thin films which are stretched within compression beams to form a ground plane, an input plane, and an output plane for a bootlace lens. The lens is contained within a compression structure supported from a deployable mast with guy wires. This structure is supported to the feed horn cluster by space-extendible beams to form an antenna with its length approximately twice its diameter. The solar arrays form two paddles to be one-axis gimballed and Sun oriented. They are sized for 65 kilowatts in LEO; the distribution conditioning and batteries are sized for 50 kilowatts at GEO. The lens portion will be closest to Earth.

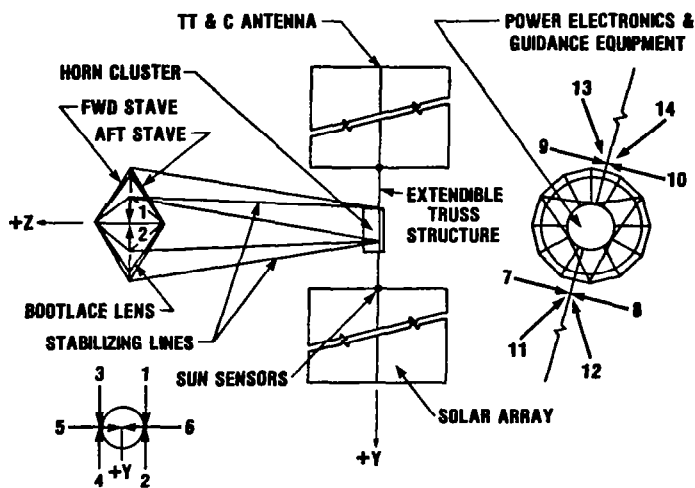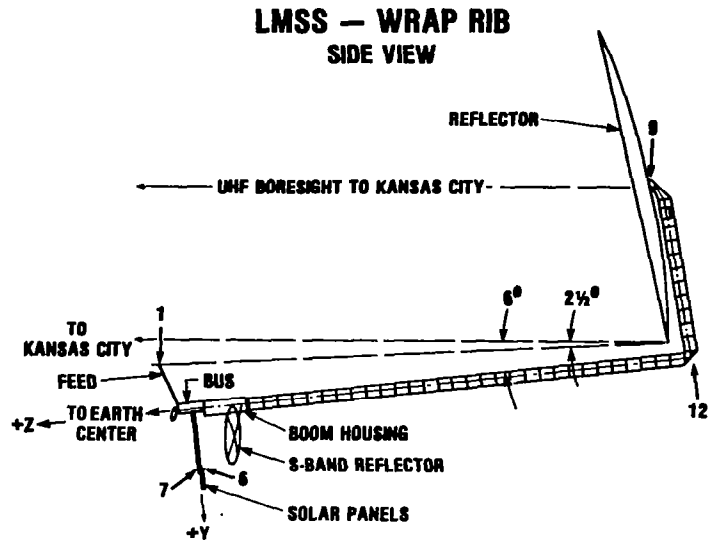## LAPAA — ELECTRONIC MAIL AND EDUCATIONAL TV

Figure 1

LAND MOBILE SATELLITE SYSTEM (LMSS) - WRAP RIB

Looking at the 55-meter offset wrap rib concept shows the long boom pointing at the Earth's center. The shorter, vertical boom at the right points to the north, supporting the antenna reflector. The large panel at the left is the ultra-high-frequency feed. It and the 55-meter-diameter wire mesh reflector are angled to point at the center of the United States near Kansas City. Multiple beams emanating from the feed panel are arranged to cover all contiguous 48 states, Alaska, Hawaii, and parts of Canada. The solar arrays are sized for 10 kilowatts.

LMSS — WRAP RIB
SIDE VIEW

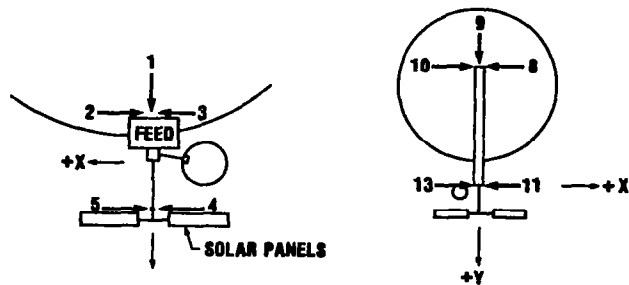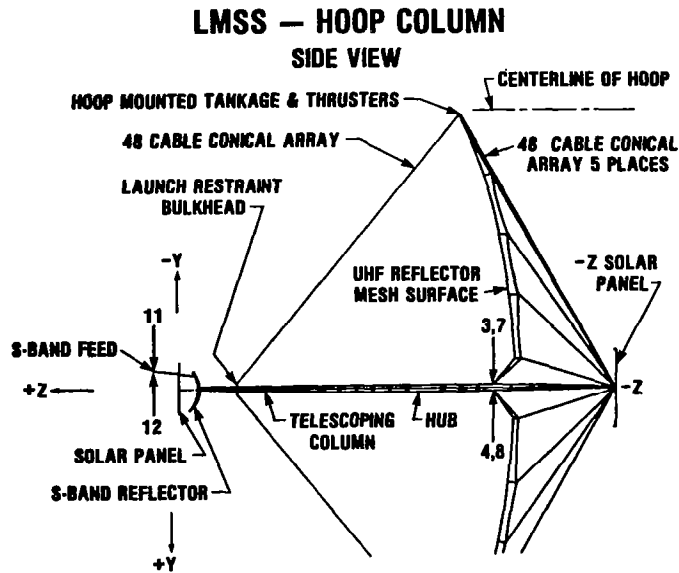REFLECTOR

UHF BORESIGHT TO KANSAS CITY

6° 2½°

TO KANSAS CITY

FEED

BUS

+Z — TO EARTH CENTER

BOOM HOUSING

S-BAND REFLECTOR

SOLAR PANELS

12

+Y

LMSS — WRAP RIB
END VIEW

FEED

+X

SOLAR PANELS

+Y

9

10 — 8

13 — 11 — +X

+Y

Figure 2

The 120-meter hoop column concept features independent power units, one at either end. The central column points at the center of the United States near Kansas City. Each of the four feed panels projects a multiple beam pattern onto its assigned quadrant on the large, molybdenum mesh reflector. There are uplink and downlink feeds for both the eastern and western halves of the country. The radio beams are arranged to cover all contiguous states, Alaska, Hawaii, and parts of Canada.
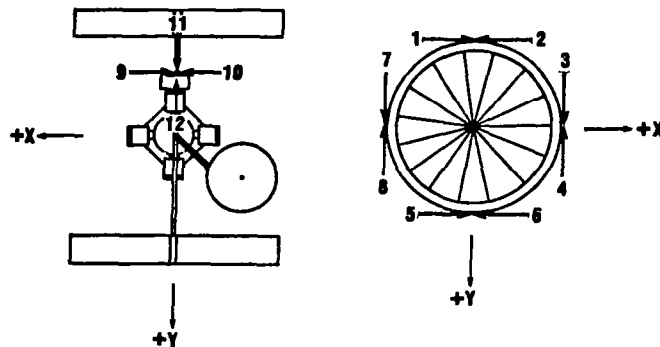
LMSS — HOOP COLUMN
SIDE VIEW

LMSS — HOOP COLUMN
END VIEW

Figure 3

The platform carries nine payloads, with the active antenna elements (feed arrays) hard-mounted to the central core and the passive (reflector) elements on a deployable structure. The wrap rib concept was used on P/L 203 and P/L 601, which also share the 15-meter antenna for their transmit operations. The 10-meter antenna is located off the East-West axis to provide an optimum location for the radiator. The solar arrays are supported by a deployable boom and are sized for 8 kilowatts. The rest of the payloads are mounted on three rigid structures. The solar arrays will be closest to Earth.

GEOSTATIONARY PLATFORM
VIEW LOOKING TOWARDS EARTH

P/L 203 - UHF TECHNOLOGY DEMONSTRATION
P/L 601 - TECHNOLOGY DEMONSTRATION (TRANSMIT, 4 GHZ)
15 M COMMON ANTENNA

22.4 M "SUNFLOWER" CONCEPT

ENVIRONMENTAL EFFECTS ON SPACE SYSTEMS

DCS

VAS

SOLAR PANELS

NORTH
+Y

RADIATOR

TECHNOLOGY DEMONSTRATION 10 M ANTENNA

LIGHTNING MAPPER

IMAGING SPECTROMETRIC OBSERVATORY

GEOSTATIONARY PLATFORM
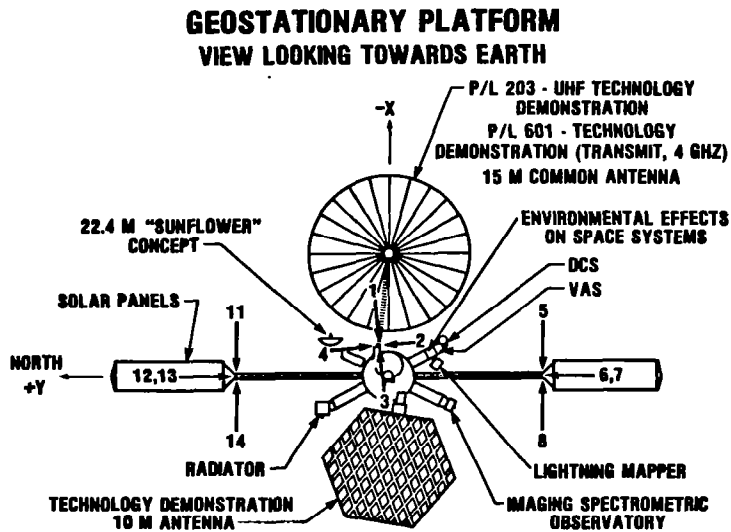
END AND SIDE VIEW

Figure 4

SCIENCE AND APPLICATIONS SPACE PLATFORM (SASP)

The first-order platform consists of three stub arms attached directly to the power system aft section. Attached to these arms are deployable, rotatable payload berthing systems to which payload elements may be connected. The deployment or rotation of the payload berthing systems will probably occur when they are being attached, and the positions will not be commandable during flight. Power system subsystems will provide payload support. The solar arrays are sized for 25 kilowatts. The vehicle orientation will be variable.
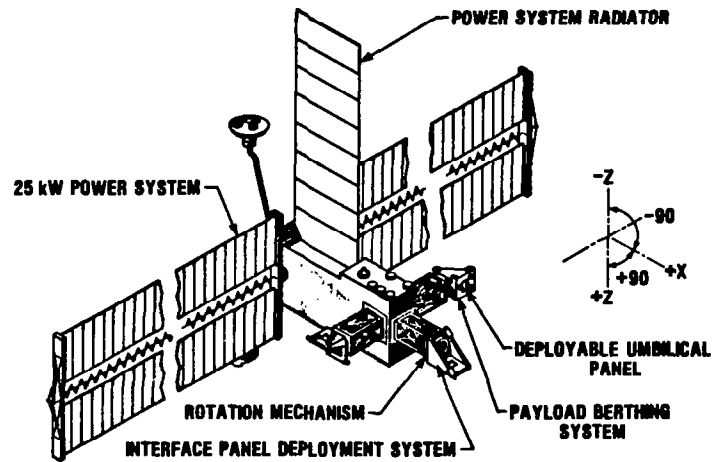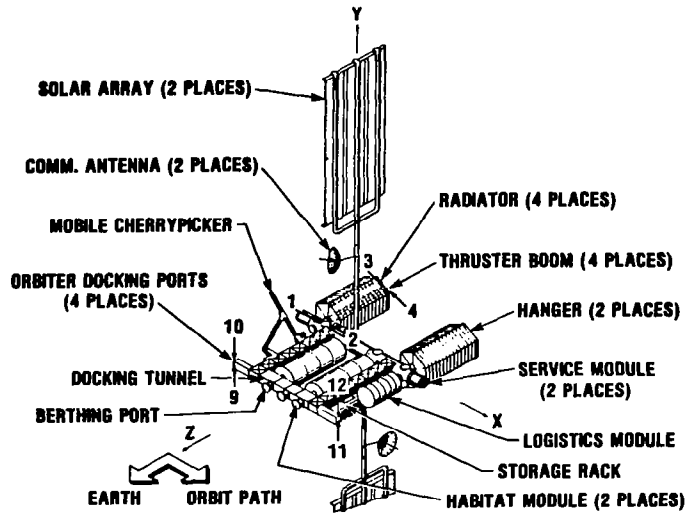
FIRST-ORDER PLATFORM CONFIGURATION

Figure 5

SPACE OPERATIONS CENTER (SOC)

The intial space operations center (SOC) configuration will essentially consist of a solar array, communication antenna, left support module, and logistics module. This configuration will support a crew of two. The operational SOC (fig. 6) will have two of each of the modules listed for the initial SOC as well as a mobile cherry picker for satellite rendevous and aquisition, two hangers, and additional docking and berthing ports. The operational configuration will support a crew of twelve.

SPACE OPERATIONS CENTER — OPERATIONAL

SOLAR ARRAY (2 PLACES)
COMM. ANTENNA (2 PLACES)
MOBILE CHERRYPICKER
ORBITER DOCKING PORTS (4 PLACES)
DOCKING TUNNEL
BERTHING PORT
EARTH   ORBIT PATH
RADIATOR (4 PLACES)
THRUSTER BOOM (4 PLACES)
HANGER (2 PLACES)
SERVICE MODULE (2 PLACES)
LOGISTICS MODULE
STORAGE RACK
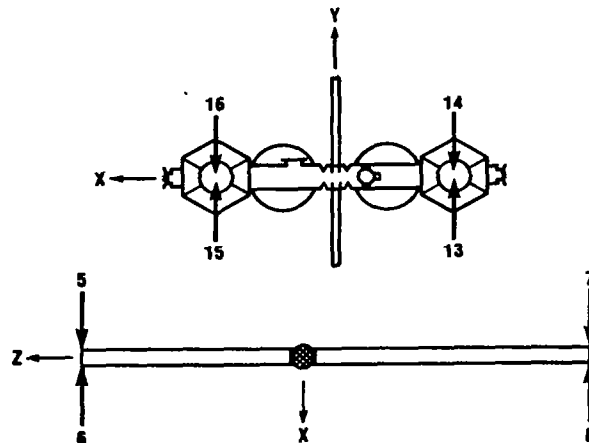HABITAT MODULE (2 PLACES)

SPACE OPERATIONS CENTER — OPERATIONAL
EDGE VIEW

Figure 6

183

For each configuration the environmental disturbance forces and
torques acting on the LSS have been determined (refs. 1 and 2). The en-
vironmental forces and torques were described using a spherical coordinate
system as shown for the SASP in figure 7. The range of environmental
forces, as a function of orientation, acting on SASP (12.5 kW) at a
300-kilometer altitude is shown in figure 8. Figure 9 shows the environ-
mental torque acting on SASP. The angles at which the sum of environ-
mental disturbance forces is greatest are 45° and 135° (fig. 8) and 210°
(fig. 7).

Tables I to III summarize the environmental disturbance torques which
must be overcome by the auxiliary propulsion system (APS) for the dif-
ferent LSS's. Nominal orientation is that in which the APS can be sized
to handle the environmental disturbance with sufficient margin to assure
control and yet not force the APS size to be unrealistic.

**SPHERICAL COORDINATE REFERENCE ANGLES FOR
MAXIMUM FORCE ON SASP (12.5 kW)**

Figure 7

FORCE UPON SASP (12.5 kW) DUE TO SUM OF
AERODYNAMIC AND RADIATION PRESSURE
300 km ALTITUDE

Figure 8

TORQUE UPON SASP
(12.5 kW) DUE TO SUM OF AERODYNAMIC
AND RADIATION AND GRAVITY GRADIENT TORQUE
300 km ALTITUDE

Figure 9

185
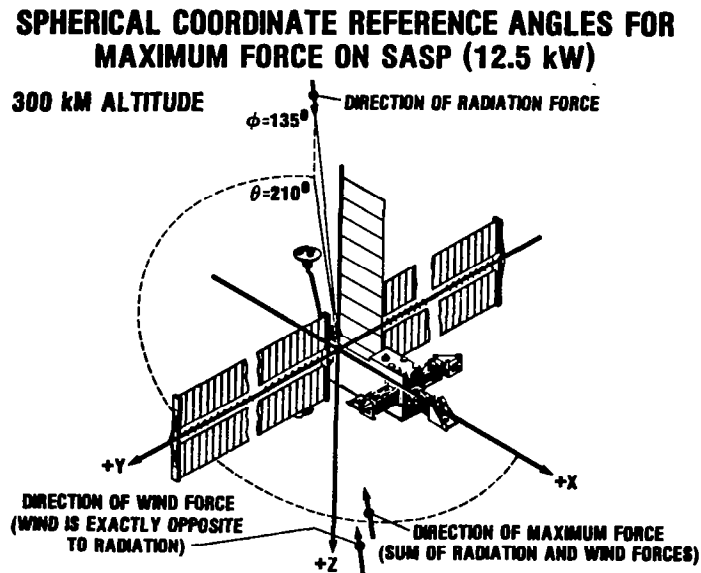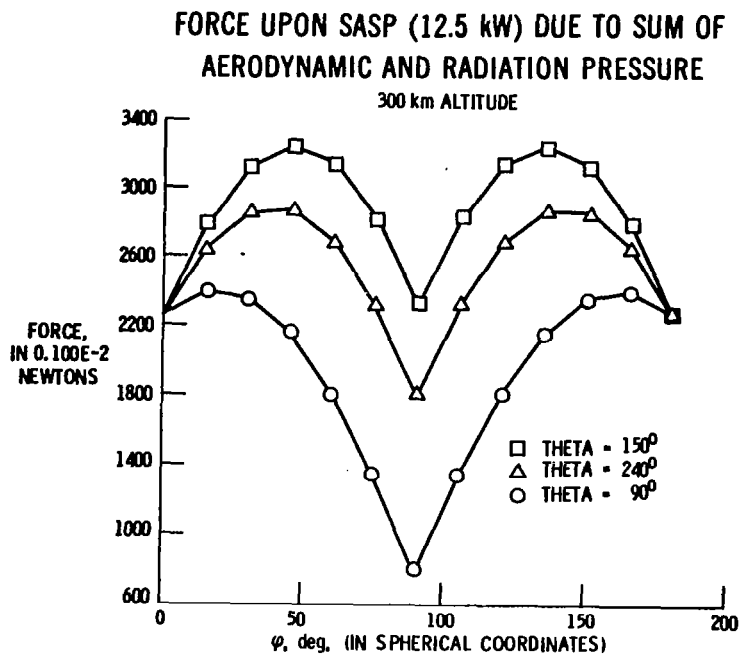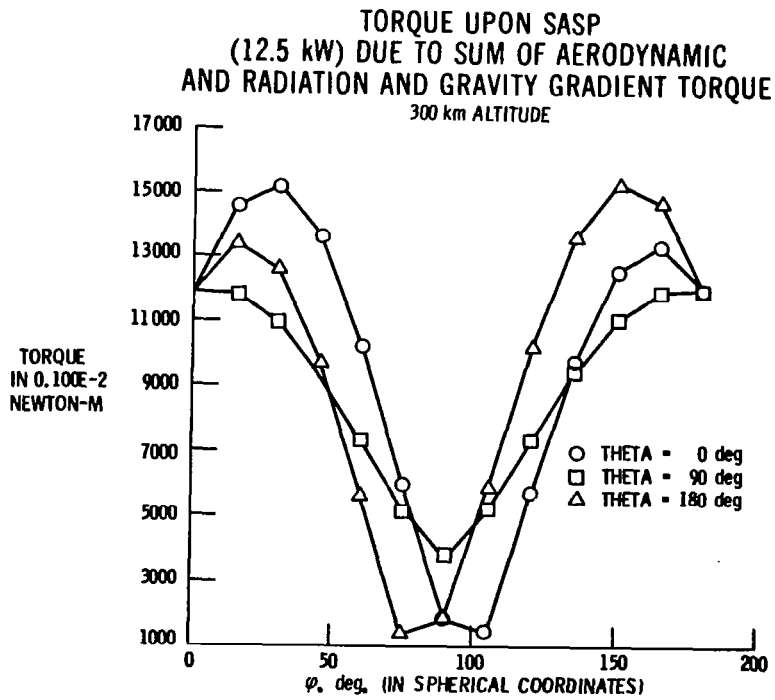
TABLE I. - LEO NOMINAL DISTURBANCE TORQUES

LSS	300 km				400 km				500 km			
	TX	TY	TZ	RSS	TX	TY	TZ	RSS	TX	TY	TZ	RSS
LAPAA 13 kw ELM												
g-load = .06	.2405	-.1201E+1	.8812E-3	.1221E+1	.9231E-1	-.3251	.8428E-3	.3366	.5772E-1	-.1276	.8065E-3	.1394
g-load = .15	-.5679	.0346E+1	.9072E-3	.3046E+1	-.1796	.7392	.8677E-3	.5464	.9336E-1	.2251	.8304E-3	.2317
g-load = 1.0	-.1560	.7253E+1	.1184E-2	.7255E+1	-.5049	.1909E+1	.1133E-2	.1924E+1	.2736	.7084	.1084E-2	.7391
LAPAA 65 kw ETV												
g-load = .06	.7476	.4891E+1	.1323E-1	.4891E+1	-.1973	.1187E+1	.1265E-1	.1187E+1	-.6281E-1	.3583	.3583	.3583
g-load = .15	.2043E+1	-.1113E+2	.1362E-1	.1122E+2	.5044	-.2717E+1	-.1303E-1	.2747E+1	.1602	-.8697	-.8697	.8795
g-load = 1.0	-.3460E+1	.1883E+2	.1744E-1	.1883E+2	-.9756	.4569E+1	.1668E-1	.4574E+1	-.4146	.1480E+1	.1480E+1	.1460E+1
Wrap Rib 55 m												
g-load = .06	.1385E+2	.4821E+2	-.1699E+2	.5198E+2	.5762E+1	.1280E+2	-.4411E+1	.1385E+2	.3848E+1	.4830E+1	.4830E+1	.5900E+1
g-load = .15	.1122E+2	.4724E+2	-.1600E+2	.5069E+2	.3454E+1	.1297E+2	-.3929E+1	.1374E+2	-.2106E+1	.5237E+1	.5237E+1	.5689E+1
g-load = 1.0	.1709E+2	.4123E+2	-.1338E+2	.4419E+2	.1037E+2	.1250E+2	-.4074E+1	.1549E+2	.8619E+1	.5964E+1	.5964E+1	.1002E+2
Hoop/Column 120 m												
g-load = .06	-.1200E+2	.6379E+2	.2670E-2	.6466E+2	-.3841E+1	.1650E+2	.1243E-2	.1687E+2	.2041E+1	.5886E+1	.8976E-3	.6176E+1
g-load = .15	-.1124E+2	.5939E+2	.2670E-2	.6022E+2	-.3690E+1	.1547E+2	.1243E-2	.1583E+2	.2032E+1	.5607E+1	.8976E-3	.5907E+1
g-load = 1.0	-.6192E+1	.2952E+2	.2670E-2	.3009E+2	.2857E+1	.8560E+1	.1242E-2	.8968E+1	.2086E+1	.3815E+1	.8974E-3	.4314E+1
Geostationary Plt.												
g-load = .06	-.6675	.3567E+1	.1235E+1	.3755E+1	-.1629	.9143	.3078	.9553	-.4499E-1	.3192	.1003	.3284
g-load = .15	-.6564	.3491E+1	.1226E+1	.3680E+1	-.1623	.8973	.3055	.9386	-.5158E-1	.3153	.9948E-1	.3247
g-load = 1.0	-.5679	.2923E+1	.1151E+1	.3116E+1	-.1448	.7858	.2904	.8261	-.5484E-1	.3048	.9749E-1	.3132
SASP - 12.5 kw	.3256	-.4826E+1	.2990E+1	.5172E+1	.8573E-1	-.1158E+1	.7199	.1244E+1	.3181E-1	-.3377	.2126	.3664
SASP - 25 kw	.4328	-.9933E+1	.5765E+1	.9933E+1	-.1042	-.2408E+1	.1395E+1	.2408E+1	-.3069E-1	-.7250	.4180	.7250
SOC - Initial	.3056E+2	.1448E+2	.1519E+3	.1522E+2	-.7563E+1	.3920E+1	.3696E+2	.3700E+2	-.2592E+1	.9344	.1127E+2	.1127E+2
SOC - Operational	-.1015E+2	.4065E+2	.6249	.4189E+2	.4097E+1	.1035E+2	.5110	.1111E+2	.2763E+1	.3563E+1	.4698	.4451E+1

TABLE II. - LEO WORST CASE DISTURBANCE TORQUES

LSS	300 km				400 km				500 km			
	TX	TY	TZ	RSS	TX	TY	TZ	RSS	TX	TY	TZ	RSS
LAPAA 13 kw ELM												
g-load = .06	.3479E+1	-.3174E+1	.1484E-1	.3480E+1	.9429	-.8811	.1419E-1	.9434	.3727	.3635	.1358E-1	.3738
g-load = .15	.2807E+1	.3046E+1	.1528E-1	.3052E+1	-.8153	.7392	.1461E-1	.8153	-.3647	-.2666	.1398E-1	.3647
g-load = 1.0	.4206E+1	-.7251E+1	.1994E-1	.7252E+1	-.1384E+1	.1982E+1	.1907E-1	.1982E+1	-.7681	.9158	.1825E-1	.9158
LAPAA 65 kw ETV												
g-load = .06	.1452E+2	.1406E+2	.2227	.1454E+2	.3526E+1	.3546E+1	.2130	.3601E+1	.1068E+1	.1190E+1	.2038	.1197E+1
g-load = .15	-.1403E+2	.1683E+2	.2294	.1691E+2	.3423E+1	.4265E+1	.2194	.4282E+1	-.1052E+1	.1449E+1	.2100	.1452E+1
g-load = 1.0	-.9524E+1	.1883E+2	.2937	.1884E+2	.2624E+1	.4592E+1	.2808	.4609E+1	-.1093E+1	.1497E+1	.2688	.1518E+1
Wrap Rib 55 m												
g-load = .06	-.5531E+2	.5301E+2	.1790E+2	.6328E+2	-.1602E+2	.1561E+2	-.5031E+1	.1769E+2	-.7418E+1	.7364E+1	.2207E+1	.7880E+1
g-load = .15	-.5409E+2	.5224E+2	.1902E+2	.6305E+2	-.1635E+2	.1597E+2	.6560E+1	.1905E+2	-.7770E+1	.7870E+1	.3695E+1	.9325E+1
g-load = 1.0	-.4203E+2	.4664E+2	-.1424E+2	.5000E+2	.1717E+2	.1803E+2	-.5600E+1	.1908E+2	.1183E+2	.1175E+2	.3805E+1	.1241E+2
Hoop/Column 120 m												
g-load = .06	.1008E+3	-.1008E+3	.1921E-1	.1069E+3	.2745E+2	-.2744E+2	-.1575E-1	.2890E+2	.1093E+2	-.1091E+2	-.1453E-2	.1135E+2
g-load = .15	.9494E+2	-.9493E+2	.1921E-1	.1006E+3	.2614E+2	-.2613E+2	-.1575E-1	.2746E+2	.1063E+2	-.1061E+2	-.1453E-1	.1101E+2
g-load = 1.0	.5554E+2	.5552E+2	.1920E-1	.5767E+2	.1760E+2	.1758E+2	-.1575E-1	.1811E+2	.8963E+1	-.8949E+1	-.1453E-1	.9089E+1
Geostationary Plt.												
g-load = .06	.5784E+1	.8242E+1	.3702E+1	.8670E+1	.1404E+1	.2135E+1	.1018E+1	.2222E+1	.4257	.7640	.4216	.7831
g-load = .15	.5725E+1	.8157E+1	.3671E+1	.8581E+1	.1396E+1	.2118E+1	.1009E+1	.2204E+1	.4285	.7632	.4173	.7815
g-load = 1.0	.5269E+1	.7533E+1	.3476E+1	.7901E+1	.1311E+1	.2033E+1	.1006E+1	.2105E+1	.4266	.8022	.4582	.8163
SASP - 12.5 kw	.4057E+1	.1760E+2	.1031E+2	.1760E+2	.9846	.4297E+1	.2552E+1	.4297E+1	.2977	.1322E+1	.8153	.1322E+1
SASP - 25 kw	.1687E+2	-.3079E+2	.1868E+2	.3079E+2	-.4094E+1	-.7465E+1	-.4520E+1	.7465E+1	-.1238E+1	-.2251E+1	-.1354E+1	.2251E+1
SOC - Initial	-.7678E+2	-.2807E+2	.1525E+3	.1529E+3	-.1902E+2	-.7590E+1	.3757E+2	.3765E+2	-.6091E+1	-.2978E+1	.1186E+1	.1188E+2
SOC - Operational	.5969E+2	.4725E+2	.1004E+2	.6561E+2	.1743E+2	.1199E+2	.8056E+1	.1956E+2	.9193E+1	.4104E+1	.7415E+1	.1006E+2

TABLE III. – GEO NOMINAL AND WORST CASE DISTURBANCE TORQUES

LSS	Nominal ± 10°				Worst case			
	TX	TY	TZ	RSS	TX	TY	TZ	RSS
Electronic Mail								
g-load = .06	.3472E-3	-.5072E-3	.3501E-5	.5692E-3	.1638E-2	-.1250E-2	.5895E-4	.1638E-2
g-load = .15	.3285E-3	.3785E-2	.3604E-5	.3658E-2	-.1563E-2	-.3784E-2	.6069E-4	.3848E-2
g-load = 1.0	.1052E-2	.9290E-2	.4706E-5	.9308E-2	.3083E-2	.9391E-2	.7923E-4	.9407E-2
Educational TV								
g-load = .06	-.1104E-3	.6020E-2	.5255E-4	.6020E-2	.3719E-2	.6020E-2	.8847E-3	.6020E-2
g-load = .15	.5289E-3	.8914E-2	.5413E-4	.8915E-2	-.3654E-2	.9463E-2	.9114E-3	.9403E-2
g-load = 1.0	.1411E-2	.2346E-1	.6929E-4	.2346E-1	.4074E-2	.2344E-1	.1167E-2	.2347E-1
LMSS - Wrap Rib								
g-load = .06	.1736E-1	.5225E-1	-.1910E-1	.5636E-1	.4949E-1	.5522E-1	-1.956E-1	.5875E-1
g-load = .15	-.9601E-2	.5359E-1	-.1735E-1	.5646E-1	-.5063E-1	.5786E-1	.2800E-1	.6286E-1
g-load = 1.0	.3753E-1	.5331E-1	-.1870E-1	.6467E-1	.6217E-1	.6828E-1	-.2327E-1	.7222E-1
LMSS - Hoop Column								
g-load = .05	.9266E-2	.4731E-1	.3675E-5	.4800E-1	.5646E-1	.5641E-1	.6268E-4	.5651E-1
g-load = .15	.9181E-2	.4413E-1	-.3675E-5	.4487E-1	.5380E-1	.5375E-1	.6268E-4	.5385E-1
g-load = 1.0	.9092E-2	.2288E-1	.3674E-5	.2448E-1	.3883E-1	-.3376E-1	.6266E-4	.3885E-1
Geostationary Plt.								
g-load = .06	-.3608E-3	.2678E-2	.1095E-2	.2852E-2	.4544E-2	.7450E-2	.2255E-2	.7469E-2
g-load = .15	-.3675E-3	.2614E-2	.1090E-2	.2792E-2	.4519E-2	.7413E-2	.2231E-2	.7432E-2
g-load = 1.0	-.3803E-3	.2208E-2	.1065E-2	.2398E-2	.4284E-2	.7207E-2	.2372E-2	.7223E-2
SASP - 12.5 kw	-.2200E-3	-.3698E-2	.6508E-3	.3731E-2	.4994E-2	.1718E-1	-.3215E-2	.1718E-1
SASP - 25 kw	-.9796E-3	-.8539E-2	.1242E-2	.8539E-2	.2076E-1	-.302E-1	.4862E-2	.3025E-1
SOC - Initial	-.9271E-2	.1260E-1	.1873	.1876	-.5173E-1	-.1875E-1	.1899	.1903
SOC - Operational	.1392E-1	.4175E-1	.2221E-2	.4373E-1	.7658E-1	.4173E-1	.3402E-1	.7746E-1

LOW ORBIT IMPACT

Preliminary calculations show that it may be unreasonable to maintain some LSS's in very low orbits (300 km). Figure 10 shows that to maintain the 12.5-kilowatt SASP in orbit would require excessive propulsion requirements. Since at a LEO of 500 kilometers the disturbance torques are a magnitude less than those at 300 kilometers (as can be seen from tables I and II), the propulsion requirements are eased.
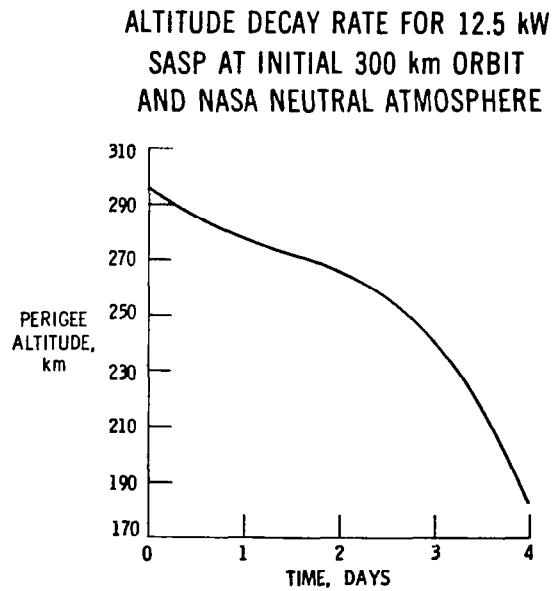
ALTITUDE DECAY RATE FOR 12.5 kW
SASP AT INITIAL 300 km ORBIT
AND NASA NEUTRAL ATMOSPHERE

Figure 10

THRUST REQUIREMENTS AND THRUSTER LOCATION

Once the disturbance forces and torques acting on the LSS were determined, the required thrust levels could be established. Station-keeping thrust level requirements were determined as a function of duty cycle (ratio of thrust on time per orbit to orbit time), frequency of correction (number of orbits between correction), and the disturbance force and torques. Table IV presents the total thrust requirements for each LSS to overcome the environmental forces and torques in GEO as a function of correction frequency and duty cycle.

From the total thrust requirements the thrust per thruster requirements can be determined. Thruster location on a LSS establishes the momentum arm which in turn impacts the required thrust per thruster. In sizing an APS a trade must be made between thruster location and the thrust per thruster. A maximum of four thrusters was used for any one operation. Consequently, an overdetermined set of equations (i.e., 6 equations, 4 unknowns) results for all calculations. The unknowns were solved using a pseudo-inverse operation:

$$AX = B$$

$$X = (A^T A)^{-1} A^T B$$

where A is the N_{xm} matrix of direction cosine/moment arm coefficients (N > M), X is the thrust requirement vector of order M, and B is the solution matrix of order N.

TABLE IV. – THRUST REQUIREMENTS FOR GEOSYNCHRONOUS STATIONKEEPING*

Correction frequency	Once per orbit				Once per week			
Duty cycle	0.01		0.4		0.01		0.4	
Perturbing forces	N/S	E/W(SP2)**	N/S	E/W(SP2)**	N/S	E/W(SP2)**	N/S	E/W(SP2)**
LSS								
Electronic Mail								
g-load = .06	0.173	0.0325	0.0046	0.87E-3	1.21	0.0325	0.0324	0.87E-3
g-load = .15	.189	.0355	.0051	.95E-3	1.32	.0355	.0354	.95E-3
g-load = 1.0	.420	.0788	.0112	.0021	2.94	.0788	.0785	.0021
Educational TV								
g-load = .06	.470	.0883	.0126	.0024	3.29	.0883	.0880	.0024
g-load = .15	.488	.0917	.0131	.0025	3.42	.0917	.0914	.0025
g-load = 1.0	.739	.139	.0198	.0037	5.17	.139	.138	.0037
LMSS Wrap Rib								
g-load = .06	.424	.0796	.0113	.0021	2.97	.0796	.0794	.0021
g-load = .15	.445	.0834	.0119	.0022	3.11	.0834	.0832	.0022
g-load = 1.0	.637	.120	.0170	.0032	4.46	.120	.119	.0032
LMSS Hoop Column								
g-load = .06	.403	.0757	.0108	.0020	2.82	.0757	.0754	.0020
g-load = .15	.426	.0799	.0114	.0021	2.98	.0799	.0796	.0021
g-load = 1.0	.731	.137	.0195	.0037	5.11	.137	.137	.0037
Geostationary Plt.								
g-load = .06	.545	.102	.0146	.0027	3.82	.102	.102	.0027
g-load = .15	.547	.103	.0146	.0027	3.83	.103	.102	.0027
g-load = 1.0	.578	.108	.0154	.0029	4.04	.108	.108	.0029

*Thrust (N), correction lasting one orbit.

**For solar pressure ΔV calculations, correction frequency is set by maximum allowed error of 0.1°.

ACCELERATION EFFECT

The g-loading characteristic of a LSS must also be considered when determining thruster size and location. LSS structures have critical components (e.g., solar array or astromast booms) whose mass and packaging characteristics are very sensitive to changes in g-loading. The critical component's sensitivity results from its low stiffness.

For the large aperture phased array antenna, LMSS with wrap rib, LMSS with hoop column, and SASP structures, g-loading designs for the three g-levels of 0.06, 0.15, and 1.0 were determined. Finite-element models using NASTRAN were constructed for these four flexible LSS's. Figure 11 shows the effect of g-loading on the LMSS - wrap rib mass. Since the SOC and SASP are relatively rigid structures and thus can stand higher g-loading, they were not studied for g-loading effect.

During the g-loading design and dynamic interaction analysis certain mass properties were determined or assumed for each configuration. The mass properties for the LMSS with wrap rib (55-m-diam. antenna) are presented in table V.

EFFECT OF G-LOAD ON MASS
25 METER WRAP RIB

$M_0 = 2041$ kg $G_0 = .15$ G

REFLECTOR

BOOMS

SOLAR ARRAYS

FEED

HUB

BUS

MASS RATIO, M/M_0

G-LOAD RATIO, G/G_0
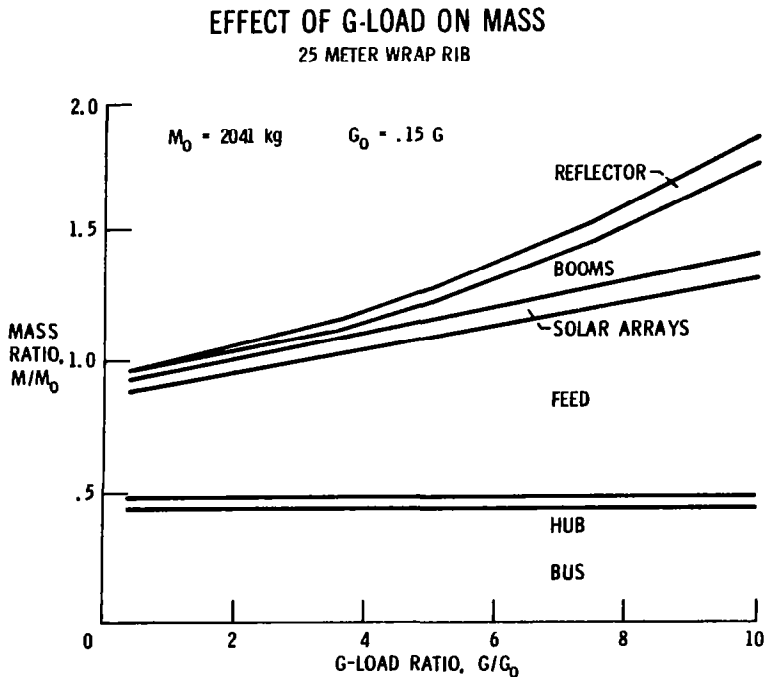
Figure 11

TABLE V. – LAND MOBILE SATELLITE SYSTEM (LMSS)

[Wrap rib, 55-m diam.]

Initial orbit	Mission orbits	Lifetime	Attitude stationkeeping and shape control tolerances
LEO	LEO (300, 400, 500 km) 5600-km polar orbit GEO (36,000 km)	10 years	Attitude control, $\pm 0.10°$ Pointing stability, $\pm 0.03°$

g-Load	Mass, kg	CG location, m		
		X	Y	Z
0.16	2897.06	-0.208	-3.823	-11.029
.15	3036.41	-.198	-4.318	-12.001
1.0	4352.52	-.138	-7.432	-18.109

g-Load	Inertias (about C_G, kg-m^2)					
	I_{XX}	I_{YY}	I_{ZZ}	$-I_{XY}$	$-I_{XZ}$	$-I_{YZ}$
0.06	2,437,290	2,223,871	275,508	4961	4032	-559,971
.15	2,781,766	2,523,995	345,003	5259	4617	-668,662
1.0	5,798,378	5,170,587	952,443	7133	8293	-1,599,345

g-Load	C_p (origin at C_G, m)								
	Plane XY			Plane XZ			Plane YZ		
	X	Y	Z	X	Y	Z	X	Y	Z
0.06	0.097	-6.380	-20.278	-0.216	-3.798	-19.263	0.0267	-19.680	-51.452
.15	.087	-5.885	-19.306	-.226	-3.303	-18.292	.0167	-19.185	-50.481
1.0	.027	-2.771	-13.198	-.285	-.189	-12.184	-.0433	-16.071	-44.373

g-Load	Area, m^2			Area/mass		
	XY	XZ	YZ	XY	XZ	YZ
0.06	270.703	206.770	99.825	0.093441	0.071372	0.034457
.15	270.703	206.770	99.825	.089152	.089152	.032876
1.0	270.703	206.770	99.825	.062195	.047506	.022935

For each LSS configuration studied, the optimum thruster locations, direction cosines for each thruster, and thrust per thruster were determined. Figures 1 to 6 show the optimum thruster locations for each LSS configuration (heavy arrows). Table VI presents the coordinates of thruster locations for the LMSS with wrap rib. Tables VII to X summarize the stationkeeping thrust per thruster requirements for the LMSS with wrap rib. Tables XI to XIII summarize the environmental disturbance torque thrust per thruster requirements for the LMSS with wrap rib. Similar results (table of thrust per thruster) have been obtained for the other five LSS configurations studied.

TABLE VI. - LAND MOBILE SATELLITE SYSTEM WRAP RIB

THRUSTER LOCATIONS

Thruster	Location, m			Direction		
	X	Y	Z	X	Y	Z
1	-0.119	-7.790	5.530	0.000	1.000	0.000
2	-1.000	-7.790	5.530	-1.000	.000	
3	1.000	-7.790	5.530	1.000		
4	-.119	11.100	.000	-1.000		
5				1.000		
6				.000	-.707	.707
7				.000	-.707	-.707
8	1.000	-29.960	-75.410	-1.000	.000	.000
9	-.119	-29.960	-75.410	.000	1.000	
10	-1.000	-29.960	-75.410	1.000	.000	
11	1.000	.000	-82.450	-1.000	.000	
12	-.119	.000	-82.450	.000	-1.000	
13	-1.000	.000	-82.450	1.000	.000	

194

TABLE VII. - LEO STATIONKEEPING THRUST/THRUSTER

REQUIREMENTS (N) AT 400 km FOR LMSS WRAP RIB

AT g-LOAD = 0.15

Thruster	Thrusting time, hr		
	0.5	5	100
1	0.000E+00	0.000E+00	0.000E+00
2	.812E+01	.727E+00	.352E-01
3	.812E+01	.727E+00	.352E-01
4	.328E+01	.294E+00	.142E-01
5	.328E+01	.294E+00	.142E-01
6	.000E+00	.000E+00	.000E+00
7	.000E+00	.000E+00	.000E+00
8	.134E+01	.120E+00	.581E-02
9	.000E+00	.000E+00	.000E+00
10	.134E+01	.120E+00	.581E-02
11	.134E+01	.120E+00	.581E-02
12	.000E+00	.000E+00	.000E+00
13	.134E+01	.120E+00	.581E-02

TABLE VIII. - GEO STATIONKEEPING THRUST/THRUSTER

REQUIREMENTS (N) FOR LMSS WRAP RIB

AT g-LOAD = 0.06

Thruster	Correction frequency			
	Once/week		Once/day	
	Duty cycle			
	0.01	0.4	0.01	0.4
1	0.232E+01	0.649E-01	0.331E+00	0.882E-02
2	.459E-01	.127E-02	.459E-01	.121E-02
3	.459E-01	.127E-02	.459E-01	.121E-02
4	.185E-01	.513E-03	.185E-01	.489E-03
5	.185E-01	.513E-03	.185E-01	.458E-03
6	.179E+01	.501E-01	.255E+00	.680E-02
7	.179E+01	.501E-01	.255E+00	.680E-02
8	.759E-02	.210E-03	.759E-02	.200E-03
9	.634E+00	.178E-01	.905E-01	.241E-02
10	.759E-02	.210E-03	.759E-02	.200E-03
11	.759E-02	.210E-03	.759E-02	.200E-03
12	.425E+00	.119E-01	.606E-01	.162E-02
13	.759E-02	.210E-03	.759E-02	.200E-03

TABLE IX. - GEO STATIONKEEPING THRUST/THRUSTER

REQUIREMENTS (N) FOR LMSS WRAP RIB

AT g-LOAD = 0.15

Thruster	Correction frequency			
	Once/week		Once/day	
	Duty cycle			
	0.01	0.4	0.01	0.4
1	0.243E+01	0.649E-01	0.347E+00	0.929E-02
2	.481E-01	.127E-02	.481E-01	.127E-02
3	.481E-01	.127E-02	.481E-01	.127E-02
4	.194E-01	.513E-03	.194E-01	.513E-03
5	.194E-01	.513E-03	.194E-01	.513E-03
6	.187E+01	.501E-01	.268E+00	.716E-02
7	.187E+01	.501E-01	.268E+00	.716E-02
8	.795E-02	.210E-03	.795E-02	.210E-03
9	.664E+00	.178E-01	.950E-01	.254E-02
10	.795E-02	.210E-03	.795E-02	.210E-03
11	.795E-02	.210E-03	.795E-02	.210E-03
12	.445E+00	.119E-01	.636E-01	.170E-02
13	.795E-02	.210E-03	.795E-02	.210E-03

TABLE X. - GEO STATIONKEEPING THRUST/THRUSTER

REQUIREMENTS (N) FOR LMSS WRAP RIB

AT g-LOAD = 1.0

Thruster	Correction frequency			
	Once/week		Once/day	
	Duty cycle			
	0.01	0.4	0.01	0.4
1	0.348E+01	0.929E-01	0.497E+00	0.133E-01
2	.692E-01	.184E-02	.692E-01	.184E-02
3	.692E-01	.184E-02	.692E-01	.184E-02
4	.280E-01	.745E-03	.280E-01	.745E-03
5	.280E-01	.745E-03	.280E-01	.745E-03
6	.268E+01	.716E-01	.383E+00	.102E-01
7	.268E+01	.716E-01	.383E+00	.102E-01
8	.114E-01	.305E-03	.114E-01	.305E-03
9	.952E+00	.254E-01	.136E-00	.363E-02
10	.114E-01	.305E-03	.114E-01	.305E-03
11	.114E-01	.305E-03	.114E-01	.305E-03
12	.638E+00	.170E-01	.911E-01	.243E-02
13	.114E-01	.205E-03	.114E-01	.305E-03

TABLE XI. - ENVIRONMENTAL DISTURBANCE THRUST/THRUSTER REQUIREMENTS (N)

FOR LMSS WRAP RIB AT g-LOAD = 0.06

Thruster	Disturbance torques					
	Nominal			Worst case		
	400 km	500 km	GEO	400 km	500 km	GEO
1	0.655E-01	0.437E-01	0.197E-03	0.182E+00	0.843E-01	0.563E-03
2	.125E+00	.472E-01	.511E-03	.153E+00	.720E-01	.540E-03
3	.125E+00	.472E-01	.511E-03	.153E+00	.720E-01	.540E-03
4	.924E-01	.332E-01	.400E-03	.105E+00	.462E-01	.410E-03
5	.924E-01	.332E-01	.400E-03	.105E+00	.462E-01	.410E-03
6	.540E-01	.361E-01	.163E-03	.150E+00	.696E-01	.464E-03
7	.540E-01	.361E-01	.163E-03	.150E+00	.696E-01	.464E-03
8	.924E-01	.332E-01	.400E-03	.105E+00	.462E-01	.410E-03
9	.764E-01	.510E-01	.230E-03	.212E+00	.984E-01	.656E-03
10	.924E-01	.332E-01	.400E-03	.105E+00	.462E-01	.410E-03
11	.125E+00	.472E-01	.511E-03	.153E+00	.720E-01	.540E-03
12	.655E-01	.437E-01	.197E-03	.183E+00	.843E-01	.563E-03
13	.125E+00	.472E-01	.511E-03	.153E+00	.720E-01	.540E-03

TABLE XII. - ENVIRONMENTAL DISTURBANCE THRUST/THRUSTER REQUIREMENTS (N)

FOR LMSS WRAP RIB AT g-LOAD = 0.15

Thruster	Disturbance torques					
	Nominal			Worst case		
	400 km	500 km	GEO	400 km	500 km	GEO
1	0.393E-01	0.239E-01	0.109E-03	0.188E+00	0.875E-01	0.575E-03
2	.127E+00	.512E-01	.524E-03	.156E+00	.769E-01	.566E-03
3	.127E+00	.512E-01	.524E-03	.156E+00	.769E-01	.566E-03
4	.823E-01	.259E-01	.363E-03	.137E+00	.774E-01	.587E-03
5	.823E-01	.259E-01	.363E-03	.137E+00	.774E-01	.587E-03
6	.324E-01	.198E-01	.900E-04	.155E+00	.722E-01	.475E-03
7	.324E-01	.198E-01	.900E-04	.155E+00	.722E-01	.475E-03
8	.823E-01	.259E-01	.363E-03	.137E+00	.774E-01	.587E-03
9	.458E-01	.279E-01	.127E-03	.219E+00	.102E+00	.671E-03
10	.823E-01	.259E-01	.363E-03	.137E+00	.774E-01	.587E-03
11	.127E+00	.512E-01	.524E-03	.156E+00	.769E-01	.566E-03
12	.393E-01	.239E-01	.109E-03	.188E+00	.875E-01	.575E-03
13	.127E+00	.512E-01	.524E-03	.156E+00	.769E-01	.566E-03

TABLE XIII. – ENVIRONMENTAL DISTURBANCE THRUST/THRUSTER REQUIREMENTS (N)

FOR LMSS WRAP RIB AT g–LOAD = 1.0

Thruster	Disturbance torques					
	Nominal			Worst case		
	400 km	500 km	GEO	400 km	500 km	GEO
1	0.118E+00	0.980E-01	0.427E-03	0.195E+00	0.134E+00	0.707E-03
2	.122E+00	.583E-01	.521E-03	.176E+00	.115E+00	.668E-03
3	.122E+00	.583E-01	.521E-03	.176E+00	.115E+00	.668E-03
4	.853E-01	.410E-01	.392E-03	.117E+00	.797E-01	.487E-03
5	.853E-01	.410E-01	.392E-03	.117E+00	.797E-01	.487E-03
6	.973E-01	.808E-01	.352E-03	.161E+00	.111E+00	.583E-03
7	.973E-01	.808E-01	.352E-03	.161E+00	.111E+00	.583E-03
8	.853E-01	.410E-01	.392E-03	.117E+00	.797E-01	.487E-03
9	.138E+00	.114E+00	.498E-03	.228E+00	.157E+00	.824E-03
10	.853E-01	.410E-01	.392E-03	.117E+00	.797E-01	.487E-03
11	.122E+00	.583E-01	.521E-03	.176E+00	.115E+00	.668E-03
12	.118E+00	.980E-01	.427E-03	.195E+00	.134E+00	.707E-03
13	.122E+00	.583E-01	.521E-03	.176E+00	.115E+00	.668E-03

PRELIMINARY CONCLUSIONS

With the information generated to date, the following preliminary conclusions can be stated:

1. Environmental forces and torques acting on LSS are significantly affected by orbit altitude, structural configuration and surface density. (Refer to figs. 1 to 6 and tables I to III.)

2. It may be unreasonable to maintain LSS in low orbits between 300 and 400 kilometers. (Refer to tables I to III).

3. With reasonable thrusting times, correction frequencies and duty cycles LSS thrust per thruster requirements (for most configurations at nominal orientation and orbit of 400 km and higher) can be met with state-of-the-art electric propulsion. (Refer to tables IV and VII to XIII.)

4. Study results can serve as a useful guideline for the initiation of future technology development programs in auxiliary propulsion.

5. Throttleable engines or separate sets of engines are required for zero torque stationkeeping capability with ratios as high as 10:1.

The work remaining under this study is to compare APS requirements for each LSS with state-of-the-art APS, assess areas of required technology improvement, and analyze APS/LSS structural dynamic interactions.

REFERENCES

(1) Maloy, J.E.; and Smith, W. W.: An Insight into Auxiliary Propulsion Requirements of Large Space Systems. NASA TM-82827, 1982.

(2) Smith, W.W.; and Clark, J.P.: Study of Electrical and Chemical Propulsion Systems for Auxiliary Propulsion of Large Space Systems. Vols. I and II. NASA CR-165502, 1981.

A SUMMARY OF MISSION AND SYSTEM PERFORMANCE REQUIREMENTS
FOR LARGE SPACE ANTENNAS

Lloyd S. Keafer, Jr., and W. R. Hook
NASA Langley Research Center
Hampton, Virginia

INTRODUCTION

Mission definition studies and system analyses have been described for a number of potential civilian missions and a few military missions. In this paper, an attempt is made to summarize the most formidable mission and system performance requirements for large space antennas. The emphasis will be on the civilian systems; only those aspects of military mission and system requirements that are unclassified are included.

"Requirements" as used here really means "needs." "Requirements" are associated with defined and approved missions to be conducted with a selected baseline system under specified space operational guidelines and with known constraints. But practically all of the large antenna missions are envisioned for the 1990's time frame. They are not fully and firmly defined and there are no firm commitments to implement them. Presently we are in the process of identifying what technology advances are needed to implement them. In so doing we examine numerous space operational scenarios and constraints and their associated system options. So "needs" is a better word than requirements at this stage.

The reason that missions requiring large antennas are not currently approved is related primarily to the cost of flight hardware, not to the importance of the data that could be collected or the communications that could take place or the intelligence that could be gathered if a large antenna were in space. The challenge, therefore, for the large space antenna technology community is the development of concepts and hardware that will be affordable. These mission requirements are set forth in a hope that they will provide realistic targets for such technology development.

POTENTIAL LARGE SPACE ANTENNA (LSA) MISSIONS

This table categorizes potential missions as either a communications, space science, Earth observations, or military surveillance application as noted and coded in the first two columns. Columns 3 and 4 further describe the application/sensing technique and identify the primary mission benefactors. In the following discussions the missions will be referred to by the codes given here. Reference is also made to a wide-band 30/20 GHz communications mission (C3), an Orbiting Deep Space Relay Mission (C4), an Earth observation Lidar mission and the Space Telescope (ST) mission. The designations used here are not the same as those used in the NASA mission model (ref. 1).

From this listing alone some systems implications can be stated. First, mission and technology relationships for the various civilian and military applications should be clearly defined in order to foster cooperation wherever possible, e.g., in the area of environmental monitoring where the military already has a policy of cooperation with civilian agencies. Second, cost analyses should be done for maturing missions. In the Land Mobile Satellite Service (CI) case such an analysis provided new insights and emphasized the need for affordable space systems. Another cost implication is that alternative and/or complementary systems for accomplishing the mission goals should be re-appraised periodically (e.g., active vs. passive systems and reflector vs. phased-array systems).

C1	COMMUNICATIONS	LAND MOBILE SATELLITE SERVICE	COMMERCIAL
C2	COMMUNICATIONS	BROADCAST	VOICE OF AMERICA
SS1	SPACE SCIENCE	RADIO ASTRONOMY (I.R. & SUB mm) (LARGE DEPLOYABLE REFLECTOR)	NASA
SS2	SPACE SCIENCE	RADIO ASTRONOMY (MICROWAVE) (VERY LONG BASELINE INTERFEROMETRY)	NASA
EO1	EARTH OBSERVATIONS	LAND, OCEAN, CRYOSPHERE PHENOMENOLOGY (RADIOMETRY, SCATTEROMETRY, RADAR)	NOAA, USDA COMMERCIAL, NASA
EO2	EARTH OBSERVATIONS	ENVIRONMENTAL MONITORING	MILITARY
MS1	MILITARY SURVEILLANCE	INTEGRATED TACTICAL SURVEILLANCE	MILITARY
MS2	MILITARY SURVEILLANCE	SPACE-BASED RADAR SURVEILLANCE	MILITARY

LARGE SPACE ANTENNA MISSION SCENARIO SUMMARY

A summary of requirements for NASA missions has been published previously.
This table, adapted from reference 2, gives requirements for communications, Earth
radiometry and radio astronomy missions. Updates were made in the radiometer column
for diameter and resolution, and a column has been added on the space-based radar to
indicate that military mission information should be included. But rather than
update and summarize the mission and system needs in detail, this paper highlights
key needs and special requirements in the hope that this may lead to better
understanding of the issues that should be addressed in the future by mission and
system analysts and technologists.

MISSION PARAMETER	COMMUNICATIONS				MICROWAVE RADIOMETER SYSTEM	RADIO ASTRONOMY (VLBI)	SPACE-BASED RADAR
	ADVANCED		PSS***				
FREQUENCY (GHz)	4-6	11-14	0.87	2.0	1.4	1.4-22, 30	VARIABLE
DIAMETER (M)	20	12	75	37	50-200	30	70
POINTING ACCURACY (DEGREES)	0.035	0.035	0.035	0.035	0.1	0.01	
F/D	>1	.>1	>1	>1	2	0.7	
BEAM NUMBER	219	219	108	108	200-300	1	1000 TRACKS
BEAM ANGLE (DEGREES)	0.256	0.256	0.5	0.256	0.06	FREQUENCY DEPENDENT	
GAIN (dB)	60.3	60.3	60.3	60.3	68	52-76	
BEAM ISOLATION (dB)	-30	-30	-30	-30	N/A	N/A	
FEEDS	OFFSET				OFFSET/ ON AXIS	ON AXIS	CONFORMAL PHASE ARRAYS
SURFACE ACCURACY	$\lambda/20$	$\lambda/20$	$\lambda/20$	$\lambda/20$	$\lambda/50$	$\lambda/20$	
ORBIT ALTITUDE	GEO	GEO	GEO	GEO	LEO	LEO	9000 Km
RESOLUTION (KM)	N/A	N/A	N/A	N/A	1-10	10^{-5}/SEC* 10^{-3}/SEC**	BOMBER - MISSILE
REVIST COVERAGE (DAYS)	N/A	N/A	N/A	N/A	3	N/A	CONTINUOUS
SWATH ANGLE (DEGREES)	N/A	N/A	N/A	N/A	± 30	N/A	
LIFE TIME (YEARS)	>20	>20	>20	>20	>20	>20	4

*TARGET
**GOAL
***PUBLIC SERVICE SATELLITE

KEY NEEDS AND SPECIAL REQUIREMENTS

At the top of the figure are listed key needs peculiar to the individual missions, such as multiple beams, along with some needs that are common to all the missions, such as deployment and long life. In order to meet these needs, advances are required in many technologies. Some areas of special importance are listed at the bottom of the chart. Orbit requirements range from very low Earth orbit (LEO) to greater than geosynchronous (GEO) altitudes, implying a need for versatile, reliable, and cost effective orbital transfer technology. Aperture and beam requirements are of high priority for all of the missions and impact numerous technology disciplines. Large space antennas which can be packaged in Space Transporation System (STS), transferred to higher orbits, deployed, and operated with precision dictate the need for special structural configurations and deployment concepts. Long lifetime or service interval requirements focus on the need for durability in the space environment.

Each of these four areas is discussed further.

MISSIONS	PECULIAR NEEDS	COMMON NEEDS
C1	97 BEAMS CONUS COVERAGE FROM GEO	• STS PACKABLE; IN-ORBIT DEPLOYABLE
C2	5 BEAMS OF 10 KW OR MORE FROM GEO	• 10-YEAR LIFETIME
EO1	HI BEAM EFFICIENCY MULTIPLE RADIOMETERS	WITH
SS2	VERY LONG BASELINE (HI ORBIT ALTITUDES); FINE POINT KNOWLEDGE	2-YEAR SERVICING INTERVALS
SS1	DIFFRACTION LIMITED OPTICS (SEGMENTED) AT 30 μm; POINTING AND VIBRATION CONTROL	

SOME SPECIAL TECHNOLOGY DRIVING REQUIREMENTS AREAS

- ORBIT REQUIREMENTS

- APERTURE AND BEAM REQUIREMENTS
  ANTENNA GEOMETRY AND TOLERANCES

- STRUCTURAL CONFIGURATIONS AND DEPLOYMENT CONCEPTS

- DURABILITY IN SPACE ENVIRONMENT

ORBIT REQUIREMENTS

Orbit requirements deal with establishing the operational orbit, precisely keeping that orbit for years, and servicing the antenna in the operational orbit or in a temporary lower orbit. Impacts are primarily in the areas of space systems, structures, and controls.

Station-keeping requirements show up primarily as a weight penalty for propellants. This is a prime consideration for Earth observation missions with their need to sense as close to the Earth as possible for maximum resolution and for precise orbit maintenence for precise geodetic registration of the data pixels.

The antenna structural system must accommodate an orbital transfer system, whether an integral part of the antenna or a separate vehicle. In its undeployed package it must sustain the potentially high thrust loads necessary to place it in its operational orbit. Even when fully deployed the antenna structure may have to sustain orbit change, docking, and servicing loads. Military requirements may be the most stringent ones. Additional controls may be required for docking of a service vehicle and for other servicing operations.

Our knowledge of large space antenna missions and implementing technologies probably has advanced to the point where structural loads and controls requirements for orbit transfer, docking, and servicing should be quantitively assessed. In particular, if military mission requirements are more stringent, NASA technologists should be made aware of the additional challenge.

OPERATIONAL ORBITS   (10-15 YEAR LIFETIME; 2-5 SERVICE INTERVALS)

- LOW   - EO1 AS LOW AS POSSIBLE, SS1, SS2

- INTERMEDIATE - MS2

- HIGH   - C1, C2

SPACE SYSTEMS

- LEO ALTITUDE MAINTENANCE IMPOSES HIGH PROPELLANT WEIGHT PENALTY

- ANTENNA SYSTEM MUST ACCOMMODATE AN ORBITAL TRANSFER SYSTEM

- UNDEPLOYED ANTENNA MUST SUSTAIN ORBIT PLACEMENT LOADS (MAY BE HIGH THRUST)

- DEPLOYED ANTENNA MUST SUSTAIN ORBIT CHANGE, DOCKING, AND SERVICING LOADS

- DOCKING AND SERVICING CONTROLS REQUIRED

- SPECIAL MILITARY REQUIREMENTS--?

206

LARGE SPACE ANTENNA MISSION REQUIREMENT TRENDS

Large space antenna requirements vary with electromagnetic wavelength. At the top of the figure the frequencies and wavelengths are shown for the microwave, infrared, and visible bands. The prime wavelength ranges of the civilian missions are plotted on the figure. Large space antenna applications focus on the microwave bands with wavelengths of 1 meter to 1 centimeter. Recently, however, some attention is being given to the shorter millimeter wavelengths. It should be noted, also, that broadcast communications (C2) users are considering wavelengths as long as 11 meters and the radio astronomers (SS1) envision using the Large Deployable Reflector (LDR) in a "light bucket" mode with wavelengths as short as 2 micrometers. Thus, the frequency or wavelength range covers almost seven orders of magnitude!

Large antennas are needed for collection energy, providing gain and obtaining good angular or spatial resolution. Resolution requirements are shown on the next line of the figure. Although the trend appears to be wavelength dependent, in reality it is more mission dependent. Space science missions demand the greatest resolution, Earth observations missions less and communications missions the least.

The spatial coverage required of the large antennas is shown on the next line of the figure. Earth observation missions in low orbit have the greatest requirement in terms of angular field of view, space science experiments are very resolution elements in the field of view space science experiments are very demanding also. To meet these requirements, slewing of the entire antenna system is usually not practical. Therefore, single beam concepts employ some sort of scanning system while multiple beam systems use an array of feeds or detectors at the focal surface. The Space Telescope (ST), for example, has a 800 by 800 pixel array of charge-coupled devices (CCD's).

Aperture size requirement trends are indicated on the next line of the figure. These requirements are related to both the spatial resolution and the spatial coverage requirements and exhibit a similar mission dependence. At a given wavelength, the greater the resolution requirement (smaller sec) the larger the required aperture. If spatial coverage dictates the use of multiple beams which cannot fully overlap an even larger aperture is required. On the wavelength scale, the longer the wavelength the greater the required aperture. The general trend for aperture size in wavelength units, however, decreases at the longer wavelengths. In this sense, the requirements presently imposed in the microwave region are not as severe as in the optical region, reflecting the shorter technology history of microwave measurements.

The electromagnetic performance of an antenna depends on its ability to collect the electromagnetic radiation with the large aperture and to feed it to the radiometer per se. If the reflecting surface is not smooth at the operating wavelength, and if its shape deviates from the design shape, energy is lost from the beam. Other factors contributing to the RF performance budget are collector-feed array alignment tolerances and stability and pointing tolerances. The tolerance criteria are expressed in terms of fractions of wavelength. For example, a surface criterion for a quality system may be $\lambda/50$ for the rms value of the random deviations from a perfectly smooth surface. Periodic variations, such as "pillowing," and large scale shape changes, although more deterministic by nature, are often judged by the same criterion, perhaps without full understanding of the implications. These tolerances, whether surface, alignment, stability or pointing,

are harder to obtain with a large system than with a small system. So the real merit of a system is judged on something like a tolerance-to-size ratio. Optical systems with their long technology history are currently better than microwave systems.

From this figure it is obvious that mission requirements and system tolerance criteria need to be established and understood across the spectral range. Furthermore, they should be relatively independent of the system concept. This would facilitate comparison of system concepts, especially with regard to error budgets that are established for reflector surface roughness and antenna component misalignment.

LARGE SPACE ANTENNA MISSION REQUIREMENT TRENDS

~0.5° (CI) 0.05° -0.1° (SS2, EOI) SPATIAL RESOLUTION 0.1 sec (SSI)   0.05 sec (ST)

~7° (CI)   30° (EOI)   15° (LIDAR)   0.5° (ST)
ARRAY   PUSH BROOM   SPATIAL COVERAGE   SCAN   ARRAY

$10^2 \lambda$'s $10^3 \lambda$'s $10^4 \lambda$'s $10^5 \lambda$'s $10^6 \lambda$'s
              200 m   APERTURE SIZE   20 m   5 m

$\lambda / 20$ (CI) $\lambda / 50$ (EOI)   SURFACE TOLERANCE $\lambda / 50$ (ST)
2×10^{-2} m 2×10^{-3} m 10^{-8} m

ANTENNA STRUCTURAL REQUIREMENTS

The question of tolerances is also noted in this figure dealing with structural requirements. Regarding collector-feed geometry, f/D, feed location (coaxial or center-fed) and slewing requirements limit structural configuration options and determine alignment tolerance budgets and frequency modes requirements. Most missions use a mesh reflector in a gore pattern, but the SS1 mission uses a solid reflecting surface in a hexagonal segmented pattern. Regardless of the structural configuration, the collector surface must be attached to it and its figure must be verified and/or controlled. Whether or not this must be done in space is a technology issue having implications for the antenna design itself, as well as for the associated measurement and control systems and the correlation of their results with the actual RF performance.

Historically, however, the structural configuration is driven by the packaging and deployment requirements. High packing density is required for transport via the STS, and obviously reliable and precise deployment is a must. The hoop-column wrapped-rib truss configurations are deployable mesh concepts while the Large Deployable Reflector is a deployable solid optics concept. Two systems points are noted:

(1) The mission depends on successful deployment and the kinetics/kinematics of deployment should be thoroughly analyzed to establish high potential reliability in space.

(2) To date packaging for deployment from the Shuttle seems to be a constraint universally accepted by the NASA missions. If postulated future systems begin to exceed the 100-200 m size class, the question of assembly or erection vs. deployment should, perhaps, be re-examined.

Finally it must be noted that meeting the requirements in these three areas-- geometry, surface, and deployment--is so important yet so difficult to verify by ground-based simulation, that there is an implied requirement for space flight experiments to verify the technology readiness. The interplay between structures, controls and RF performance must be quantitively treated by such experiments.

COLLECTOR - FEED GEOMETRY

- LARGE   f/D   CONFIGURATION

- COAXIAL VS OFF-SET FED   ALIGNMENT TOLERANCES

- SCANNING VS ARRAYS   DYNAMICS - FREQ. MODE RANGES

COLLECTOR SURFACE

- MESH, MEMBRANE, SOLID SURFACES

- GORES, SEGMENTS   FIGURE SENSING AND CONTROL

PACKAGING AND DEPLOYMENT

- HIGH PACKING DENSITY   MESH — H-C, W-R, TRUSS
                              E.G. CONCEPTS
- RELIABLE/PRECISE DEPLOYMENT   SEGMENTED SOLID — LDR

THE LIFETIME REQUIREMENT--DURABILITY IN SPACE

NASA missions, whether in geosynchronous or low Earth orbits, generally require that the large antenna systems have a lifetime of greater than 10 years, with the provision that they can be resupplied, refurbished, or serviced at intervals somewhat greater than 2 years. Some military missions may be at intermediate orbits with guaranteed lifetimes on the order of 5 years without servicing. This suggests a look at long-term changes, contamination wearout, and lifetime effects such as those caused by the space radiation environment. The figure lists, for example purposes only, some large antenna subsystems and components which, a priori, may be judged to be non-servicable, along with some that may be judged to be serviceable.

From a systems point of view, it appears that each subsystem or component should be understood well enough to know whether it must function for the whole mission lifetime without servicing or whether periodic or emergency replacement, refurbishing, or servicing is feasible. The technology implications corresponding to such classification should be assessed.

● NON-SERVICEABLE ITEMS

- STRUCTURES (CYCLING W/O FATIGUE)

- THERMAL COATINGS

- REFLECTOR SURFACE (MESH)

- FEED SYSTEM

- HEAT REJECTION SYSTEM

● POTENTIALLY SERVICEABLE ITEMS

- POWER SYSTEM ⟨ SOLAR CELLS / STORAGE

- ELECTRONICS

- CONTROL SYSTEM

LARGE SPACE ANTENNA MISSION AND SYSTEM NEEDS

This figure lists again those areas highlighted by this summary of requirements or needs for civilian and military space missions using large antennas. Although not a complete list, it does include a wide range of needs, from those associated with orbital operations to those associated with in-space RF performance. Although such needs ought to be quantified and eventually turned into specific requirements, the most formidable need is a general one--that of developing technology that will result in affordable space system concepts and hardware.

- MISSION AND TECHNOLOGY RELATIONSHIPS FOR CIVILIAN AND MILITARY APPLICATIONS

- AFFORDABLE CONCEPTS

- ALTERNATIVE APPROACHES (ACTIVE/PASSIVE, REFLECTOR/PHASED ARRAY)

- ELECTROMAGNETIC SYSTEM
    - "OPTICS" DESIGNS, TOLERANCES
    - FIGURE SENSING AND CONTROL

- STRUCTURES AND CONTROLS
    - ORBIT TRANSFER, DOCKING, SERVICING, . . .
    - PACKAGING, DEPLOYMENT/ASSEMBLY

- SUPPORTING SUBSYSTEMS
    - LIFETIME AND SERVICING

REFERENCES

1. NASA Space System Technology Model, Vol. I, Part A: Mission System Descriptions and Technology Needs, NASA TM-80473, September 1981.

2. Russell, R. A., Campbell, T. G., and Freeland, R. E.: A Technology Development Program for Large Space Antennas, IAF Paper No. 80 A-33, International Astronautical Federation, 1980.

212

SPACECRAFT MATERIALS RESEARCH — A NASA PERSPECTIVE

Darrel R. Tenney
NASA Langley Research Center
Hampton, Virginia

INTRODUCTION

Because of their unique combination of high specific stiffness and low coefficient of thermal expansion, composite materials will be used for future space missions such as communication antennae, solar reflectors, satellite power systems, and a space operations center. (See fig. 1.) For long-life space missions (10-20 years), the durability of these materials in the hostile space environment has been identified as a key materials technology need.

This paper reviews NASA's spacecraft materials research program. This is a multicenter program and includes research in the following areas: space environmental effects on materials, low expansion composites, fatigue and fracture of composites, thermal control coatings, and contamination. Research to date has concentrated on establishing a fundamental understanding of space environmental effects on current graphite-reinforced composites and polymer systems, and developing analytical models to explain observed changes in mechanical, physical, and optical properties. As a result of these research efforts, new experimental facilities have been developed to simulate the space environment and measure the observed property changes. Chemical and microstructural analyses have also been performed to establish damage mechanisms and the limits for accelerated testing. The implications of these results on material selection and system performance are discussed, and additional research needs and opportunities in the area of tougher resin/matrix and metal/matrix composites are identified.

LARGE SPACE SYSTEMS
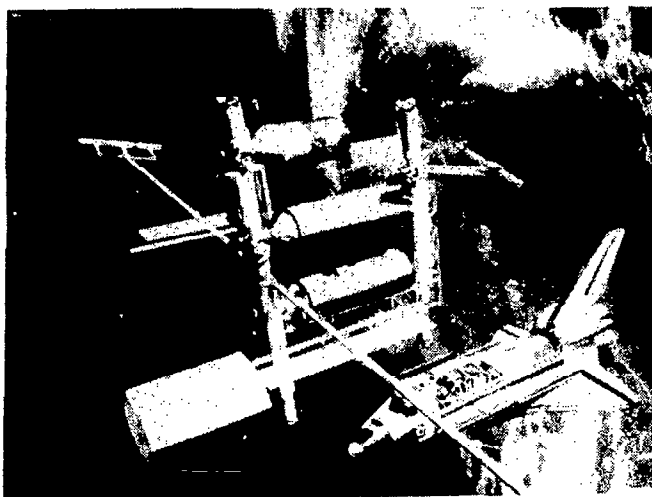
THE SPACE STATION   LARGE SPACE ANTENNA SYSTEMS

Figure 1

HIGH-STIFFNESS LOW-THERMAL-EXPANSION SPACE MATERIALS

Structural requirements generally focus on light weight, high stiffness, and dimensional stability. Conventional aerospace materials such as aluminum and titanium do not provide these characteristics, whereas advanced graphite reinforced composites do. The coefficient of thermal expansion (CTE) values and specific stiffnesses of graphite composites and selected other low-expansion materials are compared in figure 2. Quartz and ULE (titanium silicate glass) fall within the preferred range of CTE values but do not provide the needed stiffness. A range of values is shown for both the graphite/resin and graphite/metal composites, indicating the flexibility that these composites offer for tailoring properties by varying the fiber type and ply orientation. Graphite/resin and graphite/metal composites both provide the needed CTE values and can be selected for a particular application depending on the stiffness requirements. Graphite/glass has a very low CTE and high stiffness, but its low thermal conductivity may make it undesirable in applications where large thermal gradients could cause warping of the structure.

Metal matrix composites (graphite/aluminum and graphite/magnesium) research for space structures is being conducted in several Department of Defense programs. Resin matrix composites (graphite/epoxy, graphite/polyimide, and graphite/advanced resins) research is the primary focus of the NASA program. Each of the composite materials has potential advantages for large space structures. Continued research on both classes of composite materials is warranted to assure their technology readiness and to provide the designer with material options for optimum structural design.
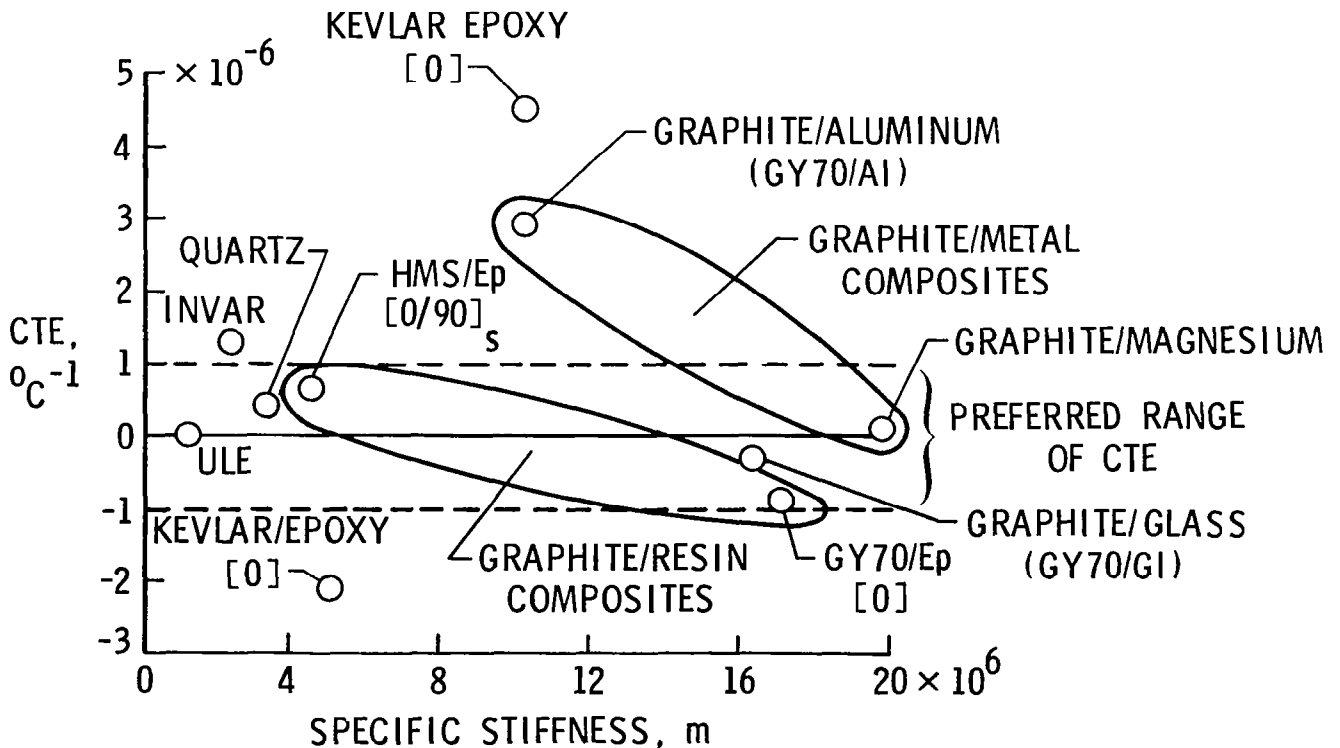
Figure 2

DURABLE SPACE MATERIALS

Space-durable materials are a necessary requirement to achieving long-life space structures. (See fig. 3.) As previously noted, materials of construction will include advanced metal and polymer matrix composites, coatings for thermal control, polymer films, and adhesives. In low Earth orbit (LEO), materials will be subjected to repeated thermal cycles from approximately +200°F to -200°F, to UV radiation, and to ultra-high vacuum. Micrometeoroids and space debris are also considered as hazards in LEO. For higher orbits, such as geosynchronous Earth orbit (GEO), the materials will also be subjected to large doses of high-energy electrons and protons (refs. 1-3). The primary concerns for resin matrix composites are radiation-induced changes in mechanical and physical properties and dimensional stability, as well as microcracking due to residual stresses produced during thermal cycling. Similarly, the residual strains produced by the thermal expansion mismatch between the fibers and the matrix in metal matrix composites are likely to affect the dimensional stability of these materials.

Long-life coatings are required to keep the spacecraft system within design temperature limits. Degradation of the optical properties of these coatings by UV and particulate radiation and by contamination appears to be a significant problem that must be solved to achieve long-life systems (10 to 20 years).

The ability to predict the long-term performance of all classes of materials in space must be a central part of any durability program and may require flight experiments for verification of ground exposure data and analytical predictions.
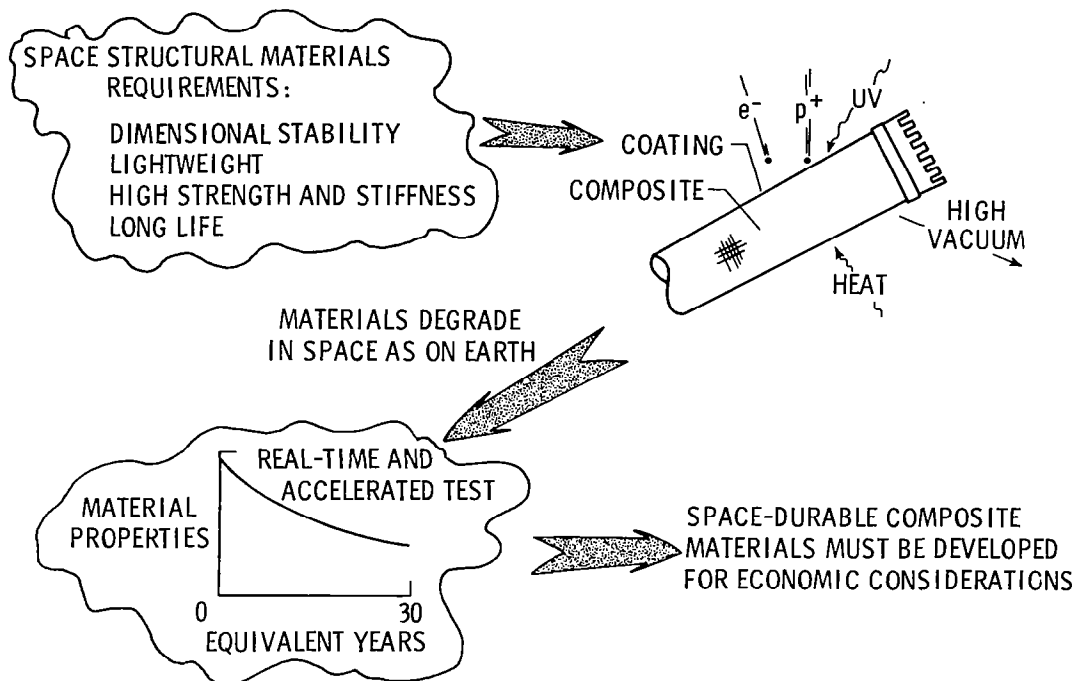
Figure 3

SPACE MATERIALS DURABILITY LABORATORY

Figure 4 shows a schematic of the Space Materials Durability Laboratory at NASA Langley. The laboratory is dedicated to the evaluation of the effects of space radiation on composite materials. This laboratory has a 2.5-MeV proton accelerator, a 1-MeV electron accelerator, and a solar simulator, all focused on a 12-inch-diameter target in a clean ultra-high-vacuum chamber. The accelerators were selected to cover the most prevalent energy range found in space for generation of bulk damage to composite materials.

Two smaller single-parameter exposure chambers have also been developed for in situ chemical characterization studies. In these chambers, polymer films are subjected to low-energy (100 keV) electrons. Chemical and physical properties such as weight loss, outgassing and condensible products, infrared (IR) absorption, and dynamic moduli are followed during the irradiation. Mechanical properties of the films are obtained after irradiation. These characterizations serve as a sensitive measure of the radiation interaction and provide data for development of mechanistic models of the interaction process.

RADIATION EQUIPMENT LAYOUT
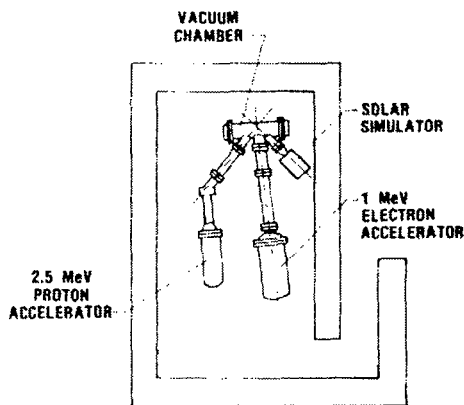
ENERGY SPECTRA FOR 30 YEARS IN GEOSYNCHRONOUS EARTH ORBIT

Figure 4

217
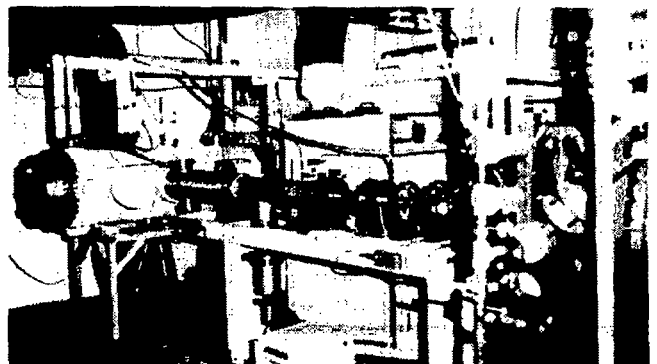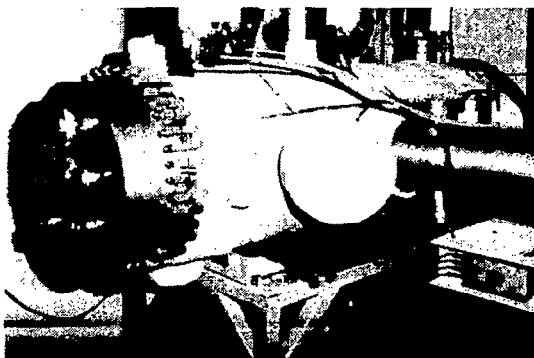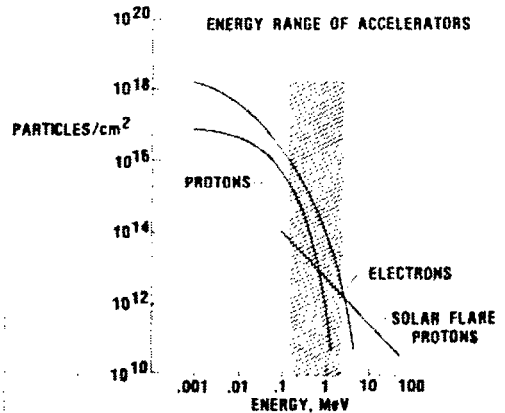
MSFC RADIATION EFFECTS FACILITY

Within the irradiation cell of the MSFC Radiation Effects Facility, the 2.5-MeV Model A2500 Van de Graaff accelerator is shown on the left and the 400-keV Model A400 accelerator is on the right in figure 5. In the photograph the A400 system is configured to produce a proton beam and pass the protons through an analyzing magnet and beam steering assembly into an irradiation chamber. The A2500 is configured to produce an electron beam and pass the electrons through a switching magnet into the irradiation chamber in the background or into a specially modified vacuum canister of the type used for the long-term thermal-vacuum exposure. Since the accelerators can be reconfigured between positive and negative modes in a few days, these configurations are often changed to meet different experimental requirements.
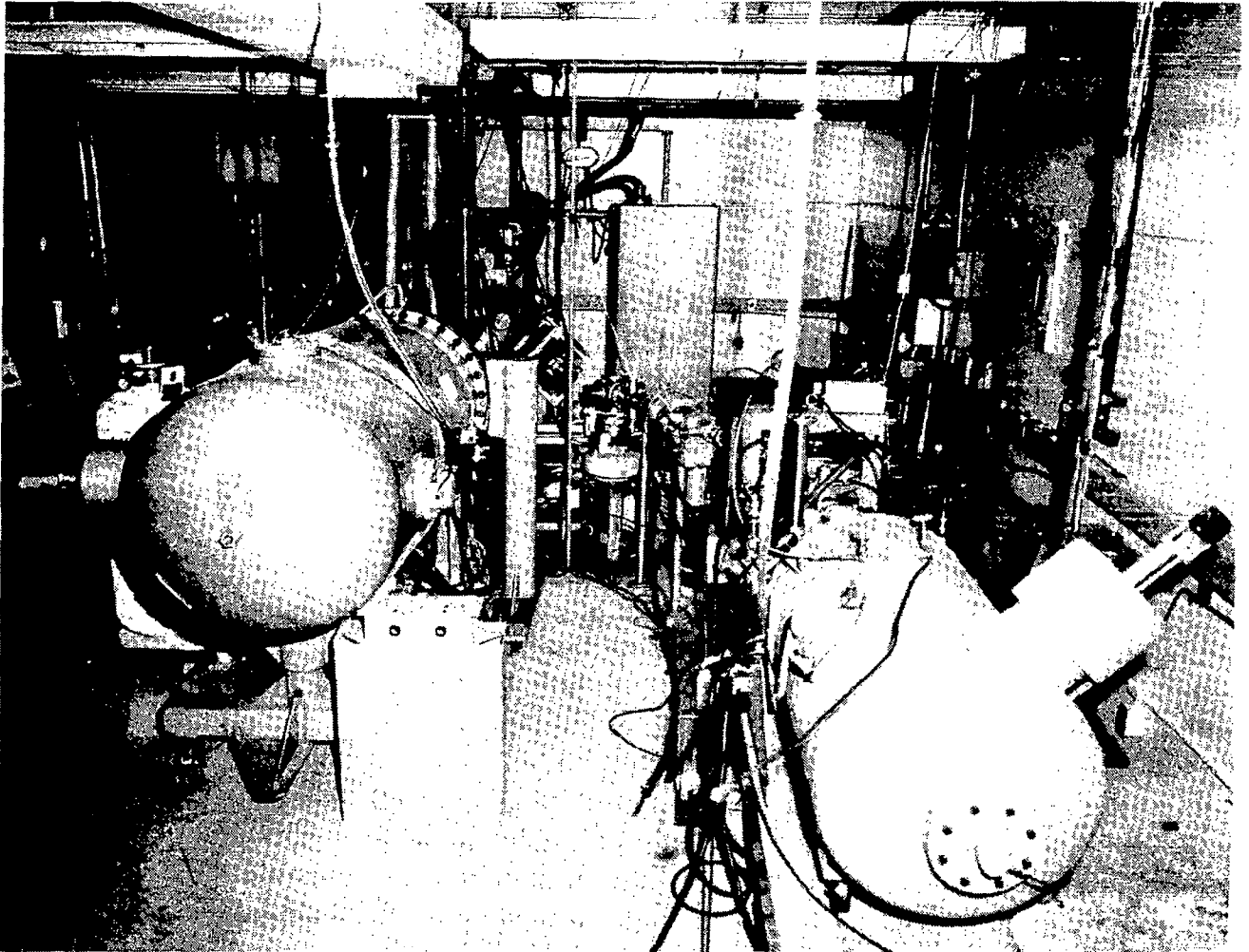
Figure 5

EFFECTS OF ELECTRON RADIATION ON INTERLAMINAR SHEAR STRENGTH

The interlaminar shear strengths of graphite fiber/epoxy (T300/5208) and graphite fiber/polyimide (C6000/PMR-15) composites are degraded by high doses of electron radiation. Typical data for C6000/PMR-15 are shown in figure 6 (ref. 4). Samples were exposed in vacuum to 0.5 MeV electron radiation up to a cumulative dose of 10 000 Mrad.

The data shown in figure 6 are for a unidirectional C6000/PMR-15 sample. The interlaminar shear strength initially increased, reaching a maximum of approximately 9% higher than the control value at 2000 Mrad, and then decreased, reaching a value at 10 000 Mrad exposure which was approximately 54% lower than the value at 2000 Mrad. Similar data collected on T300/5208 showed the same general trends except that the maximum in interlaminar shear strength occurred at approximately 1000 Mrad. For T300/5208 the values at 10 000 Mrad were considerably lower than those of the maxima for all three composite constructions evaluated: longitudinal (-34%), (0/+45/0) (-18%), and (90/+45/90) (-70%). Strength values measured by the three-point bending test do not exhibit large negative changes like those seen in interlaminar shear strength. When tested in the fiber direction (longitudinal), composites show no degradation with radiation exposure because of fiber reinforcement and matrix crosslinking. Also the transverse tensile strength of these composites did not show any large decrease due to radiation presumably because matrix crosslinking provides a stabilizing effect. Interlaminar shear strength depends only on the interfascial components, so without the stabilizing effect of fiber and matrix components, large decreases are seen in this parameter.
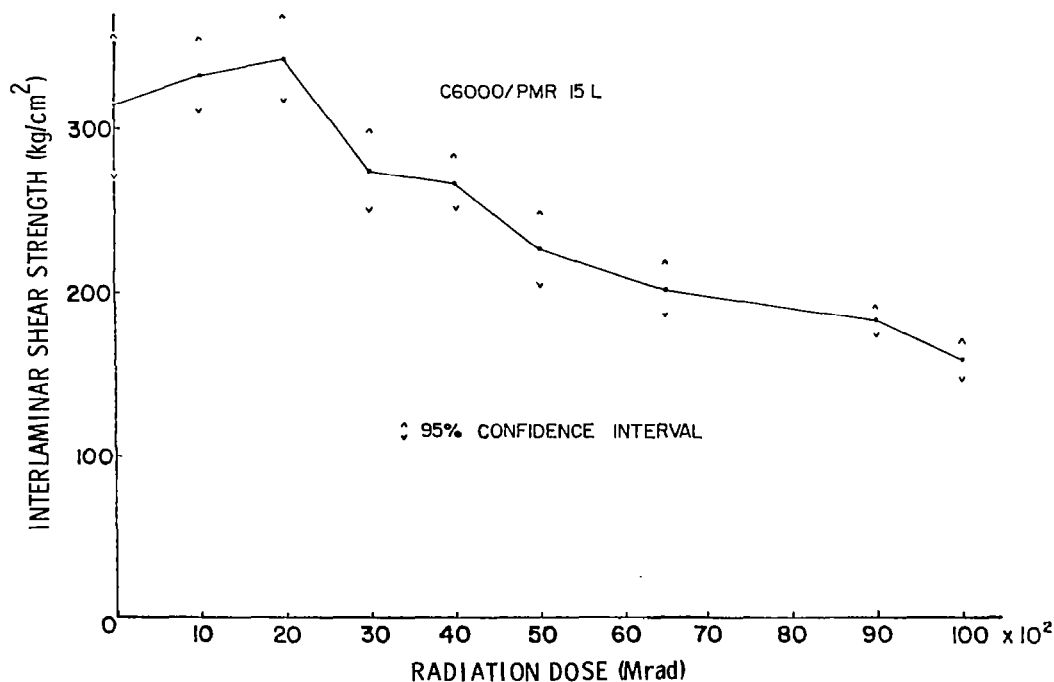
Figure 6

EFFECT OF ELECTRON RADIATION ON THE MODULUS OF POLYSULFONES

Thermoplastics with improved properties are being actively considered for structural applications. One class that has received considerable attention for space and aircraft application is polysulfones. To assess long-term durability of these materials in space, a series of four materials, each with a different chemical structure, was exposed to either an electron or a proton environment using several different dose rates and particle energy sufficient to give a uniform dose through the polymer film (ref. 5). The absorbed dose was varied between 10^8 and 10^{10} rads. Film samples of all materials were used because chemical characterization of films is much easier than chemical charac- terization of composites and provides a more sensitive measure of radiation damage.

The effect of total electron dose on the observed modulus of the four polysulfone films is shown in figure 7. Modulus values were obtained using an automated Rheovibron Dynamic Viscoelastometer with all data obtained at a frequency of 3.5 Hz. When determining modulus, the film sample was inserted, removed, and reinserted several times to eliminate sample mounting effects. All reported values are the average of at least three measurements.

For all materials, modulus increased as dose increased and the threshold value for a major change in modulus appears to be near 10^9 rad. The percent increase ranges from about 24 percent for P-1700 to 58 percent for Radel 5000. This increase with dose suggests that crosslinking is occurring in all materials, particularly above 10^9 rad.
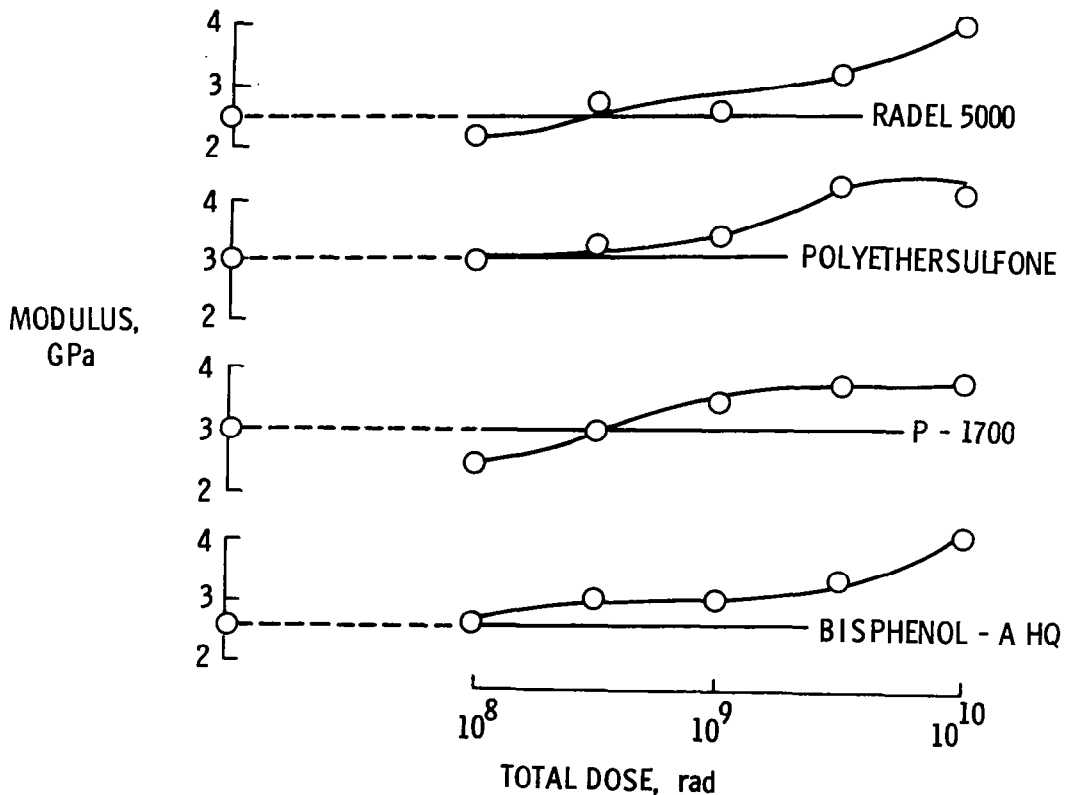
Figure 7

Following irradiation of each polysulfone film, a chemical analysis was performed to determine changes in elemental composition. Figure 8 shows this elemental composition data for one material (P-1700), normalized relative to the chemical analysis of the starting material, as a function of total dose. Similar chemical analysis data were obtained on all polysulfones studied and showed trends as presented in this figure. The analysis showed considerable loss of oxygen and moderate losses of sulfur and hydrogen. The threshold for a major decrease in oxygen occurs near 2×10^8 rads. About 24 percent of the initial oxygen content is lost for P-1700 at 10^{10} rad, and that loss could establish sites for crosslinks. This apparent loss is supported by the diminished absorption bands associated with oxygen in the IR data. The breaking of an oxygen bond by irradiation and subsequent combination of oxygen atoms to form oxygen molecules, which could then be lost to the surroundings, would explain the decrease in oxygen content and the diminished absorption bands. The loss of oxygen atoms from $-SO_2-$ linkages creates sites for crosslinking to adjacent chains and thus could explain the observed increase in modulus at high radiation doses.
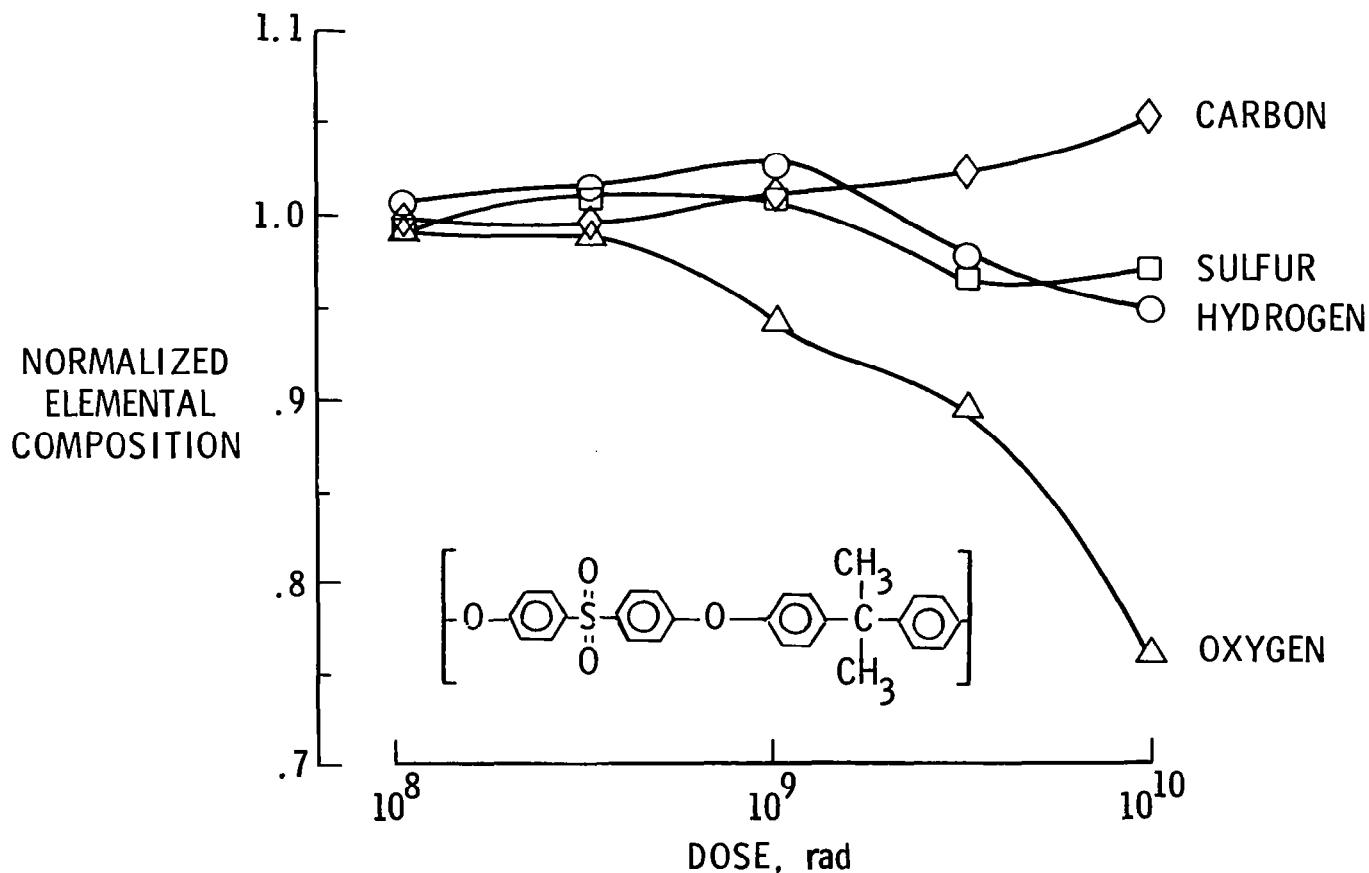
Figure 8

INFRARED SPECTRA OF ELECTRON-IRRADIATED P-1700

Two infrared spectra, each made from a film of P-1700, are shown in figure 9. This polysulfone is representative of the four materials studied. The lower curve represents the portion from 1600 to 600 cm^{-1} frequency of the IR spectrum of nonirradiated polyethersulfone. The upper curve represents that same portion of the spectrum of polyethersulfone irradiated with electrons to 10^{10} rads. The SO_2 absorption band occurs at approximately 1400 cm^{-1}, which can clearly be seen as an absorption peak (an inverted peak) on the nonirradiated curve. However, after irradiation this peak is greatly diminished. Near 1300 and 1150 cm^{-1} are the asymmetric and symmetric ϕ-SO_2-ϕ absorption bands, respectively. These bands are present in the lower curve, but they have almost disappeared in the upper curve of the irradiated material. At approximately 1070 cm^{-1}, the C-O-C absorption band that appears on the spectrum for the nonirradiated specimen is absent in the spectrum for the irradiated polyethersulfone. The spectra shown here are the two extremes of the data actually obtained. The spectra of those specimens irradiated at lower doses resemble the spectrum of the nonirradiated material, and as the dose was increased, the spectra approached that of the curve at 10^{10} rads. All four polysulfones exhibited this same basic trend, with the SO_2, ϕ-SO_2-ϕ, and C-O-C bands being the most significantly affected by the radiation. The proton data, not shown here, also followed this trend, but the magnitude of change was less.
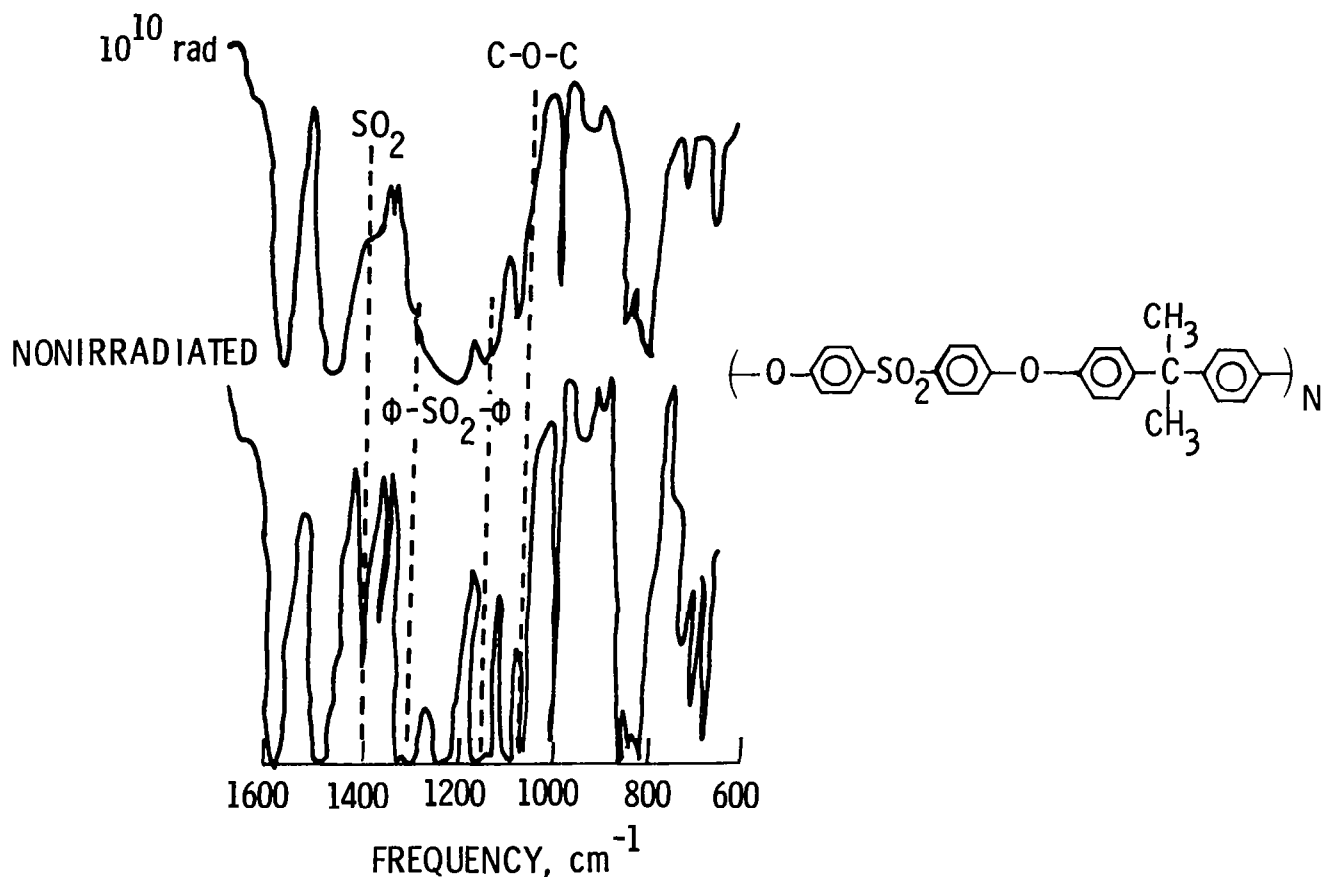
Figure 9

MODEL POLYMER RESINS FOR SPACE COMPOSITES

In addition to determining the long-term space durability of currently available polymer resins, research is also under way to evaluate new and emerging resin systems. The chemistry of two new thermoplastic polyimidesulfone resins which look promising for both aeronautical and space applications is shown in figure 10. The chemical structures of these polymers are intermediate between a thermoplastic, shown at the top of the figure, and a polyimide, shown at the bottom of the figure. The approach being followed is to first understand the behavior of the linear thermoplastic polysulfone and progress through the two intermediate polymers to a crosslinked, high temperature polyimide. Characterization of the radiation stability of each system will produce information on factors such as the effect of imide/sulfone content, structural flexibility, and aromatic content on the space durability. A generic data base on the stability of a particular group can be determined in different structural arrangements. This study and related investigations to determine the effect of molecular weight and crosslink density on each of the indicated polymers will begin to establish the required data base for development of composite materials optimized for long-term use in space.
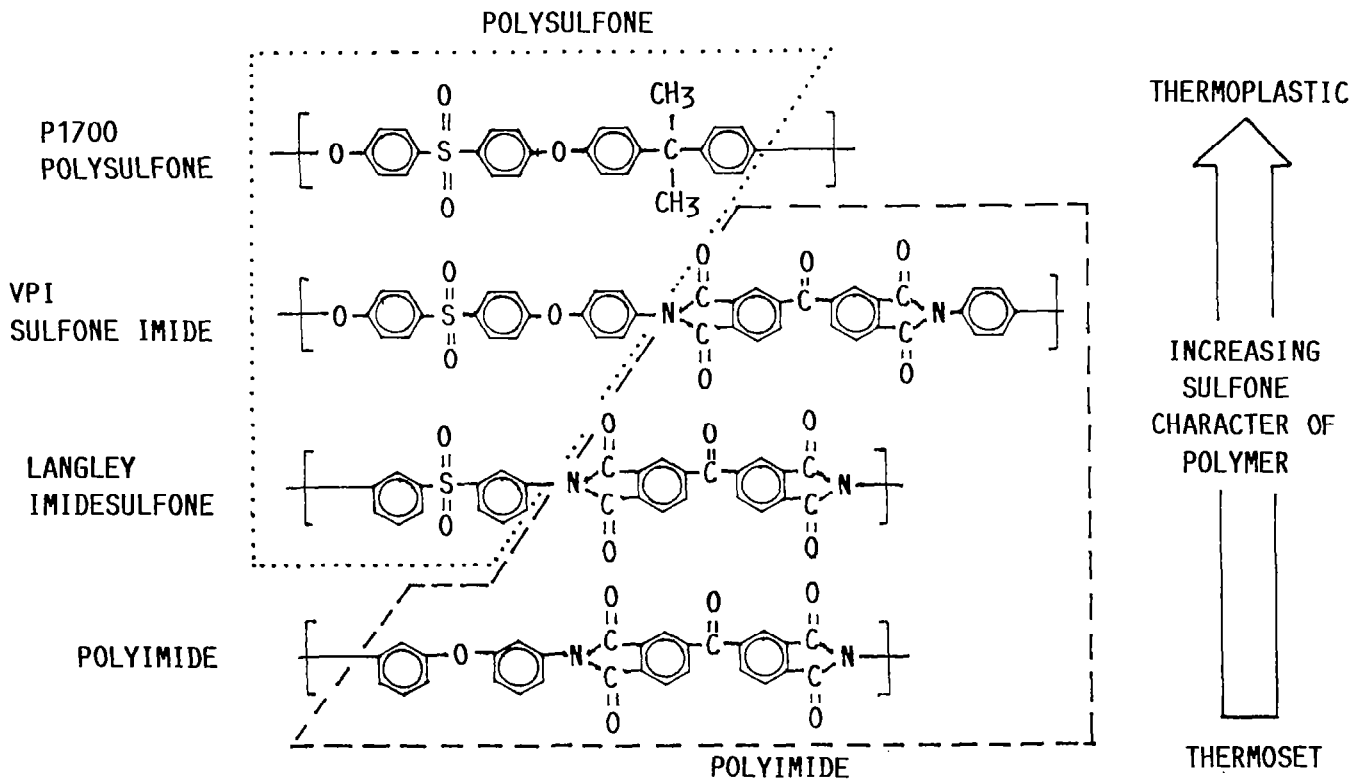
Figure 10

THERMOPLASTIC POLYIMIDESULFONE

Aromatic polysulfones, a class of high-temperature engineering thermoplastics, have a major deficiency in their tendency to swell and dissolve in many common solvents. This solvation can cause structural components which are fabricated from these polymers to be susceptible to damage by these solvents and thereby lose their structural integrity.

Aromatic polyimides, conversely, are a class of polymers which are known to be resistant to solvents, but they are generally not processable via thermoplastic means. These polyimides are known to be exceptionally thermally stable, and like polysulfones and other thermoplastics, their use temperature is governed by the softening temperature of each system.

A novel polymer system that possesses the processability of the polysulfones and the solvent resistance of the polyimides has been synthesized and characterized as a film, unfilled molding, filled molding, and adhesives. The structure of this polyimidesulfone (PISO2) is shown in figure 11 along with some adhesive and molding data (ref. 6).
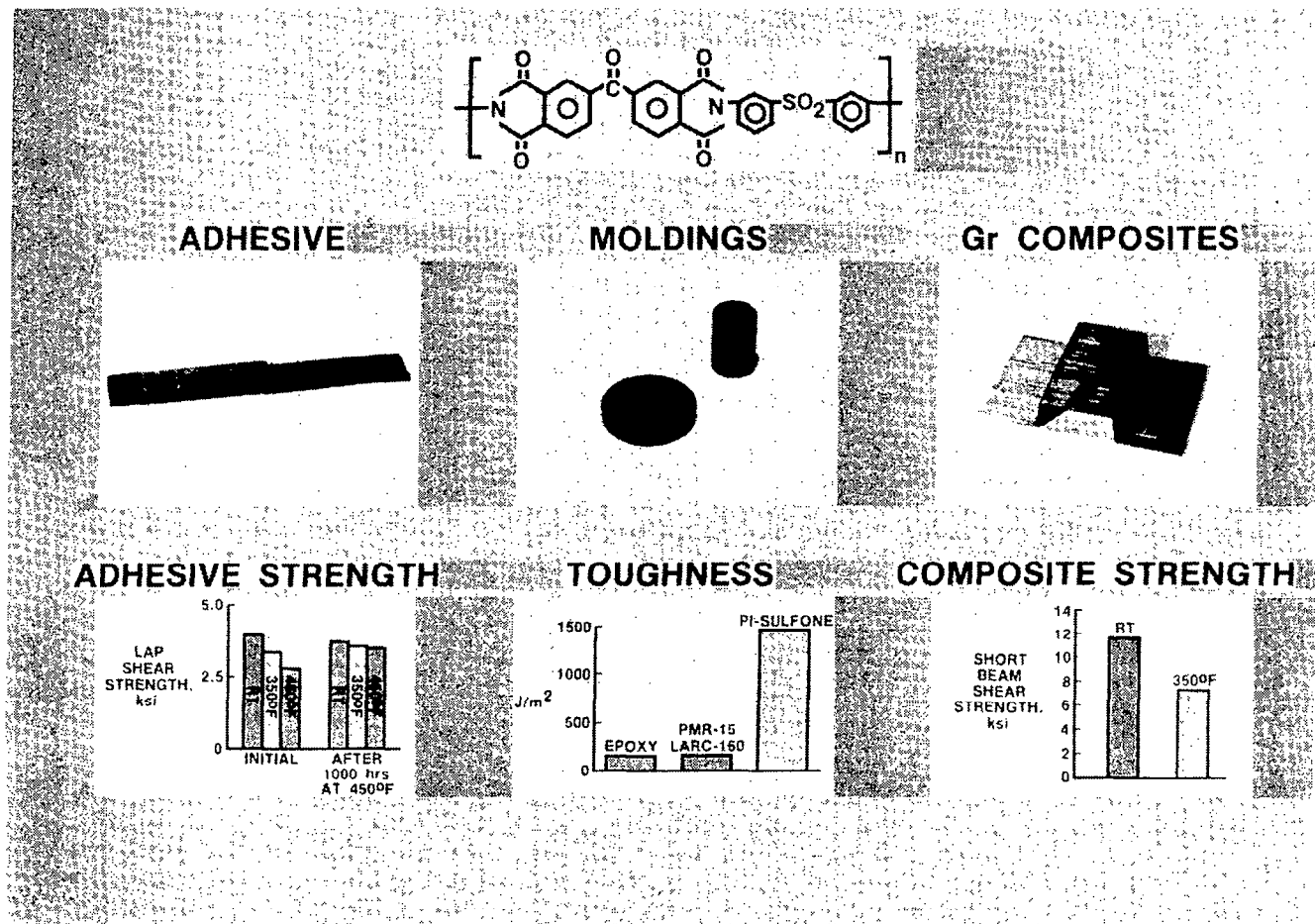
Figure 11

RAMAN SPECTRA OF KAPTON SAMPLE FROM STS-3

Significant mass loss of organic and some inorganic materials exposed in the bay of Space Shuttle was observed on the first four orbital flights. Surface erosion was observed on the materials exposed to impinging atom flux associated with the motion of the Shuttle through the ionosphere. Dr. A. Gupta at the Jet Propulsion Laboratory has undertaken a program to understand the fundamental nature of the observed mass loss from Kapton.

Oxygen atom effects on Kapton thermal blanket material aboard STS-2 and STS-3 were evaluated by monitoring the chemical changes on the etched Kapton surface by several spectroscopic techniques, including ESCA, Raman spectroscopy, surface energy analysis, reflectance UV visible spectroscopy and ATR FT-IR spectroscopy. Typical results of the Raman spectroscopic scans are shown in figure 12. Several changes are apparent, chief among them being the disappearance of the 1164 cm^{-1} line and decreased intensity of the 1630 cm^{-1} line. Assignment of these lines is still in progress, the preliminary interpretation being that C-N and C-O linkages are being cleaved without affecting C=O linkages. These interpretations are consistent with the observed evaluation of CO and CO_2 from Kapton exposure to O atoms, and surface enrichment of nitrogen detected by ESCA measurements.
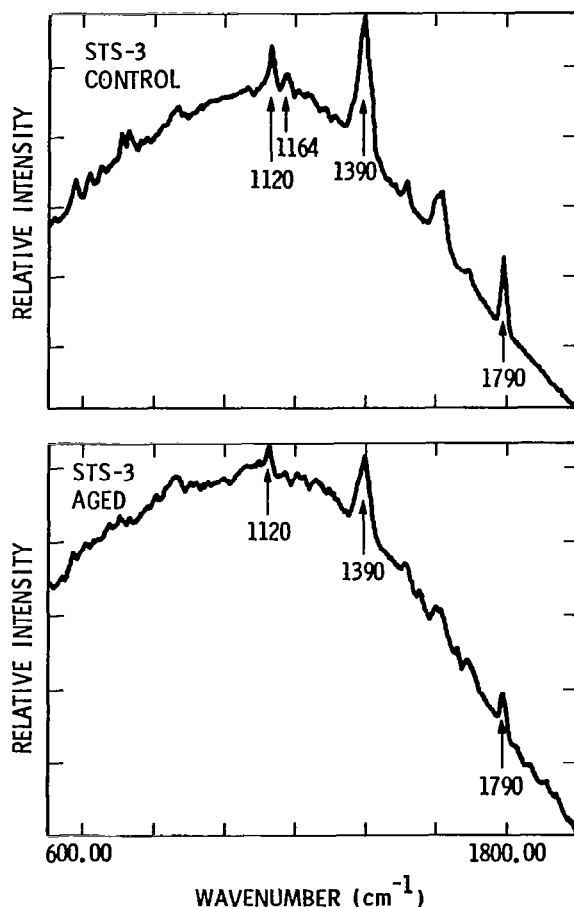
Figure 12

SURFACE ENERGY ANALYSIS OF KAPTON SAMPLE FROM STS-3

Recent work by A. Gupta, JPL, (unpublished data) on analyses of Kapton samples flown on the third Shuttle flight (STS-3) is summarized in figure 13. Results of surface energy analyses indicate an overall decrease in contact angle due to surface roughening. This is measured by the decrease in angle for PT-150. The decrease in contact angle for water is higher, indicating a significant increase in surface polarity of the aged sample. Subsequent measurements with other liquids have confirmed this conclusion and have provided a quantitative assessment of the nature of the chemical change in surface structure.

SOLVENT	SURFACE TENSION (dyne/cm)	CONTACT ANGLE		$\cos \theta_2/\cos \theta_1$
		CONTROL (θ_1)	AGED (θ_2)	
PT150	36	45°	18°	1.34
H_2O	73	70°	45°	2.07

Figure 13

MICROCRACKING IN COMPOSITES

Microcracks are small cracks that extend parallel to the fiber direction in the matrix of organic composites. They occur when the internal stresses exceed the transverse strength of an individual lamina. The two primary causes of microcracking are mechanical and thermal loads.

A limited amount of research has been conducted concerning the causes and effects of microcracking in composites. Repeated thermal cycling has been shown to cause microcracking in graphite/epoxy laminates, which causes the CTE to approach that of the unidirectional material (ref. 7). A typical example of this thermal microcracking is shown in figure 14. Research has also shown that residual strains, due to microcracking, of up to 20 $\mu\varepsilon$ may develop in graphite/ epoxy during the first cooling cycle to $-143^{\circ}C$. What has been lacking in past research is a quantitative relationship between the amount of microcracking and changes in CTE. This was the main focus of the current research.
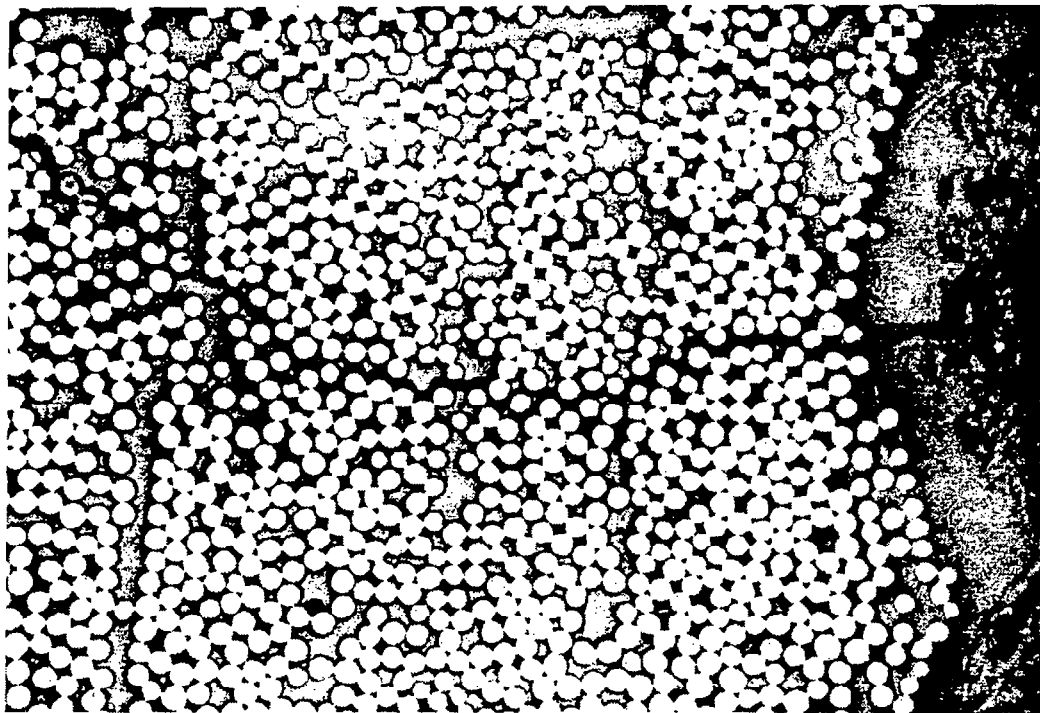
├─ 75 μm ─┤

Figure 14

MODELING THE EFFECT OF MICROCRACKING ON CTE OF COMPOSITES

The effect of microcracks on the CTE was modeled with a finite-element analysis. A generalized plane strain formulation was used with four noded linear general quadrilateral isoparametric elements capable of handling orthotropic material properties.

Numerical results were generated for the $[0_m/90_n]_s$ (m, n = 1, 2, 3) class of laminates using typical material properties for T300/5208. Results are presented in the form of CTE as a function of linear crack density in the $90°$ plies, which was varied from zero to three cracks per mm. The value of three cracks per mm was found to be an upper limit on the crack density formed in these materials during the experimental phase of this research.

The results for this family of laminates are shown in figure 15. As would be expected, the laminate configuration with the largest percentage of $90°$ plies experienced the largest reduction in CTE. The CTE at three cracks per mm for the three laminates, $[0/90_3]_s$, $[0_2/90_2]_s$, and $[0_3/90]_s$, was reduced by approximately 80, 65, and 40 percent, respectively. For all of these laminates the CTE was reduced in a direction towards the value of the CTE for the unidirectional material, -0.1×10^{-6} per $°C$, and approached a stabilized value after approximately two cracks per mm.
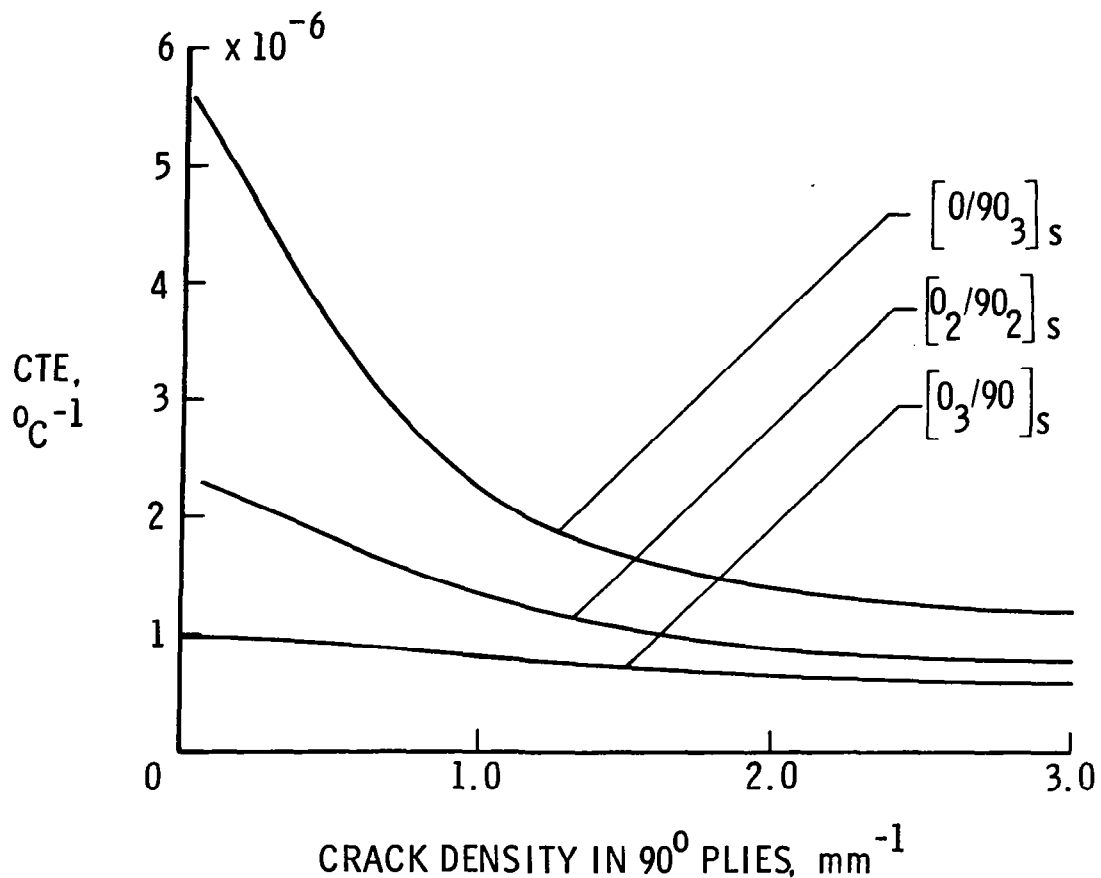
Figure 15

THERMAL EXPANSION OF P100 Gr/6061 Al TWO-PLY UNIDIRECTIONAL LAMINATE

The thermal strain of a two-ply unidirectional graphite/aluminum (P100/6061) Gr/Al composite laminate during thermal cycling is shown in figure 16. The sample was in the as-received condition and was subjected to three continuous, uninterrupted cycles from room temperature, to -225°F, to 300°F and back to room temperature. The test was conducted at atmospheric pressure in an air circulating oven which was heated by resistance heaters and cooled by liquid nitrogen. Strain measurements were made with a laser interferometer dilatometer (ref. 8). The specimen and dilatomer were at thermal equilibrium before each measurement was recorded. Strains were measured in the longitudinal direction (fiber direction).

The Gr/Al composite showed a non-linear thermal expansion which exhibits a thermal hysteresis loop. This loop became smaller with each successive thermal cycle and resulted in a permanent strain of about 20 µε after the third cycle. The loop is caused by the elastic-plastic deformation of the aluminum during thermal cycling and is very dependent upon the matrix yield strength and the residual stress in the composite. These data are similar to data by Min and Crossman (ref. 9) for Gr/Al which had been annealed. Heat treatment, which increases the yield strength of the matrix, has been found to significantly reduce the hysteresis loop of the Gr/Al composite (ref. 9). Research is needed to define the optimum thermomechanical treatment for metal-matrix composites.
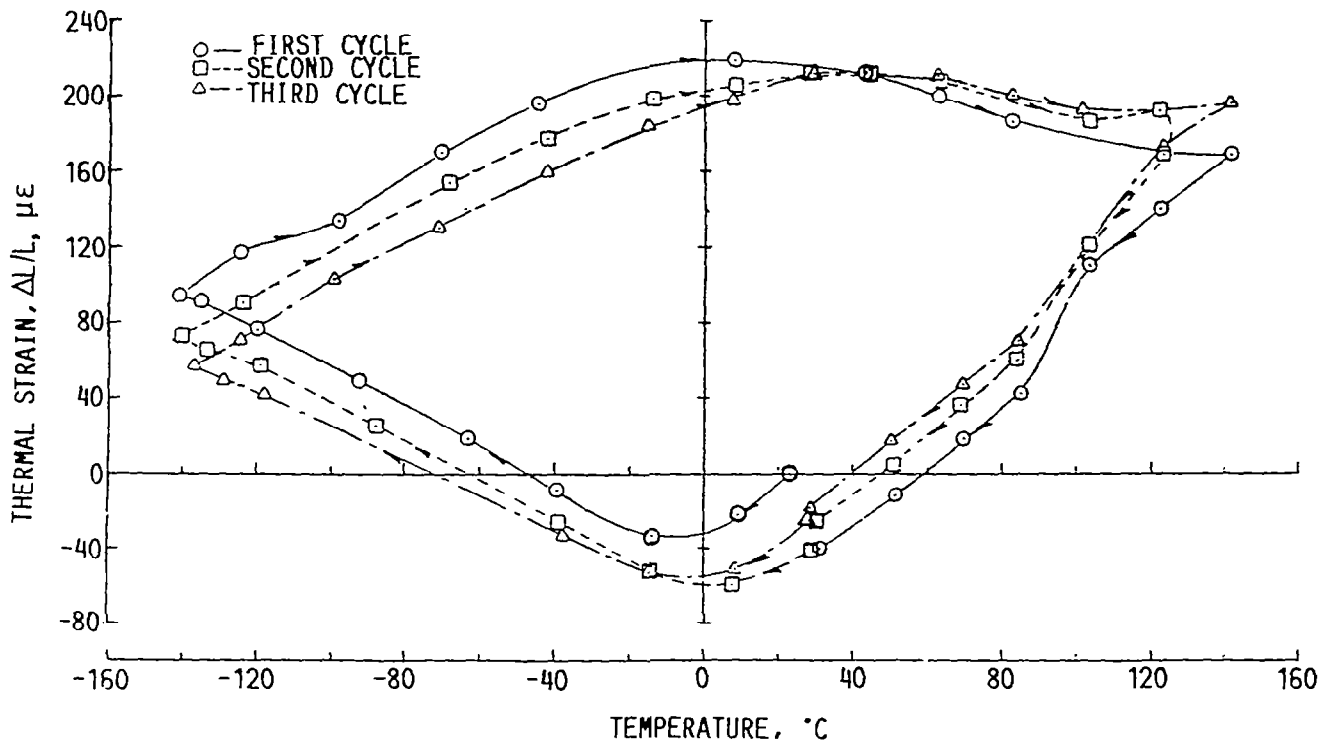
Figure 16

HYPERVELOCITY IMPACT EFFECTS ON COMPOSITE MATERIALS

Since the beginning of the space program, meteoroids (natural dust particles in space) were known to represent a potential danger to spacecraft. Studies and tests revealed that the primary danger resulted from objects smaller than a millimeter in diameter and that existing spacecraft structures, in most cases, offer sufficient protection against these particles. In 1970, several researchers estimated the probabilities for collision with the man-made objects being tracked by NORAD. These objects were larger than 10 cm in diameter, and although they represented a greater hazard than 10 cm meteoroids, the collision probabilities were sufficiently low that no further research was conducted.

However, beginning in the late 1970's, new findings combined with a possible change in future spacecraft structures caused renewed concern about space debris: (1) tests by NORAD revealed that a significant, untracked population of space debris existed, (2) most of the tracked population is accounted for by man-made objects in LEO which have exploded, and these explosions undoubtedly produce a significant population of small untracked particles, and (3) collisions between elements of the tracked debris population can be expected by the 1990's. These will result in sufficient fragments 1 mm and larger to exceed the hazard from meteoroids in certain regions of low Earth orbit. (See fig. 17). The emphasis on large, long-duration lightweight structures increases the sensitivity to spacecraft structures to collisions.

NASA/JSC is conducting studies and ground tests to determine the current and expected debris environment.

TECHNICAL HIGHLIGHTS: BACKGROUND INFORMATION ON SPACE DEBRIS

o STATISTICAL ANALYSIS OF SPACE DEBRIS SHOWS THERE IS A POTENTIAL FOR HYPERVELOCITY IMPACTS ON LARGE STRUCTURES IN 1990'S.

o 1995 FORECAST IS THAT 1 IMPACT PER YEAR OF 1 MM OBJECTS, 1 IMPACT PER 10 YRS OF 1 CM OBJECTS WILL OCCUR ON 30x30 METER STRUCTURE IN LEO.

o HYPERVELOCITY IMPACT WITH EVEN 1 MM OBJECT CAN CAUSE SIGNIFICANT DAMAGE.

o FORECAST BASED ON REASONABLE EXTRAPOLATION FROM NORAD RADAR, WHICH CAN ONLY MEASURE DOWN TO 4 CM OBJECTS.

o ACTUAL SITUATION MAY BE BETTER OR WORSE.

o MEASUREMENTS OF SMALL DEBRIS PLANNED.

Figure 17

HYPERVELOCITY TESTS

Meteoroid impact velocities range from 11 km/sec to 72 km/sec, averaging 20 km/sec. These velocities can only be duplicated in the lab for sub-micron size particles using a Van de Graaff accelerator. However, since much larger particles are likely to cause damage to spacecraft, most tests are conducted at between 5 to 10 km/sec using a light gas gun (refs. 10 and 11). Past tests usually consisted of firing either glass or metal projectiles varying in size from a fraction of a millimeter to a couple of centimeters in diameter. The target material was usually an aluminum spacecraft structure, although a significant amount of testing was conducted into glass. Figure 18 shows typical results of hypervelocity impact tests on aluminum. These tests revealed that the most effective way to protect against hypervelocity impacts is to divide the shield into 2 layers. The first layer acts as a "bumper" breaking up the projectile and spreading its energy over a larger area of the second layer. Such a design decreases the weight of an impact shield by a factor of 5 to 10 over a single layer.

Because typical space debris collision velocities average 10 km/sec, all the hypervelocity impact testing into aluminum and glass can be applied to the man-made hazard. However, little or no testing has been conducted on composite materials planned for future spacecraft. NASA/JSC plans to conduct such tests and compare the results with previous tests on aluminum. A light gas gun capable of firing a 0.15-cm projectile at 8 km/sec has been constructed. Larger projectiles, up to 2 cm in diameter, are planned to be fired at 10 km/sec using an Ames Research Center gun.

AT 10 km/sec, EVEN SMALL PROJECTILES CAUSE CONSIDERABLE DAMAGE

O

1-mm DIAMETER ALUMINUM PROJECTILE AT 10 km/sec (ENERGY = 54 ft-lb)

5-mm THICK ALUMINUM TARGET

TARGET PENETRATED, PRODUCING 100 TIMES AS MUCH EJECTA MASS AS THE PROJECTILE
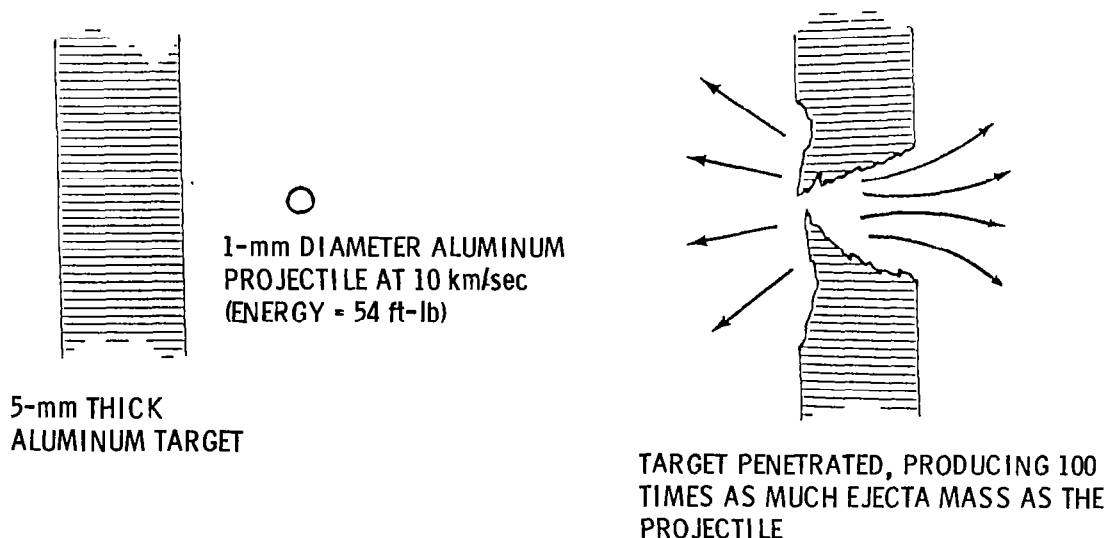
ORBITAL DEBRIS WILL PENETRATE APPROXIMATELY 5 PARTICLE DIAMETERS INTO A SINGLE SHEET TARGET.

Figure 18

EDGE DELAMINATION TENSION TEST MEASURES

INTERLAMINAR FRACTURE TOUGHNESS

A simple test has been developed for measuring the interlaminar fracture toughness of composites made with toughened matrix resins (ref. 12). The test involves measuring the stiffness, E_{LAM}, and nominal strain at onset of delamination, ε_c, during a tension test of an 11-ply $[\pm30/\pm30/90/\overline{90}]_s$ laminate (fig. 19). These quantities, along with the measured thickness t, are substituted into a closed-form equation for the strain energy release rate, G, for edge delamination growth in an unnotched laminate (ref. 13). The E* term in the equation is the stiffness of the $[\pm30/\pm30/90/\overline{90}]_s$ laminate if the 30/90 interfaces were completely delaminated. It can be calculated from the simple rule of mixtures equation shown in figure 19 by substituting the laminate stiffness measured during tension test of $[\pm30]_s$ and $[90]_n$ laminates. The critical value of G_c at delamination onset is a measure of the interlaminar fracture toughness of the composite. This edge delamination test is being used by Boeing, Douglas, and Lockheed under the NASA ACEE (Aircraft Energy Efficiency) Key Technologies contracts to screen toughened resin composites for improved delamination resistance (ref. 14).

ELEVEN-PLY $\left[\pm30/\pm30/90/\overline{90}\right]_s$ LAMINATE

LAMINATE STIFFNESS; DELAMINATION ONSET

INTERLAMINAR
FRACTURE TOUGHNESS

$$G_c = \frac{\varepsilon_c^2 t}{2}\left(E_{LAM} - E^*\right)$$

SUBLAMINATE STIFFNESS

$[\pm30]_s$

$[90]_n$

$$E^* = \frac{8E_{(\pm30)_s} + 3E_{(90)_n}}{11}$$
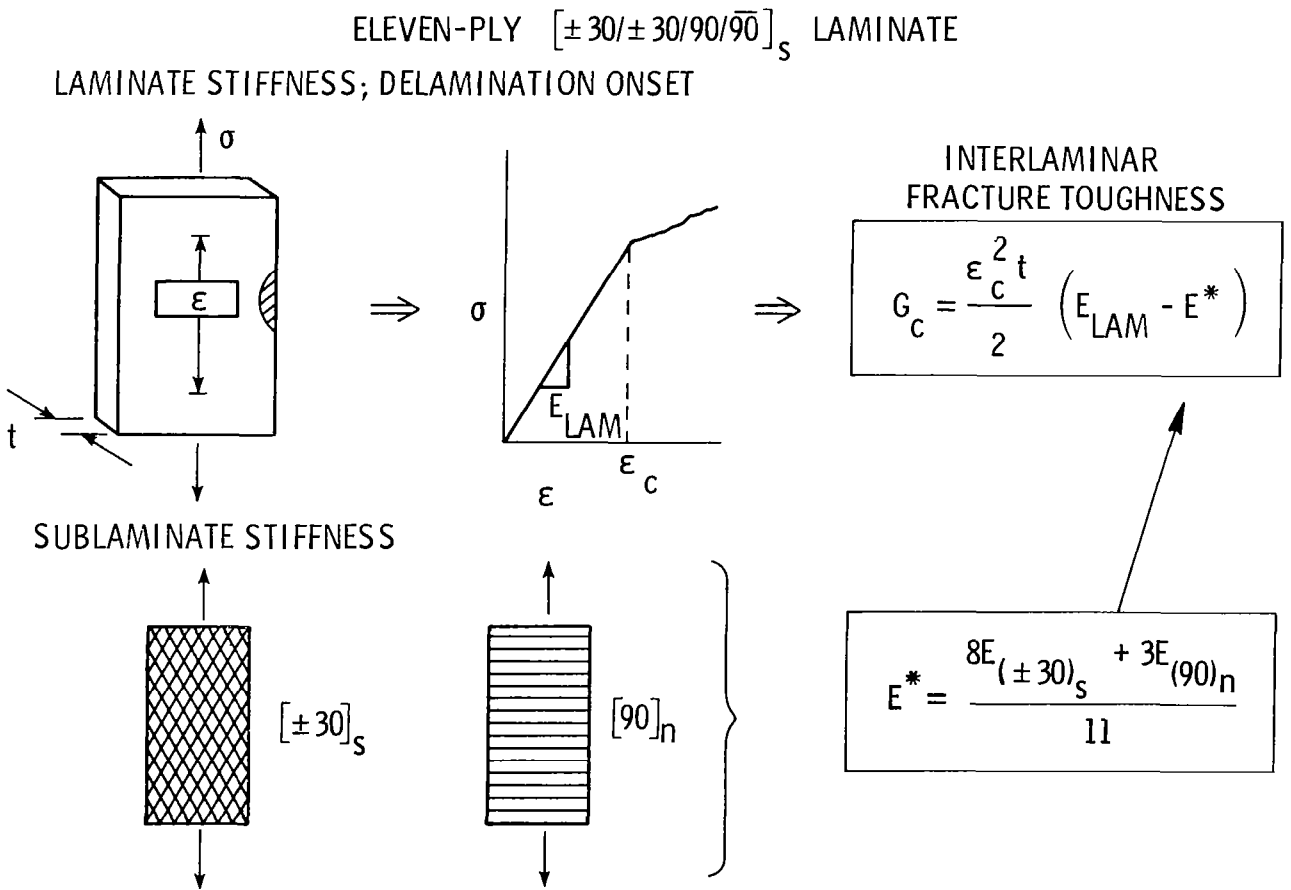
Figure 19

DELAMINATION ONSET PREDICTED

To predict the onset of delaminations in realistic unnotched laminates (ref. 13), quasi-static tension tests were conducted on the $[\pm 30/\pm 30/90/\overline{90}]_s$ laminates. The applied strain recorded at the onset of delamination, ε_c, was used to calculate a critical strain energy release rate, G_c. Then, G_c was used to predict the onset of delamination in more complex laminates. Figure 20 shows data and predictions for three $[+45_n/-45_n/0_n/90_n]_s$ laminates all having the same layup but with different ply thicknesses. For example, $n = 1$ is an 8-ply laminate, $n = 2$ is a 16-ply laminate, and $n = 3$ is a 24-ply laminate. The predictions agreed well with experimental data, indicating that G_c was a material property. Furthermore, the trend of lower ε_c for thicker laminates was correctly predicted. This trend could not be predicted by a critical interlaminar stress criterion.

$$\left[+45_n/-45_n/0_n/90_n\right]_s \quad \text{GRAPHITE EPOXY}$$

$$\varepsilon_c = \sqrt{\frac{2\,G_c}{t\left[E_{LAM} - E^*\right]}}$$

Figure 20

233
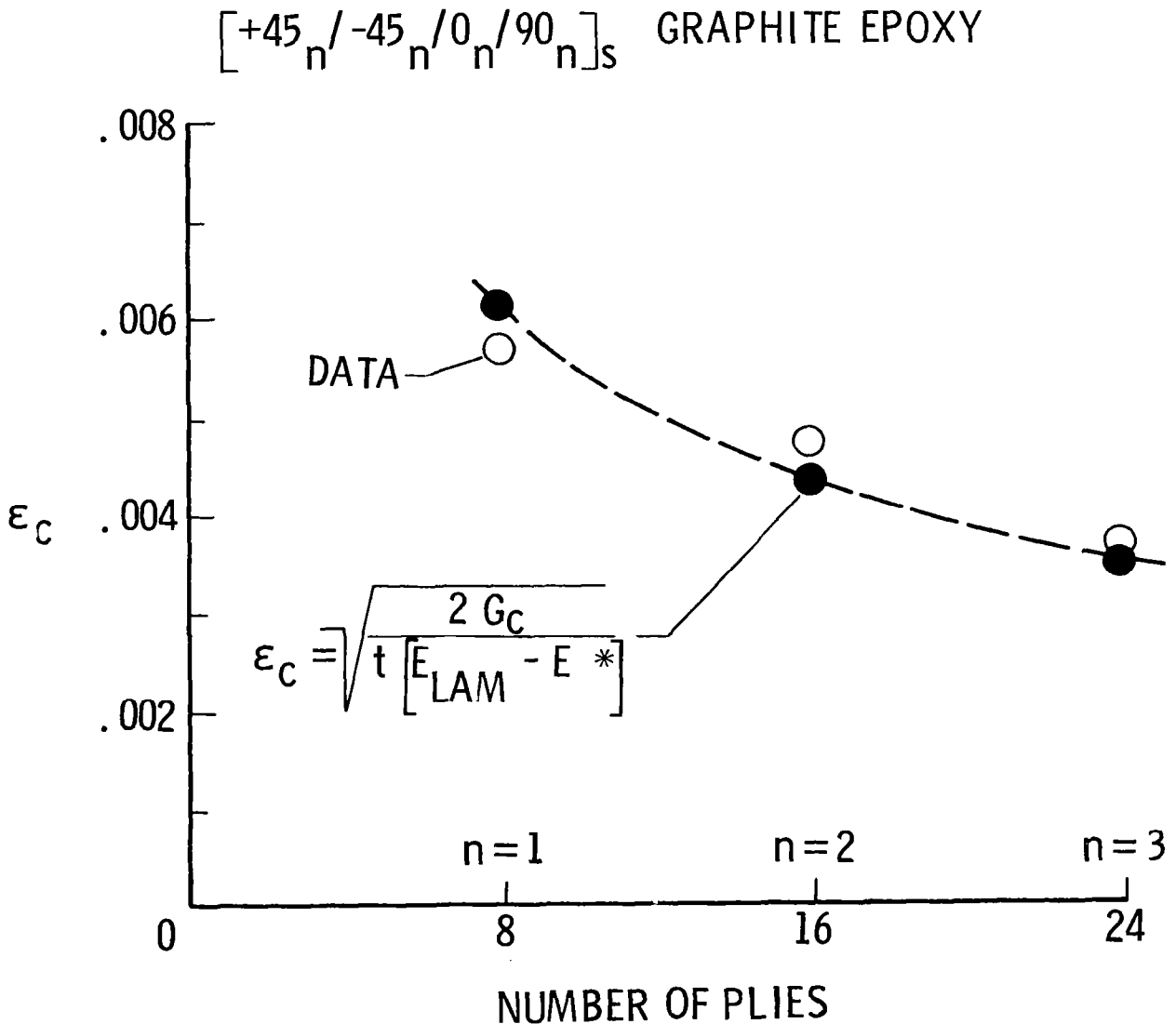
THERMAL CONTROL COATING REQUIREMENTS FOR SPACE STRUCTURES

The basic requirement for thermal control coatings is to keep spacecraft components within allowable temperature limits. Thermal designers have two major problems. The first occurs when the temperature limit is dictated only by the solar heat input (for example, large-area structures) and the second occurs when both solar and internal heat are thermal inputs (for example, a manned habitat). In each case a coating with a different ratio of solar absorptance to thermal emittance is required. In figure 21 the coating requirements for a composite structure in GEO are compared to the requirements for a manned habitat in LEO. The major differences are: (1) low-emittance coatings are required for the composite structure to reduce the extent of cooldown during a solar occult, (2) coating to be used in GEO must be able to withstand high-energy electrons and protons in addition to UV, and (3) a higher electrical conductivity is required in GEO to eliminate spacecraft charging. Contamination would be a major source of coating performance degradation for the manned habitat because of contaminants from the Shuttle. However, repair or refurbishment of coatings can be considered for this application but not for GEO.

	COMPOSITE STRUCTURE GEO	MANNED HABITAT LEO
OPTICAL PROPERTIES	α/ε – SELECTABLE WITH $\varepsilon \leq 0.3$	α/ε – SELECTABLE WITH $\varepsilon \geq 0.8$
TEMPERATURE	-100° TO $+80^\circ$C	-100° TO $+40^\circ$C
ENVIRONMENT	UV, e^-, p^+, VAC, ΔT	UV, VAC, ΔT
ELECT. CONDUCTIVITY	$\leq 10^{-8}$ (ohm^{-1} – cm^{-1})	10^{-8} – 10^{-17} (ohm^{-1} – cm^{-1})
LIFETIME	10 TO 20 YEARS	10 YEARS

Figure 21

METAL IONS IMPROVE POLYIMIDE PROPERTIES

Polymer films are attractive for various aerospace applications such as antenna surfaces, adhesives, coatings, etc. However, covalently bonded polymers inherently lack the electrical conductivity desirable to resist spacecraft charging or to act as a Faraday Cage, and even the most stable polymers developed to date have limited temperature capability.

Several options are available to increase electrical conductivity in a polymer film: (1) mix metallic flakes or powders into the formulation; (2) laminate metallic/polymer films; and (3) add complex metallic ions to the backbone of the polymer structure. The latter is a very attractive option because the potential for conductivity increases with less increase in the characteristically low polymer film density than is experienced with the other options, but this application has had relatively little attention until recently.

Recent research activity has demonstrated the potential of certain selected metallic ion additions to a polyimide to increase electrical conductivity in a film and high-temperature performance in an adhesive. The addition of the aluminum-ion complex increased adhesive shear strength significantly at 275°C and 300°C. Even more dramatic was the increased electrical conductivity of polyimide films when palladium- and palladium/lithium-ion complexes were added. Electrical conductivity at room temperature was increased by 8 orders of magnitude. (See fig. 22.)

This research is now directed towards elucidation of the mechanisms of electrical (and thermal) conductivity in these metallic ion containing polymers to provide a rational basis for the selection of the most effective ion additions for specific property improvements (ref. 15).
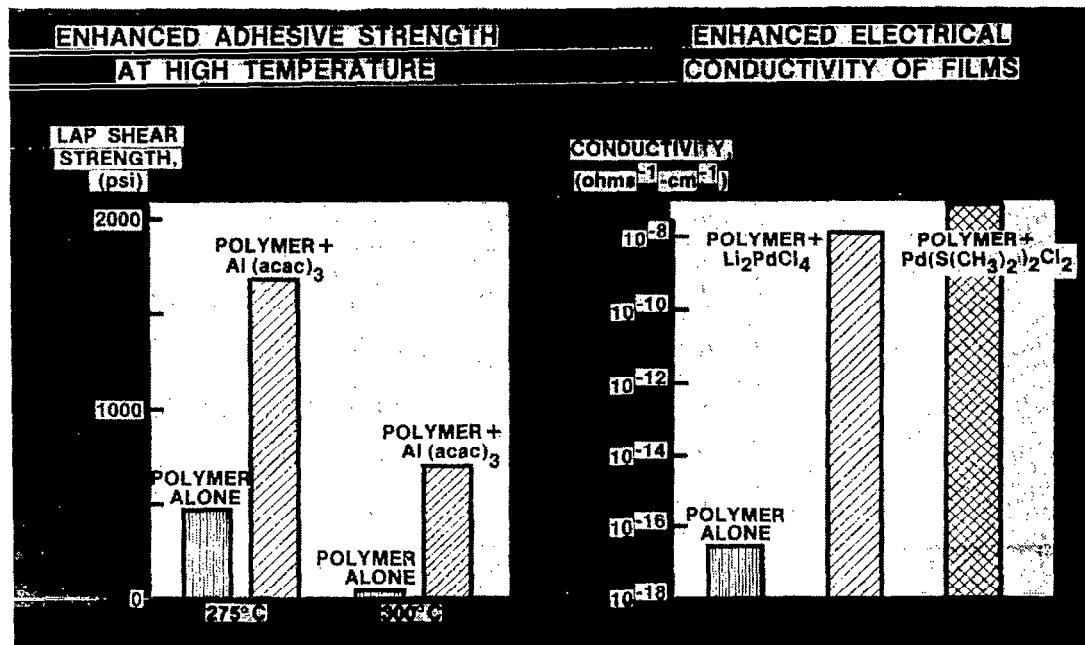
Figure 22

TAILORING POLYMER STRUCTURES TO CONTROL PROPERTIES

The oxidative stability and color (transparency) of linear aromatic polymers can be tailored by altering chemical groups that bridge the aromatic rings. In figure 23 below, the $-\overset{\overset{O}{\|}}{C}-$ (carbonyl) bridging group is in the dianhydride-derived portion of the polymer and the -O- (oxygen) bridging group is in the diamine-derived portion of the commercial polyimide. When this polyimide was tested at 350°C, the polymer film lost half of its initial weight in 80 hours. Other experimental polyimides were prepared and tested in the same manner, but the bridging groups were altered as shown in the figure. With the carbonyl bridge in both components (LARC Polyimide I), oxidative stability was improved by a factor of 2 without affecting the color transparency. Altering the structure by placing the oxygen bridge in both components (LARC Polyimide II) provided a polymer film with good transparency (colorless) and oxidative stability comparable to the commercial polyimide.

These results indicate the progress being made in understanding how to control properties by tailoring the chemical structure of the polymer. For polymer coatings good transparency can be achieved without sacrificing oxidative stability, or the structure can be altered to achieve excellent gains in thermooxidative stability (ref. 16).
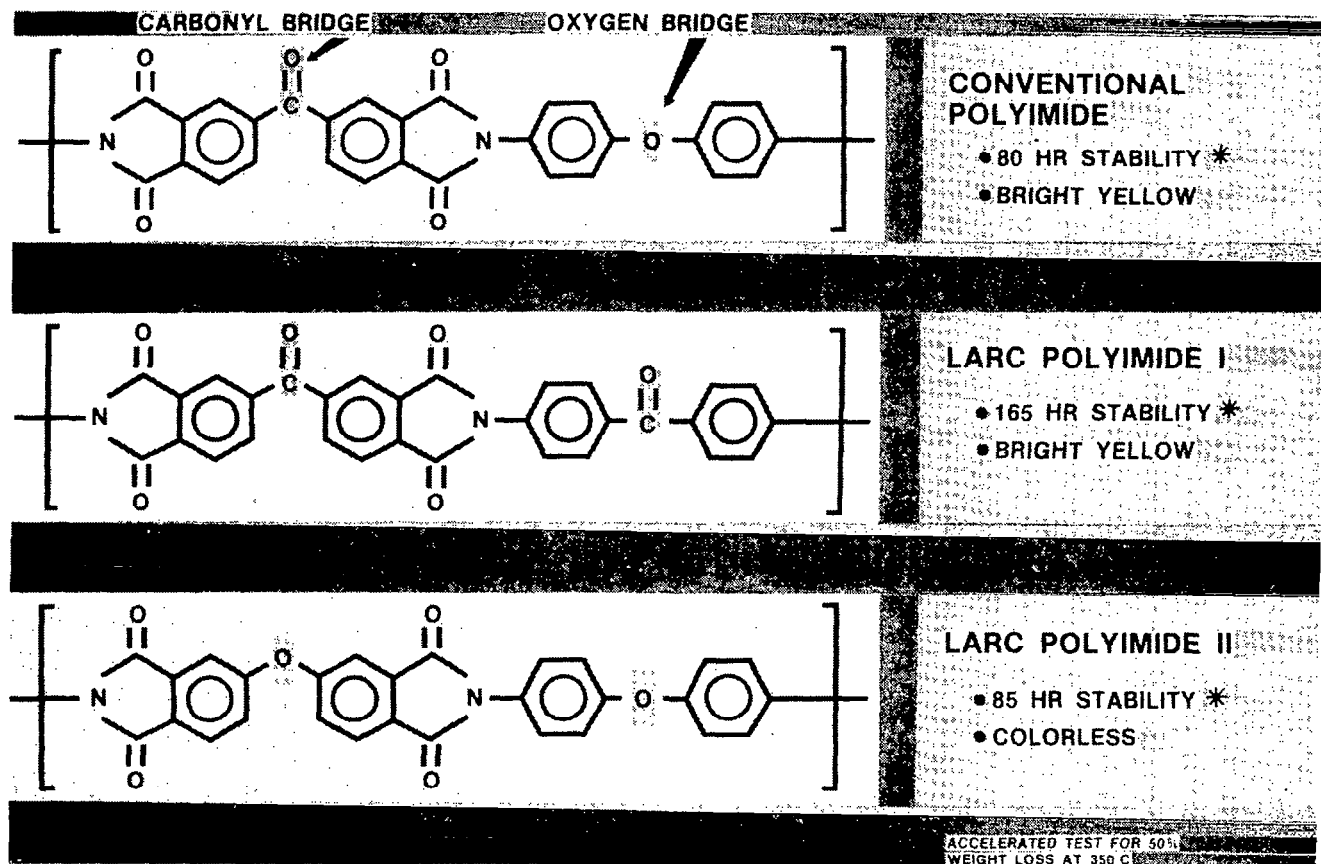
Figure 23

DEGRADATION OF THERMAL CONTROL COATINGS

The optical properties of thermal control coatings are changed by the space environment primarily because of radiation degradation. Some of the best available long-time data on coating performance in space flight are shown in figure 24. These data are from an Air Force flight experiment (AFML-TR-78-99) conducted in a polar orbit (ref. 17). The interesting part of this figure is that the 3 white paints exhibit a substantial increase (130%) in solar absorptance in 5 years and all three have about the same degradation rate. The second-surface mirror type coatings, which do not have pigments, also are grouped together in degradation but exhibit a much lower degradation of only 40% and remained stable over long periods. Because most of this degradation occurred in the first 2 or 3 months of flight, contamination is suspected as a primary source of degradation for these nonpigmented coatings.
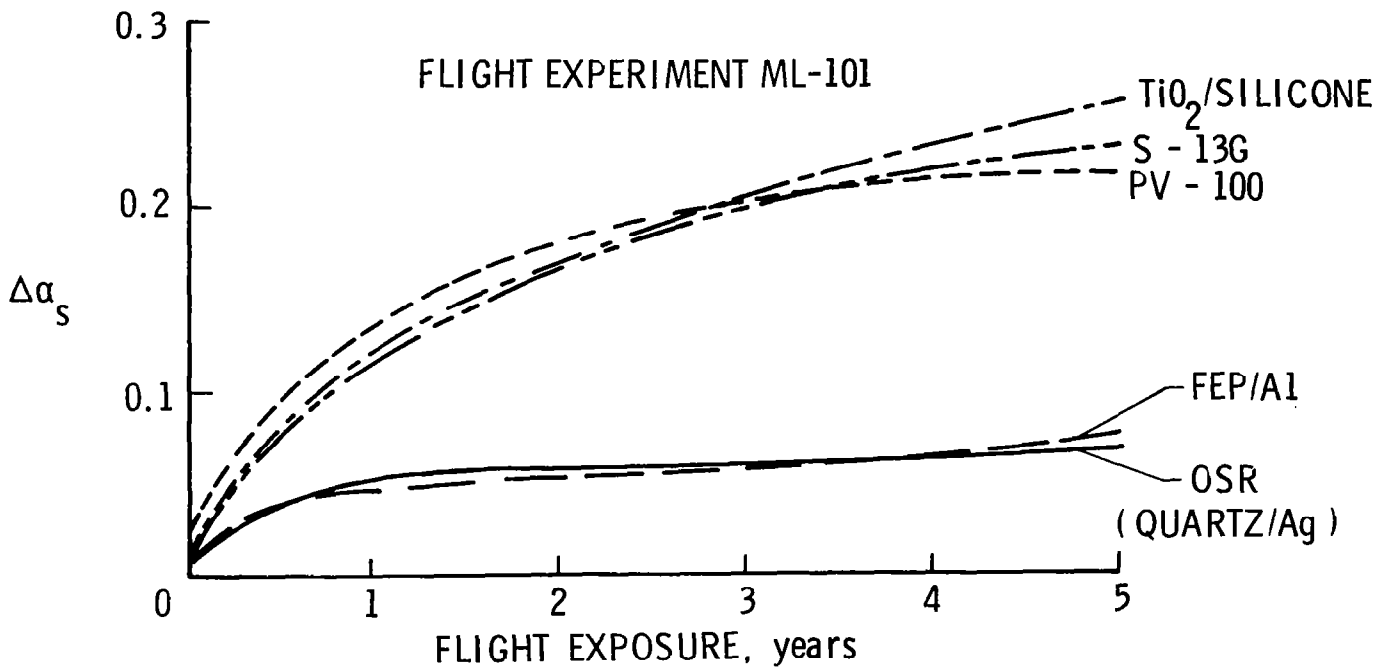
Figure 24

SUMMARY

    Spacecraft materials technology is a continuing research activity within
NASA. A coordinated multicenter research program has been undertaken to address
the key materials technology needs (see fig. 25) that have been identified for
large space structures. They include: development of space-durable graphite-
fiber-reinforced polymer and metal-matrix composites, development of long-life
thermal control coatings, and formulation of techniques and procedures to
minimize contamination of critical spacecraft surfaces. Results of ongoing
research programs are expected to significantly contribute to the data base
required for the confident design, construction, and deployment of future large
space systems.

o LIGHTWEIGHT COMPOSITE MATERIALS

       - LONG TERM ENVIRONMENTAL STABILITY
       - LOW EXPANSION/DIMENSIONAL STABILITY
       - DAMAGE TOLERANT CONCEPTS
       - PRECISION MANUFACTURING TECHNOLOGY

o COATINGS

       - TAILORED OPTICAL PROPERTIES
       - RADIATION, UV RESISTANT
       - MINIMUM SENSITIVITY TO CONTAMINATION
       - APPLICABLE TO STRUCTURAL SHAPES

o CONTAMINATION

       - EFFECTS ON MATERIALS
       - SOURCE CHARACTERIZATION
       - MASS TRANSPORT/DEPOSITION PHENOMENA

Figure 25

REFERENCES

1. King, J. H.: Solar Proton Fluences for 1977-1983 Space Missions. J. Spacecraft and Rockets, vol. 11, no. 6, June 1974, pp. 401-408.

2. West, G. S.; Wright, J. J.; and Euler, H. C.: Space and Planetary Environment Criteria Guidelines for Use In Space Vehicle Development, 1977 Revision. NASA TM-78119, Nov. 1977.

3. Schimmerling, W. S.; and Curtis, S. B.: Workshop on the Radiation Environment of the Satellite Power System. LBL-8581, Sept. 15, 1978.

4. Wolf, K. W.: Effect of Ionizing Radiation on the Mechanical and Structural Properties of Graphite Fiber Reinforced Composites. Ph.D. Dissertation, North Carolina State University, Raleigh, NC, Sept. 1982.

5. Santos, B.; and Sykes, G. F.: Radiation Effects on Polysulfone Films. Presented at 13th National SAMPE Tech. Conf. (Mt. Pocono, PA), Oct. 1981.

6. St. Clair, T. L.; and Yamaki, D. A.: A Thermoplastic Polyimidesulfone. Presented at First Technical Conference on Polyimides, Society of Plastic Engineers, Inc. (Ellenville, NY), Nov. 11-12, 1982.

7. Bowles, D. E.: The Effects of Microcracking on the Thermal Expansion of Graphite-Epoxy Composites. Large Space Systems Technology - 1981, NASA CP-2215, 1981.

8. Short, J. S.; Hyer, M. W.; Bowles, D. E.; and Tompkins S. S.: Thermal Expansion of Graphite-Epoxy Between 116K and 366K. Large Space Systems Technology - 1981, NASA CP-2215, 1981.

9. Min, B. K.; and Crossman, F. W.: History Dependent Thermo-mechanical Properties of Graphite-Aluminum Unidirectional Composites. Presented at 6th Conference on Composite Materials: Testing and Design, ASTM, May 1981. (ASTM STP-787.)

10. Meteoroid Damage Assessment. NASA SP-8040, May 1970.

11. Cour-Palais, B. G.: Space Vehicle Meteroid Shielding Design. European Space Agency SP-153, Oct. 1979.

12. O'Brien, T. K.; Johnston, N. J.; Morris, D. H.; and Simonds, R. A.: A Simple Test for the Interlaminar Fracture Toughness of Composites. SAMPE Journal, vol. 18, no. 4, 1982, pp. 8-15.

13. O'Brien, T. K.: Characterization of Delamination Onset and Growth in a Composite Laminate. Damage in Composites Materials, K. L. Reifsnider, ed., AST STP 775, American Society for Testing and Materials, 1982, pp. 140-167.

14. Standard Tests for Toughened Resin Composites. NASA RP-1092, 1982.

15. Taylor, L. T.; St. Clair, A. K.; Carver, V. C.; and Furtsch, T. A.: U. S. Patent 4,311,615, Jan. 19, 1982.

16. St. Clair, T. L.; St. Clair, A. K.; and Smith, E. N.: Structure-Solubility Relationships in Polymers. Academic Press, Chapter 15, pp. 199-215, 1977.

17. Winn, R. A.: ML-101 Thermal Control Coatings: Five Year Space Exposure. AFML-TR-78-99, July 1978.

SPACECRAFT MATERIAL APPLICATIONS -
LONG-TERM STABILITY QUESTIONS

F. W. Crossman
Lockheed Missiles and Space Co., Inc.
Sunnyvale, California

An examination of the materials concerns for a variety of spacecraft components shows that long-term stability within the space environment is a major issue in the design of large space antenna systems. This survey paper will review some of the more recent work on the effect of space environment on (1) thin films, (2) structural composites, and (3) thermal control materials. Degradation in thermal-mechanical and optical properties associated with atmospheric and trapped particles and ultraviolet light will be highlighted. Finally, the dimensional instability associated with microcracking during thermal cycling will be examined and a methodology for estimating thermal fatigue effects from results of mechanical fatigue tests will be presented.

SELECTED ANTENNA SYSTEMS COMPONENTS/MATERIALS CONCERNS

REFLECTOR RIB
     DIMENSIONAL STABILITY
     STIFFNESS
     WEIGHT
     ENVIRONMENTAL STABILITY
FEED SUPPORT BOOM
     DIMENSIONAL STABILITY
     STIFFNESS
     WEIGHT
     ENVIRONMENTAL STABILITY
SPACECRAFT SYSTEM MOUNT
     DIMENSIONAL STABILITY
     STIFFNESS
     STRENGTH
     ENVIRONMENTAL STABILITY
FOLDING SOLAR ARRAY
     DIMENSIONAL STABILITY
     STIFFNESS
     WEIGHT
     ENVIRONMENTAL STABILITY

     *** LONG TERM (3-10 YEAR) STABILITY
     (ENVIROMENTAL AND DIMENSIONAL)
     IS THE CRITICAL MATERIALS APPLICATION PROBLEM

Three potential sources of material degradation are (1) trapped electrons and protons, (2) sunlight, and (3) neutral and charged atoms associated with the upper atmosphere. Protons and electrons have a wide range of energies, but only electrons penetrate deeply enough in structural materials to have any bulk effect on properties. The effects of electrons have been investigated on a number of films and composites composed of polymer matrices. The simulation typically uses high-energy electrons at fluxes 2000 to 5000 times the natural exposure flux.

SPACE RADIATION EFFECTS ON SURFACE AND BULK PROPERTIES

THE ENVIRONMENT AT GEO
 TRAPPED ELECTRONS AND PROTONS
 SOLAR FLARES
 UV
 MICROMETEOROIDS

10^9 rad ELECTRON DOSE DURING 10 YEARS AT GEO
TEN TIMES HIGHER PROTON DOSE

EXPERIMENTAL EVALUATION OF POLYMER BASED FILMS AND COMPOSITES
IN SIMULATED SPACE ENVIRONMENT (ELECTRON, PROTON, UV, AND VACUUM)
USING HIGH ENERGY (.1-1.5 MeV PENETRATING ELECTRONS)

MATERIALS TESTED TO DATE [REFERENCES IN BRACKETS]

LOW TEMPERATURE MATERIALS
 TEFLON/VP AG/INCONEL FILM   [1]
 GY70/X30 250 DEG F CURE COMPOSITE [2]
 PITCH 75/948 "   "   "   [3]
 KEVLAR 49/E719   "   "   [3]

HIGH TEMPERATURE MATERIALS
 KAPTON/VP AL POLYIMIDE FILM   [1]
 PES   POLYSULFONE FILM [4]
 RADEL 5000   "   [4]
 P1700   "   [4]
 BISPHENOL-A HQ   FILM   [4]

 GY70/934 350 DEG F CURE COMPOSITE [1]
 HMS/934   "   [1]
 T300/934   "   [2,4]
 T300/5208   "   [4]
 T50(PAN)/P1700 POLYSULFONE COMP. [4]
 CE6000/P1700   "   [4]
 T50(PAN)/F263 BISMALEIMIDE COMP. [3]

Solar flares cause a time variation of this flux, so many investigations have examined property changes after exposure to total fluences 10 times greater than those projected for the lifetime of the spacecraft. For example, the total electron fluence at GEO (and within the Van Allen belt) is on the order of 3×10^9 rad over a 30-year period. Thus even the low-temperature materials which exhibit property changes at fluences greater than 10^9 rad are probably acceptable for 5- to 10-year orbiting lifetimes.

SPACE RADIATION EFFECTS IN GEO -- CONCLUSIONS

(1) LOW TEMPERATURE MATERIALS ARE MARGINAL FOR LONG TERM USE

    TEFLON EMBRITTLED [1]
    250 DEG F CURE COMPOSITES DIM. CHANGES DURING EXPOSURE [3]
    HIGH TEMPERATURE MECHANICAL PROPERTIES REDUCED [3]
    GLASS TRANSITION TEMPERATURES REDUCED [2,3]
    OPTICAL ABSORPTIVITY INCREASED [1]

... BUT

    THE THRESHOLD FOR ALTERED PROPERTIES IS $> 10^9$ RAD ELECTRONS

(2) HIGH TEMPERATURE MATERIALS WILL STAND UP TO >10 TIMES ANTICIPATED LIFETIME ELECTRON DOSES

    NO SIGNIFICANT CHANGES IN DIM. STABILITY [3,4]
    NO SIGNIFICANT CHANGES IN MECHANICAL PROPS. [1-4]
    SMALL INCREASE IN OPTICAL ABSORPTIVITY [1]

... BUT

    SOME CONCERN FOR SEMI-TRANSPARENCY OF COMPOSITES
    TO ELECTRON RADIATION, I. E. SHIELDING OF ELECTRONIC
    COMPONENTS MAY BE NEEDED [5]

Most thermal control materials use polymer layers, as shown below. Simulation of solar UV has been conducted on a number of thermal control materials. In all cases it is necessary to account for changes in absorptivity during the lifetime of the spacecraft.

UV DEGRADATION OF THERMAL CONTROL SURFACES IN LEO

MATERIAL	IR EMISSIVITY	SOLAR ABSORPTIVITY - INITIAL/AFTER 3 YRS
1ST SURFACE ALUMINIZED KAPTON	.03	.12/.13
2ND SURFACE ALUMINIZED KAPTON	.80	.45/.55
" " TEFLON	.80	.07/.17
1ST SURFACE GOLDIZED MYLAR	.025	.20/.21
2ND SURFACE SILVERIZED KAPTON	.80	.07/.17

UV DEGRADATION OF SOLAR ABSORPTIVITY IN GEO

MATERIAL	IR EMISSIVITY	SOLAR ABSORPTIVITY - INITIAL/AFTER 7 YRS
CLEAR ANODIZED 6061 AL	.79	.38/.55
CLEANED 6061 AL	.04	.24/.26
CLEANED TI-6-4	.10	.50/.50
Z306 BLACK CHEMGLAZE POLYURETHANE	.87	.38/.55
S13GLO WHITE SILICONE	.88	.22/.55
BARE GR/EPOXY	.78	.92/.85
2ND SURF. ALUMINIZED KAPTON	.80	.45/.77
2ND SURF. ALUMINIZED TEFLON	.80	.14/.32

Significant surface damage has been observed on organic and some inorganic materials exposed in the Space Shuttle bay on the first four orbital flights.

M A T E R I A L S   D E G R A D A T I O N   I N   L . E . O .

MATERIAL	STRUCTURE	PHYSICAL RESULTS
Carbon	Flame Sprayed Amorphous	Disappeared
Aquadag	Collodial Carbon Suspension	Disappeared
A276	Urethane Based White Paint	Apparent Rapid
A971	Urethane Based Yellow Paint	Aging
Silver	Metallic Coating	Converted to Oxide
Osmium	Metallic Coating	Disappeared
Torlon	Polyamide-imide Casting	White Powdery Surface
Kapton	Polyimide Film	Surface Appears Unevenly Eroded, Weight Loss
Mylar	Polyester Film	Comparable Weight Loss to Kapton
Teflon TFE and Teflon FEP	Perfluoroalkane Films	Slight Surface Degradation

On the STS-4 flight, experiments were conducted to demonstrate that the mass loss is associated with a combination of impinging atom flux associated with the motion of the Shuttle through the ionosphere and the simultaneous exposure to sunlight.

NASA STS-4 POST FLIGHT MEASUREMENTS

o STS-4 IECM INDUCED ENVIRONMENT CONTAMINATION EXPERIMENT (300 KM)

o PLASTIC FILM COVERED WITNESS PLATES ½" DIAMETER

o EXPOSED TO IMPINGING ATOMIC OXYGEN AND SOLAR RADIATION IN FORWARD VELOCITY VECTOR

o LUBERT J. LEGER ESTIMATES (ref. 6) 3 HOUR EXPOSURE PERIOD

Trade Name	Thickness (Mils)	Thickness Loss (Mils) Exposed Film		Protected Film	
o Mylar Film	0.5	0.073	0.071	0.007	0.003
o Kapton Film	0.3	0.073	0.068	0	0.005
	0.5	0.064	0.064	0	0.002
	1.0	0.068	0.067	0.002	0.002
o TFE Film	——	0.003	0.002	0.0009	0
o FEP Film	——	0.003	0.005	0.001	0.001

The Shuttle orbit environment includes a variety of molecules, atoms, and ions which peak in concentration at 100 to 200 km. However, the concentration levels can vary by an order of magnitude, depending on the solar flare activity level, as shown in the left-hand figure below. The concentration of charged particles is orders of magnitude less (right-hand figure) but is potentially more damaging to polymer films. Leger [6] attributes the mass loss to neutral atomic oxygen, but recent Lockheed studies (unpublished results) have shown that oxygen plasma combined with UV exposure results in similar surface degradation.

Distribution of major constituents of neutral atmosphere at extremes of solar activity

Neutral atmospheric density

Solid lines: solar maximum
Dashed lines: solar minimum

Altitude, km

Concentration, cm^{-3}
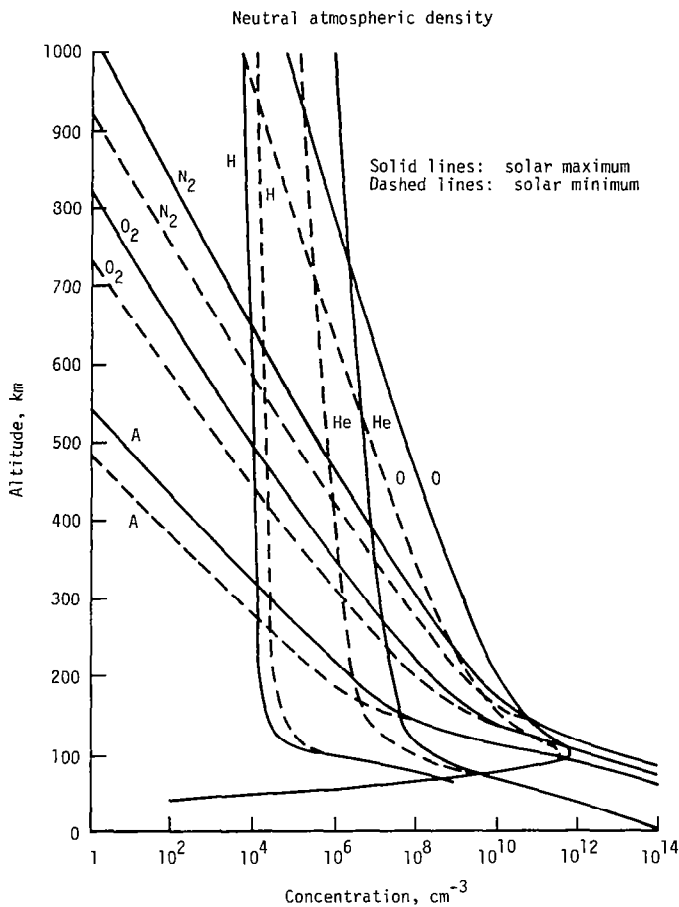
Ionic composition of solar minimum - daytime winter ionosphere

Altitude, km

Number/cm^3
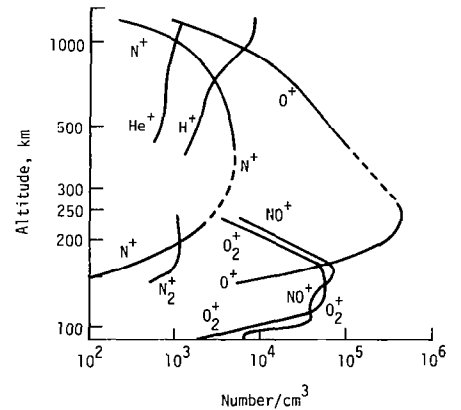
EFFECTS OF NEUTRAL AND CHARGED PARTICLES IN LEO -- CONCLUSIONS

(1) DEGRADATION GREATEST FOR CHARGED PARTICLES COMBINED WITH UV POSSIBLY ASSOCIATED WITH FLAKING OFF OF DEGRADED SURFACE BY PHOTONS

(2) MAGNITUDE OF NEUTRAL AND CHARGED PARTICLE FLUX HIGHLY DEPENDENT ON SOLAR FLARE ACTIVITY

(3) SHIELDING FROM ORBITAL FLUX INHIBITS DEGRADATION [6]

(4) DEGRADATION MECHANISM(S) AND KINETICS OF REACTION NEED FURTHER STUDY

(5) NEED TO INVESTIGATE MORE HIGHLY THERMO-OXIDATIVE RESISTANT POLYMER FILM CANDIDATES

(6) NOT A PROBLEM AT GEO SINCE THE DENSITIES OF NEUTRAL AND CHARGED PARTICLES ARE ORDERS OF MAGNITUDE LESS AT THIS ORBIT

One of the least understood contributions to dimensional instability of structural composites is the effect of microcracking. Bowles [7] was the first to show that the measured density of microcracks could be related to a change in the coefficient of thermal expansion (CTE) by properly accounting for the reduction in effective transverse modulus as a function of microcracking [8]. He was able to predict the CTE changes in quasi-isotropic laminates from microcrack densities induced by prior mechanical loading and measured by edge replication techniques.

Microcrack density is a function not only of static load level (top figure) but also of the number of mechanical fatigue cycles (bottom figure). Fatigue-induced microcracking can occur at stress levels below the threshold stress determined by static tensile loading [9, 10].
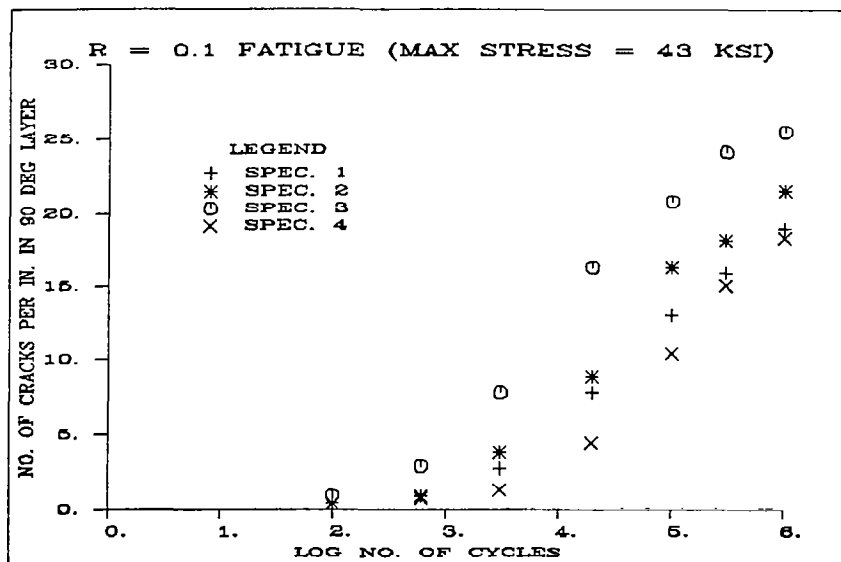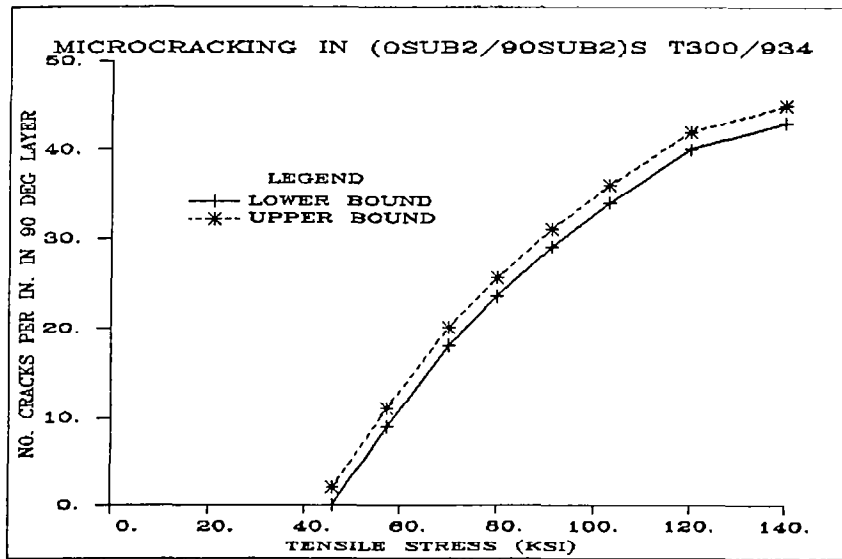
In the figures which follow, microcracking experiments on $(0_290_n)_s$ T300/934 laminates will be examined, and the CTE response during thermal fatigue will be calculated from the data associated with mechanical loading.

Laminate analysis has been employed in conjunction with experimental measurements of microcrack initiation under tensile loading to determine the "in situ" transverse stress (YT) at onset of microcracking in the 90° ply of a series of $(0_290_n)_s$ T300/943 laminates where n varies from 1 to 8 [11]. Note that the effective onset stress level depends strongly on the thickness of the 90° ply and can be as high as twice the transverse tensile strength of unidirectional specimens. This effect is associated with constraints of the neighboring plies, which act to reduce the energy release rate during microcrack formation [10]. From the laminate analysis and mechanical loading experiments it is possible to predict microcrack onset under different combinations of thermal and mechanically applied stresses. In particular, we can determine the conditions under which microcracking is induced by thermal residual stress alone.

[From ref. 9]

$(0_2/90_n)_s$

YT
(KSI)

APPLIED STRESS

RESIDUAL STRESS
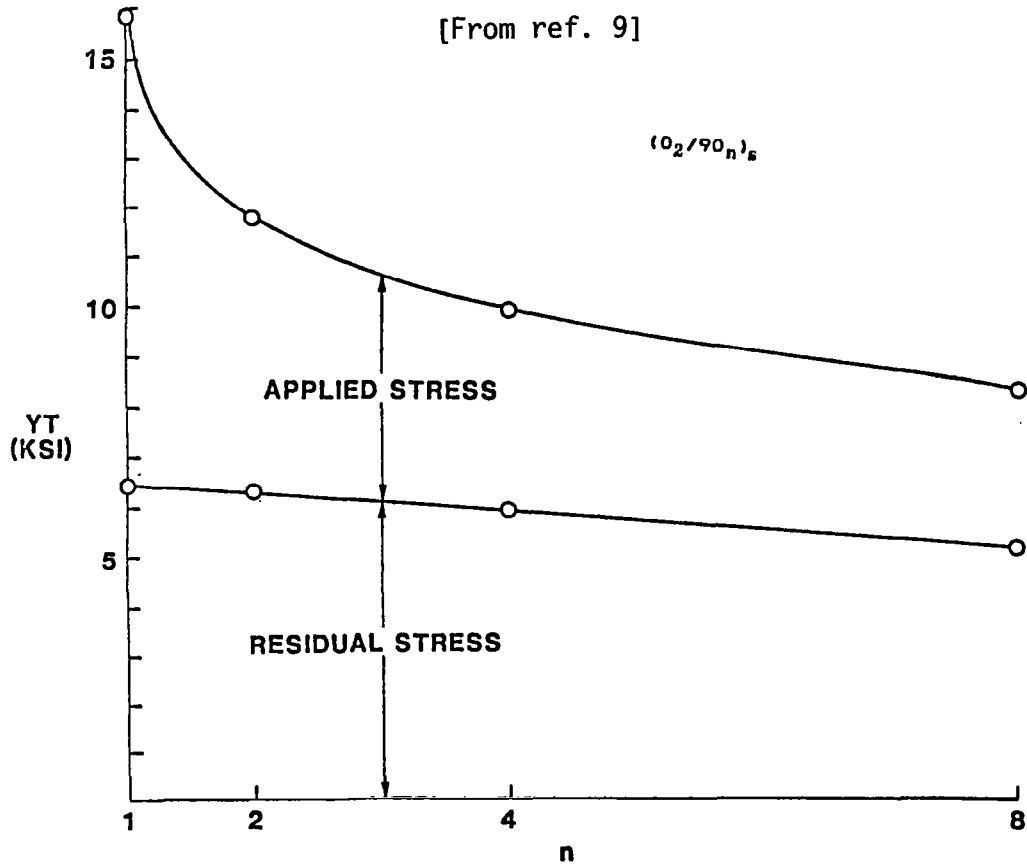
The top figure shows the relationship between microcrack density, maximum fatigue stress level, and number of fatigue cycles. Laminate analysis was used to convert the stress axis to a delta temperature scale. Delta T is defined as T - T (stress free). For T300/934, the stress free value is 340°F [11]. Given a possible thermal cycling range of -250/250°F in GEO, delta T in the bottom figure is 590° and the 3000 to 4000 thermal cycles during a 10-year GEO application can result in the buildup of 15 to 20 transverse cracks per inch in the $(0_290_2)_s$ T300/934 laminate.
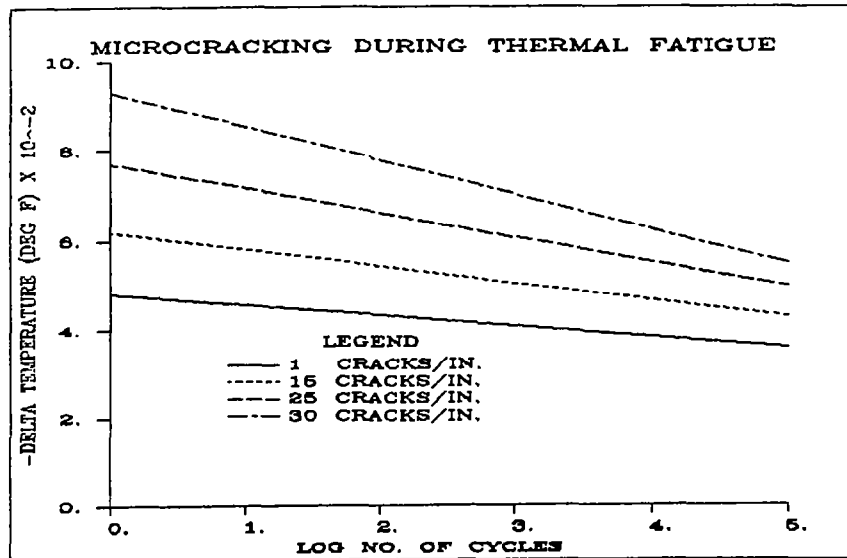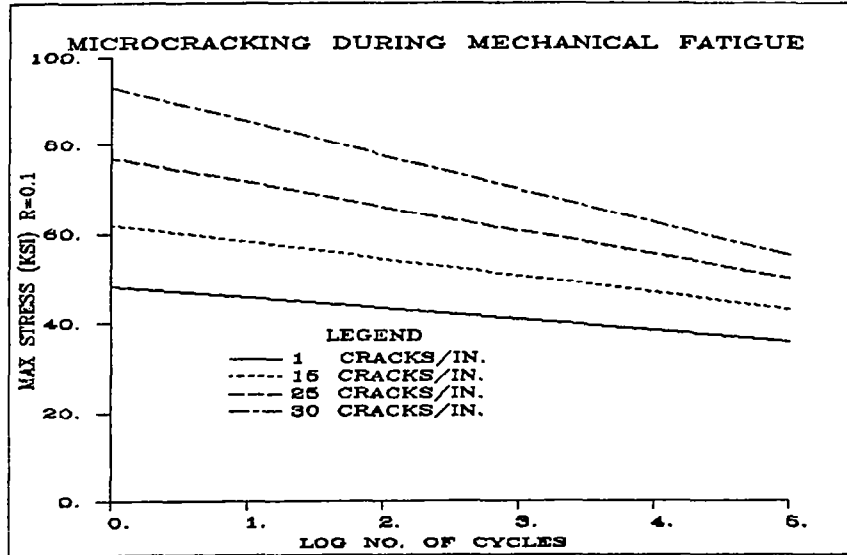
The alteration of effective transverse modulus due to microcracking was obtained by finite-element micromechanical modeling [8] and is represented in a nondimensional manner in the top figure. For the $(0_2 90_2)$ laminate, the relation between effective transverse modulus and crack density in the 90° layer is given in the bottom figure. This reduced modulus was then substituted in a laminate analysis to predict the effect of microcracking on CTE in the manner of Bowles [7]. For purposes of illustration the CTE is assumed to be constant over the temperature range $-250/340^\circ F$.

TRANSV. MODULUS OF 90 DEG LAYER VS CRACKING

LEGEND
——+—— (0/90)S LAM. [11]

CRACK SPACING/(2*PLY THICKNESS)

TRANSV. MODULUS OF 90 DEG LAYER VS CRACKING

LEGEND
——+—— FROM REF. 11

NO. OF CRACKS PER IN. IN 90 DEG LAYER
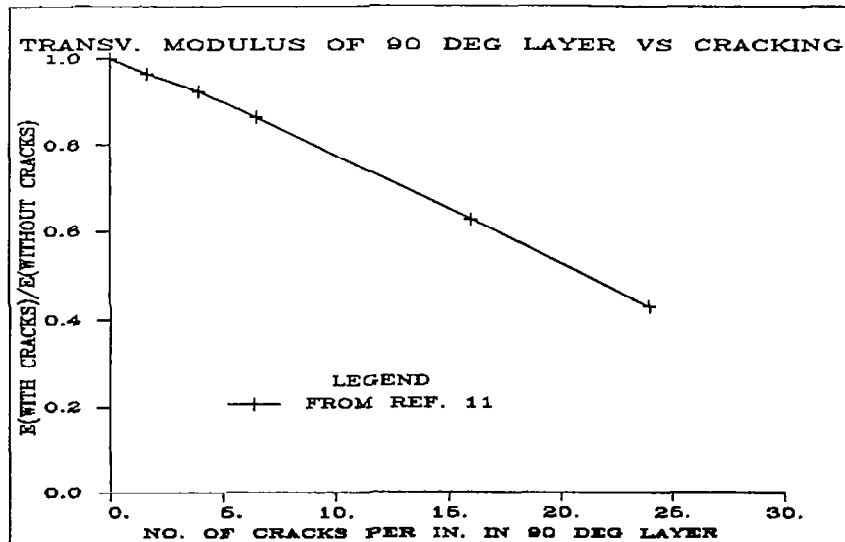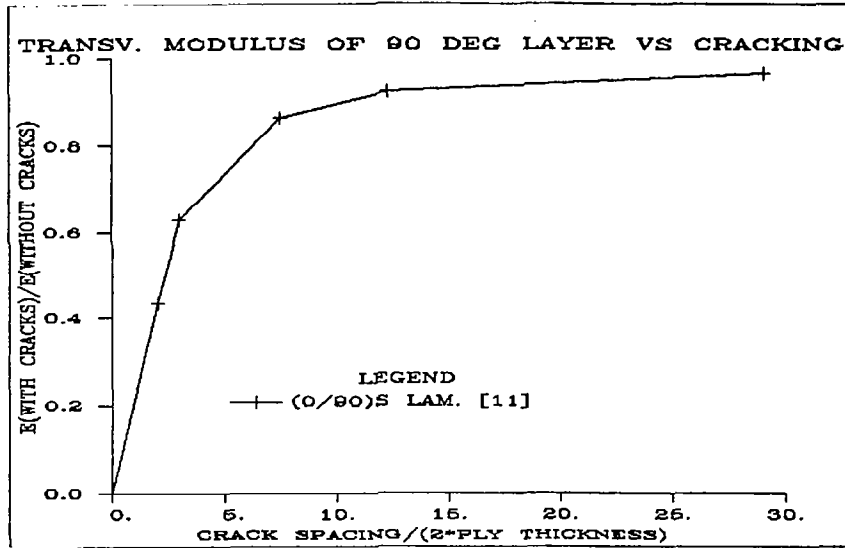
The magnitude and sign of CTE change associated with microcracking are seen to depend on the choice of materials. The stiffer GY70 $(0_2 90_2)_s$ laminate is less sensitive to microcracking. Cracking is an elastic process which does not alter the stress-free temperature of the laminate. This is illustrated in the bottom figure, where total strain is plotted as a function of temperature. The absolute dimensional change at 75°F is 140 micro-strain after 1000 -250/250°F thermal cycles and a crack density of 15/in. Microcracking has, in effect, improved the dimensional stability of this laminate.

CTE CHANGE WITH MICROCRACK DENSITY

LEGEND
—+— T300/934
--*-- GY70/339

THERMAL STRAIN VS TEMP. AND NO. CYCLES

LEGEND
—+— FIRST CYCLE
--*-- CYCLE NO. 1000
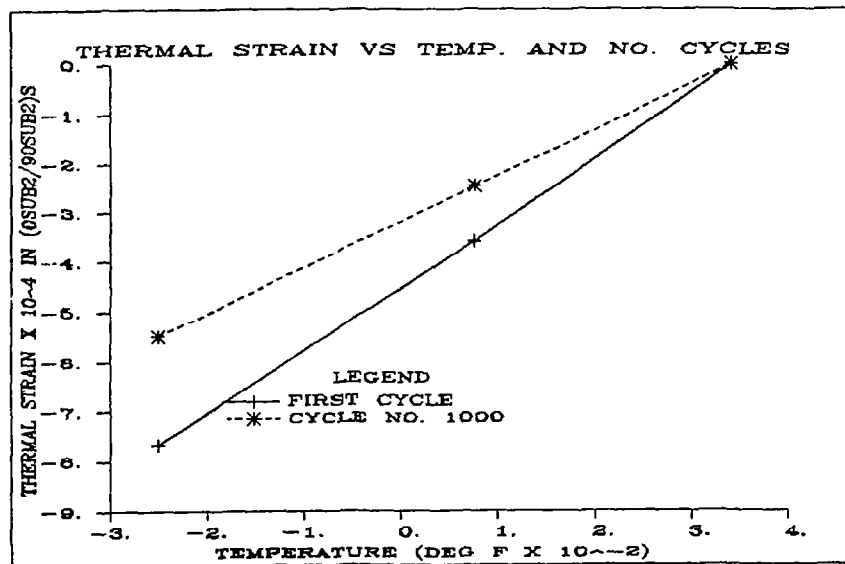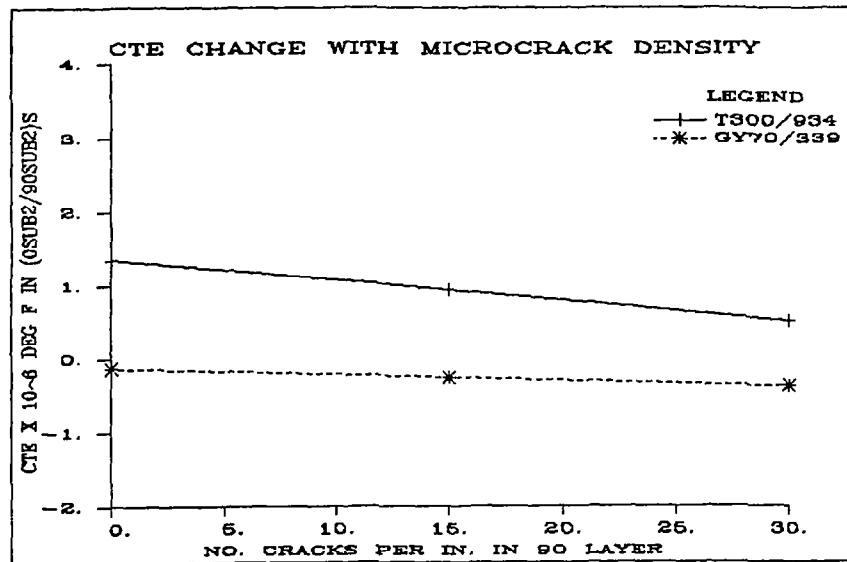
MICRO-CRACKING DURING THERMAL CYCLING - CONCLUSIONS

(1) MICROCRACK DENSITY INCREASES WITH THE NUMBER OF
    THERMAL CYCLES

(2) THE ABSOLUTE DIMENSIONAL CHANGE ASSOCIATED WITH
    MICRO-CRACKING IS ON THE ORDER OF 50-200 MICROSTRAIN,
    DEPENDING ON CRACK DENSITY AND LAMINATE STIFFNESS

(3) THE STRESS-FREE TEMPERATURE IS NOT CHANGED BY
    MICRO-CRACKING

(4) IMPROVEMENTS TO MICROCRACKING RESISTANCE CAN BE MADE
    BY USING TOUGHER MATRIX MATERIALS OR, ALTERNATIVELY,
    USING THINNER PLIES. DOUBLING THE TOUGHNESS OR HALVING
    THE PLY THICKNESS BOTH RESULT IN A 40 PERCENT
    IMPROVEMENT

REFERENCES

1. Brown, G. L., J. F. Thomasson, and R. M. Kurland, Space Radiation Effects on Spacecraft Materials. SAMPE Symp. Proc., Vol 24, 1979, p. 1024.

2. Haskins, J. F., Advance Composites Design Data for Spacecraft Structural Applications. SAMPE Tech. Conf. Proc., Vol. 12, 1980, p. 977.

3. Mauri, R. E., and F. W. Crossman, Space Radiation Effects on Structural Composites. Proc. AIAA Conf. on Space Sciences and Astronomy (Reno, Nevada), Jan. 1983.

4. Slemp, W. S., and B. Santos, Radiation Exposure of Selected Composites and Thin Films. Large Space Systems Technology - 1980, NASA CP-2168, 1980, p. 105.

5. Long, E. R., Electron and Proton Absorption Calculations for a Graphite/Epoxy Composite Model. NASA TP-1568, Nov. 1979.

6. Leger, L. J., Oxygen Atoms Reaction With Shuttle Materials at Orbital Altitudes. NASA TM-58246, May 1982.

7. Flaggs, D. L., and M. H. Kural, Experimental Determination of the In-Situ Transverse Lamina Strength in Graphite/Epoxy Laminates. J. Comp. Mat., vol. 16, 1982, p. 103.

8. Crossman, F. W., Analysis of Delamination. NASA Workshop on Failure Analysis and Mechanisms of Failure of Fibrous Composite Structures, March 23-25, 1982, Hampton, VA.

9. Chou, P. C., A. S. D. Wang, and H. Miller, Cumulative Damage Model for Advanced Composite Materials. Interim Technical Report No. 2, Drexel Univ., 23 Aug 1981 - 23 Feb 1982 (AF contract F33615-80-C-5039).

10. Wang, A. S. D., and F. W. Crossman, Fracture Mechanics of Transverse Cracks and Edge Delamination in Graphite-Epoxy Composite Laminates. Final Tech. Report, Drexel Univ., March 1982 (AFOSR contract F49620-79-C-0206).

11. Flaggs, D. L., and M. H. Kural, Experimental Determination of the In-Situ Transverse Lamina Strength in Graphite/Epoxy Laminates. J. Comp. Mat., vol. 16, 1982, p. 103.

ADVANCES IN STRUCTURAL CONCEPTS

Martin M. Mikulas, Jr., and Harold G. Bush
NASA Langley Research Center
Hampton, Virginia 23665

257

INTRODUCTION

number of different structural concepts are currently under development as a means
ʃ placing large structures in orbit. In figure 1, three commonly considered con-
epts are shown. The radial rib structure and the hoop-column structure have under-
ʃone considerable early development because of their seeming potential for providing
ʃ reliably deployable reflector surface. In the present paper, attention is focused
ʃon truss structures which historically have been widely used in ground based struc-
tures because of their inherent simplicity, versatility, and high stiffness.

REFLECTOR ANTENNA CONCEPTS

- RADIAL RIB STRUCTURE
  - FOLDABLE
- HOOP-COLUMN STRUCTURE
  - FOLDABLE
- TRUSS STRUCTURE
  - FOLDABLE
  - NESTABLE STRUTS
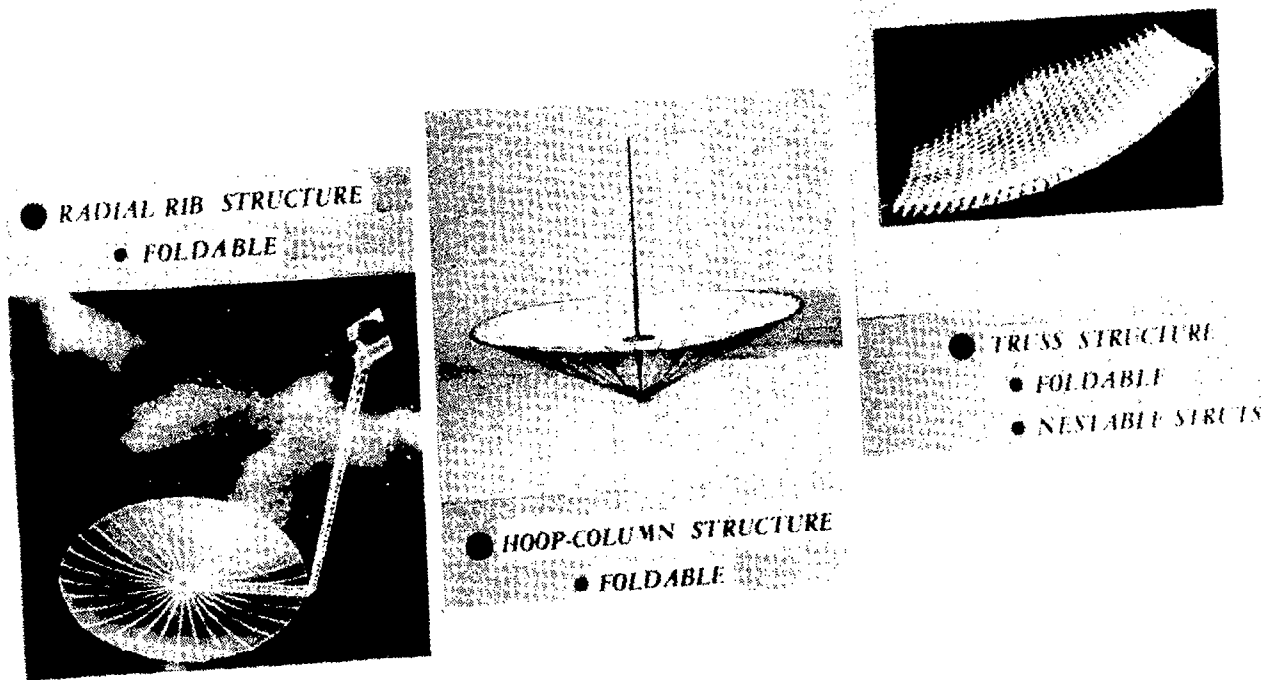
Figure 1

TRUSS CONCEPTS CONSIDERED

The truss structural concepts considered in the present paper are categorized according to on-orbit erection approach and are indicated in figure 2. The erection approach for each concept is described as the concept is discussed.

- **SURFACES/PLATFORMS**
  - **ERECTABLE**
  - **SEQUENTIALLY DEPLOYABLE**
  - **SYNCHRONOUSLY DEPLOYABLE**

- **BEAMS**
  - **ERECTABLE**
    - **TUBULAR STRUTS**
    - **NESTABLE STRUTS**
  - **DEPLOYABLE**
    - **SINGLE FOLD**
    - **DOUBLE FOLD**

Figure 2

PRIMARY DESIGN CONSIDERATIONS FOR LARGE SPACE STRUCTURES

Since most space structures are produced as one-of-a-kind systems, the high cost of design and flight qualification must be borne by a single mission. This cost can represent a substantial portion of the mission budget and as such must be dealt with early in the design process. Two main factors in the design and flight qualification costs are associated with obtaining confidence in on-orbit elastic response and in the on-orbit erection process. For large space structures (100 to 1000 meters) it is not likely that the complete structural system will be capable of being ground tested. To obtain confidence that the on-orbit elastic response of the structural system will be as expected, it is important that structural predictability be a primary design consideration. Structural predictability can be insured by such items as designing zero free-play joints, designing with highly repeatable individual members and designing such that full scale subcomponent ground tests can be conducted. Establishing high confidence in the deployment process or in predicting the assembly time is likely to be quite difficult for very large structures due to gravity effects. For this reason it would be highly desirable to conduct a series of on-orbit assembly tests to gain experience in this area. The other major cost factor associated with large space structures is that of launch costs. As with all space structures, it is important that weight be kept to a minimum; however, for very large space structures, compact packaging represents a significant challenge. In the present paper, a major emphasis is placed on the implications of compact packaging. (See fig. 3.)

MAJOR COST FACTORS   DESIGN DRIVERS
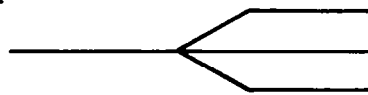
DESIGN AND FLIGHT   • STRUCTURAL PREDICTABILITY
QUALIFICATION   • SUBCOMPONENT GROUND TESTS
                                            • RELIABLE DEPLOYMENT OR
                                                EASE OF ASSEMBLY
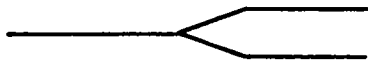
LAUNCH   • LOW WEIGHT
                                            • COMPACT STOWAGE

Figure 3

260

One structural element concept which meets the requirement for low mass and compact stowage is the nestable strut (reference 1). Figure 4 shows a 36-strut segment of a tetrahedral truss cantilevered from a structural backstop. This structural component weighs approximately 130 lbm and stows in a small volume as shown on the figure. This component was constructed using precision length half-struts and quick-attachment side entry joints. These two features are necessary to permit rapid construction of redundant structures which require the insertion of structural elements between points rapidly fixed in space. A number of struts and a smaller tri-pod sub-component were tested earlier and are reported in reference 2. The 36-strut component shown is the smallest stable truss segment which contains one complete 9-point cluster (located at the center of the bottom face). Tests have been conducted to investigate cluster joint behavior and truss structure predictability.

Figure 4

The truss segment shown in figure 4 was statically tested by applying a vertical tension load (via a hydraulic cylinder and steel rod) to the top surface node furthermost from the backstop. A compression loading occurred in certain struts connected to the 9-point cluster at the center of the bottom surface of the truss. The theoretical buckling load of the truss segment was calculated to be approximately 1500 lbf and occurred when two of the struts reached this critical buckling load. Experimental deflection of the truss component (measured at the load application point) is shown in figure 5 (circles-loading/triangles-unloading). Truss loading continued until buckling of the critical struts was observed. Analytical efforts to predict the truss deflection are shown in figure 5. Reasonable detail was used in modeling the joint features, yet the finite element model displayed a higher truss stiffness than observed experimentally. Tension and compression joint tests were conducted, from which joint stiffnesses were calculated. Use of the experimental joint stiffness in the finite element analyses resulted in an extremely close prediction of the overall truss deflection prior to the onset of strut buckling, as shown by the solid line in figure 5.
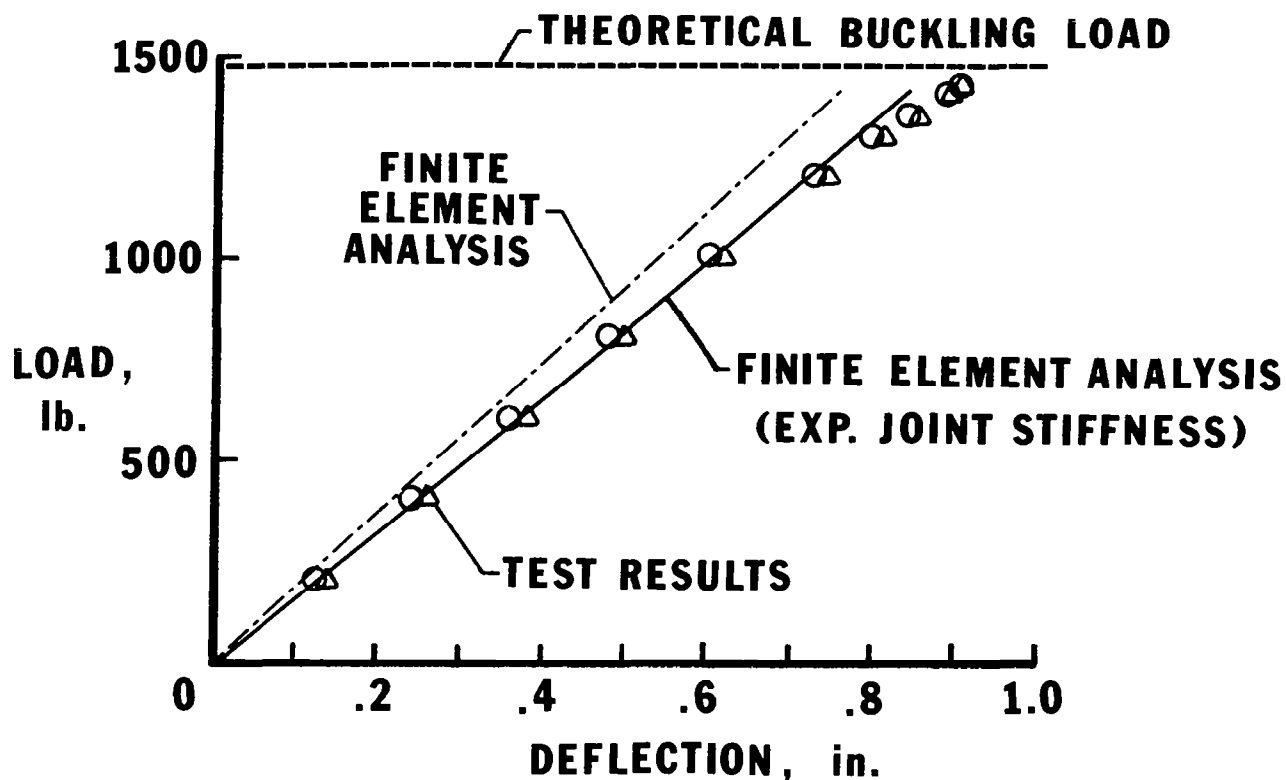
Figure 5

JOINT STIFFNESS TEST

Initial analyses of the 36-strut tetrahedral truss test included a reasonably detailed finite element representation of the nodal joint area. Due to the multiplicity of nodal joints present, an "exact" nodal joint model was not developed. The use of such detail at each node is prohibitive. Joint tests were conducted, as shown in figure 6, in both tension and compression. The displacement history was recorded during loading and unloading, and a small amount of hysteresis typically occurred, as shown. The quick attachment joint and bolted nodal cluster arrangement typically showed a small amount of non-linearity. Test results such as that shown in figure 6 were used to calculate effective joint extensional stiffnesses, which greatly simplified the analytical model and significantly improved predictability of the structural response. Such sub-element and component testing is considered imperative for any repetitive structure containing a multiplicity of complex joints between elements.
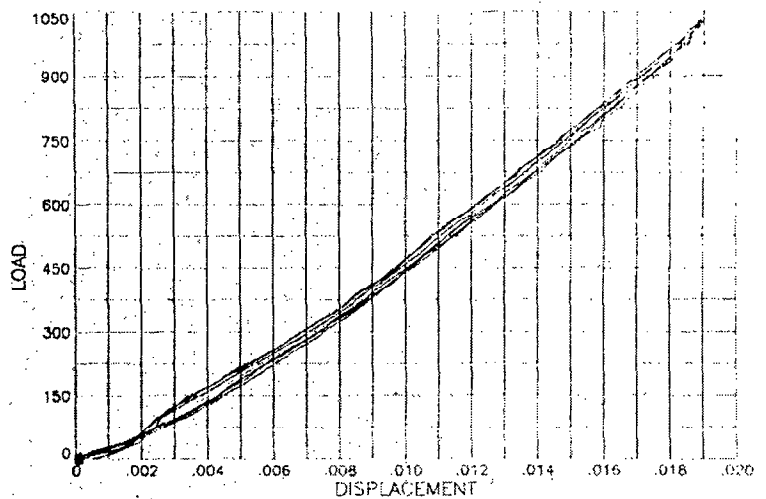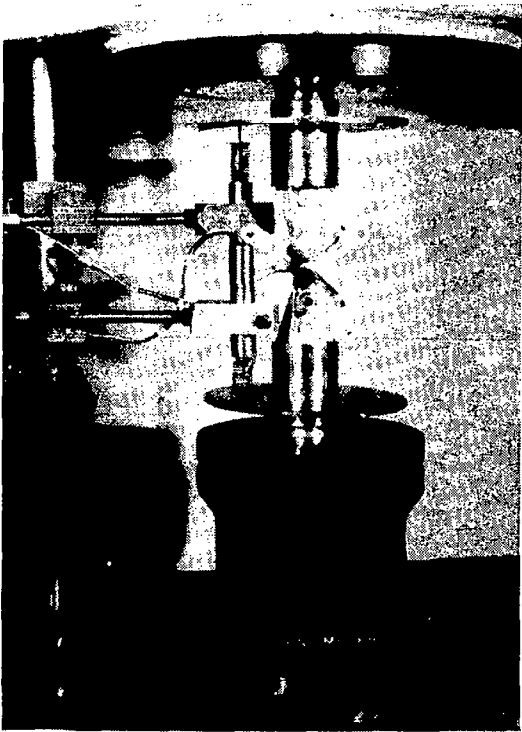
Figure 6

DEPLOYABLE TRUSS ANTENNA

The high stiffness characteristics of trusses makes them attractive candidates for those applications requiring extremely stable supporting structures, such as large antennas. For this application, it is desirable to configure the antenna reflector (and feed support) such that it may be deployed, or unfolded. An overall truss antenna arrangement which is currently being investigated is shown in figure 7. Previous studies (ref. 3) determined the mass, geometric, structural, and packaging characteristics of tetrahedral truss structure for antenna reflector application. The antenna arrangement shown in the figure has a tripod feed support for stiffness. However, ongoing and future studies will determine the feed support requirements for various missions.
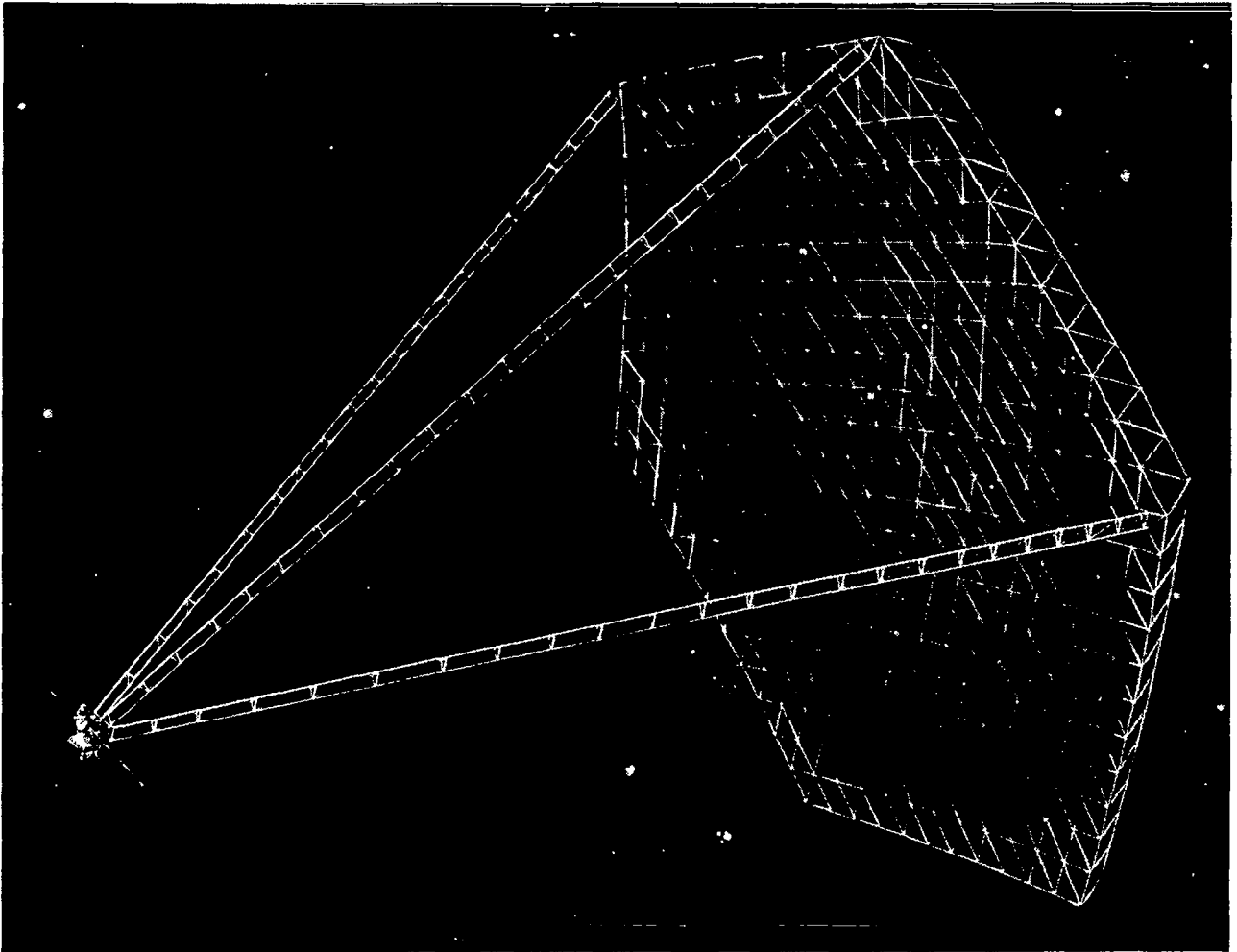
Figure 7

One method of unfolding a truss structure, which has received considerable attention, is to deploy the structure sequentially (ref. 4). The sequential deployment process is depicted in figure 8, which shows the packaged truss with face struts folded outward. Rows of truss elements are unfolded in sequence, one row after another until the final structural configuration is obtained. This deployment concept has been developed for planar, spherical and parabolic structures. Sequential deployment requires the use of external, robotic devices to unfold the stowed elements into the desired structure. However, a structurally stiff configuration is maintained throughout the deployment process.
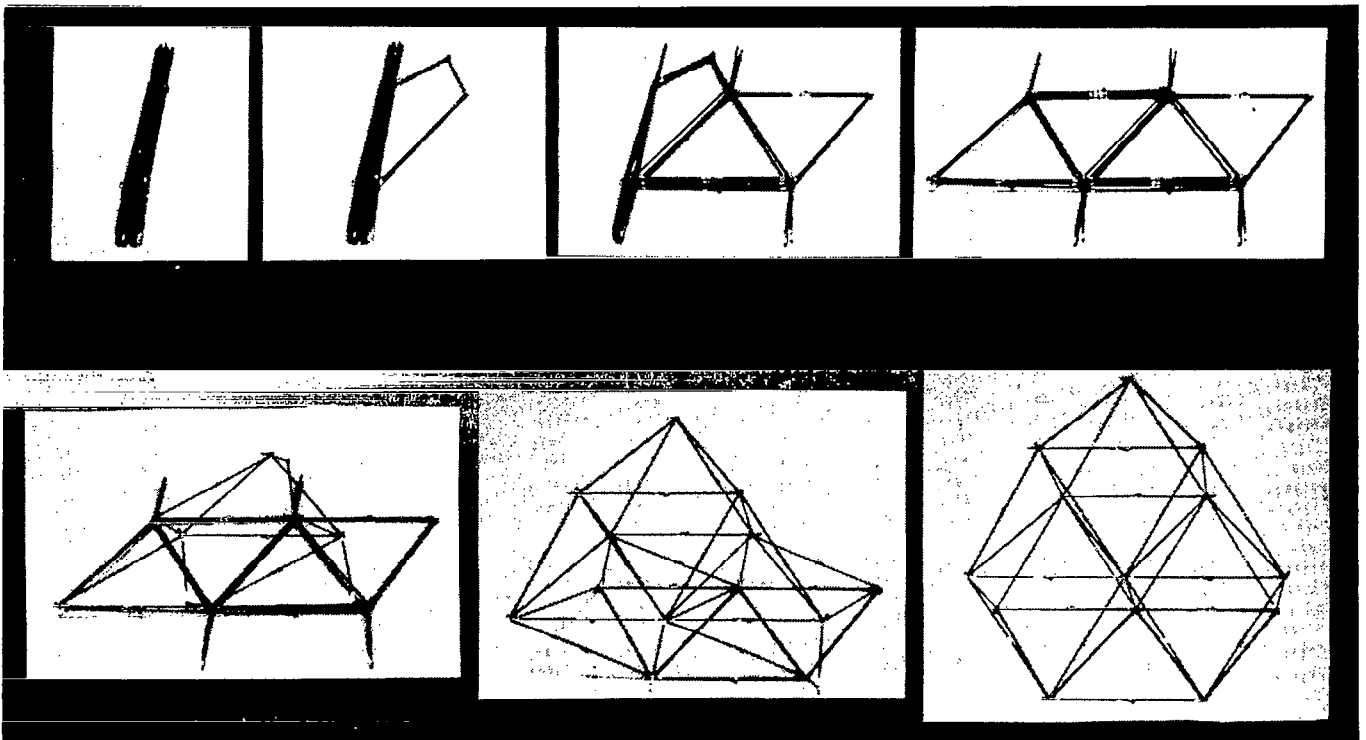
Figure 8

SYNCHRONOUSLY DEPLOYABLE ANTENNA

A method of deploying an antenna structure which is currently being studied is to unfold the stowed structure synchronously. This technique requires all elements to move simultaneously and in a regulated manner. The packaged configuration for the tetrahedral truss reflector structure is described in reference 5. The inset in figure 9 shows a tetrahedral truss segment which illustrates the inward folding surface members and the actuator/synchronization mechanism located at each node. This concept uses passive, distributed deployment energy (springs) which is released in a controlled manner at each node by dampers which regulate deployment velocity. Positioning of the face and core struts throughout the deployment process is accomplished by actuator links (or cranks) operated by a slider which is driven by the spring. Proper design of the slider-crank mechanism is possible to achieve synchronized operation between face and core struts at each node. Because the core struts extend between truss surfaces, kinematic loops are formed which provide synchronization and prevent one surface from opening faster than the other.
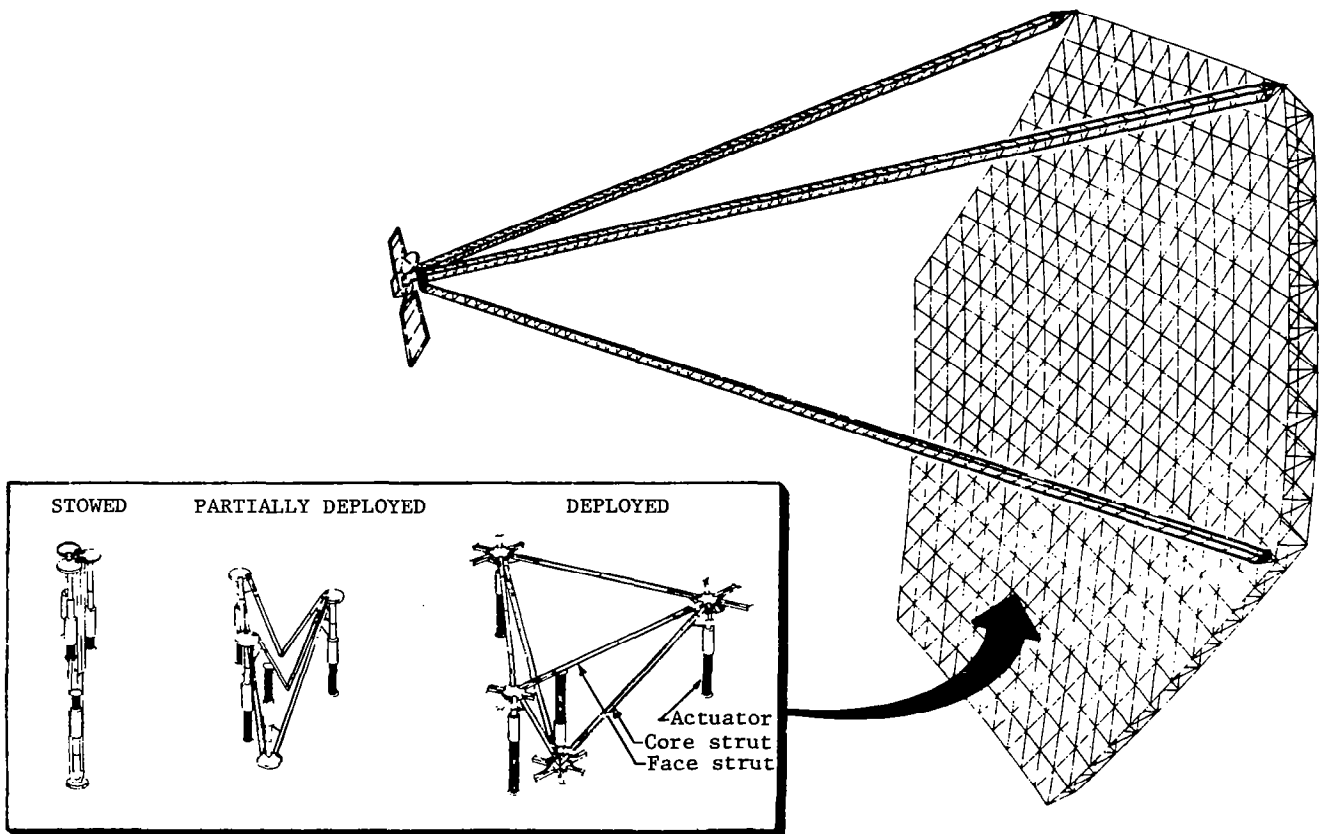
Figure 9

STOWED REFLECTOR/MAST 100 METER CONFIGURATION

In addition to detailed, technical studies of the mechanical, geometric and struc-
tural requirements of a synchronously deployable truss structure, studies are also
under way to integrate this type of reflector support structure into an antenna
system, complete with feed support, spacecraft electronics, mesh reflector systems
and orbital transfer vehicle which is transportable within the Shuttle cargo bay.
A preliminary stowed configuration for a 100 meter diameter antenna with tri-mast
feed support is shown in figure 10. Engineering estimates of component weights are
also shown on the figure. The 12,000 lb. mast weight includes the antenna feed and
electronics. This system is being investigated for applications requiring apertures
up to 300 m, or as a module from which larger apertures may be constructed.

Figure 10

267
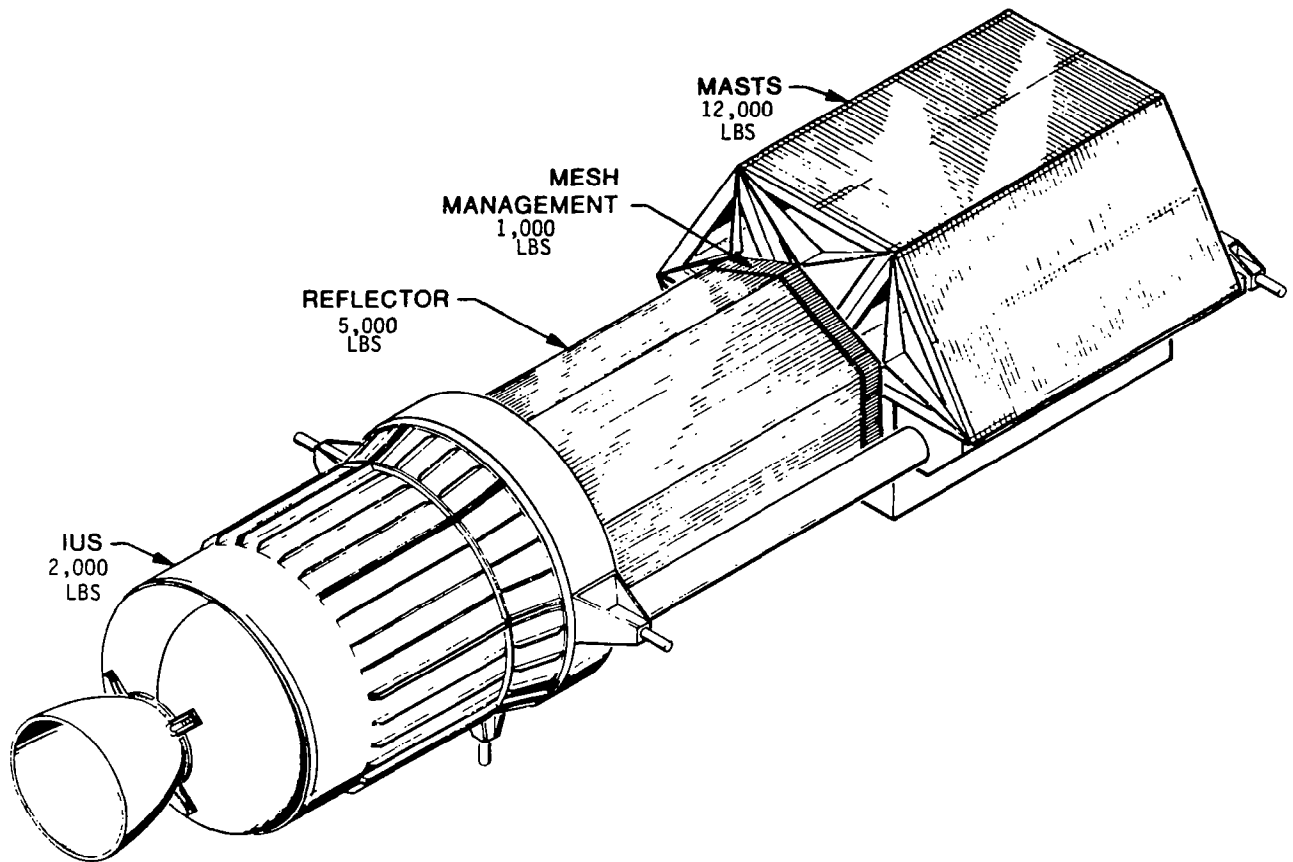
STOWED VOLUME FOR SURFACES/PLATFORMS

In figure 11, the stowed volume of two types of truss structures is plotted as a function of deployed diameter. The upper dotted area shown is for deployable or erectable trusses which are fabricated from tubular struts. The lower dotted area shown is for erectable trusses fabricated from nestable struts. As can be seen, the stowed volume of both type trusses is a strong function of the strut ℓ/ρ; however, the nestable strut trusses package about an order of magnitude better. The stowed volumes for four antennas are shown for comparison. It should be noted, however, that the feed mast is an inherent part of the hoop column, so that simple stowed volume comparisons are difficult except for antenna applications which require a feed mast where that volume could be included for all concepts.
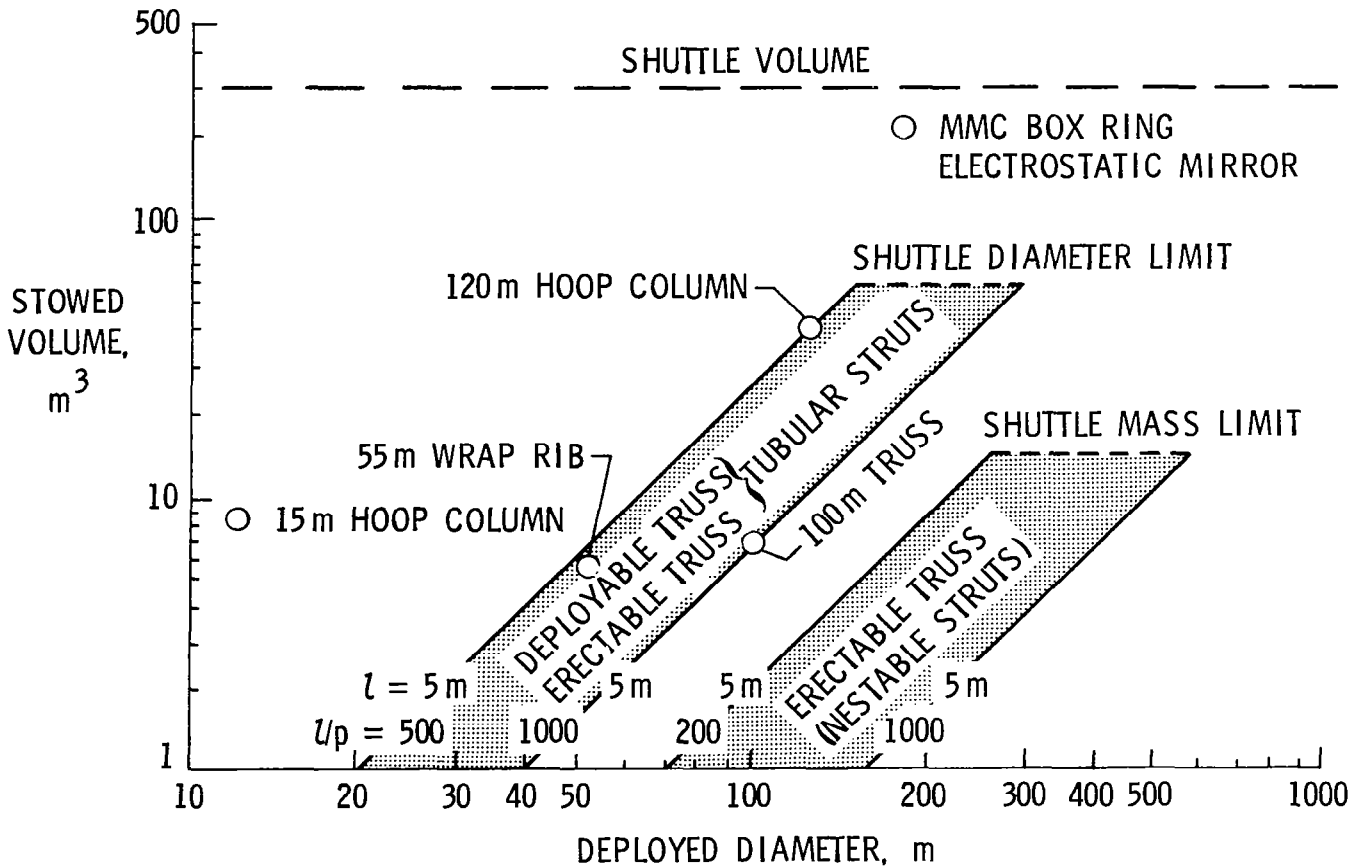
Figure 11

SURFACE/PLATFORM SUMMARY

In figure 12 some pros and cons are listed for the different concepts. It is obvious that the selection of a concept for a specific mission will be the result of a detailed system study for that application. For this reason, it is important that the base program develop the technology sufficient for each concept so that rational system decisions can be made.

CONCEPT	PROS	CONS	TECHNOLOGY READINESS
ERECTABLE TRUSS (NESTABLE STRUTS)	• SUPERIOR PACKAGING • HIGH VERSATILITY • UNLIMITED SIZE POTENTIAL • DEMONSTRATED PREDICTABILITY	• EVA REQUIRED • UTILITIES INTEGRATION REQUIRED ON ORBIT	LIMITED ONLY BY EVA READINESS
SEQUENTIALLY DEPLOYABLE TRUSS	CONTROLLED DEPLOYMENT	EXTERNAL MANIPULATOR REQUIRED	10-30 meters 1986 > 100 meters 1988
SYNCHRONOUSLY DEPLOYABLE TRUSS	UTILITIES PREINTEGRATED	• UTILITIES DEGRADE PACKAGING • SLENDER STRUTS REQUIRED FOR COMPACT PACKAGING	
	SELF CONTAINED DEPLOYMENT SCHEME	DEPLOYMENT RELIABILITY	

Figure 12

SPACE BEAM STIFFNESS REQUIREMENTS

In figure 13 a plot is made of beam bending stiffness (EI) as a function of beam depth. The points shown are requirements obtained from various mission studies and the dashed lines merely outline these points. Studies have shown that the coilable longeron beam (Astromast) is limited to beam diameters of less than 1 meter due to difficulties in packaging the stowed energy in the beam. For applications which require larger beams, deployable beams with hinged longerons or erectable beams must be developed.
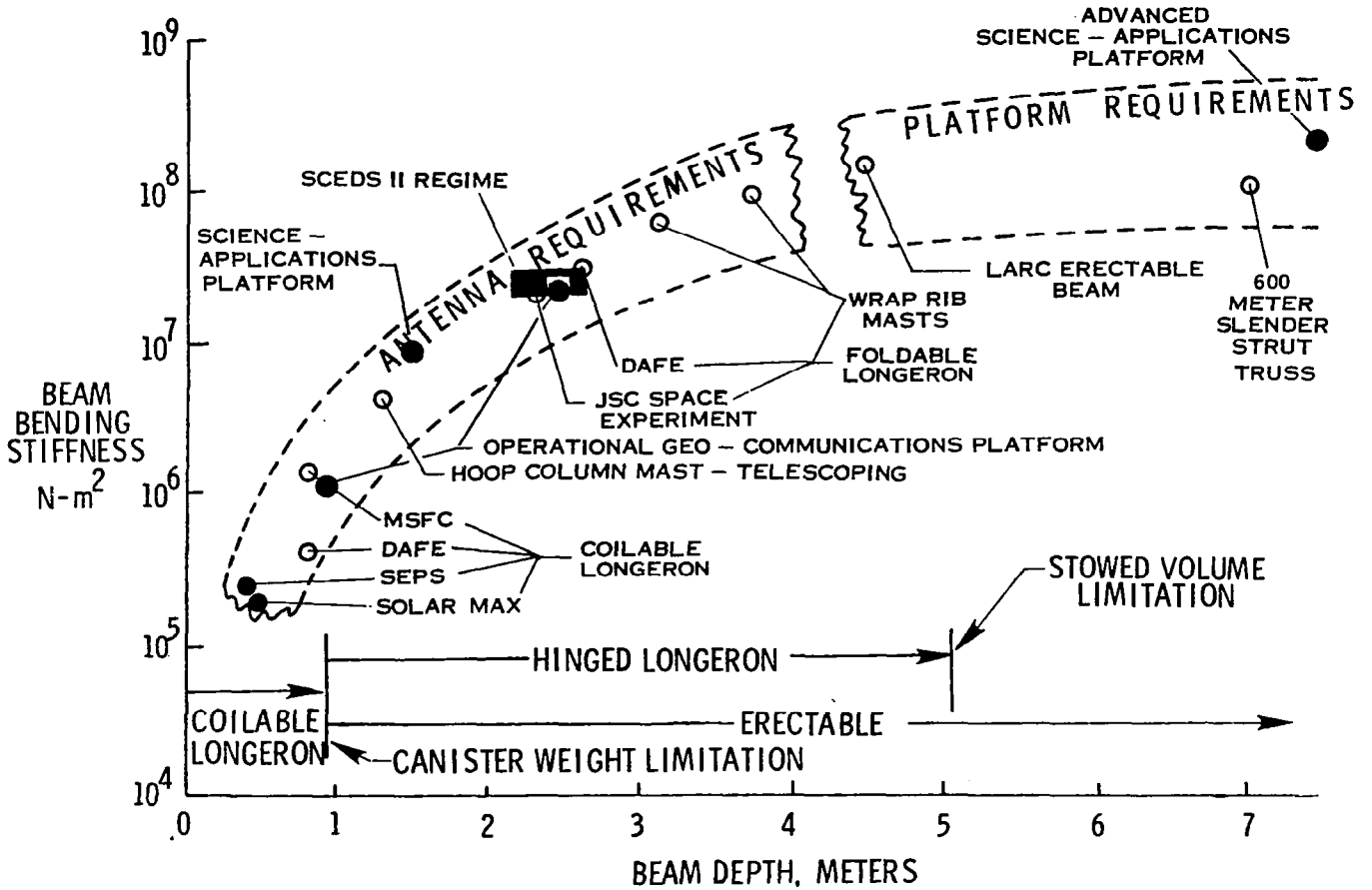
Figure 13

In figure 14 a 0.75 meter diameter Astromast, which is being developed for MSFC by Astro Corporation, is shown. The longerons of this beam are one third graphite/ epoxy sandwiched between two equal layers of fiberglass. The fiberglass was needed because of its higher failure strain which is necessary for compact packaging. This beam, which is still under development, should be available for structural testing by mid-1983.

DIAMETER = 0.75 m

LENGTH = 6.1 m

LONGERON DIAMETER = 1.1 cm

$EI = 1.37 \times 10^6 \ N\text{-}m^2$

LINEAR MASS = 4.0 kg/m
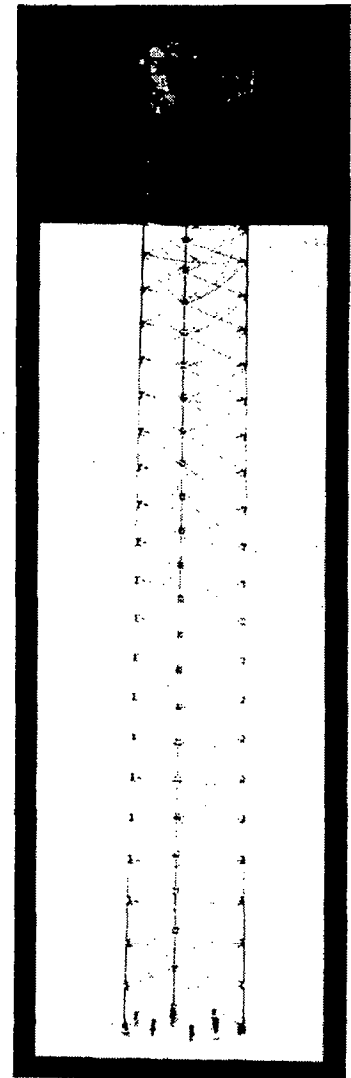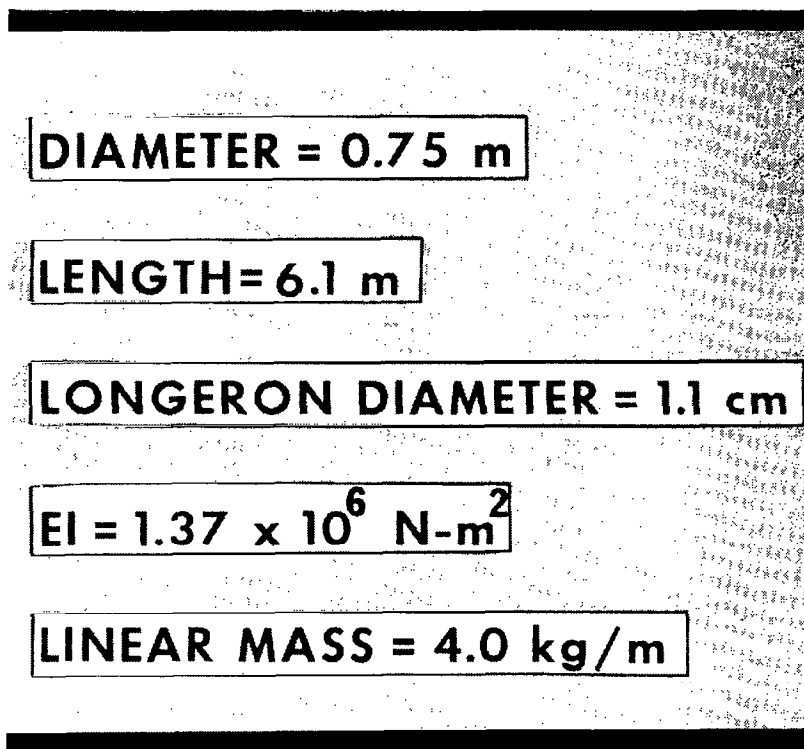
Figure 14

TYPICAL FOLDED BEAM CONCEPTS

The two major generic types of beams with hinged longerons are shown in figure 15. The beam labeled "single fold" has the feature that the length of the beam collapses while the beam cross-sectional area is maintained in the packaged condition. The beam labeled "double fold" is featured by a collapse of the beam cross-sectional area as well as its length. The packaging of both types of beams is governed primarily by the ℓ/ρ of the constituent struts.

SINGLE FOLD
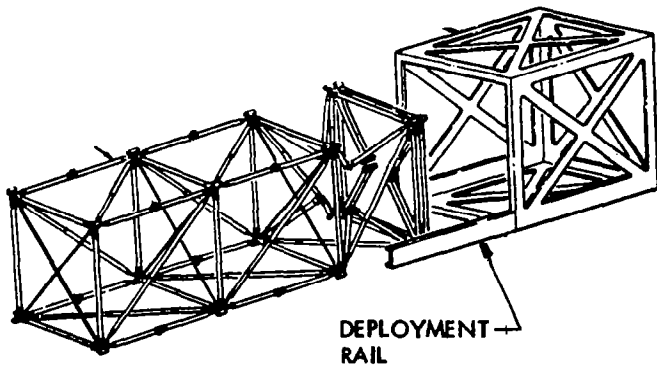
DOUBLE FOLD
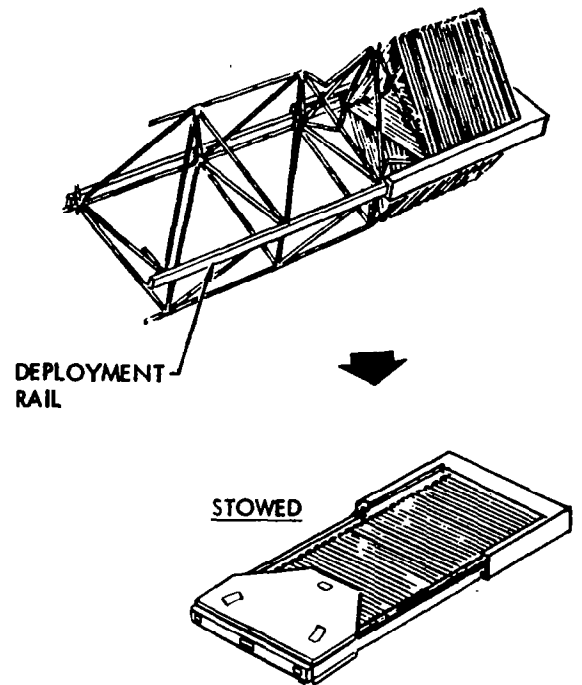
Figure 15

STRUCTURAL CONCEPTS EVALUATED - ROCKWELL

Under contract to MSFC, the Rockwell International Corporation and the Vought
Corporation studied a number of different structural concepts for fully deployable
beams and platforms. The companies reviewed the industry concepts shown in figure
16 (Rockwell) and figure 17 (Vought). The features of these concepts were subject
to a series of trade studies for specific mission requirements with utilities
integration being a primary consideration. Details of these requirements and trade
studies are given in references 5 and 6.
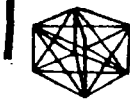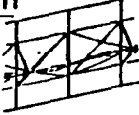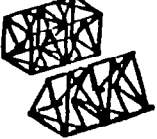
Ⓐ AstroResearch	Ⓔ Vought	Ⓘ Rockwell
CONTINUOUS LONGERON MAST	DOUBLE-CELL, DOUBLE-FOLD TRUSS	WARREN TRUSS— TRANSVERSE FOLD
Ⓑ AstroResearch	Ⓕ Martin	Ⓙ Rockwell
ARTICULATED LONGERON MAST	BOX TRUSS WITH X-BRACING	CABLE CROSS-BRACED— TRANSVERSE FOLD
Ⓒ AstroResearch	Ⓖ Harris	Ⓚ Rockwell
EXTENDIBLE SUPPORT STRUCTURE FOR SEASAT	TOWER SEGMENT	CABLE CROSS-BRACED—TRANSV. & LONGITUDINAL FOLD
Ⓓ General Dynamics	Ⓗ Lockheed	Ⓛ Ⓜ Rockwell
TETRAHEDRAL TRUSS	TAPERED TUBE	K-BRACES— LONGITUDINAL FOLD

Figure 16

Figure 17 shows the structural concepts evaluated by Vought.

VOUGHT DOUBLE FOLD   VOUGHT BIAXIAL SCISSORS   MSFC/VOUGHT SINGLE FOLD   GDC PETA

GDC DIAMOND TRUSS BOOM   MARTIN BOX TRUSS   VOUGHT INFLATABLE DOUBLE FOLD

VOUGHT BIAXIAL DOUBLE FOLD   VOUGHT PIVOTED DOUBLE FOLD   MDAC TELEFOLD   MODIFIED GDC HALF DIAMOND BEAM
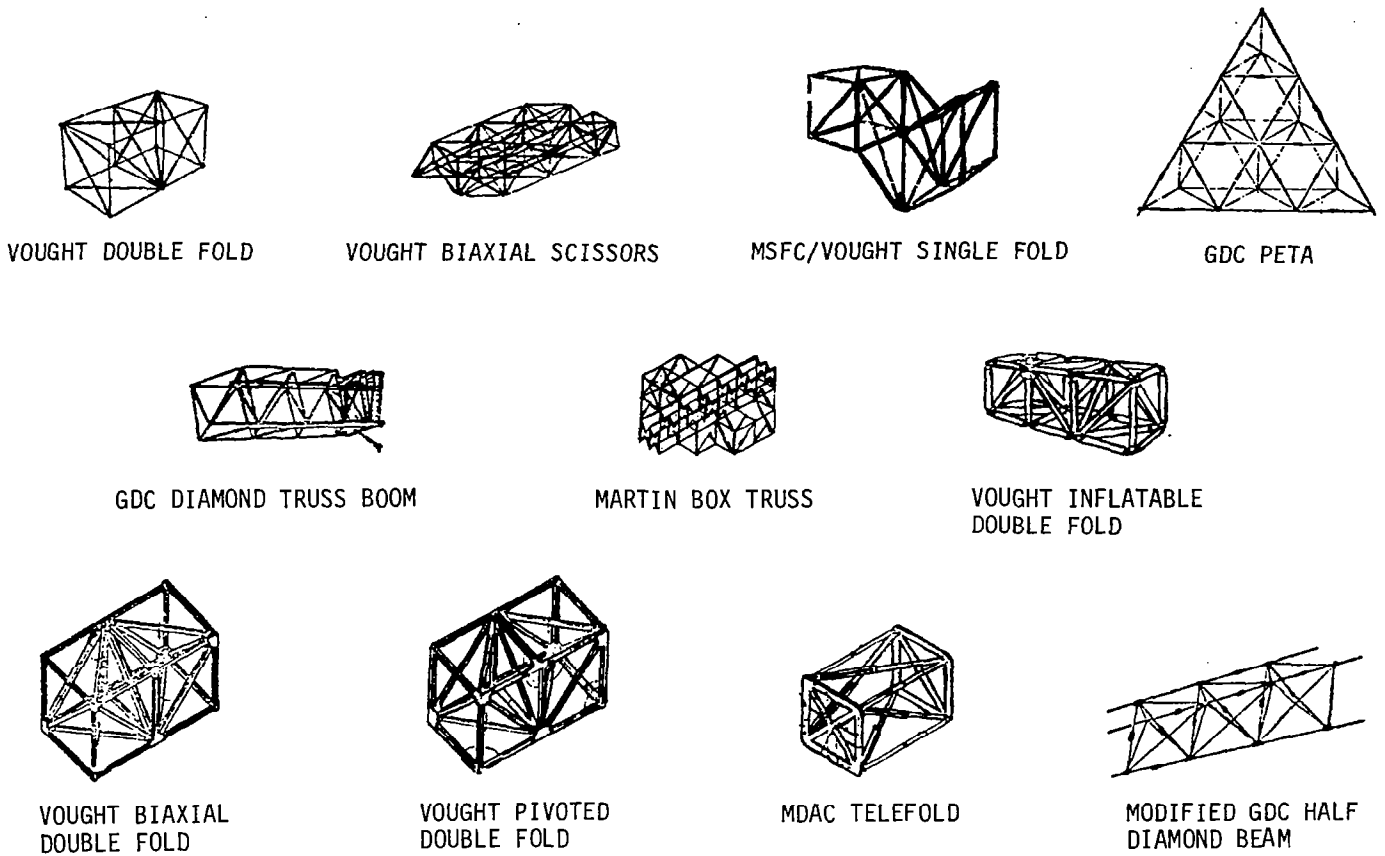
Figure 17

SELECTED CONCEPT - ROCKWELL

Of prime concern in the Rockwell studies was deployment simplicity. Accordingly, they chose a single fold beam with few joints. The selected concept, which features hinged longerons and telescoping diagonals, is shown in figure 18. Deployment of the beam is effected one bay at a time within the deployment rails so that positive control of the beam can be maintained. It also has a built in folding utilities tray which is not shown in the figure. Details of the concept are given in ref. 5.
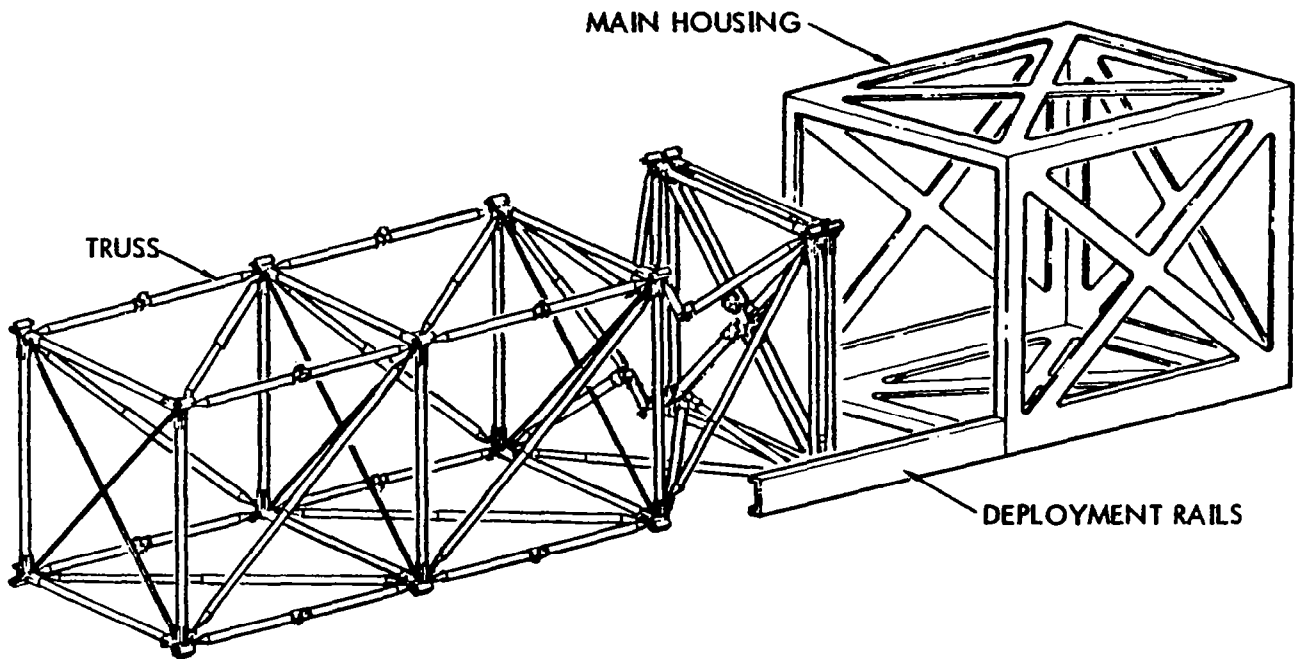
Figure 18

Of prime concern in the Vought studies were stowage volume and retraction. Accordingly, they chose a double fold beam with cable retractors as shown in figure 19. The concept has springs at the joints which power the deployment, and all bays of the beam deploy simultaneously. The vertical battens of the beam telescope, which permits the geometry change required for collapse, and cables are interlaced throughout the beam to permit control during deployment as well as a retraction capability. The details of this beam are presented in reference 6.
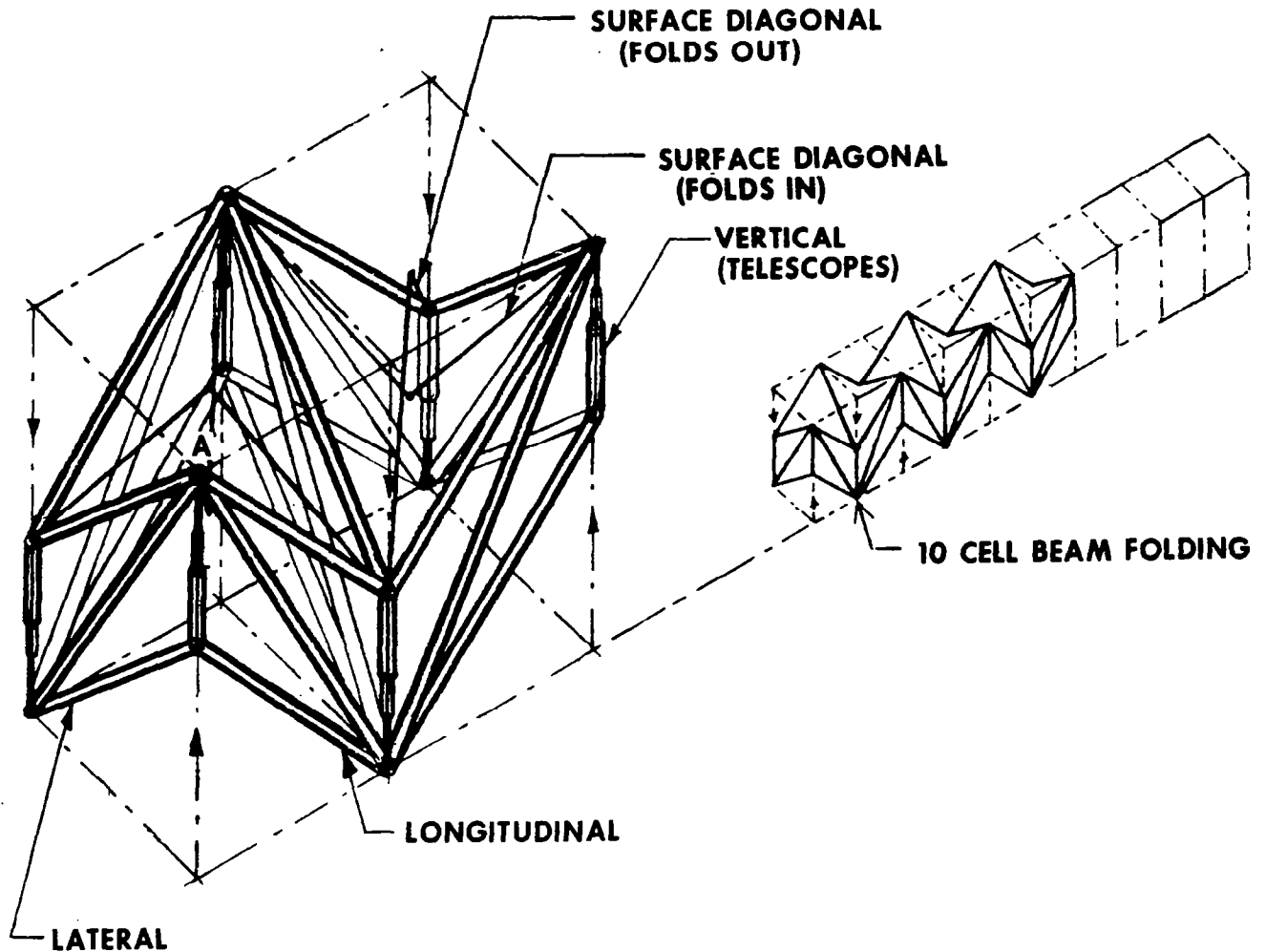
Figure 19

ERECTABLE BEAM

Beams which are erected on orbit from individual struts by astronauts offer another alternative for obtaining large beams. Erectable structures such as the truss structure discussed earlier have been under study at LaRC for several years. More recently, attention at LaRC has been focused on the technology for erecting a beam structure. An example of a 2 meter diameter 100 meter long erectable beam is shown in figure 20. The packaged beam and the erected beam are shown to scale with the Space Shuttle. The estimated assembly time of this 453 strut beam by one astronaut assisted by the assembly aid shown in the next figure is three to six hours.

ASSEMBLED **100 METER BEAM** *PACKAGED*

STRUTS
L = 2 m
DIA. = 2.5 cm
NO. = 453
ASSEMBLY TIME = 3 — 6 hrs.
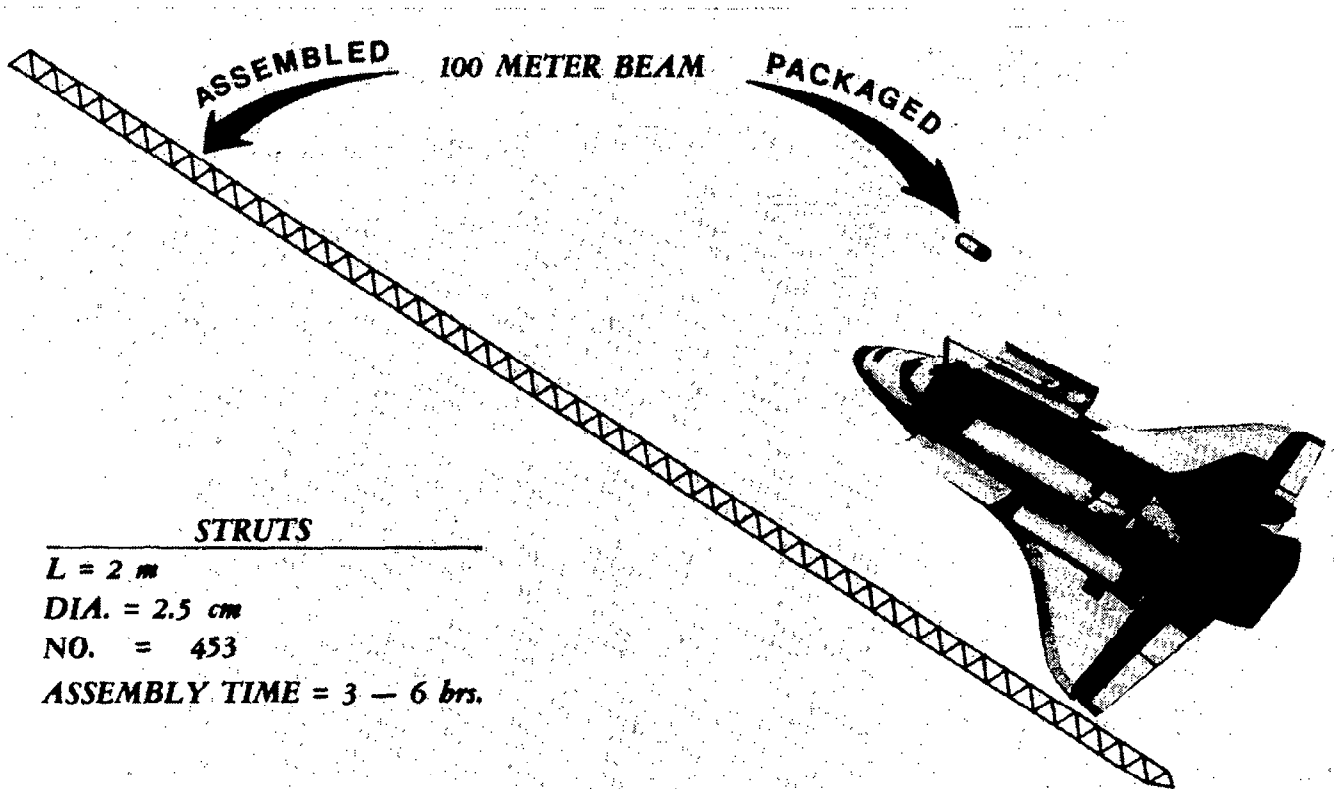
Figure 20

The erection process for a structure is strongly dependent on the structural arrangement used. To ease the erection process, a modified tetrahedral beam was selected and a mock-up of such a beam is shown on the left of figure 21. This arrangement was chosen to reduce the number of joints required in the assembly process to a minimum. A schematic of the beam assembly aid is shown on the right of figure 21. The single astronaut needed to erect the beam using struts with quick-attach joints has his boots secured to a platform which can telescope up or down and can rotate around the beam to permit ready access to all joints. As each bay of the beam is assembled, the beam is registered outward and the process is repeated one bay at a time until the beam is complete. Utilities could be readily integrated during this assembly process. The hardware for such a beam and assembly aid is being fabricated and neutral buoyancy assembly tests will be conducted in late 1983.
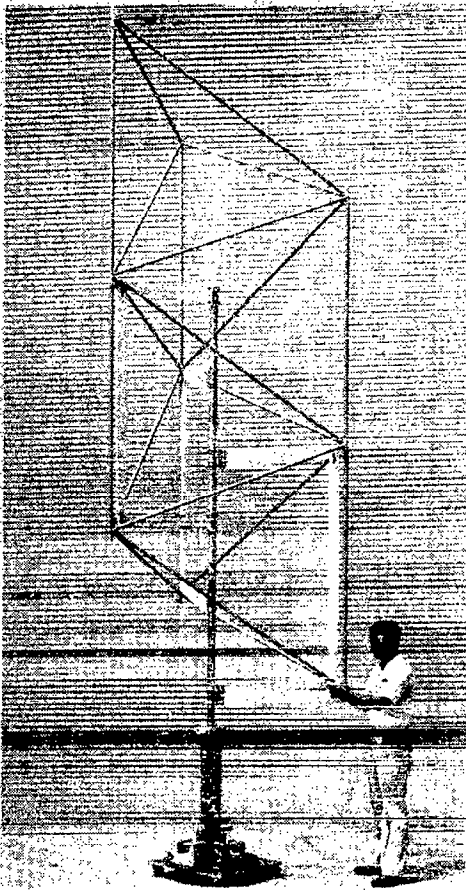
MOCKUP   **ERECTABLE BEAM EXPERIMENT**
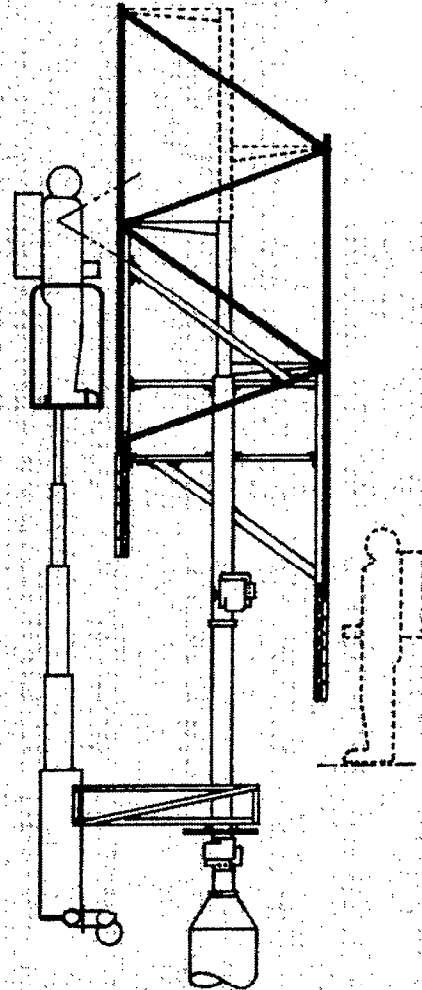
Figure 21

STOWED VOLUME FOR BEAMS

For very large space structures, a serious challenge will be presented by launch vehicle stowage volume restrictions. In figure 22, the stowed volume to deployed volume ratio on the percentage basis is presented for four generic beam concepts as a function of strut length to diameter ratio. The least efficient packaging beam is a single fold beam in which the beam cross-sectional area is doubled in the packaged state. A more efficiently stowed beam is the single fold discussed earlier in which the cross-sectional area is maintained. A double fold beam has much better stowing characteristics than the single folds; however, this beam requires many more joints and a more complex deployment. The most efficient stowable beam is an erectable using nestable struts; however, the assembly aids and EVA requirements must be considered for fair comparison. The main point to be made from this figure is that concept selection can change stowed volume by two orders of magnitude as indicated, by the example on the right.
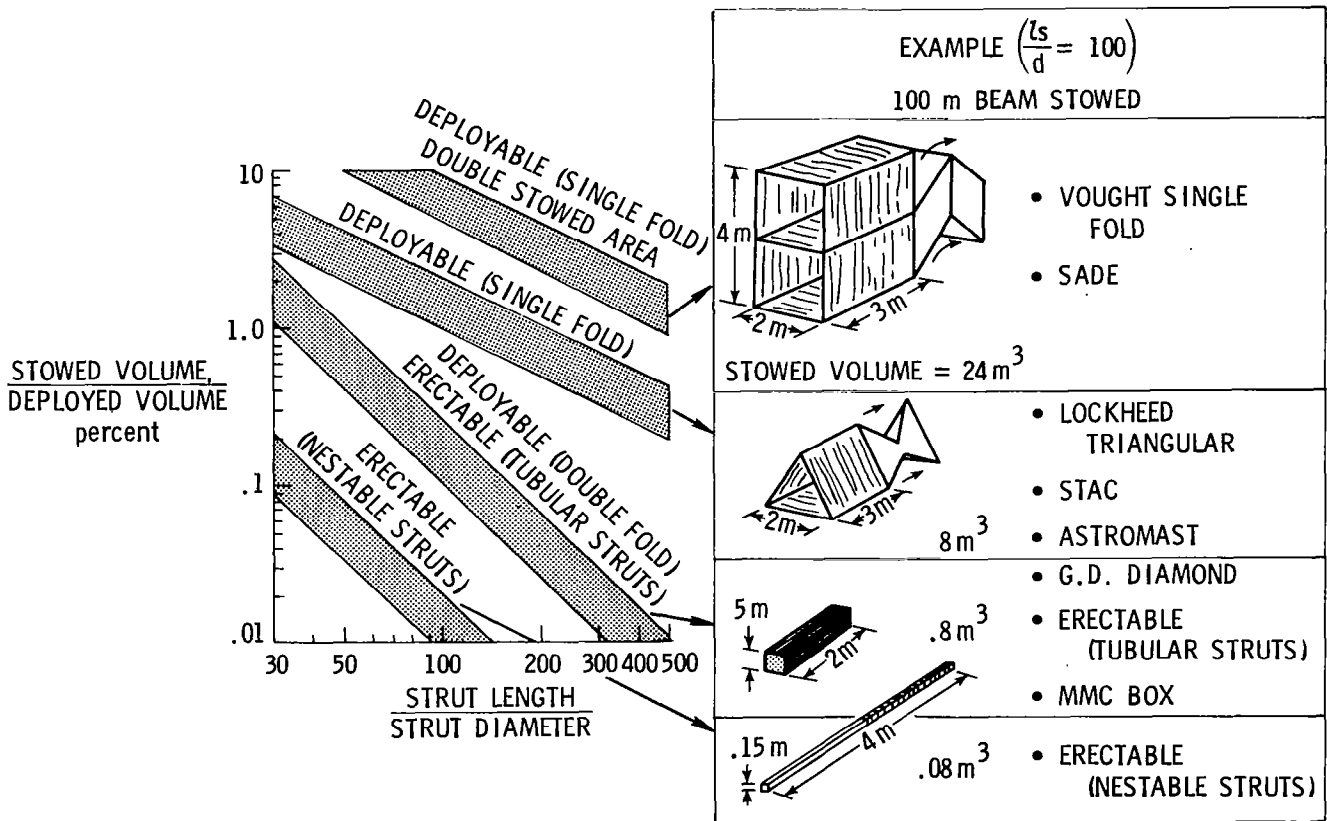
Figure 22

DOUBLE FOLD BEAM LAUNCH AND HARDWARE COSTS

Although complete system studies will be needed to make concept selections for a given mission, two major considerations will be launch costs and hardware costs. In reference 6, the launch costs and hardware costs were developed for several different double fold beam concepts and are shown in figure 23. All beams considered were package volume limited for the Space Shuttle and the spread on the launch costs is a function of how well the beam stowed. It can also be seen that the spread on the hardware costs is not great. The main point to be made from this figure is that launch costs will greatly dominate hardware costs and that a major concern should be placed upon developing efficiently packageable concepts for missions that require very large space structures. Although not shown on this figure, launch costs for single fold beams would be much greater than those shown for the double folds, while launch costs for erectables using nestable struts would be less.
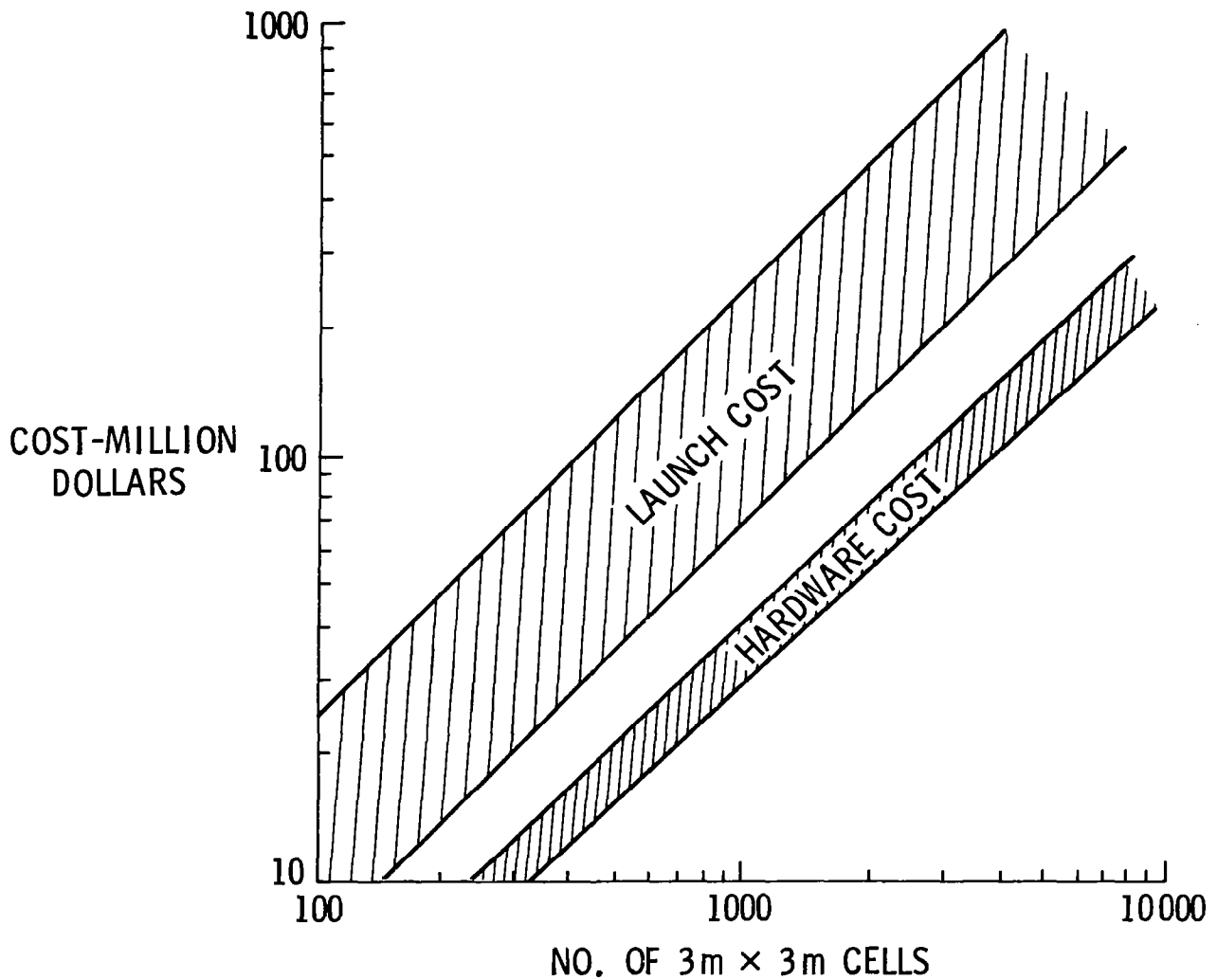
Figure 23

BEAM SUMMARY

As was the case for surfaces/platforms, the different beam concepts have pros and cons (as shown in figure 24) which must be considered during system studies for specific missions. However, since stowed volume and deployment reliability or ease of assembly will obviously be major design considerations, the base technology program should be focused on concepts to improve these features.

CONCEPT	PROS	CONS
DEPLOYABLE (SINGLE FOLD)	• SIMPLE DEPLOYMENT • SIMPLE UTILITIES INTEGRATION • FEW JOINTS	INEFFICIENT PACKAGING
DEPLOYABLE (DOUBLE FOLD)	COMPACT PACKAGING	• COMPLEX DEPLOYMENT • LARGE NUMBER OF JOINTS
ERECTABLE (TUBULAR STRUTS)	COMPACT PACKAGING	• EVA REQUIRED • UTILITIES INTEGRATION REQUIRED ON ORBIT
ERECTABLE (NESTABLE STRUTS)	HIGHLY VERSATILE	
	SUPERIOR PACKAGING	

Figure 24

Some conclusions are presented in figure 25.

- **BECAUSE OF HIGH LAUNCH COSTS, EFFICIENT PACKAGING IS A MAJOR DESIGN DRIVER.**

- **SPACECRAFT GROUND TEST DIFFICULTIES DICTATE THE DEVELOPMENT OF HIGHLY PREDICTABLE STRUCTURES.**

- **GROUND TEST NEEDED ON FLIGHT QUALITY HARDWARE TO DETERMINE POTENTIAL TECHNOLOGY PROBLEMS.**

Figure 25

REFERENCES

1. Bush, Harold G.; and Mikulas, Martin M., Jr.: A Nestable Tapered Column Concept for Large Space Structures. NASA TM X-73927, July 1976.

2. Heard, W. L., Jr.; Bush, H. G.; and Agranoff, N.: Buckling Tests of Structural Elements Applicable To Large Erectable Space Trusses. NASA TM-78628, October 1978.

3. Heard, W. L., Jr.; Bush, H. G.; Walz, J. E.; and Rehder, J. J.: Structural Sizing Considerations for Large Space Platforms. Journal of Spacecraft and Rockets, Vol. 18, No. 6, pp. 556-564, November-December 1981.

4. Hedgepeth, John M.: Sequential Deployment of Truss Structures. Large Space Systems Technology - 1981, NASA CP-2215, Part I, pp. 179-192, November 1981.

5. Greenberg, H. S.: Development of Deployable Structures for Large Space Platforms. NASA CR-170689, December 1982.

6. Cox, R. L.; Nelson, R. A.: Development of Deployable Structures for Large Space Platforms. NASA CR-170690, December 1982.

MANNED ASSEMBLY OF SPACE STRUCTURES

David Akin, Mary Bowden, and James Mar
Department of Aeronautics and Astronautics
Massachusetts Institute of Technology
Cambridge, Massachusetts

INTRODUCTION

Much ingenuity has been demonstrated in creating mechanisms and structures which have been automatically deployed in space. Indeed the success rate is so phenomenal that many engineers blanch when it is suggested that EVA be used to reduce the amount of automation. Nevertheless, the structures being contemplated are growing in size and in complexity such that the role of man in the assembly of large space structures should be an important factor in their design. People will be on board the nation's Space Transportation System and we in the structures community should make use of the innate capabilities of man. There is much research in areas which bear names like "artificial intelligence", "expert systems", "telepresence" and "robots". Those systems, when compared to the evolution of man, are still in a prehistoric stage of development. We believe the first generation of large space structures will be assembled by procedures which require EVA.

With respect to structures in space, the most unique characteristic of the environment is zero-g. This presentation will describe some results which have been obtained and the experiments which have been conducted in the Marshall Space Flight Center's Neutral Buoyancy Facility (MSFC NBF). The MSFC NBF is a tank of water 40 feet deep and 70 feet in diameter. Presently there is a mockup of the Orbiter payload bay at the bottom. There also is a Remote Manipulator System at the edge of the tank.

PRODUCTIVITY COMPARISONS

One of the primary objectives of this research was to obtain a productivity estimate for EVA assembly. Results to date have shown that productivities over 1000 kg per crew hour can be consistently demonstrated, with an average productivity of 500-600 kg per crew-hour expected for a complicated assembly task over an extended period (2 to 4 hours).

These numbers can be compared to standard productivity numbers used for terrestrial operations: 1 kg/hr for the aerospace industry (aircraft assembly); 6 kg/hr for light industry (assembly of appliances such as refrigerators); 50 kg/hr for construction operations (assembly of steel girders for skyscrapers); 2500 kg/hr for mining operations (pushing around piles of dirt with steamshovels). Clearly, based on these numbers alone, people are quite capable in space.

SIMULATED SPACE OPERATIONS:

ASSEMBLY OF LARGE SPACE STRUCTURES   1000 KG/HR

TYPICAL TERRESTRIAL OPERATIONS:

AEROSPACE	1 KG/HR
LIGHT INDUSTRY	6 KG/HR
CONSTRUCTION	50 KG/HR
MINING	2500 KG/HR

ASSEMBLY PRODUCTIVITIES IN PRESSURE SUIT

As can be seen, productivity varies with the type of structure being assembled. Currently, it is standard practice to measure productivity in terms of kilograms assembled per crew hour or operations performed per crew hour. Both of these units have drawbacks when applied to space construction. Kilograms are not as significant in space because of weightlessness, and operations are very highly dependent on the hardware and tasks involved. A better way of defining productivity for structural assembly may be in terms of rotational alignment accomplished per unit time, since aligning structural elements is one of the most critical and time consuming tasks for space construction. Another objective of this study was to identify how best to measure productivity so as to fairly assess human capabilities in EVA.

TASK	PRODUCTIVITY (KG/CREW HR.)
SIMPLE TETRAHEDRON	1000
COMPLEX STRUCTURE	600
COMPLEX STRUCTURE AT END OF 4 HR FATIGUE RUN	450
PLATFORM STRUCTURE WITH LIGHTWEIGHT ADDONS	250

LEARNING WITHOUT FOOT RESTRAINTS

Learning was found to be an extremely important factor in evaluating a person's capabilities in weightlessness. When first working in a pressure suit in zero-g, a subject tends to expend a lot of effort trying to control his body movements and make them as close to the movements he would use on the ground as possible. After 10-20 hours of working in simulated weightlessness, however, the subject instinctively adapts to the environment and learns to use it to his best advantage. Thus, while a subject is translating along a beam, for example, he will learn to rotate his body so as to be in position for performing a task upon arrival at the work station. Another important part of the learning process is to learn to work with the pressure suit rather than against it.

To establish the learning curve shown here, the subject repeatedly assembled a six element tetrahedron, without using foot restraints. The learning rate here was approximately 68%. This is to be compared with an 80% learning rate, which is standard for most ground-based operations. During the course of the MIT tests at Marshall, many learning rates were established with a low of 55%, a high of 80%, and an average of around 70%.
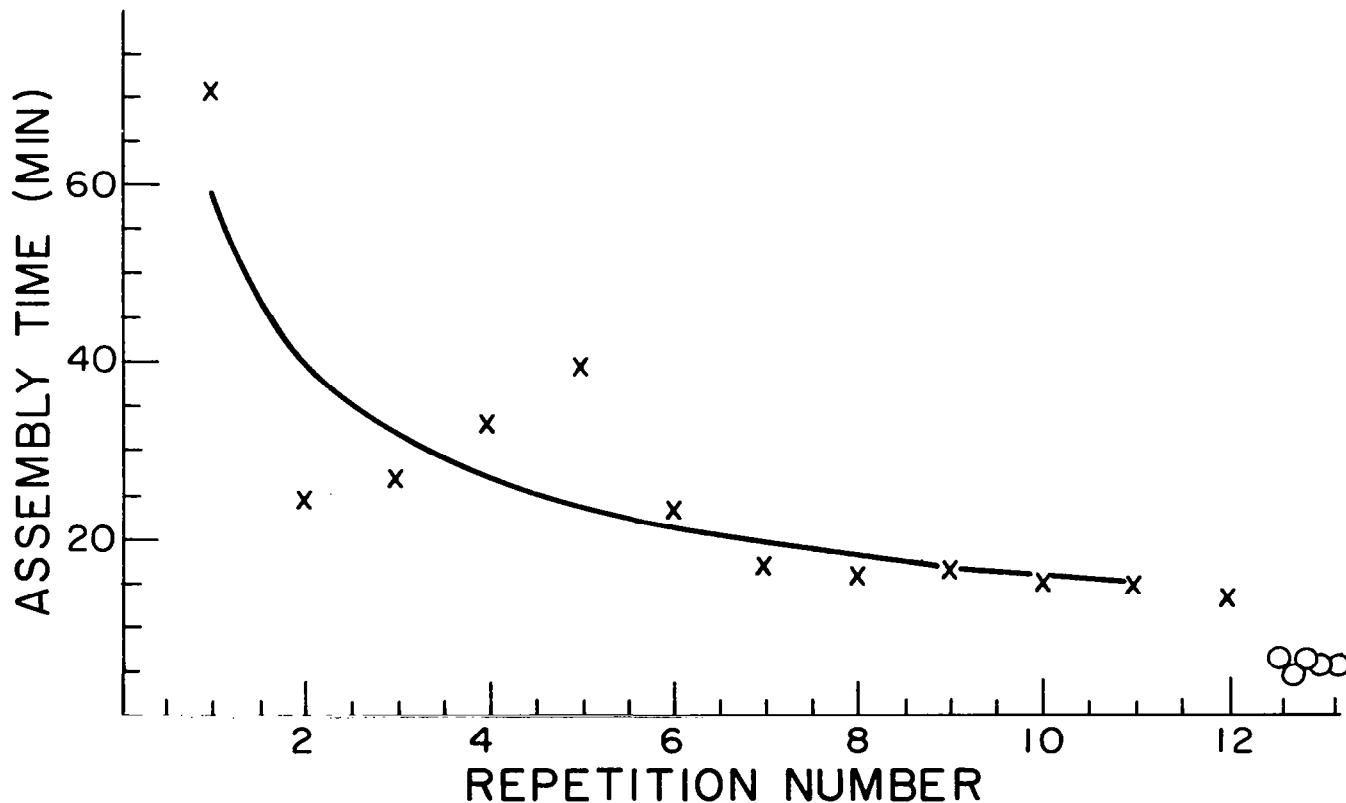
LEARNING IN FOOT RESTRAINTS

A learning curve was established in the same manner for a subject working in foot restraints at all of the work stations. Here, the learning rate was found to be about 73%. The more interesting data, however, was obtained after the subject got past the knee in the curve. The subject who had been assembling with foot restraints tried assembly without, and the subject who had been working without started assembling with foot restraints. The times obtained after this switch are shown as little circles on the graph. It is very clear that the subject who had never had to maneuver out of foot restraints still had a lot to learn, while the subject without experience in foot restraints was not hindered by using them.

In conclusion, while the task times tend to be marginally faster with the use of foot restraints, they are nevertheless not necessary at all work stations if the test subject is trained at working in weightlessness.
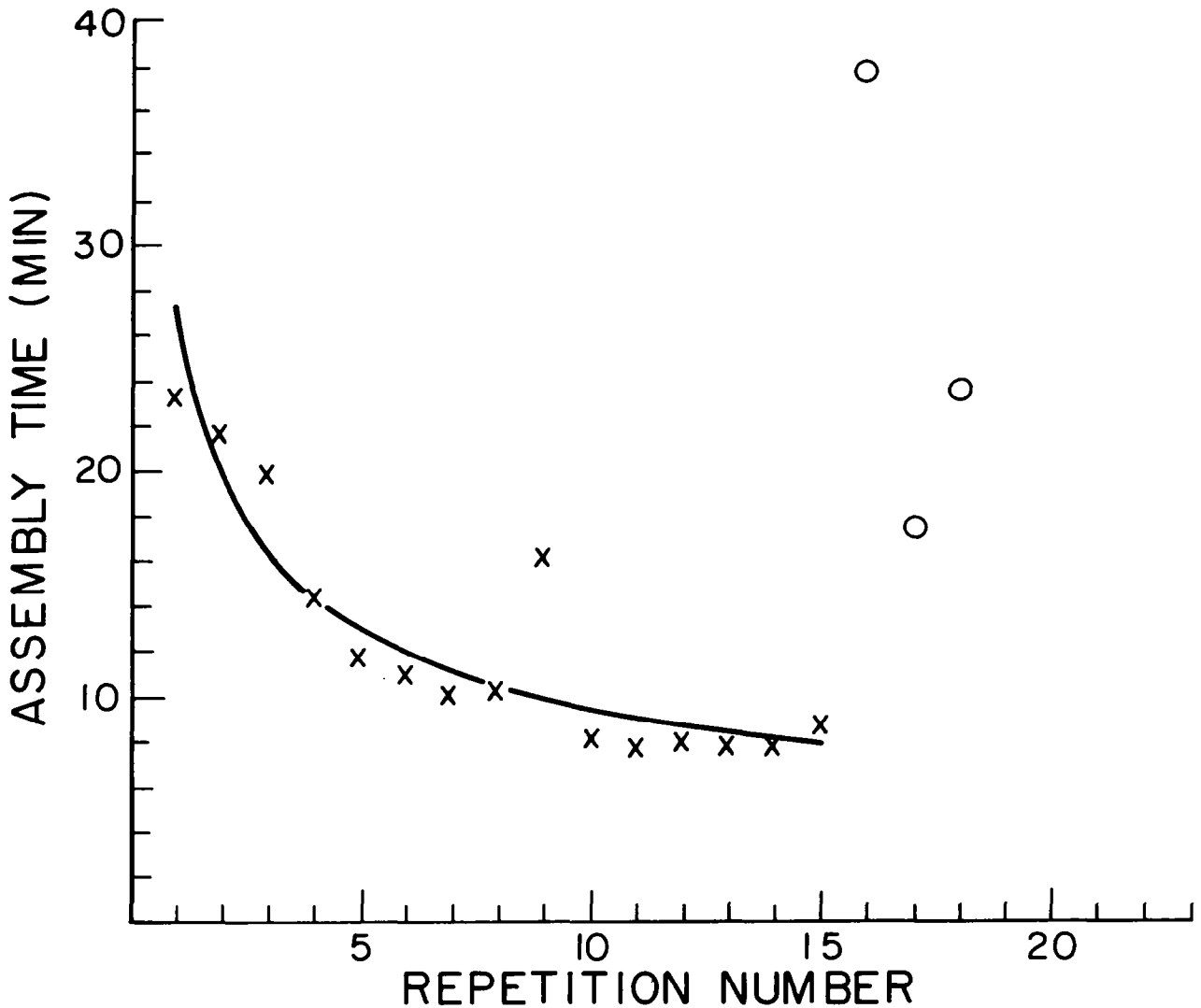
BEAM ALIGNMENT TASK

This graph shows the phase plane relationship between beam angle and angular velocity during a typical beam alignment test run. Both the beam and the test subject were neutrally buoyant for the test, but the subject, although constrained so as to prevent swimming, was not wearing a pressure suit. The objective of the task was to reach zero angle with zero angular velocity as quickly as possible. The target position was attained fairly accurately, in general, but the test subjects found it difficult to judge angular velocity. This must be taken into account when designing a connector to take assembly loads.
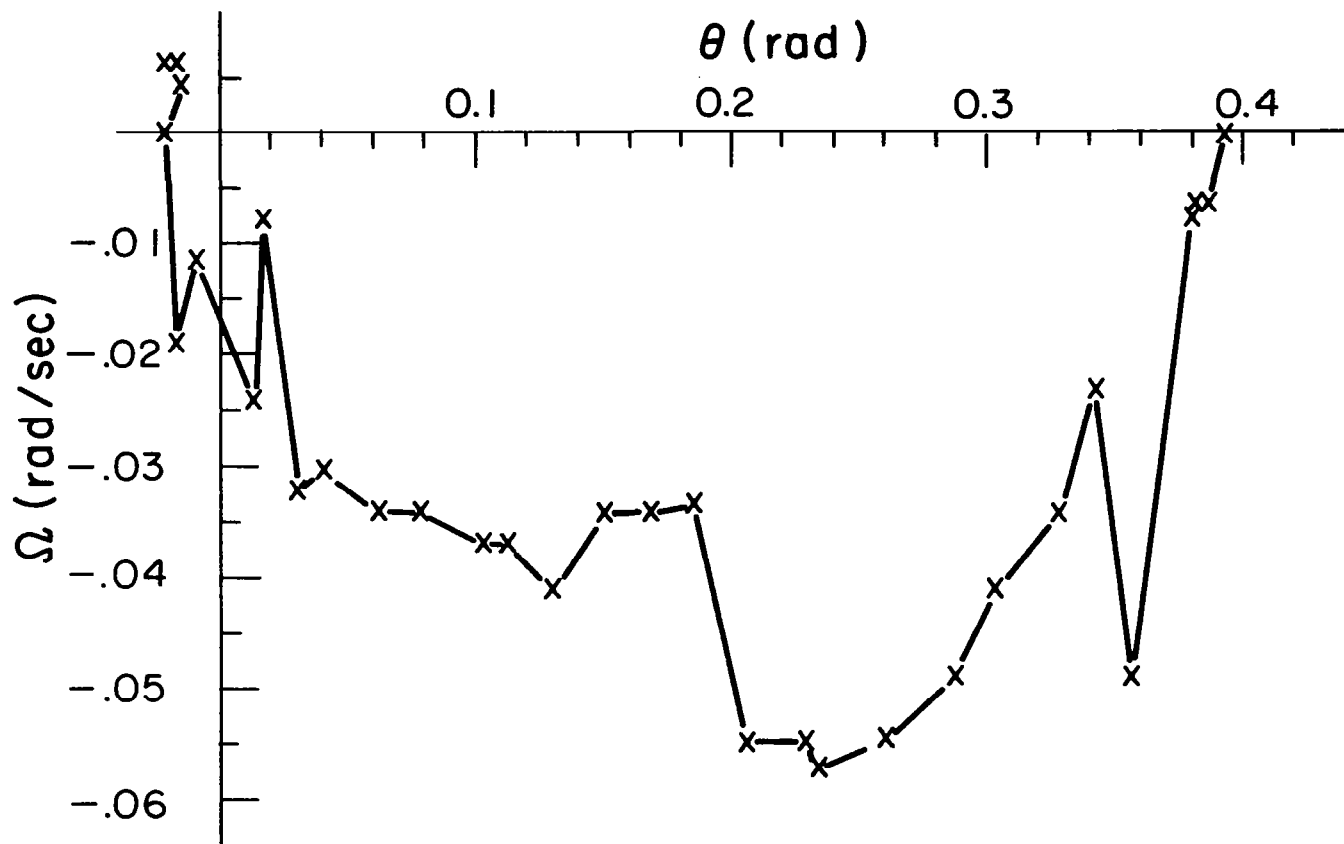
HEART RATE DURING FATIGUE RUN

In order to test the effect of fatigue on productivity during lengthy EVA operations, a four hour test session was conducted at MSFC. A single experienced test subject assembled a 36 element tetrahedral truss structure repeatedly during the run, while his heart rate and general condition were monitored. It appeared that the subject was able to pace himself quite well, so that his heart rate remained fairly steady throughout the run, even at the end when fatigue would have had the most effect. The drop in heart rate in the middle corresponds to a brief rest, during which the structure was disassembled so that it could subsequently be assembled again.
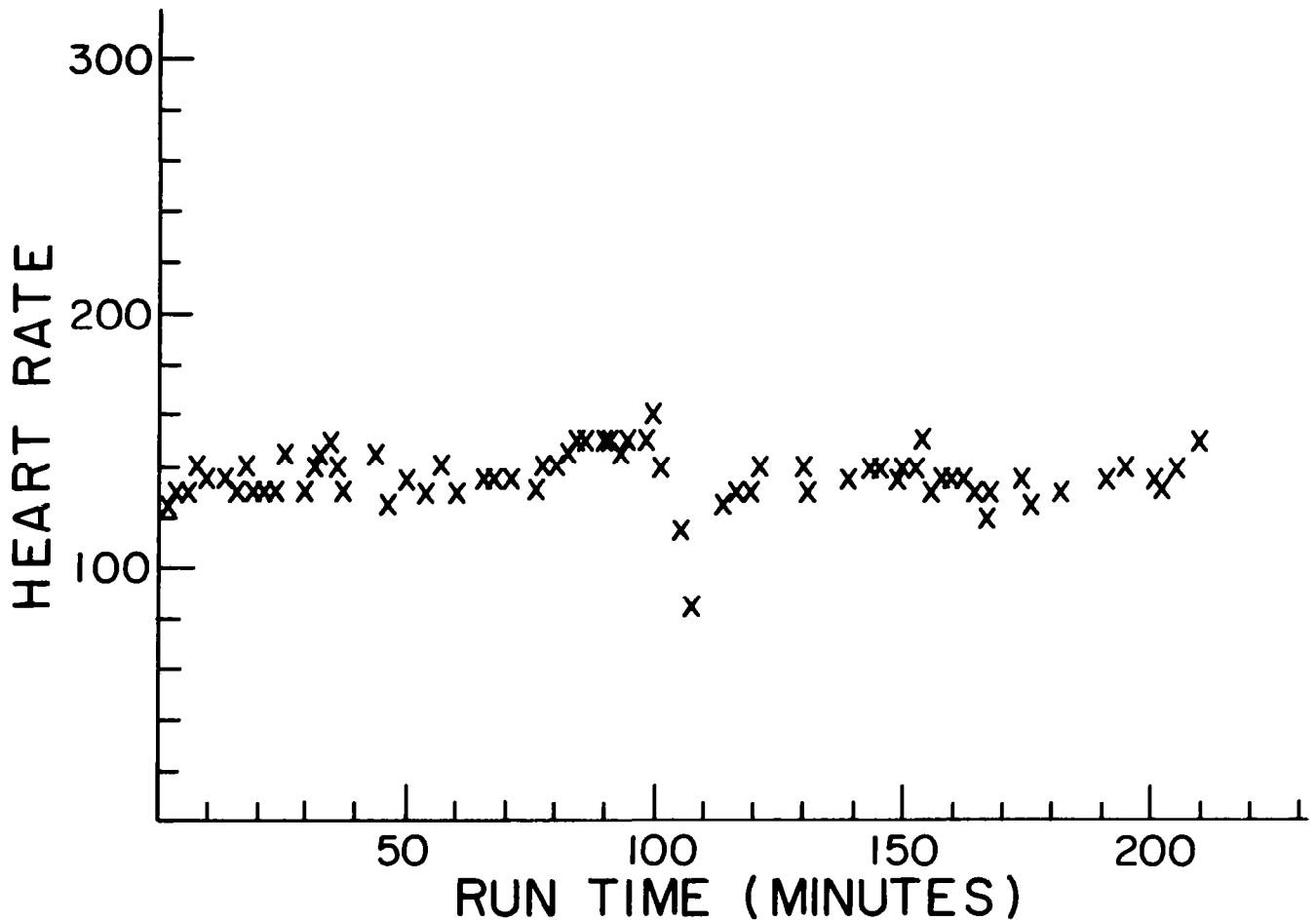
MIT CONNECTOR DESIGN

The MIT connector or joint was designed for simplicity of use and ease of manufacture. The joint is connected by placing a cylindrically shaped knob into a matching cup, and then sliding a sleeve which is locked into place by a spring-loaded button behind it. The joint requires very high angular alignment before the knob falls into place, and even more precise alignment before the sleeve can be slid. This is therefore not a very easy joint to use in weightlessness, and is thus a good test of a person's capabilities. Note also that the joint is rotationally symmetric. This reduces by one the number of alignments which must be made before the member is locked into place.

The joints were connected together on "joint clusters" at the nodes of the structure. For the tetrahedral truss structure, each joint cluster was different and had to be installed in a specific orientation; the prismatic structure had the advantage of interchangeable joint clusters.

Cup

Button Rod
Button Stem
Button

Locking Button
Sleeve
Beam End
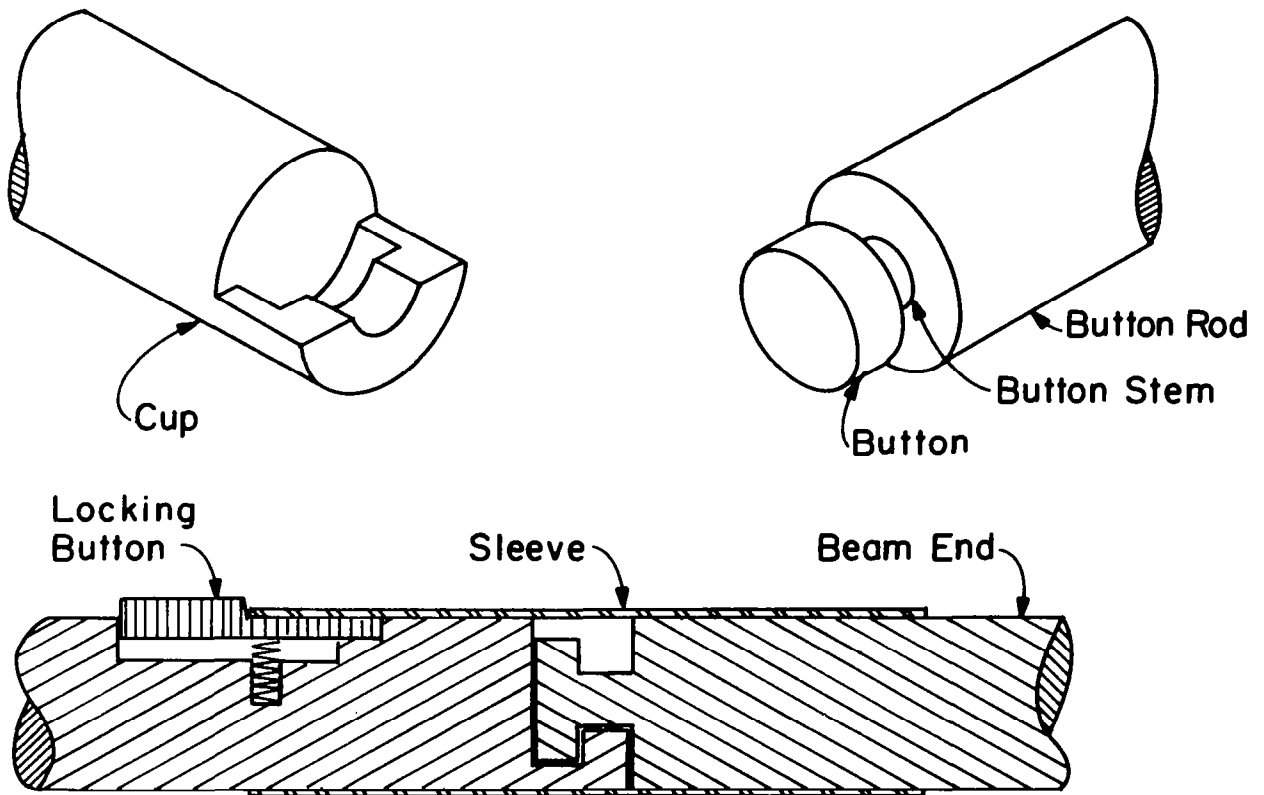
SUIT DESIGN ASPECTS FOR ASSEMBLY

Experience with pressure-suited assembly of structures in simulated weightlessness has shown that several design features of a space suit can prove limiting for that activity. Due to the constraint of the pressure garment, the work envelope for two-handed operation is much smaller than that for a shirt-sleeved subject; any incursion into that work volume is therefore deleterious to assembly performance. The Pressure Control Units (PCU) worn with the Skylab-era A7L-B suits cut into this prime volume, as does the display and control module (DCM) of the Shuttle extra-vehicular mobility units (EMU). MIT tests have shown that a head-up display is a preferable location for the functions in the current DCM.

Glove mobility is critical, as most tasks require some measure of manual dexterity. Current glove design is both restrictive on digital manipulation and tiring in that the user is performing Boyle's law work on the enclosed gases. Further research into low resistance, constant volume joints for pressure suit gloves is needed.

The design of the personal life support system (PLSS) backpack impacts much extravehicular activity, as the top corners of the backpack provide possible snag points which cannot be seen by the test subject. This suggests the need for both low-profile backpacks and greater peripheral vision capabilities from the helmets. Additional suit refinements might include low-mass boots (accidental impact from kicking motions have damaged neutral buoyancy hardware), better tether and restraint systems, and high-capacity cooling systems for extended periods of high activity.

- INCREASED MANUAL DEXTERITY NEEDED

- ELIMINATE ALL PROJECTIONS ON FRONT

- CONSTANT ARM LENGTH DURING BEND

- INCREASE VISUAL AREA AND HEAD MOBILITY

- IMPROVE PROVISIONS FOR FOOT RESTRAINTS

- INCREASE COOLING CAPABILITIES

NEUTRAL BUOYANCY FACILITY AT MARSHALL SPACE FLIGHT CENTER

This photograph shows the bottom of the NBF at MSFC. The curved ribs and other structure are a mockup of the orbiter payload bay. Our original experiments in measuring productivity and learning were accomplished on six member tetrahedral space frames. Two of these are shown being assembled. The rack on the right is a holder of the truss members which are made of PVC sewer pipe and, when filled with water, have a mass of 27 kg and a moment of inertia equivalent to a 400 foot long Grumman tri-beam. The space suits are "hand-me-downs" from the Skylab program. The scuba-equipped diver on the left is part of a team required for safety. Assembly times at the end of a two hour period were as low as 25 minutes.
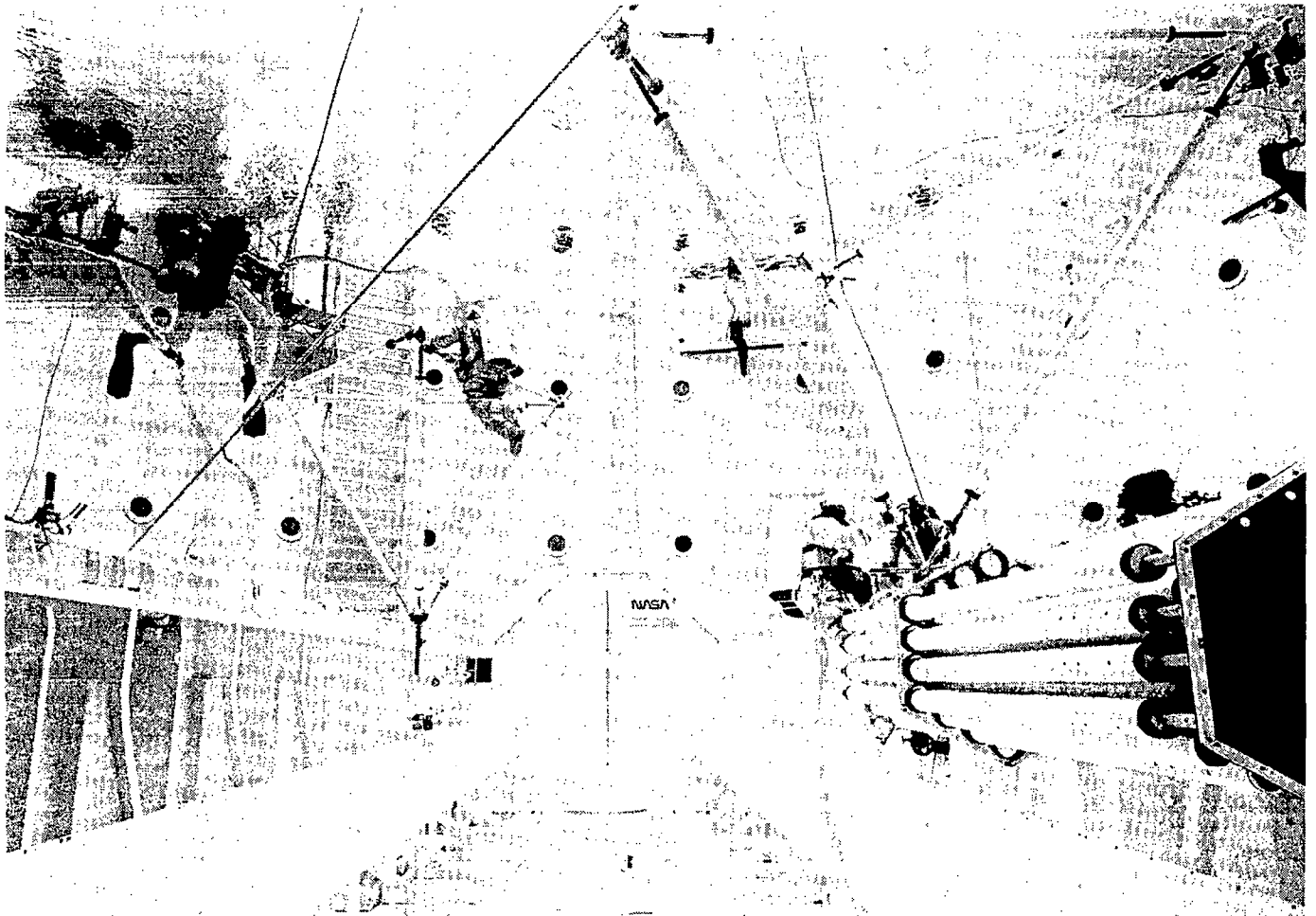
36 MEMBER TETRAHEDRAL STRUCTURE

This photograph shows a more complex structure which is being assembled by two subjects. The structure was anchored at one point. The most rapid assembly times were 1.75 hours for a single person and 45 minutes for two persons.
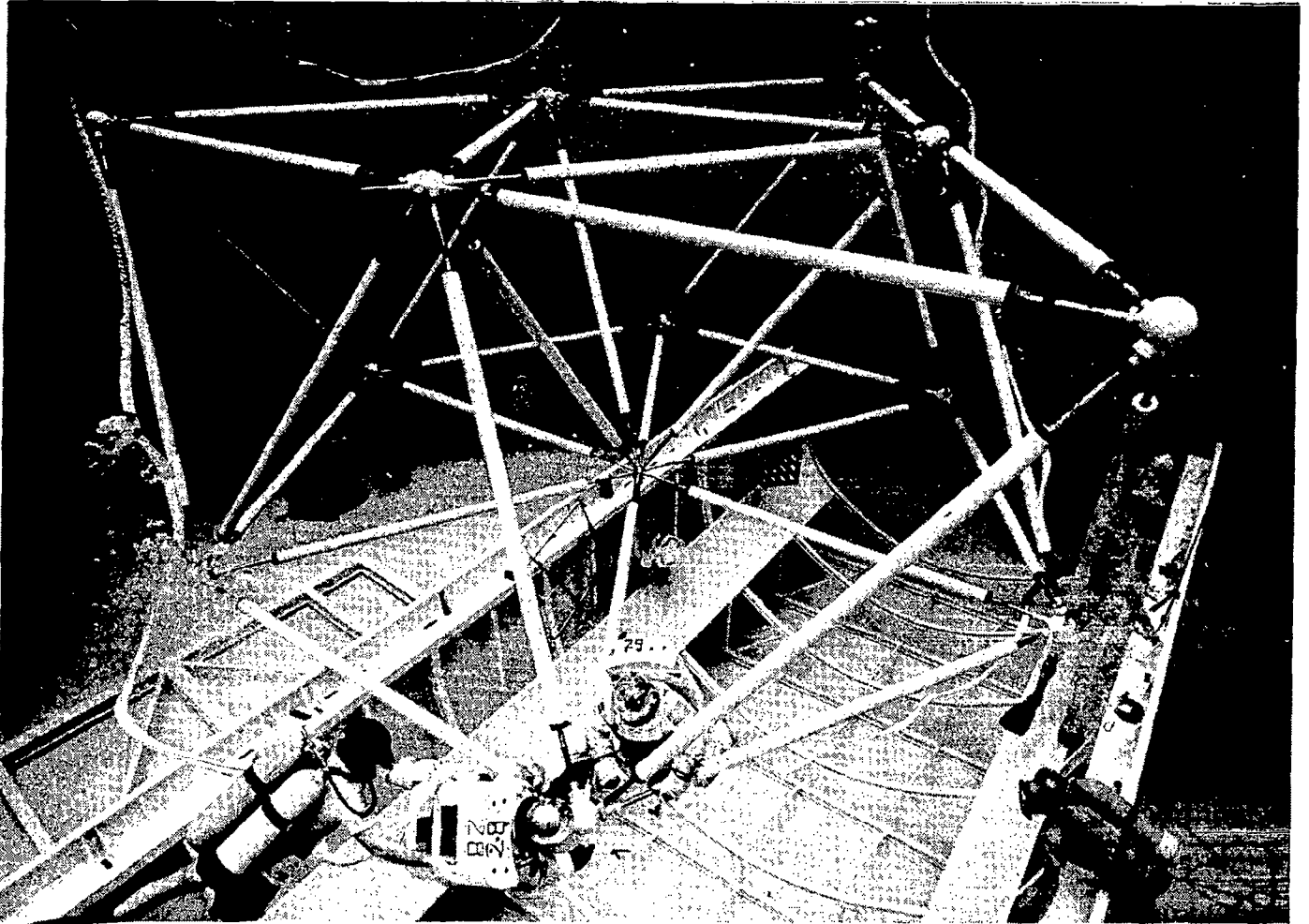
55 MEMBER STRUCTURE

The photograph represents the most complex structure thus far assembled. There are 55 members plus bracing wires, discrete payload packages (made of plastic garbage cans) as shown in the foreground, and netting which was unfurled. These different kinds of structure required different kinds of manual skills and dexterity. The measure of productivity, kilograms per hour, obviously has different meanings. Two subjects assembled the basic structure in about 112 minutes and an additional 100 minutes were required for the other hardware.

"Black Box"
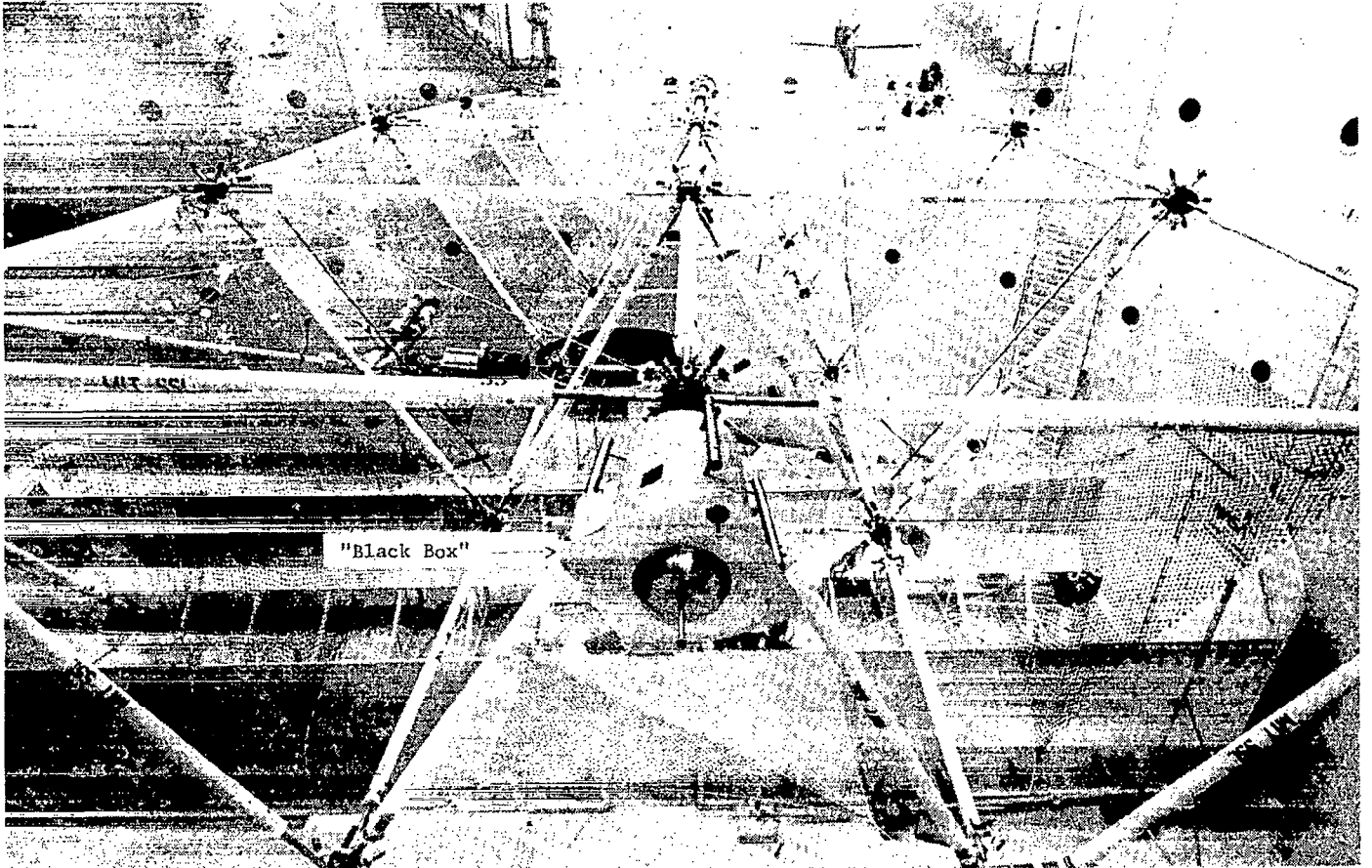
PUMA

This photograph is a closeup of the subject with the PUMA attached to provide extra mobility. The PUMA (Personal Underwater Maneuvering Apparatus) is a simulator of the Man Maneuvering Unit (MMU). Propulsive power is supplied by six electric trolling motors arranged with a control system to give five degrees of freedom. Gyros are used to maintain attitude. The right hand operates a joystick and switches, which control all the degrees of freedom.
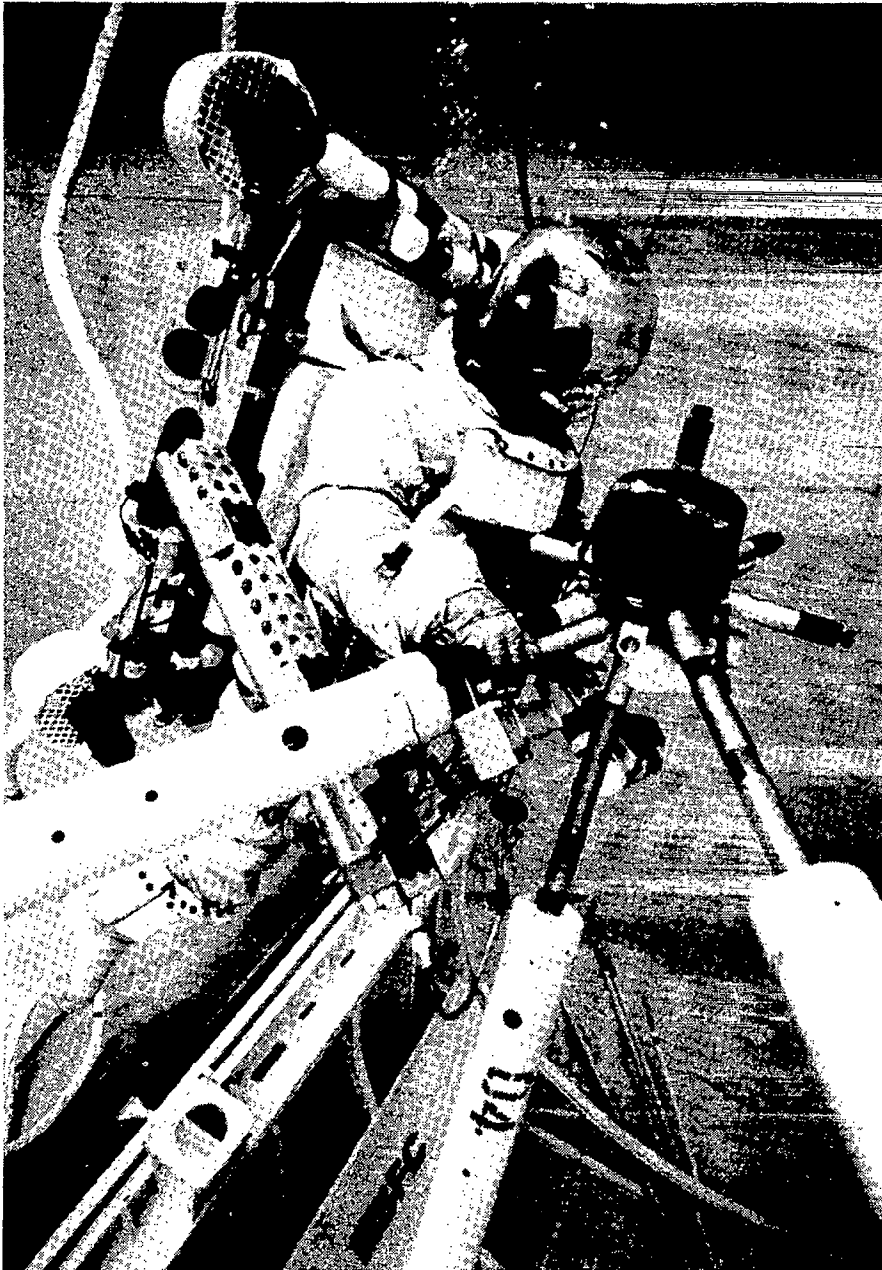
EXPERIMENTS IN SPACE

The structural design of airplanes and other structures which operate in the 1-g environment near the surface of the Earth is at the stage where the designer is not consciously aware of the machine tools being used as he prepares his design. He certainly is unaware of the capabilities of the person on the factory floor who is operating the machines or who is performing the final assembly tasks. The designer of large space structures must include in his design considerations of the capabilities of the person in space who is assembling the structure. Our best simulation of the zero-g environment is the immersion of the space construction engineer and the structure in water. Humans are nearly neutrally buoyant and it is relatively simple to neutrally balance the structure. Even though the effects of water drag can be accounted for in a rational manner, it is vitally important to determine the fidelity of the neutral buoyancy simulation of the assembly tasks by comparing results obtained in a NBF with results obtained in the real environment of space. The true productivity of man can only be validated with experiments performed in space. Such results will have important consequences for the design of space suits, the detailed design of large space structures and the directions as well as the urgency for research and development of teleoperators and robots.

REFERENCES

1. Akin, David L.; and Bowden, Mary L.: EVA Capabilities for the Assembly of Large Space Structures. IAF Paper No. 82-393, International Astronautical Federation, Oct. 1982.

2. Bowden, Mary L.: Dynamics of Manual Assembly of Large Space Structures in Weightlessness. M.S. Thesis, Dept. of Aeronautics and Astronautics, MIT, Cambridge, Mass., Jan. 1981.

3. Bement, Laurence J.; Bush, Harold G.; Heard, Walter L., Jr.; and Stokes, Jack W., Jr.: EVA Assembly of a Large Space Structure Element. NASA TP-1872, June 1981.

4. Loughead, T. E.; and Pruett, E. C.: EVA Manipulation and Assembly of Space Structure Columns. NASA CR-3285, May 1980.

5. Analysis of Large Space Structures Assembly - Large Space Systems Man/Machine Assembly Analysis. Report No. H-82-02, Essex Corp., June 1982.

6. Miller, R. H.; Minsky, M. L.; and Smith, D. B. S.: Space Applications of Automation, Robotics, and Machine Intelligence Systems (ARAMIS). Executive Summary. NASA CR-162079, 1982.

NASA/USAF RESEARCH IN STRUCTURAL DYNAMICS

L. D. Pinson
NASA Langley Research Center
Hampton, Virginia

and

A. K. Amos
Air Force Office of Scientific Research
Bolling Air Force Base, Washington, DC

301

Introduction

Work in the structural dynamics of large space structures and the associated problem of controlling response is progressing in several organizations within the NASA. The Air Force Office of Scientific Research is formulating a program of research which is to be performed in the university and industrial communities. In this paper an overview is presented of the NASA program, along with a description of the recently initiated Air Force program. Some results are presented and several assessments of technology are given.

Activities in the Dynamics of Advanced Structures

A diagram is presented in figure 1 which shows three research areas: structural response reduction, advanced structural analysis/tests and system identification. The goal of these activities is an orbit verified capability to predict closed loop dynamic response. The areas of structural response reduction and system identification are viewed as very closely related, while advanced structure analysis and test can proceed somewhat independently. Structural response reduction involves activities in the area of optimal design for dynamic response, actuator developments and a facility which could be used for doing tests of very large structures. System identification work involves automated model improvement as well as new laboratory and space dynamic test methods. Advanced analysis is being carried on in basically two ways, extension of existing analytical techniques and development of new analytical techniques.

MAJOR THRUSTS	FY82	FY83	FY84	FY85	FY86	FY87	FY88	FY89	FY90	FY91	FY92	GOALS

STRUCTURAL RESPONSE REDUCTION

OPTIMAL RESPONSE DESIGN

SPACE STATION SPECIFIC INVESTIGATIONS

ACTUATOR DEVELOPMENT

LACE

FACILITY FOR ON-LINE CONTROL

THERMAL-DYNAMICS INTERACTION

LARGE ANTENNA EXPERIMENTS

ADVANCED STRUCTURE ANALYSIS/ TEST

FLIGHT EXPER. (SAFE,MAST,STEP)

EXTEND ANAL. TECHNIQUES

NEW ANAL. TECHNIQUES

NEW PROGRAM EMPHASIS

SYSTEM IDENTIFICATION

SPACE STA. GENERIC/PATHFINDER MODEL PROGRAMS

15M HOOP COL. TEST/ANAL

AUTOMATED MODEL IMPROVEMENT

NEW LABORATORY/SPACE TEST METHODS

ORBIT-VERIFIED CAPABILITY TO PREDICT CLOSED-LOOP DYNAMIC RESPONSE

Figure 1

Goals for Structural Dynamics Technology Program

An elaboration of program goals in structural dynamics is presented in figure 2. The goals are stated for both NASA and AFOSR. The NASA goals are pursued with combinations of analysis and test programs. Design efforts in which actuators and sensors are located in an optimal manner are verified and correlated with tests. As part of the test program, actuators are being developed. The overall approach is to verify the methods developed with tests of increasingly complex structures. These tests are carried out on the ground and will be supplemented with appropriate flight tests. A goal is to develop system identification techniques to the point where timely application on orbit is possible with confidence. AFOSR objectives include the development of new materials for space stability and enhanced damping, and structural control concepts for precision performance.

NASA

ORBIT - VERIFIED CAPABILITY TO PREDICT AND CONTROL CLOSED-LOOP DYNAMIC RESPONSE:

O DEVELOP TECHNIQUES TO LOCATE AND SIZE ACTIVE/PASSIVE VIBRATION SUPPRESSORS, INTEGRATE WITH OPTIMAL STRUCTURAL DESIGN

O SUBSTANTIATE WITH GROUND TESTS OF INCREASINGLY COMPLEX STRUCTURES AND APPROPRIATE FLIGHT TESTS

O DEVELOP SYSTEM IDENTIFICATION TECHNIQUES TO THE POINT OF CONFIDENT NON-REAL-TIME ORBITAL APPLICATION

AFOSR

NEW MATERIALS FOR SPACE STABILITY AND ENHANCED DAMPING
STRUCTURAL AND CONTROL CONCEPTS FOR PRECISION PERFORMANCE

Figure 2

Presentation Topics - NASA and USAF

The order of presentation listed in figure 3 is the same for both the NASA and USAF portions of the paper.

DYNAMIC MODELING AND ANALYSIS

DYNAMIC PHENOMENA - INTERDISCIPLINARY PROBLEMS

DESIGN

EXPERIMENTAL STUDIES

Figure 3

Figure 4 shows activites in the area of dynamic modeling and analysis. As stated previously, analysis efforts are usually accompanied by a corresponding test program. Work is under way in traditional finite element methods, and in addition, equivalent continuum, repeating transfer matrices, and exact finite element activities also are under way. Tests have been performed on one dimensional and planar structures, and a test on a 15-meter hoop-column three-dimensional structure is proposed. Figures 5 through 10 indicate highlights of work in the various analysis activites.

CABLE-STIFFENED STRUCTURES

ANALYSES:

FINITE ELEMENT

EQUIVALENT CONTINUUM

REPEATING TRANSFER MATRICES

EXACT FINITE ELEMENT

TESTS:

ONE-DIMENSIONAL
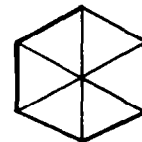
PLANAR
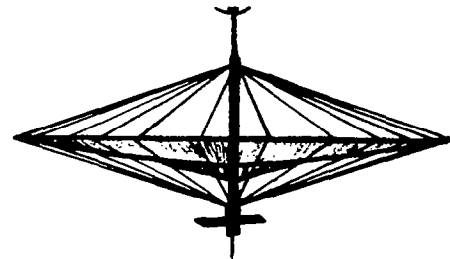
THREE-DIMENSIONAL (15-m HOOP COLUMN, PROPOSED)

Figure 4

Variation of Fundamental Natural
Frequency of a Truss Beam with Degree of Deployment

Figure 5 illustrates application of finite element techniques to the study of the important problem of deployment. The square of the natural frequency of a partially deployed truss beam divided by the natural frequency of the fully deployed beam is plotted as a function of the fraction of full deployment. Because of geometry changes that occur with deployment the natural frequency in the partially deployed configuration is less than that of the fully deployed configuration. The character of the mode shape changes from first bending to a fundamental mode of axial motion when the deployment is at very low levels.

TRUSS FUNDAMENTAL FREQUENCY DURING UNIFORM DEPLOYMENT/RETRACTION
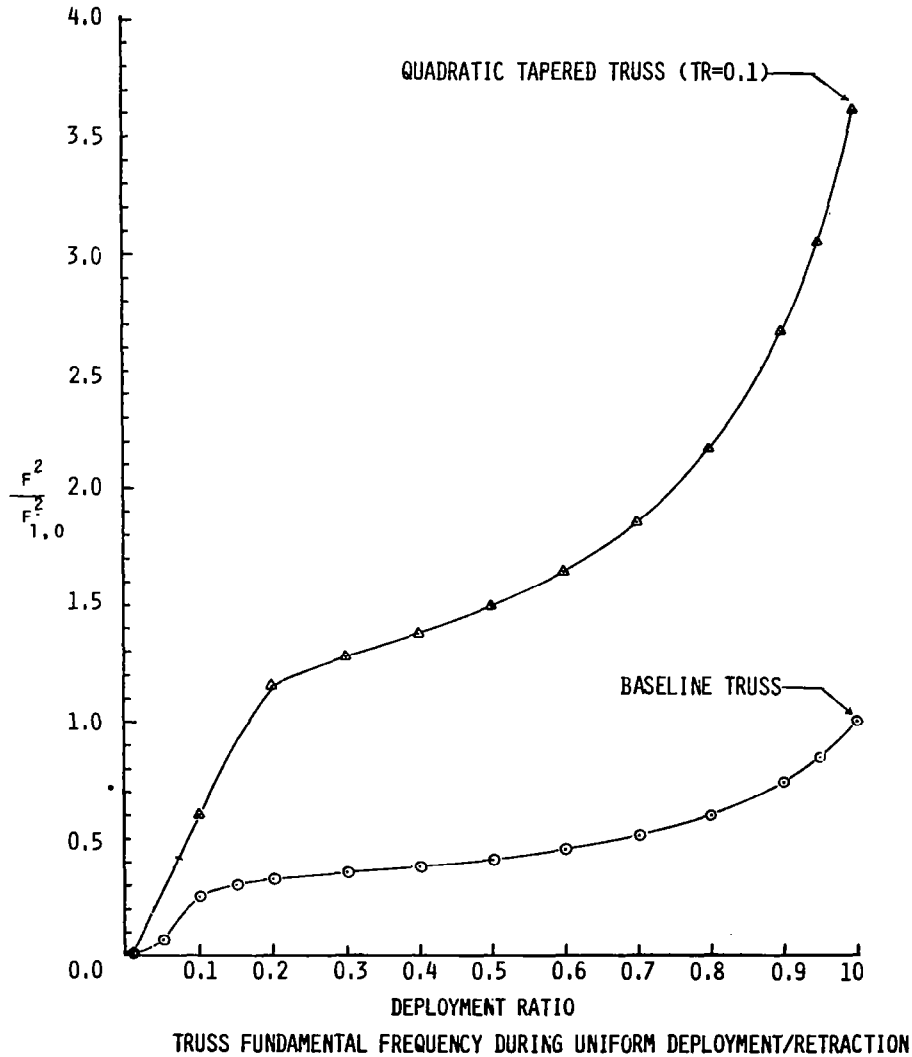
Figure 5

Reduction of Analysis Degrees of Freedom
Through the Use of Structural Repeatability

An example of the degree to which a model may be reduced by using repeatability characteristics in a structure is shown in figure 6. The general finite element analysis contained 1,848 variables whereas the repeatability feature allowed reduction to 84 degrees of freedom. Other techniques were used to reduce the problem further to 36 degrees of freedom.

TOP VIEW OF 100m TRUSS STRUCTURE

CROSS SECTION WITH PARABOLIC
UPPER SURFACE

PERIODIC STRUCTURE ANALYSIS
USES 14 NODES

PERIODIC STRUCTURE ANALYSIS
WITH INTERPOLATION PROCEDURE
USES 6 NODES
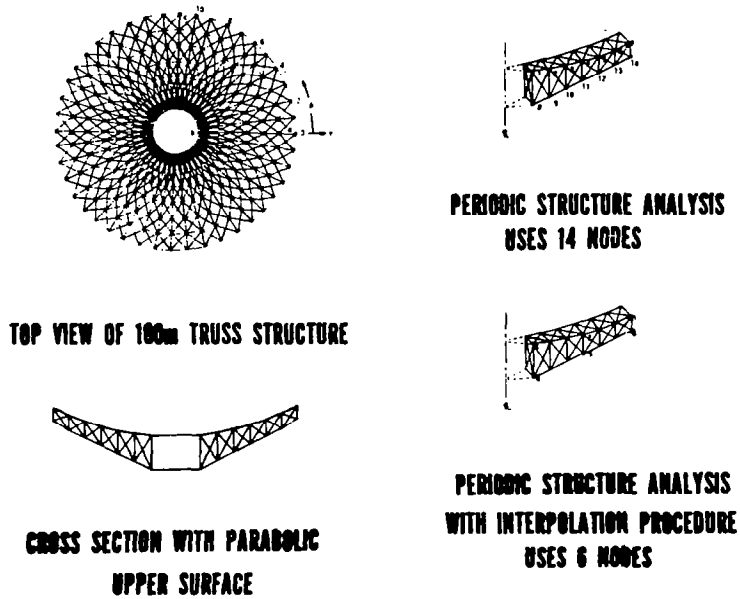
TABLE I

ANALYSIS PROCEDURE	VARIABLES
GENERAL FINITE ANALYSIS	1848
PERIODIC STRUCTURE ANALYSIS	84
PERIODIC STRUCTURE ANALYSIS WITH INTERPOLATION PROCEDURE	36

Figure 6

Axial Compressive Load/Natural-
Frequency Interaction for a Stayed Column

Results of a correlation between test and analysis of a cable stiffened column
are shown are shown in figure 7. The natural frequency is plotted as a function
of the axial compressive load in the figure and the correlation with analysis
is considered good. Difficulties with testing were encountered when the axial
load in the column reached about 60 percent of the Euler buckling load. Small
vibrations were amplified to the point where slackening of the pretensioned stays
occurred causing decidedly nonlinear behavior in the column.

VIBRATIONS OF STAYED COLUMN
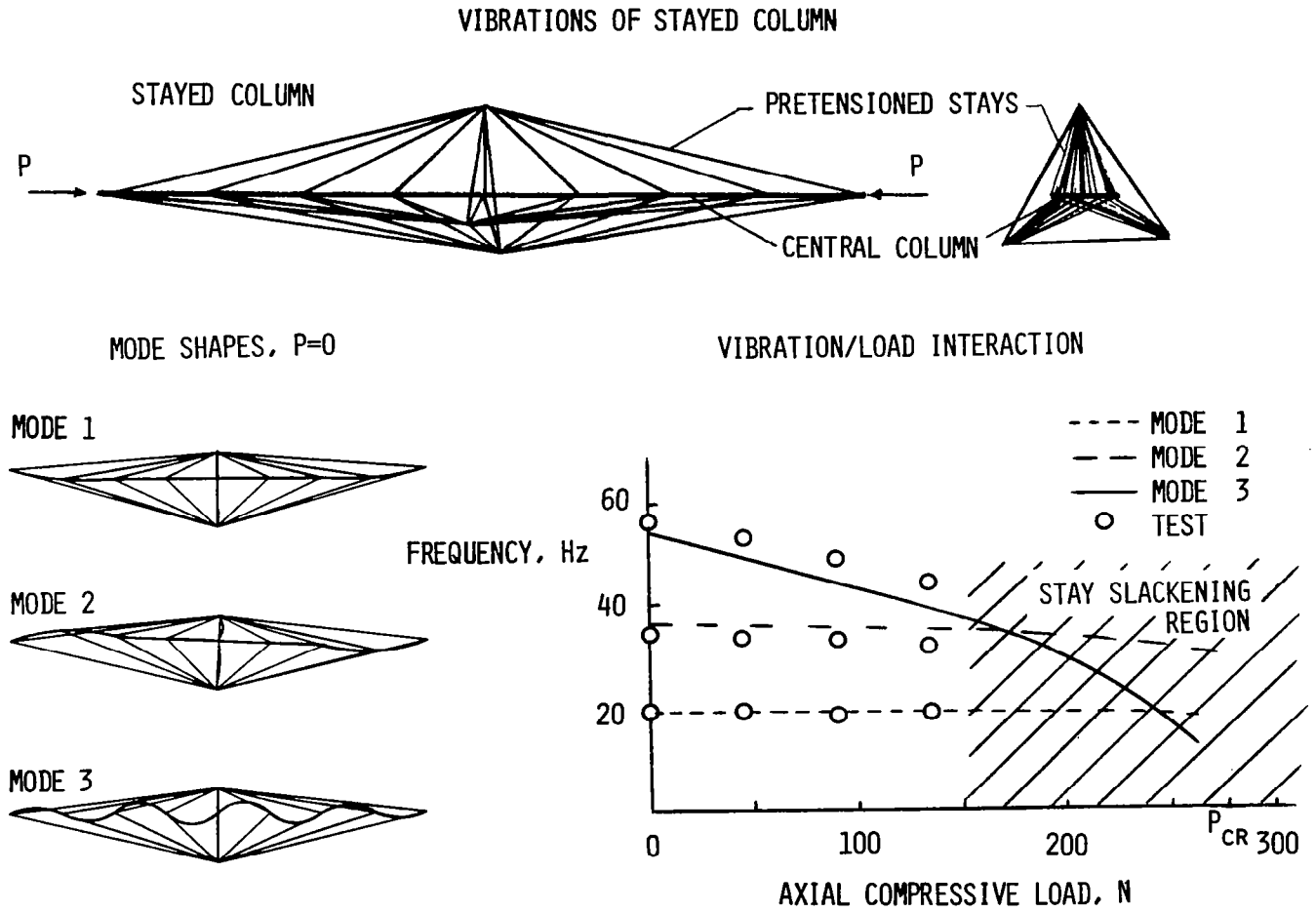
Figure 7

Experimental Frequency Response From
Pretensioned Structure Showing Clusters of Resonances

Another difficulty with testing of pretensioned structures is illustrated in figure
8. The plot shows a standard frequency response from which natural frequencies
usually may be obtained. A cluster of peaks occurs near the resonant conditions
indicating that small variations in the cable tensions may cause several resonances
to occur. Difficulty in deciding the overall resonant frequency thus is a poten-
tial problem area for more complex cable-stiffened structures.
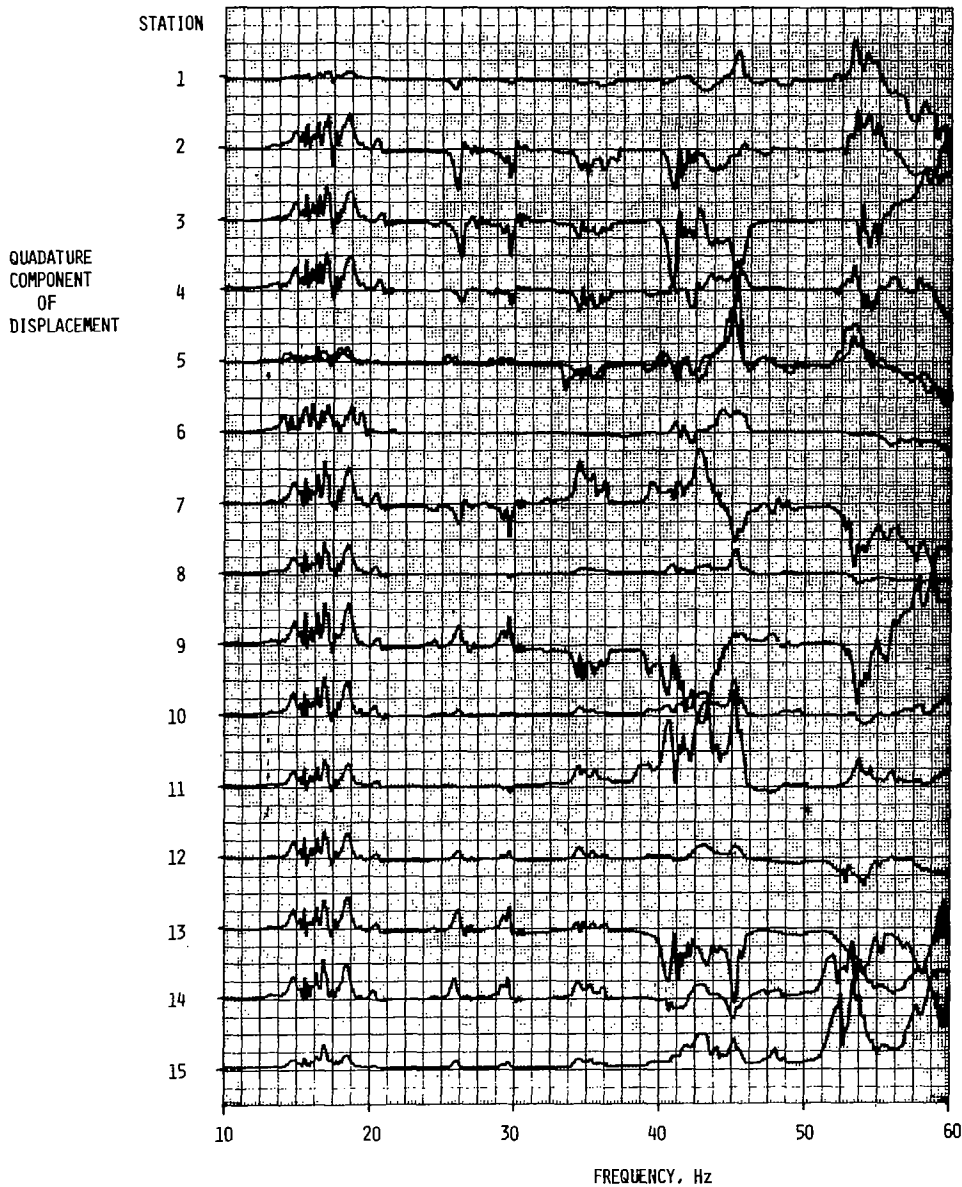
Figure 8

Load/Natural-Frequency
Interaction for Pretensioned Planar Structure

In figure 9, experiment and analysis are compared for two planar structures which are stiffened with cables. Again difficulty was encountered in performing tests when the load reached approximately 65 percent of the Euler buckling load. Correlation with analysis is considered to be good. Analyses were performed using exact finite elements.

RADIAL RIB AND HOOP PLATFORM VIBRATION STUDY
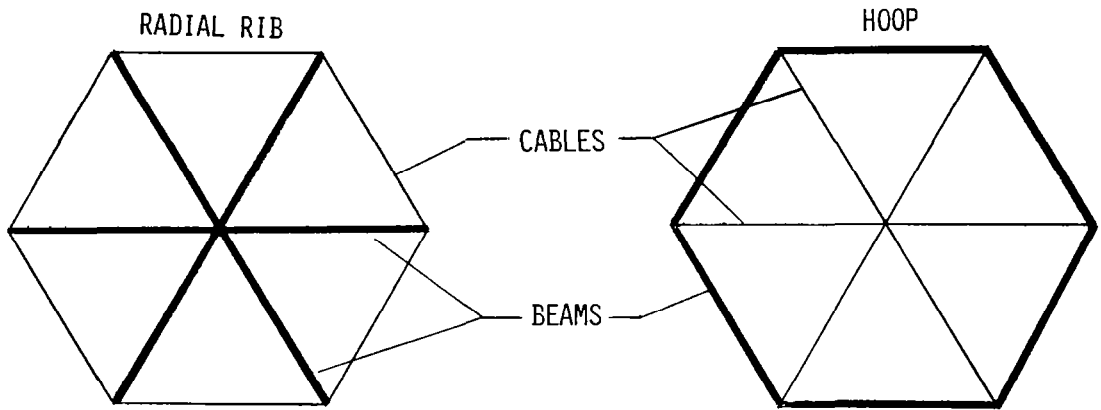
EXPERIMENT AND ANALYSIS CORRELATION
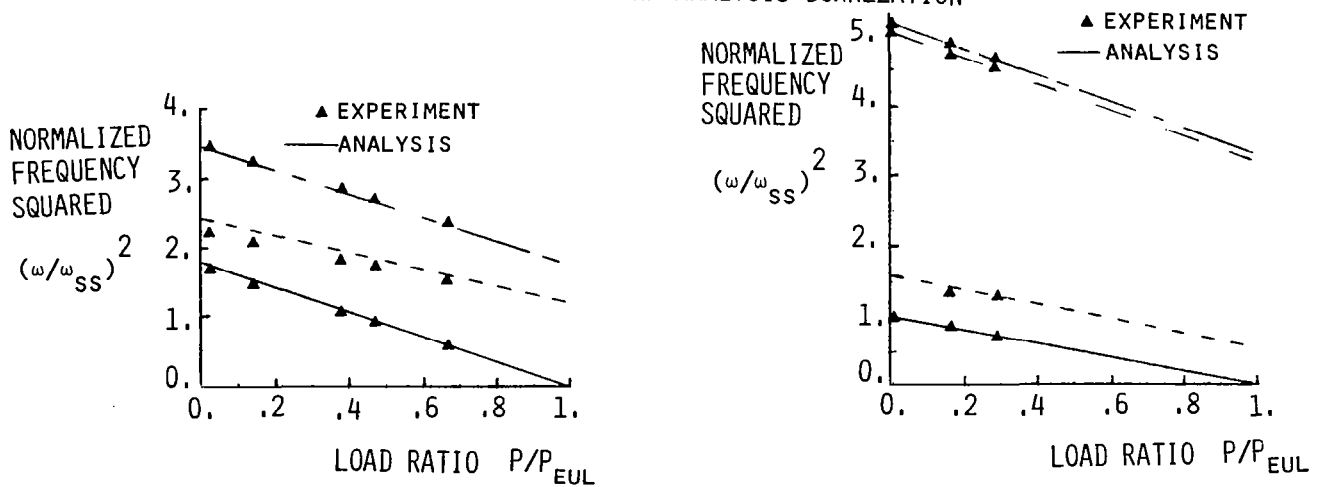
Figure 9

Model of a Cable-Stiffened
Antenna Concept for Possible Vibration Tests

To gain a better understanding of the behavior of complex cable stiffened structures, dynamic testing of a 15-meter model of the hoop column antenna concept is proposed (fig. 10). Based on results of testing and analysis of less complex structures, the correlation between analysis and test data will present a challenge.
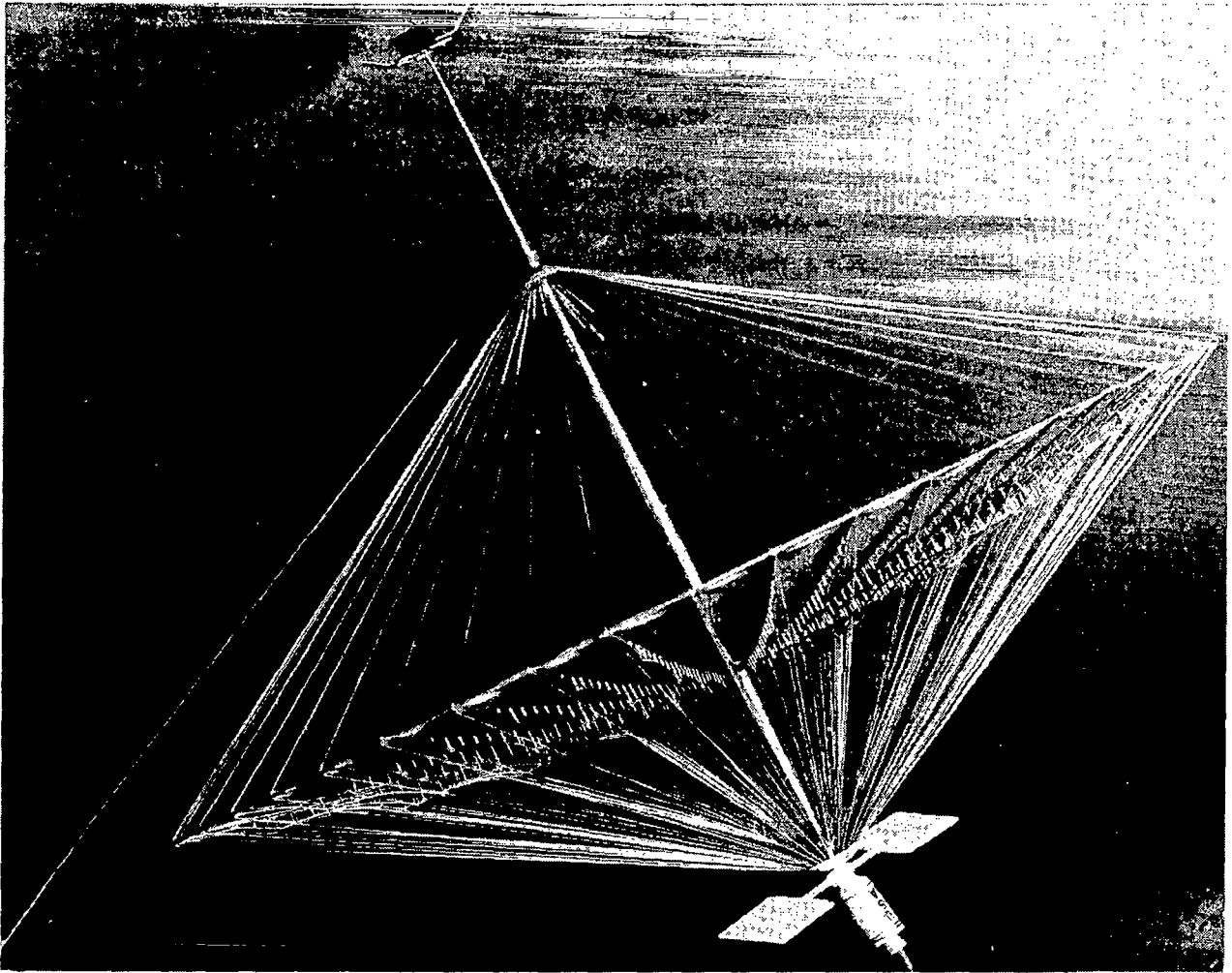
Figure 10

Summary of Dynamic Modeling and Analysis Area

Some results of the dynamic modeling and analysis efforts are presented in figure 11. In general, correlation between test and analysis has been good. However, to achieve this correlation it was necessary to consider the nonlinear behavior of the structure. Indications are that structural dynamics response must be considered early in the design of such structures to allow for potential applications of small dynamic inputs. Both analysis and tests show that cable stiffened structures are very modally dense and that modes occur in clusters. These characteristics make experimental identification and correlation with analysis very difficult. Another feature of large cable stiffened structures is the presence of a huge number of members which probably precludes the straightforward application of finite element analyses. A challenge is reduction to standard practice of imaginative approaches to this problem. Some approaches have been formulated but the methods are currently not widely used throughout industry.

O TEST-ANALYSIS CORRELATION VERY GOOD. MUST CONSIDER NONLINEAR BEHAVIOR AND
   DYNAMICS EARLY IN DESIGN.

O CABLE-STIFFENED STRUCTURES VERY MODALLY DENSE. GET "CLUSTERS" OF MODES.
   EXPERIMENTAL IDENTIFICATION DIFFICULT WITH CORRESPONDING DIFFICULTY IN
   COMPARISONS WITH ANALYSIS.

O LARGE NUMBER OF MEMBERS MAY PRECLUDE STRAIGHTFORWARD FINITE ELEMENT ANALYSES.
   A CHALLENGE IS REDUCTION TO STANDARD PRACTICE OF IMAGINATIVE ANALYTICAL APPROACHES.

Figure 11

Some Interdisciplinary Problems in Large Space Structures

Discussion of interdisciplinary problems is presented in two parts. The first is the formal correlation between analysis and test data and the second topic is called system identification (fig. 12). For this paper, system identification is taken to be the extraction of structural dynamic characteristics from time histories of responses measured on a structure.

Formal correlation between analysis and test data began in the early seventies with a theory presented by Collins et al. (ref. 1). The method was called minimum variance estimation. Another approach has been presented by Chen at JPL (ref. 2) in which a least squares method is used to revise physical dimensions and properties of finite elements. A revision of stiffness and mass matrices based directly on a least squares approach is presented by Berman of Kaman Aerospace (ref. 3).

The earliest approach to extracting structural dynamics characteristics experimentally involved applying sinusoidal forces to a structure and then measuring the response of the structure with an accelerometer. This approach is widely accepted and is even required by some government agencies. Burgeoning computer capabilities and algorithms for performing Fourier transforms in a timely manner led to the development in the early seventies of frequency domain analysis of response to random forces. This method has become known as the single-point-random method and is becoming more widely used in industry because of the time that can be saved with this approach, particularly the time during which actual hardware is being used. An alternate approach was devised in the mid-seventies by Ibrahim, in which the transformation to the frequency is avoided. This method, known as the Ibrahim Time Domain Method, is becoming increasingly used. Time domain methods are also used for on-line model updates in the process of adaptive control. These methods are not discussed in this paper.

Figures 13-17 present technical explanations and highlights in this area.

DYNAMIC PHENOMENA - INTERDISCIPLINARY PROBLEMS

O ANALYSIS - TEST CORRELATION

- MINIMUM VARIANCE ESTIMATION - J. H. WIGGINS CO. - MSFC

- REVISE FINITE ELEMENT PHYSICAL PROPERTIES - JPL

- DIRECT STIFFNESS AND MASS MATRIX REVISION - KAMAN - LaRC

O SYSTEM IDENTIFICATION

- SINE TESTING (TRIED-AND-TRUE)

- FREQUENCY DOMAIN ANALYSIS OF RESPONSE TO RANDOM FORCES

- TIME DOMAIN

= ON-LINE GAIN UPDATES (ADAPTIVE CONTROL)

= IBRAHIM TIME DOMAIN (ITD) METHOD OFF-LINE EXTRACTION OF MODE SHAPES, NATURAL FREQUENCIES AND DAMPING

Figure 12

Completed and Ongoing Work in Mathematical Model Update

Figure 13 presents an example of completed and ongoing work in the area of formal correlation between analysis and test data. This particular research is being performed by the Kaman Aerospace Company and has resulted in a program for Automated Model Improvement (AMI). In this method, modes and frequencies from tests are supplied along with stiffness and mass matrices. The program automatically corrects the stiffness and mass matrices to provide an improved set of matrices subject to constraints of symmetry and orthogonality. These improved models contain finite values in elements of the matrices which previously were zero, implying a coupling that is not present in the physical model. To correct for this, work is ongoing to provide constraints to the improvement process which will be consistent with physical reality. In addition, an algorithm to identify a damping matrix is also being pursued. This method may also be used to improve the accuracy of a reduced model which has been obtained from a more complex model by a reduction process. Modes and frequencies could be extracted once from the more complex model and then the reduced stiffness and mass matrices corrected to match the modes and frequencies of the more complex model.
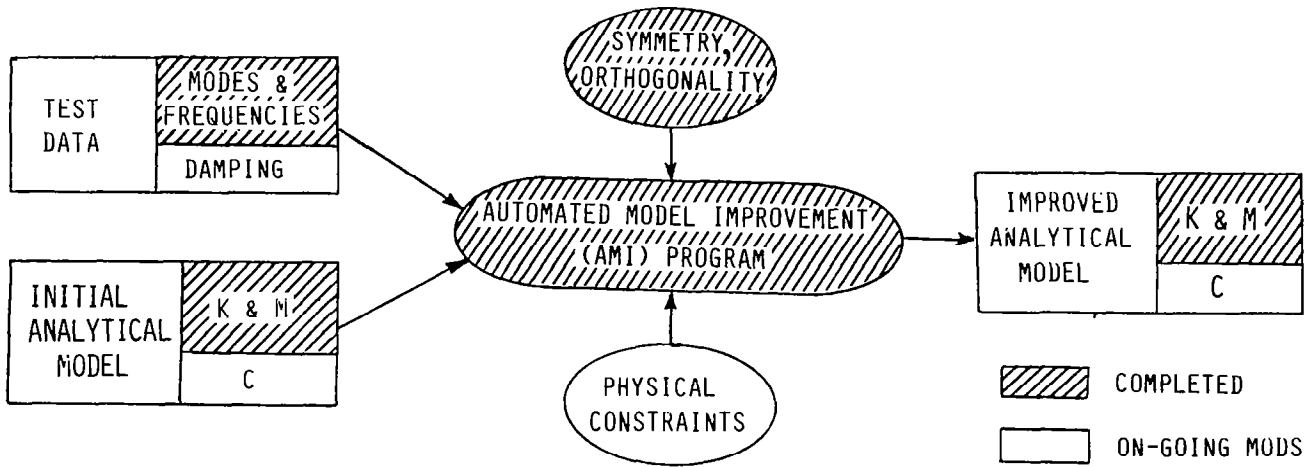
DEMONSTRATED: ANALYSIS/TEST AGREEMENT WITHIN 2%, FIRST TEN MODES, 508-D-OF-F UNDAMPED MODEL

PLANS: - APPLY TO MODEL SIZE REDUCTION

  - IMPROVE OPERATING EFFICIENCY & CONVENIENCE

Figure 13

Summary of Past and Ongoing
Research in a Time Domain Modal Identification Technique

Figure 14 is a list of activities that have been performed in connection with development of the Ibrahim time domain identification technique. The work ranges from very fundamental studies with numerical simulations to practical applications such as Voyager and a flight vehicle failure. A goal is to complete data analysis in an order of magnitude less time than is presently required.

O ANALYSIS OF VOYAGER, LDEF, AND LAB MODELS SHOWED POTENTIAL OF ITD METHOD TO SIGNIFICANTLY REDUCE COMPLEXITY OF MODAL SURVEY TESTS

O NUMERICAL SIMULATIONS AND SIMPLE LAB STRUCTURES ARE BEING USED TO VALIDATE AND OPTIMIZE IDENTIFICATION ACCURACY

O FLTSATCOM FAILURE: NOSE-FAIRING-JETTISON DATA ANALYSIS DEMONSTRATED CLOSE-MODE IDENTIFICATION PERFORMANCE

O ON-GOING WORK INCLUDES STUDIES OF:

- OPTIMUM DATA SAMPLING RATES, TIME SHIFTS, AND DEGREES OF FREEDOM TO ALLOW IN ANALYSIS

- METHODS TO ESTIMATE THE ACCURACY OF IDENTIFIED PARAMETERS

- THE EFFECTS OF STRUCTURAL NONLINEARITIES

- TECHNIQUES TO TOTALLY AUTOMATE OPERATION OF THE IDENTIFICATION PROCESS

Figure 14

A Comparison of Results from Fourier Transform Analysis
of Free Response Data and Analysis by the Ibrahim Time Domain Method

Figure 15 shows one comparison of results from the Ibrahim method with results from the more standard Fourier transform approach. The chart indicates that the FFT method will produce good results with sufficient record lengths. When the length of record is limited, however, deficiencies are apparent. A low level mode, for example, may be indistinguishable from the leakage effects which occur with the FFT method. In addition, close modes may be indistinguishable. This problem, however, is not apparent with the ITD method.

Figure 15

Reconstruction of a Segment of Flight Data from Identified Modes

Figure 16 is a display of flight data from a FLTSATCOM anomaly from which modes are extracted and the original data then reconstructed. The reconstruction is almost indistinguishable from the original data. The method successfully detected the presence of two modes closely spaced in frequency and having almost equal amplitude but opposite phase.

Figure 16

318
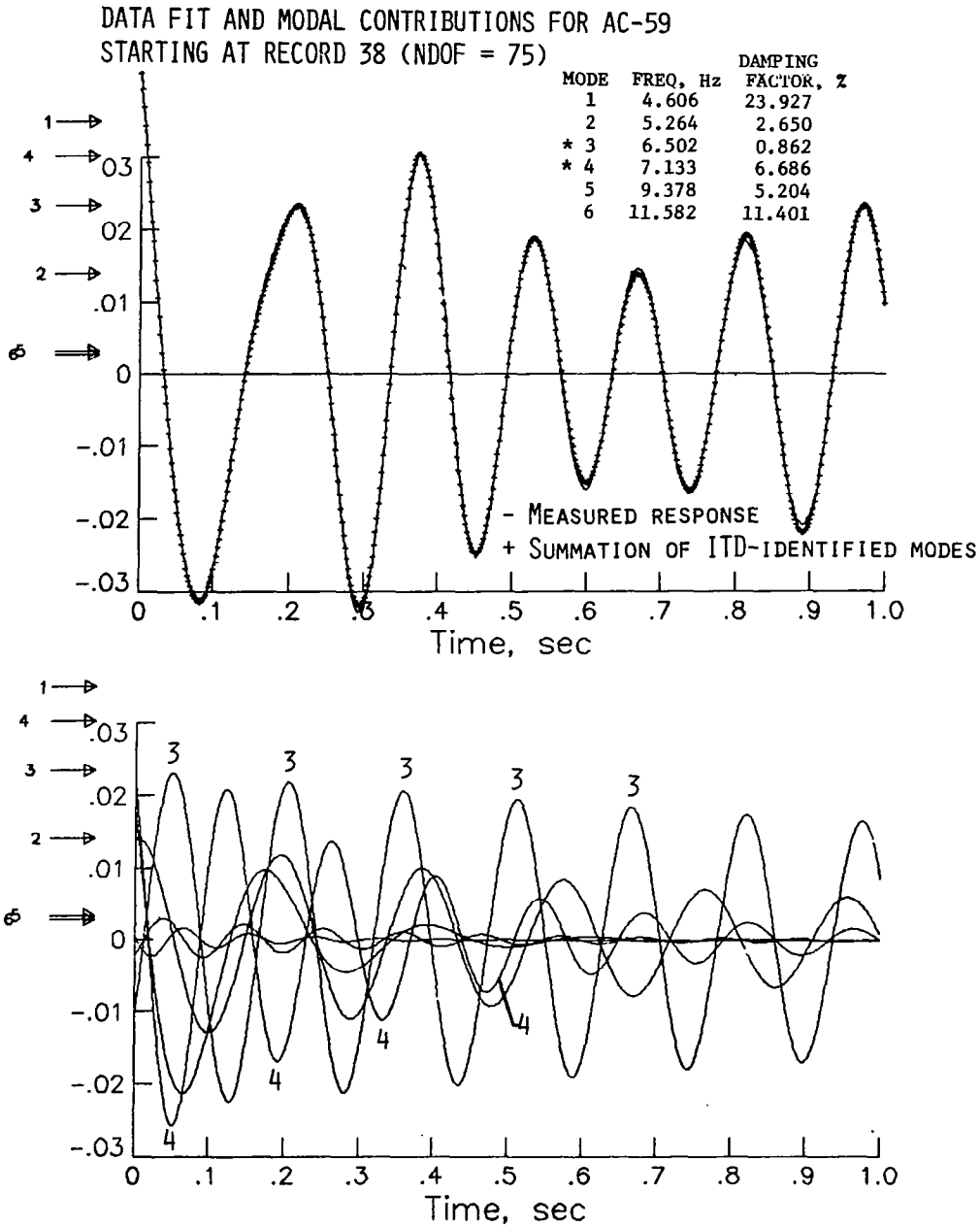
Effect of Cubic Nonlinearity on
Identification Results of Ibrahim Time Domain Technique

Figure 17 shows results of an analytical study of a single degree of freedom
system with a cubic nonlinearity in which simulated data was analyzed with the ITD
method. The result of the study with the nonlinearity was to produce not only
identification of the fundamental mode, but also identification of harmonics. The
nonlinearity produces distortions on the basic sinusoidal response and these dis-
tortions are detected as modes. An analytical and experimental study was performed
on a simple torsional structure having both a linear mode and nonlinear mode.
Results indicates that even with the presence of the nonlinear mode the linear
mode is detected accurately. The nonlinear mode is detected, as are harmonics
of the nonlinear mode. At higher amplitudes multiple frequencies are detected at
a single resonance because of the variation of frequency with amplitude. When
damping is present the average amplitude is different for successive blocks of
data resulting in the identification of a band of frequencies. Thus a result is
that identification of multiple frequencies closely spaced in combination with
other resonances at a multiple of three from the cluster of frequencies may in-
dicate the presence of nonlinearities.

SINGLE DEGREE OF FREEDOM: $X = A_1 \sin 2\pi f_1 t + A_2 \sin 2\pi f_2 t + A_3 \sin 2\pi f_3 t + \ldots$

	f_1	f_2	f_3
ANALYSIS	.304	.913	1.52
ITD	.303	.897	1.56
% DIFFERENCE	0.39	1.72	2.76

TWO DEGREES OF FREEDOM:

LINEAR MODES AT .1&.19HZ
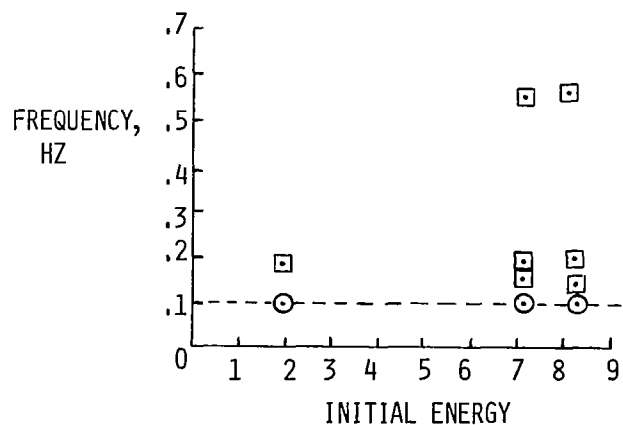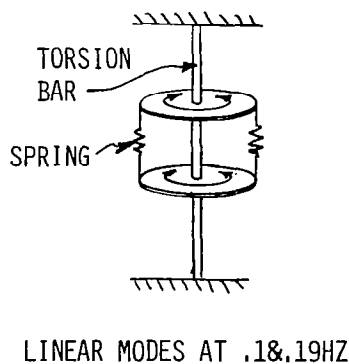
Figure 17

Status of Some Interdisciplinary Problems

In figure 18 a subjective evaluation is presented of the area of interdisciplinary problems. Formal updating of a mathematical model of a structure is considered to be immature. The problem is quite difficult and more experience is needed with practical structures. There should be tradeoffs among various approaches to performing this update. Sensitivity studies are needed to investigate the effects of errors in modal amplitude, phase, and frequency on changes that are made to mass and stiffness matrices. Most existing methods are based upon a form of a least squares criterion. Investigation should be made to determine whether this criterion is most appropriate.

Technology for extracting structural dynamics characteristics from test data is good but time involved in data analysis is still extensive. Therefore laboratory methods are considered to be adequate but the time involved in performing any on-orbit modal test is still too great; thus a need is to reduce this time. Although not discussed here, the ability for on-line correction of more than a few modes does not exist. This limitation needs correction.

O ANALYSIS - TEST CORRELATION - TECHNOLOGY IMMATURE. PROBLEM IS DIFFICULT. NEED MORE EXPERIENCE WITH PRACTICAL STRUCTURES:

- TRADE-OFFS AMONG METHODS

- SENSITIVITY STUDIES SHOWING EFFECTS OF ERRORS IN MODAL AMPLITUDE, PHASE, AND FREQUENCY

- SELECTION OF MATCHING CRITERION - WHY LEAST SQUARES

O SYSTEM IDENTIFICATION - GOOD LABORATORY METHODS. PRINCIPAL NEEDS:

- REDUCE DATA ANALYSIS TIME TO ENABLE USE ON-ORBIT (OFF-LINE)

- EXPAND ON-LINE CAPABILITY TO MORE DEGREES OF FREEDOM

Figure 18

Activities in Design
and Optimization of Structures for Dynamic Forces

Figure 19 indicates work areas for optimization of structures for dynamics response.

PASSIVE TECHNIQUES
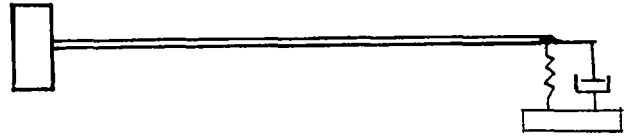
DAMPING DISTRIBUTION:

    ONE-DIMENSIONAL
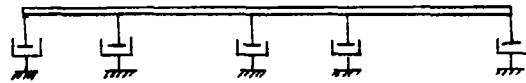
    PLANAR
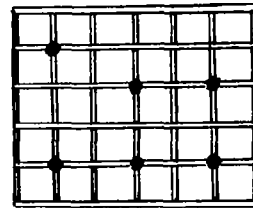
STRUCTURAL OPTIMIZATION:

    PASSIVE OPTIMAL CONTROL
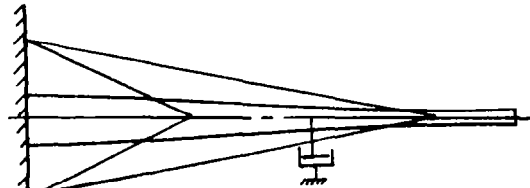
    NONLINEAR SEARCH METHODS
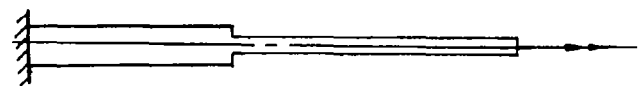
Figure 19

Plot of Vibration Absorber Mass Required for Harmonic
Response To Be Less Than a Specified Value for a Long Slender Beam

Figure 20 shows the mass required in an application of the tuned vibration absorber concept to a long mast. The chart indicates that the absorber mass required to limit responses to harmonic input becomes exorbitant at a length of approximately 60 meters.

Figure 20

Outline of Inertial Damper Optimization Problem

A method has been devised to both size and locate dampers required to achieve a specified minimum value of damping in certain modes. In this method changes in the complex modes are considered which result from changes in location and size of the damping actuators (fig. 21).

GIVEN: ζ_i, $i = 1, 2, \ldots,$ NUMBER OF MODES

FIND:

$$C = \begin{bmatrix} \ddots & & & O \\ & C_1 & & \\ & & C_2 & \\ O & & & \ddots \end{bmatrix}$$

SUCH THAT:

$$\sum_j C_j = \text{MINIMUM}$$

WHILE:

$$C_j \geq 0$$

$$\overline{\zeta_i} \geq \zeta_i, \quad \overline{\zeta_i} = \text{SOLUTION MODAL DAMPING RATIO}$$

Figure 21

323

Some Results of Damper
Optimization Analysis and Corresponding Beam Experiment

Some results from the application of the optimal damping method are shown in figure 22. A picture of a slender beam to which actuators are attached for the purpose of providing the damping force is shown and on the right side of the picture several noncontacting displacement probes are indicated. In the left of the figure some typical results are presented for damping of several modes. The method first extracts a symmetric distribution of dampers, and then a nonsymmetric arrangement is investigated to determine if the objective function can be further reduced.
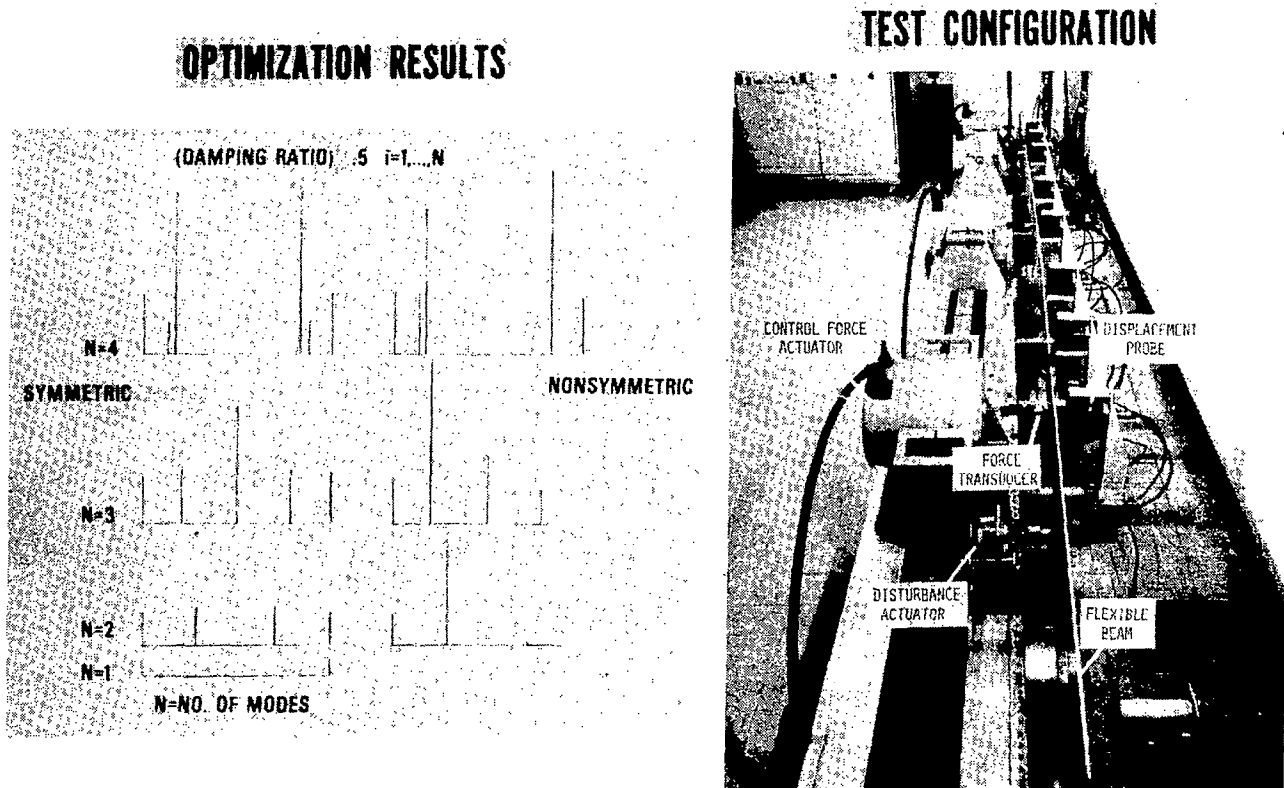
Figure 22

Comparison of Analysis With Test for Various Damping Ratios

Some experimental results from the experiment shown in figure 22 are presented in figure 23. The figure indicates good correlation between experiment and analysis. For higher damping, extraction of actual damping characteristics is quite difficult because of limited record lengths available for analysis. Thus a potential problem for investigation of closed loop structural dynamic characteristics on orbit is revealed.

ACTIVE DAMPING RESULTS
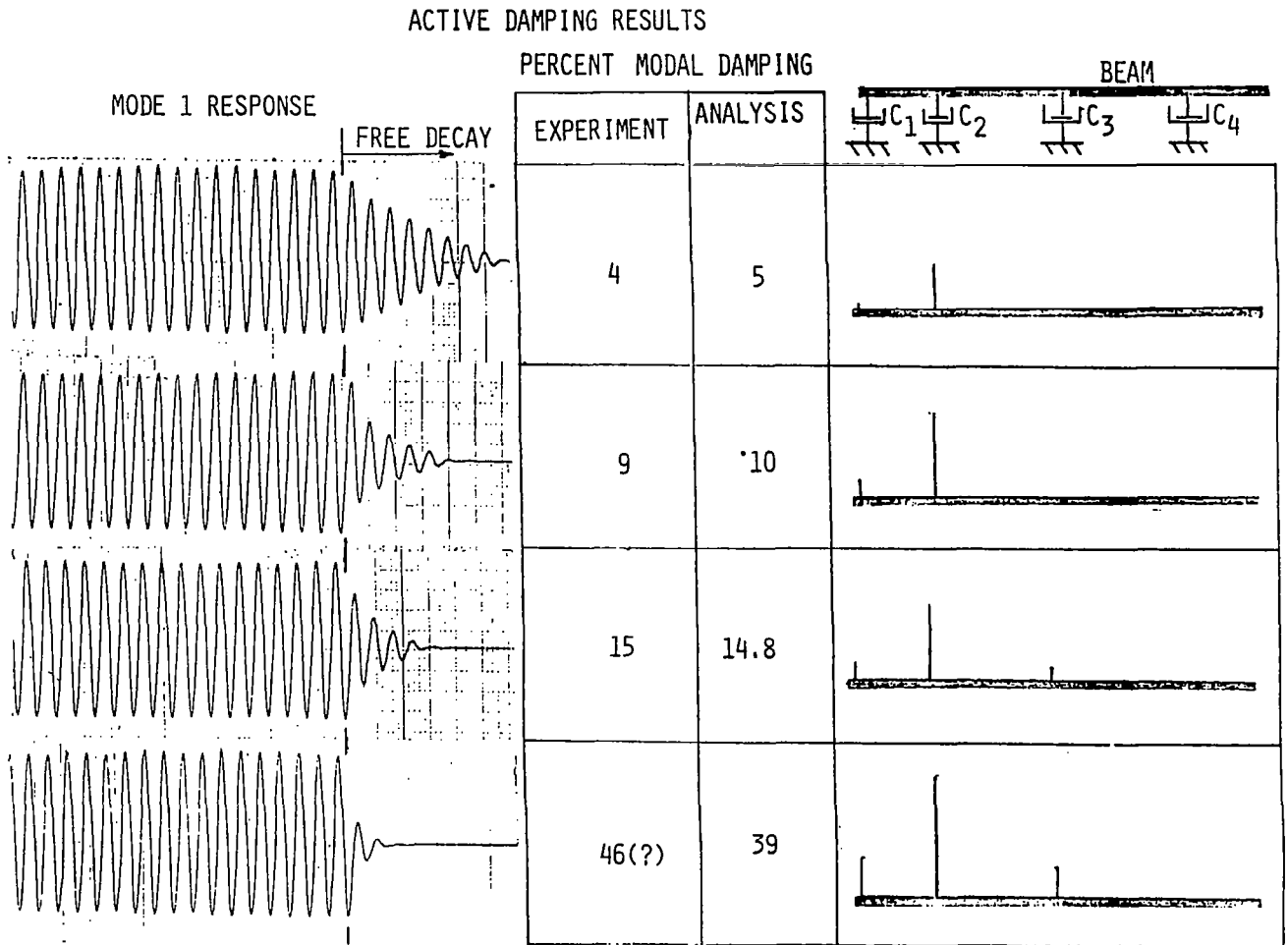
Figure 23

Grillage Structure To Be Used in Optimal Damping Experiment

Extension of the optimal damping research to a more modally dense structure, the grillage, (fig. 24) is under way.
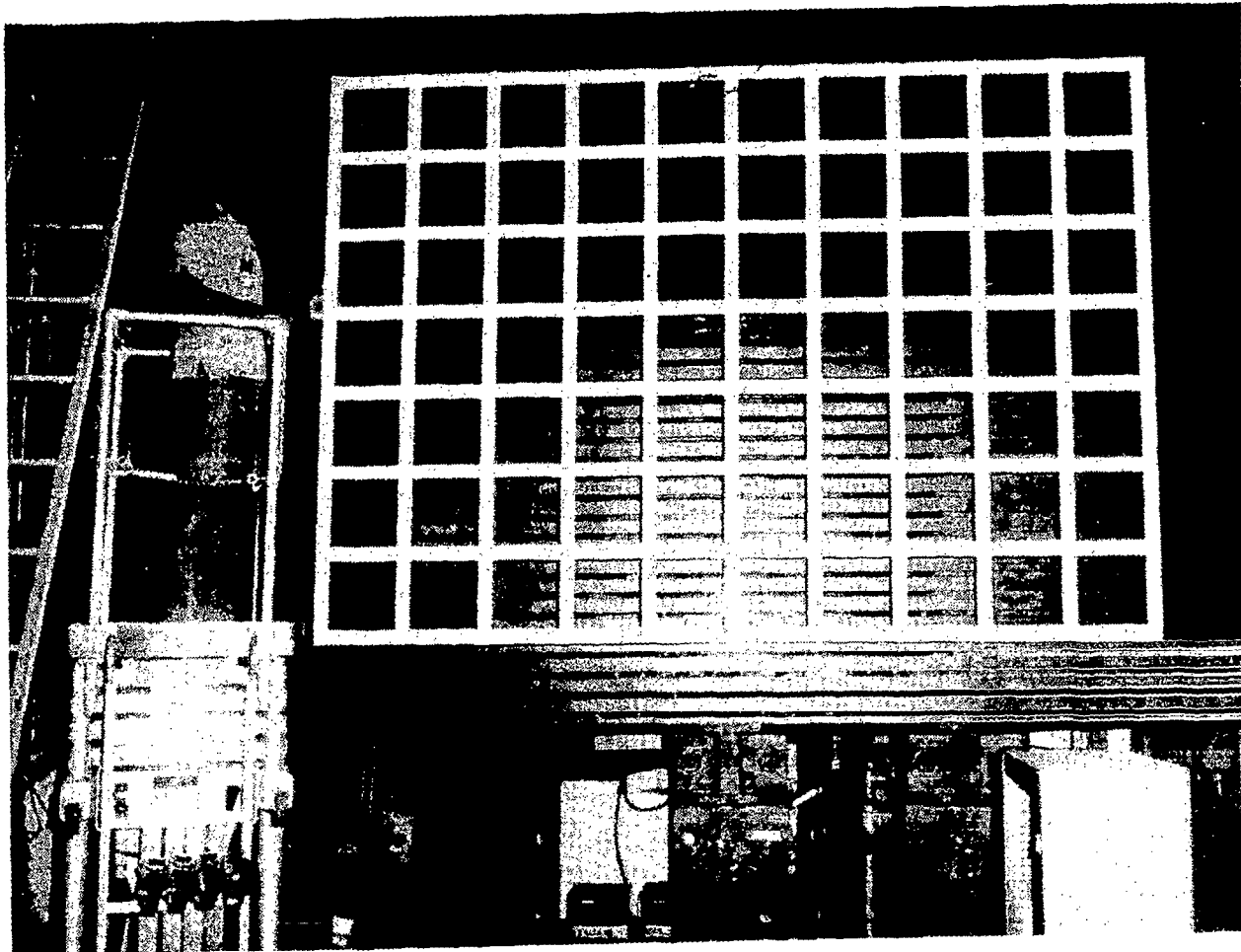
Figure 24

One Optimal Damping Design for Grillage
(Line Length Indicates Damper Magnitude)

An example optimal distribution of damping devices is indicated for the grillage in figure 25. This distribution and a set of magnitudes would be very difficult to determine by trial and error methods.

OBJ. =.09902
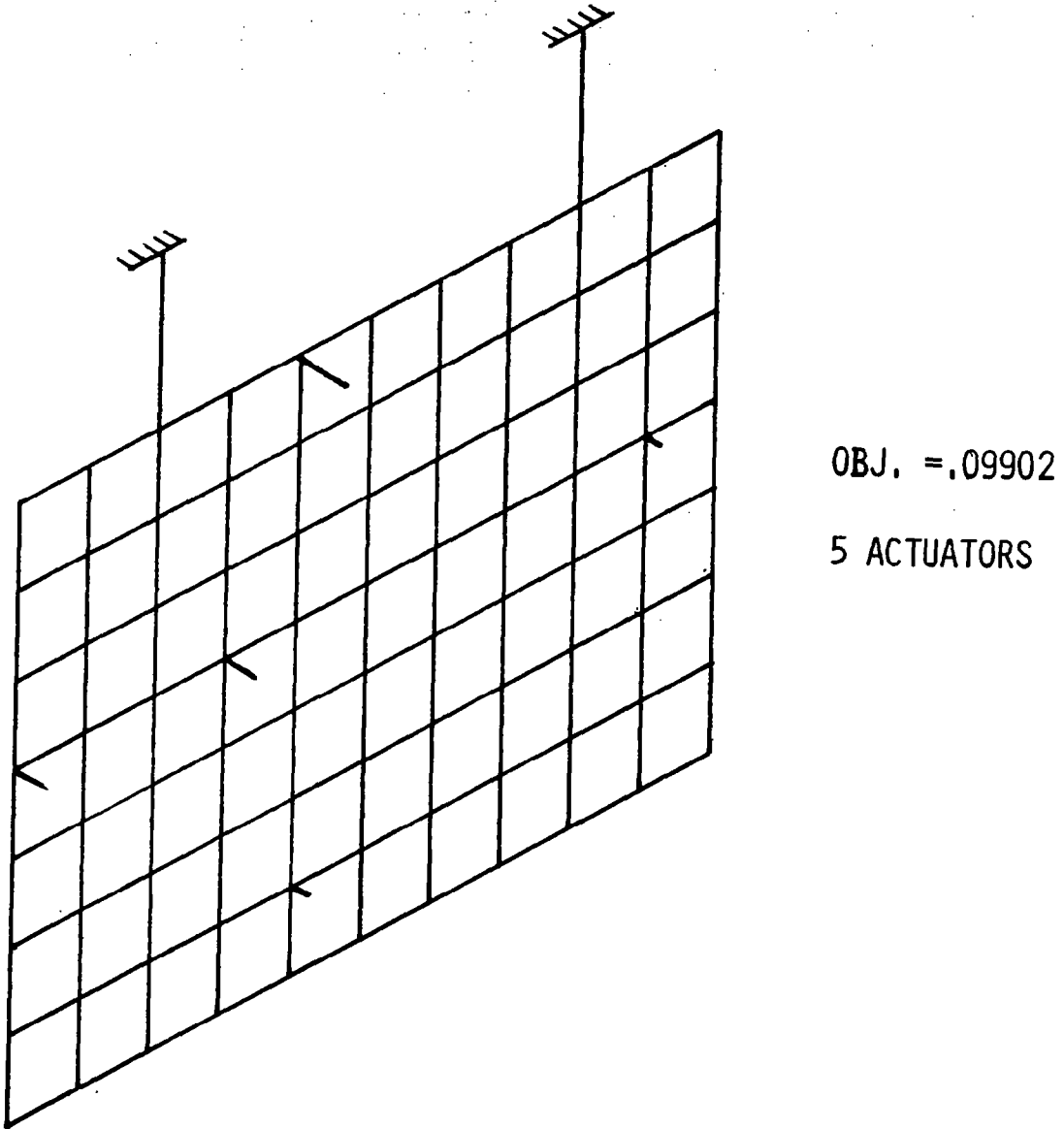
5 ACTUATORS

Figure 25

Prototype of Integrated Damping Device

As part of the test program for the grillage, new actuators are under development. Shown in figure 26 is a candidate prototype actuator. The actuator has integrated electronics so that it may be placed on the structures, and once the gain is adjusted, the device operates with only power supplied.
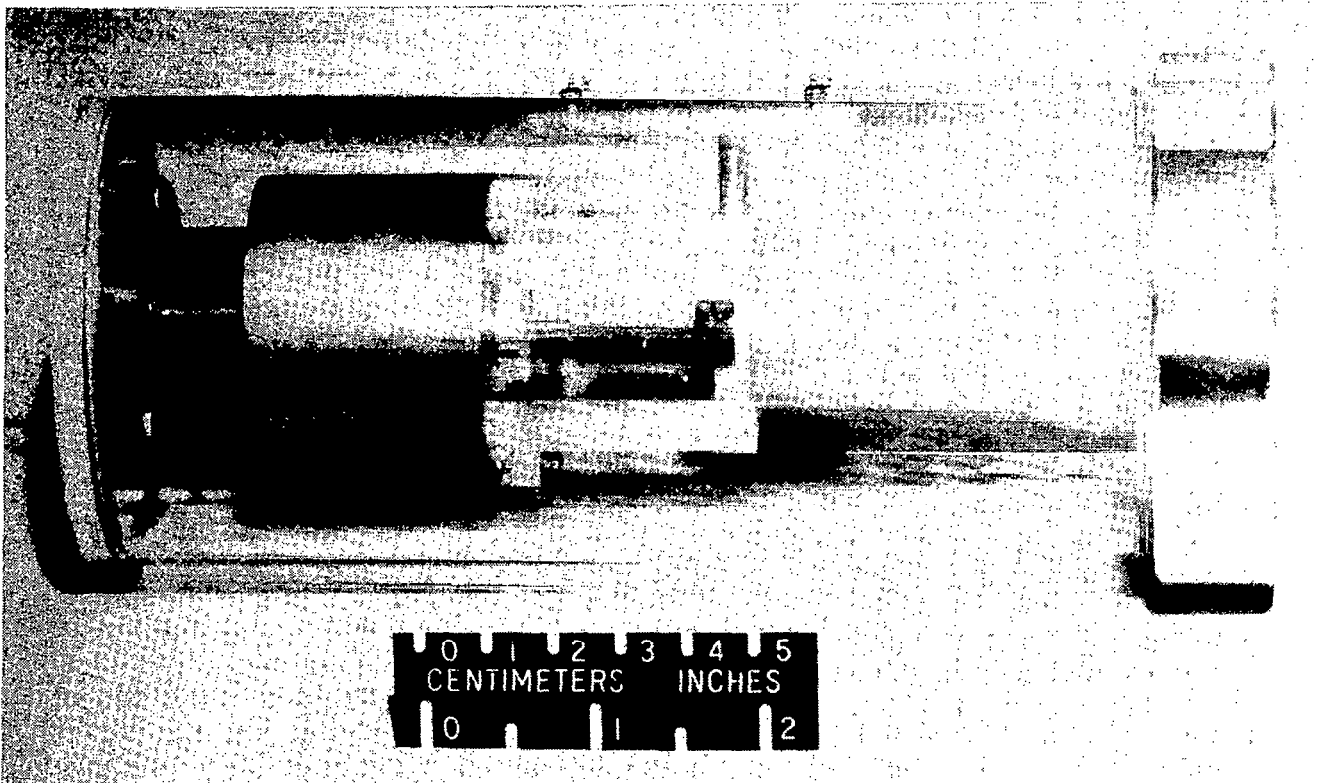
Figure 26

Overall Process for Design
of Structures by Optimal Control Theory

Efforts are under way to apply methods of modern control theory to the design of structures. Several options may result from this approach; for example, a revised mass and stiffness distribution, as well as coupling of nodes which previously were uncoupled (fig. 27).

REDESIGN OF PASSIVE STRUCTURES BY CONTROL THEORY

INITIAL STRUCTURE

$F(T)$

DESIGN PROCEDURE

| ANALYTICAL MODEL $M\ddot{X}+KX=F(T)$ | $\Rightarrow$ | CONTROLS ANALYSIS MIN $J(X,\dot{X},\Delta M,\Delta K)$ | $\Rightarrow$ | REVISED MODEL $(M+\Delta M)\ddot{X}+(K+\Delta K)X=F(T)$ |
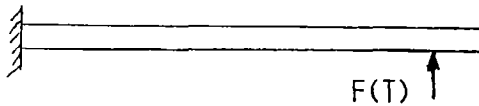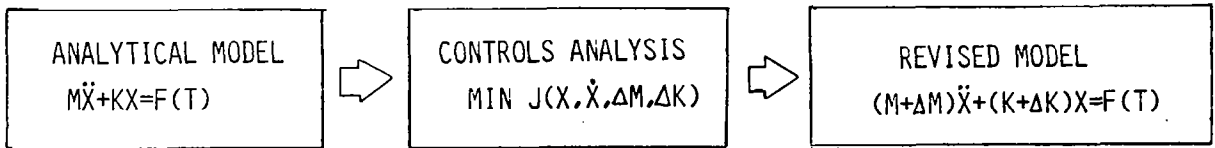
REVISED STRUCTURE

CABLES

REDISTRIBUTED MASS & STIFFNESS   CROSS-COUPLING
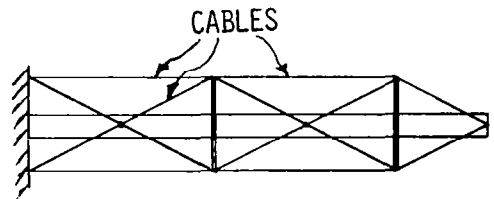
Figure 27

Simple Design Problem Indicating
Difficulties Encountered in Design for Dynamic Loads

A difficulty which arises in design for dynamic response is indicated in figure 28. Shown in this figure is a design space which is disjointed. There are two separate design subspaces in which a minimum relationship among the design variables may occur. The method for circumventing this problem in the present case is to perform the search for the optimum design in the frequency domain. As shown by the figures in the lower right, two designs can result depending upon the domain which is optimized. In the first, the shaft which is subjected to a harmonic torsional input is seen to be an approximation to a tapered shaft. The design constraints are met fundamentally through the strength of this shaft. In the other design space, a different design results in which a slender shaft supports a massive segment; thus, the constraints are met through the increase in mass moment of inertia of the larger segment. Extension of this design process to many degrees of freedom presents a great challenge.
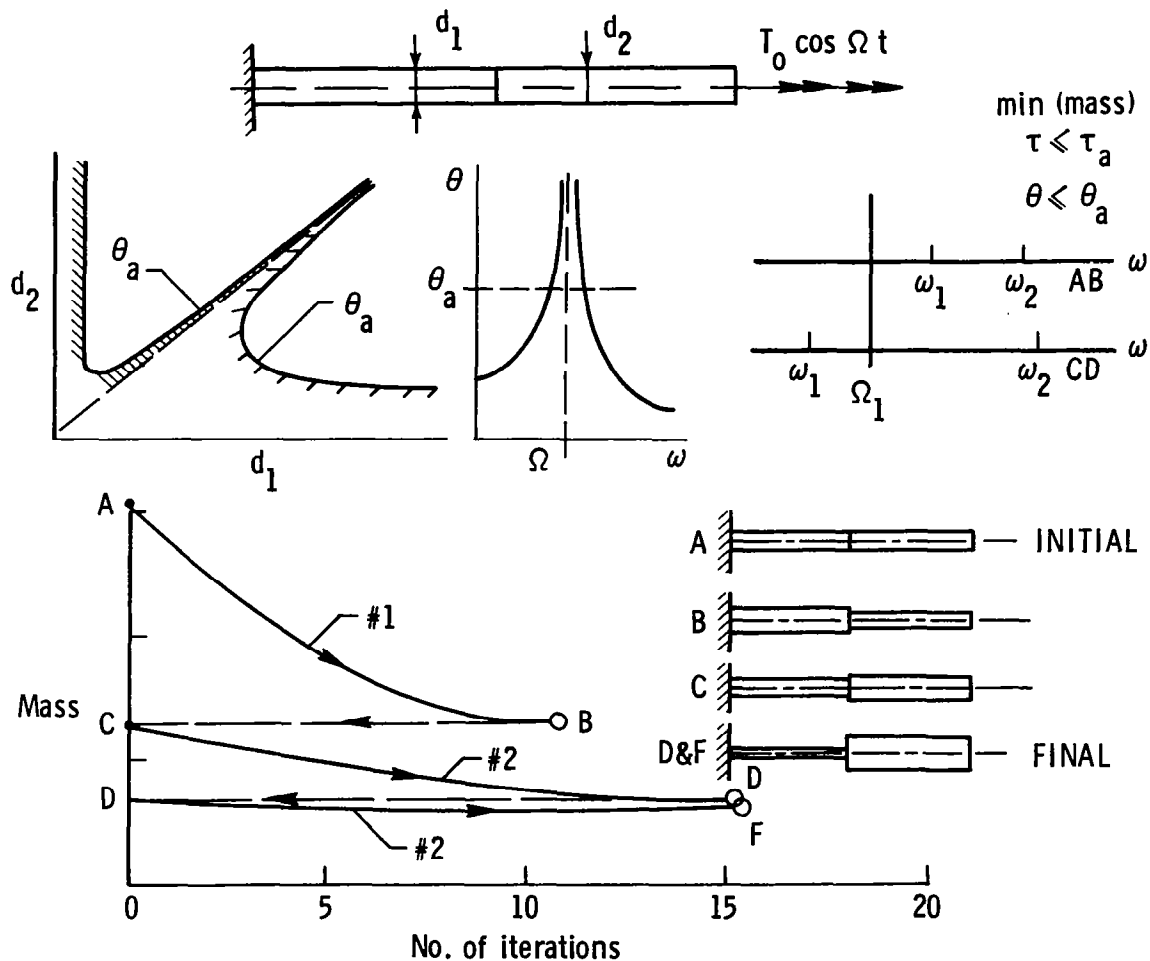
Figure 28

Status of the Area of Optimal Design for Dynamic Loads

A subjective evaluation of the area of design for dynamic response is presented in figure 29. Design of systems for harmonic inputs using tuned vibration isolation and absorber techniques is well understood. Effectiveness of such methods in the presence of rigid body modes, however, is questionable. A fundamental method for optimal damping has been developed but the method should be extended to more practical implementation. That is, account should be taken of physical characteristics of actuators such as actuator bandwidth and actuator mass. In addition, the method needs extension to actuation systems in which different parts of the structure are connected. A promising technique for design of structures is the application of theory developed within the controls community; however, experience needs to be gained with this method. Some difficulties with traditional search techniques have been indicated. Thus further evaluation of these approaches is needed.

DESIGN - STATUS

O ISOLATION/ABSORBER TECHNIQUES UNDERSTOOD - QUESTION EFFECTIVENESS IN
   PRESENCE OF RIGID BODY MODES

O FUNDAMENTAL METHOD FOR OPTIMAL DAMPING DEVELOPED - NEEDS PRACTICAL IMPLEMENTATION:
   MORE GENERAL DESIGN SITUATION AND PHYSICAL ACTUATION SYSTEMS

O WORK UNDERWAY FOR APPLICATION OF CONTROLS TECHNIQUES TO STRUCTURAL DESIGN
   FOR DYNAMIC LOADS

O TRADITIONAL METHODS NEED EVALUATION

Figure 29

Two Shuttle Attached Flight Experiments

Discussion of experiments will focus specifically on flight experiments. Two
flight experiments are being contemplated as indicated in figure 30. Other flight
experiments also are being considered but are not discussed in this paper. The
SAFE (Solar Array Flight Experiment) will fly on the Space Shuttle in 1984. In
one dynamics experiment on the SAFE, structural dynamics characteristics will be
extracted by photogrammetric tracking of targets on the array. This approach,
though inexpensive, is limited in resolution potential. Another experiment spon-
sored by the NASA Marshall Space Flight Center involves a more expensive but higher
resolution experiment. In the other experiment it is proposed that a long mast
between 60 and 100 meters be developed, ground tested, and flown on the Space
Shuttle. Multiple flights are contemplated for the mast on the space technology
experiments pallet (STEP). Emphasis in early flights would be on structural dynam-
ics objectives, leading to more comprehensive experiments in which various levels
of control complexity are investigated. An essential part of this program is a
comprehensive ground test experiment which can be correlated with results of flight
tests.

SAFE

    SYSTEM IDENTIFICATION

MAST

    MULTIPLE FLIGHTS ON STEP

    STRUCTURAL DYNAMICS —CONTROLS

    GROUND TEST METHODS

Figure 30

332
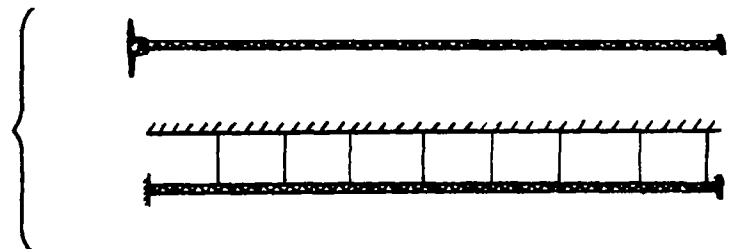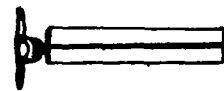
Partially Deployed Solar Array To Be Used in Flight
Experiment Showing Targets To Be Tracked Photogrammetrically

Figure 31 is a photograph of the solar array for the Solar Array Flight Experiment in a deployment test. Shown in the picture are the white targets which are tracked by on-board Shuttle television cameras. Videotapes of structural response will be returned to Earth for analysis to obtain time histories of the response of each target.
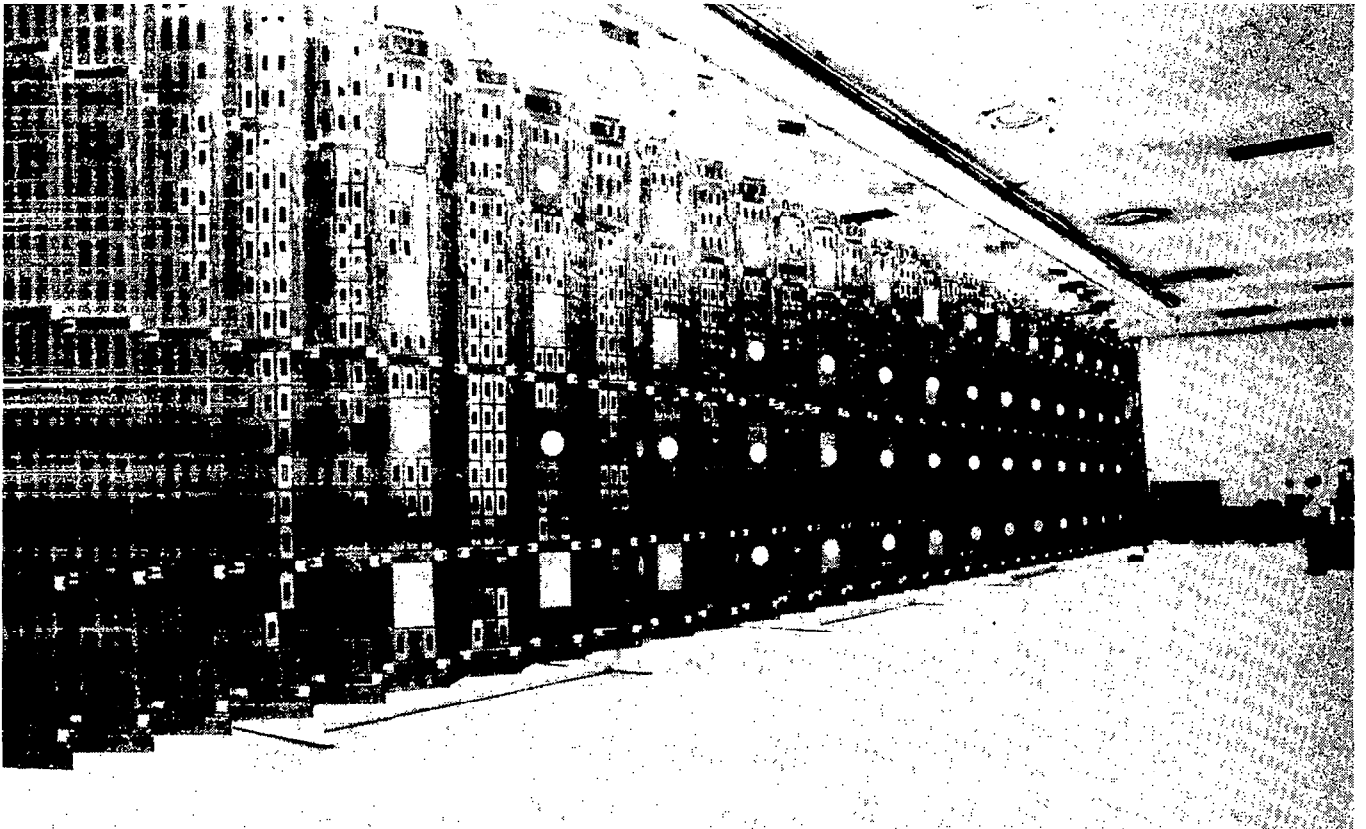
Figure 31

A Proposed Large Lightweight Mast Design

Figure 32 is an artist's conception of a mast. This mast would have a large added weight at the end to simulate perhaps an antenna feed.
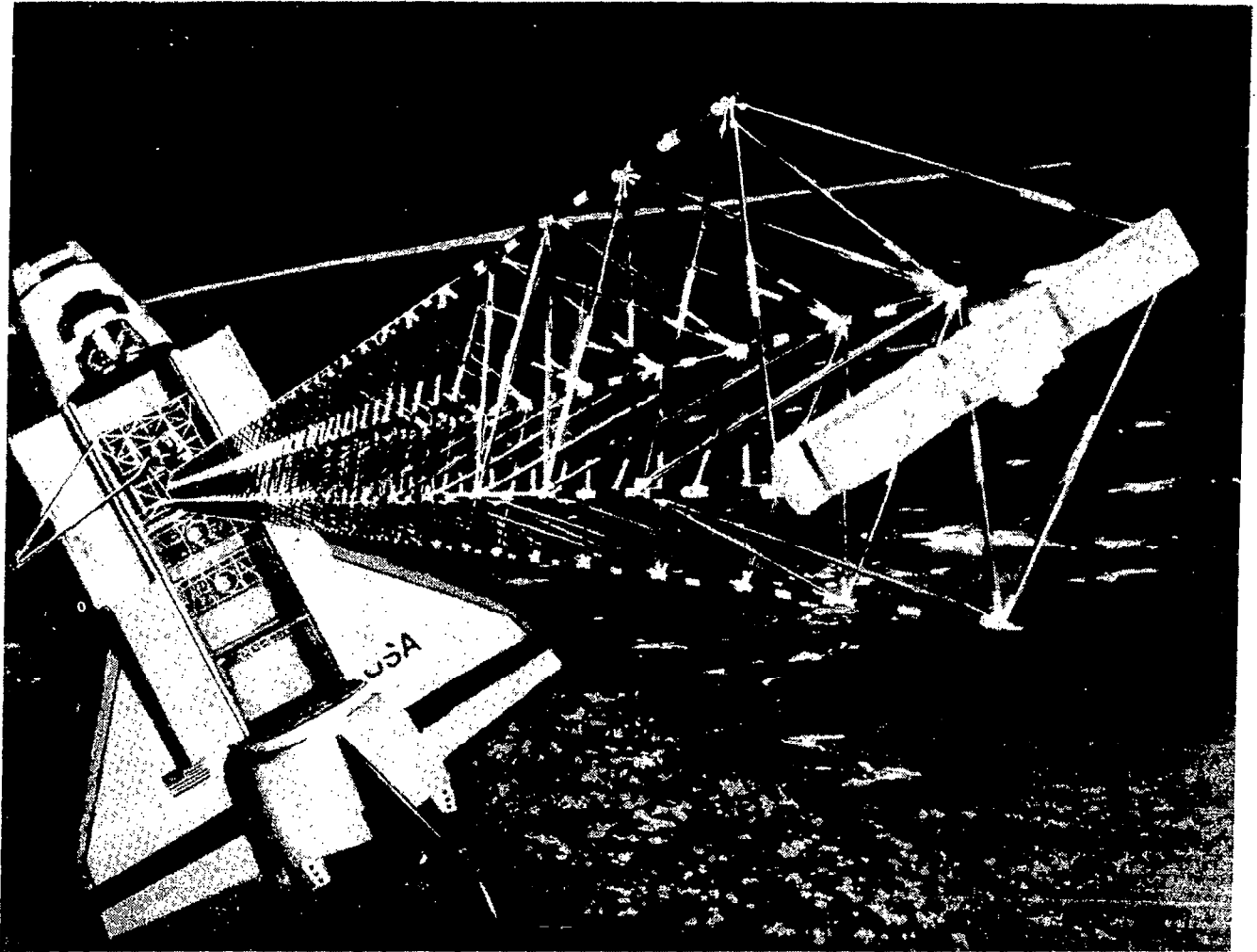
Figure 32

Some Needs and Issues Involved in Space Flight Experiments

Discussion of the area of experiments is presented in figure 33. The overall need is to gain experience which yields confidence that predictions of on-orbit structural behavior are valid even with very limited verification through ground tests.

NEEDS:

o TO BE ABLE TO CHARACTERIZE ACCURATELY THE STRUCTURAL SYSTEM BEFORE FLIGHT THROUGH MODELING, ANALYSIS, AND GROUND TEST

o TO BE ABLE TO CHARACTERIZE THE FLIGHT SYSTEM ON-ORBIT VIA PARAMETER IDENTIFICATION (SYSTEMS IDENTIFICATION TECHNIQUES)

o TO ASSESS STRUCTURE-CONTROL INTERACTIONS AT LOW FREQUENCIES IN PRESENCE OF TRUE RIGID BODY MOTIONS

ISSUES:

o STATE-OF-THE-ART MODELING TECHNIQUES QUESTIONABLE:

- NON-LINEAR EFFECTS (GEOMETRIC, INERTIAL, JOINTS)

- NON-UNIFORMLY DISTRIBUTED DAMPING

o FULL SCALE GROUND TESTING MAY PROVIDE IMPRECISE DATA:

- SUSPENSION SYSTEM IN ONE-G HAS SIGNIFICANT EFFECTS ON MODE SHAPES AND DAMPING

o SUB-SCALE STRUCTURAL GROUND TESTING PROVIDES QUESTIONABLE, INCOMPLETE INFORMATION

- ALLEVIATES ONE-G EFFECTS (BENEFIT)
- MINIMUM GAGE MATERIALS
- UNSCALABLE MANUFACTURING TOLERANCES
- UNSCALABLE ACTUATION SYSTEMS

Figure 33

335

A new basic research initiative at AFOSR in spacecraft materials and structures is being implemented in FY 83 as part of the overall Air Force thrusts in space. The major goals are to develop new structural materials uniquely tailored to space application requirements (e.g. stability and damping) and to the development and validation of passive and active control concepts for achieving high precision performance (fig. 34).

Spacecraft Materials and Structures
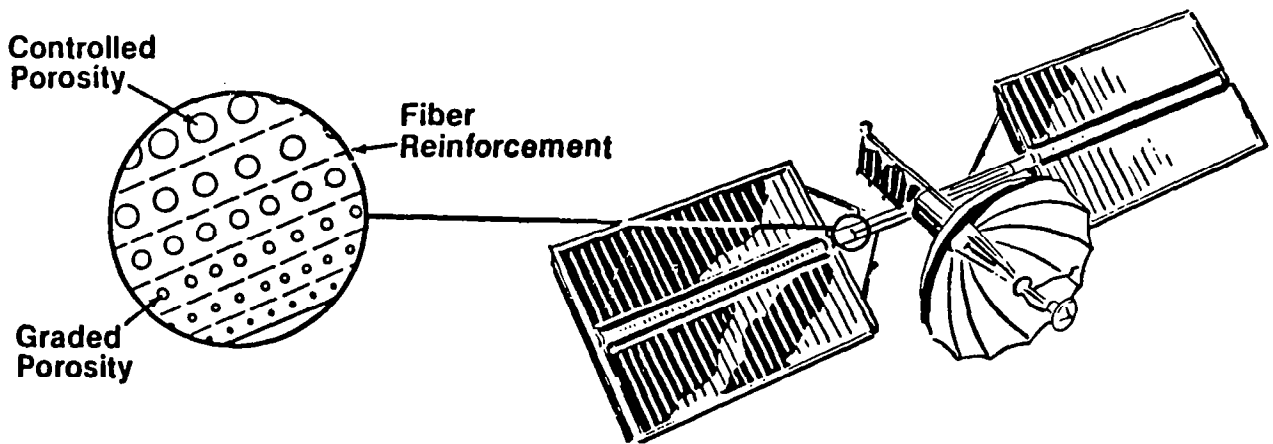
FY 83 INITIATIVE

GOALS
● **New Materials for Space Stability & Enhanced Damping**
● **Structural & Control Concepts for Precision Performance**

Figure 34

The programmatic goals listed in the previous chart translate to research require-ments in structural dynamics aimed at:

- characterization of dynamic response
- development of active and passive dynamic control methods
- formulation of multi-disciplinary optimization procedures and analytical tools

In recognition of similarly oriented programs by other organizations and in an effort to complement such activities, the AFOSR program will concentrate on basic research issues with long range payoff potentials (fig. 35).

DYNAMICS RESEARCH GOALS

TECHNICAL:

        DYNAMIC RESPONSE CHARACTERIZATION

        ACTIVE/PASSIVE CONTROL METHODOLOGY

        MULTI-DISCIPLINARY OPTIMIZATION

PROGRAMMATIC:

        COMPLEMENT ONGOING PROGRAMS

        LONG RANGE PAYOFF

        EMPHASIZE BASIC RESEARCH

Figure 35

Several of the basic research issues in structural dynamics are listed in figure 36. These have been selected on the basis of perceived deficiencies in current technology to support high precision performance goals requiring shape control, dimensional and line-of-sight stability, and rapid maneuverability. A few of these are discussed in more detail in the following figures.

SPECIFIC OBJECTIVES

DYNAMIC MODELING AND ANALYSIS:

- FRICTION MECHANISMS
- JOINT FLEXIBILITY/INERTIA

- LARGE MOTION DYNAMICS

DYNAMIC PHENOMENA:

- WAVE MECHANICS
- ENERGY DISSIPATION

- DEPLOYMENT DYNAMICS
- DYNAMIC BUCKLING

DESIGN METHODOLOGY:

- INTEGRATED STRUCTURE/CONTROLS MODELS
- INTEGRATED SYNTHESIS OBJECTIVE FUNCTIONS
- ACTIVE CONTROL CONSTRAINTS

FLIGHT EXPERIMENTS:

- TECHNOLOGY DEMONSTRATIONS
- GROUND VALIDATION CONCEPTS

Figure 36

A major thrust of the base problem is the modeling of frictional mechanisms in dynamic and contact problems. Two examples of this thrust are depicted here. The first deals with frictional damper devices used in turbomachinery rotor blades, and the second represents a theoretical derivation that properly accounts for the asperities of the contact surfaces and the resulting non-uniform contact pressure distributions and micro-deformations and motions. New efforts planned within the AFOSR initiative will extend and use these models to study the effects of joint friction on the dynamic response of lattice type space structures (fig. 37).

Dynamic Modeling and Analysis

- **Dynamic Finite Elements**
  - **Coupled Rigid/Flexible Dynamics**
- **Frictional Mechanisms**
  - **Frictional Damper in Turbomachinery**
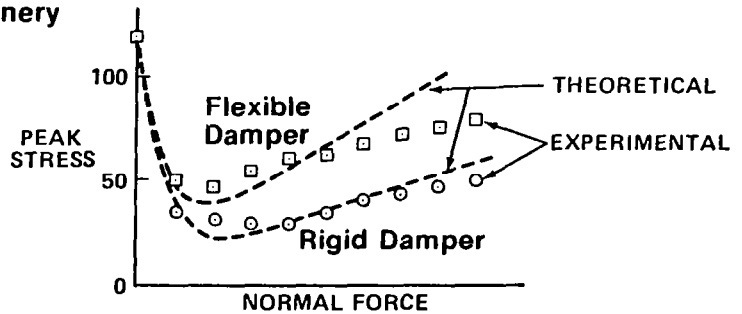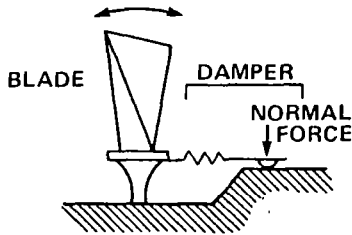
- **Non-Classical Friction Model**

Classical (Coulomb)
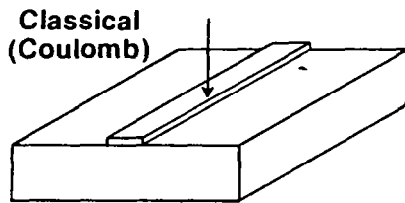
$$\sigma_T(x) = \nu_F \sigma_N(x)$$

Non-Classical
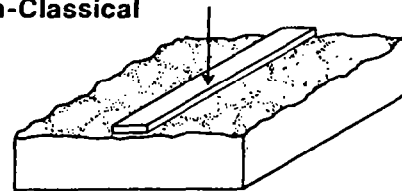
$$\sigma_T(x) = \nu \int^{S_\lambda} \sigma_N(x - \lambda_x)\,dx$$

SIGNIFICANCE: Realistic Modeling for Sliding Contact Problems

Figure 37

Wave propagation mechanisms are expected to play a major role in the on-orbit response of spacecraft structures to control inputs and other dynamic excitations. Studies to understand and model such mechanisms are being pursued. Figure 35 shows a preliminary result from an ongoing effort which clearly illustrates a wave filtering property characteristic of periodic structures (here represented by regularly spaced spring-mass systems along the length of a rod carrying a longitudinal traveling wave).

FILTERING PROPERTY OF PERIODIC STRUCTURES
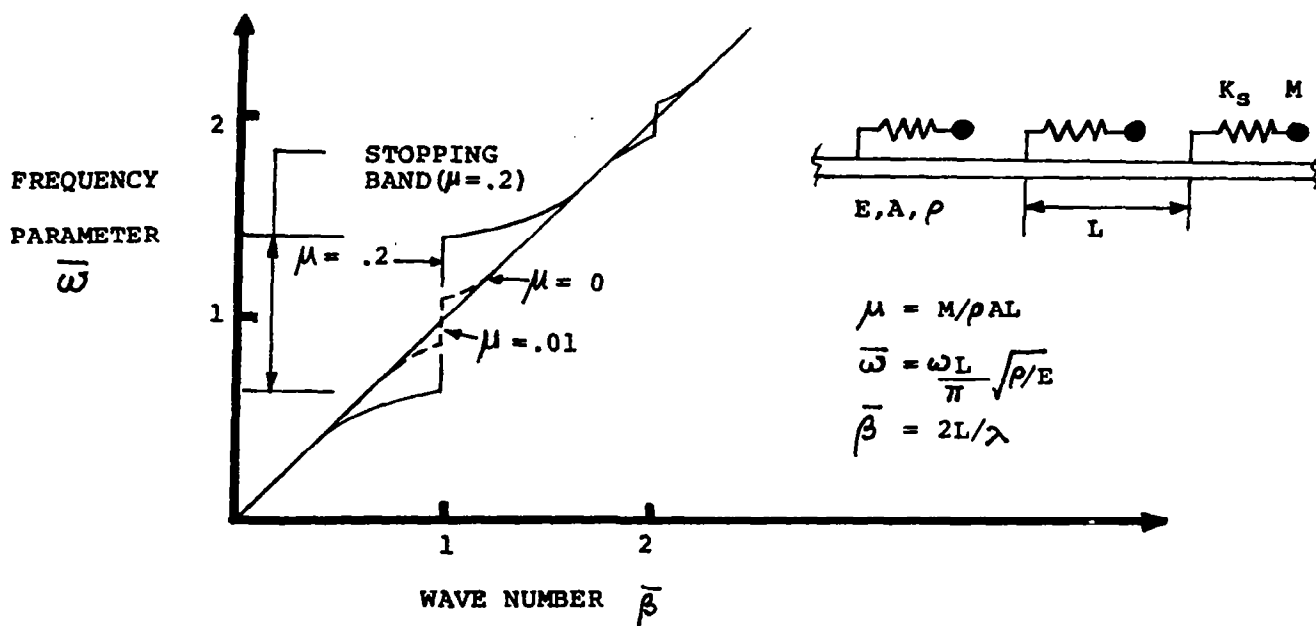
Figure 38

Idealization of Structure and
Control System for Integrated Synthesis

A generic concept of an actively controlled structure is shown schematically in figure 39. A distributed multi-processor hierarchical control system operating on a flexible spacecraft is idealized in a manner that promotes a truly integrated structure/controls modeling for analysis of the closed system and for the synthesis of both the structure and controls subsystems.

INTEGRATED CONCEPT OF ACTIVELY CONTROLLED STRUCTURE
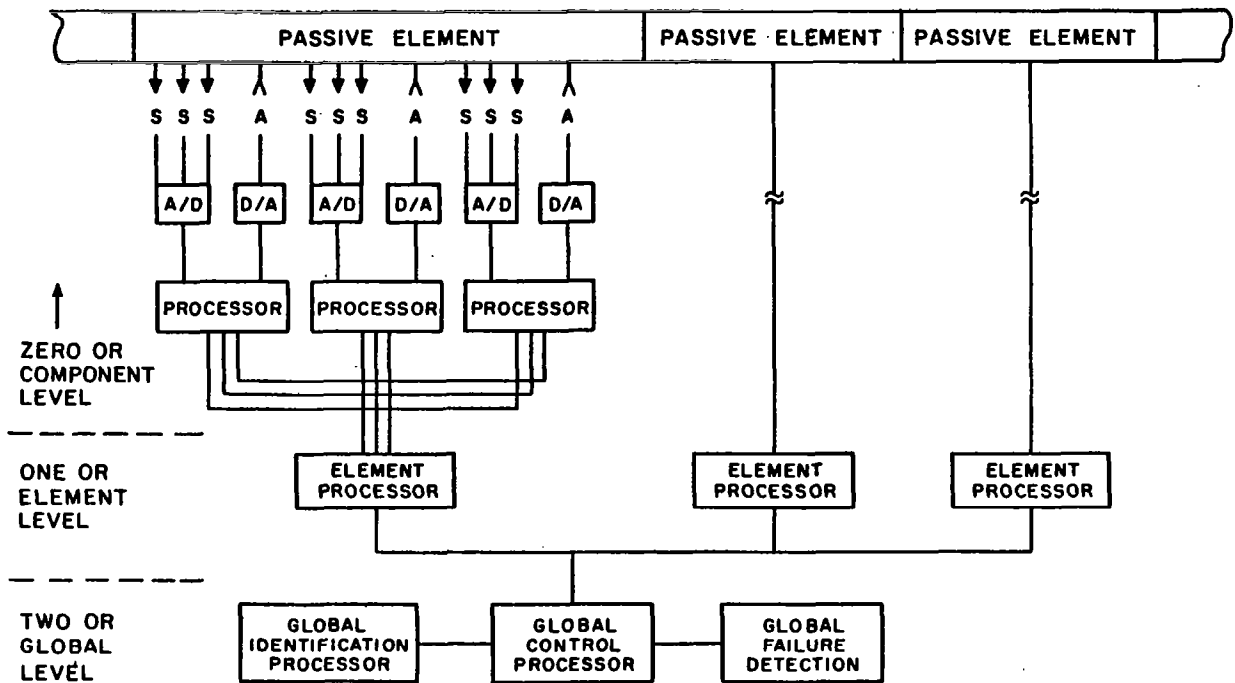
Figure 39

A listing of near term activities planned for both the NASA and AFOSR Dynamics programs is given in figure 40.

NASA:

    INITIATE EXPLORATION OF MORE COMPLEX CABLE STIFFENED STRUCTURES

    MAKE MATHEMATICAL MODEL UPDATES AND SYSTEM IDENTIFICATION TECHNIQUES MORE ACCURATE AND PRACTICAL

    DEVELOP ACTUATORS AND PERFORM VERIFICATION OF VIBRATION SUPPRESSION DESIGN ON MORE MODALLY DENSE STRUCTURE

    EXPLORE METHODS FOR OPTIMAL DESIGN FOR DYNAMIC LOADS

    EXPLORE TECHNICAL PROBLEM AREAS ASSOCIATED WITH LARGE SPACE STRUCTURES WHICH REQUIRE COMBINATIONS OF GROUND AND SPACE TESTING (SAFE, STEP, & MAST)

AFOSR:

    EVALUATION OF SEVERAL PROPOSALS IN PROGRESS FOR FY 83
    NEW PROPOSALS BEING SOUGHT FOR FY 84 PROGRAM

Figure 40

Summary State-of-the-Art Assessment

Figure 41 provides a summary assessment of current SOA by identifying two cat-
egories of technology research issues. The first represents those receiving
attention within the aerospace community. In contrast, the items of the sec-
ond category have received only casual attention and thus represent targets of
opportunity for innovative and creative research.

O SOME TECHNOLOGY NEEDS RECEIVING HEALTHY RESEARCH & DEVELOPMENT
   ATTENTION - NASA, AIR FORCE, DARPA AND OTHER PROGRAMS

        - STRUCTURAL CONCEPTS - DEPLOYABLE AND ERECTABLE STRUCTURES

        - ACTIVE & PASSIVE CONTROL MECHANISMS

        - FLIGHT EXPERIMENTATION

O OTHER AREAS STILL NEED NOVEL BASIC RESEARCH IDEAS AND TECHNOLOGY
   DEVELOPMENT APPROACHES

        - SIMULATION OF ON-ORBIT DEPLOYMENT AND DYNAMICS

        - STRUCTURES - THERMAL - PROPULSION INTEGRATION

        - STRUCTURE/ELECTROMAGNETIC INTERACTIONS

        - DESIGN VALIDATION

Figure 41

REFERENCES

1. Collins, J. D.; Hart, G. C.; Hasselman, T. K.; and Kennedy, B.: Statistical Identification of Structures. AIAA J., vol. 12, no. 2, February 1974, pp. 185-190.

2. Chen, J. C.; and Garba, J. A.: Matrix Perturbation for Analytical Modal Improvement. AIAA/ASME/ASCE/AHS 20th Structures, Structural Dynamics and Materials Conference, St. Louis, MO, April 1979. (AIAA Paper No. 79-0831.)

3. Berman, Alex; and Wei, Fu Shang: Automated Dynamic Analytical Modal Improvement. NASA CR-3452, 1981.

PROGRESS IN THERMOSTRUCTURAL ANALYSIS
OF SPACE STRUCTURES

Earl A. Thornton, Pramote Dechaumphai, Jack Mahaney
and Ajay K. Pandey
Old Dominion University
Norfolk, Virginia

INTRODUCTION

The authors are conducting finite element space structures research focused on the interdisciplinary problems of heating, thermal, and structural analysis. Detailed results of recent research activities appear in references 1-3. In this paper two research studies in progress for improving analysis capabilities are described (figure 1).

RECENT PROGRESS IN THERMAL−STRUCTURAL ANALYSIS

- ODU SPACE STRUCTURES RESEARCH
  - −Finite element method
  - −Interdisciplinary problem of heating, thermal and structural analyses

- DESCRIBE TWO RESEARCH ACTIVITIES IN PROGRESS
  - −Slender member shadowing effects
  - −Cable-stiffened structures

Figure 1

346

SLENDER MEMBER SHADOWING EFFECTS

A video tape of a rotating space truss model in sunlight presented at the conference demonstrated qualitative aspects of slender member shadowing (figure 2). Shadowing effects were shown to be in two categories: cross member and parallel member shadows. The tape demonstrated that cross member shadowing effects are highly transitory and that shadow widths are small compared to shadowed member lengths. Multiple shadows progressively moving across a shadowed member were demonstrated. Parallel member shadowing where complete member lengths are shadowed was demonstrated by the model and shadow durations were observed to be small in comparison to transit times for cross member shadows.

• Video tape will show shadow characteristics

• Simplified analysis will demonstrate preliminary thermal-structural results

Figure 2

TYPICAL TRUSS SHADOWING

Studies are currently in progress to assess the effect of slender member shadows on the thermal-structural response of an orbiting truss. The thirty-six member graphite-epoxy truss shown in Figure 3 is used as the analytical model. Subsequent figures will present results of quantitative analyses of the cross member shadows cast by the four shadowing members on the shadowed member. The Earth-facing truss shown is assumed to be in a geosynchronous orbit in the ecliptic plane.
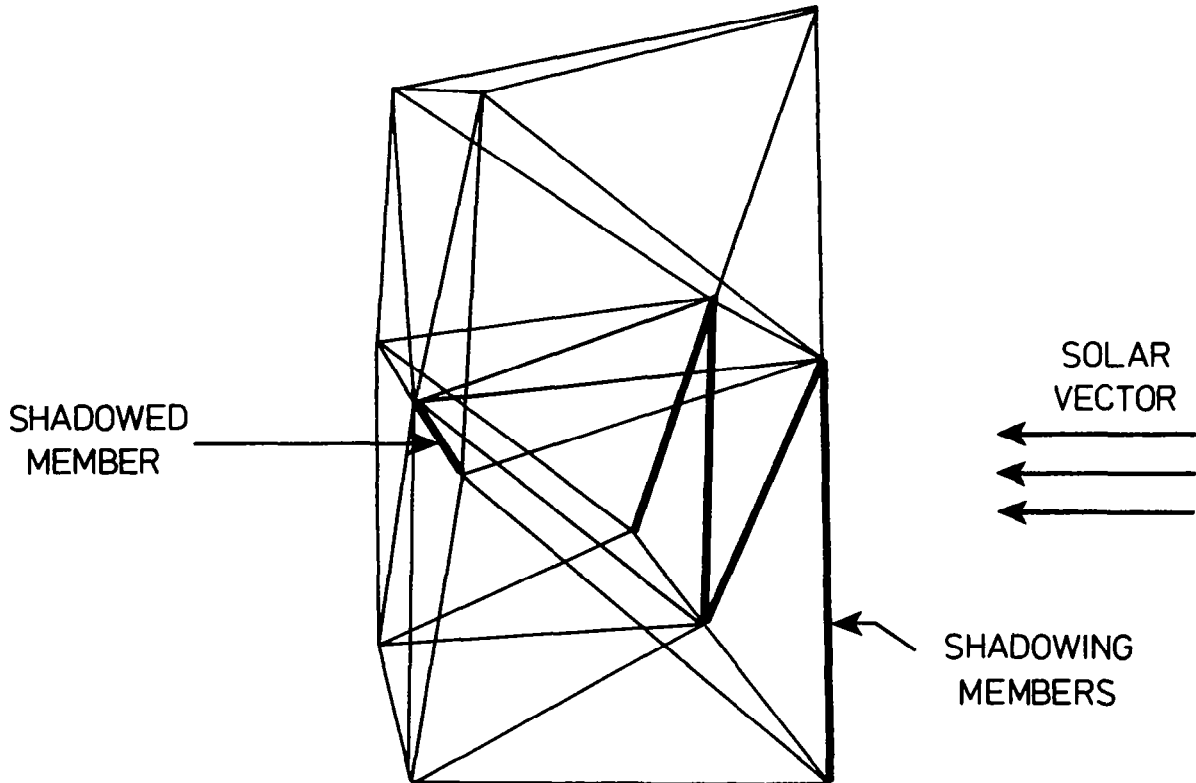
Figure 3

A numerical analysis procedure for shadowed space heating of sparse structures is presented in reference 4. The steps in this general approach are shown in Figure 4. If applied to a space truss with a large number of members, such an analysis will be very expensive. An objective of the current research is to determine if or when such highly detailed analyses are required to predict structural deformations accurately.

GENERAL APPROACH (REF. 4)
1. Subdivide each member
2. Determine when sub-elements shadowed
3. Determine reduced solar heating
4. Compute transient member temperatures

Figure 4

TRUSS MEMBER SHADOW MOVEMENT PREDICTIONS

Cross member shadow movements were analyzed by sub-dividing the shadowed member into 100 sub-elements. Predicted shadows and shadow movements are shown schematically in Figure 5. Shadow widths typically span three sub-elements for the truss analyzed. Thus when two shadows are traversing the shadowed member only six percent of the member length is shadowed.
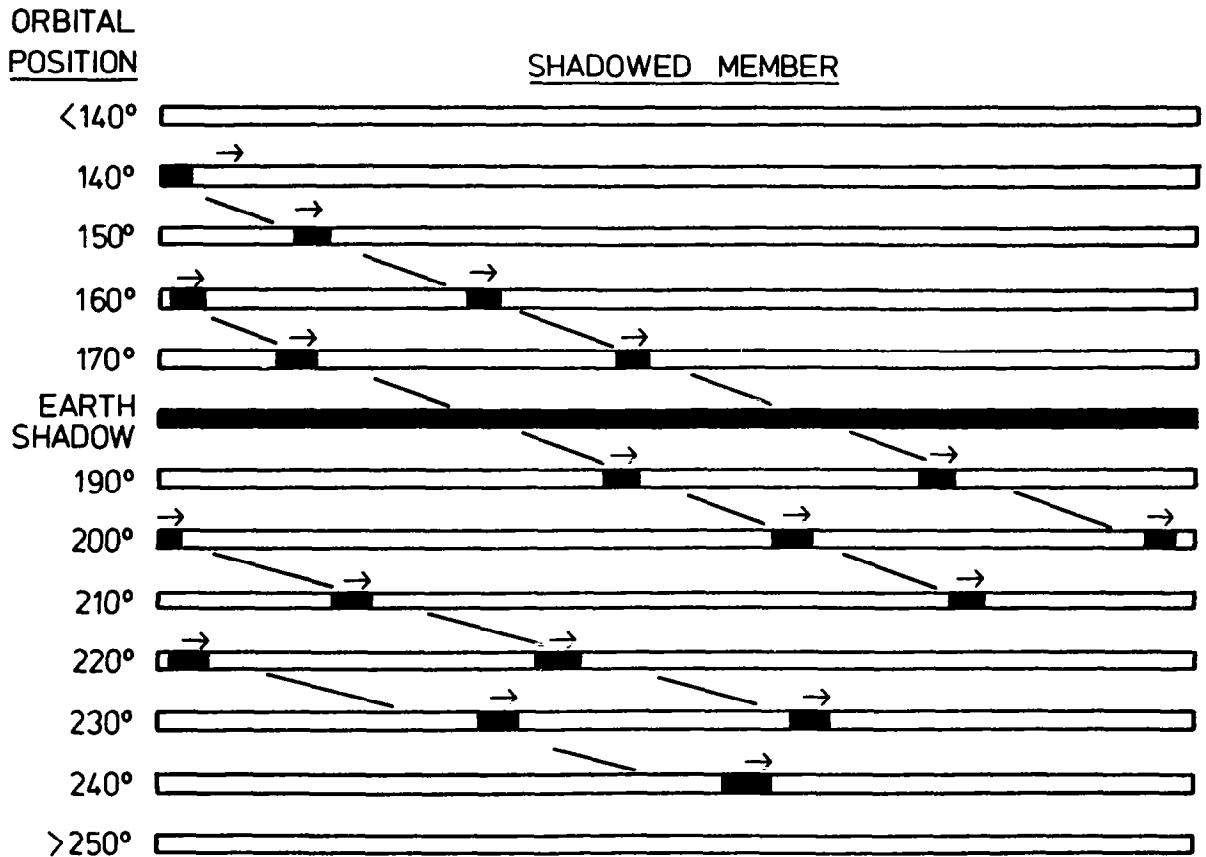
Figure 5

ASSESSMENT OF SHADOWING EFFECTS ON THERMAL RESPONSE

To assess the effects of the cross-member shadows on the shadowed member thermal response a simplified approach was employed. The simplified approach (Figure 6) gives insight into the member thermal-structural response without the programming complexity of the general approach. A "worst case" condition of complete (umbra) shadowing with fixed shadows is assumed for the heating analysis. Transient temperatures for the all graphite-epoxy member were computed considering combined conduction and radiation using 100 conventional (linear temperature distribution) finite elements.

SIMPLIFIED APPROACH

1. Subdivide member

2. Determine when sub—elements shadowed

3. —Neglect solar heating on shadowed sub—elements

— Fix typical shadows on member

— Apply shadows for proper duration

4 Compute transient member temperatures

Figure 6

TRUSS MEMBER FIXED SHADOW MODEL

The fixed shadow model shown in Figure 7 simplifies the thermal analysis but maintains the proper shadow width, spacing and duration. Using this model, heating histories for the 100 sub-element model were computed for one orbit and used as input to compute the transient thermal response of the composite member.
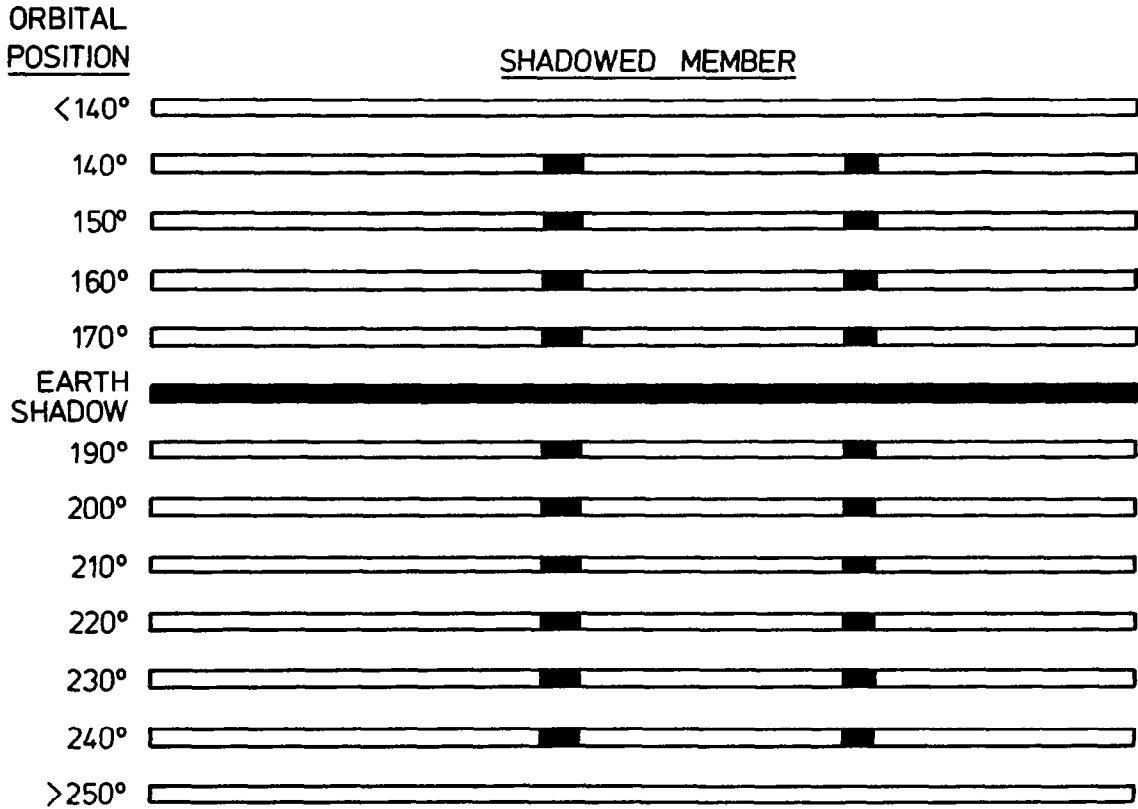
Figure 7

SHADOWED MEMBER THERMAL RESPONSE

The temperature history for a typical shadowed sub-element is shown by the solid line in Figure 8. The dashed line shows the temperature history of a typical unshadowed sub-element. The figure shows that there is a significant alteration of the temperature history during the local shadowing duration, although this result probably exaggerates the shadow effect on the thermal response because of the assumptions of fixed, umbra shadows.
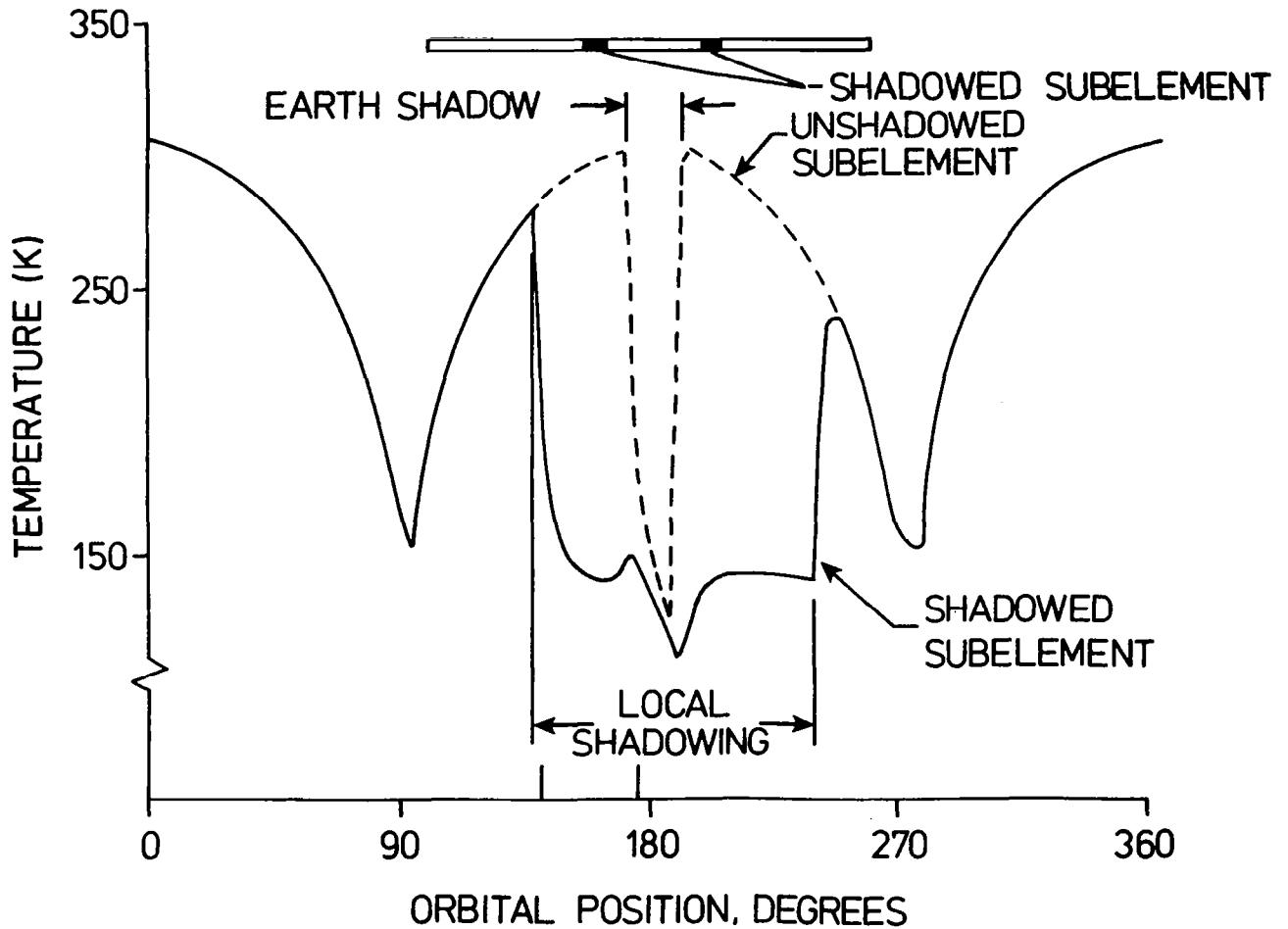
Figure 8

SHADOWED TRUSS MEMBER TEMPERATURE DISTRIBUTION

The shadowed member temperature distributions at the 140° and 175° orbit positions are shown in Figure 9. There are two significant results to be observed. The loss of heating in the shadowed sub-elements causes temperature to drop in these sub-elements, but the temperature drops are confined to only the shadowed sub-elements. The reason that the temperature drops are locally confined is the low thermal conductivity of the composite material, which minimizes member axial heat conduction. Thus only about six percent (the percent length shadowed) of the member experiences a temperature drop. The figure shows that the average temperature of the member is reduced only slightly. Consequently, the structural response will be affected only slightly by the cross-member shadowing.
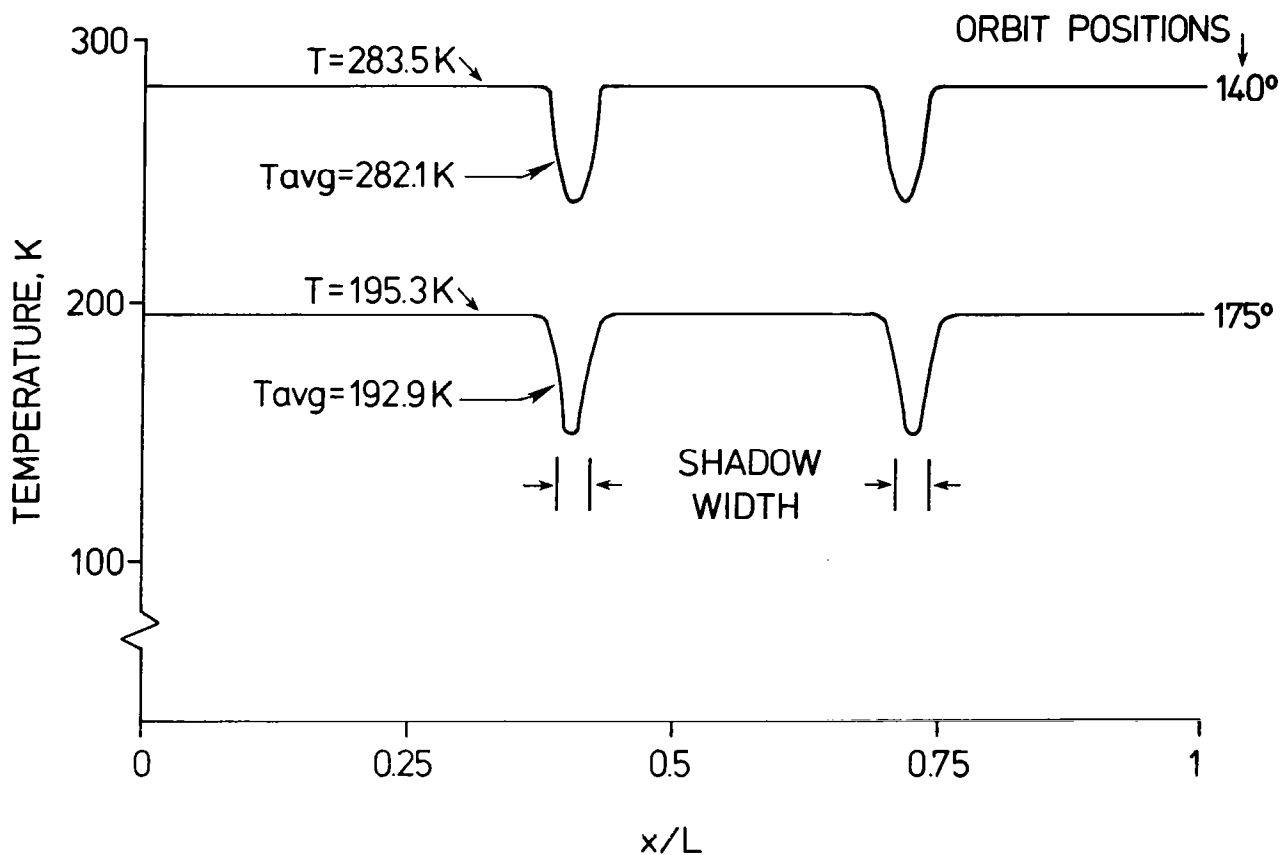
Figure 9

FINITE ELEMENT MODELING OF CABLE-STIFFENED STRUCTURES

Thermal-structural analysis of orbiting cable-stiffened structures depends on effective modeling of both the thermal and structural behavior (Figure 10). The thermal response depends strongly on the structural materials, and the following figures will demonstrate effective finite element thermal models. The structural response depends strongly on the cable behavior. Standard finite element production programs can analyze small deflection problems, but only a few proprietary programs (e.g., McNeill-Schwindler Corp. NASTRAN and ANSYS) are available to perform the nonlinear analysis required when cables experience large transverse deformations.

- **THERMAL RESPONSE DEPENDS STRONGLY ON MATERIAL**
  - Member temperature distributions different for aluminum and composites
  - Specialized finite element thermal models effective

- **STRUCTURAL RESPONSE DEPENDS STRONGLY ON CABLE BEHAVIOR**
  - Cable elongation primary deformation (no slackening)
    - Rod element—linear analysis
  - Cable elongation with large transverse displacement
    - Cable element—nonlinear analysis

Figure 10

To demonstrate two finite element thermal models a stayed column (Figure 11) is analyzed. The stayed column consists of composite spokes, battens and cables with a column of either aluminum or graphite-epoxy. The analyses to be described assume the stayed column to be Earth-facing in a geosynchronous orbit in the ecliptic plane.

Analytical and experimental studies of the vibration and buckling behavior of the stayed column (reference 5) have shown that stay (cable) pre-tension and slackening have a significant effect upon the structural response. The thermal analyses to be demonstrated are a first step in a determination of the role of thermal effects on the vibration and buckling behavior of the stayed column.

Figure 11

356
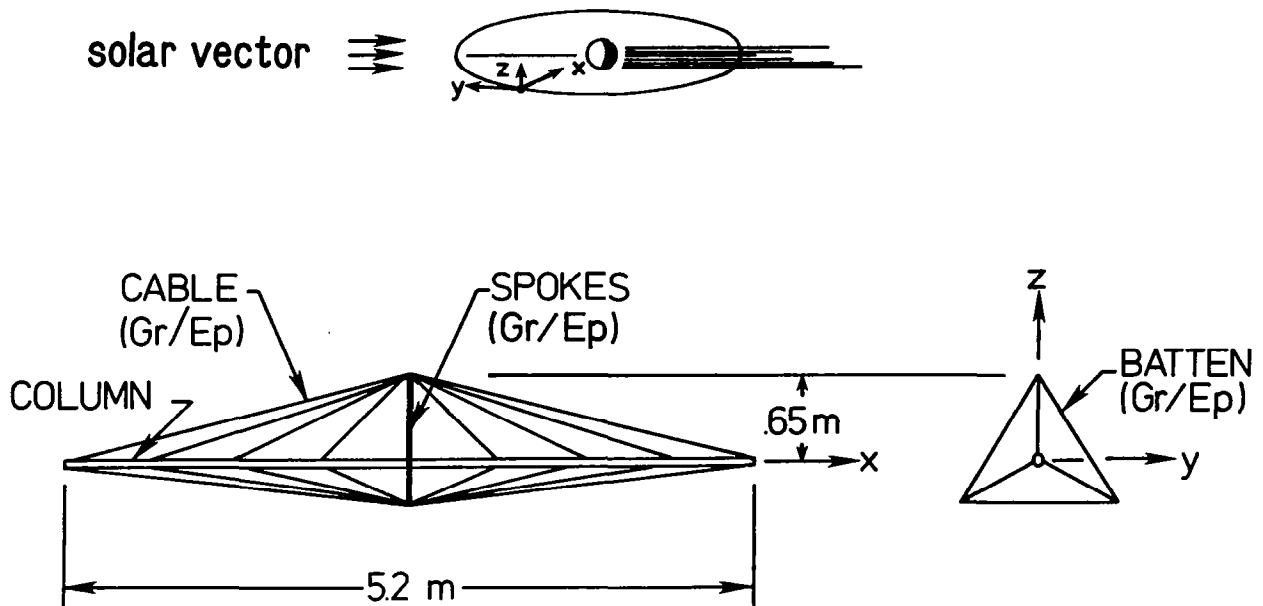
ALUMINUM COLUMN TEMPERATURE DISTRIBUTION

A stayed column design consisting of an aluminum column with composite cables, spokes and battens was thermally analyzed with a refined mesh of 380 conventional (linear temperature distribution) finite elements. The solid line in Figure 12 shows the temperature distribution in the aluminum column. The scalloped temperature distribution results from the relatively high thermal conductivity of the aluminum. Low points on the curve occur at cable attachment points indicating heat conduction to the cable. The stayed column was also analyzed with a nodeless variable (quadratic temperature distribution) finite element thermal mode with 38 elements. (See reference 2 for details.) The dashed line shows the good agreement between the predicted temperature distributions. Use of the nodeless variable elements reduces computer costs by a factor of about ten and permits use of a common discretization for an integrated structural analysis.

Figure 12

357
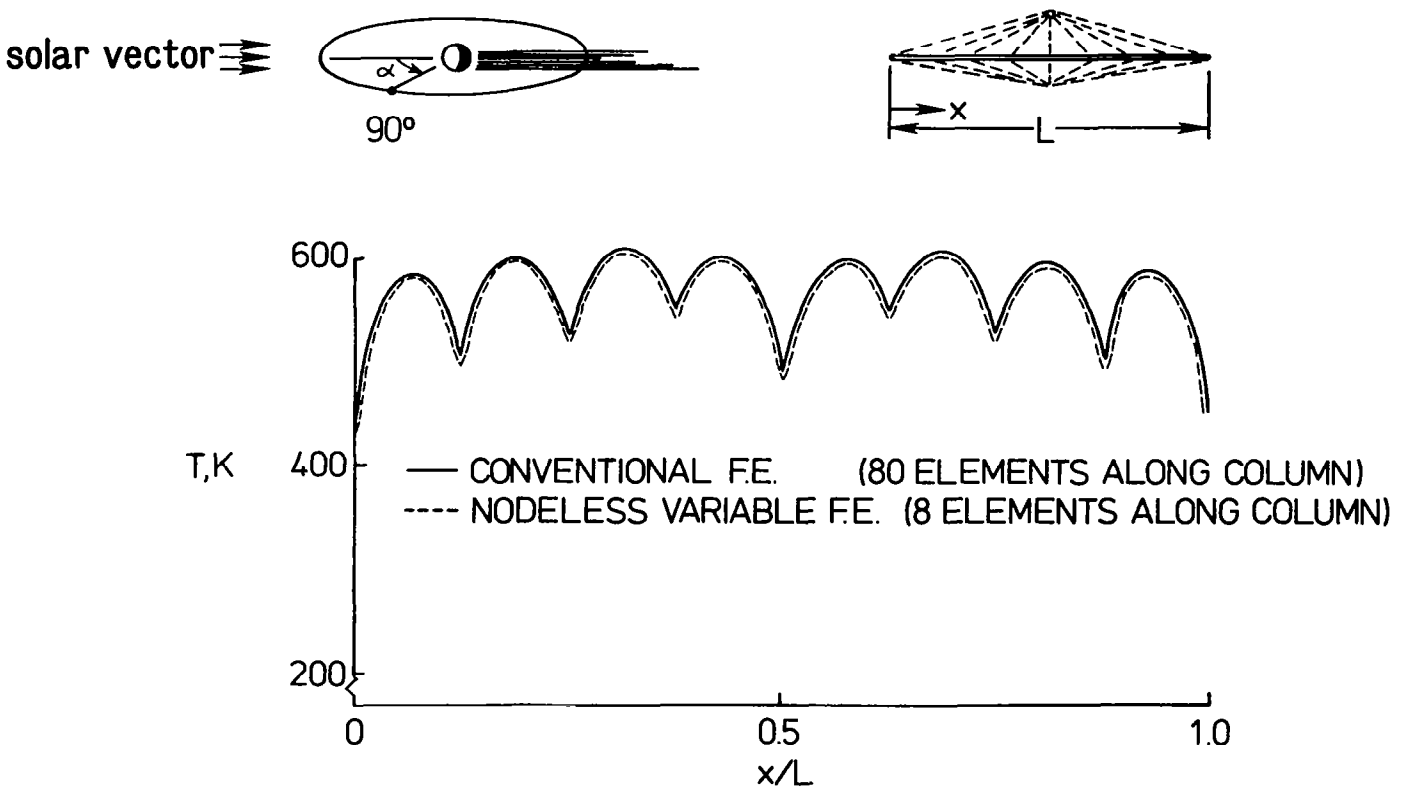
GRAPHITE/EPOXY COLUMN TEMPERATURE DISTRIBUTION

A stayed column design (Figure 13) consisting of all composite components was analyzed with the refined conventional thermal element model (380 elements) and with a mesh of 38 isothermal elements. Isothermal elements (references 1-2) neglect member conduction heat transfer and permit efficient analyses for average member temperatures. The dashed line shows the good agreement between the predicted temperature distributions along the column. The column temperature is almost constant and temperatures computed by the isothermal element are in excellent agreement with the refined conventional element solution. The use of isothermal elements reduces computer costs significantly (by about 100 for this problem) and also permits use of a common discretization for an integrated structural analysis.
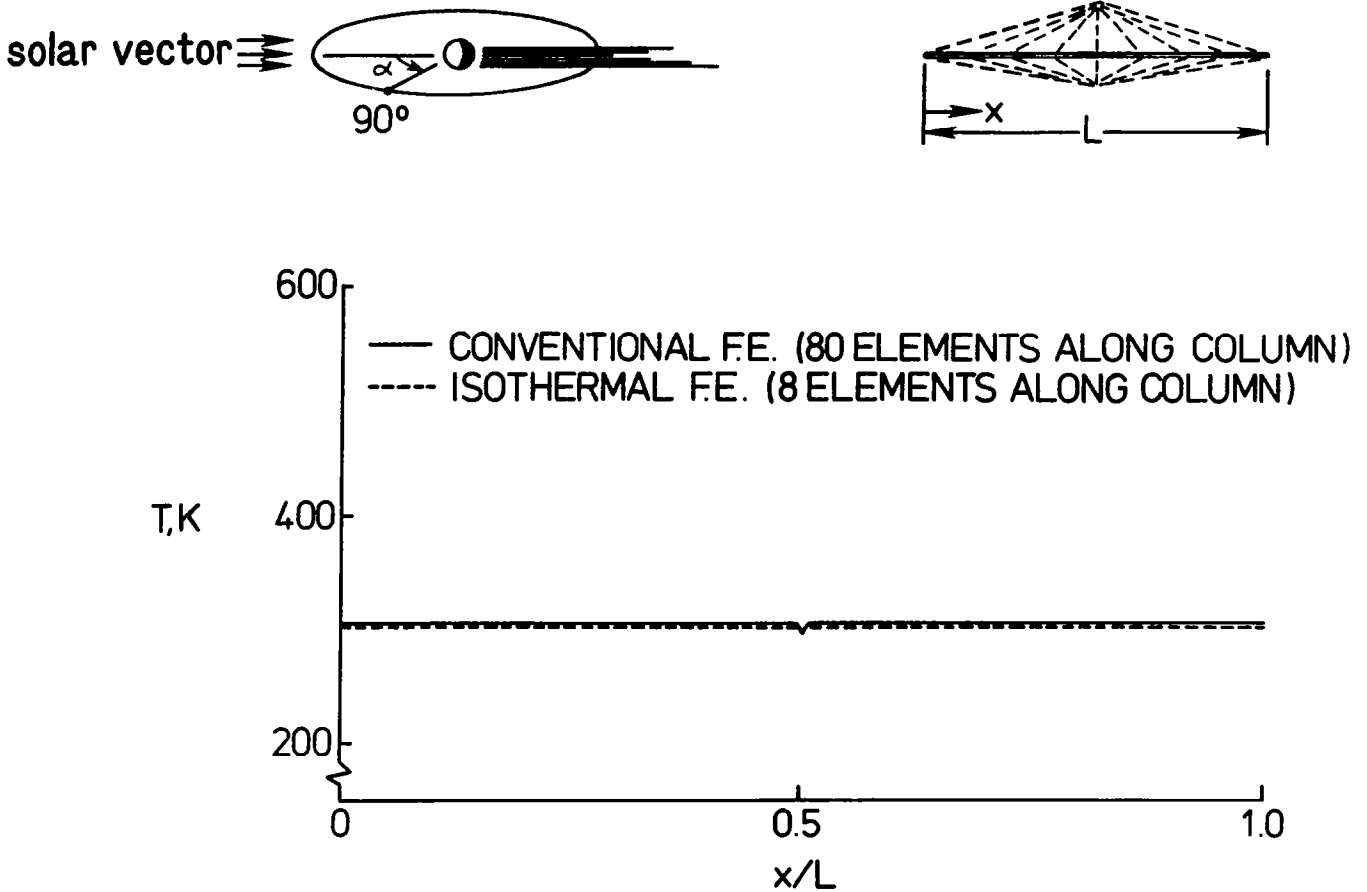
Figure 13

As structural designs for complex large space antenna systems evolve, greater reliance than ever before is being placed on analysis methods implemented in large computer codes. It is becoming increasingly important to understand the limitations and uncertainties of the analytical methods and the computer programs. Recent research aimed at understanding two interdisciplinary problems of heating, thermal, and structural analysis of orbiting space structures was described briefly in this paper. Work on these problems continues with the goal of removing uncertainties in thermal-structural modeling and analysis.

- ## THERMAL–STRUCTURAL RESEARCH DESCRIBED
  - –Slender member shadowing effects
  - –Cable-stiffened structures

- ## SLENDER MEMBER SHADOWING
  - –Cross member shadow effects appear small
  - –Work continues including parallel member shadowing

- ## CABLE STIFFENED STRUCTURES
  - –Specialized thermal models effective
  - –Need further study on nonlinear structural response with cable elements

Figure 14

359

REFERENCES

1. Mahaney, Jack and Strode, Kim B.: Fundamental Studies of Thermal-Structural Effects on Orbiting Trusses. AIAA/ASME/ASCE/AHS 23rd Structures, Structural Dynamics and Materials Conference, AIAA, 1982. (AIAA Paper No. 82-0605.)

2. Thornton, Earl A., Dechaumphai, Pramote and Wieting, Allan R.: Integrated Finite Element Thermal-Structural Analysis with Radiation Heat Transfer. AIAA/ASME/ASCE/AHS 23rd Structures, Structural Dynamics and Materials Conference, AIAA, 1982. (AIAA Paper No. 82-0703.)

3. Thornton, Earl A.: Thermal-Structural Analysis of Large Space Structures: A Review of Recent Advances. AFWAL-TR-82-3048, Air Force Wright Aeronautical Laboratories, 1982.

4. O'Neill, R. F. and Zich, J. L.: Space Structure Heating (SSQ), A Numerical Procedure for Analysis of Shadowed Space Heating of Sparse Structures. AIAA 16th Thermophysics Conference, (Palo Alto, California), June, 1981. (AIAA Paper No. 81-1179.)

5. Belvin, W. K.: Vibration and Buckling Studies of Pretensioned Structures. Large Space Systems Technology-1981, NASA CP-2215, Part 1, pp. 109-121.

STRUCTURES FOR LARGE PRECISION REFLECTORS

J. M. Hedgepeth
Astro Research Corporation
Carpinteria, California
and
W. H. Greene
NASA Langley Research Center
Hampton, Virginia

LARGE SPACE ANTENNA REQUIREMENTS

Figure 1 shows various ranges of radio frequencies and sizes that are of interest for future large space antennas. Note that the bulk of requirements involve ratios of diameter to wavelength (D/λ) < 10,000. Much more precise antennas are required for submillimeter and infrared astronomy as can be seen from the figure. This higher accuracy requirement is the subject of this paper.
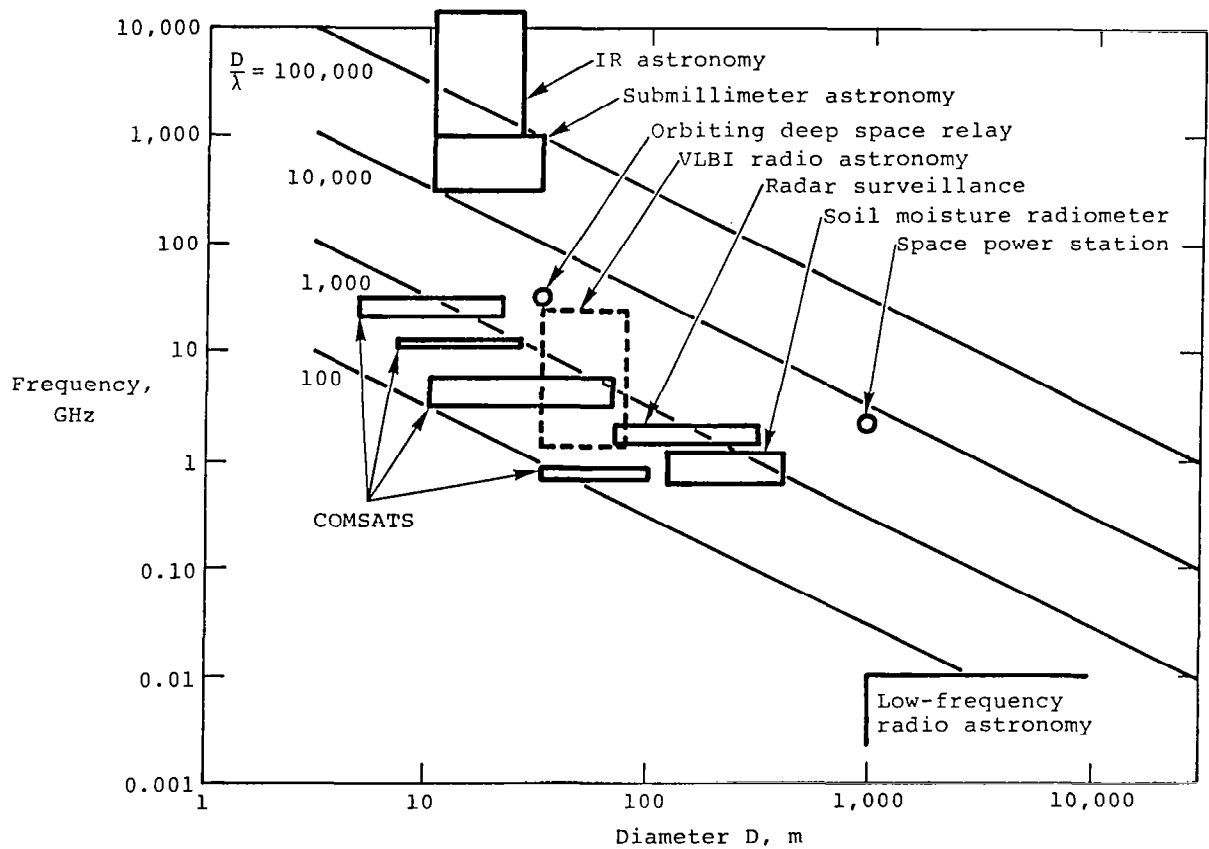
Figure 1

BASELINE LARGE DEPLOYABLE REFLECTOR

An example mission which requires very high accuracy is large-aperture infrared astronomy. The instrument for this scientific mission has been under consideration for several years; it is called the Large Deployable Reflector (LDR). In June a workshop was held at Monterey, California, for both experimenters and technologists to investigate what this instrument should be. Figure 2, which is based on the findings of that workshop, presents the requirements for the baseline design of the antenna structure that is discussed in this paper.

DIAMETER	20 m PRIMARY, 1 m SECONDARY
FOCAL LENGTH	20 m PRIMARY, 200 m SYSTEM
DIFFRACTION-LIMITED WAVELENGTH	50 MICROMETERS
POINTING	0.05 ARCSEC ABSOLUTE 0.02 ARCSEC JITTER
SCAN	1 DEGREE/MIN
ORBIT	750 km, 28° OR POLAR
TEMPERATURE	150K PRIMARY 125K SECONDARY
REFLECTOR SEGMENTS	2-m SIZE, 1.5 MICROMETER ACCURACY

Figure 2

BASELINE PRECISION REFLECTOR

The chosen structural concept for the infrared reflector telescope is shown in Figure 3. This is an off-axis Cassegrainian design with a focal length equal to the aperture diameter (the Monterey workshop recommended an on-axis fed primary reflector with an F/D = 0.5). The Cassegrainian design enables the system to have an F/D = 10 which is necessary to assure a sufficiently wide field of view. The primary mirror is made up of approximately 120 hexagonal 2 m panels. These reflector panels are assumed to be very accurately shaped and very stable in dimensions. Panels are mounted to the truss backup structure with three-point adjustable attachments and an active control system is used to position the panels in such a way as to yield the required very accurate surface. The subreflector located at the focus of the primary reflector is mounted to the main reflector by a tripod formed of lattice columns. The scientific package is contained in the main spacecraft represented by the 4-sided block at the lower left.
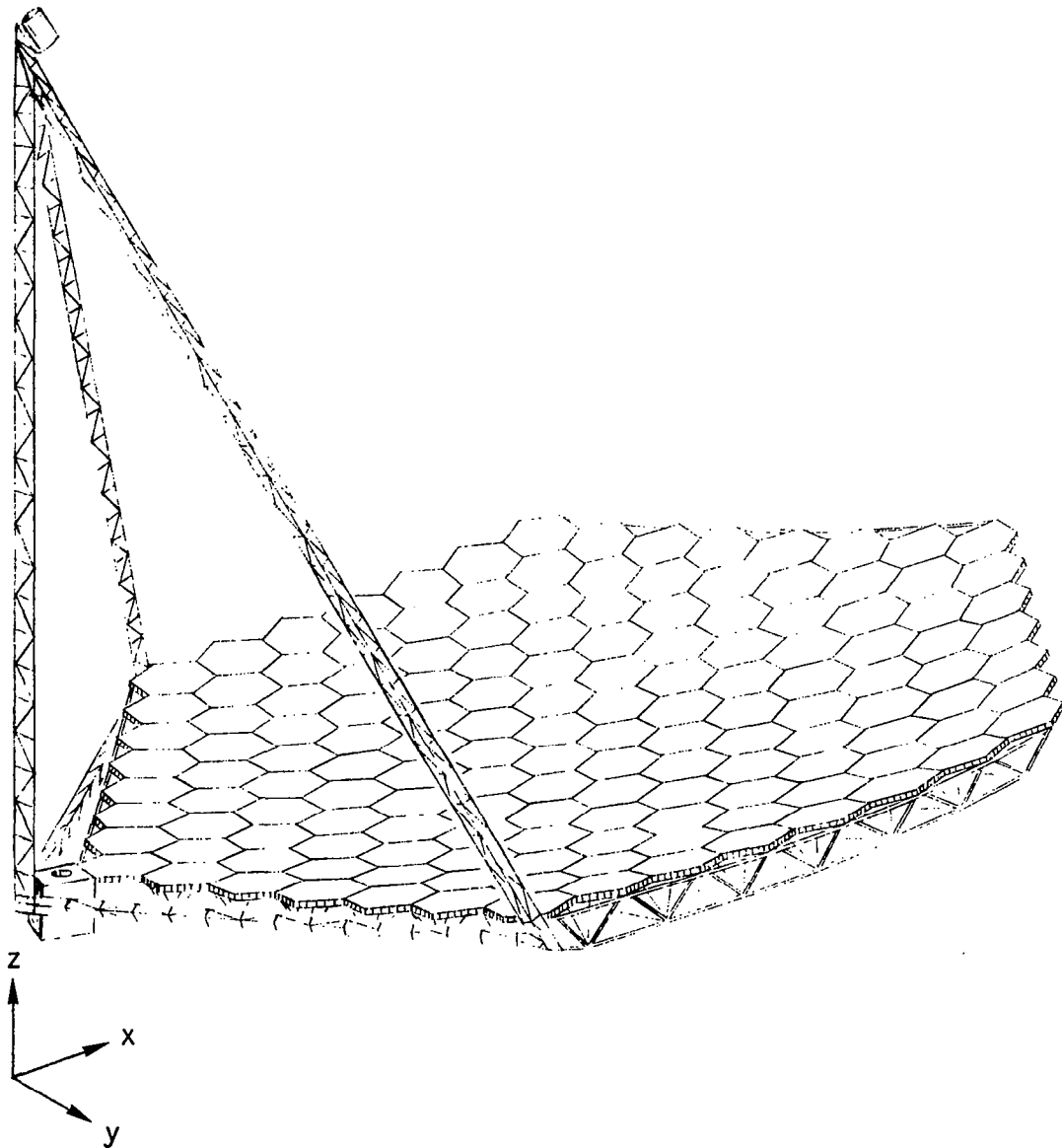
Figure 3

In order to reduce the system noise, the reflecting surfaces need to be kept very cold (see Fig. 2). This can be accomplished passively by excluding external radiation to the primary mirror. A concept of a thermal shield to exclude this radiation is shown here. This shield is assumed to be composed of highly efficient multilayer insulation on all sides, including the lower surface of the primary mirror truss. The subreflector and instrument package is assumed to be located opposite to the Sun at all times. Studies show that a serious problem occurs when the spacecraft is on the Sun return side of the Earth. Orienting the spacecraft to avoid the impingement of solar radiation in the cavity involves the capture of a significant amount of infrared Earth radiation and albedo. Consequently the interior of the thermal shield on the side away from the Earth is composed of corner reflectors so that radiation entering the cavity will be reflected out again. (See figure 4.)
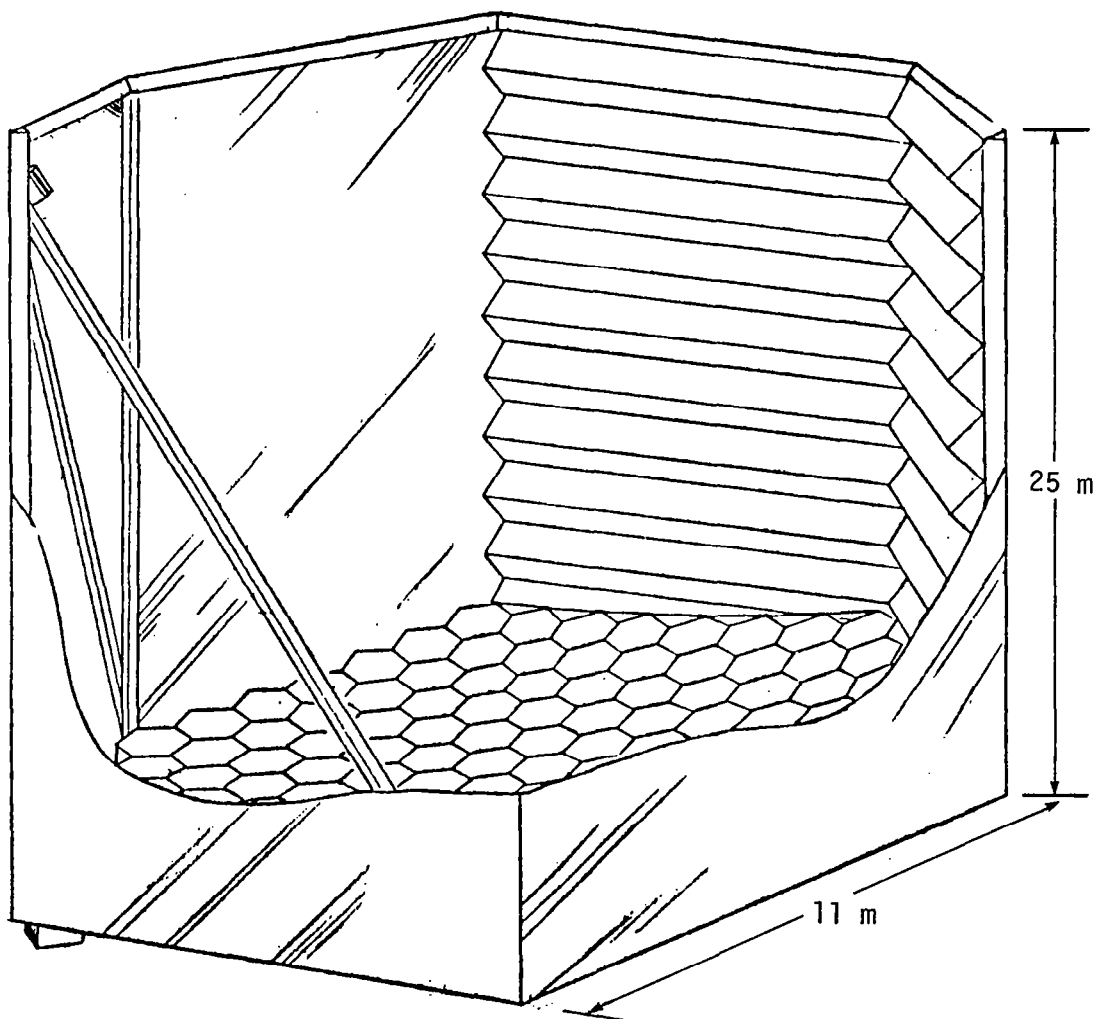
Figure 4

PEAK HEAT FLUXES ON REFLECTOR

Managing the heat load is a significant problem for the LDR. An estimate of the heat flows outside and inside the LDR is shown in Figure 5. Note that at times the amount of energy impinging on the LDR from the Earth is quite large. These results assume that the solar energy is excluded from the cavity; there may then be a total of 110 W/m^2 from earthshine that enters the cavity through the open end. The majority of this gets reflected and eventually only about 2 W/m^2 (peak) gets absorbed by the primary reflector. When this is combined with 1 W/m^2 that reaches the reflector through the multilayer insulation on the rear surface and the energy is averaged over the orbit, the result is a temperature of 150 K.

Figure 5

366
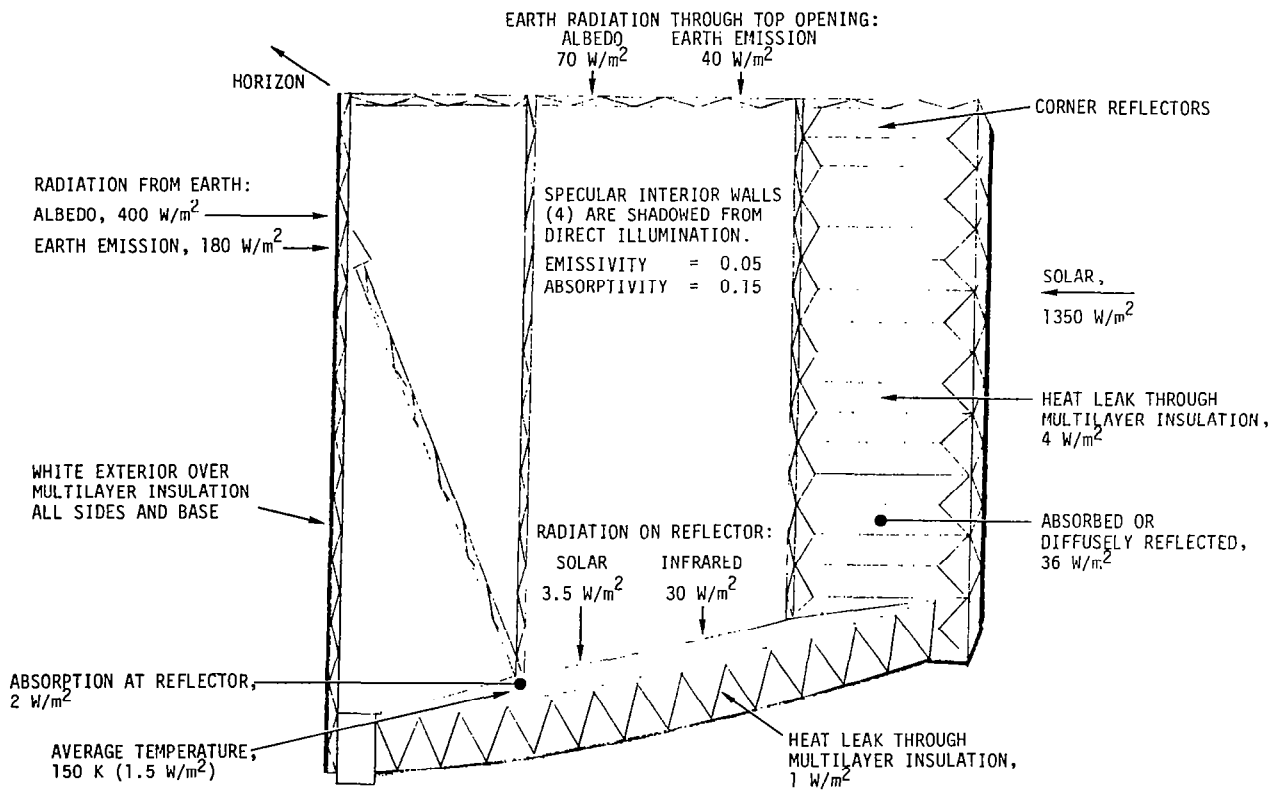
MOSAIC REFLECTOR OF SPHERICAL SEGMENTS
ASSEMBLED BY RMS FROM SHUTTLE

Various means exist for constructing the LDR in space. One approach is illustrated in Figure 6. In this approach the structural truss would be deployed and then the reflector panels would be mounted to that truss. Figure 6 shows the mounting being done by the Shuttle Remote Manipulator System (RMS). Other approaches could use EVA.
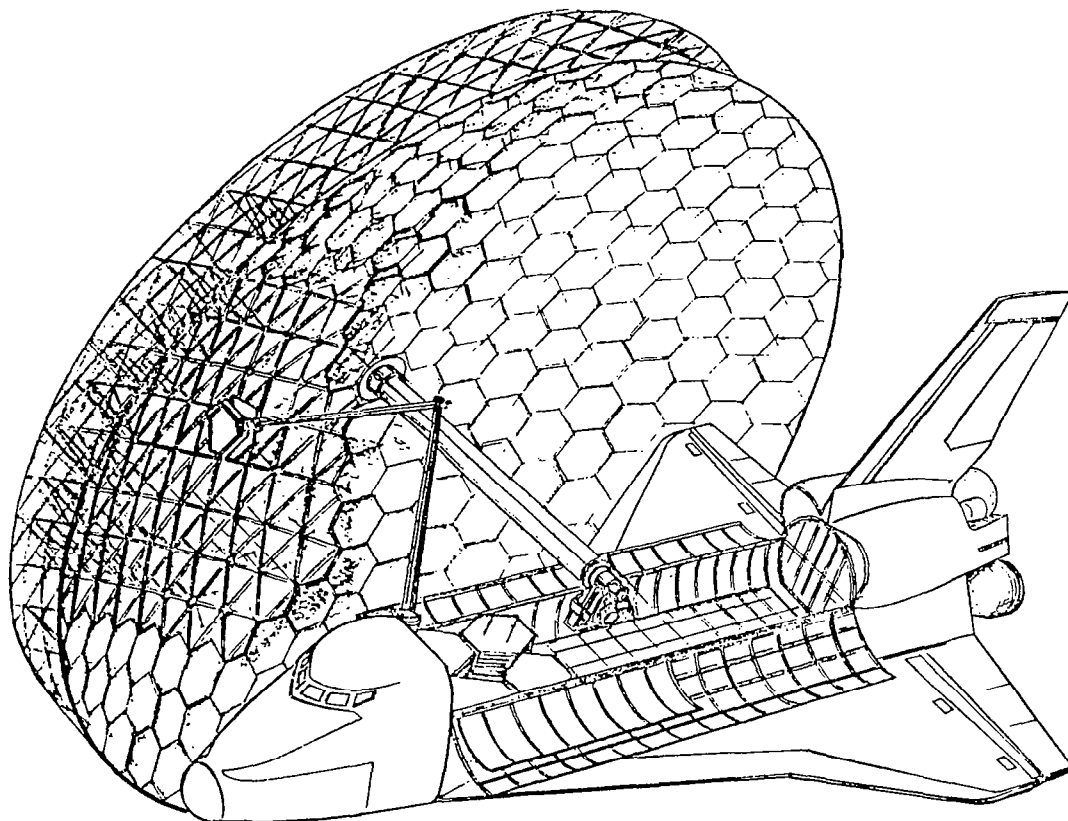
Figure 6

Figure 7 illustrates another approach, in which each reflector panel would be attached to a packaged module of the structural truss. Each module would then be deployed and assembled to its neighbors to create the entire reflector. Again, this assembly work would be done by remote manipulators or by EVA.
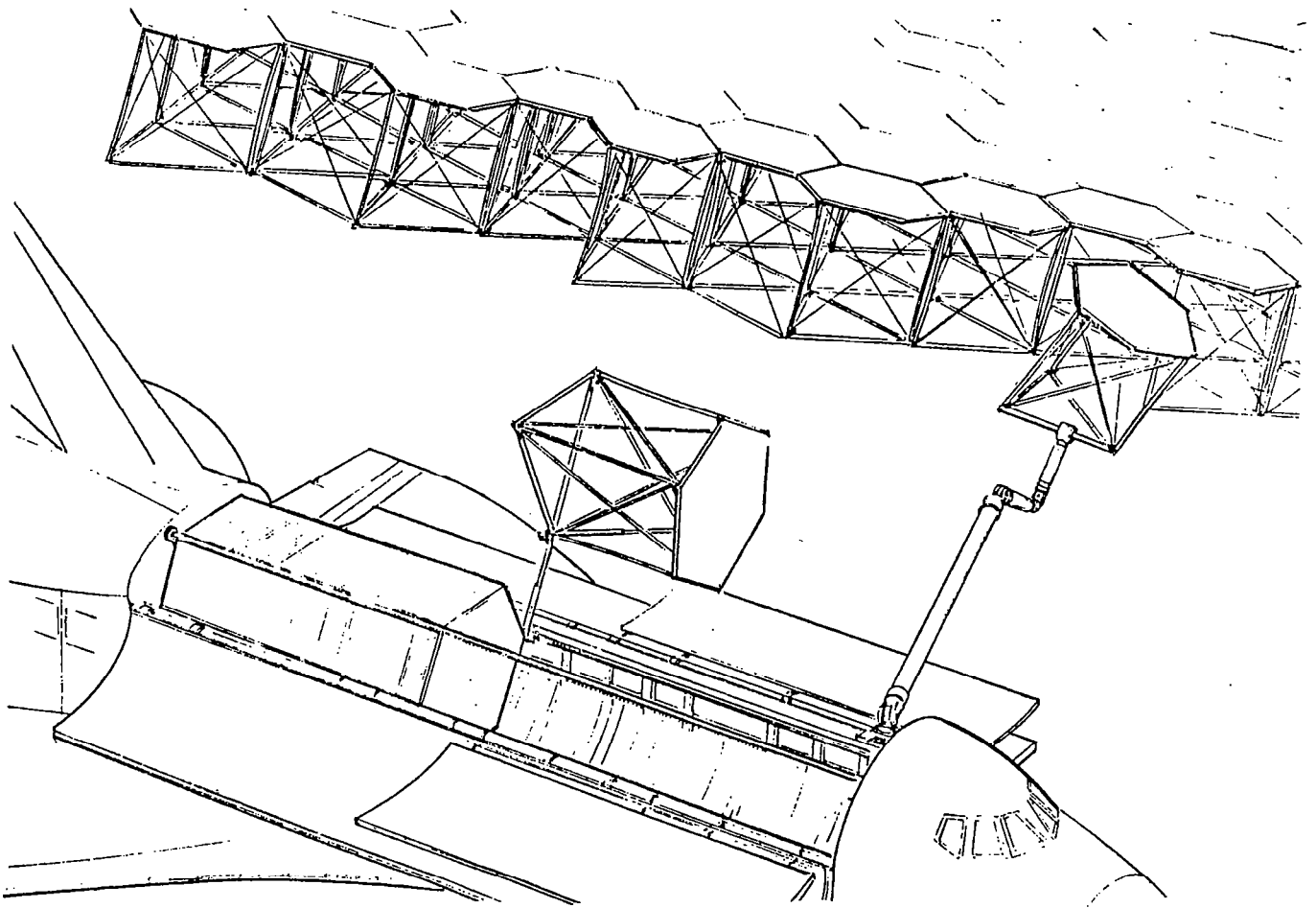
Figure 7

TYPICAL STRUCTURAL/ELECTRICAL JOINT

When structural joints are to be made on assembly, their design becomes an important consideration. One possible design is shown in Figure 8. The structural connection is made by means of a drogue and probe arrangement. A mechanical fastener of some sort would lock the joint together. Also shown here is an electrical connector which would enable the proper routing of power and signal leads as necessary.
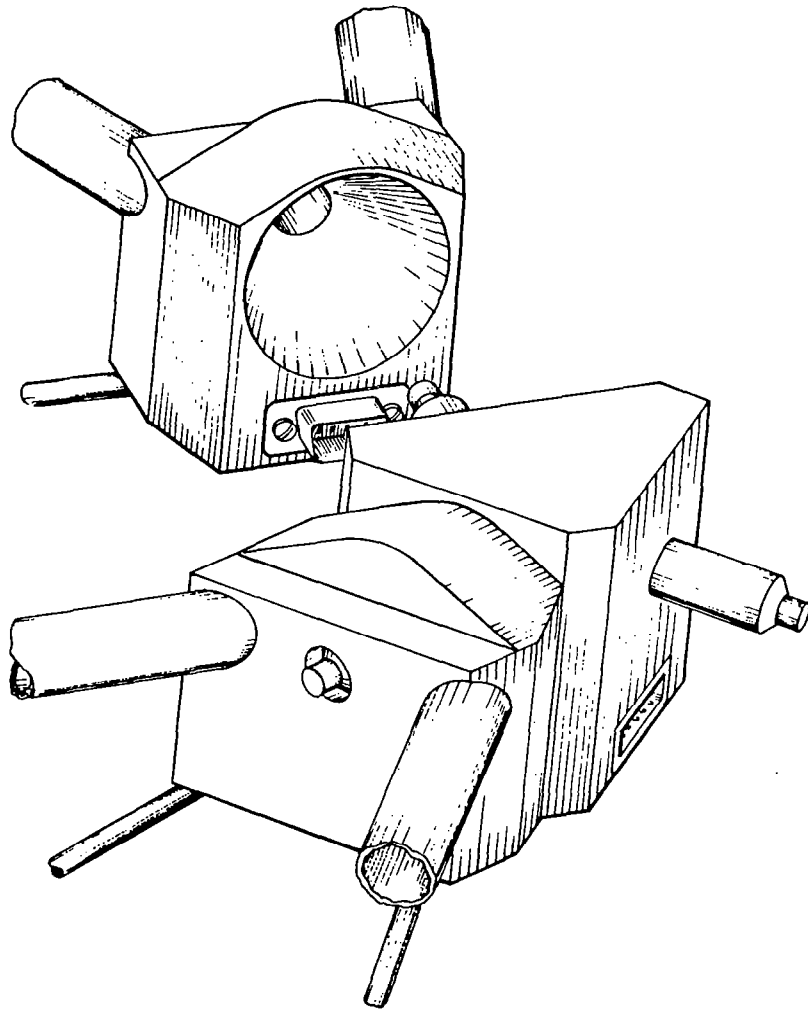
Figure 8

SEQUENTIALLY DEPLOYABLE PRECISION REFLECTOR

The assembly tasks in the foregoing concepts are characterized by a large ratio of the distance traveled to the dimensional precision of mating the parts. The concept shown in Figure 9 avoids this disadvantage. All the modules are interconnected so that the hinges in the structure furnish a large amount of control to aid the assembly of the modules. This allows the use of a fairly simple special-purpose assembler mounted to the deployment canister which needs only to do the final close-proximity attachment operations. This concept, which was developed several years ago, is described more fully in refs. 1 and 2.

Fundamentally, the interconnected reflector-truss modules are packaged in a canister and caused to deploy one at a time as the canister walks itself around the structure. The example shown in Figure 9 is appropriate to a Shuttle-based experiment.
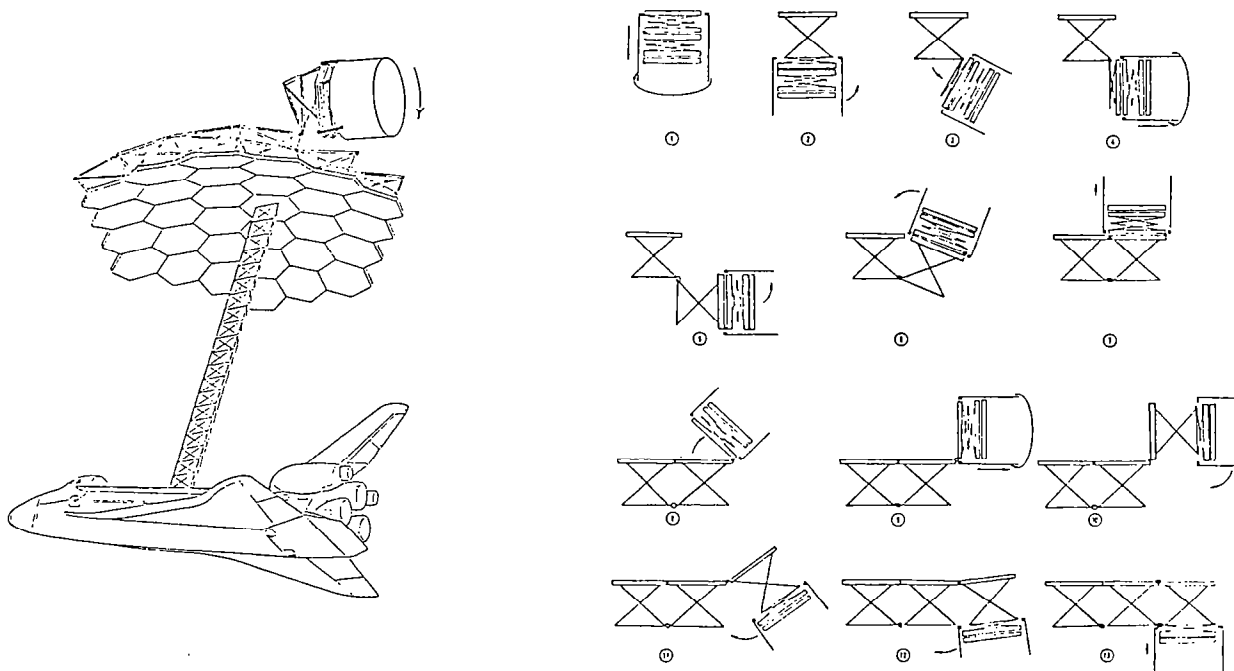
Figure 9

DEPLOYMENT SEQUENCE

The sequential deployment design for the LDR would take the form shown in Figure 10. Here the primary reflector is packaged in a canister about 10 m long. Each stowed reflector truss module would thus be about 8 cm thick. The lattice columns which support the subreflector would be folded at appropriate knee joints and the packaged telescope without thermal shield would appear as at the top left of the figure. Ample room exists in the Shuttle bay for stowage. The sequence of deployment would be first to put the subreflector into its proper position by releasing appropriate knee hinges. Then the primary reflector canister would construct that portion of the primary reflector until a corner is reached. At that time the lattice tripod would be further unfolded to reach that corner, the manipulator on the canister being available to help in making the structural joint properly. The canister would then proceed to the other tripod corner with a similar subsequent deployment of the tripod on that side. The remainder of the primary reflector would then be constructed.

Note that no work has yet been done to develop a means to package and deploy the thermal shield. It is expected that it is possible to accomplish this together with the reflector in a single Shuttle payload.
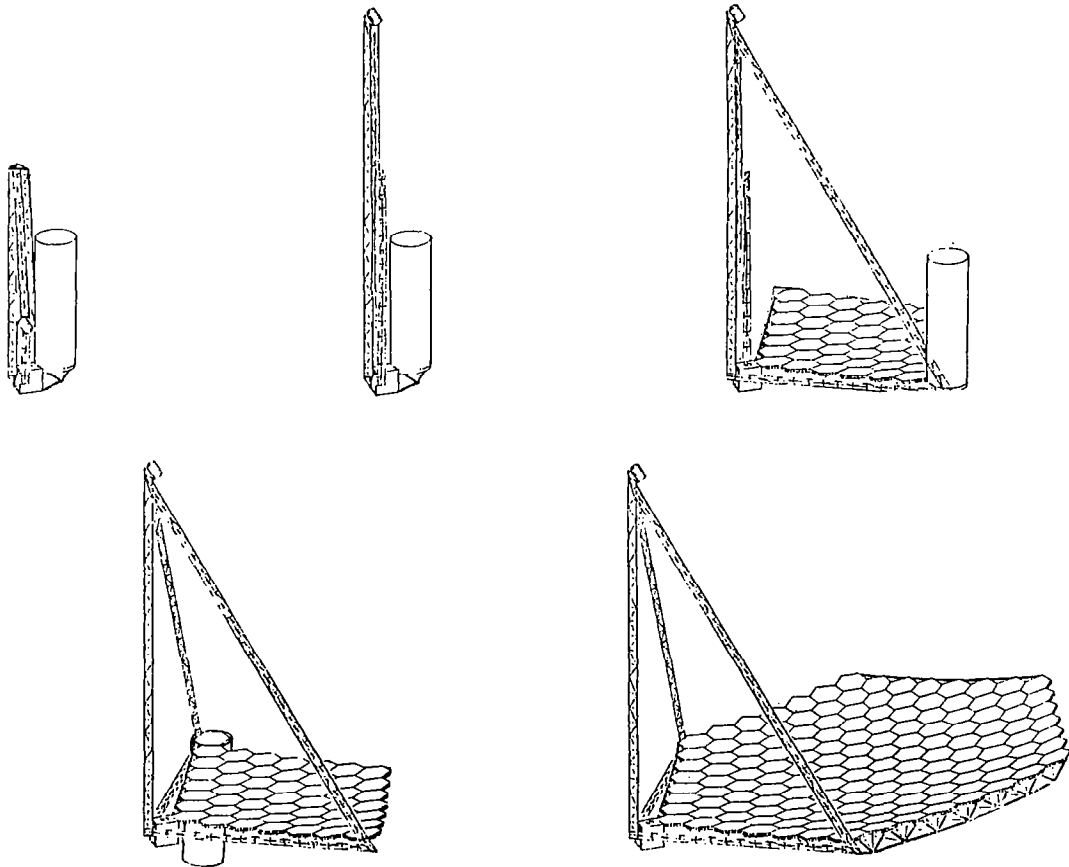
Figure 10

ACTIVE CONTROL TASKS

The LDR must use active control in order to achieve the high degree of accuracy that is required of it. The needed capability of that active control system is dependent on how well the structure itself maintains the precise geometry. The conclusion from the argument in Figure 11 is that cost depends on the required improvement in accuracy. Thus, if one micron accuracy is required, for example, a control system which must operate over a range of a centimeter would be considerably more expensive than one whose stroke, and sensor capability, would be less than a millimeter.

- SENSING DIFFICULTY IS DIRECTLY DEPENDENT ON THE FIELD OF VIEW AND INVERSELY DEPENDENT ON THE ABSOLUTE ACCURACY DESIRED.

- COMPUTATION BECOMES MORE LENGTHY AS THE RATIO OF LARGEST TO SMALLEST QUANTITY INCREASES.

- ACTUATORS ARE MORE COMPLICATED AS THE STROKE INCREASES RELATIVE TO THE REQUIRED MOVEMENT ACCURACY.

- CONCLUSION IS THAT THE EXPENSE OF ACTIVE CONTROL IS DEPENDENT ON ITS BASIC TASK OF IMPROVING ACCURACY.

Figure 11

TRANSIENT COOLING RATES OF REFLECTOR

An additional element in determining how complex the control system needs to be is the rate at which changes in geometry of the structure would occur. A very low control bandpass could be tolerated if the geometry would vary at a slow rate. An estimate of how rapidly geometry would change can be inferred from Figure 12. A simple calculation was made of the rate of decrease of temperature if one assumes that the radiation impinging on the reflector was totally removed, and the reflector allowed to cool radiatively. As can be seen for reflector masses on the order of 10 or more kg/m^2, the rate of temperature change is very low indeed. It is expected that similar results would be obtained for other time-varying phenomena so that a low bandpass control system would be possible.
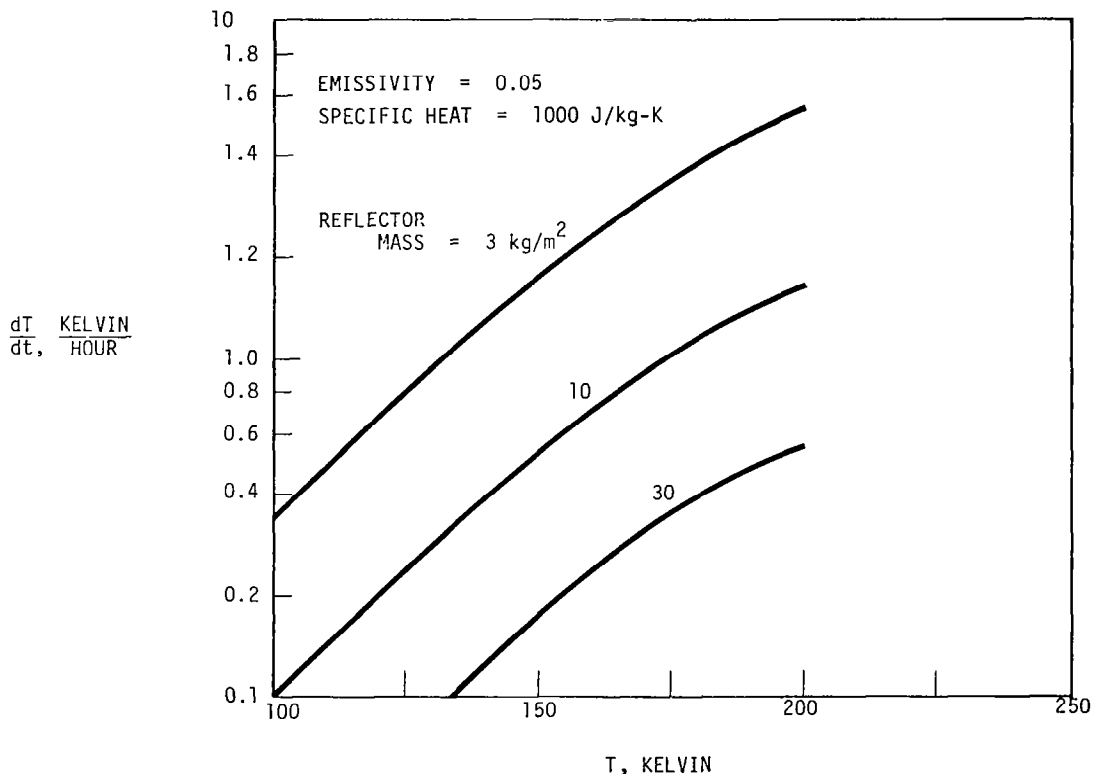
Figure 12

Estimates have been made of how accurately truss-type reflector structures can be built for space applications. Because of the difficulty of constructing and measuring large structures in a 1 g environment, the assumption is made that the structural components will be manufactured to high accuracy and then assembled without further adjustment. The final structure then will exhibit a surface precision which depends on the way in which the individual inaccuracies combine. In ref. 3 an estimate is made of this error by assuming that the truss structure has many cells, and therefore can be approximated by a continuous structure. Recently another analysis has been made which treats example trusses such as the one shown in Figure 13 in a direct fashion by using the Monte Carlo technique. Thus, a specimen structure is assumed to be built up of struts of random lengths which scatter about their norm. The distorted geometry is then calculated by finite-element truss analysis. An average of the squared error over the surface of the truss is determined.

Figure 13

374
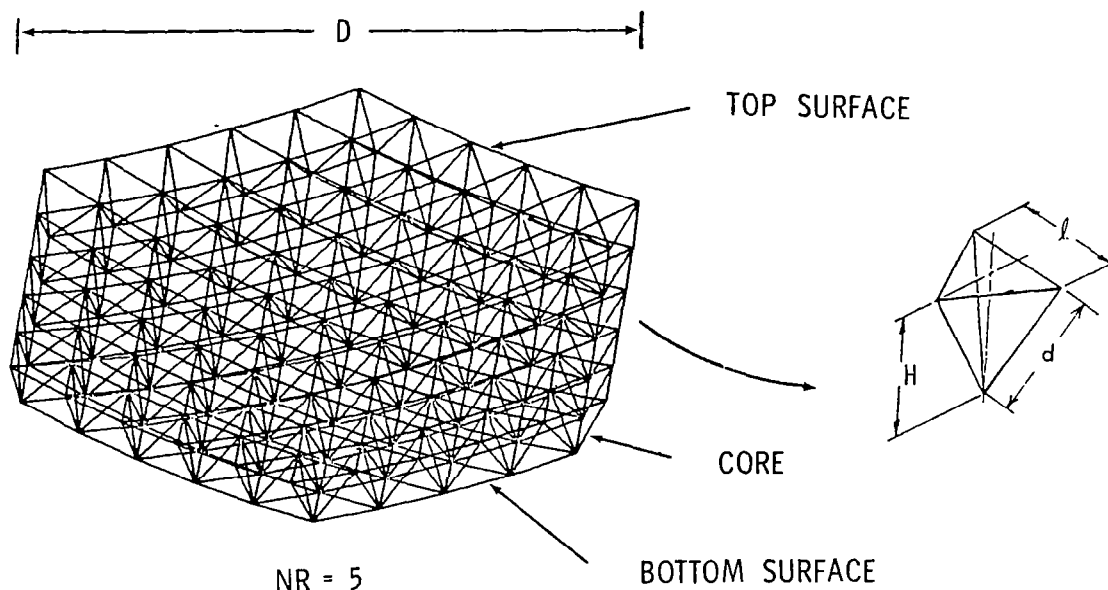
SURFACE ERROR OF A TETRAHEDRAL TRUSS ANTENNA

The variation of the rms surface error as a function of the number of rings in the truss structure is shown in Figure 14. The curve with circles is the mean of 100 trials. The extent to which the rms surface error varies from specimen to specimen is indicated by the 1 σ deviation which is shown as the difference between the square and the circle points. Also shown in the figure is the continuum analysis estimate of ref. 3. It is seen that the previous work furnishes a reasonable estimate of the mean error, but does not include the important effects of sample-to-sample variation.

$$\frac{F}{D} = 1.0$$

$$\frac{H}{\ell} = 0.816$$

O — MEAN

□ — MEAN + 1σ

SURFACE ERROR PARAMETER,

$$\frac{w_{rms}}{D\,\sigma_\epsilon}$$

CONTINUUM-ANALYSIS ESTIMATE

NUMBER OF RINGS, N_r
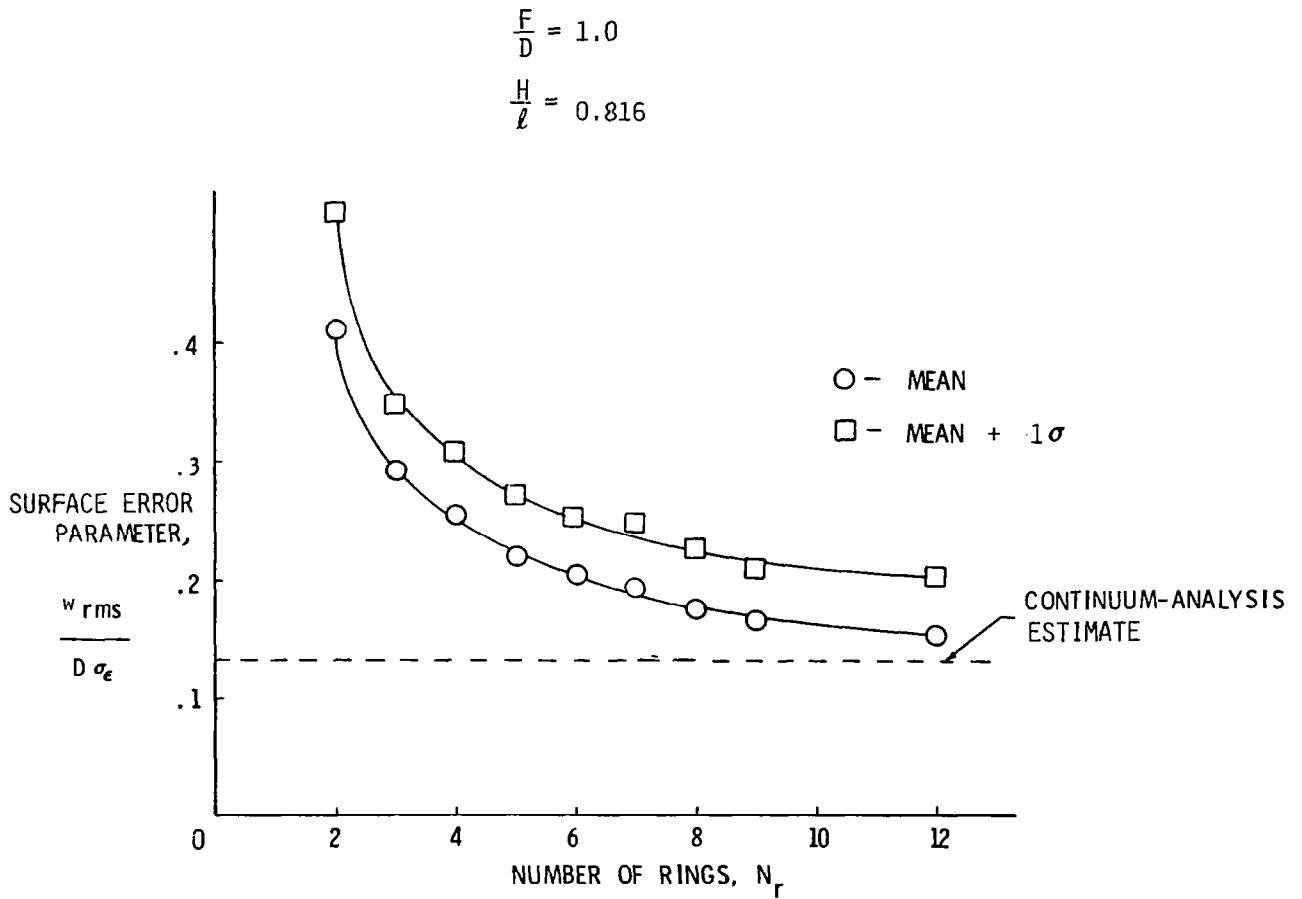
Figure 14

FABRICATION TOLERANCE INDUCED ERRORS FOR SIX-RING LDR

Detailed results for a 6-ring LDR with an offset focal point are shown in Figure 15. The nondimensional average rms for 100 structures is shown to be 0.245. If we include three standard deviations of the mean square, then the average turns out to be 0.385. This worst-case structure exhibits an error of 2-1/2 times that previously predicted by ref. 3.

Note that the rms errors are nondimensionalized with respect to the reflector diameter and the rms unit error in the length of the individual truss members σ_ε. For the LDR size and for a reasonable value of σ_ε, the product $D\sigma_\varepsilon$ is about 1 mm. For this case, the aforementioned numbers can then be interpreted as being the physical rms in millimeters.

Also shown in Figure 15 is data for the rms deviations at individual points on the reflector. This deviation is a function of the position of the point on the truss and tends to grow as the boundary of the reflector is reached. Note that the scatter-bands show how much variation exists as points around an individual ring are considered. Presumably, taking a multiple of the rms deviation would give a basis for designing the required stroke of the active control system actuators. This information indicates that a stroke of about 3 mm might be required.

$$\frac{\sqrt{\langle \overline{w^2} \rangle}}{D\sigma_\varepsilon} = 0.245$$

(AVERAGE STRUCTURE)

$$\frac{\sqrt{\langle \overline{w^2} \rangle + 3\sigma}}{D\sigma_\varepsilon} = 0.385$$

(WORST-CASE STRUCTURE)

NOTE: FOR $D = 20$ m, $\sigma_\varepsilon = 5 \times 10^{-5}$

THEN $D\sigma_\varepsilon = 1$ mm
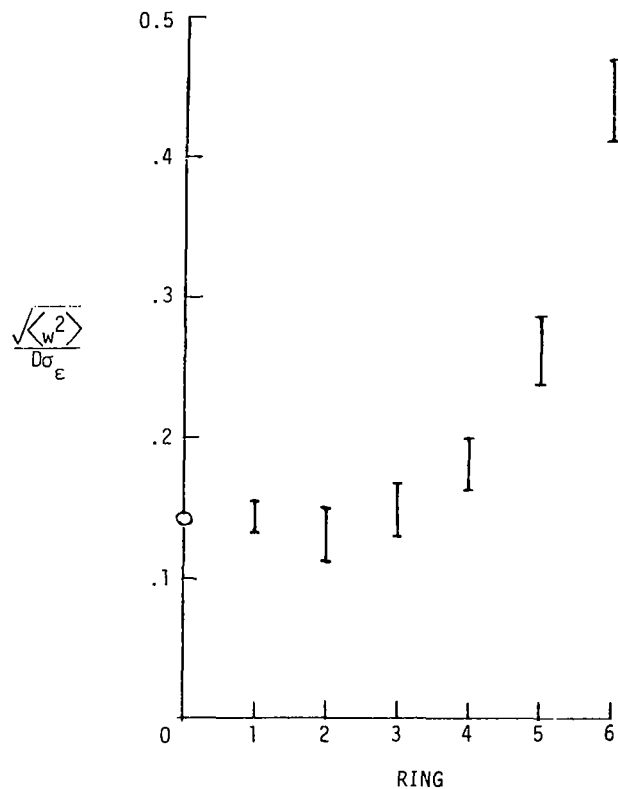
Figure 15

LIMITATIONS DUE TO FABRICATION ERRORS FOR BASELINE LDR – ALLOWABLE ERROR = WAVELENGTH/100

The results shown on Figure 15 are summarized in Figure 16. The dotted line shows the wavelengths of radiation that could be handled by the structure if no active control were employed. The improvement in capability for active control systems of various refinement as measured by ratio of accuracy to full-scale stroke is shown by the solid lines. Examination shows that a control system accuracy of one part in 2000 would be required in order to handle a wavelength of 50 μm with reasonable fabrication tolerances.

Figure 16

377
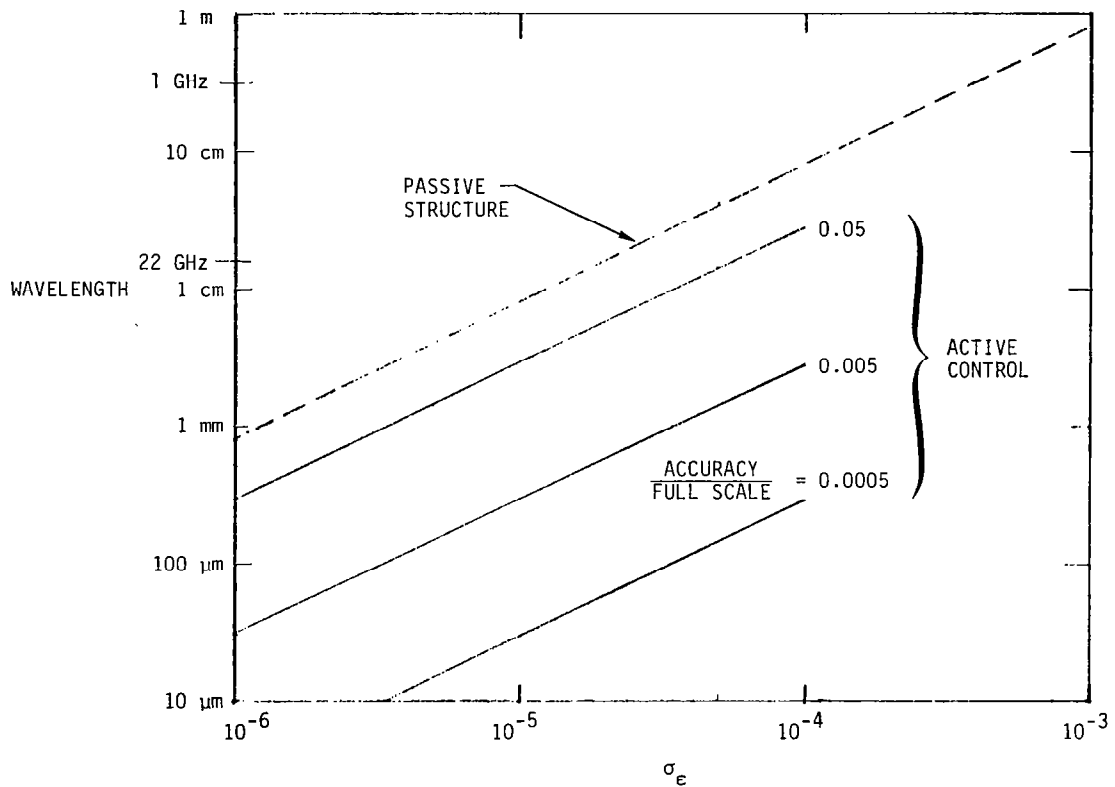
POSSIBLE EVOLUTIONARY SCENARIO

One of the problems that exists for large structures in space is how to achieve technology validation.

- Program Managers are reluctant to pursue programs involving unvalidated new technology.

- Potential users are reluctant to insist on advanced capability involving new technology for fear that they will get nothing.

- The validation cost is frequently higher than can be afforded on a stand-alone basis.

The question is, how can we cope with this vicious cycle? A possible approach is to use evolutionary development of mission and technology together. The factors are listed below.

- Technology can be proven as part of advanced missions.

- Missions must not place high demands on performance of new technology.

- Mission performance can be upgraded as new technology is proven.

- Symbiosis is enabled by recovery and reflight capability of Shuttle.

An attractive candidate for this type of development would be the LDR. A possible evolutionary scenario is shown in Figure 17.

MISSION	REFLECTOR TECHNOLOGY
L-BAND SHUTTLE-EARTH VLBI ● MEASURE ACCURACY ● OPTION OF X-BAND AND UP ● REFLY AFTER IMPROVING TO 0.25 MM GUARANTEED ACCURACY	10 METER DEPLOYABLE REFLECTOR ● 61 1-METER PANELS ● 1 MM ACCURACY ● PASSIVE CONTROL
SUBMILLIMETER RADIO ASTRONOMY	● ADD ACTIVE CONTROL AND IMPROVED PANELS TO EXISTING STRUCTURE ● 25 MICRON ACCURACY
	● 30 METER DEPLOYABLE REFLECTOR ● 0.25 MM PASSIVE ACCURACY AFTER REFLIGHT IMPROVEMENT ● 25 MICRON ACCURACY WITH ACTIVE CONTROL
INFRA RED RADIO ASTRONOMY	● IMPROVE PANELS AND ACTIVE CONTROL ANOTHER ORDER OF MAGNITUDE ● ADD THERMAL SHIELD

Figure 17

EVOLUTIONARY LDR DEVELOPMENT

One of the advantages of developing LDR in an evolutionary fashion would be that it would be possible to concentrate on the development of the antenna as an entity and thereby investigate the submillimeter wavelength regime. Subsequently, thermal shielding can be added and the reflector panel system improved so as to enable infrared astronomy to be conducted.
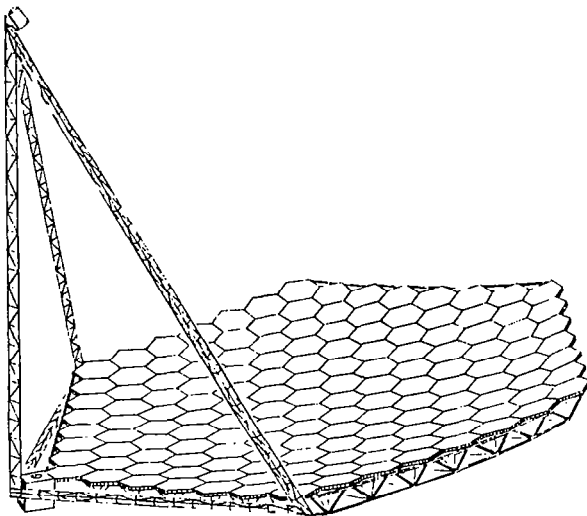
SUBMILLIMETER
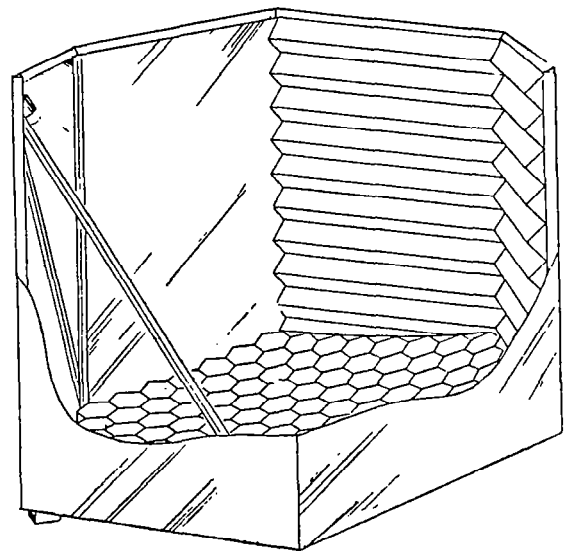
INFRARED

Figure 18

REFERENCES

1. Hedgepeth, John M. and Finley, Laurence A.; Deployable Structures for Millimeter-
    Wave Antennas. Astro Research Corp., ARC-TN-1087, April 14, 1980.

2. Finley, Laurence A.; The Geometry of the 37-Tile Microwave Antenna Support
    Structure. Astro Research Corp., ARC-TN-1083, March 5, 1980.

3. Hedgepeth, John M.; Influence of Fabrication Tolerances on the Surface Accuracy
    of Large Antenna Structures. AIAA Journal, vol. 20, no. 5, May 1982, pp. 680-686.

SURVEY OF DEPLOYABLE ANTENNA CONCEPTS

R. E. Freeland
Jet Propulsion Laboratory
Pasadena, California

SEQUENTIALLY DEPLOYED PRECISION REFLECTOR

A deployment scheme was developed by Astro Research Corporation specifically for the segmented reflector class of telescopes. The deployment approach is based on breaking up the truss structure into a number of separate deployable tetrahedral cells. Each of these individually deployable truss modules is attached to a single reflector element. These modular elements (i.e., truss and reflector element) are hinged together and stored and supported in a deployment canister during launch. This canister contains the hinging, extension and latching mechanisms to accommodate the automated deployment of the reflector portion of the telescope.

- UNIQUE FEATURES OF CONCEPT
    - AUTOMATED DEPLOYMENT FOR SEGMENTED REFLECTOR
    - TETRAHEDRAL TRUSS STRUCTURE
    - REFLECTOR ELEMENTS AND TRUSS DEPLOYED FROM SINGLE CANISTER
    - SUITABLE FOR ACTIVE CONTROL
    - REQUIRES INTELLIGENT DEPLOYER
    - INTENDED FOR REFLECTORS UP TO 30 METERS

- CONCEPT LEVEL OF MATURITY
    - FORMULATED DEPLOYMENT SEQUENCES
    - ESTABLISHED JOINT REQUIREMENTS
    - JOINT FEASIBILITY ESTABLISHED ON RELATED TECHNOLOGY DEVELOPMENT

- CONCEPT DEVELOPMENT STATUS
    - CONCEIVED AT ASTRO RESEARCH CORPORATION
    - DEVELOPED WITH NASA FUNDING
    - CONCEPTUAL DEMONSTRATION MODEL NEXT LOGICAL DEVELOPMENT STEP

SEQUENTIALLY DEPLOYED PRECISION REFLECTOR

This figure shows a segmented reflector antenna capable of precision surface applications. The off-axis feed is supported by a deployable tripod from the corners of the truss. The reflector itself is deployed sequentially from a canister. In order to provide a high level of confidence in the automated deployment process, the mechanisms for deploying, extending, and latching the structure and reflector elements should be as simple as possible. Generally, this means that all these operations be performed as close to the canister as is practicable, thereby eliminating long arms and awkward mechanisms. The outside rim of the open end of the canister is the best region available to contain the necessary sensors and mechanisms. The deployment sequence keeps this area in close proximity to the majority of the extending and latching operations.

The deployment sequence, in combination with the overall structural requirements, places certain restrictions on the types of joints possible in this structure. Briefly, the criteria for the joints require (a) that they y be as self-aligning as possible and present a good "target" as adjoining hardware is brought together, (b) that they be capable of being rigidized either by the action of the canister or the motion of the structure into the joint area, (c) that they be identical insofar as possible so that the modularity will increase reliability and decrease cost, and (d) that the final joint configuration take up a small volume in comparison with the overall structure, both stowed and deployed.
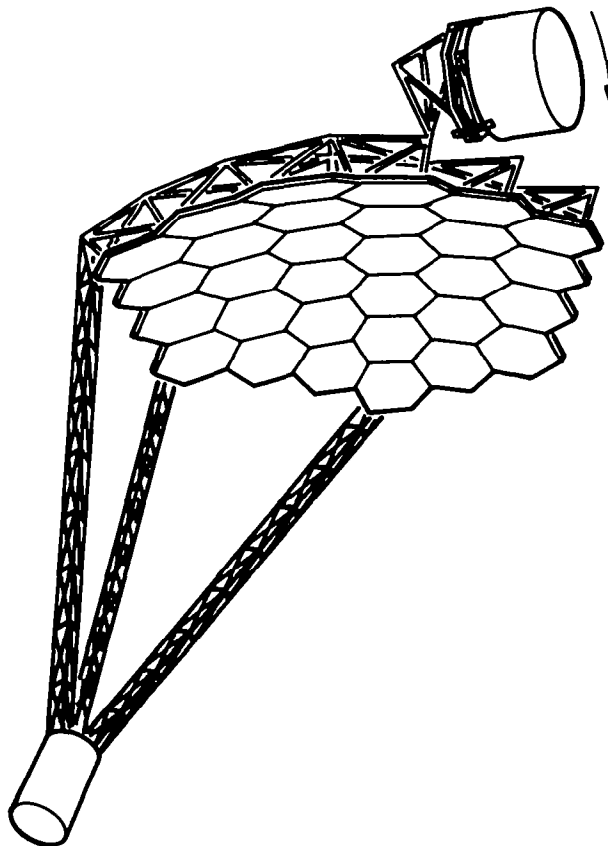
SPIN STIFFNENED MEMBRANE ANTENNA

The antenna concept utilizes the forces of rotation to deploy and dynamically stabilize a thin RF reflective membrane. Theoretically, the membrane does not require a conventional surface support structure to maintain the desired reflector shape. The basic surface shape is determined by (a) the initial static shape of the membrane, (b) the elastic properties of the membrane and (c) the rate of spin of the structure.

- UNIQUE FEATURES OF CONCEPT

  - DEPLOYED AND STABILIZED WITH CENTRIFUGAL FORCES

  - LOW WEIGHT AND EXCELLENT MECHANICAL PACKAGING EFFICIENCY

  - PARABOLIC REFLECTOR CURVATURE RESULTS FROM INITIAL MEMBRANE SHAPE, ELASTIC PROPERTIES AND RATE OF SPIN

  - INTENDED FOR SIZES UP TO 300 METERS FOR mm WAVE RF OPERATION

- CONCEPT LEVEL OF MATURITY

  - CONFIGURATION DESIGN FOR VARIETY OF SIZES

  - ONE METER CONCEPT EVALUATION HARDWARE MODEL

  - ANALYTICAL PERFORMANCE PREDICTION MODELS

- CONCEPT DEVELOPMENT STATUS

  - CONCEIVED AT LOCKHEED MISSILES AND SPACE COMPANY, INC.

  - FUNDAMENTAL CONCEPT EVALUATION ACCOMPLISHED WITH IR&D FUNDING

SPIN STIFFENED MEMBRANE ANTENNA

The concept evaluation included (a) the development of a baseline system configuration for various sizes of antennas, (b) identification and characterization of numerous membrane candidate materials for the reflector, (c) development of a manufacturing plan to accommodate the fabrication, assembly and handling of large size structures and (d) the refinement of analytical performance prediction models to reflect the physical characteristics of the test hardware.
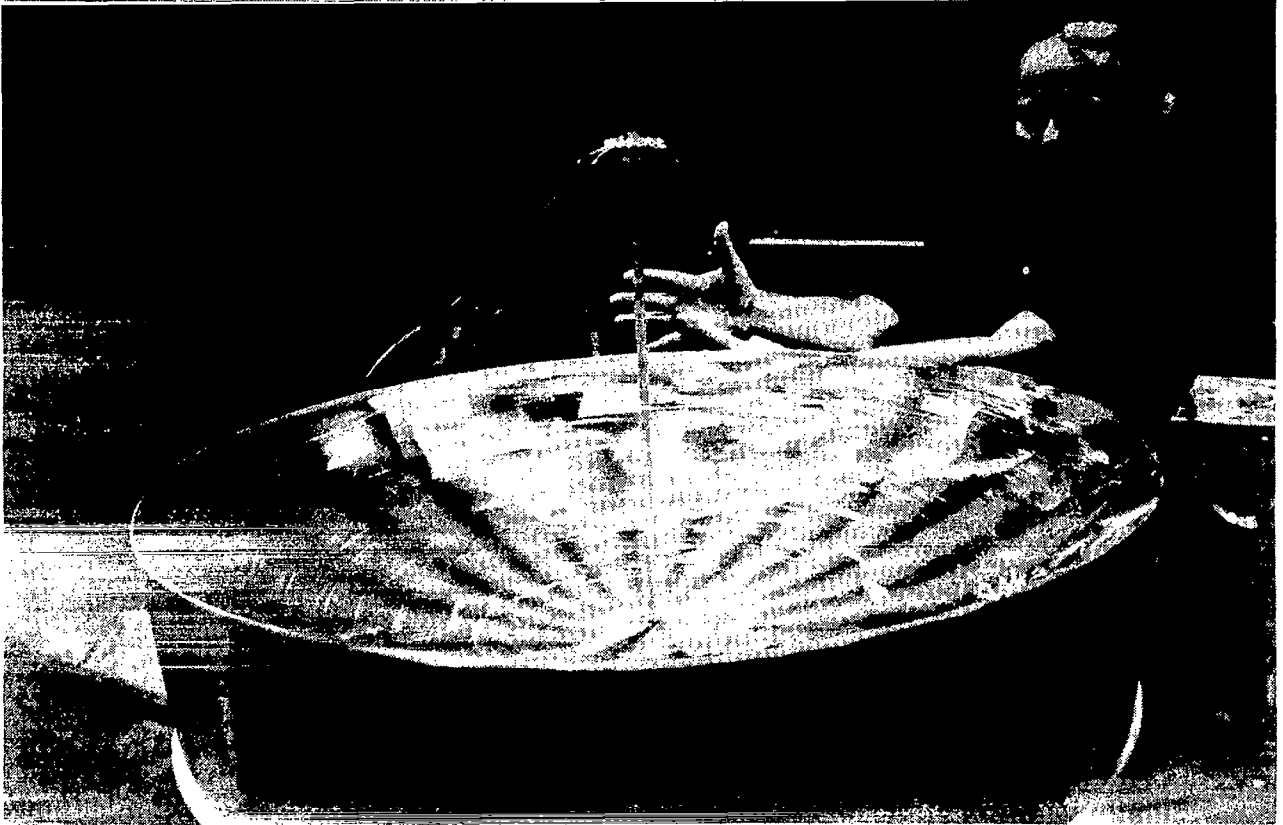
ONE-METER SPIN STIFFENEND MEMBRANE ANTENNA CONCEPT EVALUATION MODEL

A one-meter concept evaluation model was developed to (a) investigate the performance characteristics of the membrane concept and (b) identify effects of materials properties, processes and spin dynamics.
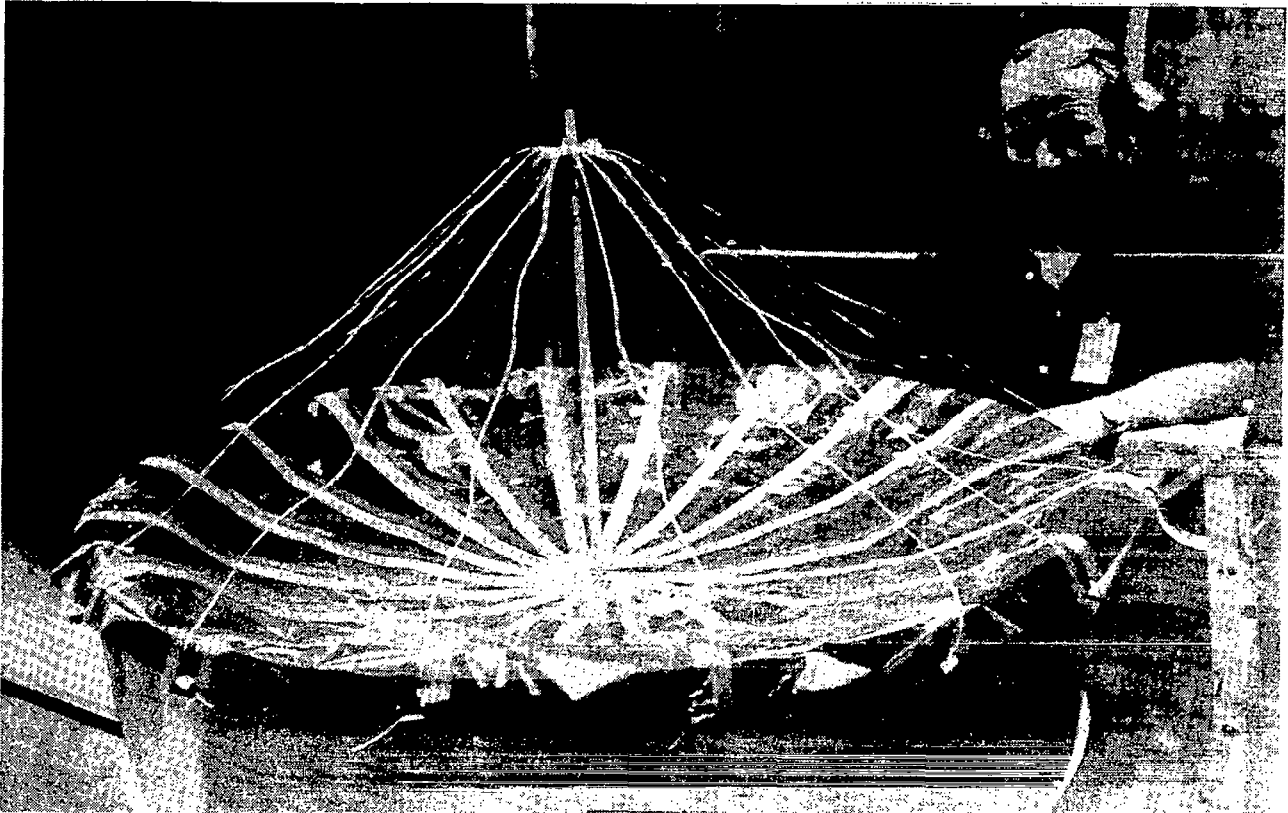
SYNCHRONOUSLY DEPLOYABLE TRUSS ANTENNA

Tetrahedral truss structures offer the advantages of low mass, high stiffness and structural redundancy. The high bending stiffness and multiplicity of hard points for surface attachment made this truss an attractive candidate for antenna reflector application. Conceptually, a triangulated feed support (possible with truss configurations) coupled with a tetrahedral truss reflector could eliminate or reduce the active vibration control requirements. Peripheral hard points offer the potential of assembling modules to construct larger aperture sizes than can be achieved with a single module.

- UNIQUE FEATURES OF CONCEPT
  - UNBLOCKED APERTURE
  - SYNCHRONIZED TRUSS DEVELOPMENT
  - HIGH DEPLOYED STIFFNESS
  - ADAPTABLE TO MODULAR SPACE CONSTRUCTION
  - INTENDED FOR SINGLE MODULE SIZES UP TO 300 METERS FOR RF OPERATION UP TO X-BAND AND BEYOND AT 100 METERS

- CONCEPT LEVEL OF MATURITY
  - CONFIGURATION DESIGN FOR 300-METER STRUCTURES
  - PRELIMINARY DESIGNS FOR CRITICAL COMPONENTS
  - HARDWARE MODELS OF TRUSS JOINTS
  - SEVENTEEN-METER PLANAR BEAM SYNCHRONIZATION MODEL
  - ONE-HUNDRED-METER BASELINE SYSTEM DEFINITION IN PROGRESS

- CONCEPT DEVELOPMENT STATUS
  - CONCEIVED BY LANGLEY RESEARCH CENTER
  - UNDER DEVELOPMENT AT LaRC AND LMSC
  - DEVELOPMENT OF FUNCTIONAL SCALE MODEL IN PROCESS
  - FLIGHT TECHNOLOGY READINESS BY 1988 - 1990

SYNCHRONOUSLY DEPLOYABLE TRUSS ANTENNA
DEPLOYMENT SCHEME

From an orbital operations viewpoint, the most desirable method for achieving a functioning spacecraft is to automatically deploy it. The design and construction of a large doubly curved reflector surface which will fold compactly and deploy reliably is a formidable challenge. The approach illustrated in the figure shows that core and face strut deployment kinematics are mechanically synchronized at each node (i.e., a slider crank mechanism). Kinematic loops are formed via the struts to synchronize the deployment of both faces. Sufficient deployment force is supplied at each node, preferably with passive springs, to overcome any joint friction present and insure lockup. Controlled release of deployment energy (via "dampers") further reduces the potential for dynamically induced mechanical anomalies to occur and enhances reliability. Nodal and joint hardware designs are under development, including actuators and dampers that do not violate the minimum packaging envelope defined by the struts.
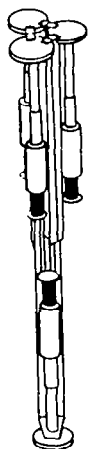
STOWED   PARTIALLY DEPLOYED   DEPLOYED

ACTUATOR

CORE STRUT

FACE STRUT
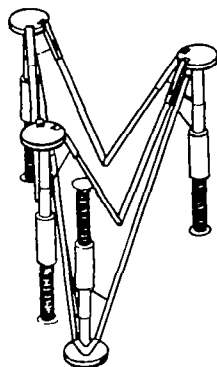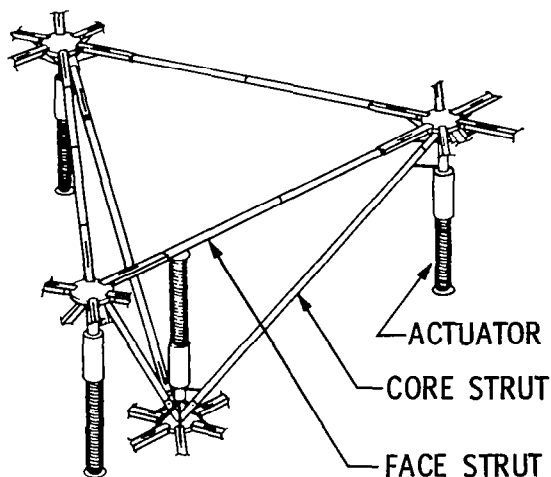
SYNCHRONOUSLY DEPLOYABLE TRUSS ANTENNA

This figure depicts various mechanical and functional features of the synchronously deployable truss antenna. Achievement of the maximum single module diameter requires the use of slender struts. Higher frequency operation requires a surface enhancement system to reduce mechanical deviation from the desired shape.
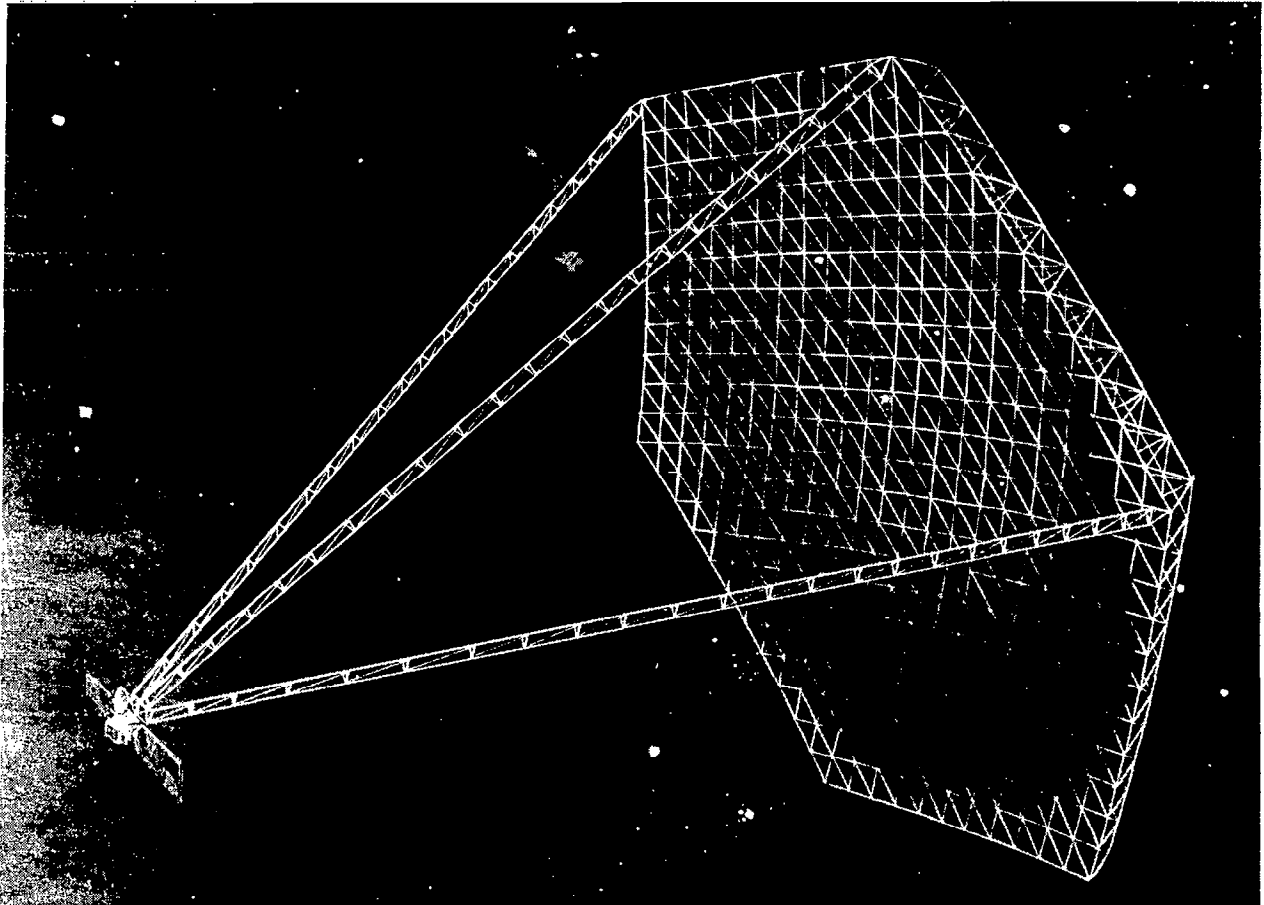
INFLATABLE PARABOLIC REFLECTOR ANTENNA

The basic concept, based on combining a rigidizing torus with a parabolic shaped and conical shaped membrane, is intended for antennas from 10 to 1000 meters in diameter. The limiting factor for launching such a large antenna structure is the STS payload weight limit. For example, a stowed 1000-meter-diameter inflatable antenna would utilize less than half of the STS payload compartment, but would use most of its payload weight capability.

- UNIQUE FEATURES OF CONCEPT
    - DEPLOYMENT BY INFLATION OF THIN FILM
    - SELF-RIGIDIZING STRUCTURAL ELEMENTS
    - MEMBRANE SHAPE MAINTAINED BY INTERNAL PRESSURE
    - LOW WEIGHT AND EXCELLENT MECHANICAL PACKAGING EFFICIENCY
    - INTENDED FOR ANTENNAS UP TO 1000 METERS FOR RF OPERATION
      (10 GHz AT 10 METERS AND LOWER FREQUENCIES AT LARGER SIZES)

- CONCEPT LEVEL OF MATURITY
    - SPACE FLIGHT EXPERIENCE WITH ECHO SERIES
    - CONFIGURATION DESIGNS FOR SIZES UP TO 1000 METERS
    - INFLATABLE AND SELF-RIGIDIZING COMPONENTS BUILT AND EVALUATED
    - ANALYTICAL PERFORMANCE PREDICTION MODELS
    - THREE-METER ANTENNA MODEL PRODUCED 0.76 mm rms SURFACE

- CONCEPT DEVELOPMENT STATUS
    - UNDER DEVELOPMENT BY L'GARDE, INC.
    - INTERIM NASA FUNDING
    - FIFTEENTH-METER GROUND TEST MODEL 2 YEARS DEVELOPMENT TIME
    - SIXTY-METER FLIGHT TEST MODEL 3 YEARS DEVELOPMENT TIME
    - THREE-HUNDRED-METER OPERATIONAL ANTENNA 3-5 YEARS DEVELOPMENT TIME

BASELINE INFLATED ANTENNA CONFIGURATION

The baseline configuration shown is the basis of the current design and is applicable for a variety of antenna sizes using the film thicknesses shown. Large microwave space antennas that are shaped and maintained by gas pressure have many advantages. They are not susceptible to launch vibrations and acoustics, and they have excellent on-orbit dynamics. Large antennas can be placed into space without extravehicular activity. Typically, inflatables have a low cost for both development and production. Gas pressure attempts to perfect bodies of revolution, enhancing accuracy in the presence of thermal distortions or manufacturing inaccuracies.

Inflatable antennas have low weight and package volume. Overall system cost is reduced substantially if fewer Shuttle launches are required to put a large system into orbit.

For inflatables, the reliability of release mechanisms is high because of the simplicity of such mechanisms and the large forces available. The advantages of inflatable antennas in dampening out oscillations led L'Garde to assign a, low error in positioning. Inflatable structures have demonstrated highly reliable erection.

Fully inflated antennas can be subjected to accurate ground electronic testing. Zero-g environment can be simulated through the use of helium. Such an antenna would have to be designed to a higher pressure than that desired for space.

FEED LOCATION

INFLATED CONE
0.006-mm FILM

FOCAL LENGTH

H_2O INFLATANT
0.001 Pa PRESSURE

SELF-RIGIDIZING TORUS
t = 0.066 mm COMPOSITE

INFLATED PARABOLOID
0.006-mm VDA FILM
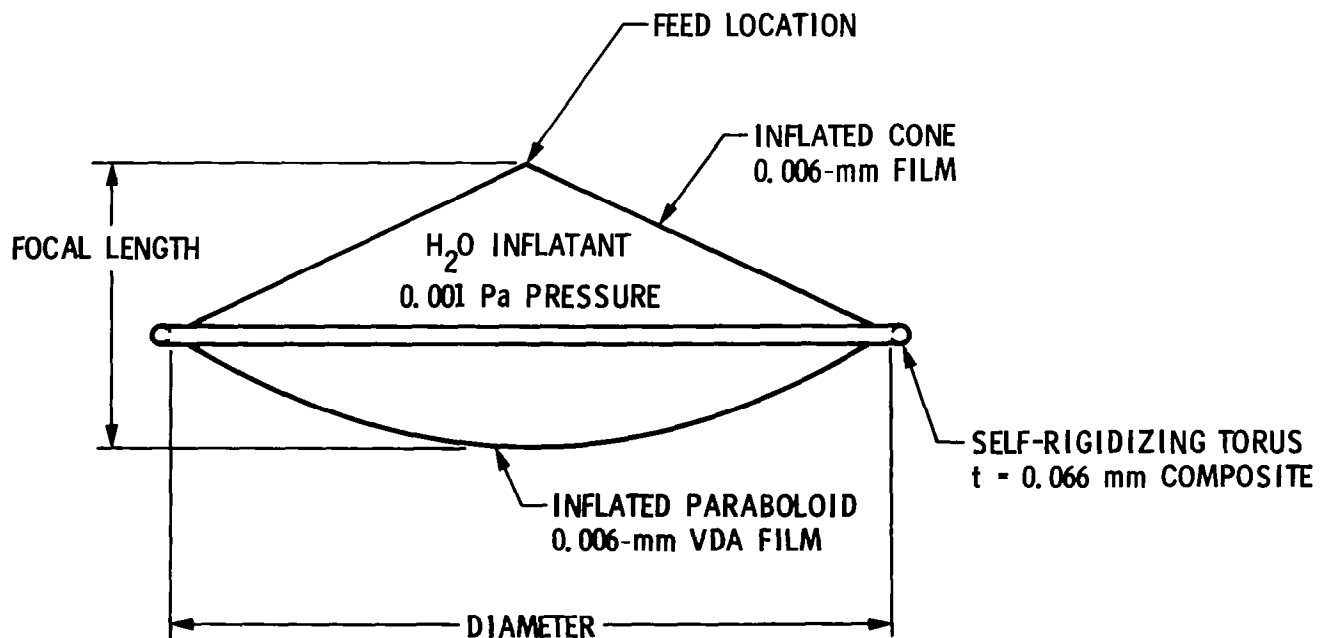
DIAMETER

THREE-METER INFLATED PARABOLIC ANTENNA

A 3-meter-diameter parabola was constructed from polyester thin film. It had a 3-meter design focal length, and was constructed of gores held together with 0.013-mm by 19-mm polyester tape and heat-sensitive adhesive. The paraboloid was inflated to 2-3 mm H_2O differential pressure. It was constructed of 32 gores of 0.006-mm polyester film coated with about 2×10^{-5} mm of vapor-deposited aluminum (VDA).

Accuracy was determined with the help of a laser test set-up. The local angles of a set of horizontal points about 680 mm below the paraboloid center were measured. The shape of this line was then determined by numerical integration. It was determined that the accuracy of these data points with respect to a best-fit parabolic shape was 0.76 mm rms. This indicates that the inflated antenna can be used at wavelengths on the order of 10 mm or more. A sensitivity study was conducted which showed that internal pressure, film thickness or film elastic modulus could change by +20% and still handle 10 mm-wavelengths. Such parameters could change by +50% and still accurately receive/transmit 30-mm wavelengths without any need to adjust the feed location.
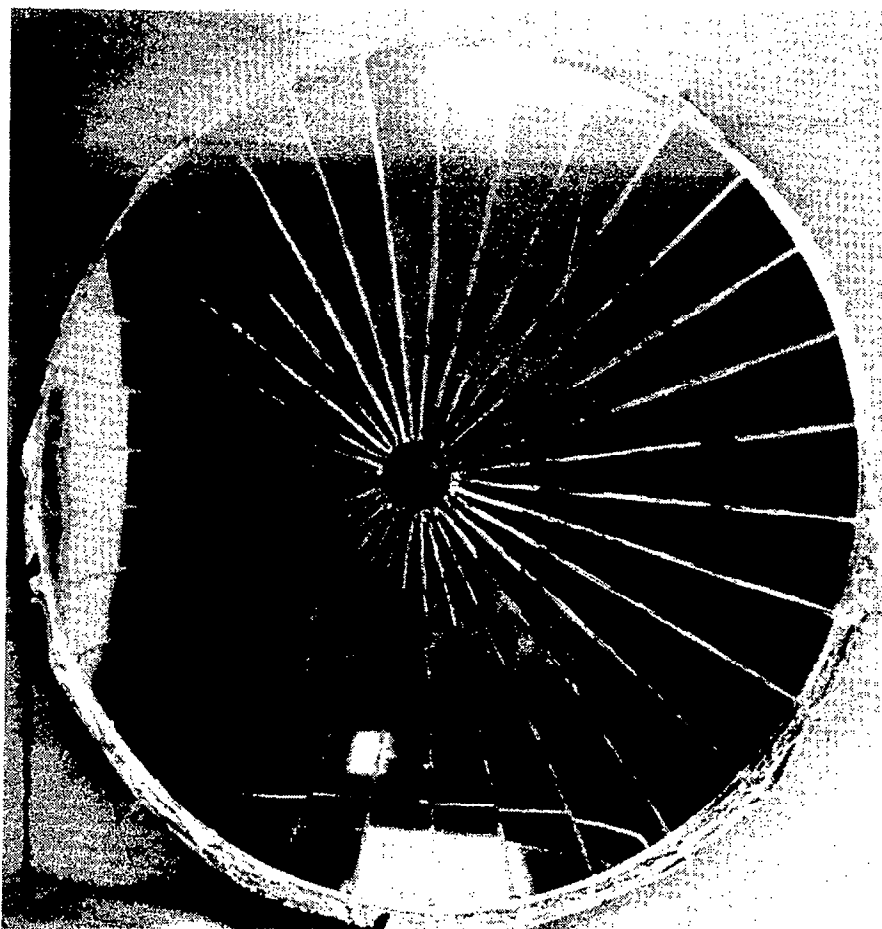
ELECTROSTATICALLY FIGURED MEMBRANE REFLECTOR

The MIT Electrostatically Figured Membrane Reflector (EFMR) Program combines closely coupled fundamental theoretical and experimental research on electromechanics and control systems in the development of very large low-mass high-precision space-based reflecting antennas. The program was first funded in January 1978 by the U. S. Joint Services Electronics Program. Since September 1980 the program has been supported by the Lockheed Missiles and Space Company.

- UNIQUE FEATURES OF CONCEPT
    - CONTINUOUS LOW-MASS MEMBRANE REFLECTING SURFACE
    - HIGH RATIO OF REFLECTOR DIAMETER TO SURFACE TOLERANCE, 10^5 TO 10^6
    - ELECTROSTATIC MEMBRANE FIGURE CONTROL
    - LOW-TOLERANCE REFLECTOR SUPPORT STRUCTURE
    - INTENDED FOR REFLECTORS 30 TO 300 METERS

- CONCEPT LEVEL OF MATURITY
    - ANALYTICAL MODELS FOR MEMBRANE ELECTROMECHANICS
    - DESIGNED CONTROL SYSTEM FOR REFLECTOR FIGURE CONTROL
    - ONE METER MESH MODEL TO VERIFY ANALYTICALLY PREDICTED ACCURACY
    - TWO METER MEMBRANE ANTENNA TO VALIDATE DYNAMIC AND CONTROL MODELS

- CONCEPT DEVELOPMENT STATUS
    - UNDER DEVELOPMENT BY MASSACHUSETTS INSTITUTE OF TECHNOLOGY
    - CURRENTLY FUNDED BY LOCKHEED MISSILES SPACE COMPANY, INC.
    - ADVANCED CONTROL SYSTEM DESIGN DURING 1983
    - ENGINEERING MODEL TO BE BUILT AND TESTED DURING 1984

EFMR FUNCTIONAL SCHEMATIC

The EFMR is specifically designed to permit the construction of self-deployable low-mass antennas with reflector diameters between 30 and 300 meters. For example, a 300-meter EFMR would have a mass of approximately 700 kg.; the complete antenna would have a mass of approximately 3,000 kg. In addition, EFMRs are expected to exhibit a high surface precision, and this should be accomplished with relatively few and simple actuators. In particular, diameter-to-surface tolerance ratios of 10^5 to 10^6 are expected, and this corresponds to antenna beamwidths of 60 to 6 arc seconds and antenna gains of 2×10^8 to 2×10^{10}. Consequently, antennas utilizing EFMR's appear to be well suited to a variety of missions, including terrestrial and space communications, terrestrial remote sensing, radio astronomy, and military missions.

COMPUTER

DEFLECTION, VELOCITY

POSITION

RIGID COMMAND SURFACE

POSITION, VOLTAGE

FLEXIBLE REFLECTOR

MEASUREMENT SYSTEM

CONTROL VOLTAGES

BIAS
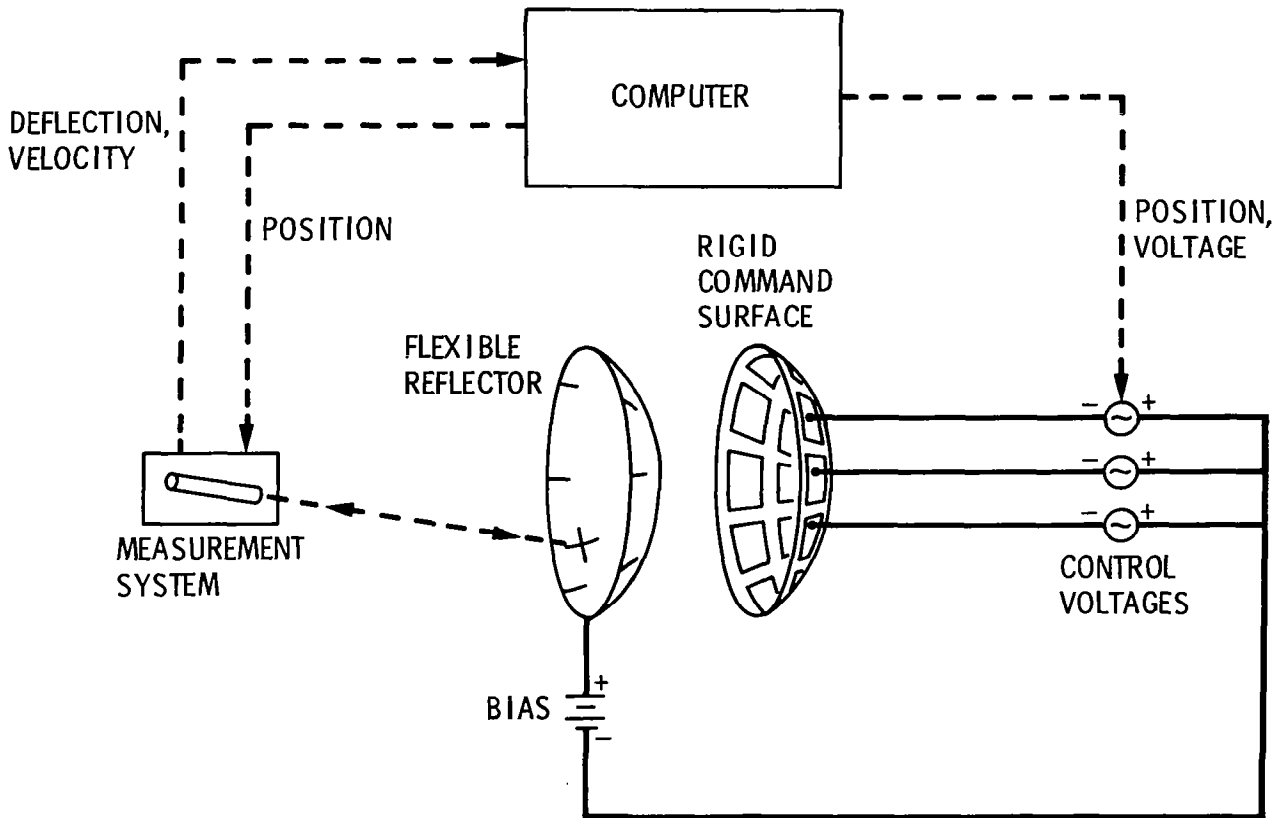
REFLECTOR TECHNOLOGY COMPARISON

The viewgraph is intended to compare the projected performance of the EFMR with well-known ground-based and space-based reflectors. It is interesting to note that the anticipated performance of EFMR's is well beyond demonstrated hardware technology.

1	ARECIBO 305-m
2	PARKS 64-m
3	GOOD 26-m
4	HAYSTACK 37-m
5	HRAO 90-m
6	LEBEDEV 22-m
7A	NRAO 11-m
7B	NRAO 11-m, DOME CLOSED
8	NRAO VLA 24-m
9	OVRO 40-m
10	NASA DSN 64-m
11	CRIMEA 22-m
12	U. TEXAS 4-m
13	MIT 1-m MEMBRANE CONTROL EXPERIMENT
14	BONN 100-m
15A	OVRO 10-m
15B	OVRO 10-m, ULTIMATE GOAL
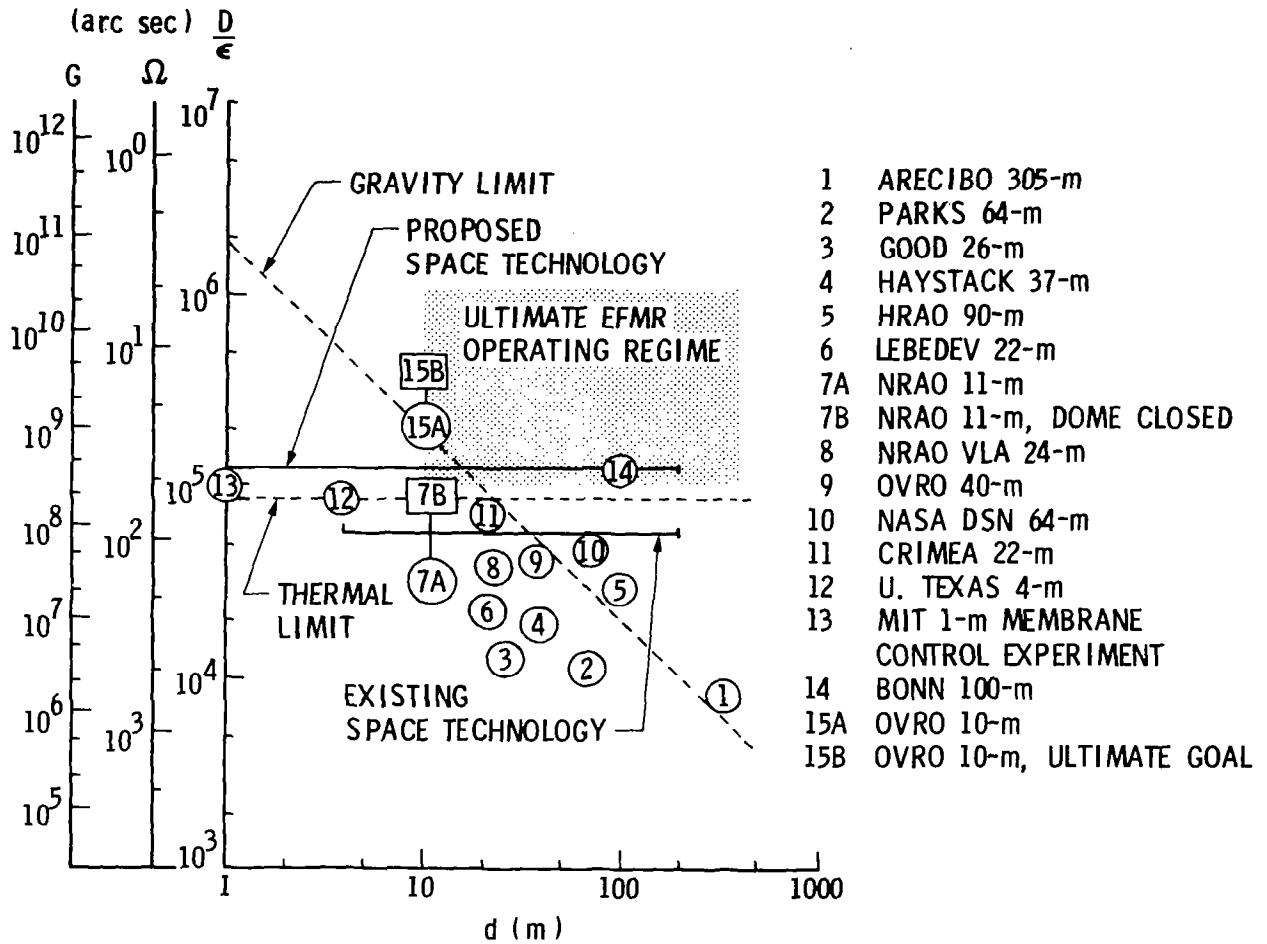
PRECISION DEPLOYABLE ANTENNA

This deployable antenna concept provides a large, lightweight, precision contour parabolic reflector. The design is applicable to multibeam configurations. The reflector is constructed of graphite/epoxy facesheets and aluminum core sandwich to provide an extremely lightweight reflector. The center section is a one-piece honeycomb sandwich construction. The folding panels are rigid honeycomb sandwich. The main panels hinge from a support ring under the center section. The two intermediate panels lie between the main panels, and are connected to the main panels and to each other with two or more hinges. The hinges have adjustable stops to locate the panels accurately in the deployed configuration. Springs are used in the hinges to drive the panels to the deployed position. Adjacent inboard hinges of the main panels are interconnected with a compound universal coupling to insure synchronization of all panels during deployment. The deployment rate is controlled by a geared motor.

A full-scale 10.0 meter model development has now been undertaken to demonstrate the manufacturability, kinematics, and reliability of the proposed design. In the first year of the study, 1980, a mechanical design was established and detailed manufacturing drawings were prepared. In 1981, the tooling concept was definitized, the tooling was designed and major lay-up tooling for panel fabrication was designed. In 1982, the reflector fabrication was initiated.

- UNIQUE FEATURES OF CONCEPT
  - PRECISION ELEMENT REFLECTOR
  - NEAR CONTINUOUS REFLECTOR SURFACE
  - AXISYMMETRIC OR OFFSET CONFIGURATION
  - HIGH DEPLOYED STIFFNESS
  - INTENDED FOR SIZES UP TO 15 METERS FOR RF OPERATION UP TO 60 GHz

- CONCEPT LEVEL OF MATURITY
  - CONCEPT FEASIBILITY BASED ON 2.1-METER DEPLOYABLE MODEL
  - PRELIMINARY DESIGN BASED ON 7.3-METER STRUCTURE
  - FULL SIZE 10-METER DEPLOYABLE DEMONSTRATION UNIT UNDER DEVELOPMENT
  - PERFORMANCE PREDICTION MODELS FOR EACH PHASE OF DEVELOPMENT

- CONCEIVED DEVELOPMENT STATUS
  - CONCEIVED BY TRW
  - INITIAL DEVELOPMENT WITH IR&D FUNDING
  - INTERIM STUDY WITH NASA FUNDING
  - DEMONSTRATION MODEL FUNCTIONAL BY 1984
  - FLIGHT TECHNOLOGY READINESS BY 1986

396

PRECISION DEPLOYABLE ANTENNA

Concept feasibility was demonstrated with a 2.1-m (7-ft.) mechanical model and development of the preliminary design was accomplished for a 7.3-m (24-ft.) diameter precision deployable antenna reflector capable of operation at frequencies up to 60 GHz and above. The antenna design provides RF efficiency of 70%, with a beam pointing error less than 0.04 degree. The estimated 72.5-kg. (160-lb.) weight for this design includes the subreflector, support structure and communication beam autotrack feed package. The deployed natural frequency is estimated at 5 Hz. The mechanical design features graphite/epoxy composite hinged-panel construction. The design is capable of withstanding conventional or Shuttle launch loads.

30 FOOT DIAMETER DEPLOYABLE SOLID REFLECTOR
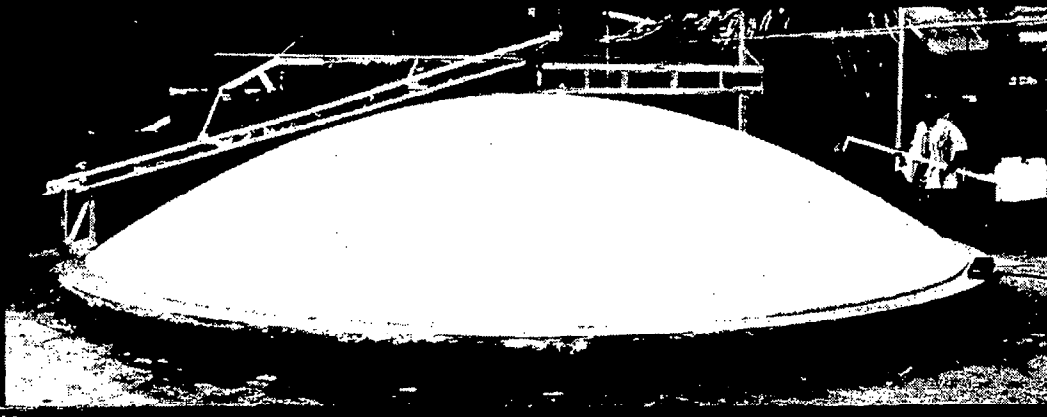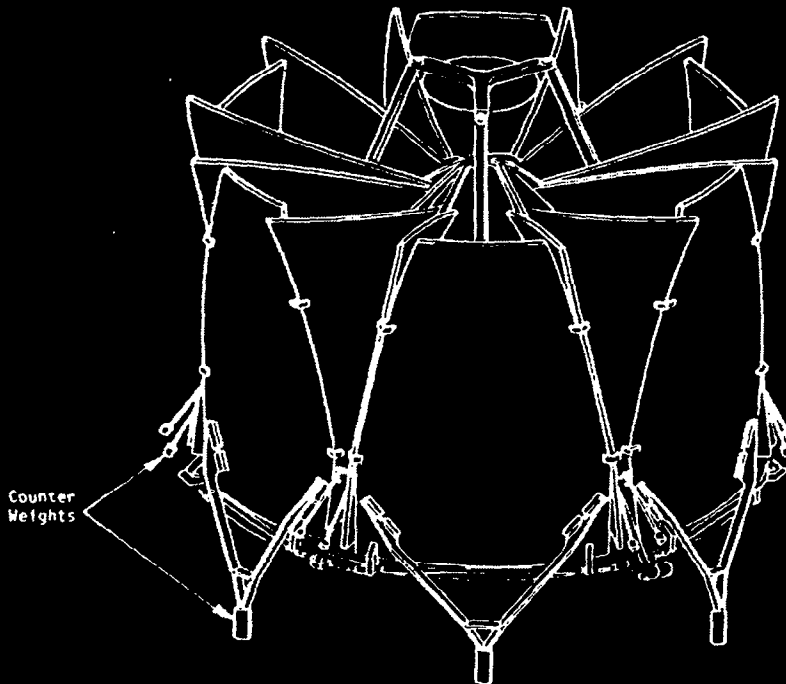
PRECISION DEPLOYABLE ANTENNA

Depicted is a 10-meter precision deployable reflector aboard the Space Transportation System as part of an experiment to demonstrate technology and functional capability for such applications as (a) radio astronomy, (b) advanced communications and (c) radiometry.
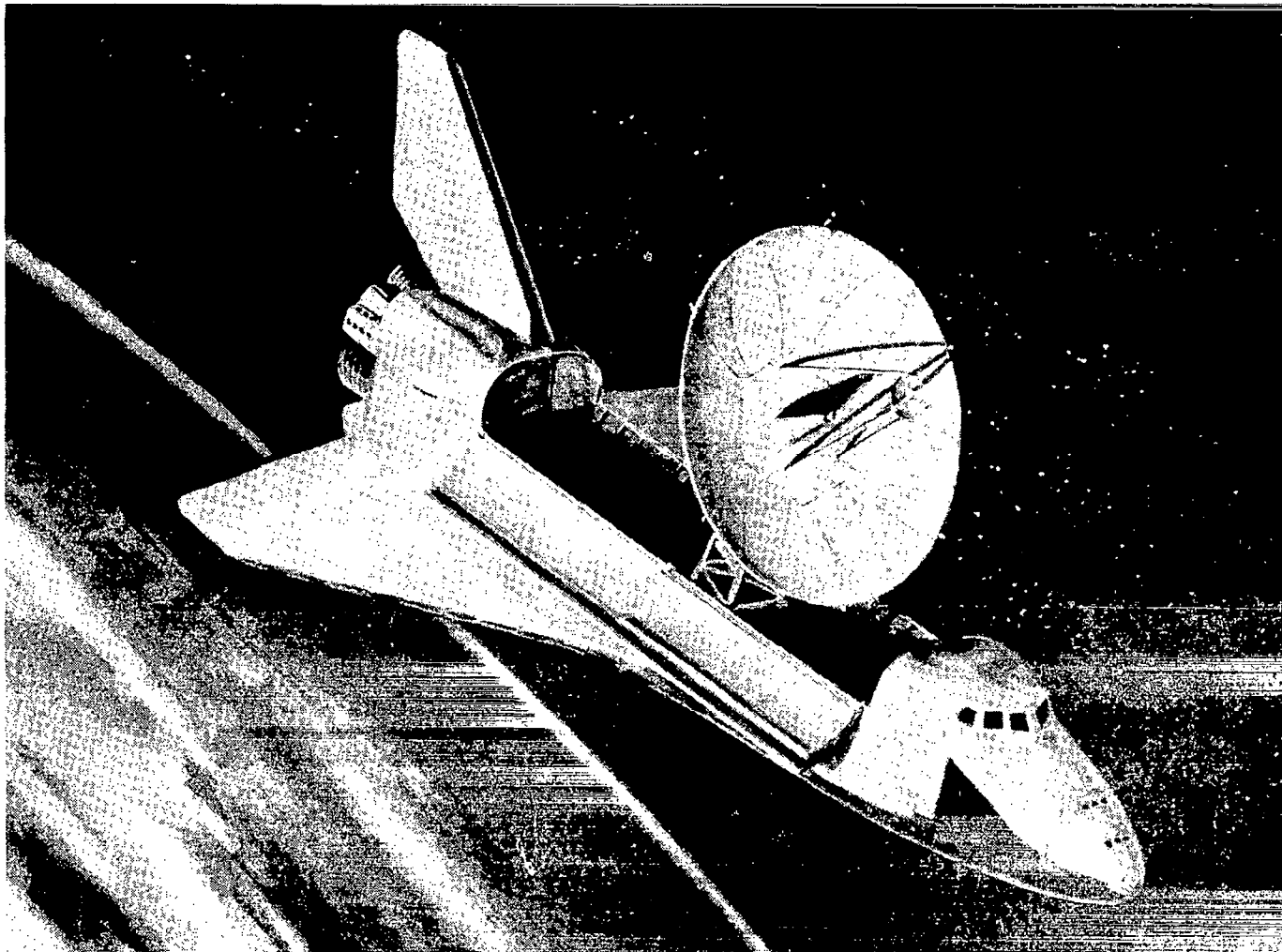
DEPLOYABLE ANTENNA FLIGHT EXPERIMENT ANTENNA

The Deployable Antenna Flight Experiment (DAFE) Antenna was developed by the Harris Government Systems Division for applications such as communications, radar, radiometry, and interferometry. This concept maintains stiffness through all stages of deployment. It is applicable to both axisymmetrical and offset configurations. The concept development benefited extensively from technology developed by the TDRSS and LSST programs. The configuration is essentially a radial rib structure to which additional members have been added to convert ribs into trusses. However, the rib segments for this concept are straight. This concept is intended for antennas up to 50 meters and possibly larger.

- UNIQUE FEATURES OF CONCEPT
  - HIGH DEPLOYED STIFFNESS ACCOMMODATES EDGE MOUNTING
  - GOOD MECHANICAL PACKAGING EFFICIENCY
  - CONTROLLED DEPLOYMENT SEQUENCE
  - UNBLOCKED APERTURE
  - INTENDED FOR ANTENNAS UP TO 50 METERS

- CONCEPT LEVEL OF MATURITY
  - UTILIZES TDRSS AND LSST MECHANISMS TECHNOLOGY
  - BASED ON TDRSS AND HOOP/COLUMN SURFACE SHAPING STRUCTURE DESIGNS
  - KINEMATIC RIB MODEL FOR 10-METER STRUCTURE
  - ANALYTIC PERFORMANCE PREDICTION MODELS

- CONCEPT DEVELOPMENT STATUS
  - CONCEIVED BY HARRIS GOVERNMENT SYSTEMS GROUP
  - DEVELOPED WITH NASA AND IR&D FUNDING
  - FLIGHT TECHNOLOGY READINESS BY 1986

DAFE ANTENNA CONFIGURATION

The DAFE antenna structure consists of radial segmented ribs and circum-ferential cords that structurally link the ribs together. The upper compressive portion of the ribs is segmented to allow accordian-type folding. Vertical rib elements extend from appropriate mid-rib joints to the lower tensioned members of the rib to complete the truss arrangement. The configuration combines the superior performance of the radial rib antenna with the efficient packaging of a folded truss.

RIBS – RADIAL ARTICULATING TRUSS MEMBERS PROVIDE SUPPORT FOR THE MESH

RF REFLECTIVE SURFACE – GOLD PLATED MOLYBDENUM MESH IS SHAPED BY CIRCUMFERENTIAL CATENARIES (SIMILAR TO TDRSS)

HUB – AN INTERFACE FOR THE RIBS AND A HOUSING FOR THE CENTRAL DEPLOYMENT SYSTEM
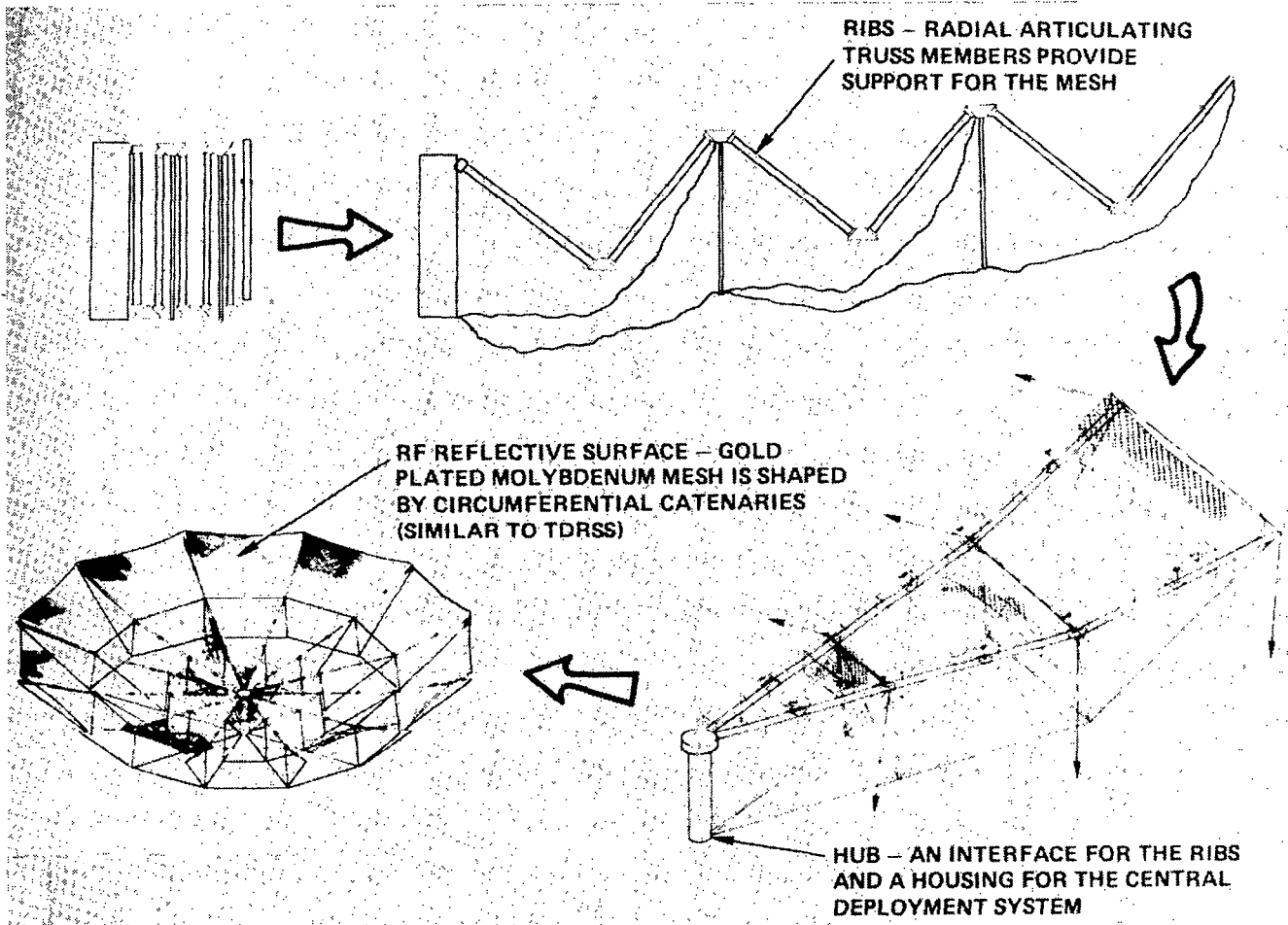
DAFE ANTENNA

The antenna concept shown below was developed by Harris Corporation to meet the requirements of the NASA MSFC Deployable Antenna Flight Experiment (DAFE) for a 50-meter single offset antenna. The truss type structure provides high stiffness and is naturally adaptive to edge-mounted feed configurations.

By virtue of the similarity between the DAFE concept and the radial rib configuration, several desirable features are evident. Deployments are synchronous and rate controlled by a central deployment mechanism. The surface design is very similar to that of the radial rib; therefore, the technologies developed on the radial rib are applicable for DAFE.
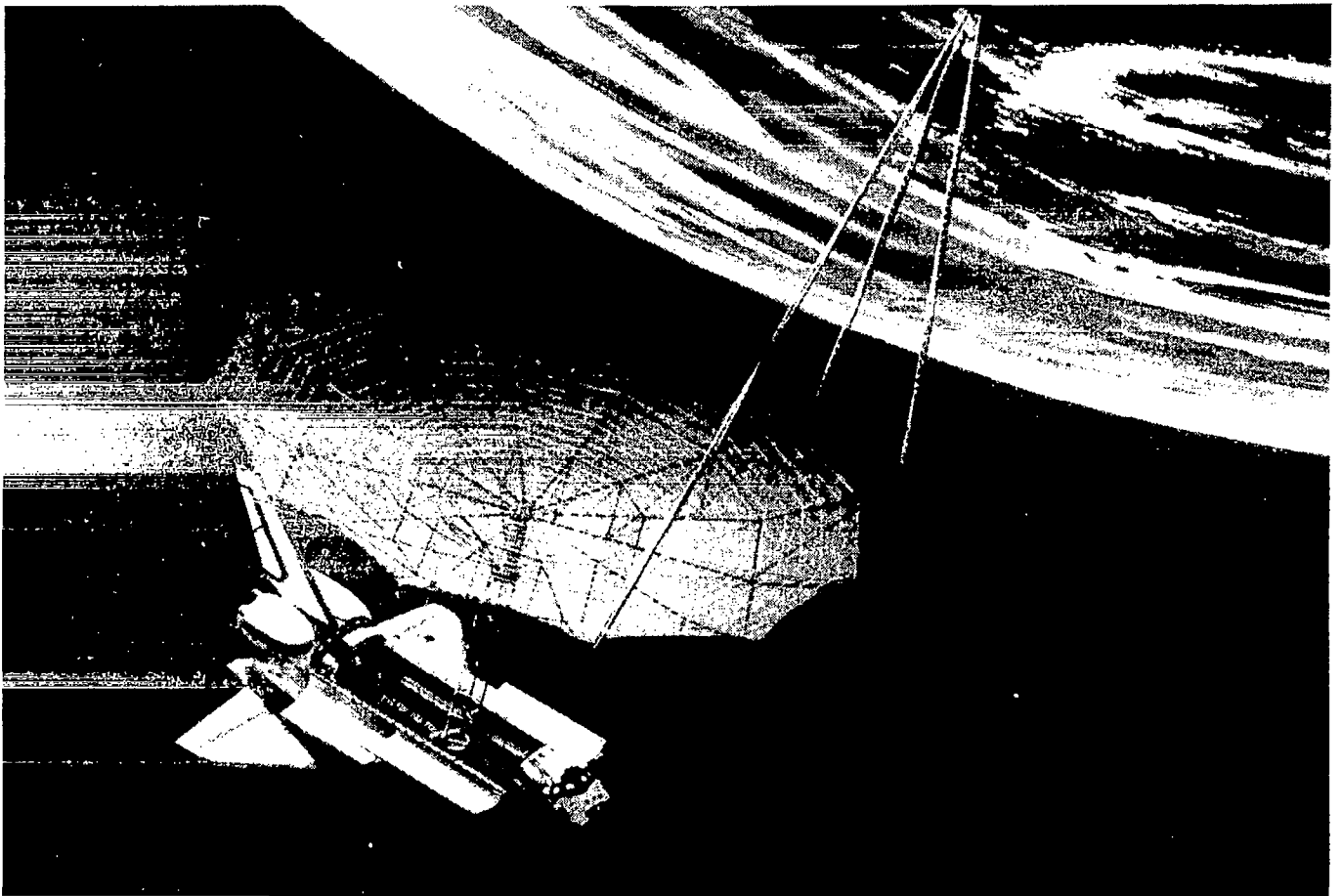
DEPLOYABLE BOX TRUSS ANTENNA

Martin Marietta is developing a deployable box truss structural system applicable to flat and curved antennas, platforms and beams. Originally proposed for the Air Force's On-Orbit Assembly program, the system is currently being developed with prototype beam and truss segments. The system features compact, stowable, step-by-step deployment, high deployed precision, convenient payload attachment points, and adaptability to a wide variety of structural configurations. One STS orbiter will be able to deliver either a truss 300 meters in diameter by 15 meters deep or a beam 3300 meters long, 15 meters high, and 15 meters deep to low Earth orbit.

- UNIQUE FEATURES OF CONCEPT

  - BASIC BOX TRUSS CUBE USES REPETITIVE ELEMENTS

  - HIGH DEPLOYED STIFFNESS

  - ACCOMMODATE MODULAR SPACE CONSTRUCTION

  - INTENDED FOR STRUCTURES UP TO 250 METERS FOR RF OPERATION UP TO 18 GHz AT 15 METERS AND 1 GHz AT 250 METERS

- CONCEPT LEVEL OF MATURITY

  - CONFIGURATION DESIGN FOR SIZES UP TO 250 METERS

  - DETAILED DESIGN FOR ALL CRITICAL COMPONENTS

  - DEVELOPED 4.5-METER DEPLOYABLE GRAPHITE CUBE MODEL

  - FIFTEEN METER, HALF SCALE, DEPLOYABLE ANTENNA TO BE COMPLETED DURING 1983

- CONCEPT DEVELOPMENT STATUS

  - CONCEIVED BY MARTIN MARIETTA DENVER AEROSPACE

  - DEVELOPED WITH IR&D, DoD AND NASA FUNDING

  - DEPLOYABLE/RESTORABLE BEAM APPROPRIATE FOR FLIGHT EXPERIMENT

  - FLIGHT TECHNOLOGY READINESS BY 1987 - 1988

BOX TRUSS FUNDAMENTAL BUILDING BLOCK

The fundamental building block of the structure is a deployable frame consisting of two equal-length structural members ("verticals"), two structural members hinged in the middle ("surface tubes") that connect the ends of the verticals and fold inward to stow between the adjoining verticals, and telescoping diagonal braces that lie in and control the shape of the deployed frame. Such frames were combined to form a kinematic scale-model parabolic reflector. The first dynamic model of a box truss cube utilized foreshortened graphite/epoxy tubes with tube diameters and aluminum fittings sized for cubes up to 8 meters across. Subsequent prototype hardware is being fabricated with all-composite tubes and fittings. Low cost manufacturing processes are being developed for all repetitive components.

The shape and stiffness of a box truss beam, antenna or platform are controlled by the diagonal tension braces in each frame face. The diagonals are multi-ply graphite/epoxy tapes that telescope for stowage and deployment. Both diagonal tapes in each frame face can lie flat in the plane of the frame, thereby equalizing solar input to the two tapes and minimizing thermal distortions.
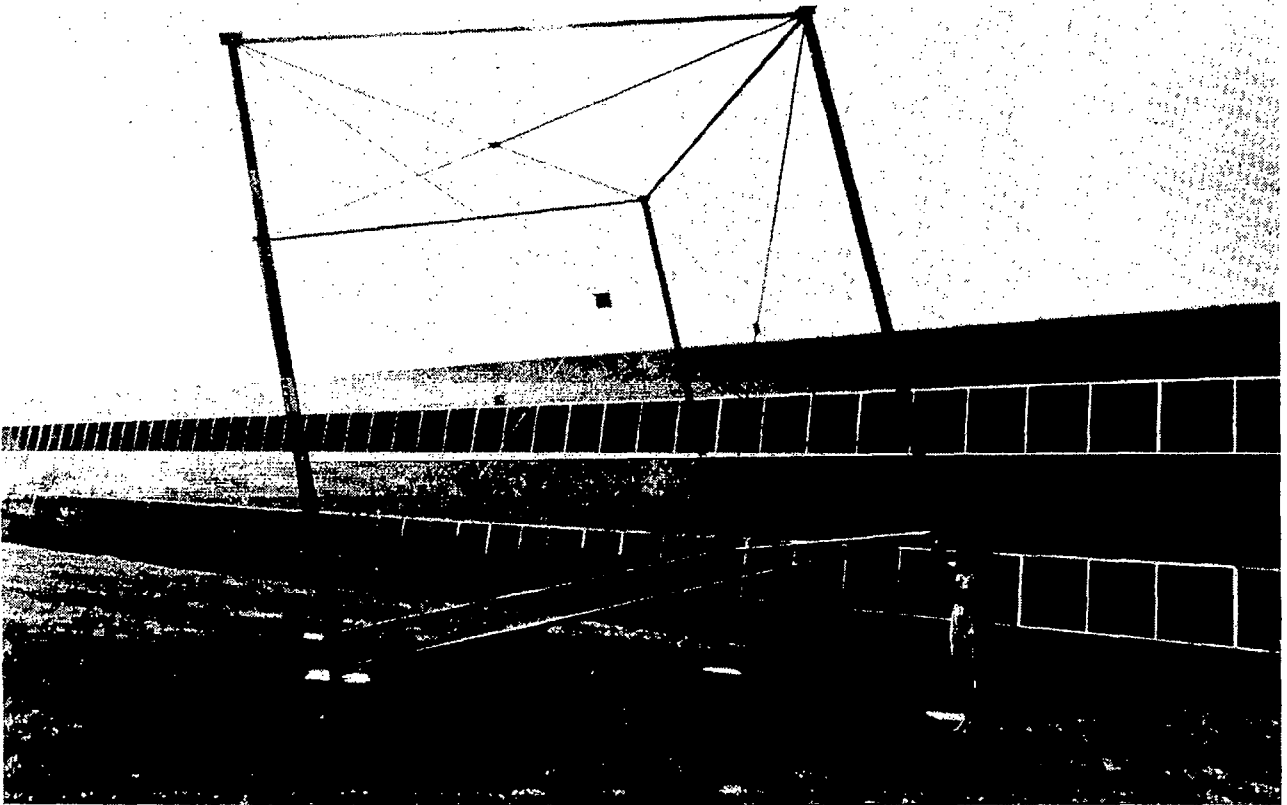
STOWED BOX TRUSS

A key feature of the truss is the hinge/latch in the middle of each folding surface tube. All moving parts are in the hinge/latch interior. This eliminates proturberances that could interfere with the diagonal braces or an antenna surface during deployment. Redundant coil springs in the hinge are sized to produce the desired deployment rate. A separate spring-driven over-center latch engages when the deploying tube is approximately 10^0 from full deployment. The latch spring is sized to meet diagonal brace and antenna surface tensioning requirements. A redundant mechanical catch functions in parallel with the over-center latch.

Deployment is accomplished in a controlled sequence of steps. Beams are deployed one cube at a time and trusses are deployed one row of cubes at a time. In the latter case, the steps are accomplished in a preselected sequence in the two orthogonal deployment directions. This type of deployment is compatible with flat, cylindrical and parabolic trusses and virtually any beam shape. Cylindrical trusses and circular beams can be implemented readily using unequal-length surface tubes in each frame.
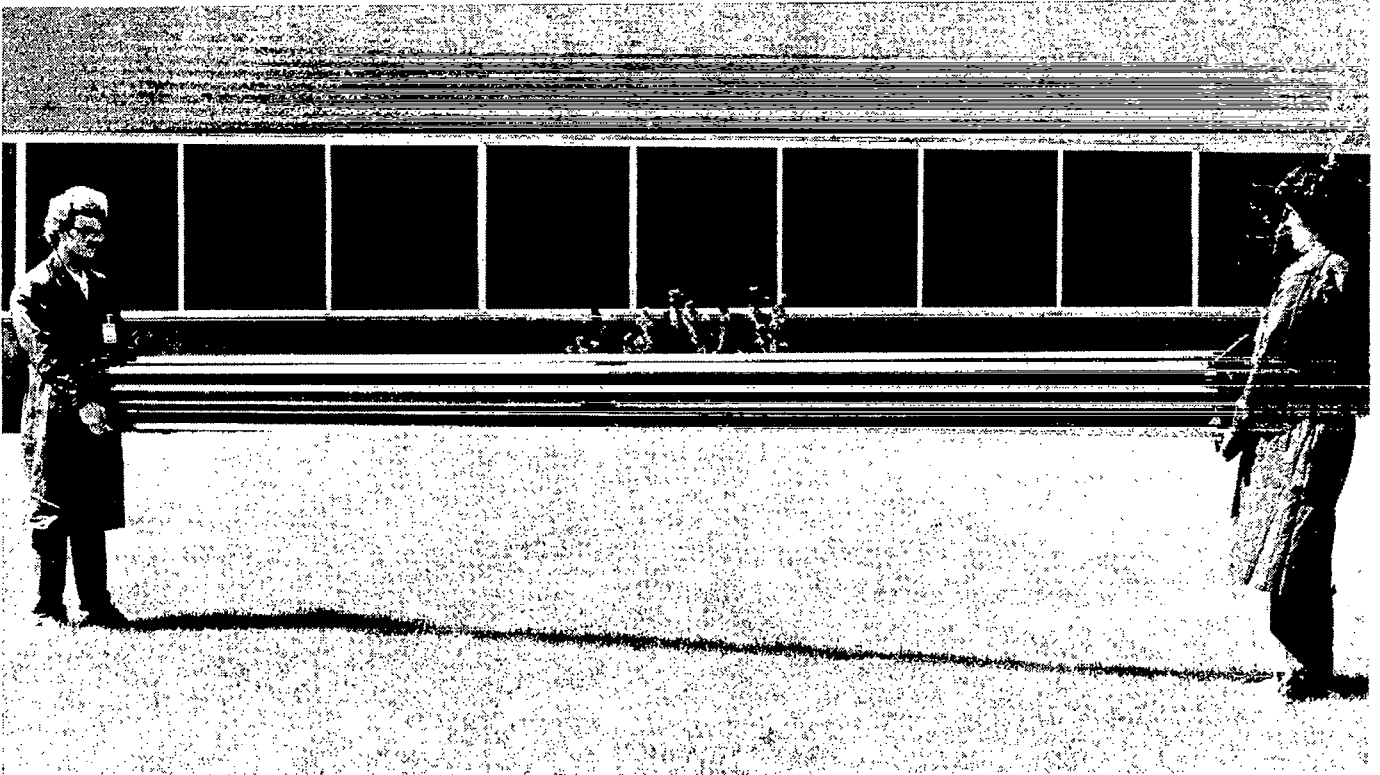
ACTIVE PHASED-ARRAY LENS ANTENNA

The active phased-array lens antenna concept for self-deployable antennas is under development by the Grumman Aerospace Corporation. The basic mechanical concept was evaluated and demonstrated with a 2-meter kinematic deployment model. Preliminary designs were developed for 50- and 70-meter antennas. Functional models were built for all critical electronic components as well as for a 3-meter prototype phased-array aperture membrane. The concept is intended for antennas up to several meters in diameter for RF operation at gains of up to 84 dB.

- UNIQUE FEATURES OF CONCEPT
  - WIDE-ANGLE ELECTRONIC BEAM SCAN CAPABILITY
  - ACTIVE RF AMPLIFIERS THROUGHOUT APERTURE
  - EXCELLENT MECHANICAL PACKAGING EFFICIENCY
  - REMOTE-CONTROLLED BEAM POSITION
  - INTENDED FOR ANTENNAS UP TO 600 METERS FOR POTENTIAL GAINS OF 84 dB

- CONCEPT LEVEL OF MATURITY
  - TWO METER KINEMATIC DEPLOYMENT DEMONSTRATION MODEL
  - PRELIMINARY DESIGNS FOR 50- AND 70-METER ANTENNAS
  - THREE METER PROTOTYPE PHASED ARRAY APERTURE MEMBRANE MODEL
  - FUNCTIONAL MODELS OF ALL CRITICAL ELECTRONIC COMPONENTS

- CONCEPT DEVELOPMENT STATUS
  - CONCEIVED BY GRUMMAN AEROSPACE CORPORATION
  - INITIALLY DEVELOPED WITH IR&D FUNDING
  - TRANSMITTER AND RECEIVER PHASE SHIFT MODULES UNDER DEVELOPMENT BY DoD
  - FLIGHT TECHNOLOGY READINESS REQUIRES 3 YEARS DEVELOPMENT

ACTIVE PHASED-ARRAY LENS ANTENNA

The basic concept is based on a "wire-wheel" type support structure for the aperture and an Astromast to support the antenna feed. The basic elements of the aperture include the hub, rotating drums, gores, rim members, and upper and lower stays. The gores, which are made up of the dipoles and the ground planes, wrap around the drum structure. The compression rim assembly is located and supported about the drum by the upper and lower radial stays that extend from reels located on the drum assembly. An Astromast, which locates and supports the antenna feed system, interfaces with the hub structure along the antenna axis.
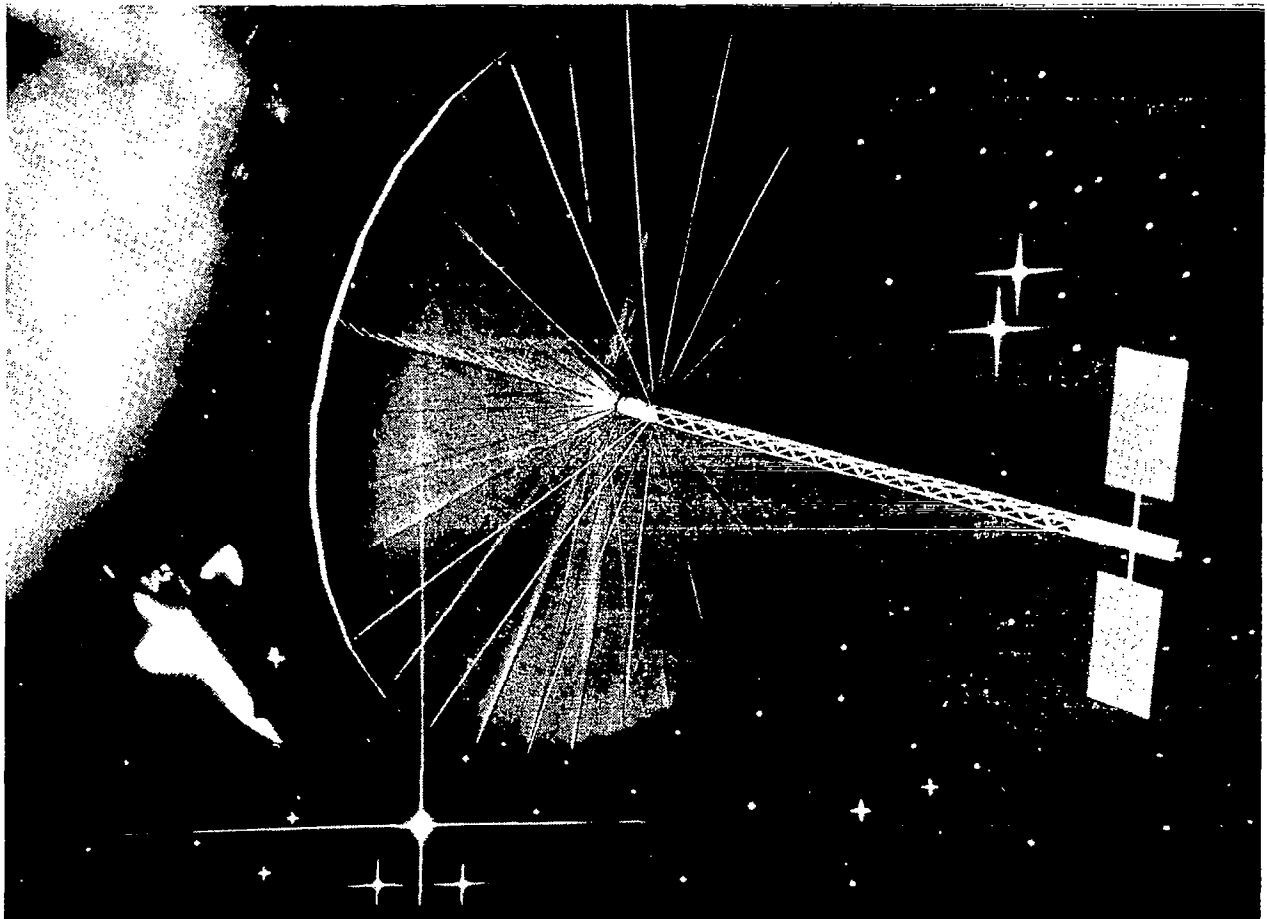
ACTIVE PHASED-ARRAY LENS ANTENNA DEPLOYMENT

Deployment of the structure is initiated by extending the Astromast and then deploying the aperture. Aperture deployment is powered by synchronized electric motors that open the rim hinges, causing the rim to unfold and move radially outward. The rim members pull on the gore panels, causing them to unroll from the central revolving drum. Simultaneously, the rim-hinge assemblies draw the stays from revolving upper and lower stay reels. Both the drum and the stay reels revolve about a central hub. Stalled AC induction motors between the drum and the hub and between the stay reels and the hub apply constant torques to these members. Thus, the actual deployment power is provided by the motors in the rim hinges; the hub and stay reel motors are only used to maintain tension in the gores and stays. After the rim has been fully deployed, the hinges are latched against stops by a linkage mechanism which also clamps the hinge joints to remove any play. The tension in the gores and stays is increased by the the drum and stay reel motors, and then the drum and stay reels are locked into place. To retract the structure, the above sequence of events is reversed. The deployment and retraction concepts have been successfully validated with an engineering model.

The stored strain energy of the Astromast provides the capability of self-deployment which can be easily achieved in a controlled way. The deployment rate is governed by a central lanyard which restrains the tip plate; the lanyard is payed out from its spool which is either motor driven or is linked to a viscous rotation damper. The motor-driven spool is the selected method since automatic retraction is required.

DEPLOYMENT AND WRAP-UP
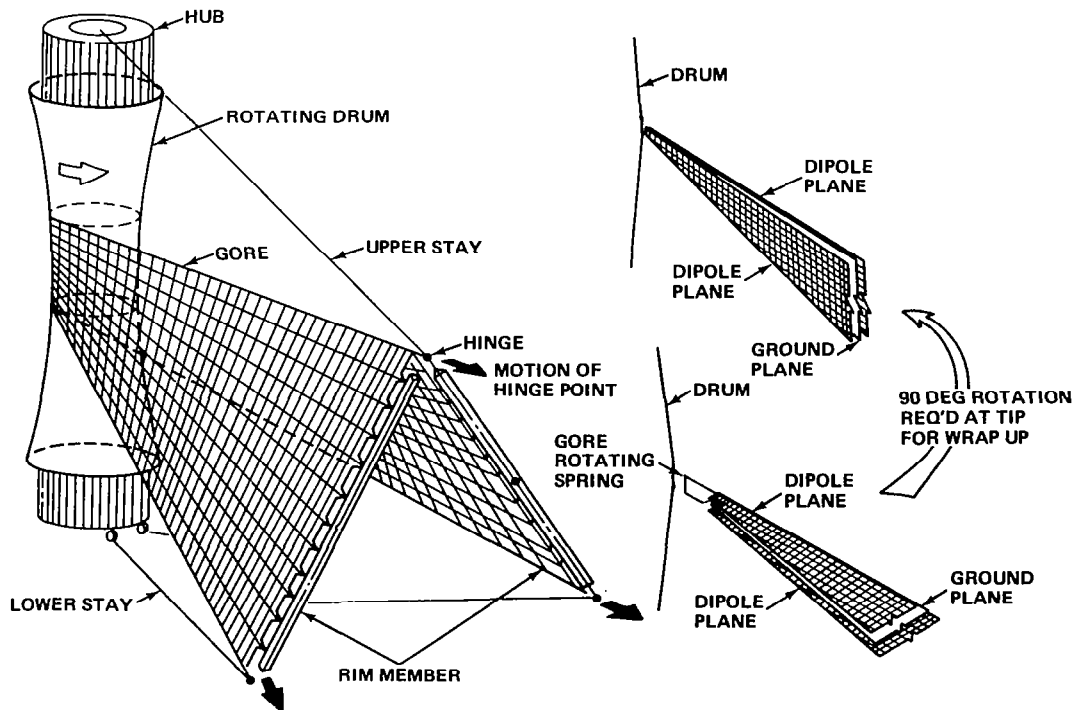
HOOP/COLUMN ANTENNA

The hoop/column antenna design was developed to provide the compact stowage and low reflector area density required by future large space antenna missions. The concept is a simple tension and compression preloaded structure. A central column and a large-diameter hoop are the compression members which maintain pretension in a highly efficient and stable graphite cable network. The cable network supports and contours the delicate RF reflective mesh surface, in addition to making structural contributions.

- UNIQUE FEATURES OF CONCEPT
  - QUAD-APERTURE CAPABILITY
  - EXCELLENT MECHANICAL PACKAGING EFFICIENCY
  - HOOP AND COLUMN ONLY COMPRESSION ELEMENTS IN ANTENNA
  - CONTROL CORDS PROVIDE SYNCHRONIZATION OF MAST AND HOOP DEPLOYMENT
  - INTENDED FOR ANTENNAS UP TO 300 METERS

- CONCEPT LEVEL OF MATURITY
  - HOOP DEPLOYMENT DEMONSTRATED WITH 2-METER MODEL AND LARGE SIZE CRITICAL COMPONENTS
  - DETAILED DESIGN FOR STRUCTURES UP TO 122 METERS
  - SURFACE FORMING STRUCTURE DEMONSTRATED WITH 50-METER STATIC MODEL
  - INITIATED DEVELOPMENT OF 15-METER FUNCTIONAL PROOF OF CONCEPT MODEL

- CONCEPT DEVELOPMENT STATUS
  - CONCEIVED BY THE HARRIS GOVERNMENT SYSTEMS GROUP
  - UNDER DEVELOPMENT BY HARRIS WITH NASA FUNDING
  - FLIGHT TECHNOLOGY READINESS BY 1985

HOOP/COLUMN ANTENNA PROGRAM DEVELOPMENTS

Depicted below are some of the major milestones of the Harris Hoop/Column Antenna Program. The program is moving steadily toward a goal of a flightworthy system by the mid-1980's. This is accomplished by development of large antenna designs, component demonstration models, large-scale test models, and a fully operable 15-meter engineering model.

1981

1982

1980

1983-1984

MAST MODEL

50 METER
SURFACE MODEL

PRELIMINARY
DESIGN

APPLICABLE FOR DIAMETERS
UP TO 122 METERS

15 METER
ENGINEERING
MODEL

HOOP JOINT MODEL

COMPONENT
DEVELOPMENT
MODELS

RF VERIFICATION
MODEL

TEST
MODELS
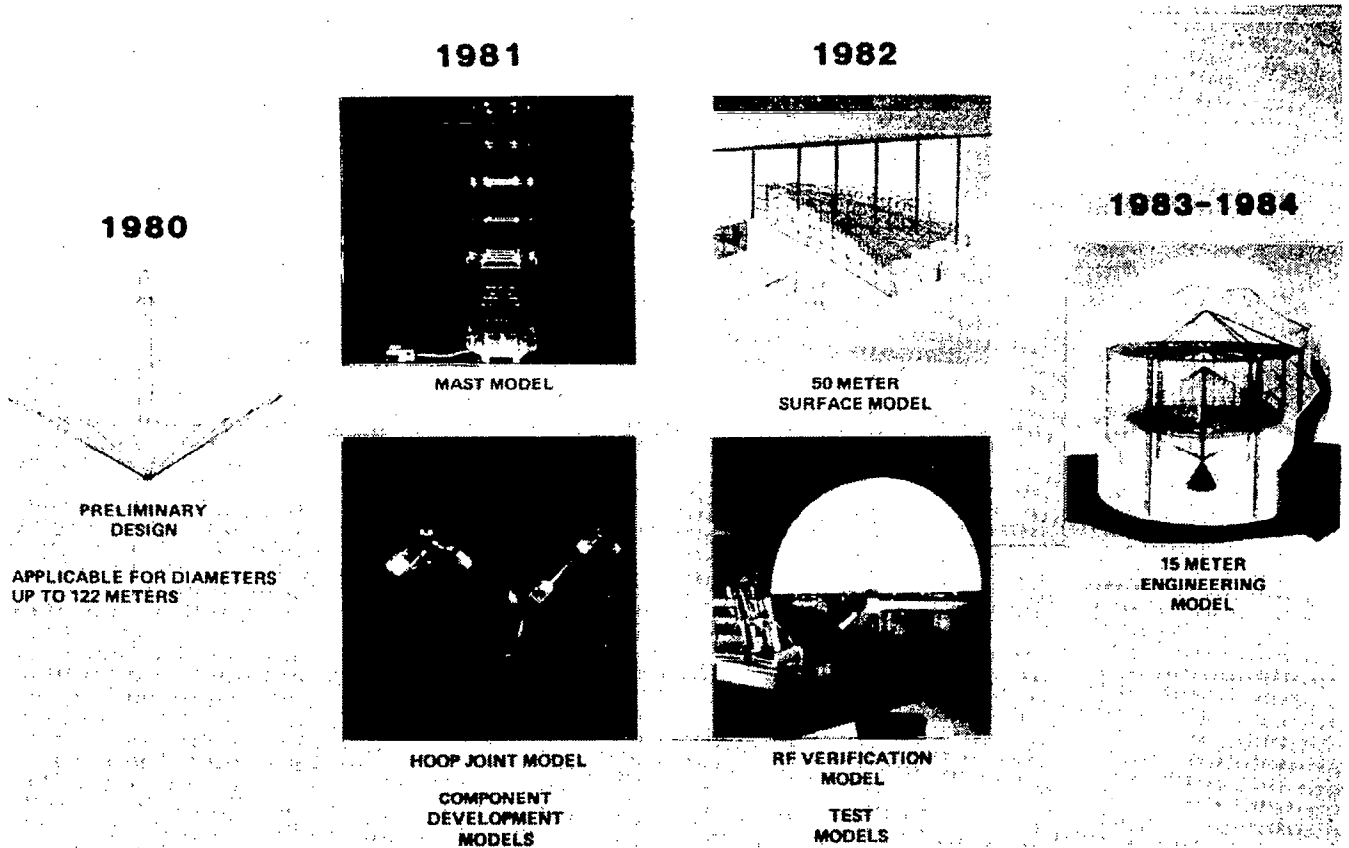
HOOP/COLUMN ANTENNA

Illustrated below are the various stages of a typical hoop/column antenna mission. The first stage is insertion into low Earth orbit by the Space Shuttle. The stowed antenna, spacecraft, and orbital transfer vehicle are then separated from the Shuttle and boosted to geosynchronous orbit where the antenna is deployed and operated. Antenna deployment is initiated by extension of the mast, followed by the controlled synchronized deployment of the hoop.

Identified space-borne focus missions for the hoop/column antenna include *Soil Moisture Radiometer*, *Land Mobile Communications* and *Very Long Baseline Interferometry (VLBI)*.
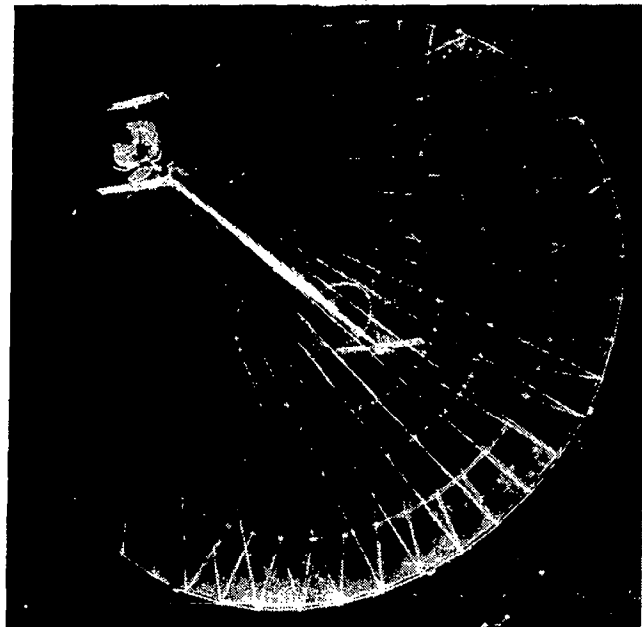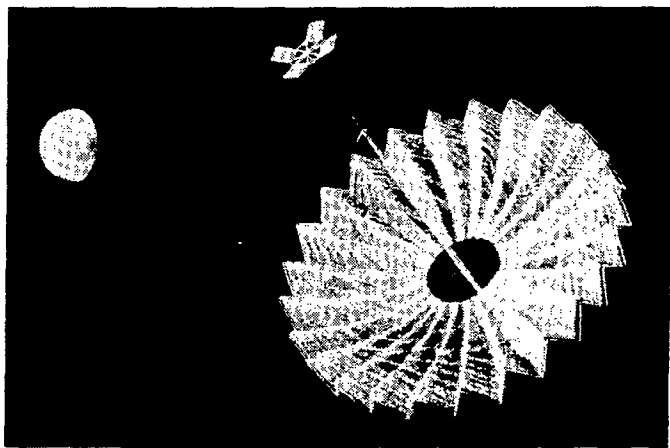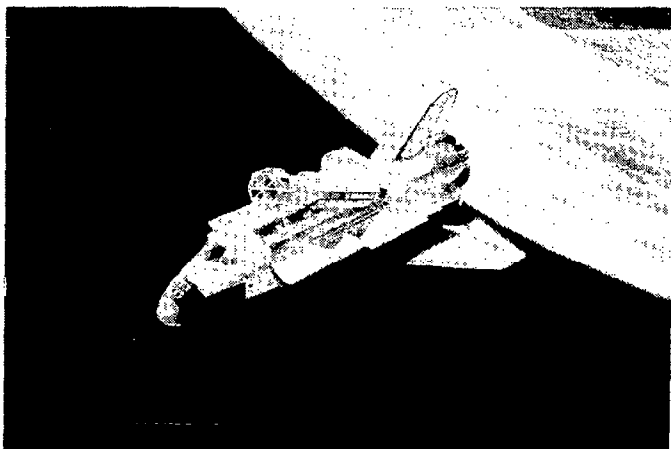
DEPLOYABLE GEO-TRUSS CONCEPT

The General Dynamics Convair Geo-Truss Concept is entering its third
generation of development. The early aluminum antenna models demonstrated
that the mechanisms' concept worked and a viable mesh system could be
integrated into the geo-truss substructure. In the second generation,
thermally stable, lightweight, rigid, graphite components enhanced the
structure. Graphite grid cable and low CTE molymesh enabled the mesh to be
contoured to a 30-GHZ operational level. Refinements in analytical tools,
deployment analysis, transient thermal shadowing interaction, and thermal
distortion models were made to accurately ($\pm$10 - 15%) predict the solar
thermal vacuum simulation performance. Thermal distortion of the reflector
surface using analytical models was predicted to within a $\pm$3.5 mil accuracy.
The stowed reflector, which has been tested with over 150°F thermal grad-
ients throughout the structure, was deployed successfully.

The third evolving generation of geo-truss concepts that can be considered includes
large offset reflectors, multi-reflectors in a common structure and multi-beam
systems with secondary antennas mounted to the periphery of the base
geo-truss. A 500-ft. reflector and a Centaur G Booster can be placed in an
STS payload area.

- UNIQUE FEATURES OF CONCEPT

    - TETRAHEDRAL ELEMENT BASIC BUILDING BLOCK

    - HIGH DEPLOYED NATURAL FREQUENCY

    - DEPLOYMENT MECHANISM INTEGRAL PART OF STRUCTURE

    - ACCOMMODATES MODULAR SPACE CONSTRUCTION

    - INTENDED FOR NUMEROUS APPLICATIONS UP TO 300 METERS; e.g.,
      RF OPERATION OF 1 GHz AT 300 METERS AND EHF AT 30 METERS

- CONCEPT LEVEL OF MATURITY

    - ENTERING THIRD GENERATION OF DEVELOPMENT

    - CONCEPT FEASIBILITY DEMONSTRATED WITH 6-METER ALUMINUM MODELS

    - GRAPHITE 5.5-METER MODELS VALIDATED THERMAL AND DYNAMIC ANALYSIS

    - CONCEPTUAL DESIGN, CRITICAL COMPONENTS AND ANALYTICAL MODELS
      FOR OFFSET ANTENNAS UP TO 200 METERS

- CONCEPT DEVELOPMENT STATUS

    - CONCEIVED BY GENERAL DYNAMICS CONVAIR

    - INITIALLY DEVELOPED WITH NASA FUNDING

    - FLIGHT TECHNOLOGY READINESS BY 1982

411

DEPLOYABLE GEO-TRUSS DESIGN

The basic building block of the geo-truss is the tetrahedron. Multiple tetrahedrons can then be assembled into a large structure as the size and number of tetrahedrons are increased. Weight, diameter and structural frequency of the antenna are a function of the ratio of the depth to the base of the basic tetrahedron.

The geo-truss design is predicated on a fail-safe approach. The weakest link in the structure is the titanium "carpenter tape" curved-leaf spring. Any overload in the structure will buckle this "fused" element and return to shape after the load is gone with no damage to the basic truss. The second level of fail-safe design is in the strut element. If an external load damages or fails an element, an interior Kevlar cable will prevent it from separating and damaging any other element. Since nine elements (six surface and three diagonal) are attached at a common spider, no loss in structural integrity or mesh stability is sustained. As long as three elements hold the spider in position the mesh will retain its contour.

Reproducibility of mesh contour is excellent since the "carpenter tape" drive is a zero-tolerance hinge. The end joints at the diagonal and surface members are tight-tolerance bushings that are taken out of tolerance budget by the mesh grid system (drum head) that bottoms the bushing out in one direction. Mesh grid cables have a 50-lb. capacity with a maximun load in the 12-lb. range so that the cable remains well within the elastic limit.

1ST GENERATION
ALUMINUM 20 MIL RMS

EDGE HELD

SECTION OF REFLECTOR

2ND GENERATION
THERMALLY STABLE GRAPHITE/EPOXY

TDRSS 20 MIL

MULTI-REFLECTOR IN ONE STRUCTURE

3RD GENERATION

LARGE OFFSET

LARGE MULTI-BEAM COMMUNICATION
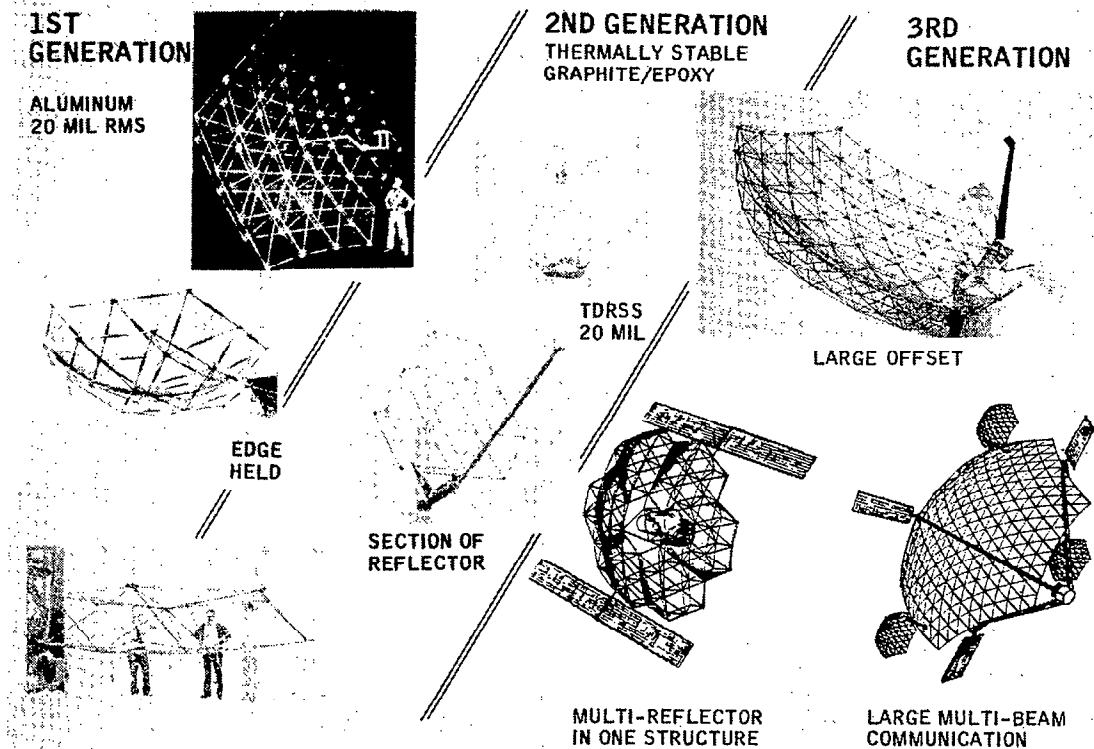
DEPLOYABLE GEO-TRUSS CONCEPT

Deployment is obtained by cutting the bands that hold the top and bottom spiders together in the packaged condition. The carpenter tape springs drive out the structure with full static deployment margin on lockup. No other drive mechanism or motor is required. Rate of deployment is at a moderate walking pace and is completely predictable.

A full computerized deployment will predict loads and position of all elements throughout the deployment cycle. Prediction of strain gage readings matched to within 15% range. Deployment times and position of members were predicted even more accurately. This tool is used to size the carpenter tape hinges to ensure a smooth uniform deployment. Because the energy of the carpenter tapes is known, the deployment loads are highly predictable. In many components, minimum gage thickness of graphite assemblies is the critical design condition.

In GD Convair's several hundred deployment tests, no carpenter tape, "fused", surface members ever failed because of deployment loads. GDC deployment analysis predicts loads throughout every phase of deployment and combines both axial and bending moments at whatever instantaneous deployment intervals are selected. Overlays of analytical computer predictions of deployment closely match frames of the deployment movie.

This basic concept can accommodate a variety of applications, from offset configurations to space platforms and modular space construction.
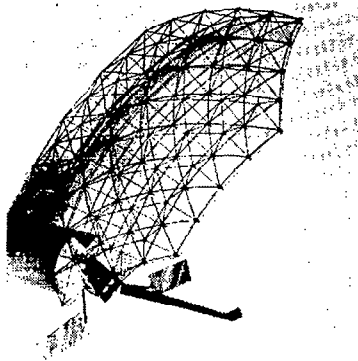
OFFSET COMMUNICATION ANTENNA
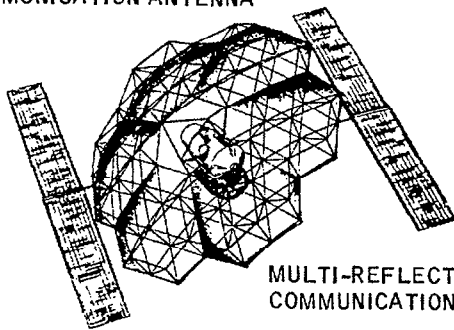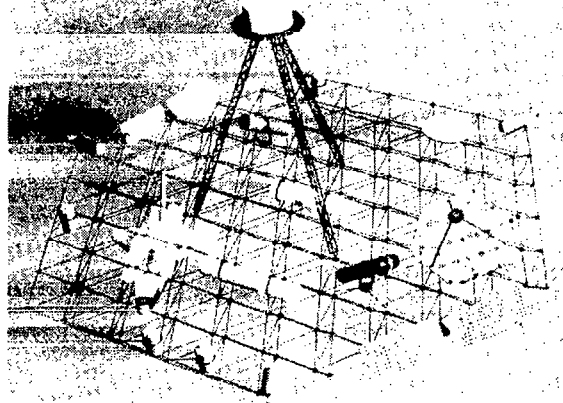
SPACE DOCK
O STABILIZED PLATFORM
O GROWTH SPACE STATION

MULTI-REFLECTOR LARGE
COMMUNICATION ANTENNA

413

RADIAL RIB ANTENNA

The radial rib antenna combines precision surface accuracy with compact packaging. This approach is presently utilized on the Tracking and Data Relay Satellite System operating at S- and Ku-band frequencies, and on the Galileo-Jupiter probe which operates in the S- and X-band range.

The precision surface accuracy of the radial rib antenna is obtained by surface shaping ties which minimize "reverse bulging" inherent in mesh antennas. Highly sophisticated analytical models are also used in obtaining and verifying the high surface accuracy of the TDRSS/Galileo systems.

- UNIQUE FEATURE OF CONCEPT
  - SIMPLE RIB DEPLOYMENT SCHEME
  - SURFACE PRECISION NOT DEPENDENT ON RIB CURVATURE
  - FEED TOWER SUPPORTS STOWED RIBS
  - HIGH DEPLOYED STIFFNESS
  - FIVE METER DIAMETER FOR RF OPERATION UP TO 15 GHz

- CONCEPT LEVEL OF MATURITY
  - TDRSS ANTENNA DERIVATIVE OF EARLY NASA TECHNOLOGY DEVELOPMENT
  - TDRSS FLIGHT ANTENNAS READY FOR FIRST LAUNCH
  - GALILEO ANTENNA MODIFICATION OF TDRSS DESIGN
  - GALILEO FLIGHT ANTENNAS DELIVERED

- CONCEPT DEVELOPMENT STATUS
  - CONCEIVED BY THE HARRIS GOVERNMENT SYSTEMS GROUP
  - INITIALLY DEVELOPED WITH NASA FUNDING
  - FLIGHT HARDWARE TECHNOLOGY DEMONSTRATED ON TDRSS AND GALILEO PROGRAMS

RADIAL RIB ANTENNA CONFIGURATION

The major elements of the radial rib antenna are the hub, ribs, reflective structure, and antenna primary structure. The antenna primary structure is comprised of the support struts, the radome, and the upper support structure.

The hub provides the base ring for the pivot points of the rib as well as the housing for the Mechanical Deployment System (MDS). The MDS employs a ball screw and a carrier with independent linkages to each rib pivot arm. The linear translation of the ball screw mechanism accomplishes a controlled synchronous deployment of the antenna. The energy necessary to deploy the antenna comes from a dual DC motor drive unit.

The ribs, which serve as the structural support for the reflective surface, are curved multi-layup graphite epoxy tubes. In the stowed configuration, the ribs fold around the central feed support system to form a stiff structure for launch.

TIP RESTRAINT

RIB ASSEMBLY – RADIAL TUBULAR GRAPHITE EPOXY MEMBERS PROVIDE SUPPORT OF THE SURFACE

SUBREFLECTOR ASSEMBLY

RADOME ASSEMBLY

RF REFLECTIVE SURFACE

RADOME ASSEMBLY

FEED SUPPORT STRUCTURE - SIX TUBULAR STRUTS AND A RADOME PROVIDE STOWED ANTENNA STIFFNESS AND SUPPORT FOR THE FEED AFTER DEPLOYMENT

MECHANICAL DEPLOYMENT SYSTEM

GOLD PLATED MOLYBDENUM MESH IS SHAPED BY A SERIES OF CIRCUMFERENTIAL QUARTZ CORD CATENARIES

MECHANICAL DEPLOYMENT SYSTEM

DEPLOYED ANTENNA

HUB – CENTRAL STRUCTURE PROVIDES PIVOT ATTACHMENT OF THE RIBS AND HOUSES THE ANTENNA'S DEPLOYMENT SYSTEM

STOWED ANTENNA

RADIAL RIB ANTENNA

GRAPHITE/EPOXY
TUBULAR RIBS AND
MESH SEAM STRIPS

GOLD PLATED
MOLYBDENUM
WIRE MESH

QUARTZ
CONTOURING
CORDS

416

OFFSET WRAP-RIB ANTENNA

The Jet Propulsion Laboratory (JPL) is responsible for the development of the offset wrap-rib deployment antenna concept, which was conceived by the Lockheed Missiles and Space Company (LMSC) of Sunnyvale, CA. The development of the concept and the demonstration of technology readiness with proof of concept hardware models are based on a JPL contract with LMSC. The development of technology requirements and the analytical projection of antenna performance are being accomplished by JPL.

The current ground-based antenna technology development program consists of three major elements: (a) the development of candidate system-level configurations to identify and characterize the subsystem interfaces so they can be accounted for in the antenna conceptual design, (b) the development of the offset wrap-rib antenna concept at LMSC and (c) the development of analytical capability at JPL for the prediction of antenna performance in order to understand the basic concept and determine the concept's potential for different applications.

- UNIQUE FEATURES OF CONCEPT
    - SURFACE QUALITY FUNCTION OF NUMBER OF RIBS AND THEIR PRECISION
    - UNBLOCKED APERTURE
    - SIMPLE REFLECTOR STRUCTURAL DESIGN AND DEPLOYMENT MECHANISM
    - REFLECTOR HAS EXCELLENT PACKAGING EFFICIENCY
    - APPLICABLE FOR NUMEROUS APPLICATIONS UP TO 300 METERS

- CONCEPT LEVEL OF MATURITY
    - FLIGHT PROVEN REFLECTOR DESIGN
    - DETAILED DESIGN FOR STRUCTURES UP TO 100 METERS
    - LARGE SIZE FUNCTIONAL CRITICAL HARDWARE COMPONENTS
    - FUNCTIONAL 55-METER PROOF OF CONCEPT MODELS
    - PERFORMANCE PREDICTION MODELS FOR STRUCTURE, CONTROL AND RF SUBSYSTEMS

- CONCEPT DEVELOPMENT STATUS
    - DEVELOPED BY LOCKHEED MISSILES SPACE COMPANY, INC.
    - CURRENT TECHNOLOGY PROGRAM FUNDED BY NASA
    - FLIGHT TECHNOLOGY READINESS BY 1985

PROOF OF CONCEPT REFLECTOR STRUCTURE

The concept development of the offset wrap-rib antenna is focused on (a) the development of "proof of concept" hardware characterizing the deployable reflector and feed structure, (b) a ground-based evaluation of these major antenna components and (c) the development of a preliminary design for a full-scale antenna whose performance and cost are based on validated analytical models.

The ribs for the offset reflector have a lenticular cross section and are based on graphite/epoxy technology. The hub structure is the basic load-carrying element for the reflector. It also incorporates the deployment control mechanism which has the capability of automated restowing of the reflector structural elements on-orbit. The "proof of concept" reflector hardware model is a 55-meter-diameter partial reflector structure. The model is composed of four ribs, three mesh panels and a simulated hub structure.

The feed support structure is basically a tetrahedral-type truss. The longerons and batten members are thin-walled, tapered graphite/epoxy tubes. The longerons are hinged with preloaded joints at their centers. The tension-carrying diagonals are based on high-modulus graphite/epoxy rods. Deployment of the feed support tower is accomplished with the aid of its deployment cage which supports the stowed truss and maintains design stiffness during deployment.

The ground-based test program is intended to demonstrate technology readiness of the basic antenna concept with large-size hardware models and validate the analytical models used to predict full-scale antenna cost performance with component and scale model testing.
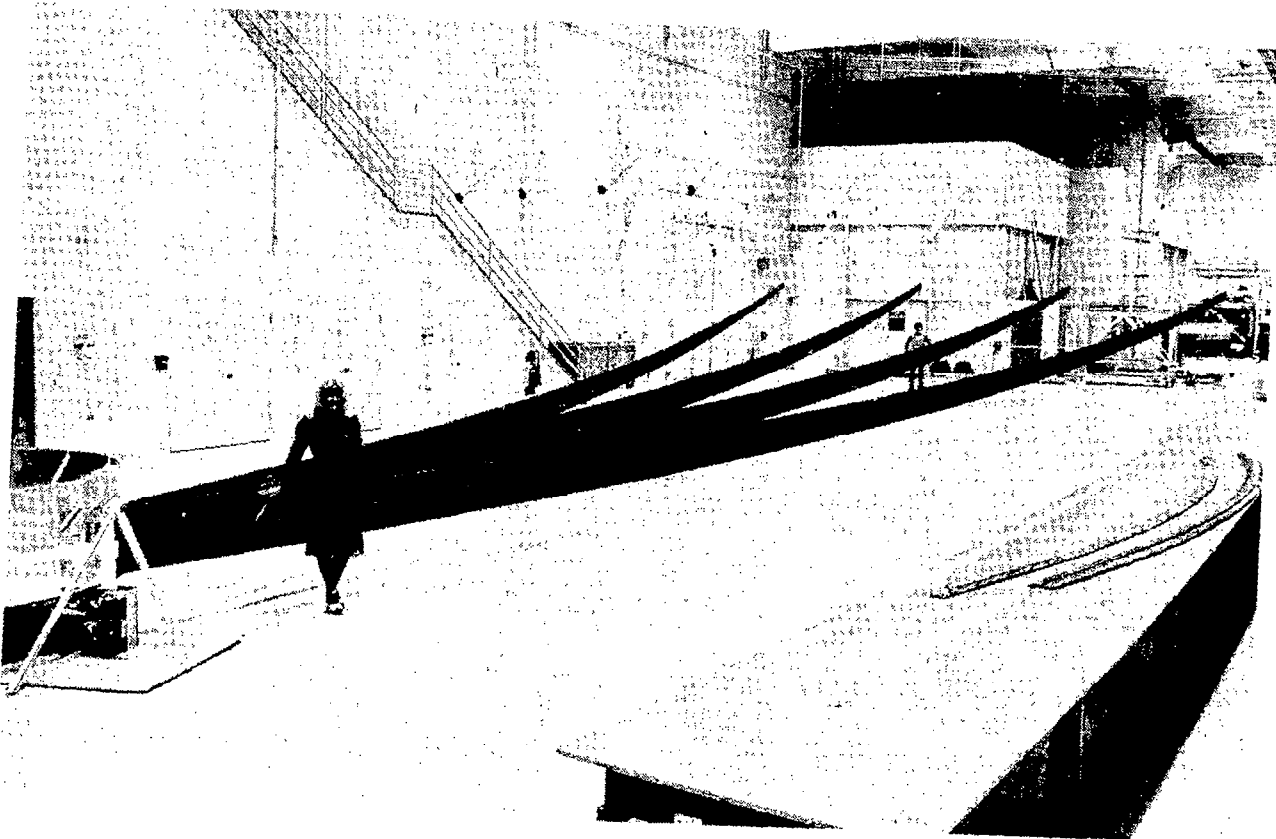
LMSS OPERATIONAL CONFIGURATION

The antenna technology development requirements such as diameter, feed
configuration, allowable surface error, weight, packaging efficiency, etc.
are not sufficient to focus the development of a specific concept for
particular applications. The interactions of the antenna structure with other
subsystems comprising the spacecraft, such as control, power, RF, thermal
control, data handling and others, need to be accounted for by the antenna
conceptual development. The Land Mobile Satellite Service (LMSS) was used as
the basis of a single-point system-level configuration design. The LMSS is a
concept developed to provide a voice communication capability between a
geosynchronous satellite and mobile receivers anywhere in the continental
United States. The relay satellite uses a large multiple-beam antenna at UHF
frequencies for uplink and downlink with ground receivers and a smaller antenna
at S-band for the base stations. The system configuration, which was based on
a 55-meter-diameter offset wrap-rib reflector, was developed by the Boeing
Company of Seattle, Washington, with technical support from LMSC and JPL.
Subsystem interfaces and constraints were identified and accounted for in the
antenna concept development.
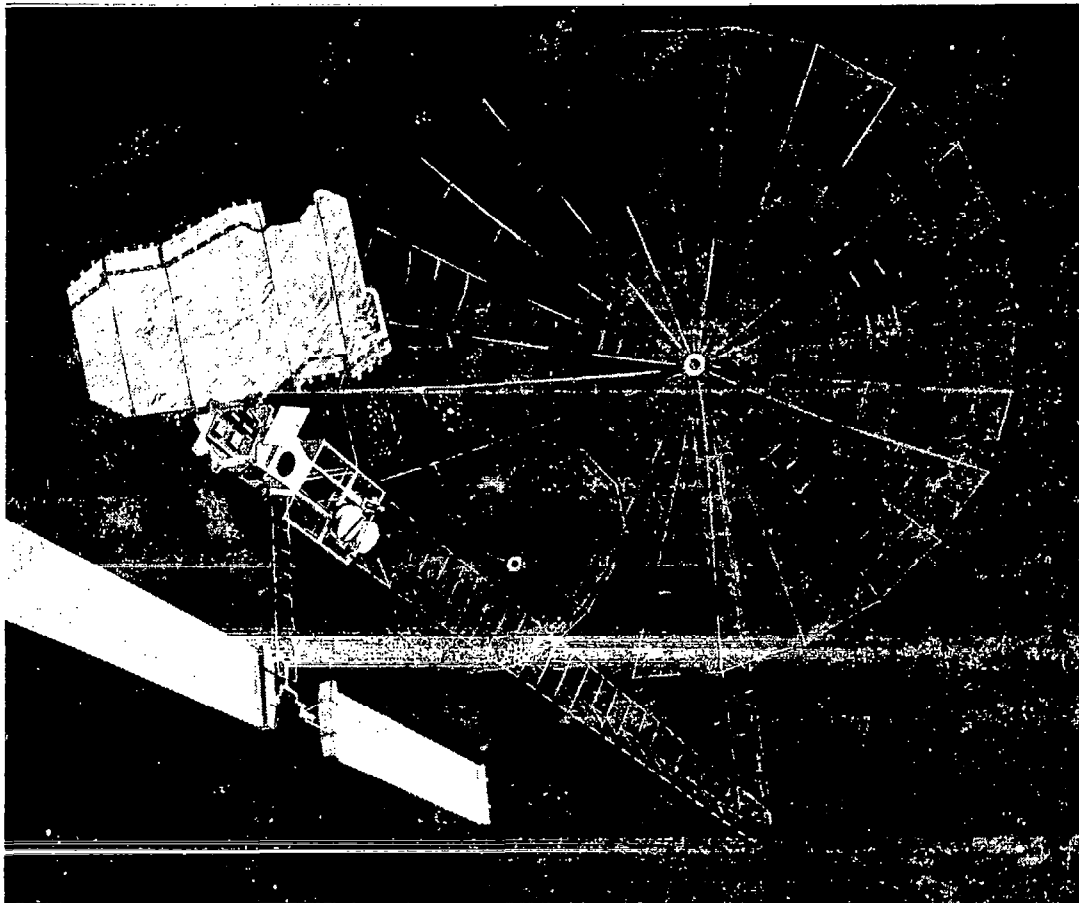
FLTSATCOM RADIAL-RIB ANTENNA

The TRW FLTSATCOM spacecraft 4.9-m-diameter antenna operates at UHF frequencies. The reflector consists of a 2-m solid center dish and a deployable outer ring of rib-supported mesh. A central mast supports the feed and also provides support for the outer ribs in the stowed configuration. The reflector weight without feed, support or thermal insulation is 14.9 kg. The initial FLTSATCOM was launched as an Earth satellite in the fall of 1977 for operation at 300 MHz. Five spacecraft are now in orbit.

- UNIQUE FEATURES OF CONCEPT
    - SIMPLE RADIAL RIB DEPLOYMENT SCHEME
    - CENTRAL MAST SUPPORTS FEED AND STOWED RIBS
    - MESH IS SILVER-PLATED WELDED STAINLESS STEEL
    - DEPLOYMENT CONTROLLED BY HYDRAULIC DAMPERS
    - PARABOLIC REFLECTOR IS 4.9 METERS AND OPERATES AT 300 MHz

- CONCEPT LEVEL OF MATURITY
    - CONCEPT DEVELOPED TO THE POINT OF FLIGHT APPLICATION
    - FLIGHT EXPERIENCE BASED ON FIVE SUCCESSFUL FLIGHTS STARTING IN 1977

- CONCEPT DEVELOPMENT STATUS
    - CONCEIVED BY TRW
    - MANUFACTURED BY TRW FOR CURRENT DoD APPLICATIONS

FLTSATCOM FLIGHT ANTENNA

The 12-ribs are hinged at the periphery of the center dish and support a silver-plated, welded, stainless-steel mesh that provides the RF reflective surface. The ribs can be folded toward the central mast for stowage in the launch configuration, and are retained in this configuration by a retention cord around the rib tip fittings. The deployment mechanism, provided at the rib hinges, consists of redundant spring actuators and a viscous damper to control deployment motion. Deployment of the ribs is initiated by a pyrotechnic cord cutter severing the retention cord. Detent latch springs lock the ribs in the deployed position. The ribs are made of thin-walled aluminum tubing formed to provide a parabolic shape under the deployed mesh tension.
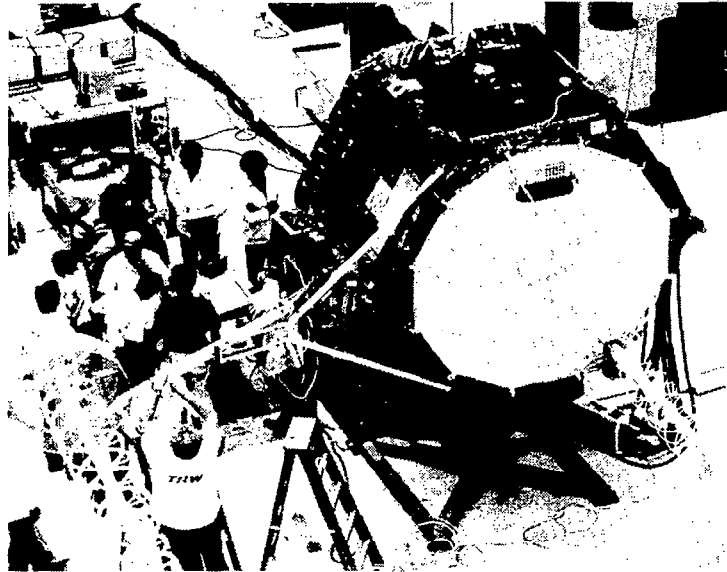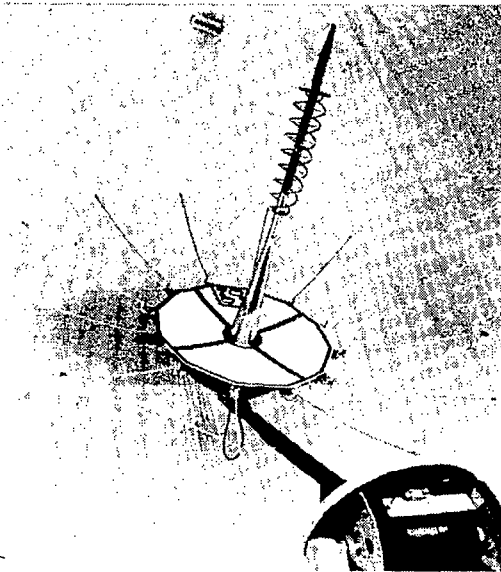
WRAP-RIB ANTENNA CONCEPT
DEVELOPMENT OVERVIEW

A. A. Woods, Jr., and N. F. Garcia
Lockheed Missiles and Space Company, Inc.
Sunnyvale, California

PROGRAM ROADMAP

The current NASA-sponsored Antenna Technology Development Program of the offset wrap-rib antenna concept (developed by the Lockheed Missiles and Space Company) is based on a ground test program of "proof of concept" hardware whose potential on-orbit performance is based on analytical estimates. The ground demonstration hardware represents a partial 55-meter diameter reflector and feed support structure. Testing will include automated deployment, reflector surface quality evaluation and validation of analytical performance models. Test results and hardware fabrication costs will be used to refine the models that will be the basis for the preliminary design of a 100-meter diameter wrap-rib antenna system. Additionally, the design, processes, tooling, fabrication techniques, fixturing and assembly approaches used for the "proof of concept" hardware are directly applicable to building flight systems up to 100 meters in diameter (Figure 1).
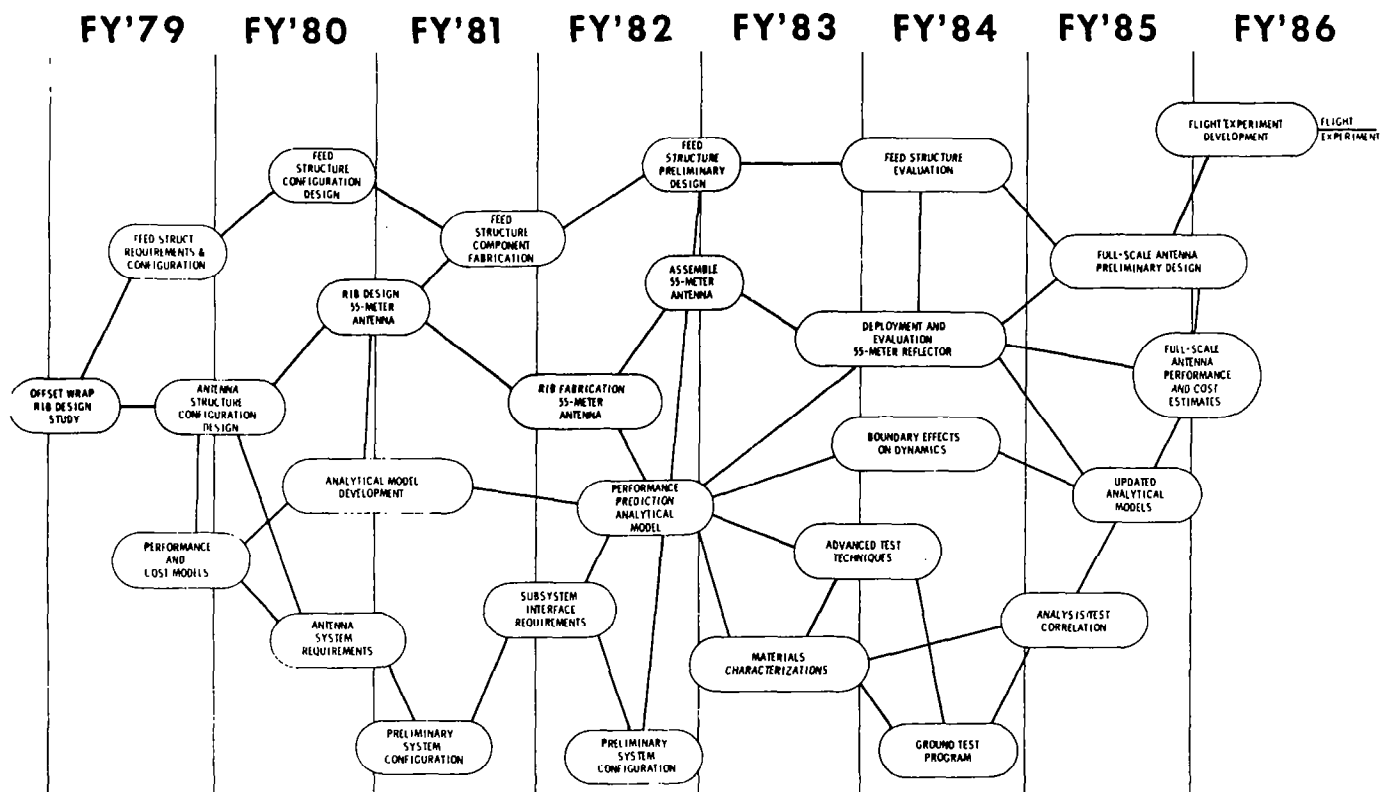
Figure 1

BACKGROUND AND INITIAL STUDY OBJECTIVES

An initial ten month contract for "Study of Wrap-Rib Antenna Design" was undertaken by Lockheed Missiles and Space Company, Inc. in January 1979. This contract was originated by Jet Propulsion Laboratory in direct support of the Large Space Structures Technology Program.

The objectives of the contract are summarized in Figure 2. LMSC was to perform a study of the Wrap Rib Antenna Design and determine the applicability of the design for offset feed configurations for antennas up to 300 meters in diameter. In addition, a technical approach was to be developed and costed which would provide a high degree of confidence for the space flight application of a large wrap-rib antenna.

- ● CHARACTERIZE OFFSET AND SYMMETRIC WRAP-RIB REFLECTORS

- ● IDENTIFY AND QUANTIFY CRITICAL DEVELOPMENT TECHNOLOGIES

- ● IDENTIFY ROM COST AND SCHEDULES FOR DEVELOPMENT

- ● DEVELOP A TECHNOLOGY PLAN FOR LOW RISK DEMONSTRATION

Figure 2

To date the large antenna systems are most commonly constructed as symmetric reflector systems. This geometry is shown at the left of Figure 3. Concerns with efficiency and side lobe levels have recently placed emphasis on the offset feed configuration shown at the right of the figure.

Geometrically an offset reflector is described by a paraboloid where the geometric centerline is not coincident with the parabolic axis of symmetry. In order to gain the electrical advantages of reduced blockage, the parabolic axis and, therefore, the focal point must in fact be located external to the section aperture. This section can most easily be visualized by forming a large paraboloid of diameter D and then passing a cylinder, with a parallel axis of symmetry, through the paraboloid. If the cylinder has a diameter d less than D/2 and its radius is common with the radius of the parabola, the section of the paraboloid bounded by the cylinder is representative of the desired offset reflector surface. Further, if D/2 - d is larger than the radius of the feed and the feed support structure is attached external to the radius of the offset section, there is no blockage of the electrical field of view.
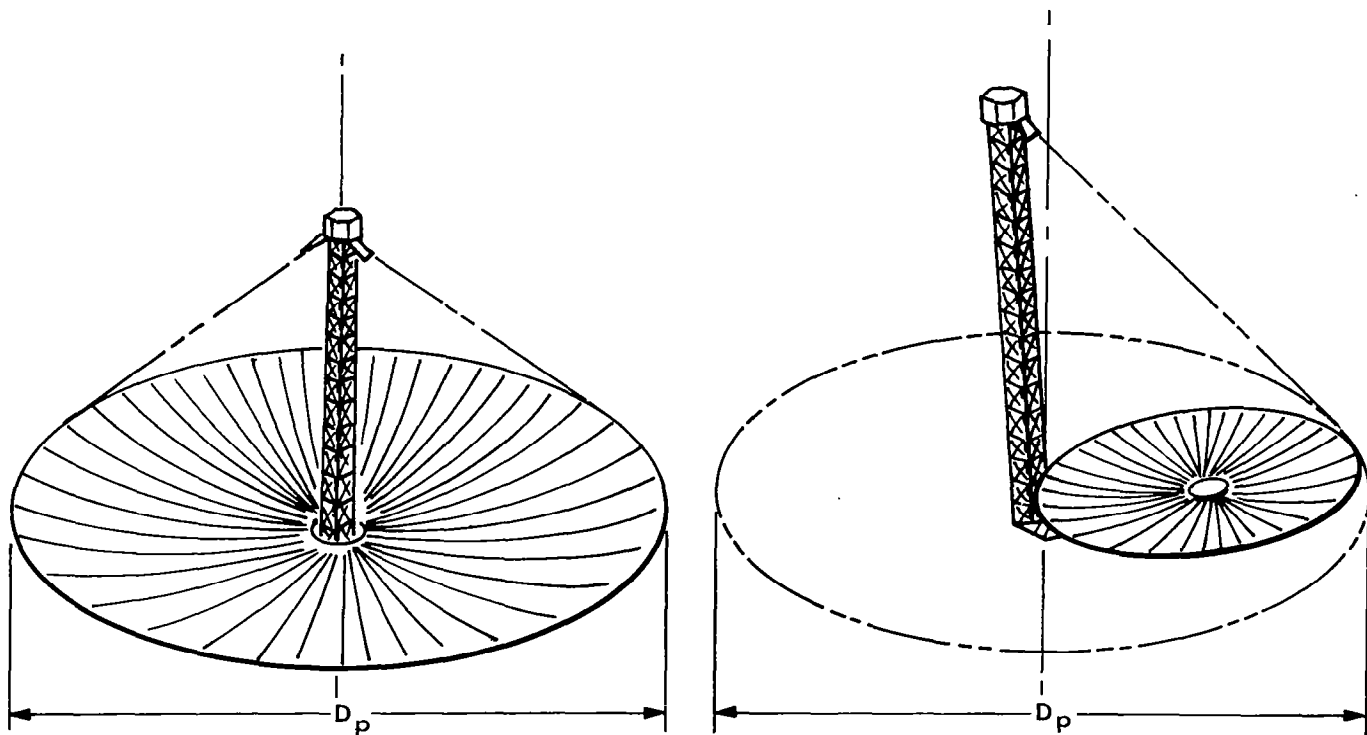
Figure 3

STUDY APPROACH

The approach taken to develop the parametric design and performance data focused on the construction of a computer aided reflector and mast design packages. The reflector design package was constructed to accept basic material and structural element characteristics and develop design solutions which satisfied these inputs and the mission constraints of weight, stowed diameter and antenna system geometry. The developed designs were then analyzed to determine the extent of orbital and assembly surface errors, deployment integrity, and development costs.

Having defined the reflector size and operational frequency, a mast design could be developed with a design constraint that the pointing error be held to less than 0.05 beam widths. The mast design package approach was similar to the reflector package.

This developed program is overviewed in Figure 4.
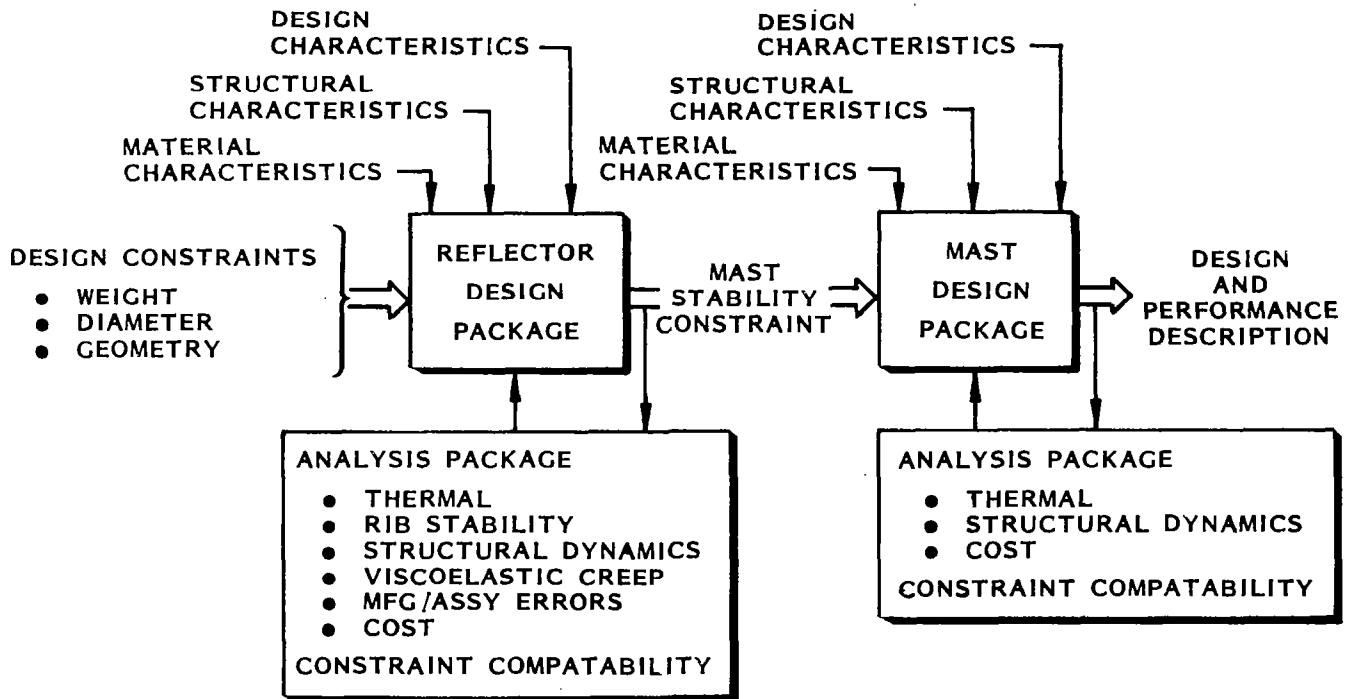
Figure 4

The initial study activity identified the growth limits of the offset wrap-rib design. These limits are presented in Figure 5 along with the data point which locates the 55 m data base design. The three major mission regions of interest are also presented to provide an appreciation for the projected design capability with respect to the defined mission models. The results show that the design potential comfortably envelops the defined near term mission zones as well as the projected far term missions (dotted projections).
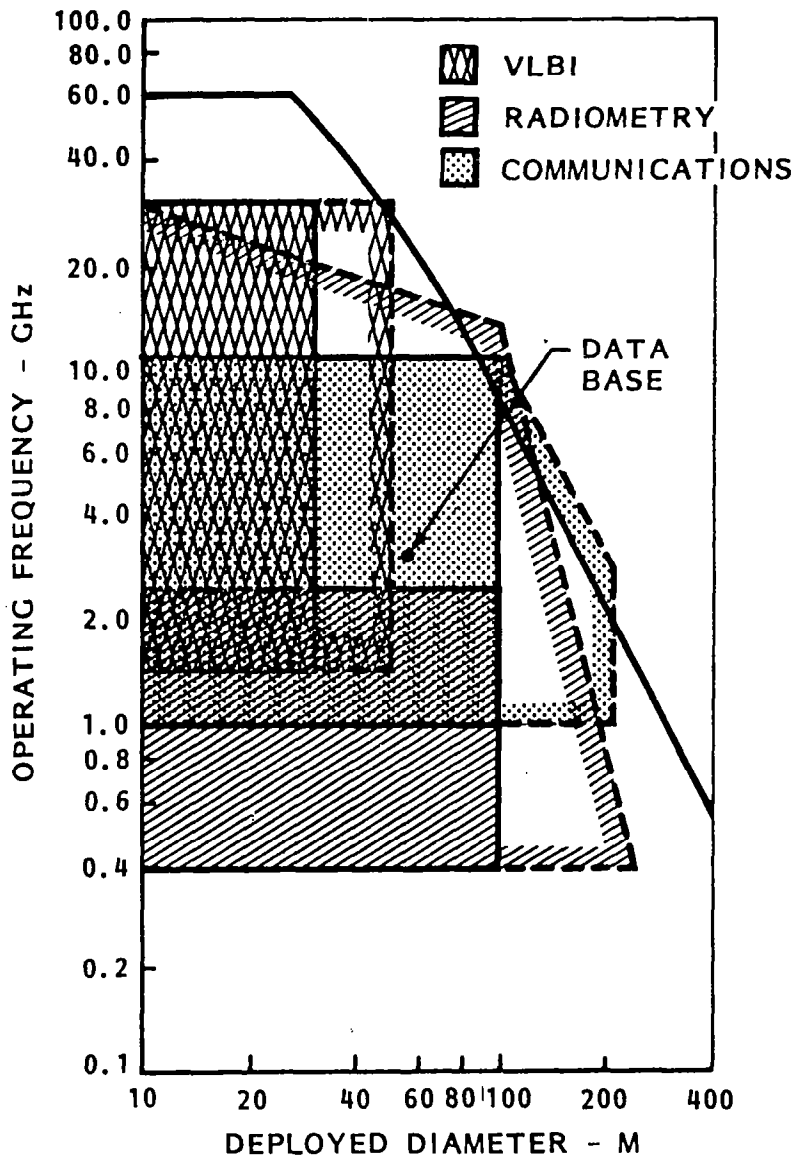
Figure 5

Figure 6 presents the projected cost for an offset antenna as a function of aperture size and operating frequency. The data show that for low frequency apertures the cost is reasonably proportional to diameter. As operating frequency limits are pushed the costs start to rise rapidly. This seems to occur in the 50 to 100 million dollar range for frequencies greater than 2 GHz.

The dotted curves present the cost projection of the initial study activity. The solid curves are revisions to the cost projections which resulted from the hardware development phases. This cost revision reflects the technology benefit afforded a development program through the new tool design approach developed under the study activity.
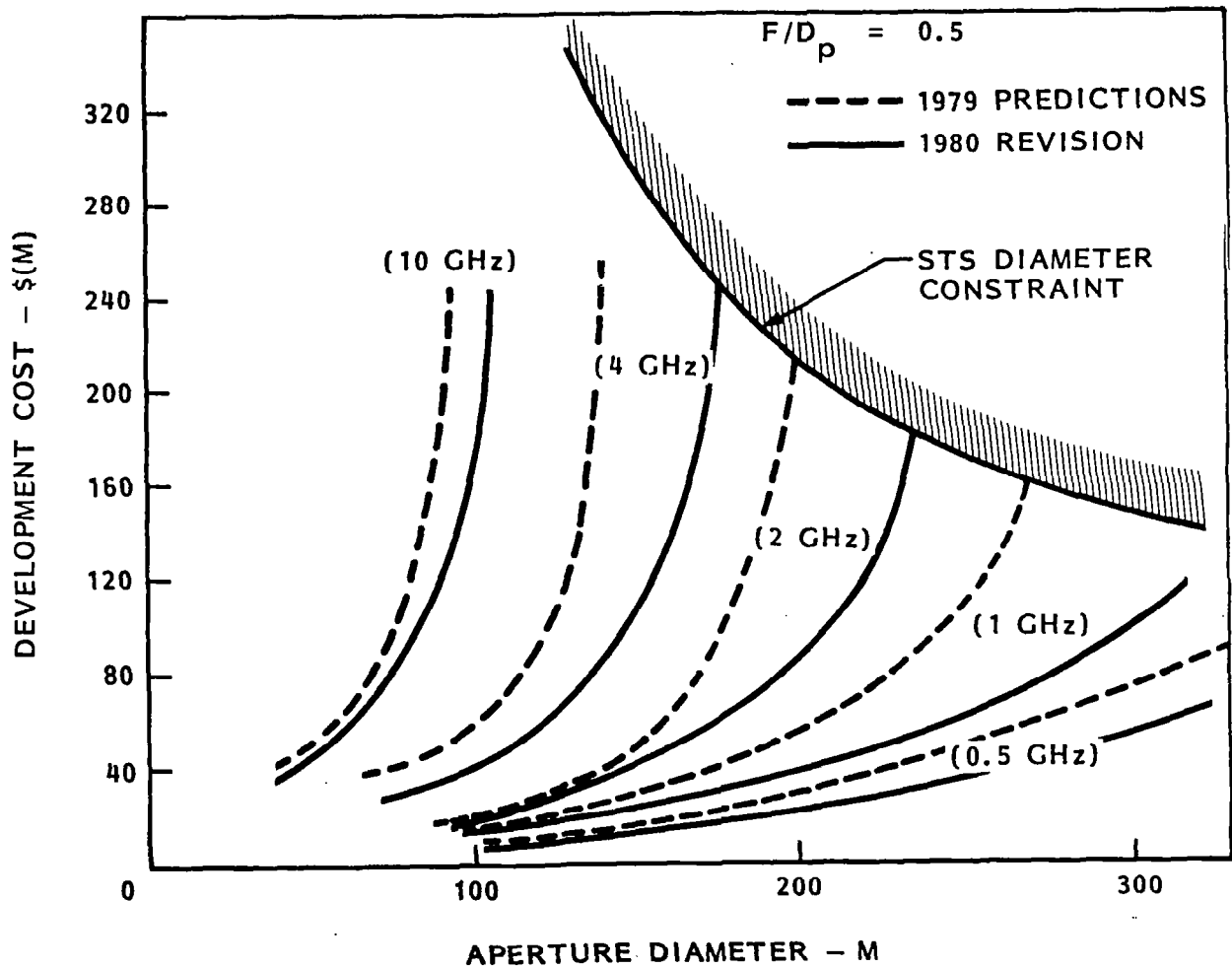
Figure 6

OFFSET ANTENNA SYSTEM OVERVIEW

The system concept developed is presented in Figure 7 which depicts a
100 m diameter communication antenna. The reflector is of the offset wrap-rib
design with the hub structure located at the center of the offset section.
The cantilevered rib surface support structure can be seen radiating from this
central hub. The spacecraft, which contains the control, communications, and
power subsystems, is located in the focal point area but out of the microwave
aperture to assure optimum performance. A deployable truss mast connects the
reflector to the spacecraft and maintains system alignment. The mast is also
configured to remain outside of the microwave path.
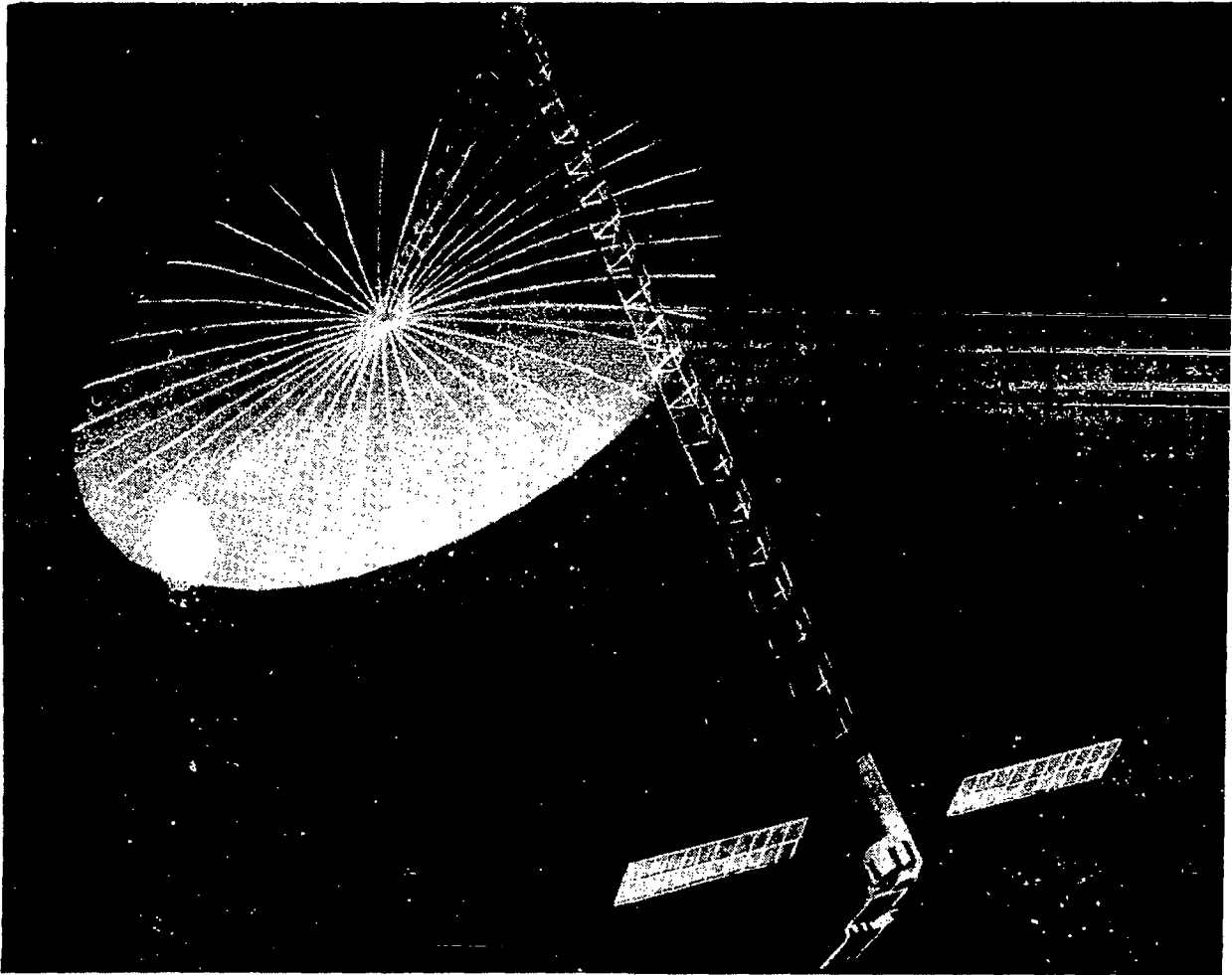
Figure 7

OPERATIONAL DEPLOYMENT SEQUENCE

Figure 8 presents the stowed spacecraft configuration as it is being deployed from the Shuttle. The stowed reflector seen as a flat cylinder is shown at one end of the spacecraft, and the IUS, used for orbit transfer, is on the opposite end. The spacecraft segment is depicted next to the IUS with the feed system and solar array panels folded forward toward the reflector. In this configuration the mast is stowed in the triangular section hidden by the spacecraft equipment.
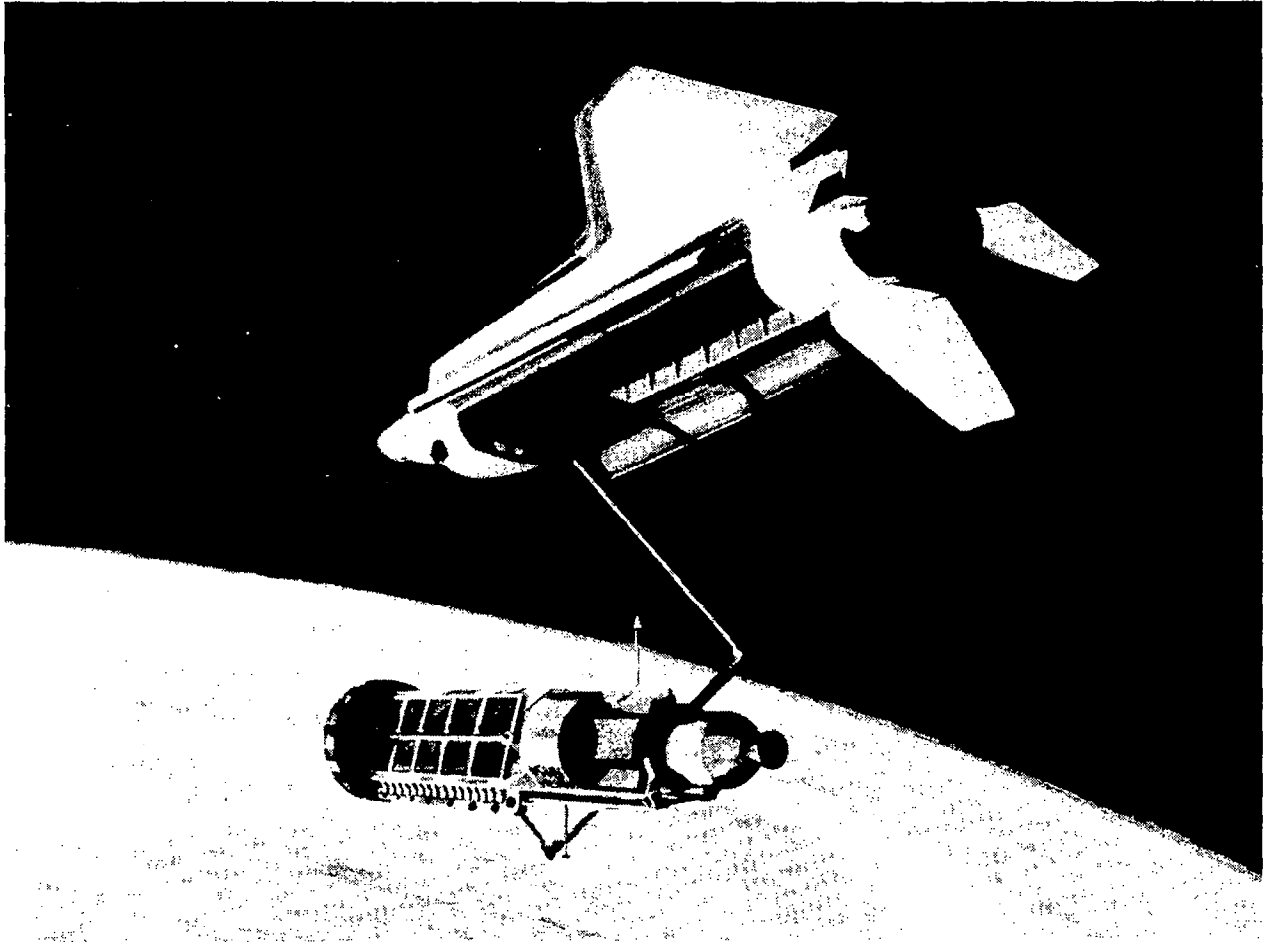
Figure 8

After the spacecraft has achieved operation orbit (Figure 9), the IUS is separated and the deployment sequence initiated. The first deployment is that of the mast. This activity can be seen in the figure as the reflector is being moved away from the spacecraft segment.
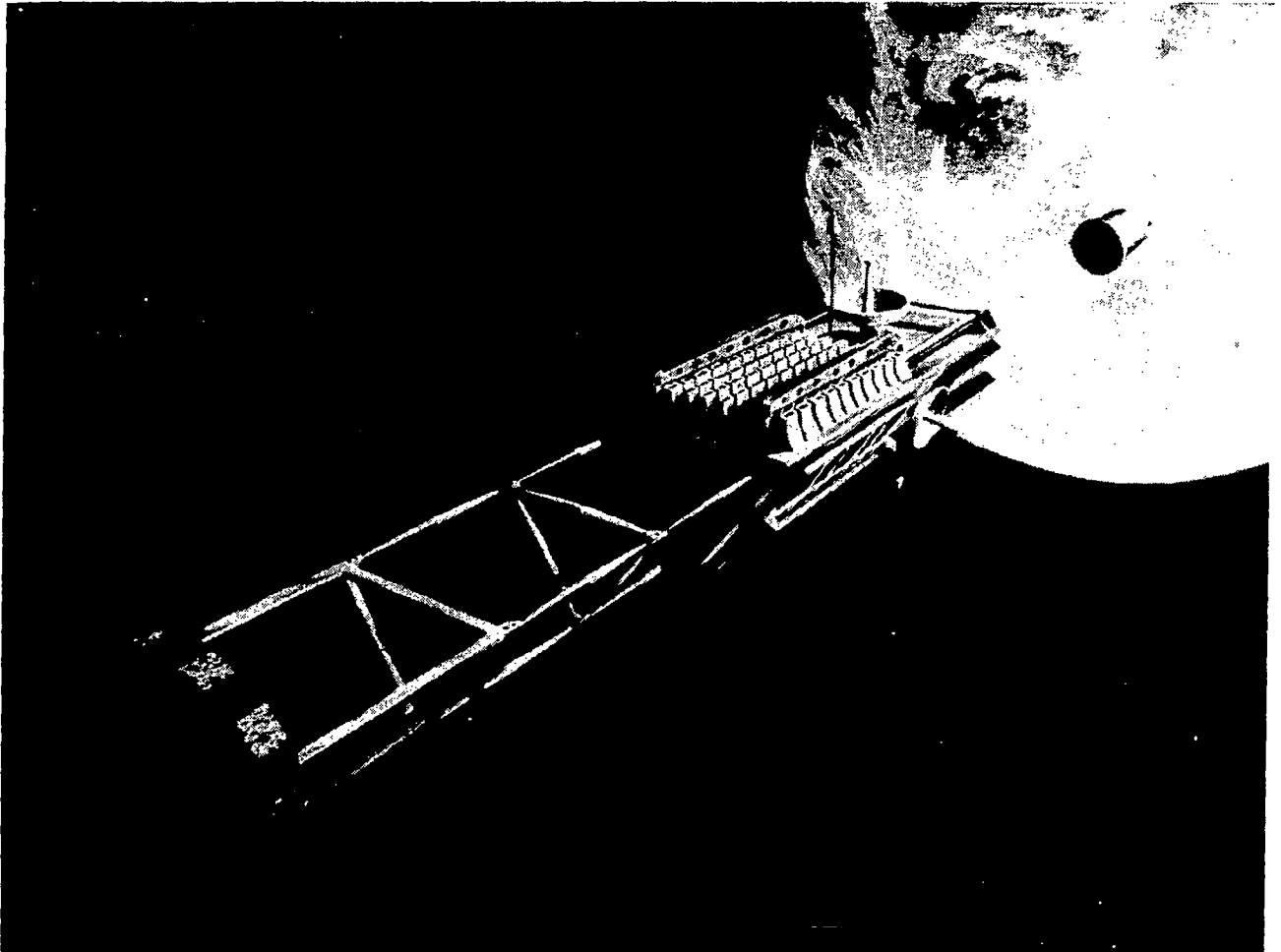
Figure 9

REFLECTOR DEPLOYMENT

The final operation is that of reflector deployment. Figure 10 depicts this event at about the one-third point. The reflective surface and ribs can be seen unwrapping off the hub at the end of the fully deployed mast.
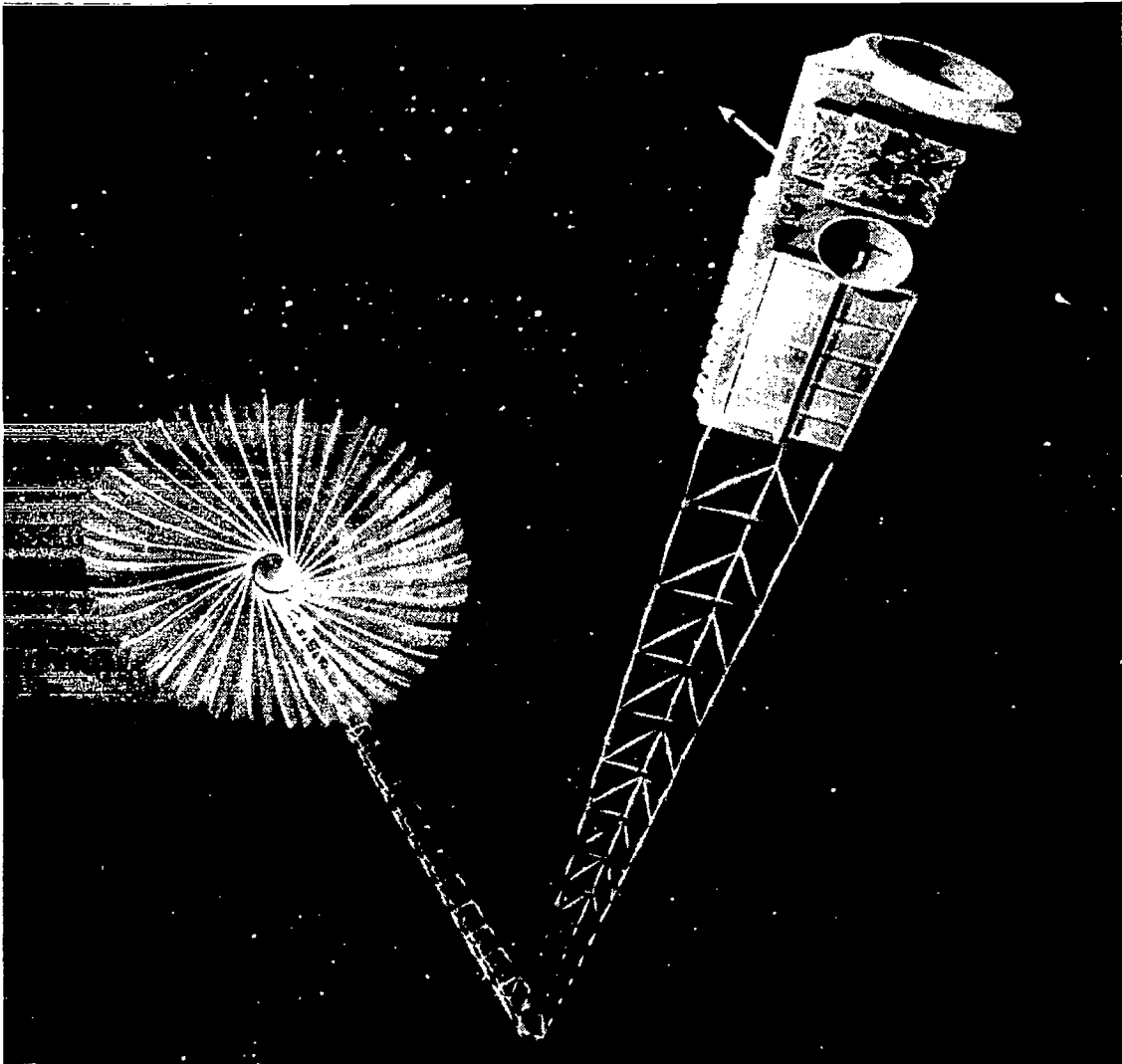
Figure 10

PROGRAM PLAN

    The initial study activity resulted in a review of the concerns involved with undertaking a space flight program demonstration of a large diameter wrap-rib antenna. The projected costs and technical risks identified the necessity of developing an early data base at a size which could comfortably be analytically scaled and which would reduce risk through demonstration. This program, identified in Figure 11, would involve developing a testable segment of a 55-m aperture. This would be used to validate the design and provide a scaling factor of 2 or 3 for the 100- to 150-m missions. The dominant effects of thermal distortions in the performance projections indicate orbital surface adjustment may prove cost effective and should be investigated. Finally, since the design is being defined, the stability and control system interactions and limitations should be identified.

ESTABLISH A 55-M DATA BASE OFFSET REFLECTOR

- MANUFACTURE AND TEST COMPONENTS/PROCESSES
- ASSEMBLE I-G TESTABLE SEGMENT
- DEMONSTRATE DEPLOYMENT AND RETRACTION
- MEASURE DEPLOYED CONTOUR WITH OFFLOADING TEST AID
- UPDATE DESIGN AND DESIGN ALGORITHM

DESIGN A COMPATABLE FEED SUPPORT STRUCTURE

- EVALUATE CANDIDATES
- SELECT CONCEPT WHICH EXPLOITS LSST
- CHARACTERIZE DESIGN
- UPDATE DESIGN ALGORITHM

EVALUATE BENEFITS OF INCORPORATING ACTIVE FIGURE CONTROL

- ONE TIME ADJUSTMENT
- CONTINUOUS ADJUSTMENT
- COSTS

Figure 11

GROUND BASED TEST PROGRAM

The ground-based test program is intended to demonstrate technology readiness of the basic antenna concept with large-size hardware models while validating the analytical models used to predict full-scale antenna cost and performance. This test program was started after the concept definition effort concluded with growth potential identified through 150 meters. The risk and technology items were reviewed within the scope of available information and program constraints, and a hardware oriented data base program was evolved (Figure 12). The following summarizes the objectives of the working program.

Static testing of antenna rib components will be accomplished for comparison with analysis. The partial reflector structure hardware will be used for repeated deployments of the single-rib structure and the multiple-rib configuration. Special test equipment to support the rib structure during automated deployment has already been demonstrated with a single-rib structure. The precision of the mesh surface will be measured for comparison with design requirements and analytical projections. Mesh management and packaging efficiency will be evaluated. The deployment control system will also demonstrate refurling capability.

The deployable feed support structure hardware components will be statically tested to determine stiffness characteristics for comparison with analysis. The multiple-bay structure will be deployed repeatedly to validate kinematic design and establish dimensional repeatability. Additionally, static influence coefficients will be determined for the multiple-bay model to support refinement of the analytical models.

Figure 12

435
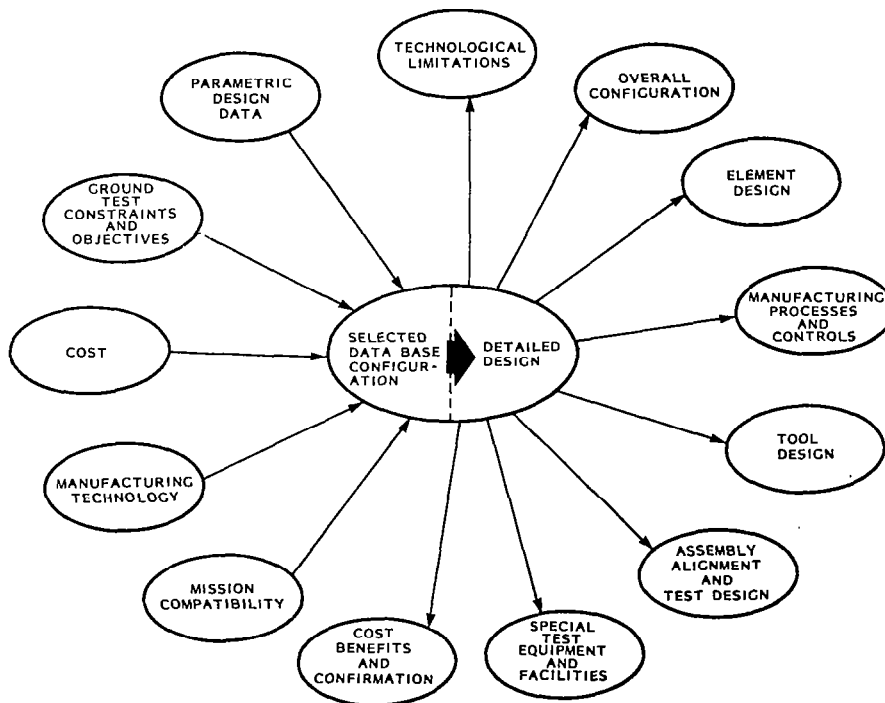
The ground test of the 55-meter diameter proof-of-concept model represents the largest ground-based demonstration for this concept. Further ground test programs will include the deployment and repeated refurling of the 4-rib partial antenna and measurement of rib stiffness and surface contour for comparison with analytical predictions. The reflector ribs will be supported during deployment and furling operations (Figure 13). The rib support system consists of four sets of balance beam/carriage assemblies for each rib. These assemblies ride on fixed rails that are located radially with respect to the antenna. The deployment displacements of the ribs will be tracked by the carriage assemblies in the radial direction and by the balance beams in the vertical and lateral directions. This passive support system progressively offloads the weight of the ribs and mesh as they unfold from the central hub. To maintain the rib positions approximately collinear with the overhead support rails, the hub will be mounted on a platform that rotates during deployment. The three degrees of freedom accommodated to the ribs during deployment by the support system results in a controlled deployment sequence where the unfolding mesh is not affected by the rib support system. Since the effect of gravity loading on the mesh will tend to force the mesh against the deployment control devices, the ground demonstration of mesh management with respect to identifying snagging problems is considered conservative.
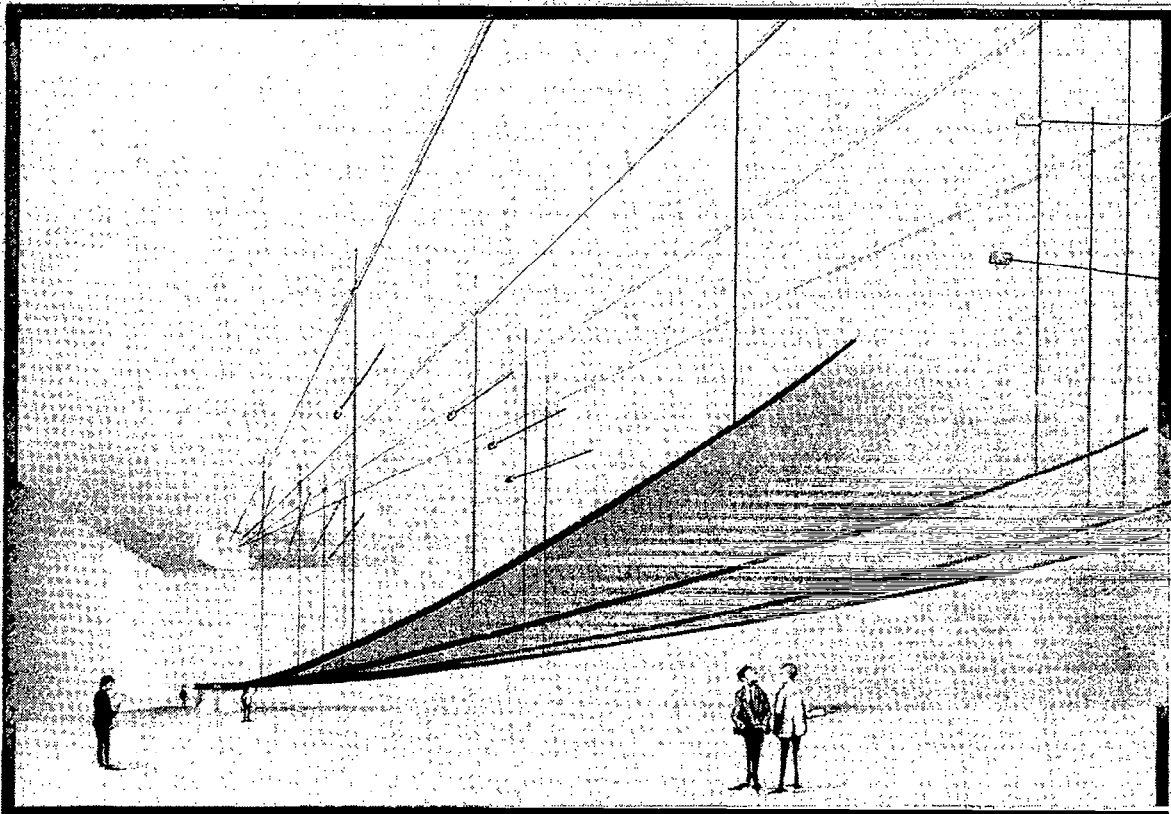
Ground Test of 55 Meter Reflector

Figure 13

Significant progress was made this year in the fabrication of the 55 m proof-of-concept reflector hardware. The completion of the four rib structure assembly validated the fabrication and assembly processes. Assembly of the hub and deployment control device and integration of these components into the four rib deployment test article allowed for initial functional testing of the integrated reflector design, which was successfully accomplished (Figure 14).

55 M DATA BASE OFFSET REFLECTOR

- COMPONENT/PROCESSES EVALUATION COMPLETE

- HUB/DEPLOYMENT/RIB ASSEMBLY COMPLETE

- FOUR RIBS AUTOMATICALLY DEPLOYED AND RESTOWED

Figure 14

RIB TOOL DESIGN AND DEFINITION

The rib layup tool design, engineering and manufacturing definition was accomplished using CADAM (Computer Graphics Augmented Design And Manufacturing System). Engineering tool definition (reflector shape, three-dimensional tool contour and tool segments) was created on CADAM. CADAM then produced numerical control (N/C) tapes which defined the flat pattern part to be scribed, contour templates to be used in bump forming, and bump forming guidelines (Figure 15).
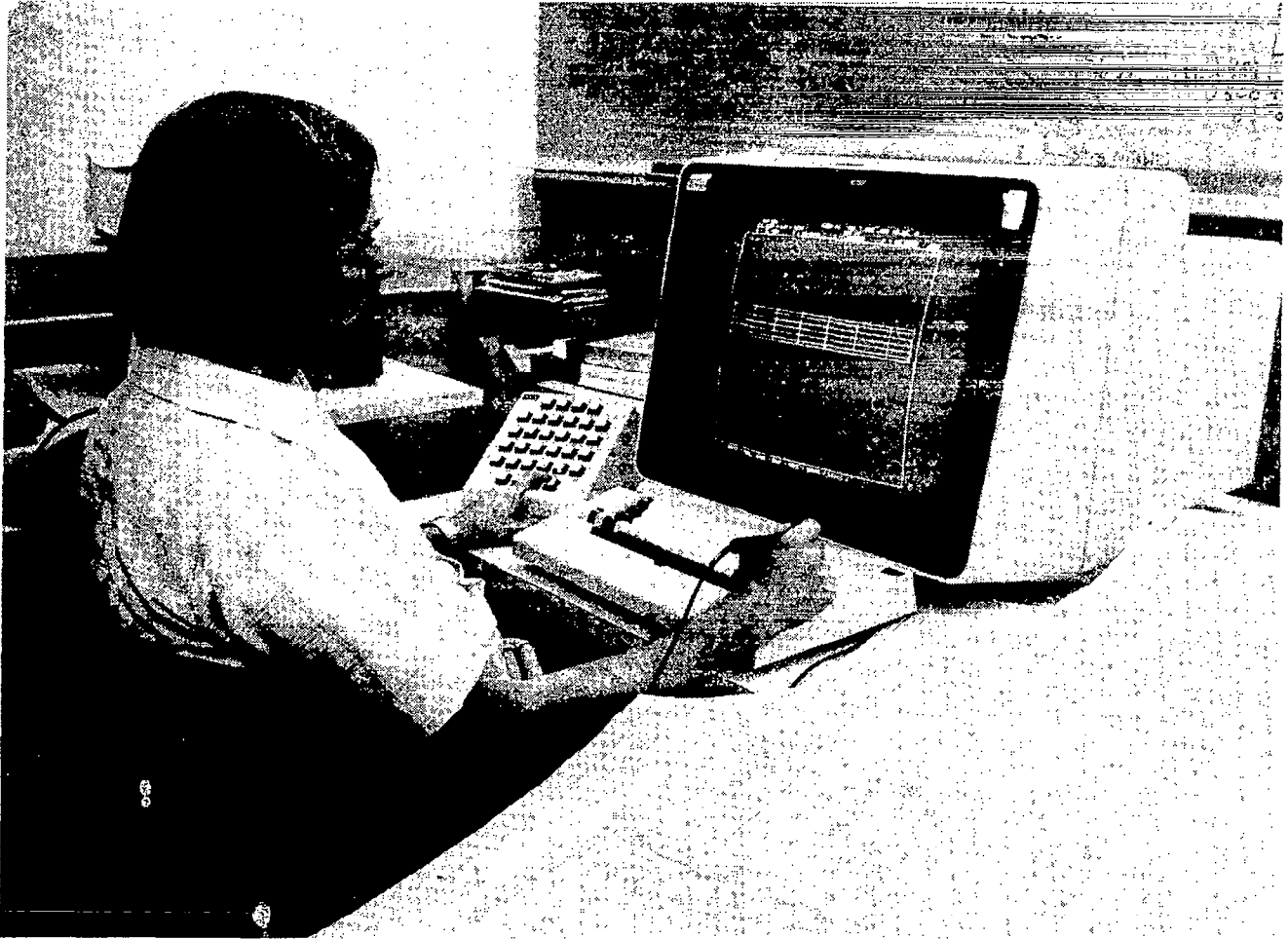
Figure 15

TOOL SURFACE FORMING

Scribed Invar sheets were bump formed in a hydraulic brake using steel dies against a hard rubber reactor. The three dimensional variation of tool layup surface was maintained using the bump forming guidelines for reflector curvature and the cross-sectional rib contour templates at intervals along the length of the tool (Figure 16).
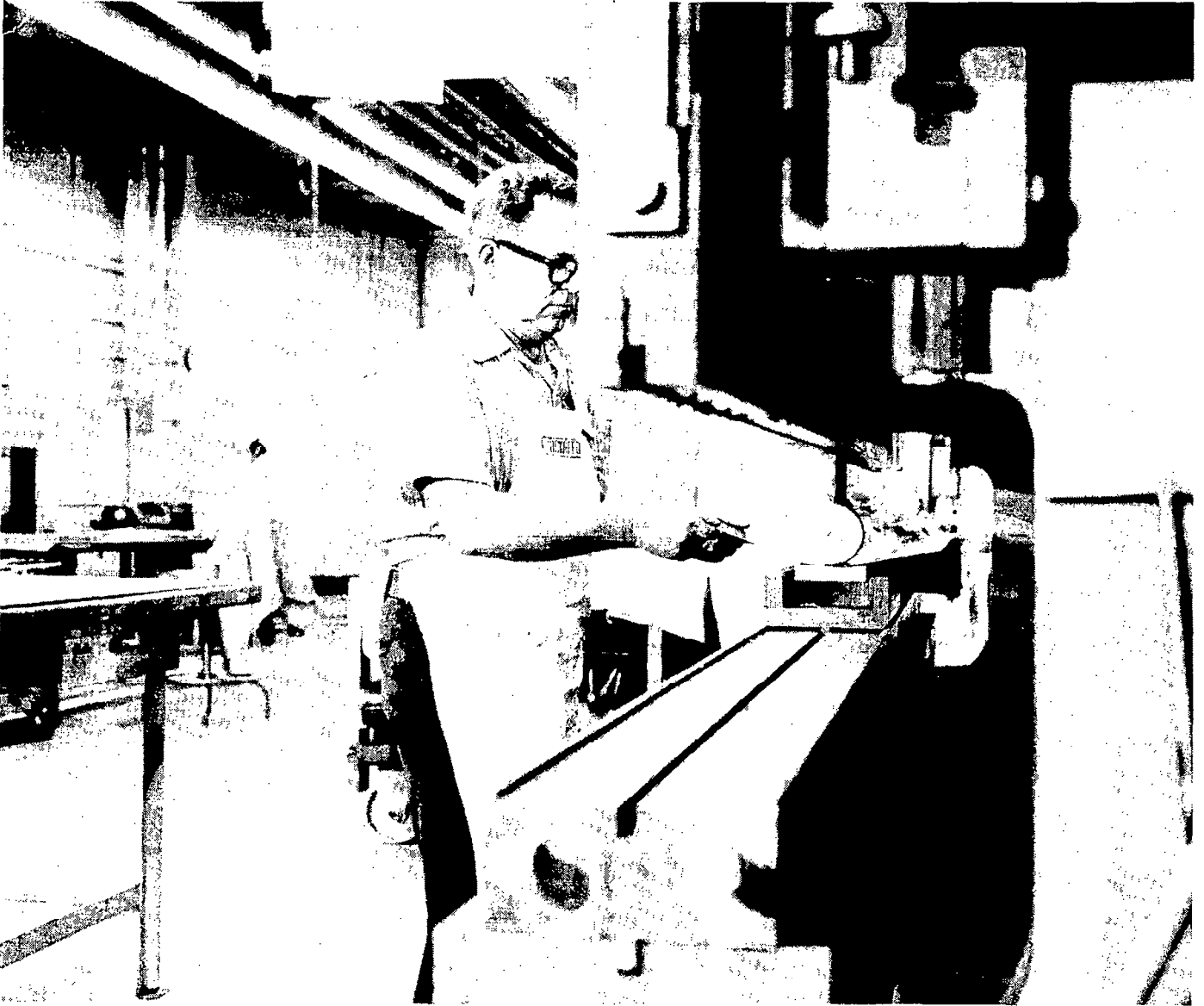
Figure 16

TOOL ASSEMBLY

The finished formed Invar layup surface is placed in position over the Invar tool base. Templates are used to check the surface contour of the formed top and the top is firmly clamped in place to the base for welding (Figure 17).

Figure 17

TOOL COMPLETION

Assembled and clamped tool segments are spot welded at intervals along the
edges to hold the assembly together. Seam welding along the edges completes
the tool (Figure 18).
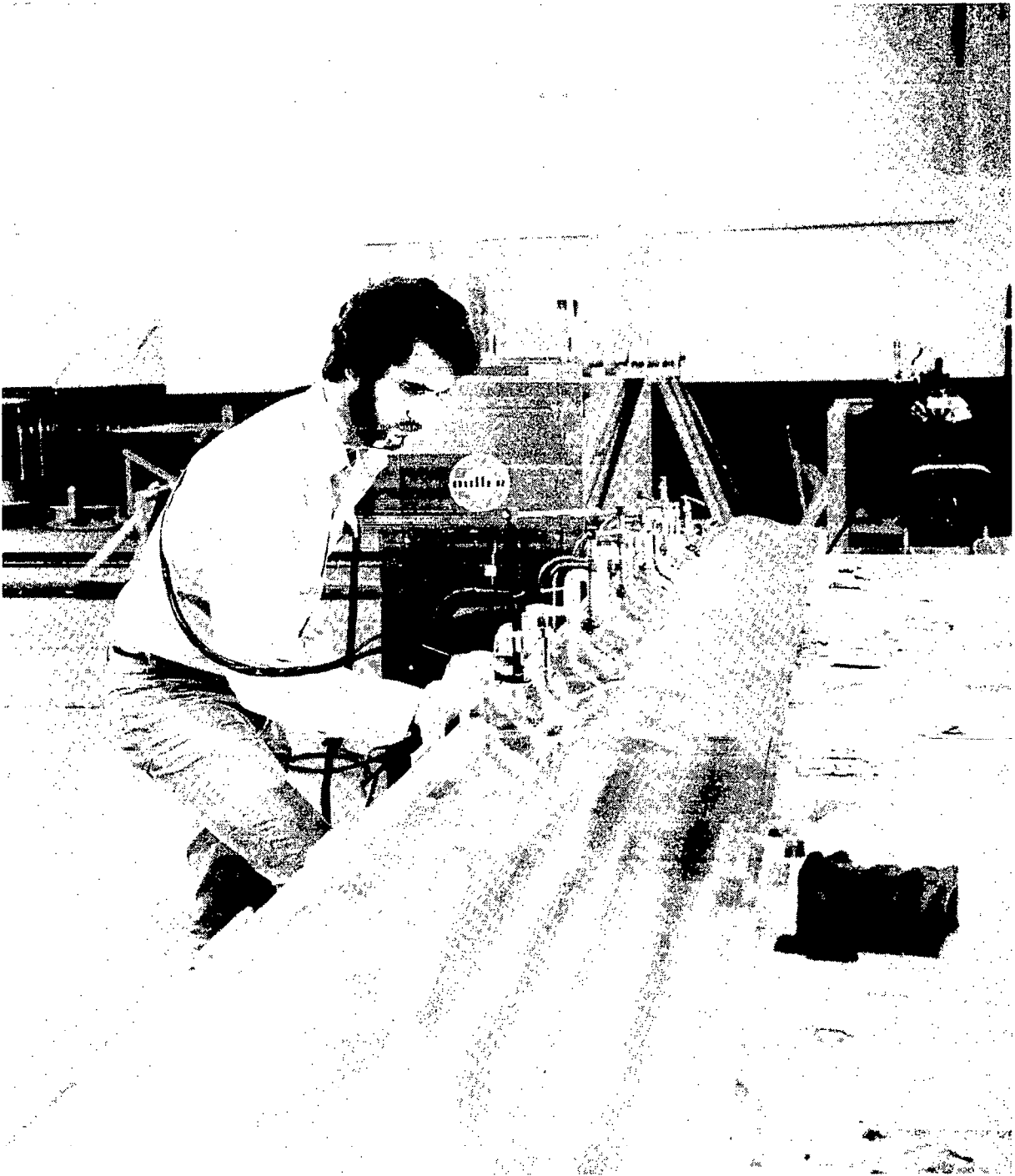
Figure 18

Epoxy impregnated graphite is placed on the layup tool in three layers. The first and third layers are graphite fabric while the second layer is unidirectional graphite tape (Figure 19).
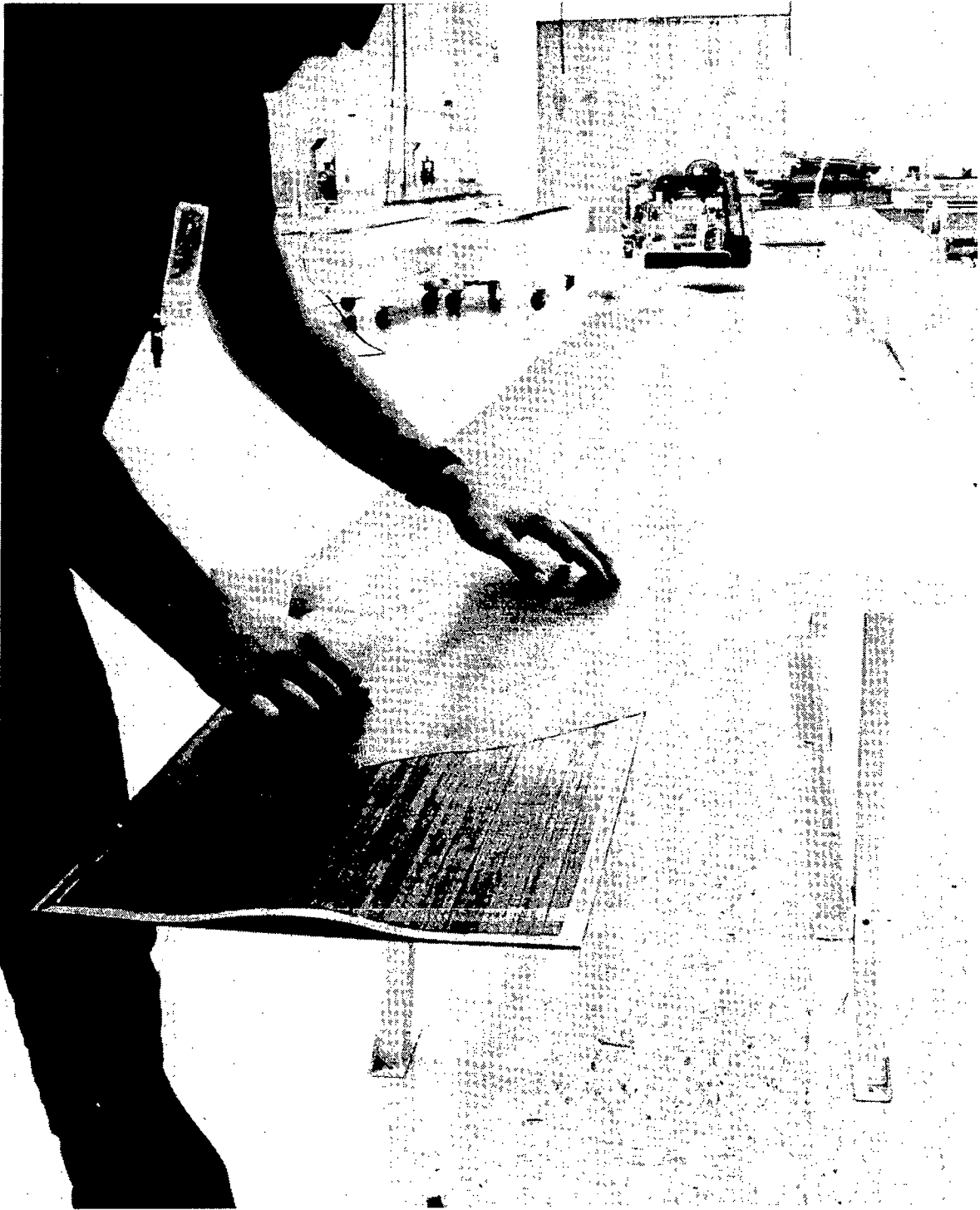
Figure 19

A bump formed titanium doubler is placed at the root end of the layup tool. The graphite layup is performed over the doubler so that curing bonds the titanium to the graphite (Figure 20).
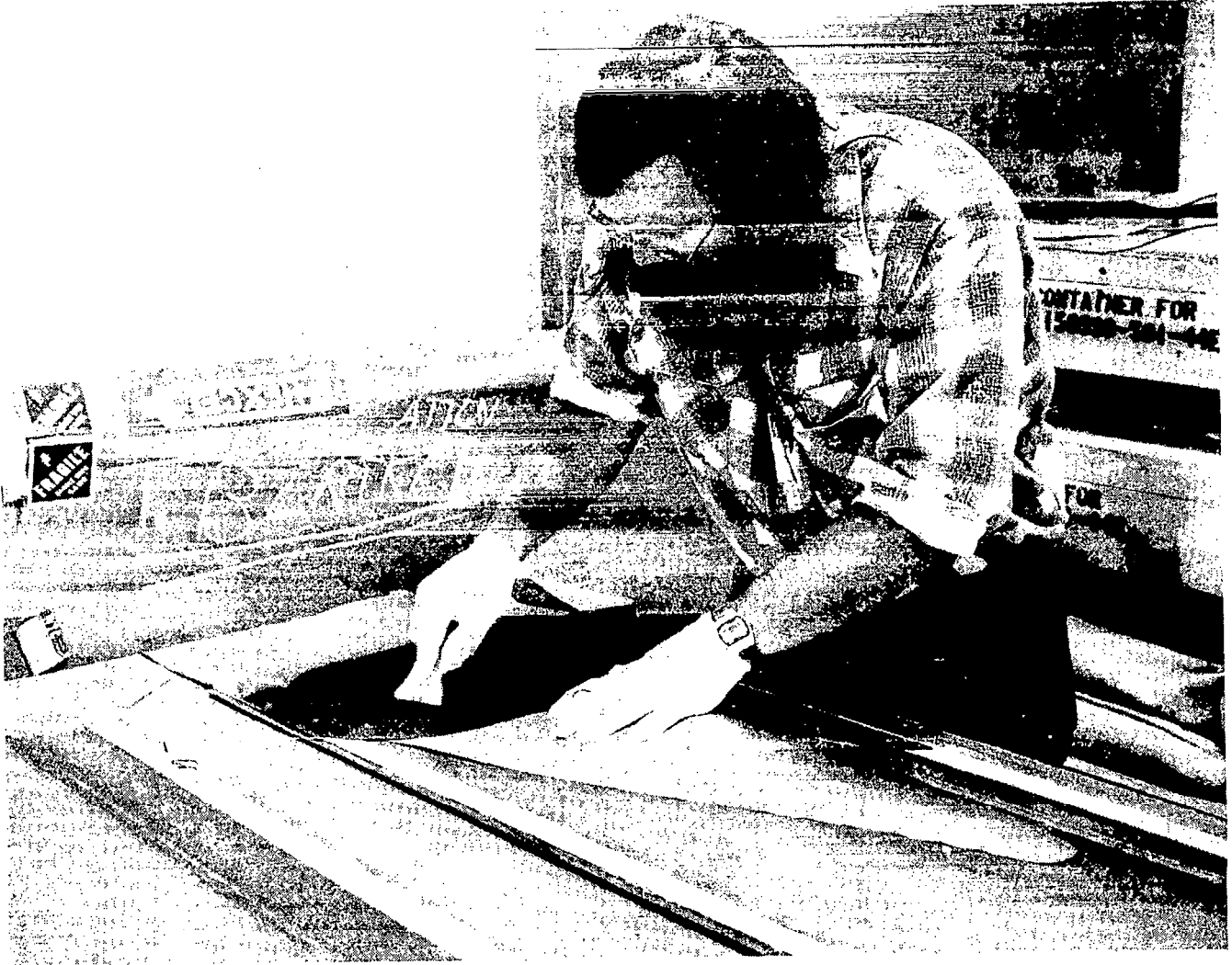
Figure 20

CURE PREPARATION

Completed graphite-epoxy layups are prepared for curing by covering them with layup release cloth, a bleeder sheet, and breather cloth. A vacuum bag is then placed over the assembly and thermocouples installed (Figure 21).

Figure 21

Temperature and pressure are applied in an autoclave to cure the assembly (Figure 22).
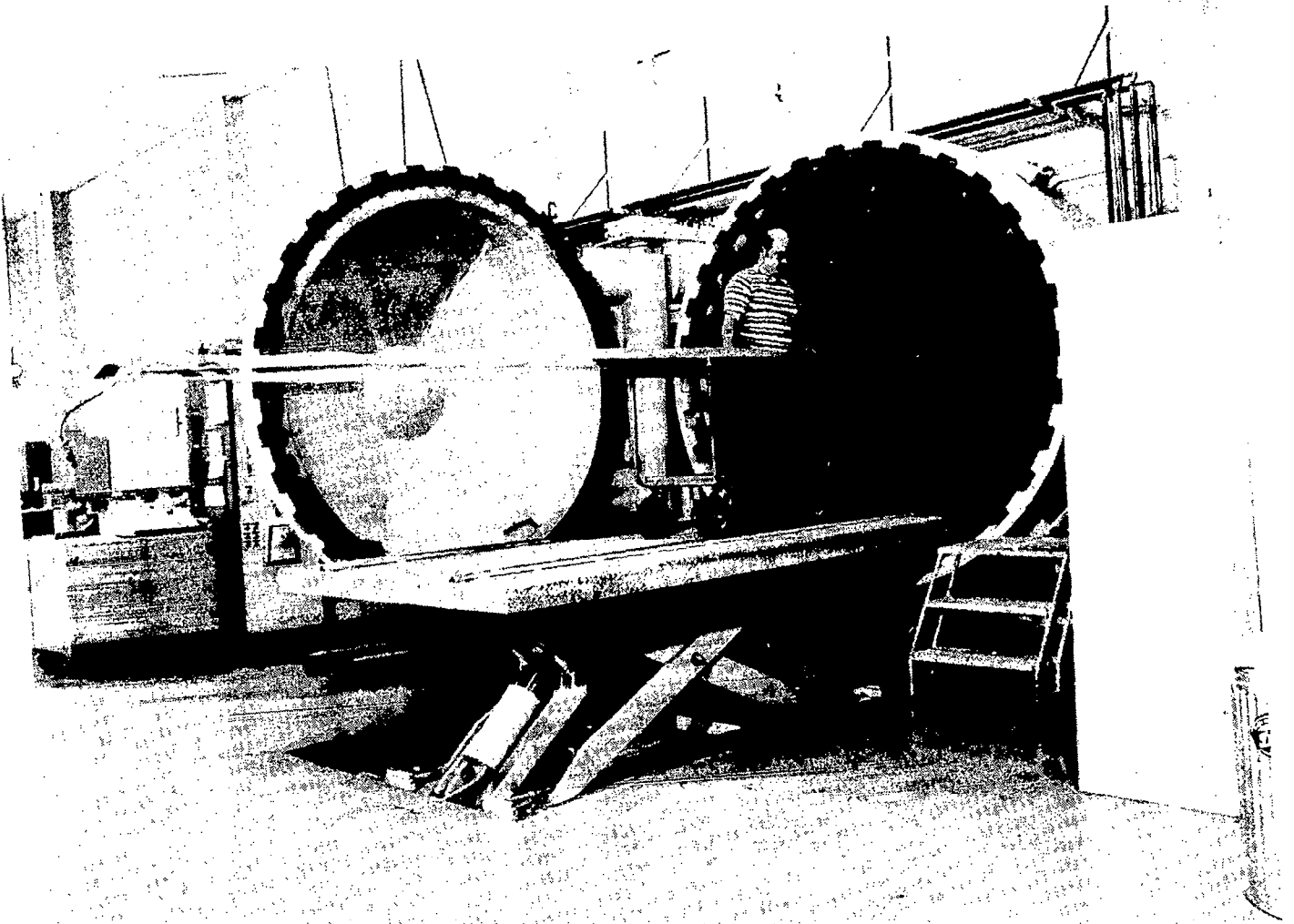
Figure 22

COMPLETED RIB SEGMENT

A cured part is removed from the autoclave and stripped of the vacuum bag assembly. The exposed cured rib segment is then easily removed from the tool (Figure 23).
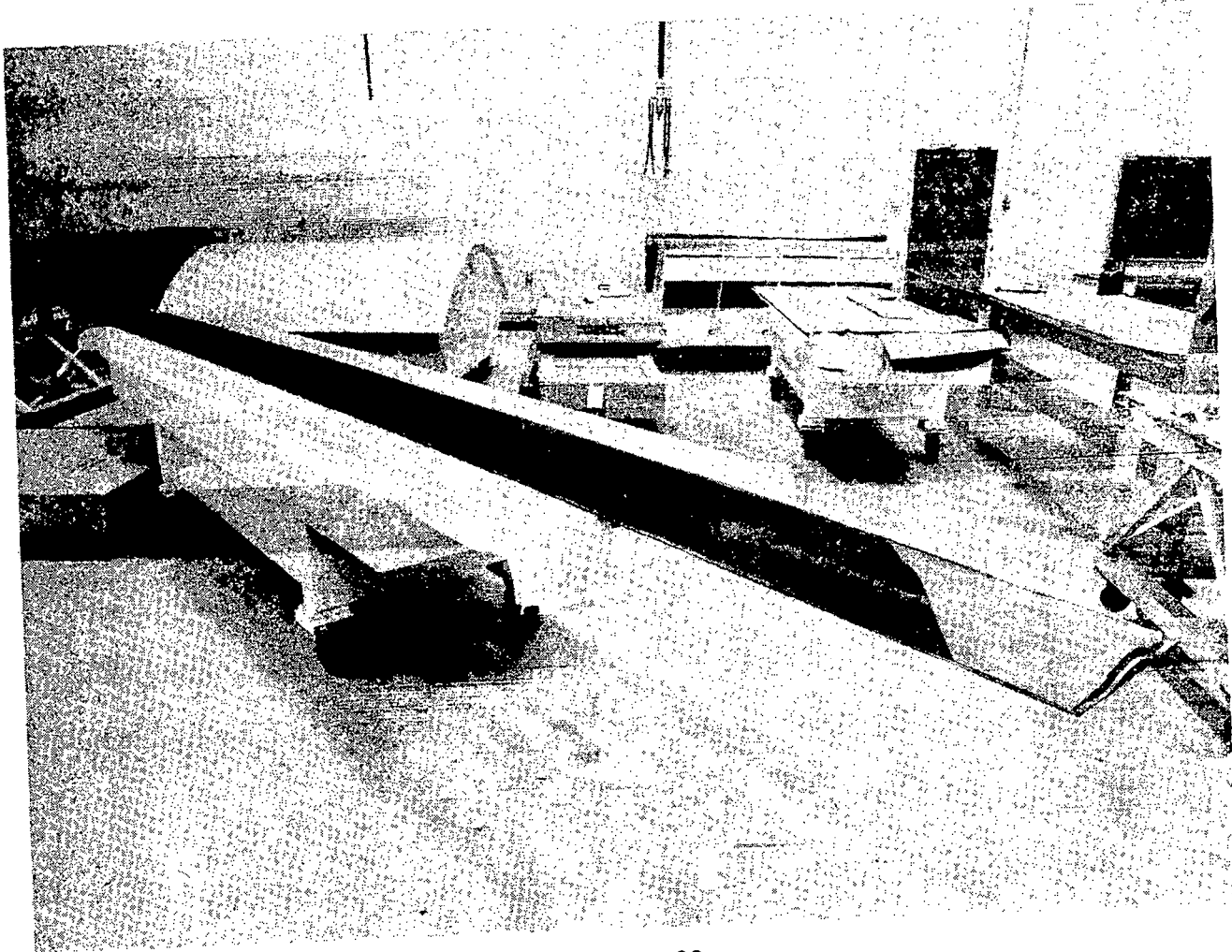
Figure 23

Rib segments are placed end to end and marked for the trim operation. Pins protruding from the table mate with locating holes in the segments, insuring accurate alignment of the parts (Figure 24).
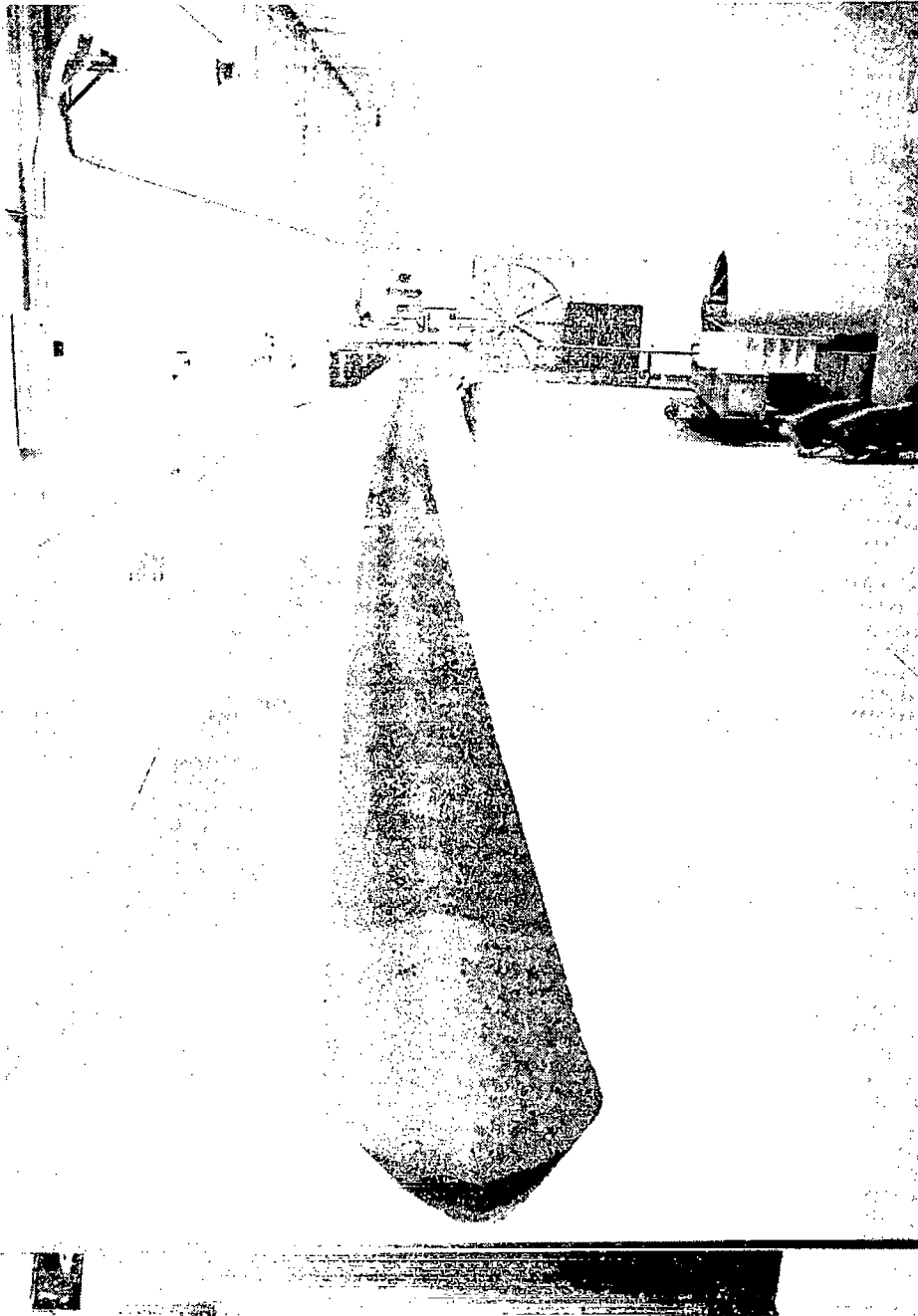
Figure 24

SPLICE BONDING

Adhesive is applied to the surface of butted segments and a splice strap is positioned over the joint (Figure 25).

Figure 25

LENTICULAR BOND PREPARATION

The semi-lenticular rib halves are bonded together along the upper and lower longitudinal edges to generate the full lenticular cross-section. Teflon tape is applied adjacent to the bond area for the full length of the segment (Figure 26).

Figure 26

Each semi-lenticular rib half is spliced with the inside face down on the work table. To complete the full lenticular cross-section one semi-lenticular rib half must be turned face up. This manuever is accomplished with the aid of a large diameter spool on which the proper segment is coiled. Placing the loaded spool appropriately on the table and unrolling the segment positions both semi-lenticular rib halves in the required orientation for lenticular bonding (Figure 27).
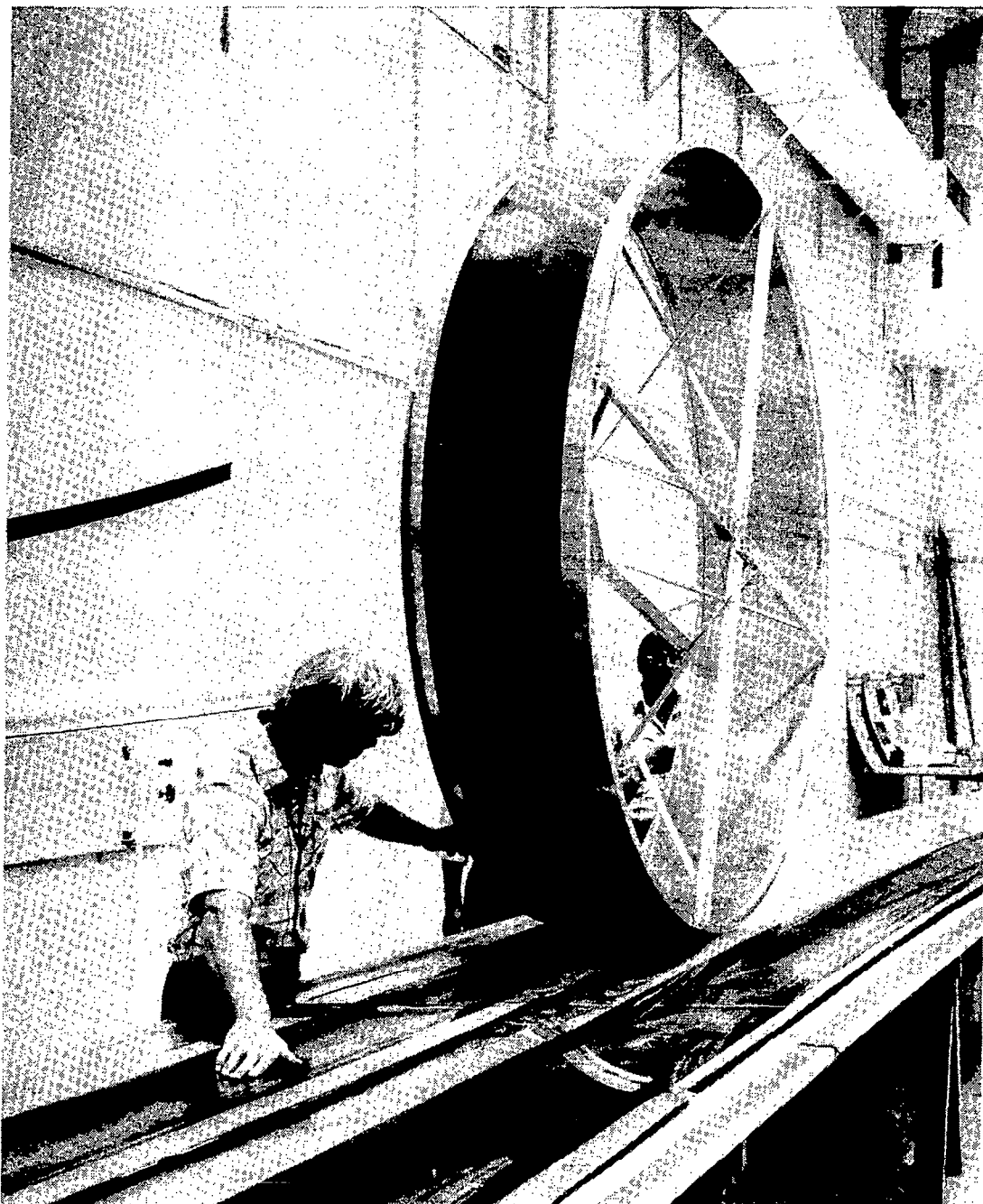
Figure 27

LENTICULAR BONDING

The two rib segments to be bonded along the longitudinal edges are positioned on the work table over location pins. Once in position, the peel ply is removed, exposing the bond area and the adhesive applied along the length of the rib. The segments are then bagged, full vacuum is applied, and the adhesive is allowed to cure (Figure 28).

Figure 28

SINGLE RIB DEPLOYMENT

A single rib was integrated with a simulated reflector hub and special test equipment (STE). On November 6, 1981, the system was successfully cycled through the deployment and stowing operations (Figures 29 and 30).
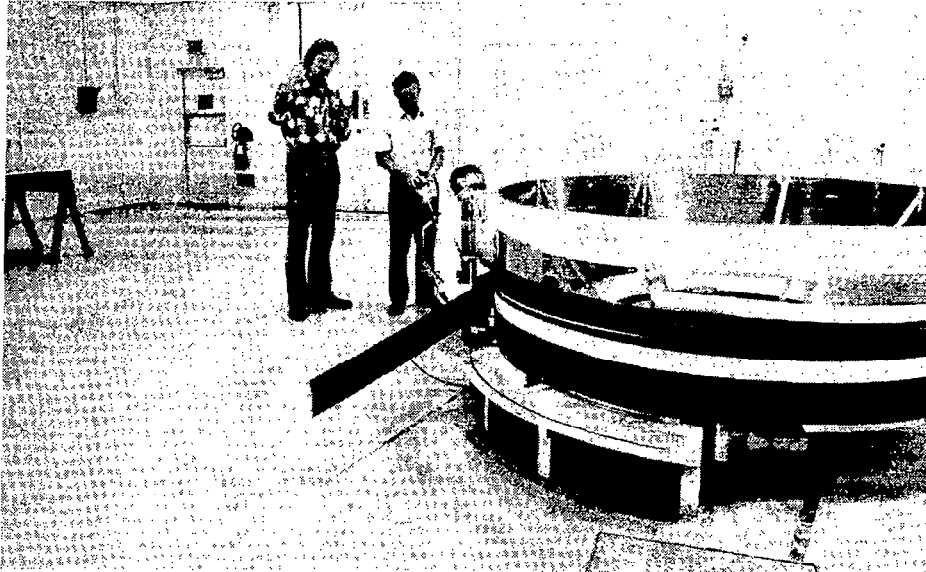
Figure 29
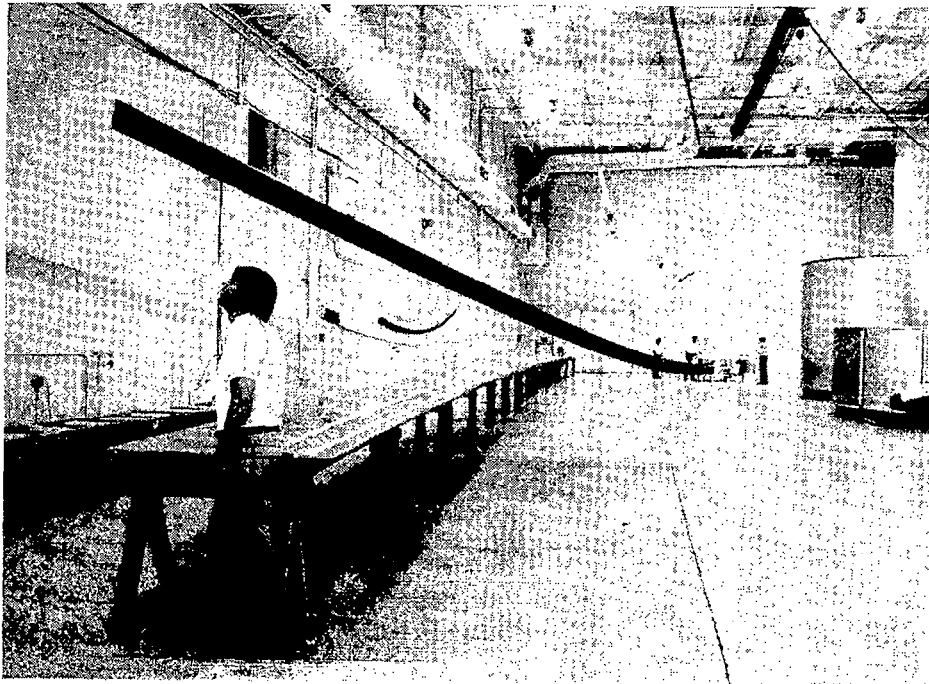
Figure 30

RIB INSTALLATION

Completed ribs are assiduously removed from the work tables by hand and placed across the facility in position for mounting on the simulated reflector hub (Figure 31).
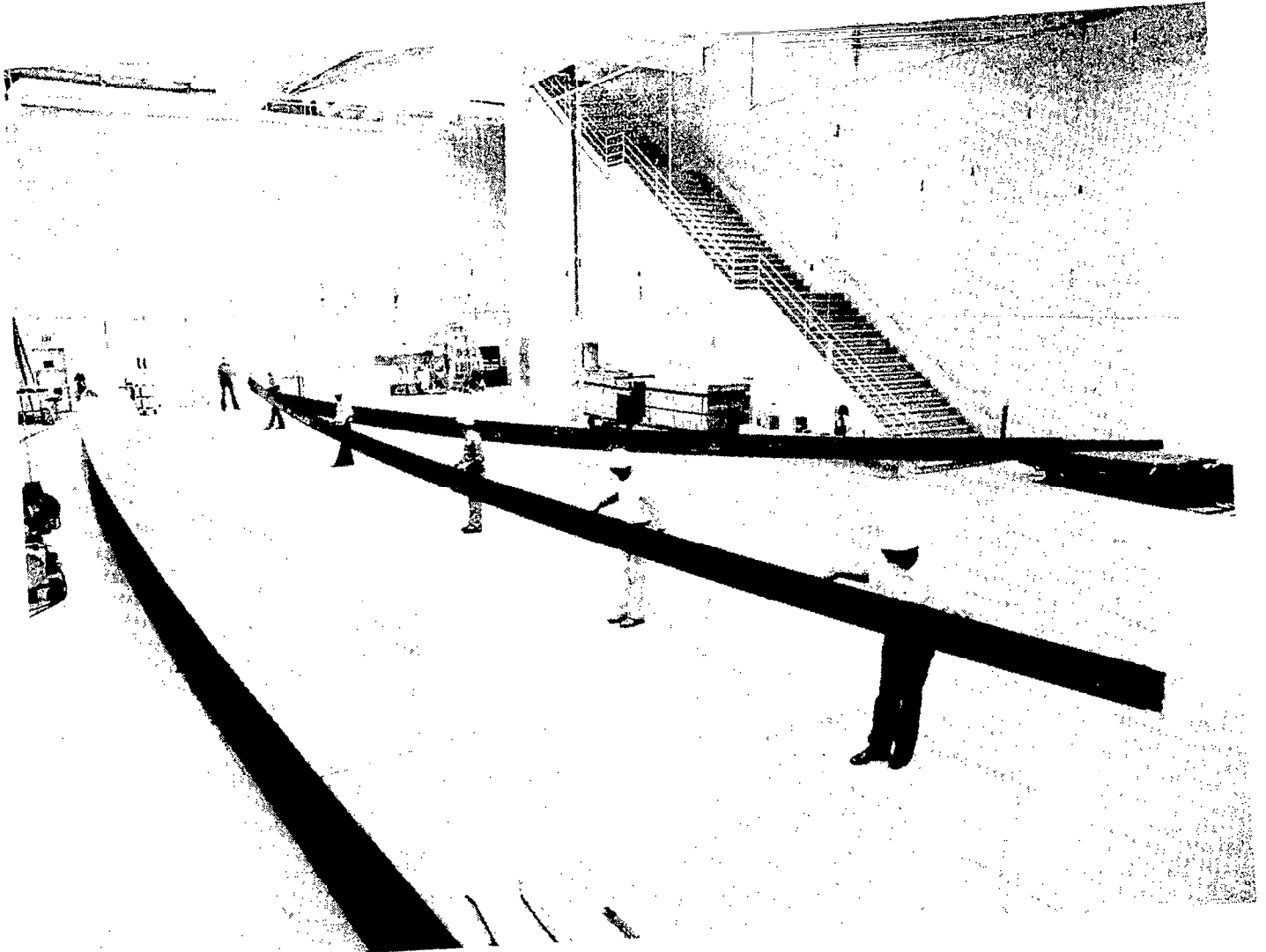
Figure 31

RIB ROOT HINGE ATTACHMENT

Hinge plates bonded and riveted at the upper and lower longitudinal edges of a rib mate with a clevis arrangement on the simulated hub. This scheme permits rib rotation and collapsing motions necessary for stowing (Figure 32).

Figure 32

SIMULATED HUB AND DEPLOYMENT MECHANISM

The simulated hub and deployment mechanism consists of a rotating hub powered by a flexible belt drive system and a tape deployment mechanism. When energized the hub rotates and the tape is drawn off the hub onto a take up reel, allowing the ribs to deploy tangent to the hub (Figures 33 and 34).
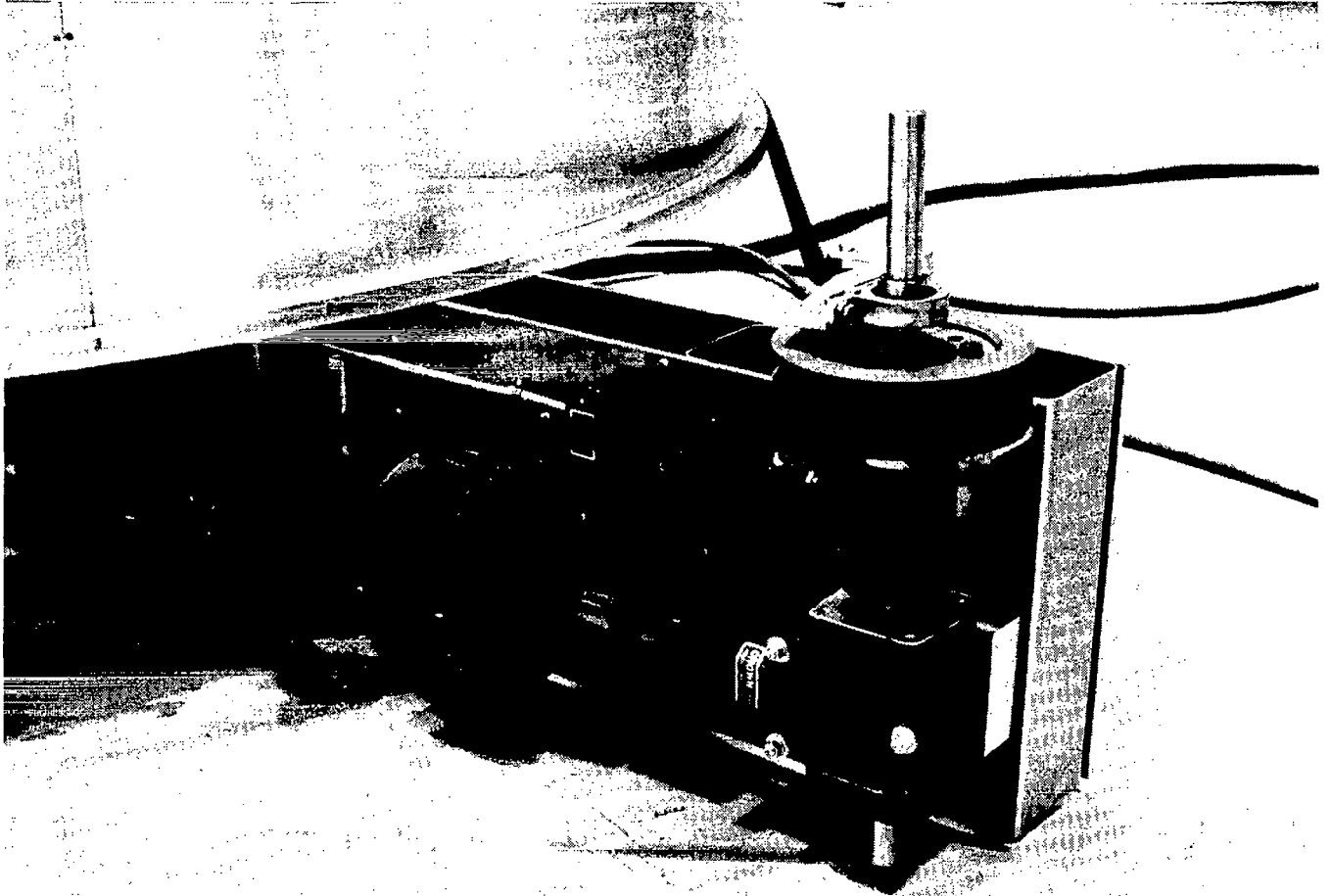
Figure 33
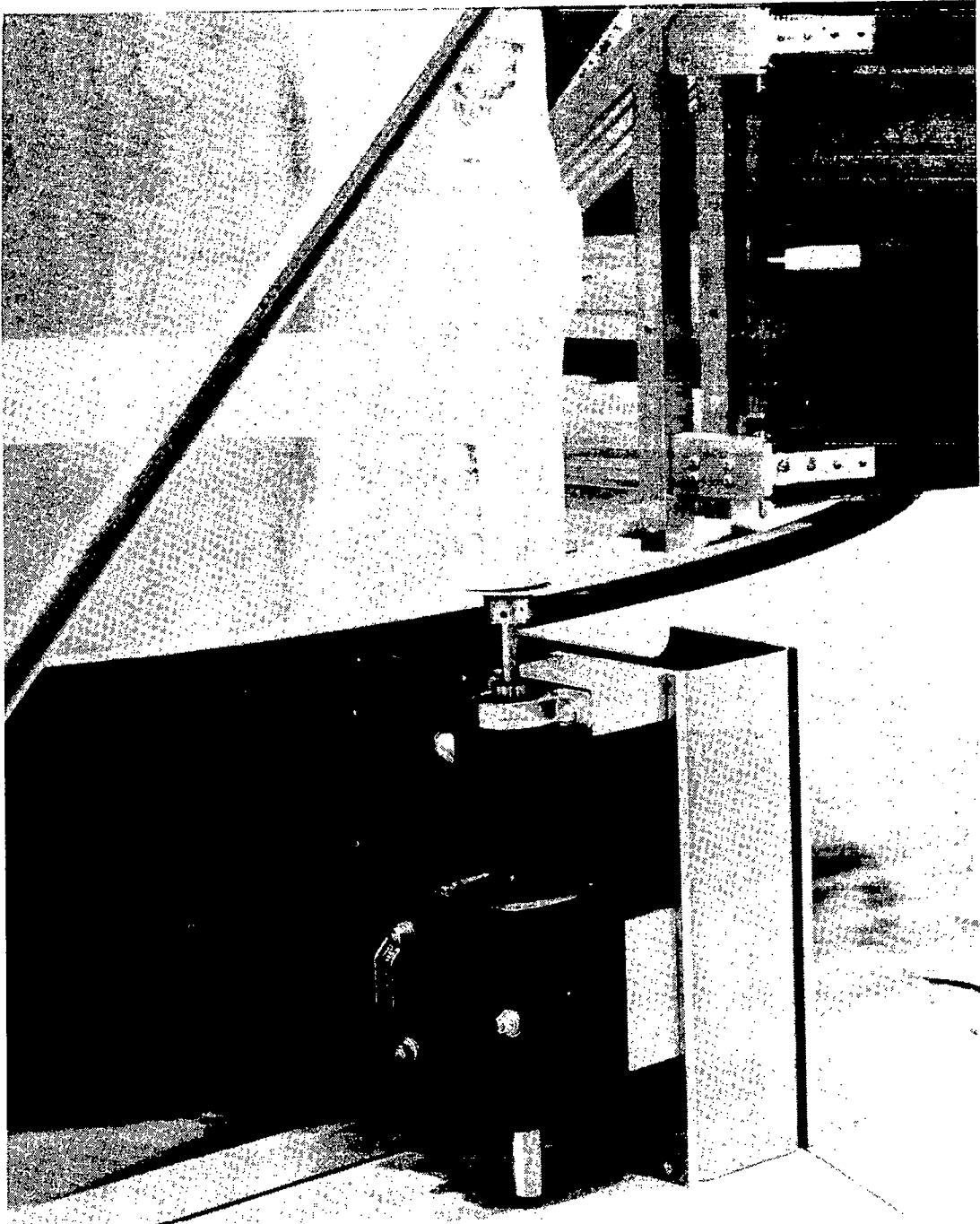
Figure 34

PARTIAL REFLECTOR DEPLOYMENT

A four rib partial reflector was successfully cycled through deployment and stowing cycles on November 4, 1982 (Figures 35 to 37).
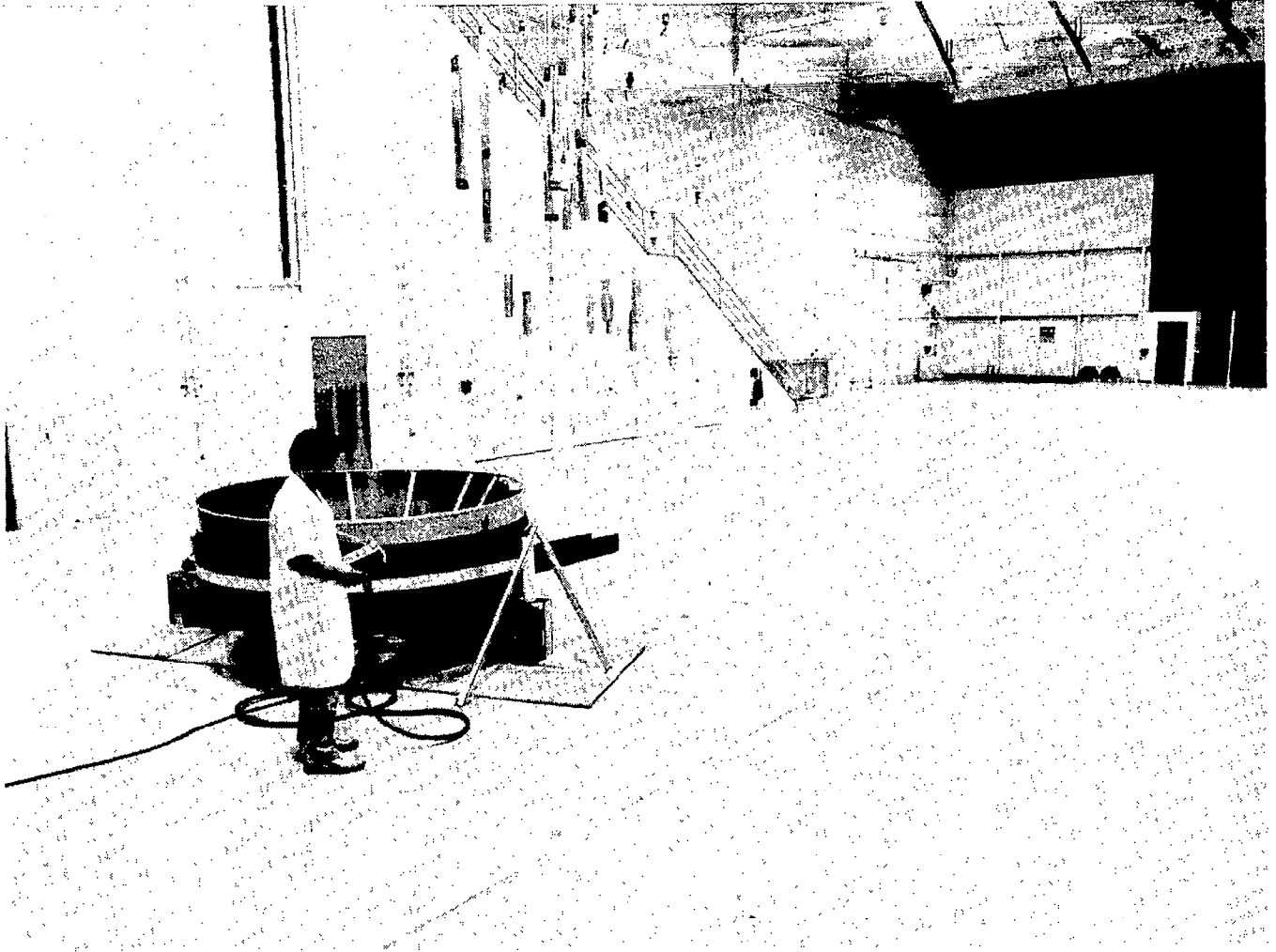
Figure 35
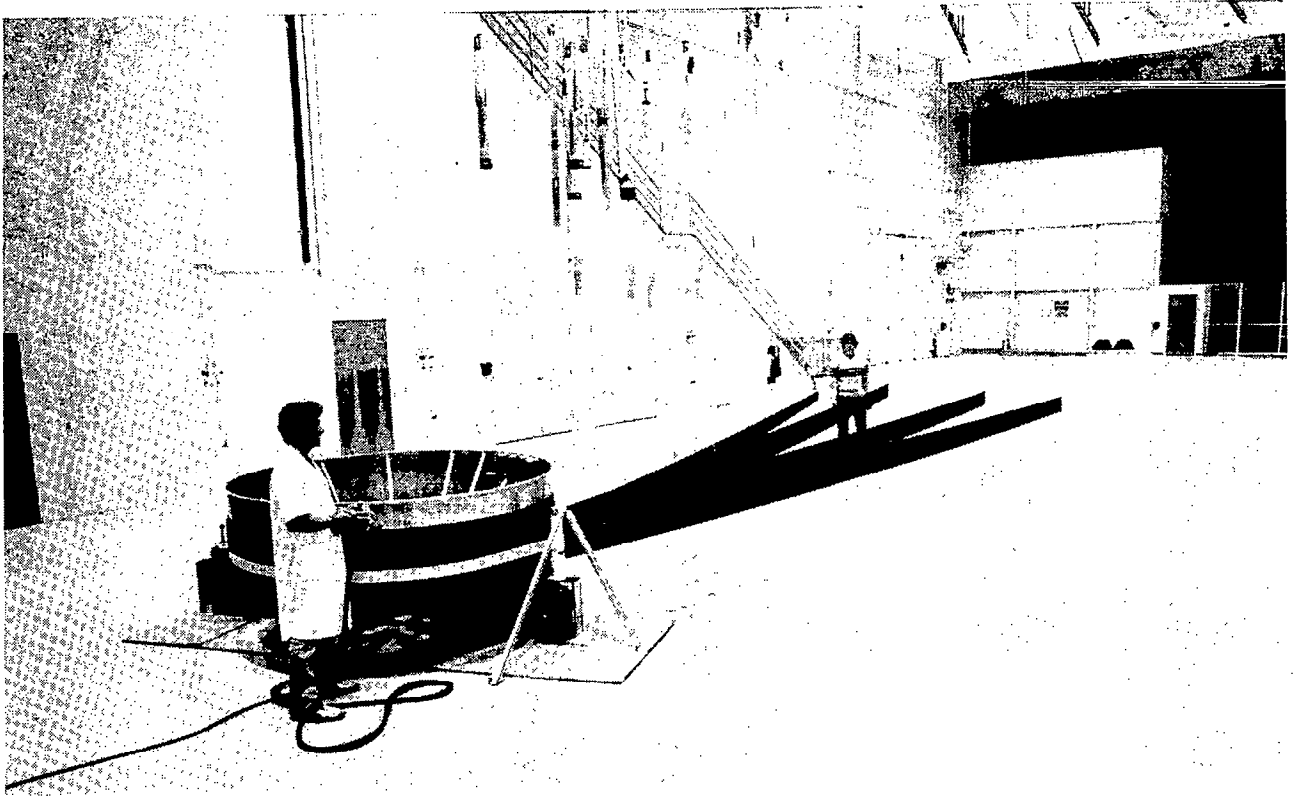
Figure 36

Figure 37

458
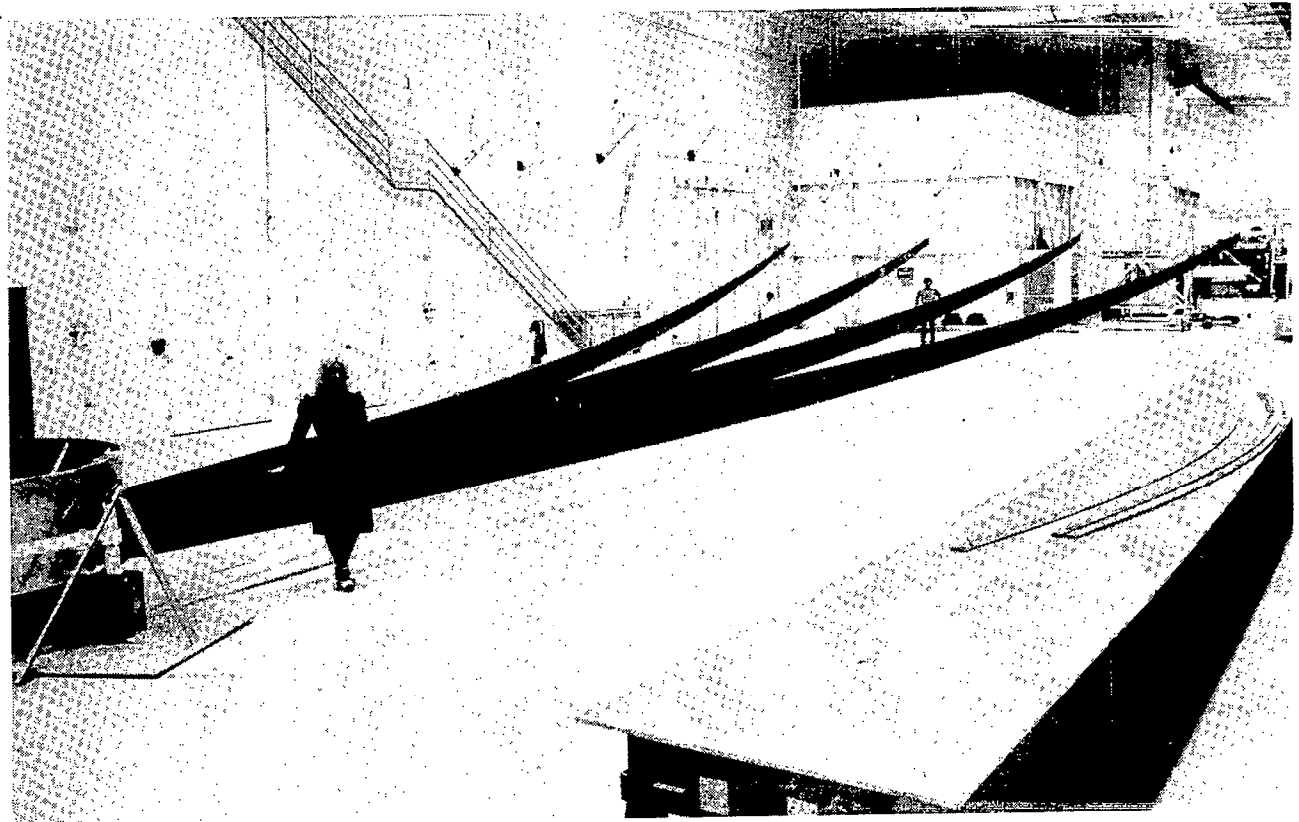
The remaining activities include assembly and installation of the mesh surface and the testing of the complete three gore, four rib reflector segment. This testing will be oriented toward deployment and retraction of the assembly to study mesh management, deployment repeatability and contour measurement.

Anticipating successful accomplishment of this testing and recognizing that program emphasis has been on hardware, additional objectives must now be identified. The primary structural components are in need of further analytical characterization through test and analysis correlation at both the component and assembly level. This would also bring forward the challenge of addressing the methods development for characterizing large space structures in the presence of ground based support constraints. The final objective of full qualification of hardware and software is gained through a flight experiment, which is the final program step (Figure 38).

CONCEPT

- INSTALL MESH SURFACE

- INVESTIGATE MESH MANAGEMENT

- DEMONSTRATE DEPLOYMENT/RESTOW

- SURFACE MEASUREMENT

TECHNOLOGY

- COMPONENT CHARACTERIZATION

- ASSEMBLY CHARACTERIZATION - STATIC AND DYNAMIC

    - WITH 1G SUPPORTS AND ANALYTICAL CORRELATION
    - WITH ACTIVE CONTROL OF SUPPORTS AND DIRECT MEASUREMENT

- CONFIRM ANALYTICS AND PERFORMANCE IN SPACE

Figure 38

Physical size and limited strength of large deployable space structural hardware constrain the application of available ground facilities and ultimately dictate requirements which can not presently be satisfied. These requirements concern not only size but environmental control of temperature, temperature gradients, and pressure gradients due to airflow and gravity. If advanced test facilities are to be constructed to satisfy these requirements we must recognize that the costs of constructing, instrumenting and controlling such a facility are extremely high even with respect to STS flight costs. An additional limitation which directly impacts the measurable hardware performance characteristics in the terrestrial environment, even if deployment of the large hardware can be accomplished on the ground, is that the measured parameters must be validated against mathematical models which include the effects of the local environment. This means that mode shape, stiffness and coupling characteristics are validated at best against models of a constrained, artificial structure. With the exception of the deployment function validation, the more significant performance metrics are significantly compromised. This suggests the use of the STS as a demonstration or qualification test facility. Based on facility costs alone this appears to be a justifiable decision. When the artificial analytical constraints are removed from the test environment, allowing direct measurement and validation of performance, the technological benefits become apparent (Figure 39).

OBJECTIVE

- STS SORTIE PAYLOAD FLIGHT VERIFICATION:
  - OFFSET 55 METER REFLECTOR
  - ACTIVE CONTROLS OF SPACE STRUCTURES (ACOSS)
  - RADIOMETER PAYLOAD

ADDITIONAL BENEFITS

- ENTERS THE TECHNOLOGIES INTO THE MAINSTREAM OF SPACE PROGRAMS

- REDUCES TO PRACTICE THE APPLIED TECHNOLOGY FEATURES ASSOCIATED WITH SUPPORTING HARDWARE/SOFTWARE AND OPERATIONAL USE

Figure 39

GROUND TESTING AND FLIGHT DEMONSTRATION

The programmed ground testing of the partial reflector and feed support structures recognizes the high cost/low benefit return of full ground qualification of this technology and, as a result, terminates short of a full hardware set completion. The objectives are mechanism demonstration, proof of overall concept and limited identification of performance characteristics. The ground test hardware has, however, been constructed to permit completion of both the 55-meter offset reflector and the feed support structures. This capability had led to the emergence of a program plan leading to a complex flight experiment which will involve the validation of the full spectrum of performance characteristics.

The objectives of the flight demonstration experiment which could be conducted as early as 1988 are (a) deployment and re-stow verification of both the reflector and feed support structure, (b) measurement of static surface figure, (c) measurement of thermal figure as a function of Sun orientation, (d) measurement of deployment repeatability effects on figure, (e) structural dynamics characterization for open- and closed-loop control, (f) evaluation of active figure control techniques, and (g) demonstration of in-flight processor modification. These objectives of necessity involve far more technology than exists in the reflector and feed support structure alone. These additional enabling technologies are absolute and relative precision measurement of deflection, velocity and acceleration, multiple input/output distributed control processor, sensors and actuators, and open- and closed-loop structural characterization techniques. These supporting technologies have been developed at the Jet Propulsion Laboratories and Lockheed Missiles and Space Company to the level required to support a 1988 flight experiment, assuming a Fiscal Year 1984 program commitment (Figure 40).

- ACOSS

- REFLECTOR

- RADIOMETER

- OPERATIONAL TIMELINE

Figure 40

ACTIVE CONTROL OF ANTENNA SYSTEMS

Introducing and demonstrating active control of space structures on an antenna flight experiment affords confirmation of our ability to integrate the technologies of structural design and controls. These benefits in the development of "control configured" systems design can allow orders of magnitude of performance improvement in dynamically critical structures which are weight or volume critical, and conversely can allow weight and volume savings to be realized (Figure 41).

CONTROL SYSTEM PERFORMANCE

● RANDOM DISTURBANCE REJECTION, SLEW

    – RESPONSE; 2 ORDERS OF MAGNITUDE

    – DELAY; 25% CRITICAL DAMPING

● NON-RANDOM, ONBOARD DISTURBANCE REJECTION

    – RESPONSE; 5 ORDERS OF MAGNITUDE (SINGLE FREQUENCY)

    – RESPONSE; 3 ORDERS OF MAGNITUDE (NARROWBAND)

    – RESPONSE; 2 ORDERS OF MAGNITUDE (BROADBAND)

HIGH GAIN ANTENNA VIBRATION CORRECTION

● BEAM POINTING

    – ERROR REDUCTION OF 10^2 TO 10^4

    – EG; 0.1 DEG → 10^{-3} TO 10^{-5} DEG

● SURFACE FIGURE

    – ERROR REDUCTION OF 10^4 TO 10^{10}

    – EG; 3 dB → 0.2 TO 0 dB

Figure 41

ACTIVE CONTROLS DEVELOPMENT STATUS

The ACOSS technology is on a parallel with the reflector development program. The theory has been developed. implemented and tested on ground validation simulations. The final verification is being accomplished on a test item which replicates an offset antenna spacecraft. Anticipating successful conclusions of this testing, the ACOSS technology is awaiting final qualification in a flight test program (Figure 42).

Figure 42

SCIENCE MISSION

Considering the overall expense of a large structures and controls flight experiment a science payload should be incorporated. A radiometer payload has been selected as best satisfying the overall mission objectives, allowing further antenna and controls validation and developing useful science data (Figure 43).

COOPERATIVE TARGET

TARGETS OF OPPORTUNITY
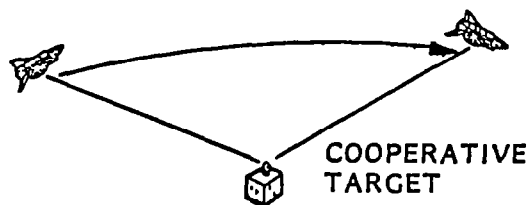
- STS POINTS AT GROUND TARGET OR FIXED PITCH/ROLL ANGLE

- TOTAL OPERATIONAL TIME/TASKING:

    <30 MIN FOR FIXED TARGET

    <25 MIN + DATA TAKE FOR TARGETS OF OPPORTUNITY
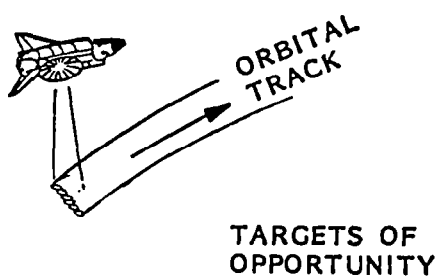
- DATA; TAPE RECORDED/REAL TIME TLM

    - P/L STATUS AND DIAGNOSTICS
    - RADIOMETER
    - 35 mm CAMERA FILM

Figure 43

OPERATIONAL TIMELINE

The mission timeline has been reviewed to determine viability with a seven day orbit timeline. The initial review indicates that the program elements can be accomplished within 9% to 20% of the total orbit timeline (Figures 44 and 45).

- OPERATIONAL SEQUENCE AND TASKING TIME (MINUTES)

- TOTAL TIME

EVENT	TIME (MIN)
INITIAL C/O/DEPLOY	35
RADIOMETER MISSION	420 TO 1,260
ACOSS	160 TO 360
REFLECTOR	250
STOW	20
	870 TO 1,925

- ELAPSED TIME

  - 4 DAYS MINIMUM
  - 6 DAYS MAXIMUM

8.7% TO 19.1% OF
7 DAY ON-ORBIT TIME
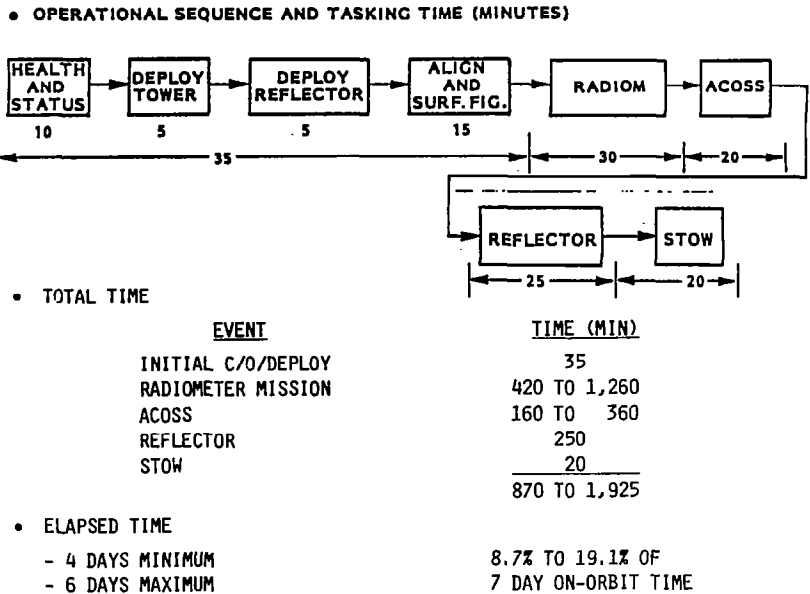
Figure 44

Figure 45

465
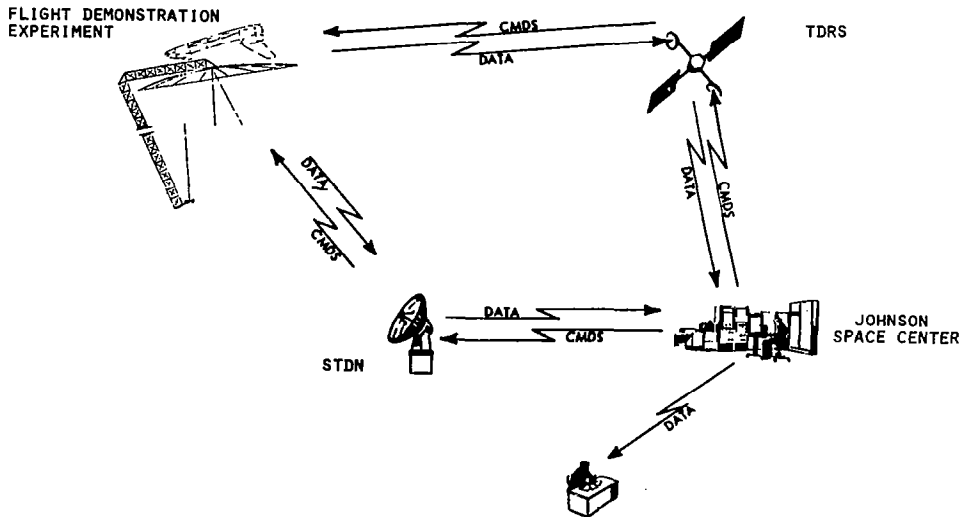
The experiment compatibility with the STS has also been reviewed. The volume, weight and power requirements are within operational constraints as are the interfaces as indicated by a review of a complete experiment block diagram (Figures 46 and 47).

VOLUME, WEIGHT AND POWER SUMMARY

STOWED VOLUME

REFLECTOR	13 FT DIA BY 2 FT LONG
MAST	9 FT DIA BY 23 FT LONG
P/L	14 FT DIA BY 4 FT LONG
	14 FT DIA X 23 FT LONG

OPERATING POWER

FEED & RADIOMETER	550 WATTS
ACOSS	2,400
TLM & CMD	30
THERMAL	400
PWR DIST/INTERCONNECT	220
CONTINGENCY (20 %)	720
	4,320 WATTS

WEIGHT

REFLECTOR	1,250 LBS
MAST	600
FEED & RADIOMETER	400
ACOSS	250
TLM & CMD	20
STRUCTURE	900
THERMAL	150
PWR DIST/INTERCONNECT	200
CONTINGENCY (20%)	750
	4,520 LBS

Figure 46

466

EXPERIMENT PAYLOAD BLOCK DIAGRAM
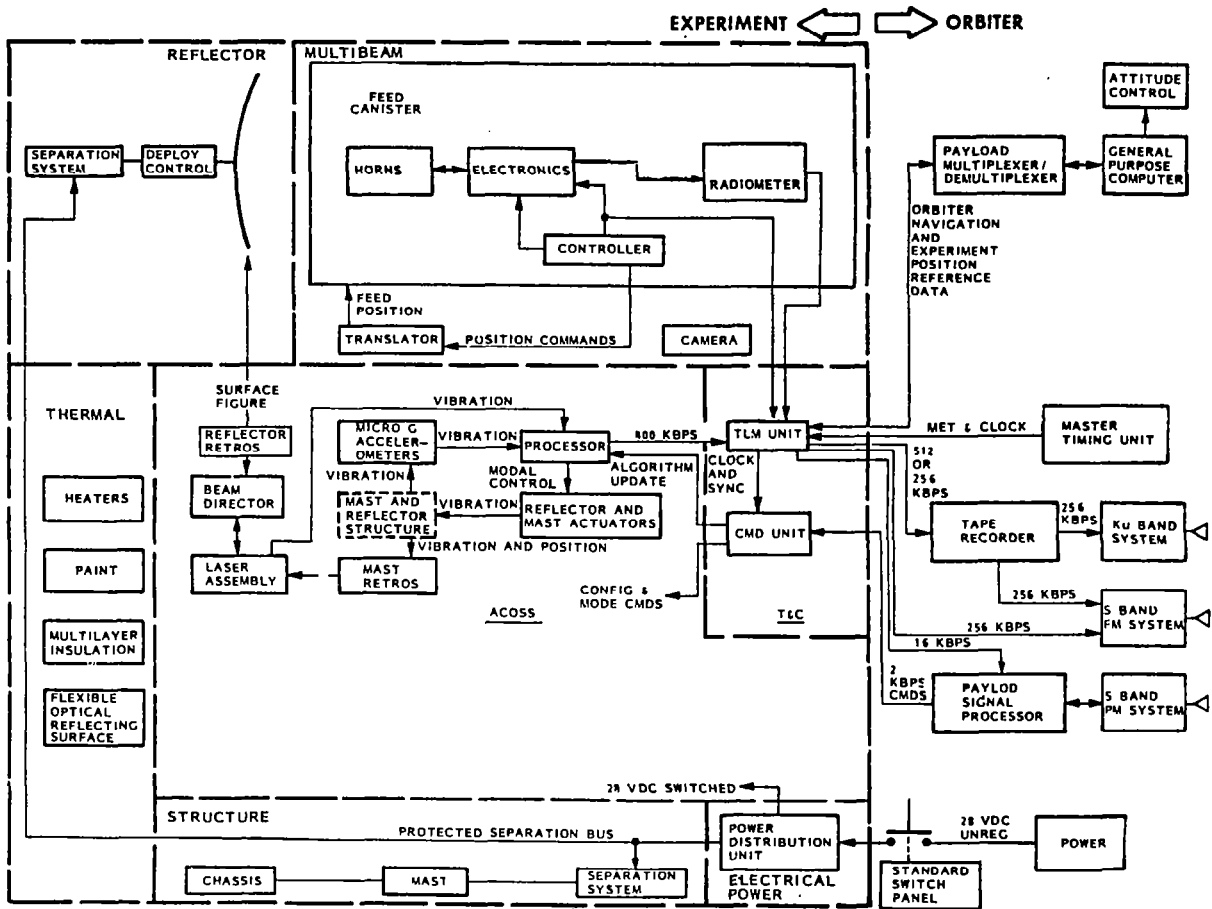
Figure 47

467

FLIGHT DEMONSTRATION EXPERIMENT SCHEDULE

A review of the technology program status and identification of the development timelines for the experimental subsystems and interface and ground support subsystems has been accomplished. The timeline developed indicate that an experiment can be flown in the last quarter of FY 1988 providing the program is initiated in FY 1984 (Figure 48).

FY

1984	1985	1986	1987	1988
▽ GO AHEAD ▽ PDR	▽ CDR			SHIP ▽ ▽
				LAUNCH

55 M REFLECTOR

ACOSS

MODEL TEST

ASSEMBLY

MAST, STRUCTURE

FEED AND RADIOMETER

FINAL ASSEMBLY

FAR FIELD TEST

SYSTEM TEST

ELECT., THERMAL, TUM. AND CMD.

STS MATE TEST

GSE, TEST S/W, PROCEDURES

FLIGHT ANALYSIS & REPORT

PIP   ICD   ▽▽▽   CIR ▽   FINAL PIP FRR ▽ ▽

STS INTEGRATION
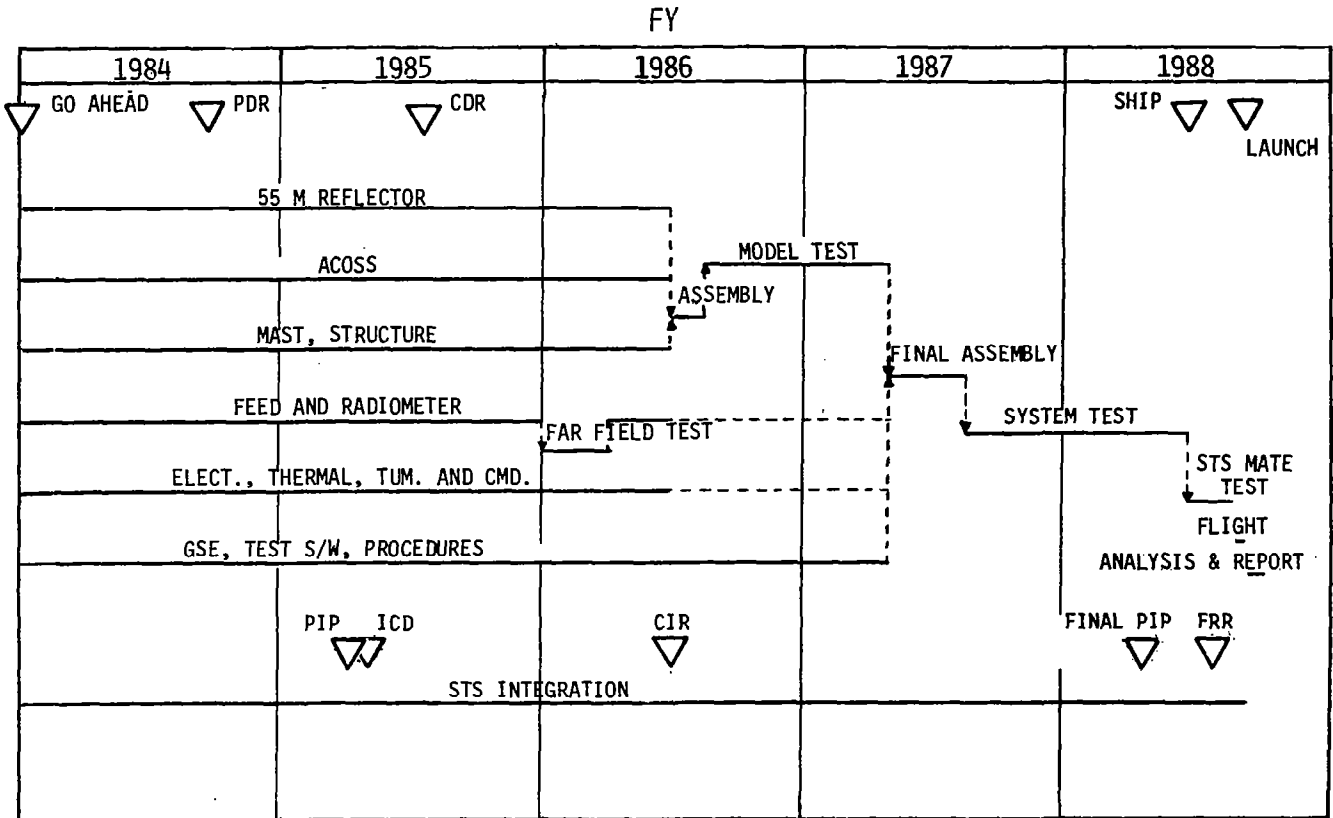
Figure 48

HOOP/COLUMN ANTENNA
DEVELOPMENT PROGRAM

M. R. Sullivan
Harris Corporation
Melbourne, Florida

HOOP/COLUMN ANTENNA DEVELOPMENT PROGRAM

   The results of the development program to date indicate the versatility
of the generic concept. Performance evaluations of the hoop/column concept
have shown that it is capable of meeting the requirements of future identified
large antenna missions.
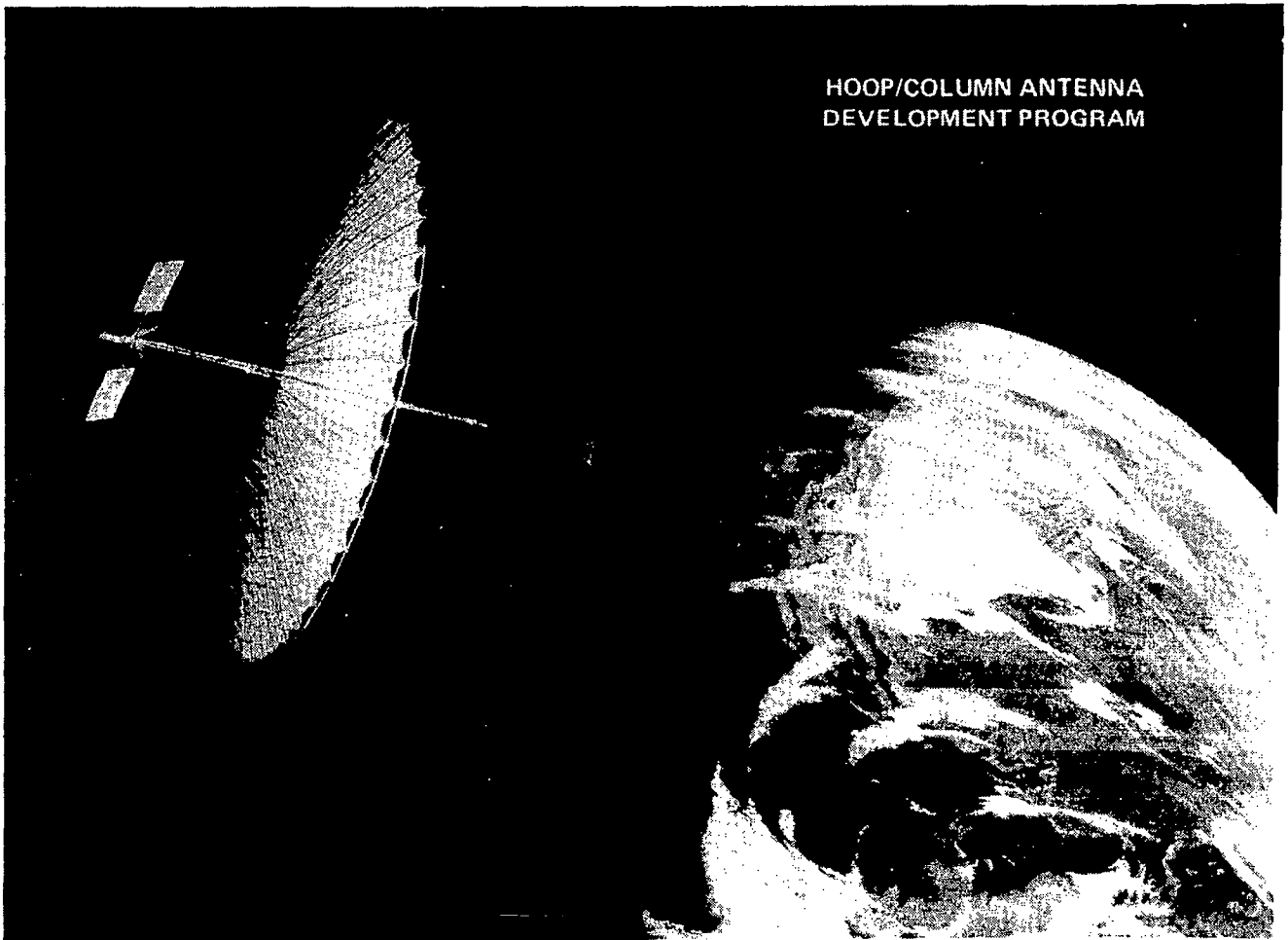
TASK DESCRIPTIONS AND PROGRAM OBJECTIVES

The hoop/column antenna development program is divided into six tasks. All six tasks support the main objective of the program, which is to develop the technology necessary to evaluate, design, manufacture, package, transport, and deploy the hoop/column reflector by means of a ground-based test program.

TASK 1: PRELIMINARY DESIGN AND PERFORMANCE

TASK 2: MATERIALS DEVELOPMENT

TASK 3: ADVANCED CONCEPTS

TASK 4: ECONOMIC ASSESSMENT

TASK 5: DEMONSTRATION/ VERIFICATION MODELS
- COMPONENTS
- 50-METER SECTOR
- RF TEST MODEL

TASK 6: 15-METER ENGINEERING MODEL

PROGRAM OBJECTIVE

DEVELOP THE TECHNOLOGY NEEDED TO:
- EVALUATE
- DESIGN
- MANUFACTURE
- PACKAGE AND TRANSPORT
- DEPLOY

THE HOOP/COLUMN REFLECTOR VIA A GROUND-BASED TEST PROGRAM

SCHEDULE SUMMARY

The total program length is approximately 5 1/2 years, and the program culminates with the design, fabrication, and test of a fully operable engineering scale model.

	FY 79	FY 80	FY 81	FY 82	FY 83	FY 84
TASK 1: ANTENNA DESIGN AND PERFORMANCE						
TASK 2: MATERIALS DEVELOPMENT		GRAPHITE CABLES	QUARTZ CABLES		TESTING	
TASK 3: ADVANCED CONCEPTS						
TASK 4: ECONOMIC ASSESSMENT						
TASK 5: MODELS o DEMONSTRATION o 50-METER SURFACE o RF VERIFICATION		HOOP MAST	DESIGN FAB AND TEST APPROACH ANAL, FAB AND TEST			
TASK 6: 15-METER ENGINEERING MODEL		CONCEPT		DESIGN	FAB AND TEST	

POINT DESIGN SELECTION

The program began with a review of the NASA-supplied mission scenarios for the communications, radiometry, and radio astronomy missions. The study of these mission scenarios led to specific hoop/column antenna configurations for each mission. The mission configurations were then evaluated to identify specific technology items that required further development. The compilation of these technology drivers resulted in a specification of a point design. All design and performance estimates for the program were made for the point design.

REVIEW MISSION
        SCENARIOS: COMMUNICATIONS   RADIOMETRY   RADIO/ASTRONOMY

DEVELOP CONFIGURATIONS:

IDENTIFY TECHNOLOGY DRIVERS:

POINT DESIGN SPECIFICATION

REFLECTOR
REQUIREMENTS
DOCUMENT

MATERIALS
DEVELOPMENT

CONCEPTUAL DESIGN

PRELIMINARY ANALYSIS

MANUFACTURING PLAN

VERIFICATION MODELS

TEST PLAN

PERFORMANCE ESTIMATES

PRELIMINARY
DESIGN

PHASE I
DESIGN REVIEW
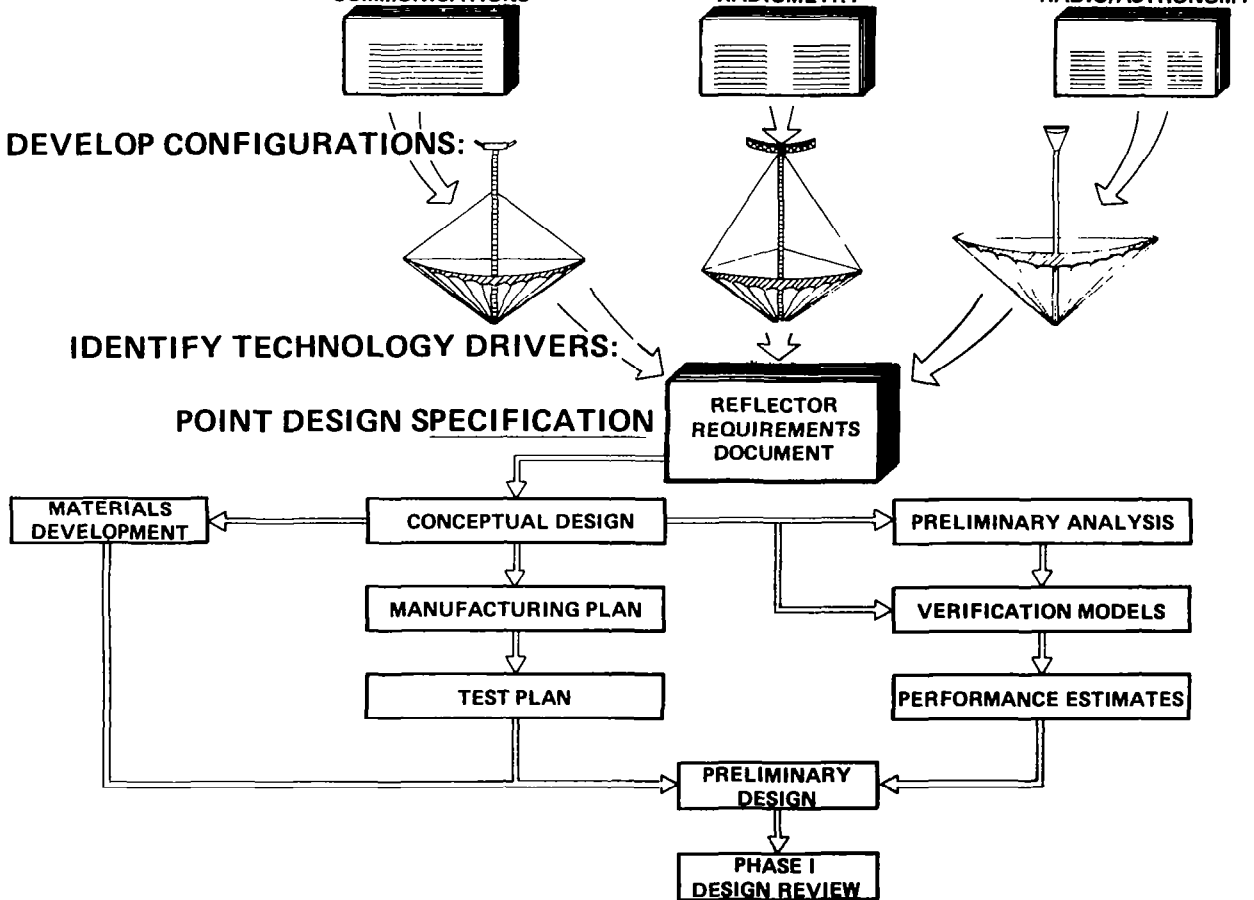
STS COMPATIBILITY

A study of the hoop/column antenna for the Land Mobile Satellite System application determined that a 122-meter-diameter reflector can be packaged in the STS cargo bay along with the multiple-beam feed, spacecraft, and booster (IUS) for transportation to high Earth orbit.
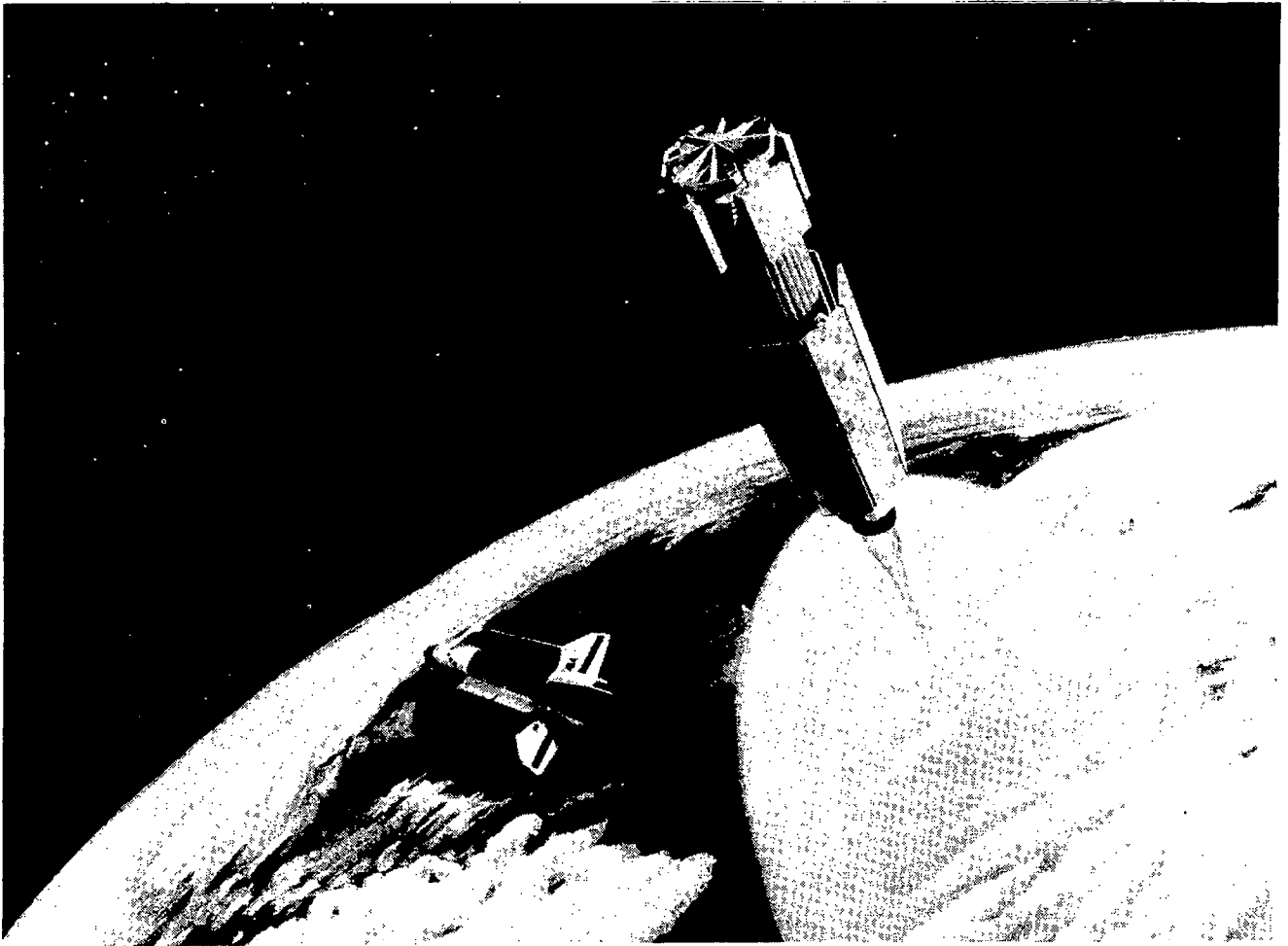
HOOP/COLUMN ANTENNA DEPLOYMENT SEQUENCE

The deployment sequence of the hoop/column antenna is initiated by the extension of the main structural mast. Once this mast extension is completed, the hoop begins to deploy outward. The energy for deployment is provided by four separate drive units located on joints 90^0 apart around the hoop. Once the hoop is deployed to its full circular approximation, a separate section of the mast called the preload section is deployed. This motion tensions all of the hoop support cables and thus preloads the system.

475
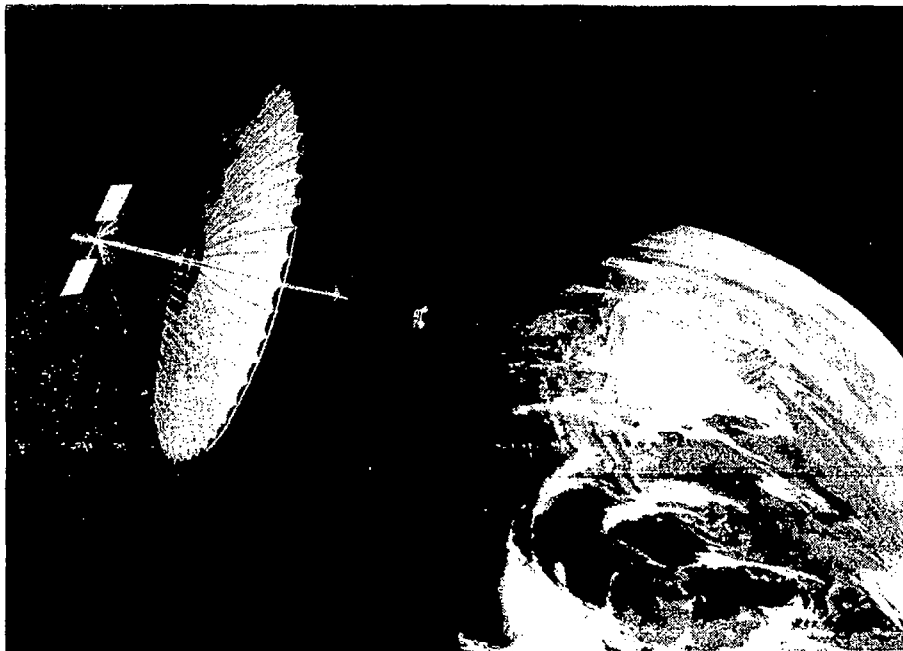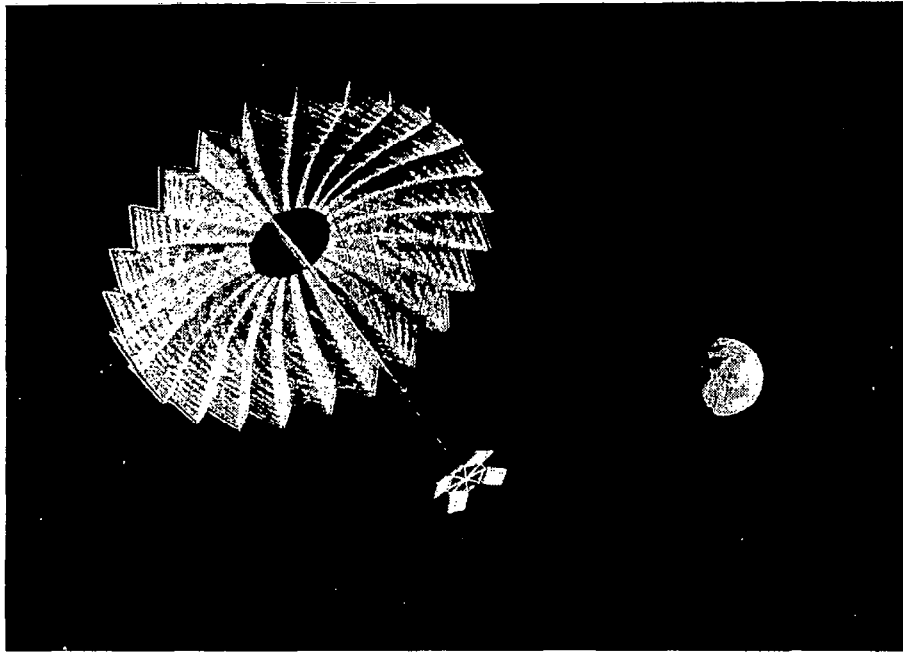
CONFIGURATION OF HOOP/COLUMN
POINT DESIGN - DEPLOYED CONFIGURATION

The deployed configuration of the hoop/column point design is shown below. A 100-meter point design has been selected which provides the quad aperture reflector system.

ANTENNA GEOMETRY
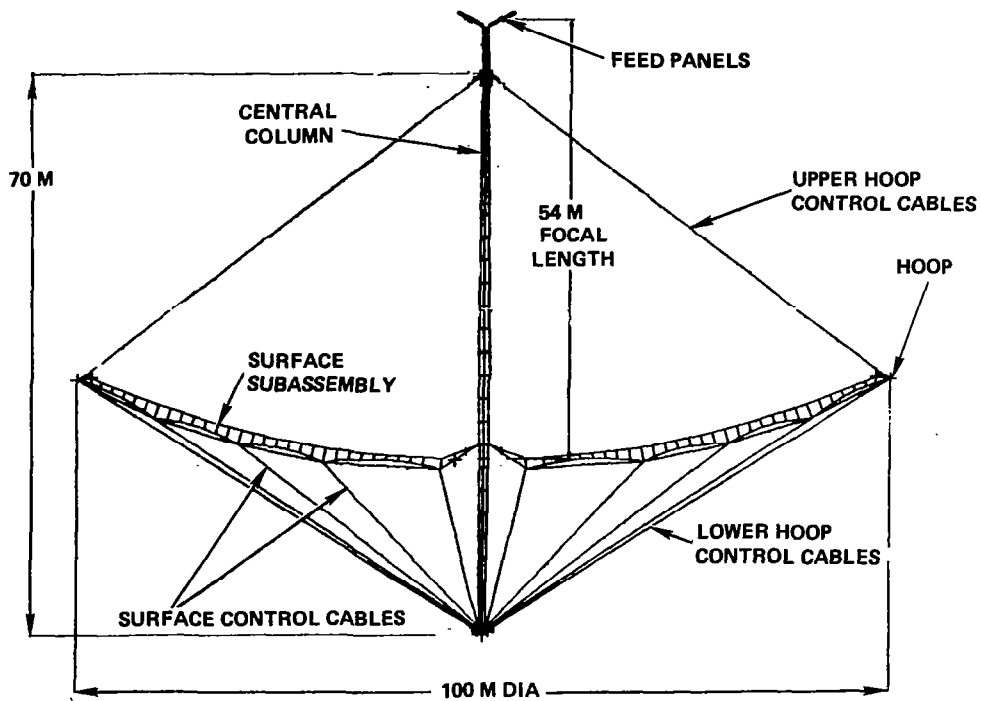
REFLECTOR SURFACE

The point design is a multiple-beam/multiple-quadrant offset reflector system. Four separate areas of illumination or aperture areas on the parent reflector are shown by imaginary lines. The surface is shaped as if it were four offsets; thus the parent reflector is cusped.

SURFACE - PLAN VIEW

VERTEX (TYP 4 PLACES)

SURFACE OF ILLUMINATION (IMAGINARY LINES)

90°

RADIAL CORD
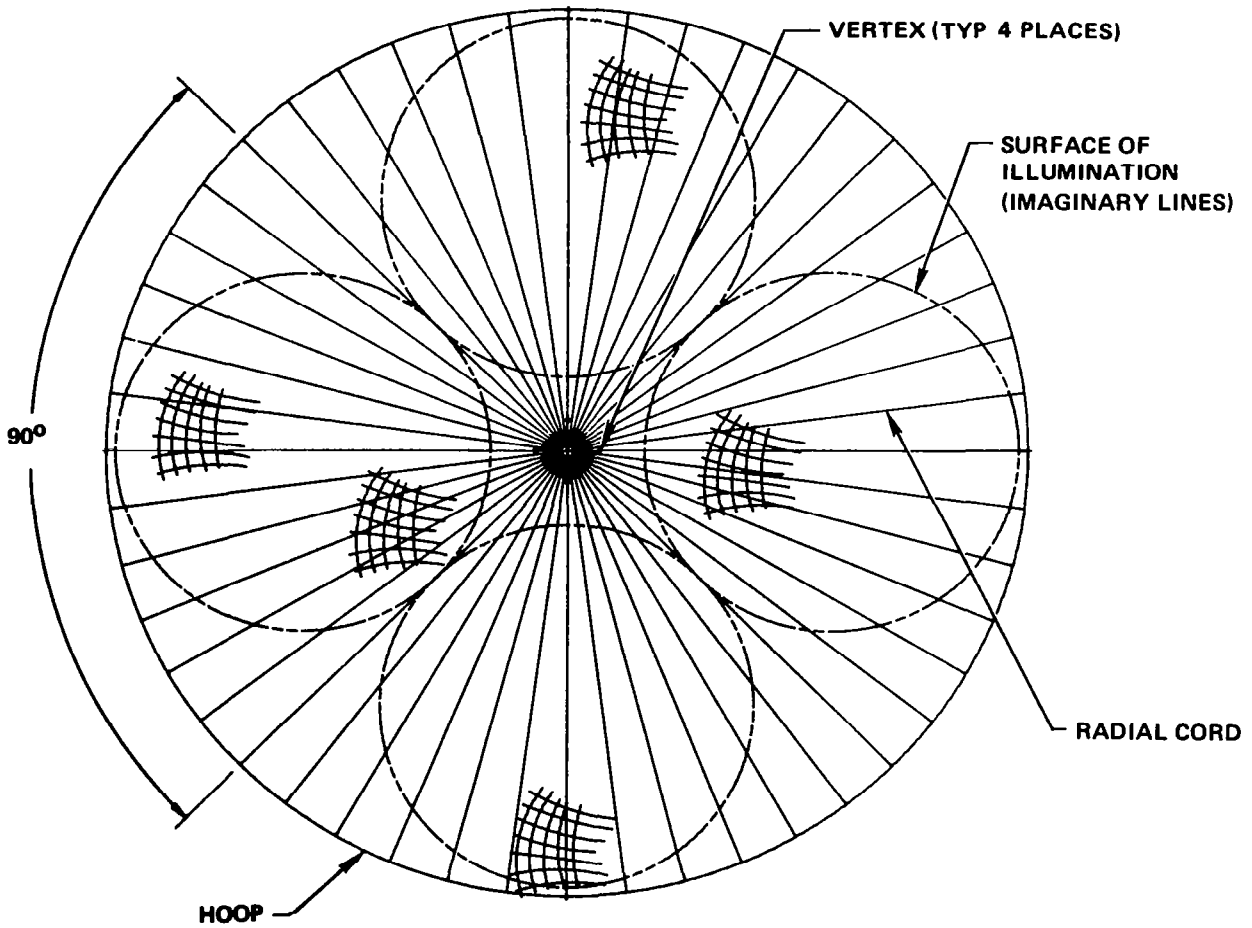
HOOP

POINT DESIGN STOWED CONFIGURATION

The stowed hoop/column antenna packages vary efficiently within the constraints of the Shuttle bay. The configuration selected for the point design, which is a 100-meter diameter deployed reflector, utilizes 48 articulating hoop segments. This dictates the aspect ratio of length to diameter of the stowed package. The aspect ratio can be modified for any given deployed diameter by changing the number of hoop segments.

STOWED GEOMETRY (100-METER DESIGN)

(15')
4.56M
SHUTTLE MAX PAYLOAD ENVELOPE

FEED PANELS

HUB

SKEWER (TYP)

STOWED MESH

HOOP

6.32 M (20.7')

7.20 M (23.6')

1.98 M (6.7')

SIDE VIEW
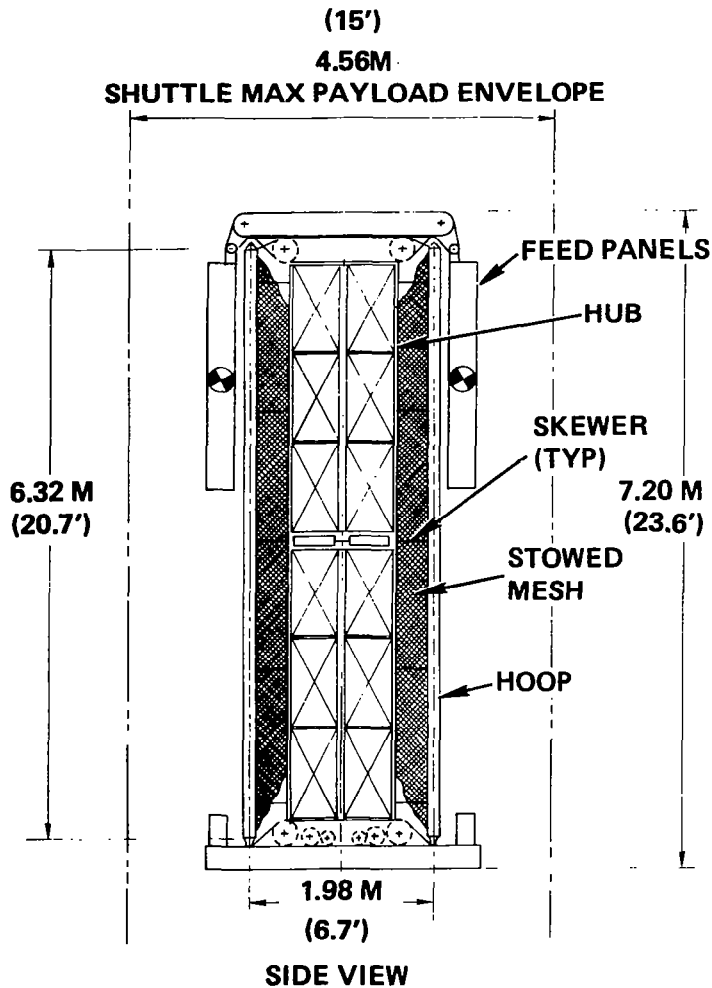
CABLE DEVELOPMENT

Extensive research of cable materials and constructions led to the selection of continuous graphite fiber cables that were impregnated with Teflon while under load to improve fiber load sharing and handling toughness. The cables have demonstrated a combination of low thermal expansion and residual strain unique to flexible cable materials.

TEFLON-COATED GRAPHITE CORD PRODUCTION

SPECIAL ACRYLIC FIBRE

OXIDATION
INERT GAS
CARBONIZATION
INERT GAS
GRAPHITIZATION
SURFACE TREATMENT
GRAPHITE FIBER PRODUCTION
CONTINUOUS FIBRE TOW (TYPICALLY) 800 to 1200 METERS BETWEEN SPLICES)
HIGH E
MED E
LOW E
TEFLON IMPREGNATION
DRYING
SINTERING
SPOOLING
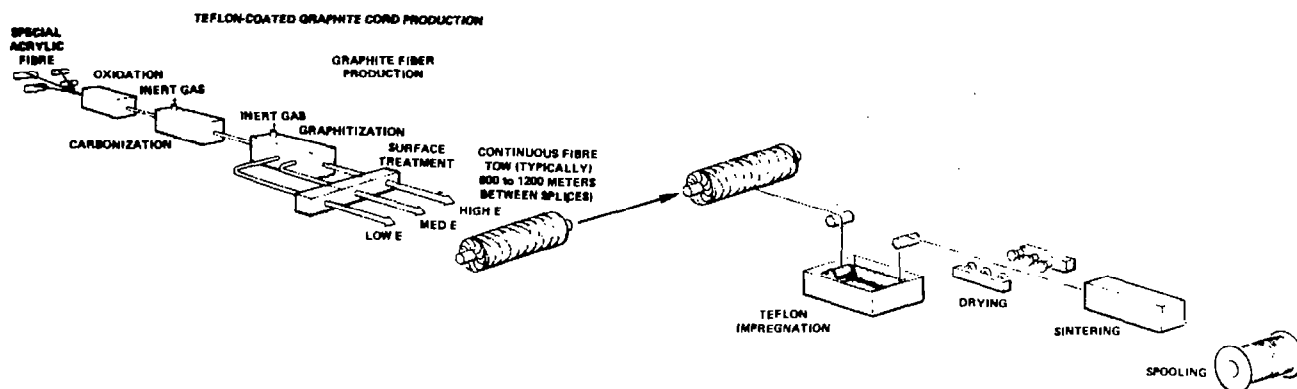
CABLE MANUFACTURE IS VERIFIED

CABLE PROPERTIES ARE VERIFIED

- STRENGTH
- STIFFNESS
- RESIDUAL STRAIN
- COEFFICIENT OF THERMAL EXPANSION (CTE)

CURRENT CABLE RESEARCH

The final phase of the cable development task consists of process and material optimization and statistical base testing.

- PROVIDE MORE OPTIMUM COATING PROCESSES AND MATERIALS

    - HANDLING TOUGHNESS

    - SURVIVABILITY (RADIATION)

- PERFORM STATISTICAL DATA BASE TESTING USING IMPROVED EQUIPMENT

    - RESIDUAL STRAIN

    - CTE

    - EA

    - STRENGTH

    - ENVIRONMENTAL TESTING

THERMAL CYCLE CHAMBER

A Harris-built thermal cycle chamber will be used for future cord CTE and creep testing. The chamber is a Harris capital expenditure that will greatly reduce the cost and increase the accuracy of future cable testing.

HARRIS BUILT THERMAL CYCLE CHAMBER WILL BE USED FOR FUTURE CABLE AND MMC MATERIALS TESTING

VACUUM CHAMBER

LIQUID NITROGEN SHROUD AND RADIANT HEATERS

TEST SPECIMEN (WIRE OR OTHER STRUCTURAL SHAPES)

SLVC LENGTH MEASUREMENT SENSOR
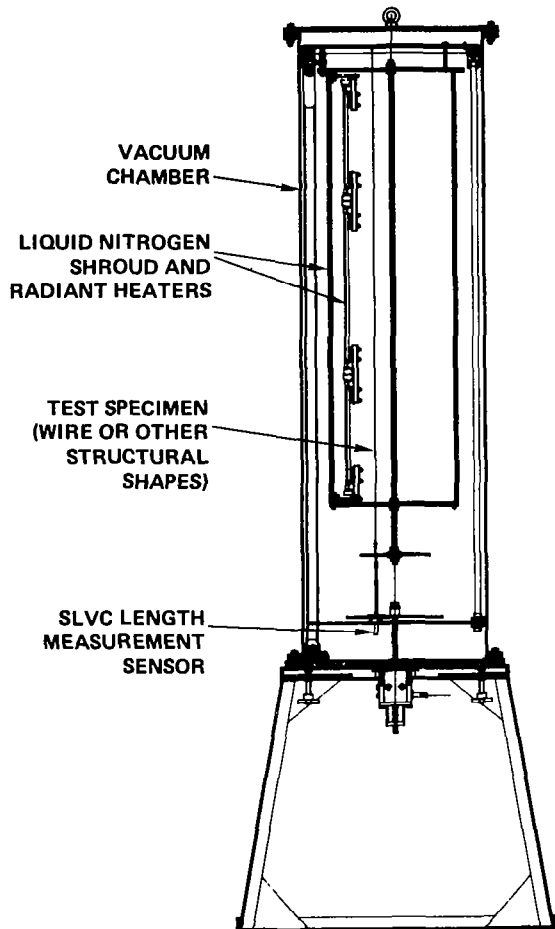
SPECIFICATIONS
- TEMPERATURE RANGE: -185°C TO 150°C (-300°F TO 300°F)
- PROGRAMMED TEMPERATURE PROFILES
- CYCLE TIME: 40 MINUTES
- NUMBER OF SPECIMEN PER TEST: 12
- STRAIN MEASUREMENT ACCURACY: $\pm 1\mu\epsilon$
- TEMPERATURE ACCURACY CONTROL: ± 3°C (5°F)
- SPECIMEN MAXIMUM LENGTH: 127 cm (50 IN)

OUTPUTS
- CONTINUOUS PLOTS OF TEMPERATURE AND LENGTHS
- COEFFICIENT OF THERMAL EXPANSION
- STRAIN VERSUS NUMBER CYCLES
- CREEP VERSUS TEMPERATURE AND/OR TIME

DEMONSTRATION MODELS

Hoop Model: A model of three full-scale hinge joints with truncated
hoop segments was fabricated to evaluate the hoop's deployment, synchroni-
zation, and repeatability. A single drive unit deploys the model; synchroni-
zation is accomplished by means of synchronizing strips that connect adjacent
hinge platforms, and drive motion is accomplished by means of a push-rod
link.

Mast Model: Design verification of the mast was accomplished by means
of a deployment model that represents an approximate one-fifth scale of the
point design.

Stowage Model: A method of stowing and deploying the mesh in an
organized and unobstructed manner has been preliminarily confirmed by a
NASA-developed mesh management model.

Surface Model: A 30-degree sector of a 50-meter diameter reflector
surface was fabricated to demonstrate the ability to fabricate very large
antenna surfaces.

DEMONSTRATION MODELS

HOOP
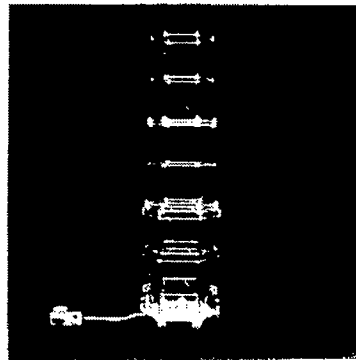
MAST

STOWAGE
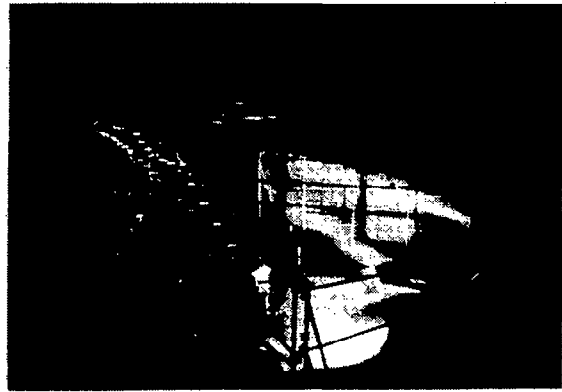
SURFACE

50-METER SURFACE MODEL OBJECTIVES

This model represents a logical step toward the eventual goal of fabrication of very large antenna surfaces. The objectives of the task are defined in the figure below.

OBJECTIVES:

- DEMONSTRATE SURFACE ACCURACY AND ADJUSTMENT CAPABILITY
- VERIFY ANALYTICAL MODELS
- EVALUATE FABRICATION AND ASSEMBLY TECHNIQUES
- PROVIDE TEST BED FOR OPERATIONAL DEMONSTRATION OF SAMS
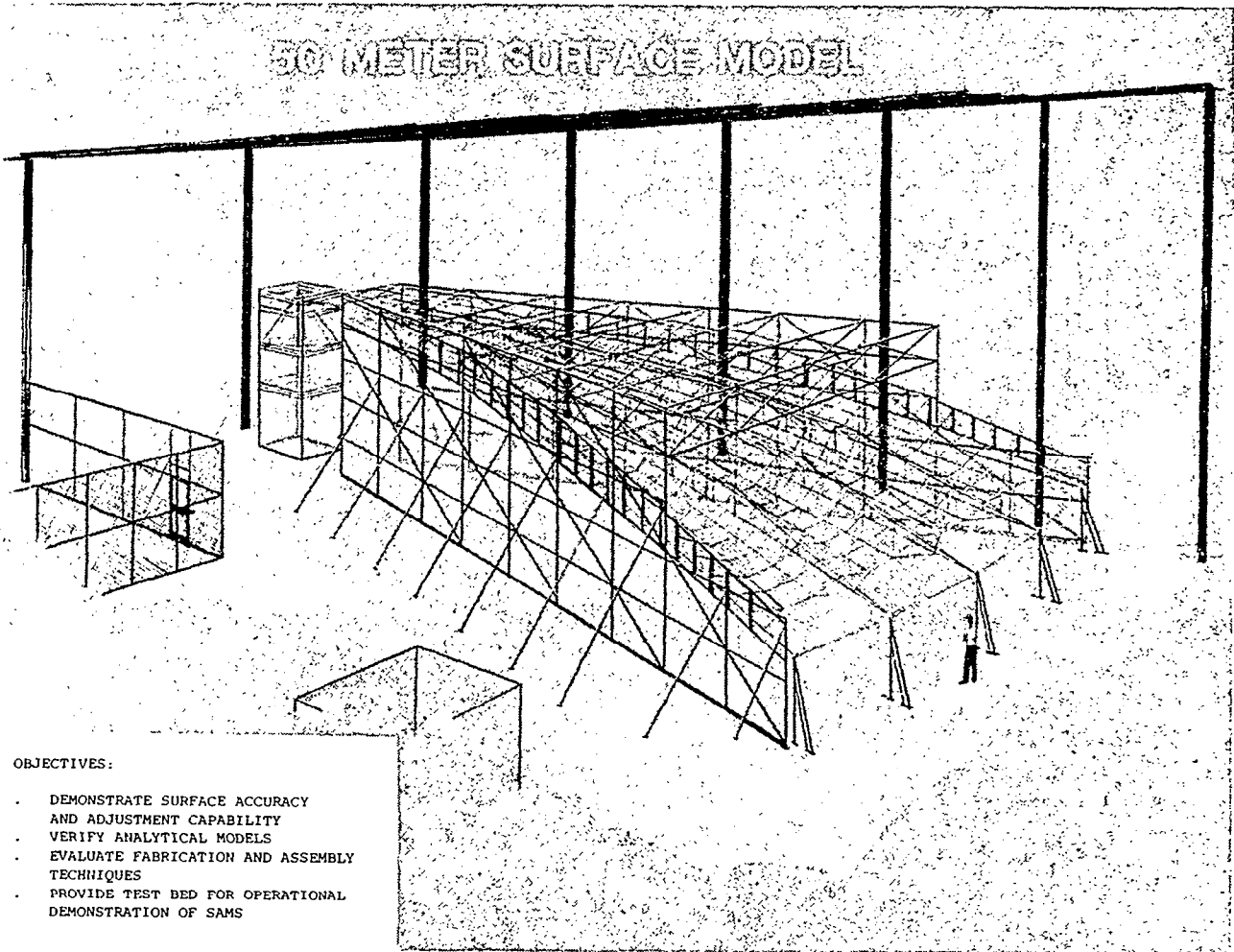
SURFACE MODEL FINITE ELEMENT MODEL

Detailed analytical models were made to fabricate and assess the performance of the 50-meter surface model. The figures below are graphic representations of the four-gore finite element model used in analysis.

484
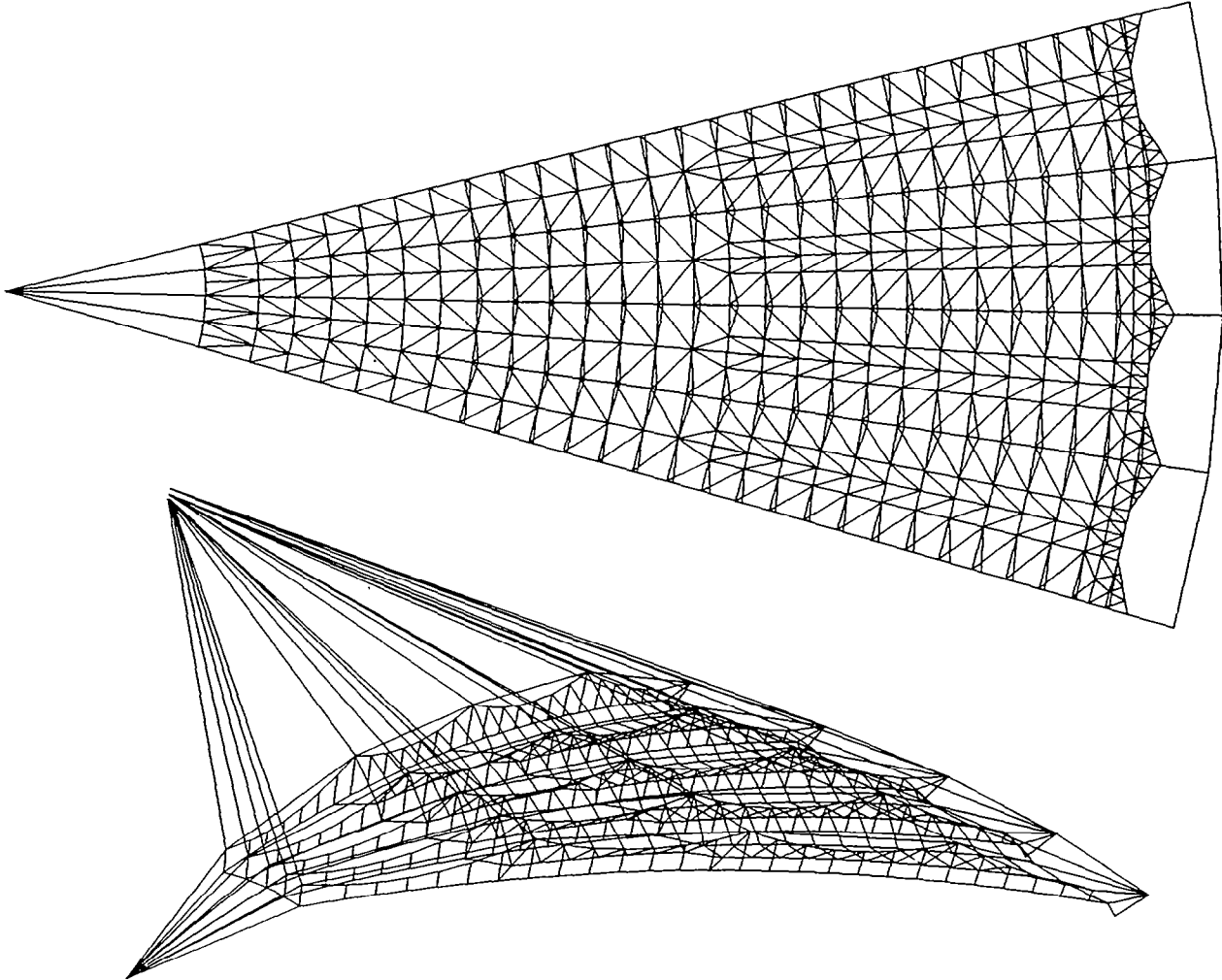
50-METER SURFACE MODEL
FABRICATION AND ASSEMBLY

The 50-meter surface model is fabricated from flat patterns developed by means of analytical models. The boundary structure, which simulates the hoop, column, and adjacent gores, is a fixed boundary to which the surface attaches. To meet the primary goal of build to dimension for the point design, an assembly method was devised which would yield the lowest manufacturing tolerances. The method selected involves maintaining control of both geometry and preload during the manufacturing process. Individual cords are loaded and positioned over accurately placed tooling pegs at each cable junction.

485
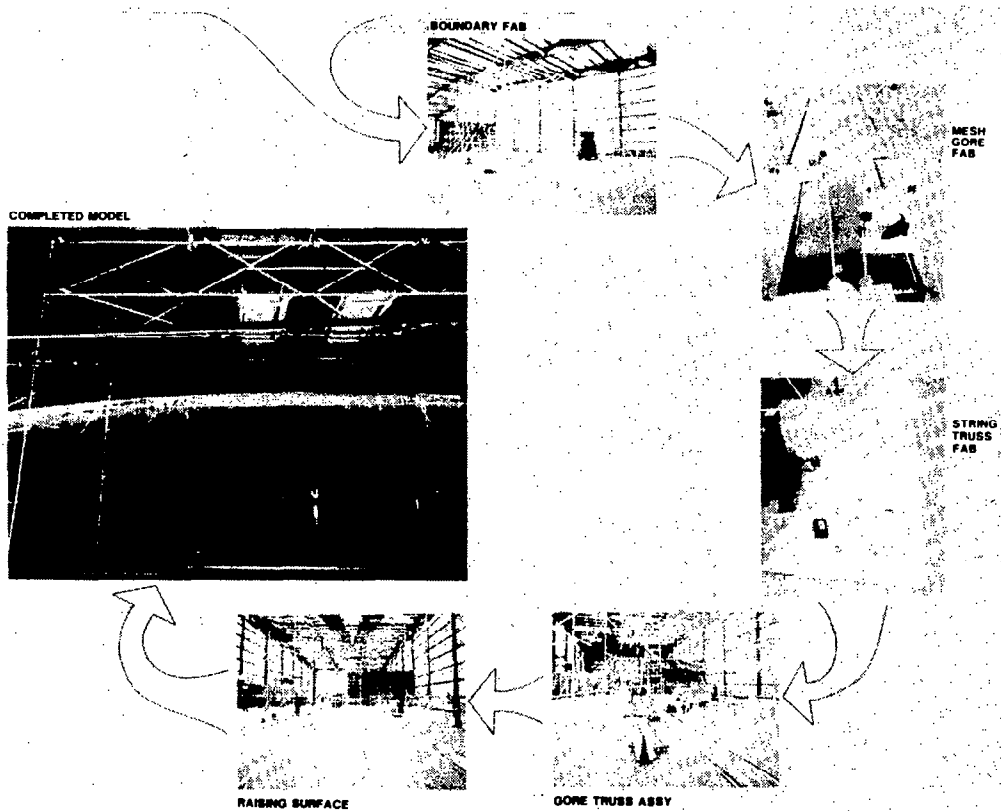
TYPICAL JOINT

This illustration shows a typical front cord joint consisting of two fiberglass plates that sandwich and bond the graphite front cords. This joint is located with pegs to an accuracy of ± 0.020 inch. Mesh can also be seen tensioned and laced to the cables.
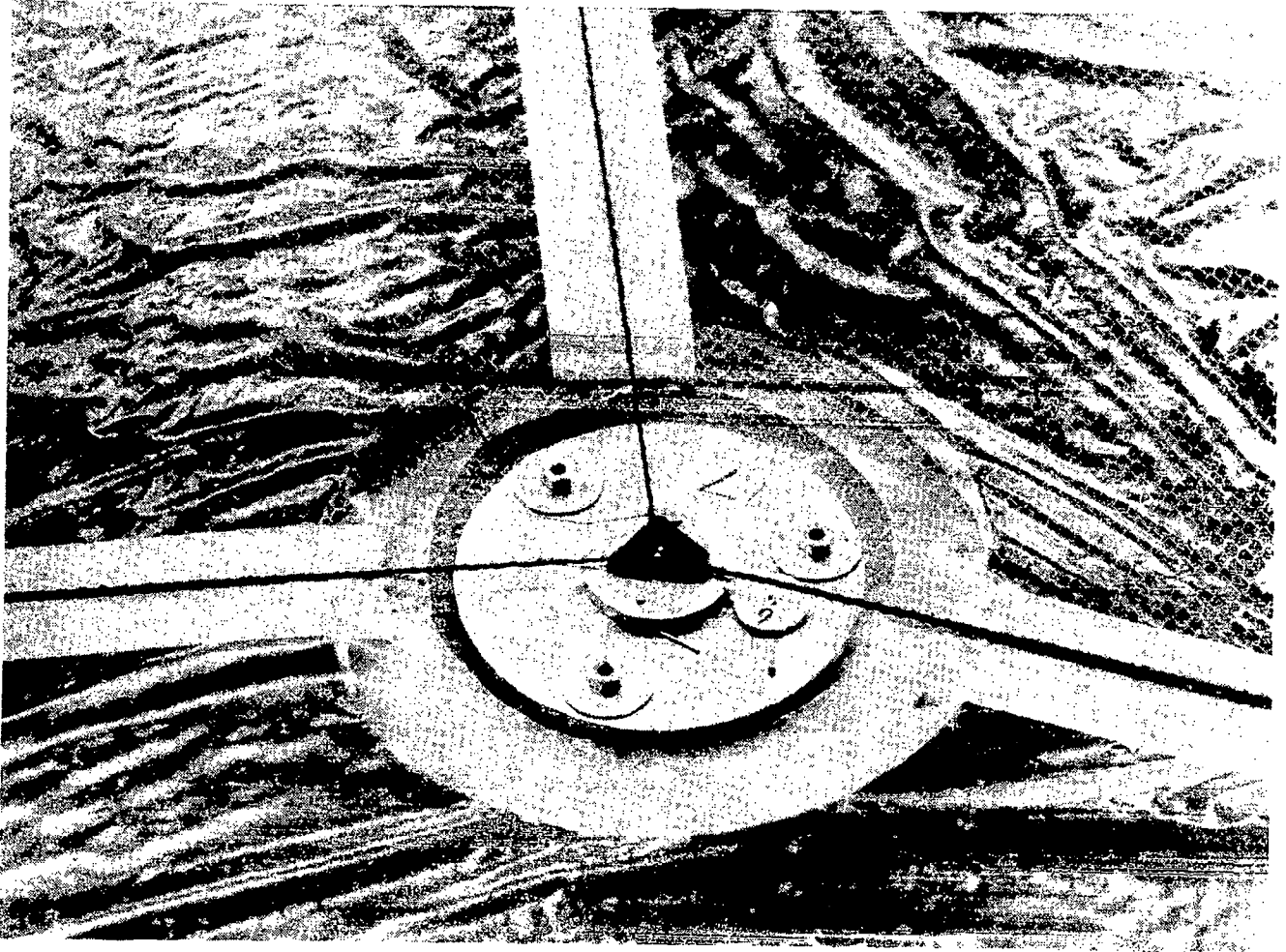
MAJOR SUBASSEMBLIES

The mesh gores and string trusses are laced together at their common interface lines.

GORE ASSEMBLIES AND STRING TRUSS ASSEMBLIES
ARE LACED TOGETHER AT TOP ASSEMBLY

MESH AND CORD
GORE ASSEMBLY

STRING
TRUSS
ASSEMBLY
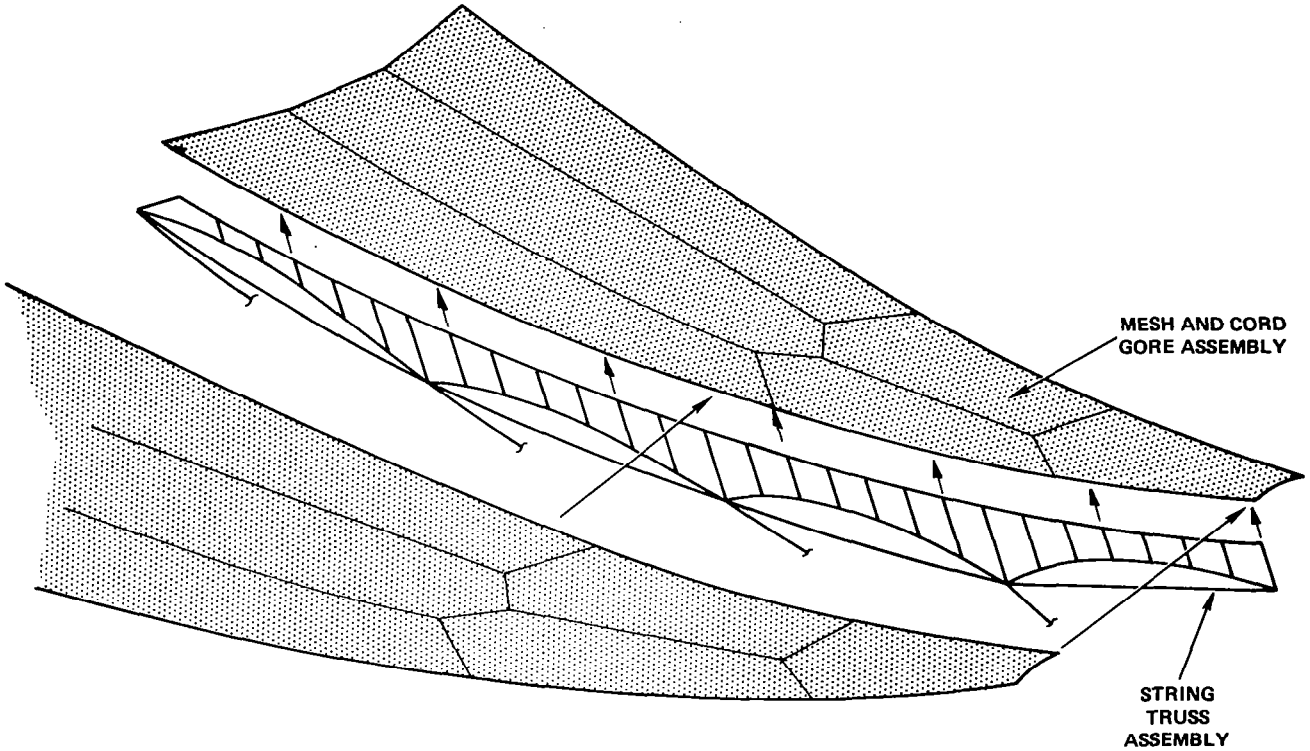
COMPLETED 50-METER SURFACE MODEL

The completed model is approximately 80 feet long and consists of four mesh gores. The two outer gores are considered boundaries for the center two gores which are used as the test bed.

488
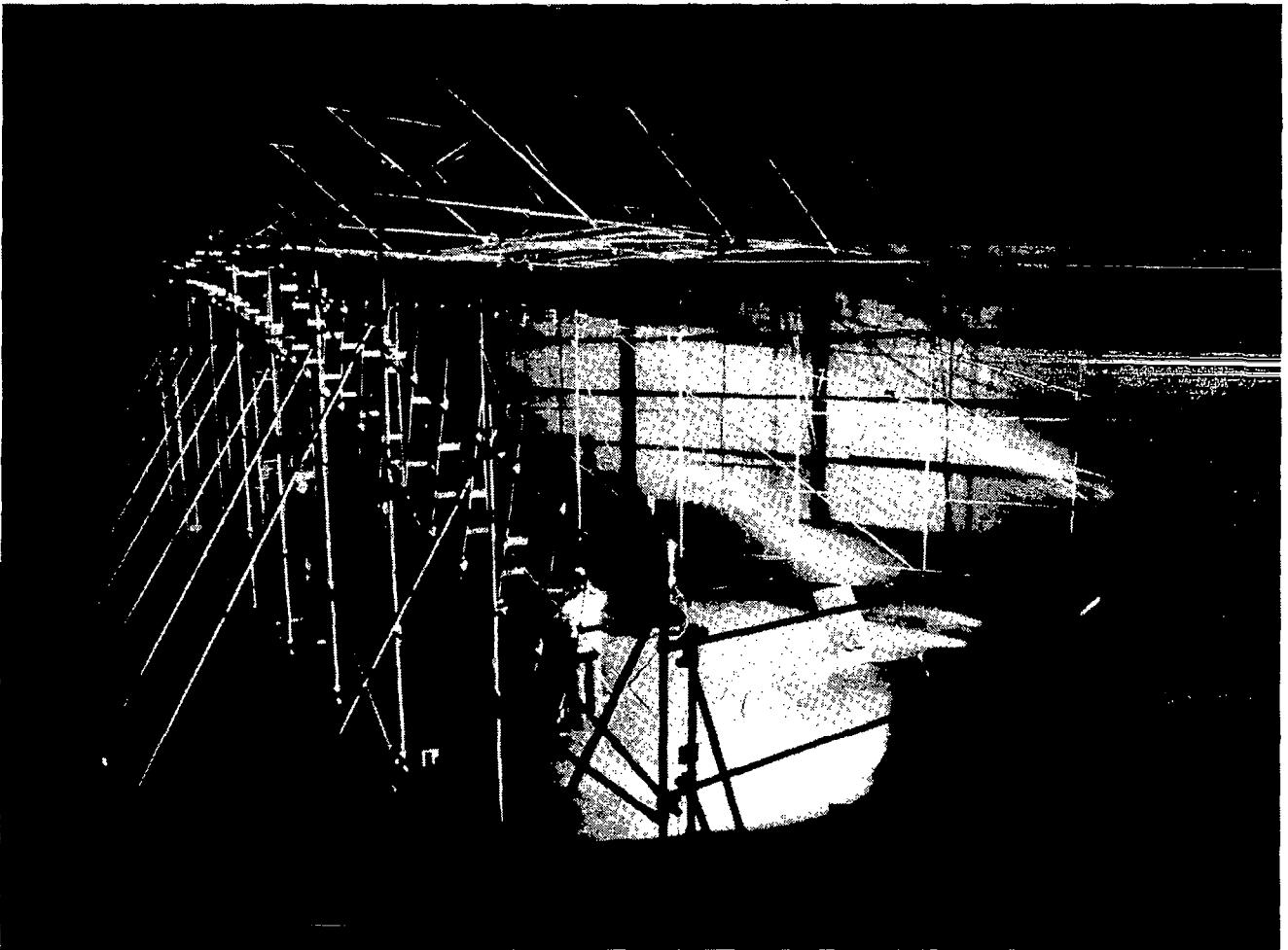
SURFACE MODEL CONTOUR

The black graphite cable network behind the mesh surface provides a smooth contour and is difficult to photograph.
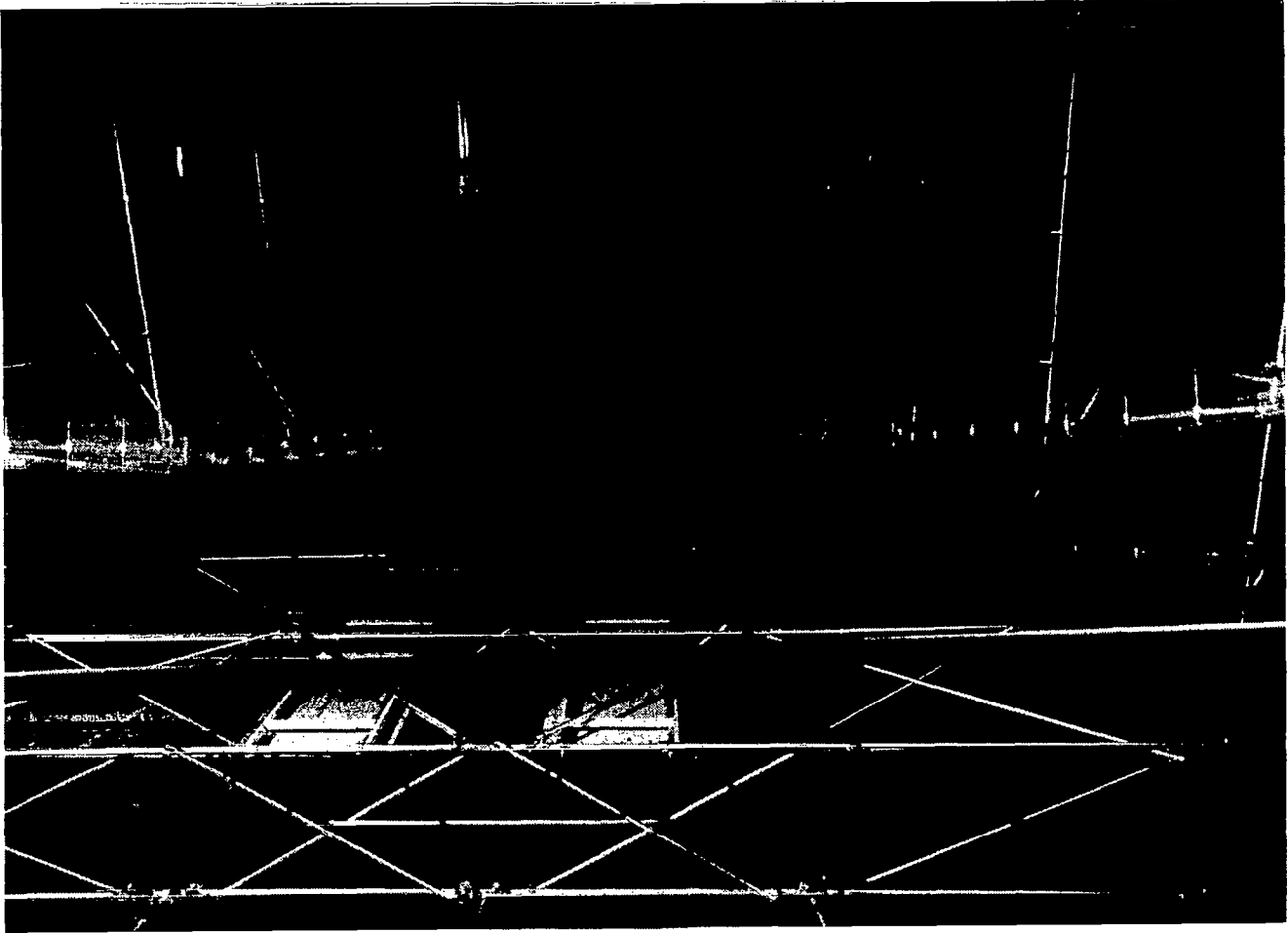
SURFACE MODEL VIEWED
FROM CENTER

This photograph shows the surface as it would be viewed from the central column of a full reflector.
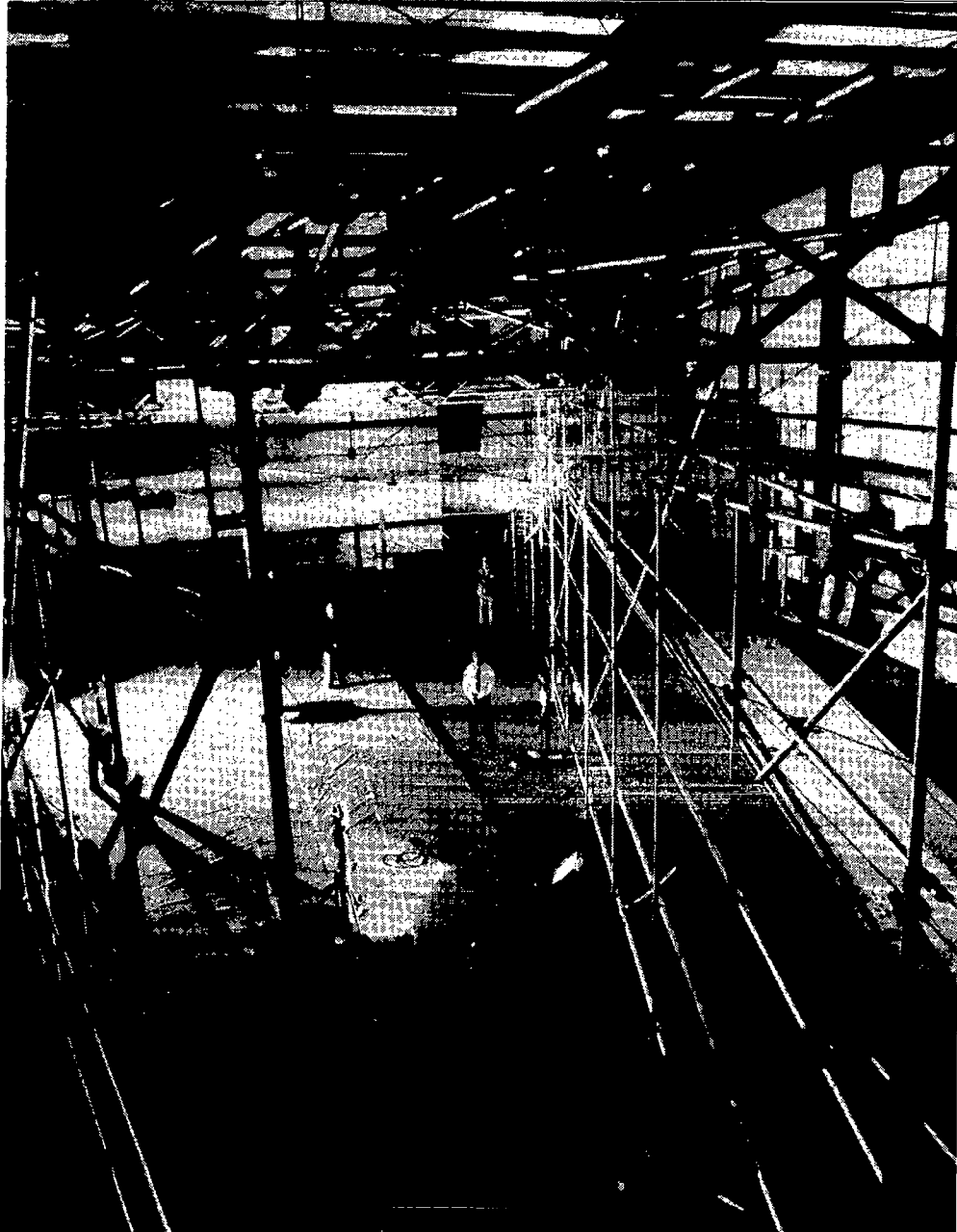
TARGET

Targets are located in predesignated areas on the surface to characterize the contour. They are constructed of printed thin film which sandwiches the mesh.
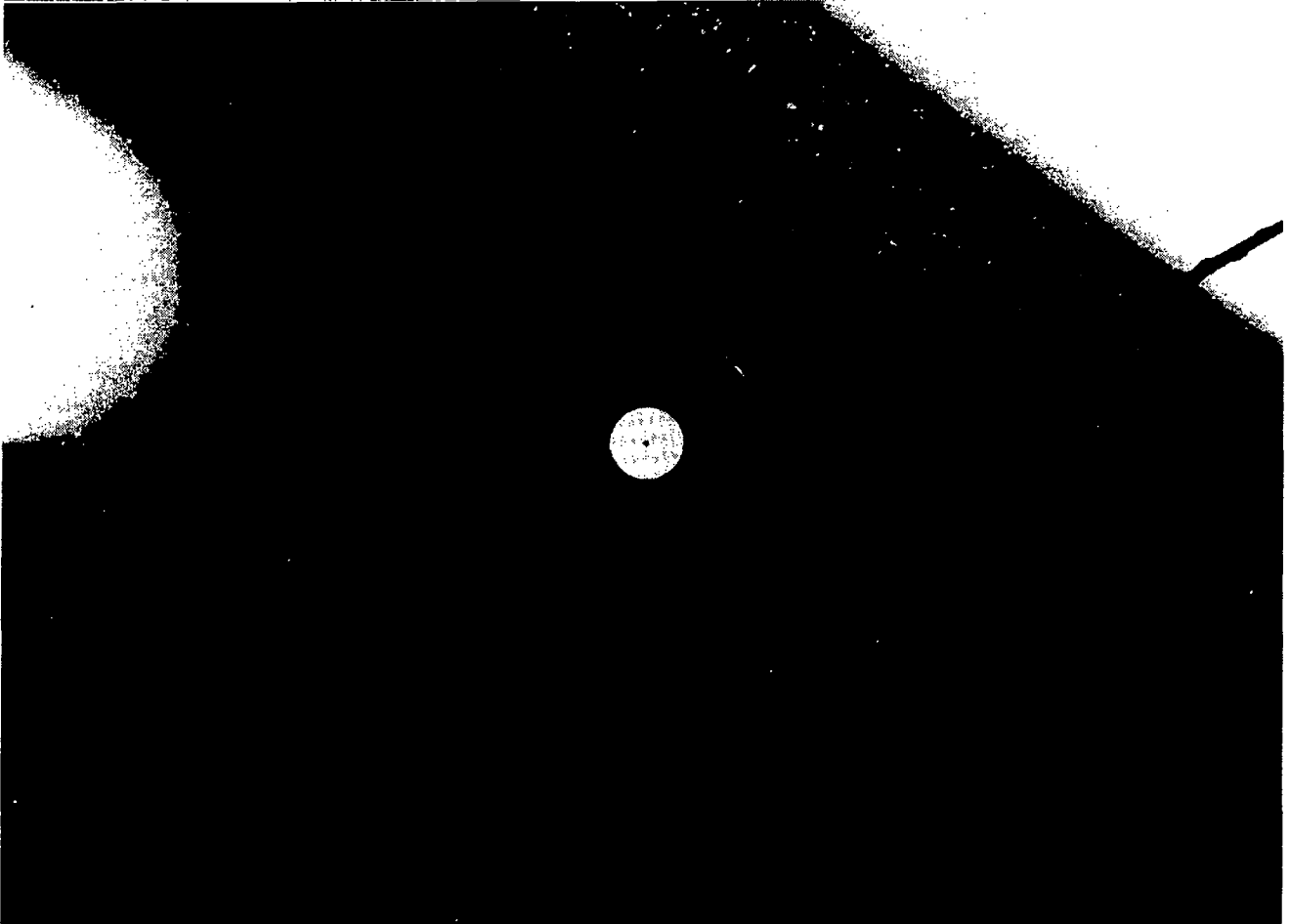
50-METER MODEL VERIFIES
100-METER POINT DESIGN

Harris has generated an analytical model that takes into account gravity and actual boundary conditions of the 50-meter model. This analytically generated contour is compared to the as-measured contour to ascertain the actual as-built error. Measured deviations from the 1-g ideal 50-meter surface are extrapolated and used to verify the predicted deviations of the 0-g 100-meter point design surface.
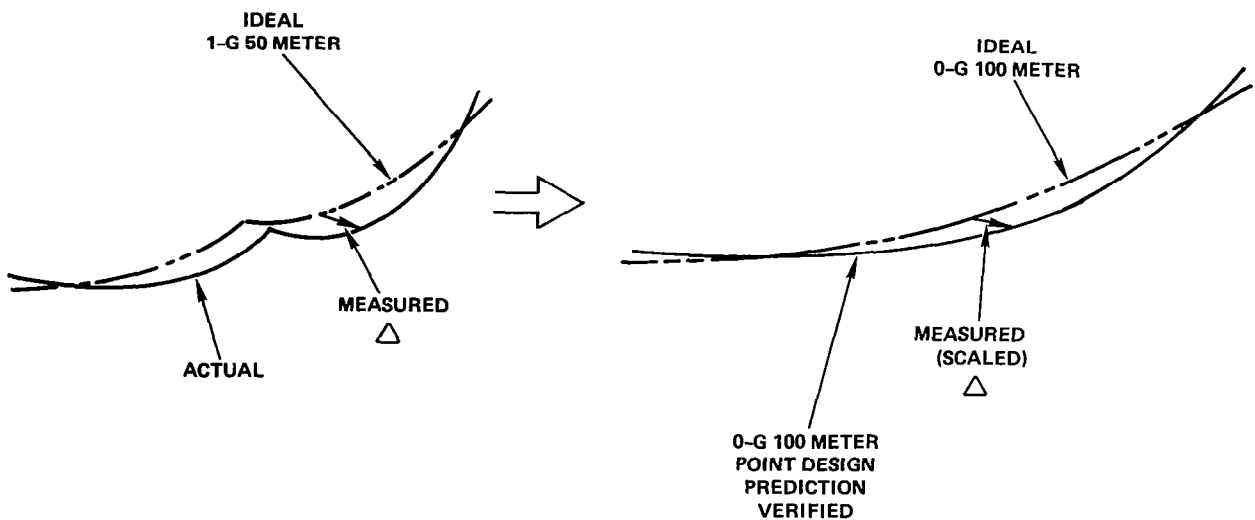
$\triangle$ = MANUFACTURING + MATERIAL PROPERTIES + MEASUREMENT
ERROR   ERROR   ERROR

50-METER SURFACE MODEL
MEASUREMENT RESULTS

Measured results are presented below along with the 100-meter point design requirements.

(INCHES)

	PRETEST GOAL	MEASURED	TRANSLATED TO 100-METER	REQUIRED ON 100-METER
SURFACE ACCURACY RMS	0.083*	0.102	0.256	0.300**
DEFOCUS	1.554	0.556	4.622	10.000

* THE PRETEST SURFACE ACCURACY GOAL WAS NOT REALIZED
BECAUSE IT DID NOT REFLECT UNCERTAINTIES DUE TO:

- WEIGHT
- THERMAL GRADIENTS
- BOUNDARY VARIATIONS

** SURFACE ACCURACY REQUIREMENT OF 100 METER IS BASE
ON A λ/80 QUALITY.

50-METER MODEL SURFACE
ADJUSTMENT VERIFICATION –
ANALYTICAL

The first verification of the analytical model was the demonstration of a predictable surface contour quality as presented on the previous page. A second analytical model verification was accomplished by adjusting one of the primary surface support cables on the model assembly and comparing the resulting contour distortion with the distortion predicted by the analytical model.

The analytically predicted results caused by displacing a single rear support cable 0.10 inches are shown below.

ANALYTICAL NORMAL DISPLACEMENTS CAUSED BY ANALYTICALLY
ADJUSTING THE OUTBOARD CENTER SUPPORT CABLE

◯ CORD PULL POINT

```
                                                                    -6      0
                                                         -12
                                                 -19            -25    -11
                                          -16         -33              -17
                                    -14        -34           -54
                              -12       -31         -86  -83      -47       0
                        -11      -26         -71              -83
                  -11       -19    -56             -86  (-104)      -54   -17
              -9       -30  -39      -68            -83
          -9       -28    -38  -48        -86           -54     -25      -11
      -9       -24  -28  -35  -40  -56    -71     -33
  -7       -22    -33         -32      -35           -6      0
-5    -19    -25  -28  -31  -20  -26        -16  -19  -13
-4   -16          -28    -12 -12  -12  -14
-2  -12                -9  -10  -12 -12
-10     -6  -8      -9
  -4
```

The following shows the measured results after adjusting the same support cable used in the analysis of the previous page by 0.10 inches.

**MEASURED NORMAL DISPLACEMENTS CAUSED BY ADJUSTMENT OF
OUTBOARD CENTER SUPPORT CABLE OF 50-METER MODEL**

-7

2

-19

CABLE PULL POINT

-1   -20

-8   -29   -19

-57

-9   -18   -19

-15   -101

-94   -11

5   -4   -104

-2   -64   -51

0   -6   -105   -36

2   -27   -84

-20   -55   -86   -70

8   -50   -100

-10   -57   -2

-1   -28   -35   -5   -17

3   -16   -20   -15   2   -5

1   -3   4   -3   8   5   17   -23

-1   -18   -11   4   5   -1

-11   3   7   0

-5   -4   3   -7   6

8   -6   3

-1   3

-1

495

50-METER MODEL SURFACE
ADJUSTMENT VERIFICATION –
ANALYTICAL AND MEASURED
DIFFERENCE

The following shows the difference between analytical and measured adjustment results. The correlation is considered acceptable if the difference between measured and predicted contours is no greater than 0.64 mm (0.025 inch) rms. This number was derived by taking the rss of a 0.50-mm (0.020 inch) measurement error and a 0.38-mm (0.015-inch) manufacturing uncertainty error which included boundary position and mass properties uncertainties.

**DIFFERENCE IN NORMAL DISPLACEMENTS OF MEASURED AND ANALYTICAL VALUES
IS 0.017 INCH RMS COMPARED TO 0.025 INCH GOAL**

⬭ CORD PULL POINT

SURFACE ACCURACY MEASUREMENT
SENSOR (SAMS) SYSTEM TEST ON THE
50-METER MODEL

The SAMS system was installed and demonstrated on the 50-meter model. The sensor measured the relative deflections of two LED targets on the antenna surface as the surface was manipulated by structural surface control cables. An additional LED target, located on the stable hoop portion 21 meters from the sensor, was used as a reference. The mesh targets were positioned 10.5 and 15.7 meters from the sensor. A goal of 0.75-mm rms accuracy was met with a 12 to 1 margin.
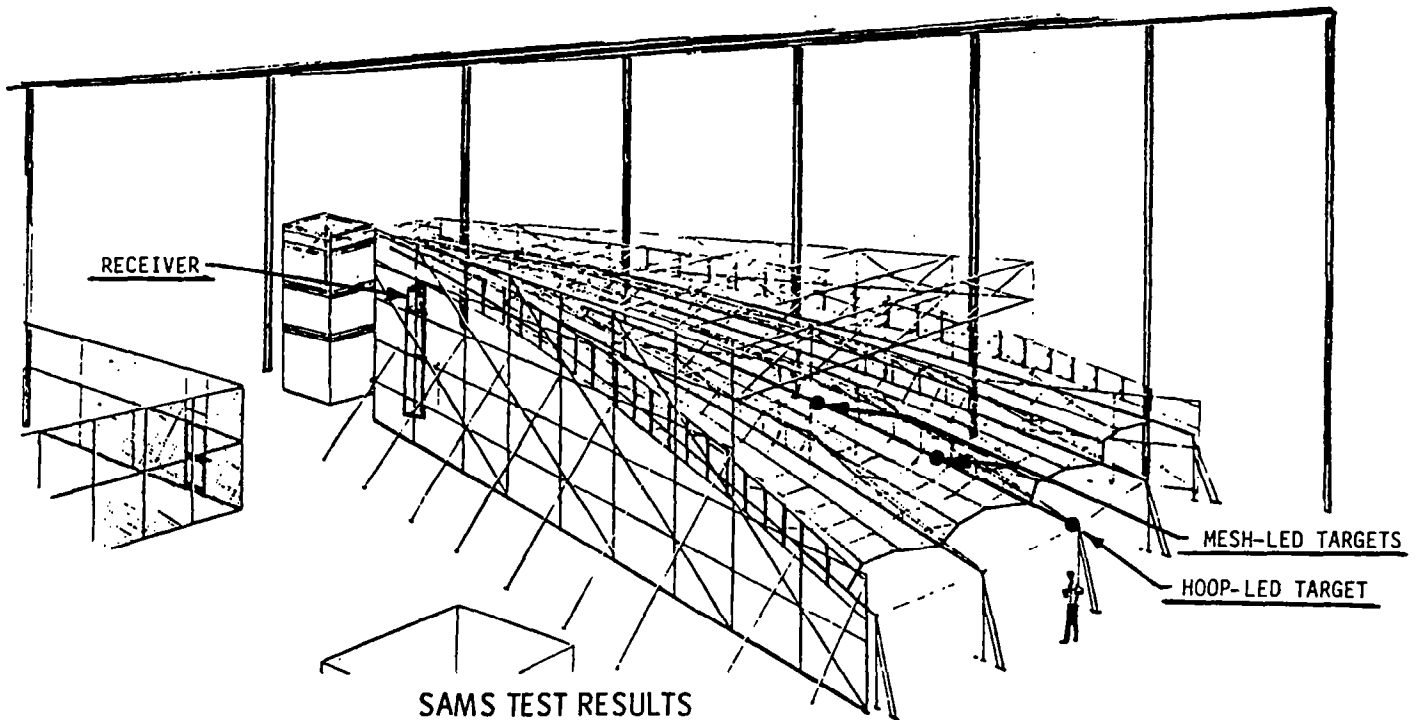
SAMS TEST RESULTS

SENSOR	RANGE		ACCURACY (RMS)	
LOCATION	METERS	FEET	MM	INCHES
MESH	10.5	34.5	0.015	0.000604
MESH	15.7	51.5	0.029	0.001129
HOOP	21.0	69.0	0.060	0.002361

50-METER SURFACE MODEL – CONCLUSION

The conclusions from the 50-meter surface model design, analysis, fabrication, and test are given below.

- DEMONSTRATED THE CAPABILITY TO "BUILD TO DIMENSION" LARGE PRECISION ANTENNA REFLECTORS WHICH CANNOT BE VERIFIED IN A GRAVITY ENVIRONMENT

- VERIFIED ANALYTICAL MODELS THAT CAN BE USED TO BUILD AND PREDICT ORBITAL PERFORMANCE OF THE HOOP/COLUMN ANTENNA DESIGN

- ACHIEVED REQUIRED SURFACE ACCURACY WITHOUT ADJUSTMENT

- DEMONSTRATED ON-ORBIT ADJUSTMENT CAPABILITY AND PREDICTABILITY FOR HIGH-PRECISION APPLICATIONS

- VERIFIED ACCURACY OF ON-ORBIT SURFACE ACCURACY MEASUREMENT SENSOR SYSTEM (SAMS)

RF VERIFICATION MODEL OBJECTIVES

An RF verification model was designed to study the parameters critical to the multibeam quad–aperture antenna performance and to verify RF analytical methods.
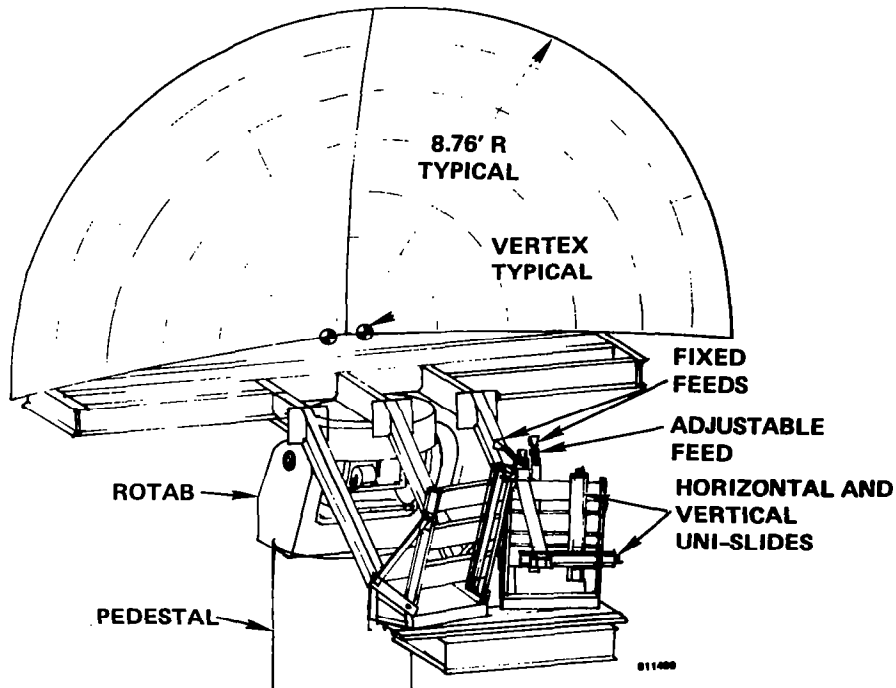
OBJECTIVES:

- EVALUATE RF PARAMETERS CRITICAL TO THE MULTIBEAM QUAD-APERTURE ANTENNA PERFORMANCE
- PROVIDE VERIFICATION OF CRITICAL PARAMETERS THROUGH TEST AND ANALYSIS
- VERIFY ANALYTICAL METHODS

RF VERIFICATION MODEL FABRICATION

The photographs below show key steps in achieving a reflector model with a 0.010-inch rms surface accuracy requirement.

FABRICATION OF PRECISION RF VERIFICATION MODEL

A MOLD WITH 0.05 mm (0.002 IN.) RMS ACCURACY IS USED TO BUILD FIBERGLASS FACE SKINS

FACE SKINS ARE ASSEMBLED TO RIGID BACKUP STRUCTURE

ASSEMBLED ANTENNA TEST MODEL

ADJUSTMENT SCREWS BETWEEN FACE SKINS AND BACKUP STRUCTURE PROVIDE A REFLECTOR ACCURACY OF 0.2 mm (0.008 IN.) RMS

RF VERIFICATION MODEL ASSEMBLY

The model is composed of two removable quadrant reflectors and an aluminum base and feed structure that supports fixed and movable offset feeds in both quadrants.
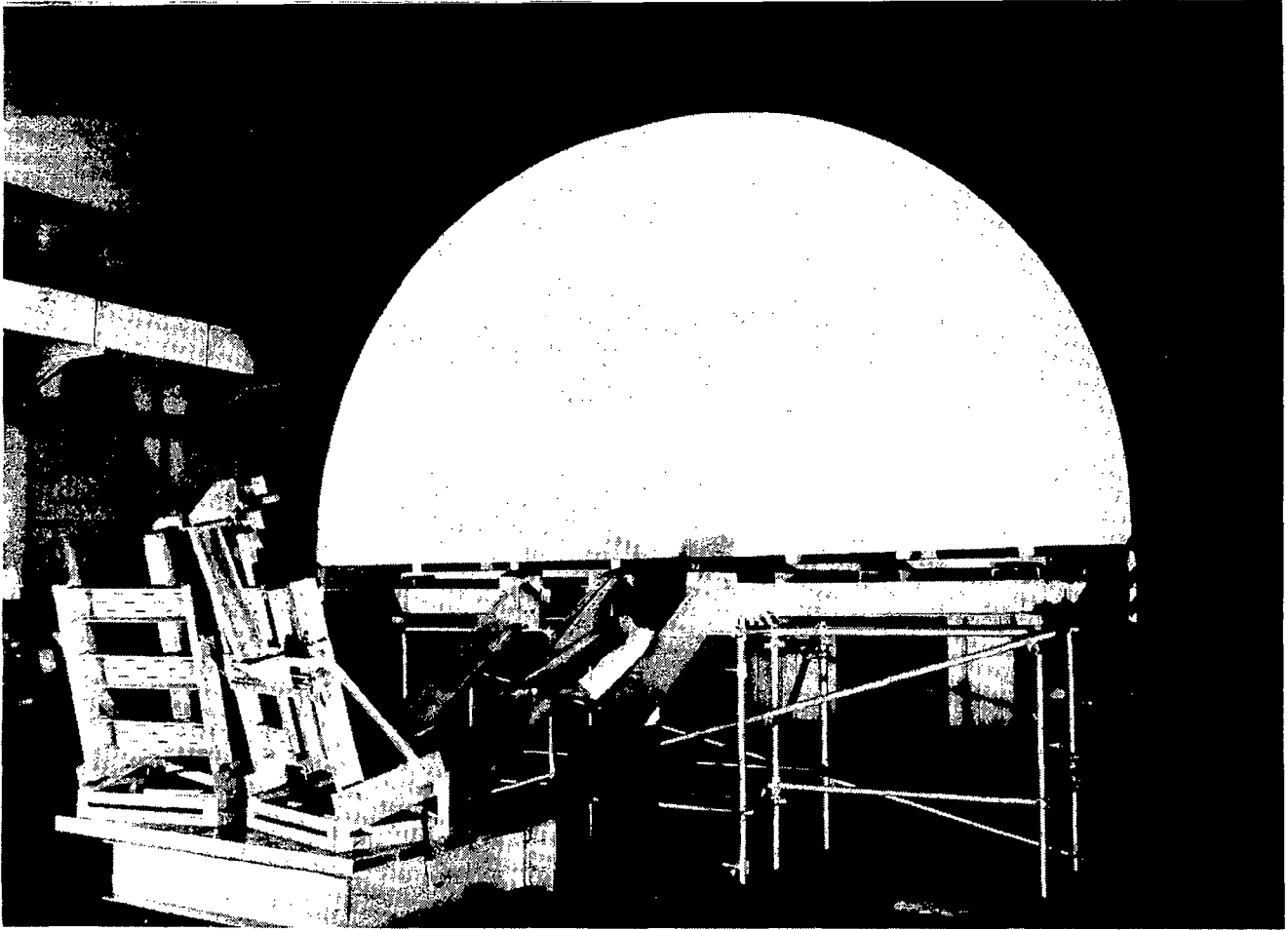
FEED ALIGNMENT

Feed alignment was accomplished on the antenna range using a large triangular truss tool shown below.
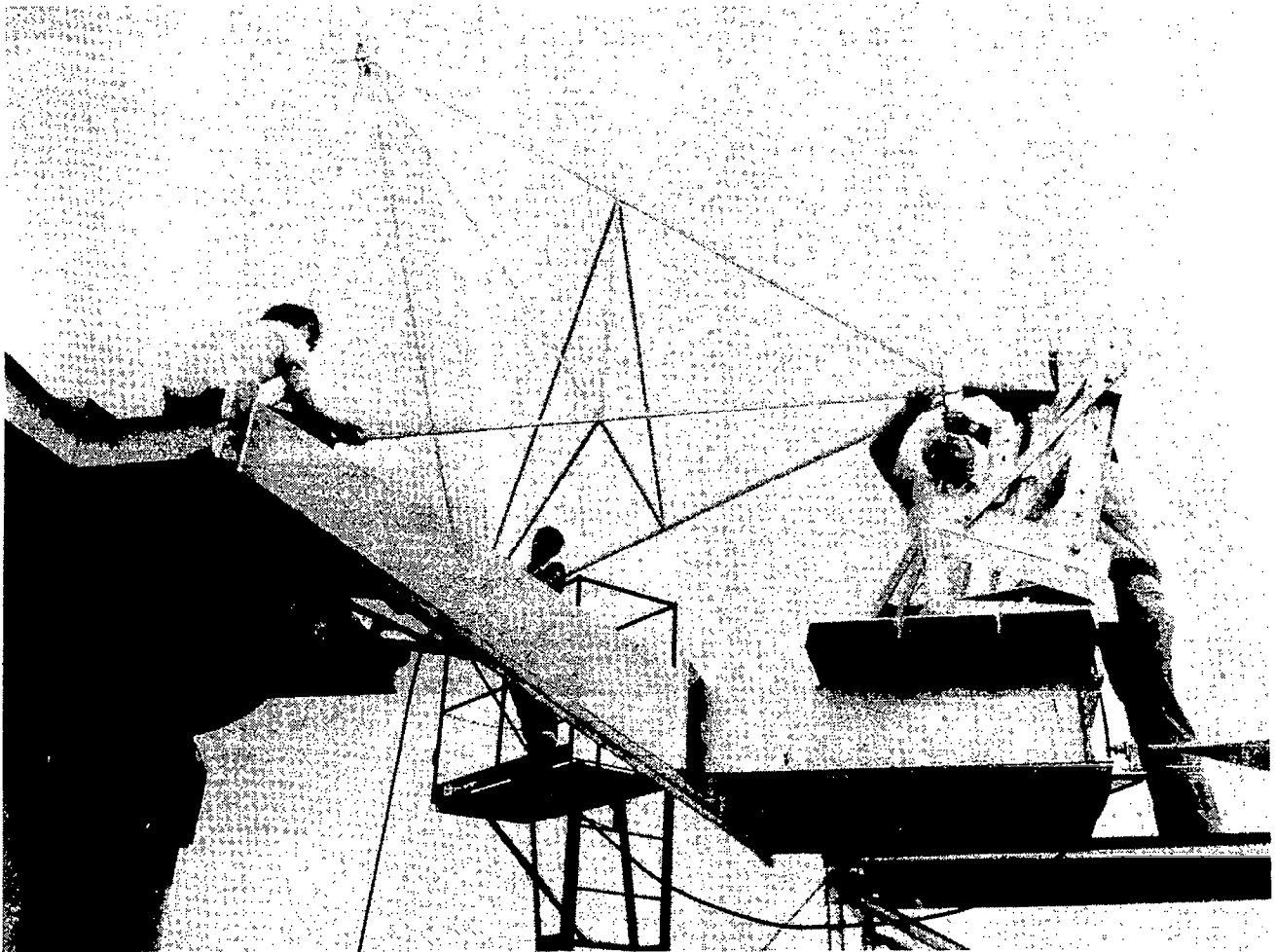
TEST CONFIGURATION

The photograph below shows the test configuration on the range. White quartz cables stretched across the test aperture are barely visible.
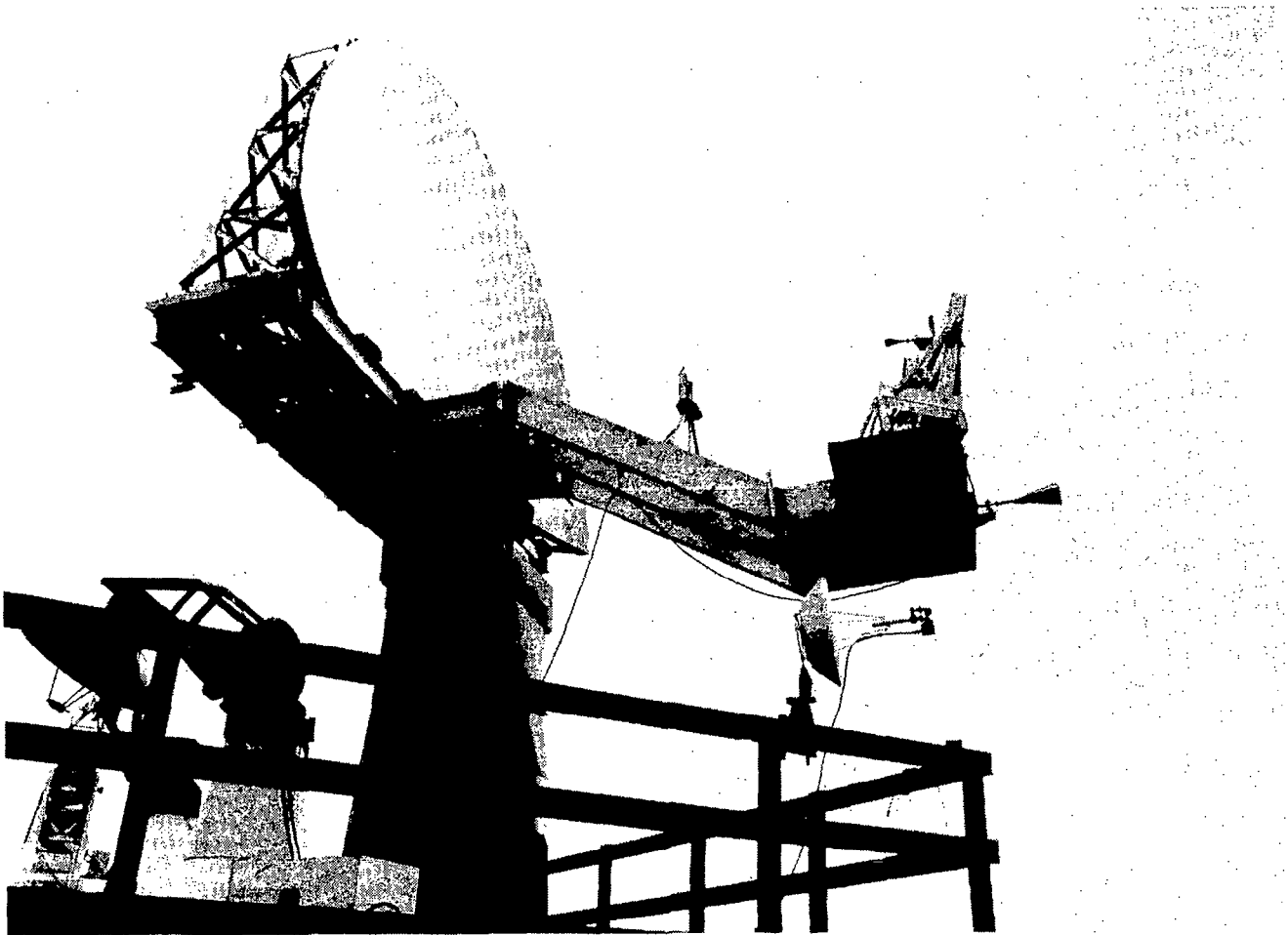
POINTING ACCURACY

Accurate pointing of the RF verification model toward the source antenna was achieved using a scope mounted on the model base shown below.
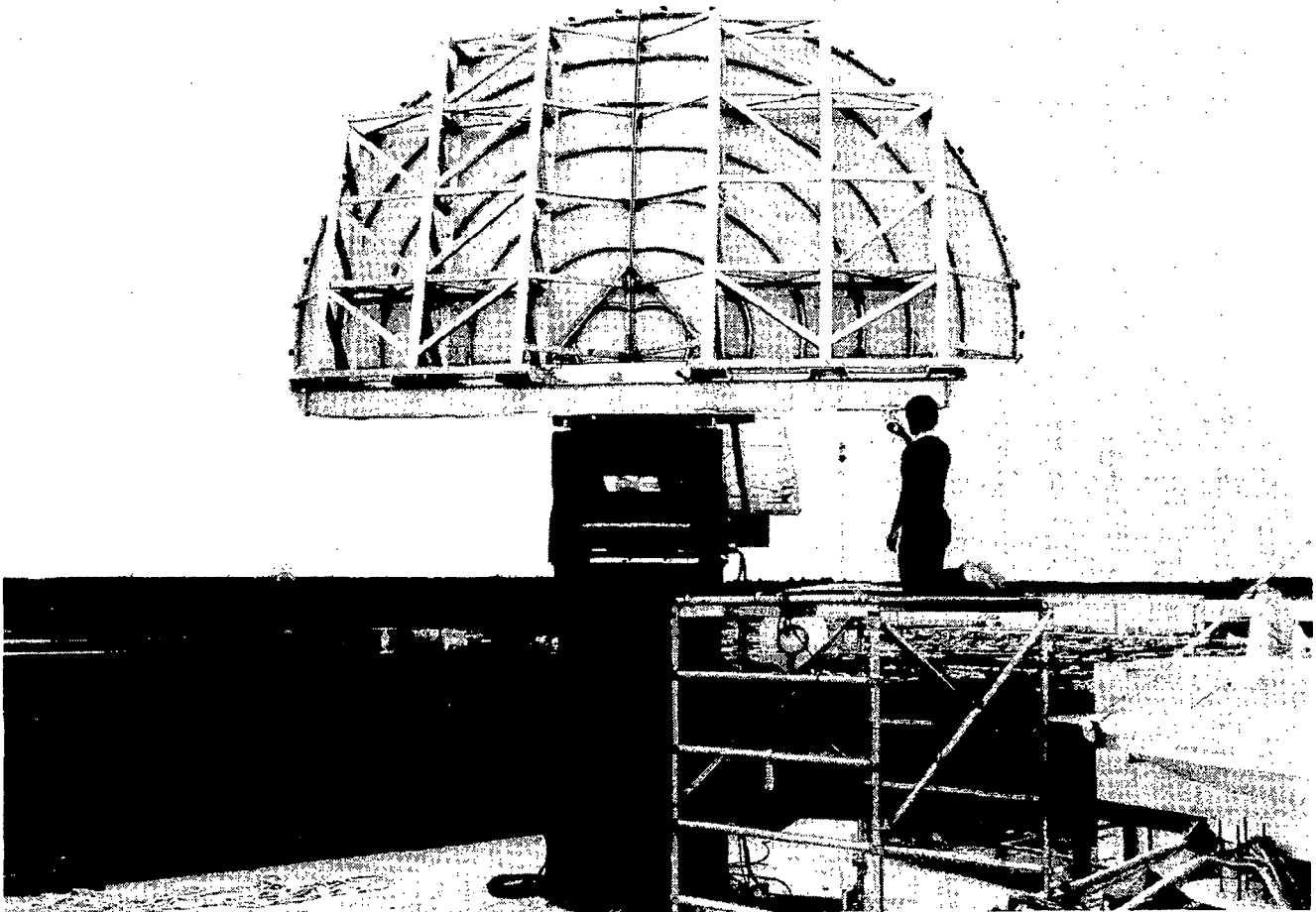
SINGLE-QUADRANT CONFIGURATION

Reflector quadrants are removable so either or both quadrants can be tested.
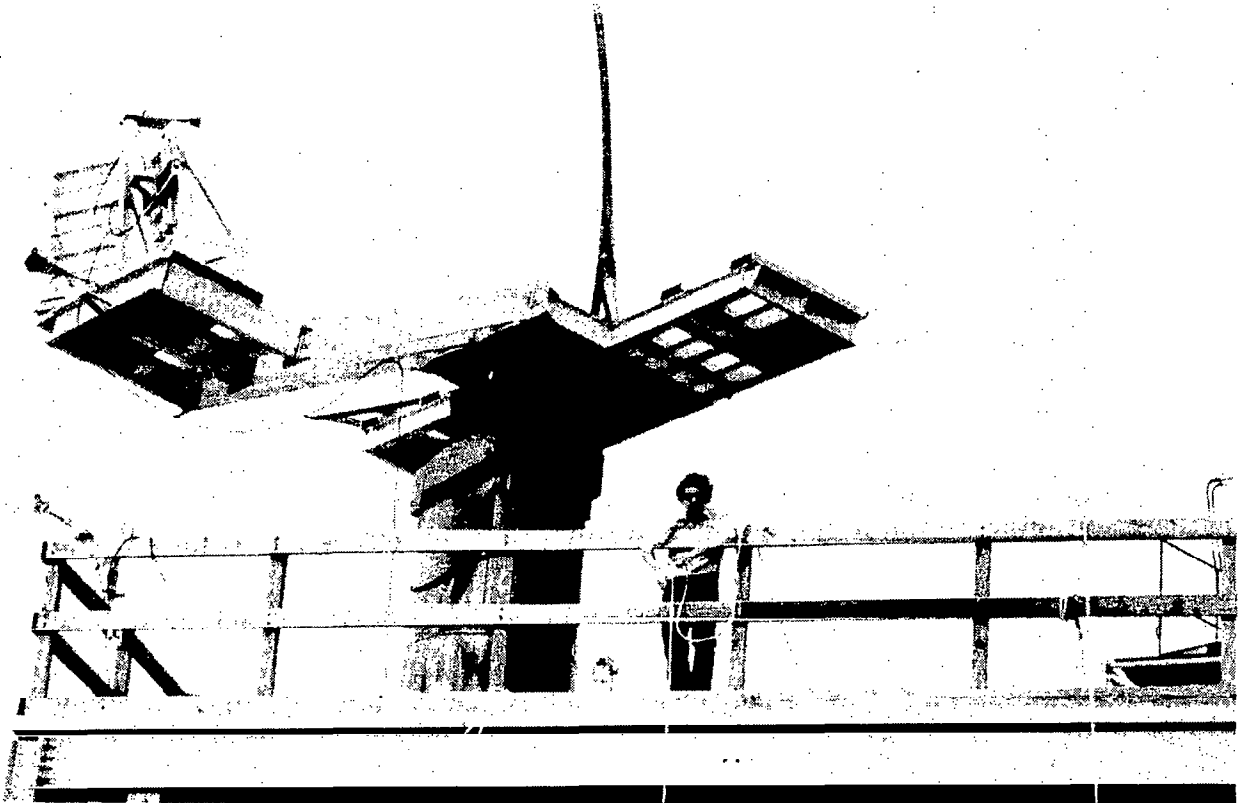
15-METER MODEL

The 15-meter kinematic model will verify the overall deployment scheme of the hoop/column antenna. The model will be capable of deployment and stow cycles, repeatability measurements, cup-up/cup-down measurements, and a series of deployment and failure modes testing. It will be fabricated in the Harris radome as shown below.
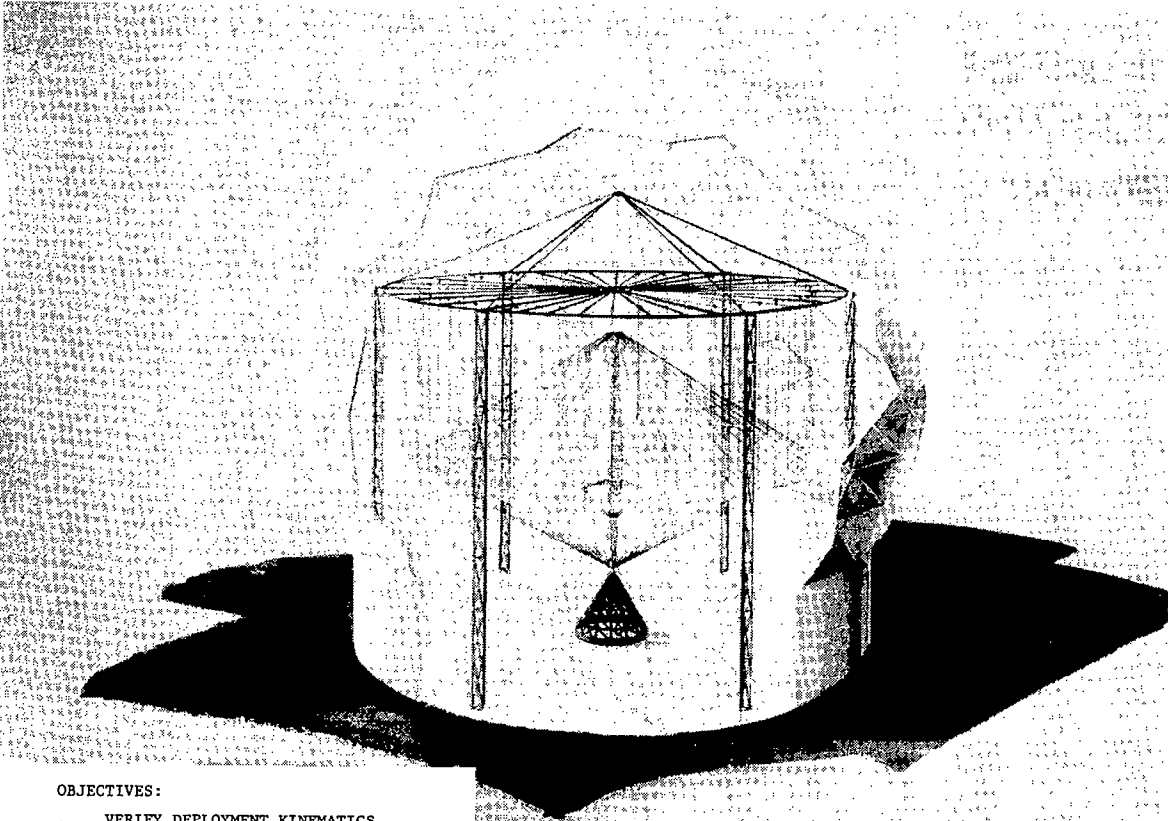
OBJECTIVES:

- VERIFY DEPLOYMENT KINEMATICS AND RELIABILITY
- INVESTIGATE SURFACE INTERACTION AND REPEATABILITY
- VERIFY ANALYTICAL MODELS
- VERIFY MANUFACTURING TECHNIQUES

15-METER MODEL GEOMETRY

The 15-meter model geometry shown below is based on the 100-meter point design.

**DIMENSIONS IN INCHES
UNLESS SPECIFIED OTHERWISE**
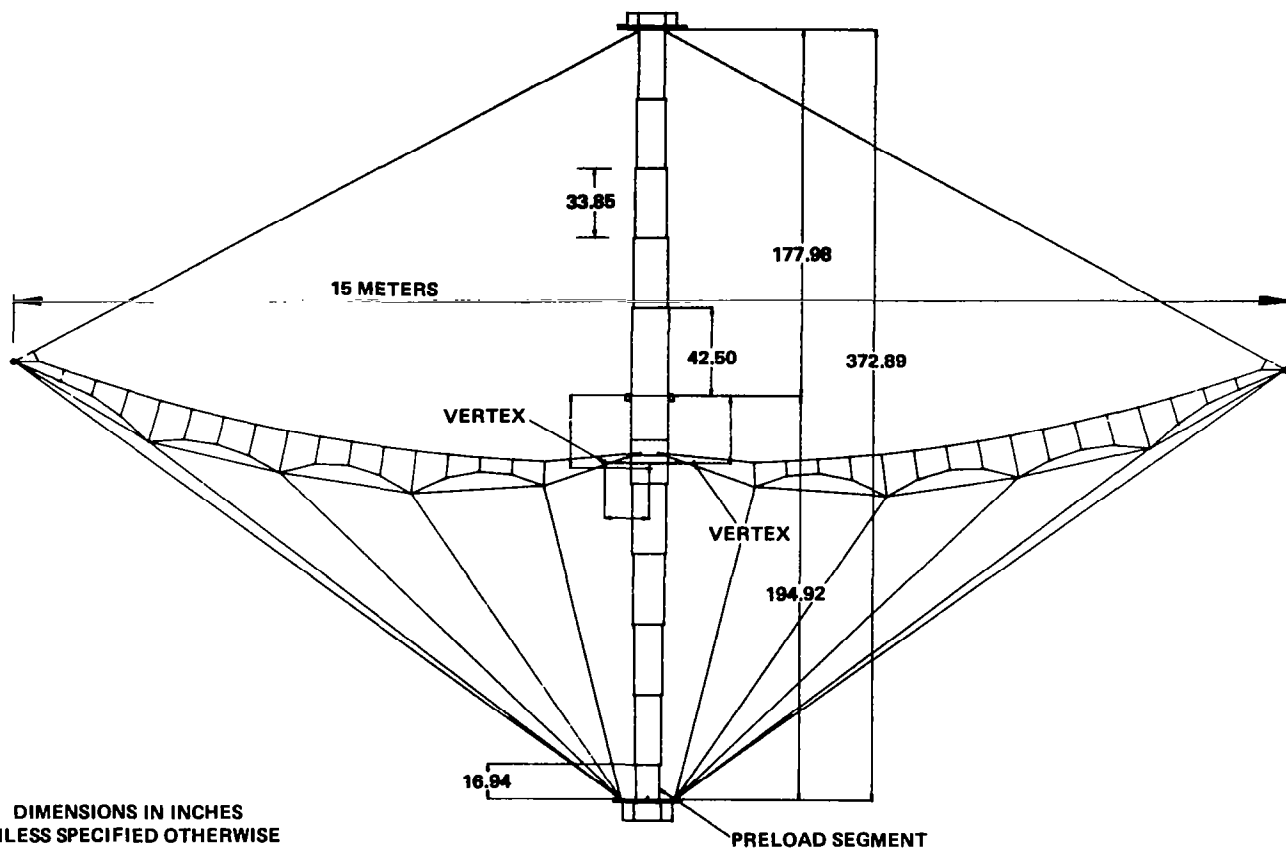
The model has a 24-segment hoop and a four-quadrant contoured mesh surface.
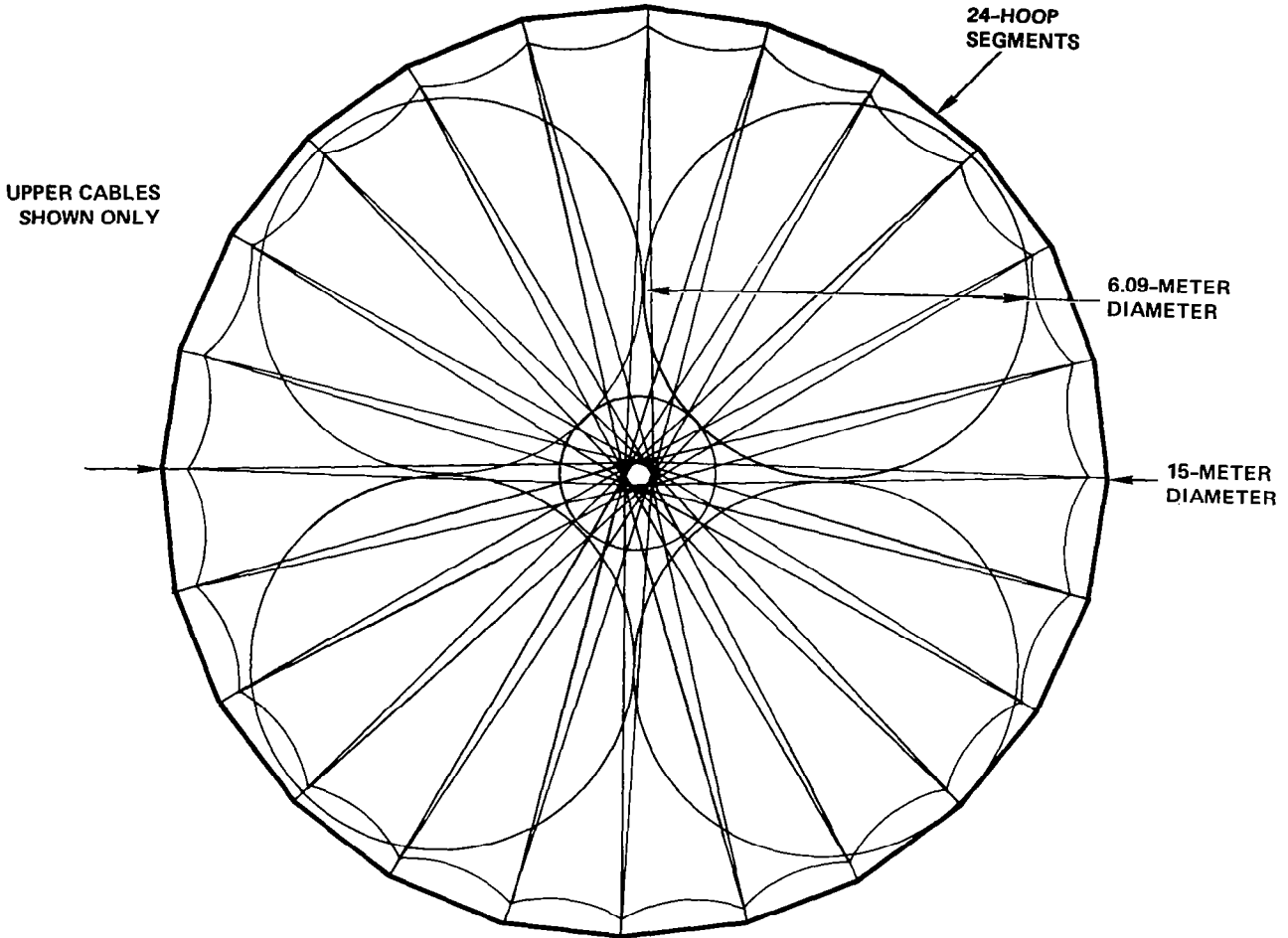
STOWED 15—METER MODEL

The 15-meter model stowed configuration is shown below.
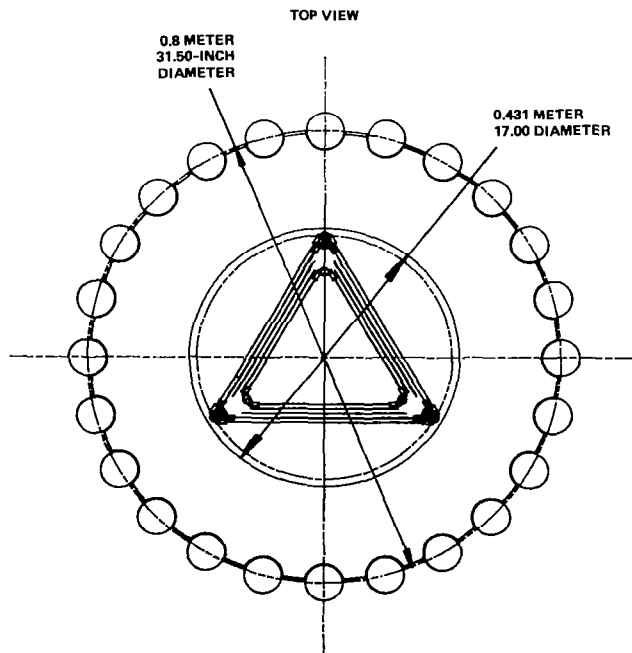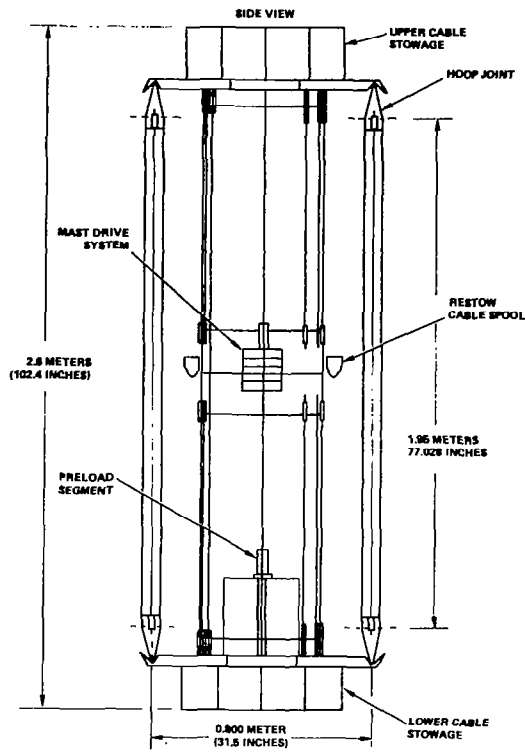
A counterbalance system will be used on the hoop to deploy and stow the 15-meter model. In the fully deployed configuration, the hoop does not require counterbalancing.

15-METER MODEL-STOWED

C/B SYSTEM
- DP

15-METER MODEL

MODEL SUPPORT TUBES
- DP
- MEASUREMENT

MODEL HANDLING FIXTURE
- TURNOVER
- TRANSPORT
- ROTAB MOVEMENT

510
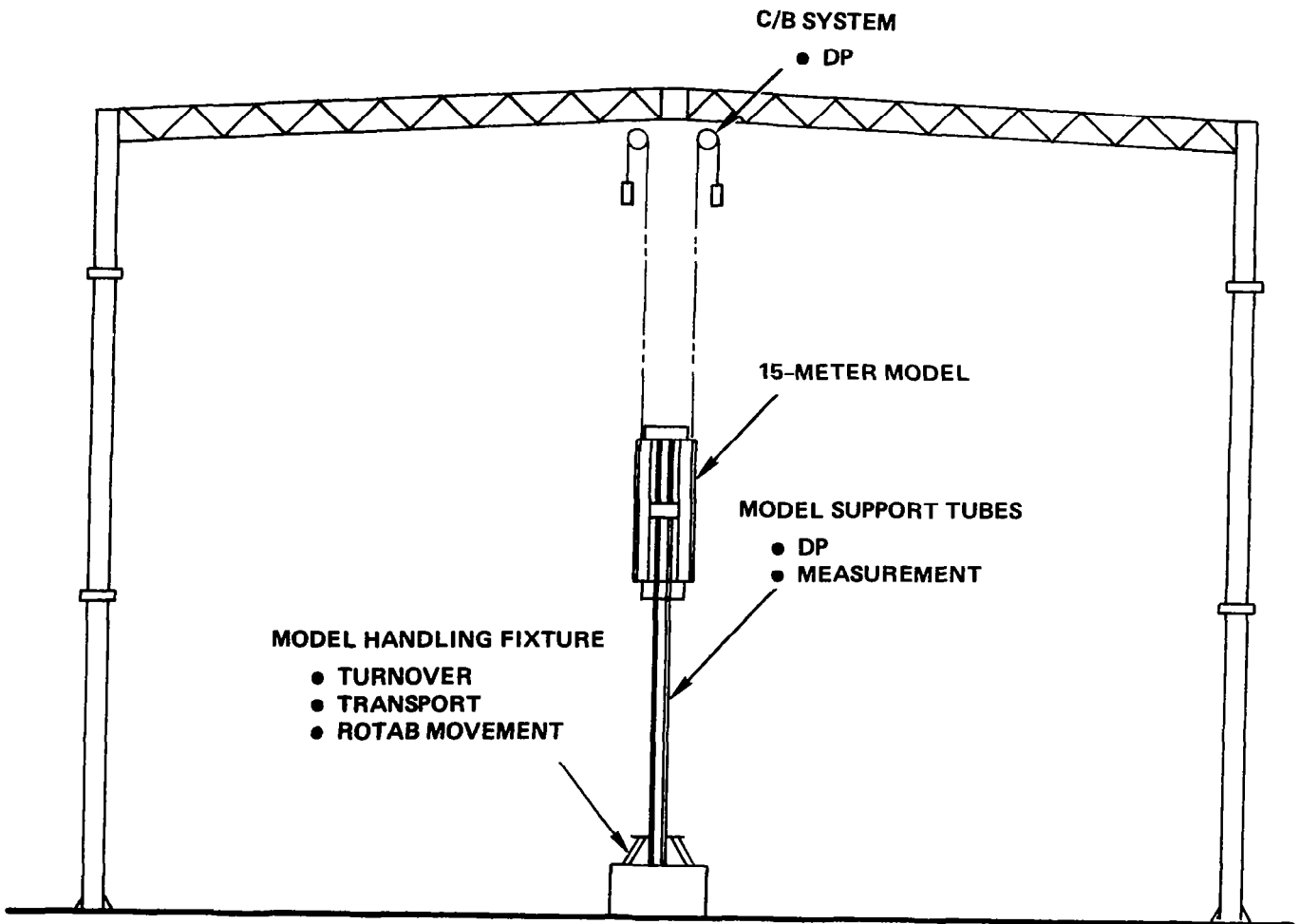
15-METER MODEL-PARTIALLY DEPLOYED

C/B SUPPORT
PEDESTAL (6 PL)

MODEL HANDLING FIXTURE

15-METER MODEL-DEPLOYED

C/B SYSTEM (24 PL)

C/B SUPPORT
PEDESTAL (6 PL)

MODEL SUPPORT TUBES

MODEL HANDLING FIXTURE

511
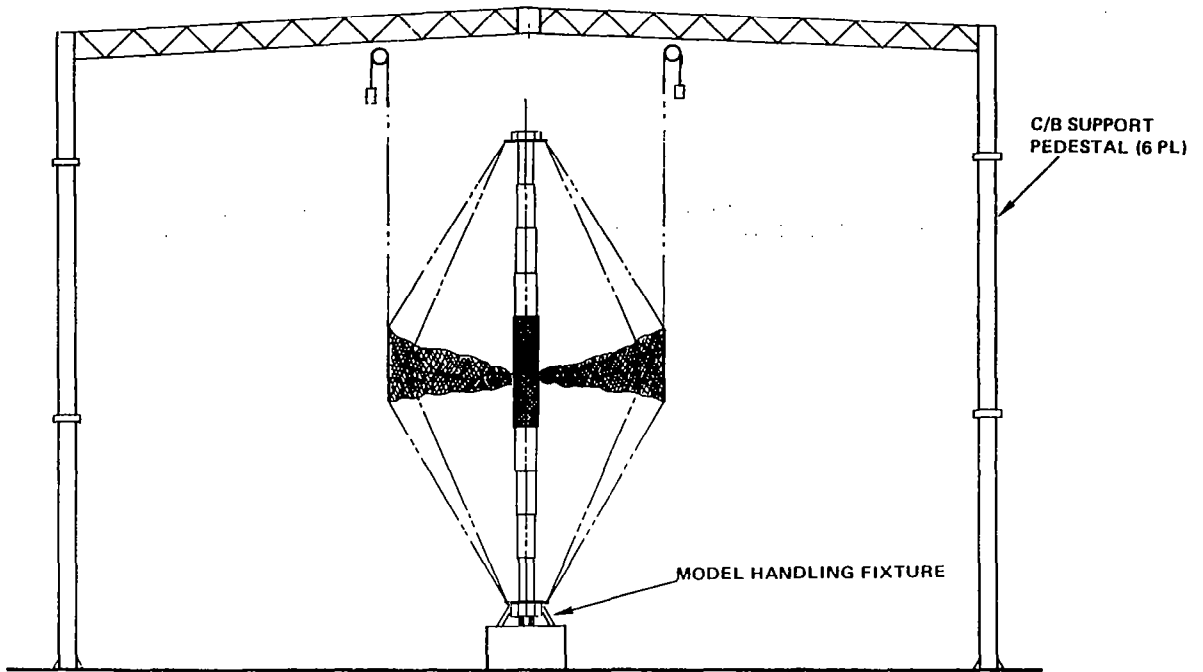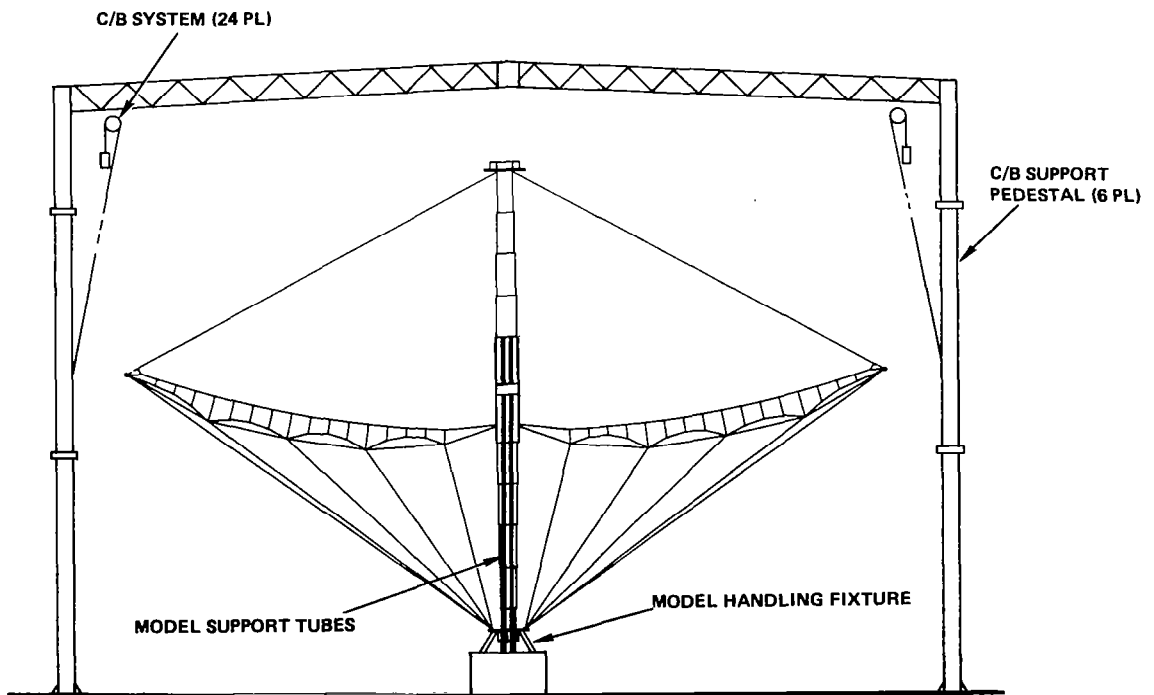
15-METER MODEL SCHEDULE

The 15-meter model is scheduled for fabrication and testing of the model less the surface in FY'83. The surface will be fabricated and assembled to the model in FY'84.

	FY 1983				FY 1984			
	1	2	3	4	1	2	3	4
DESIGN AND ANALYSIS	△——▽ STRUCTURE				△——▽ SURFACE			
PROCUREMENT		△——STRUCTURE——▽				△—SURFACE—▽		
PRODUCTION		△——STRUCTURE——▽				△——SURFACE——▽		
ASSEMBLE STRUCTURE AND SURFACE							△——▽	
TEST				STRUCTURE KINEMATIC △—▽			DEPLOYMENT RF △▽——▽	
FINAL REPORT								▽
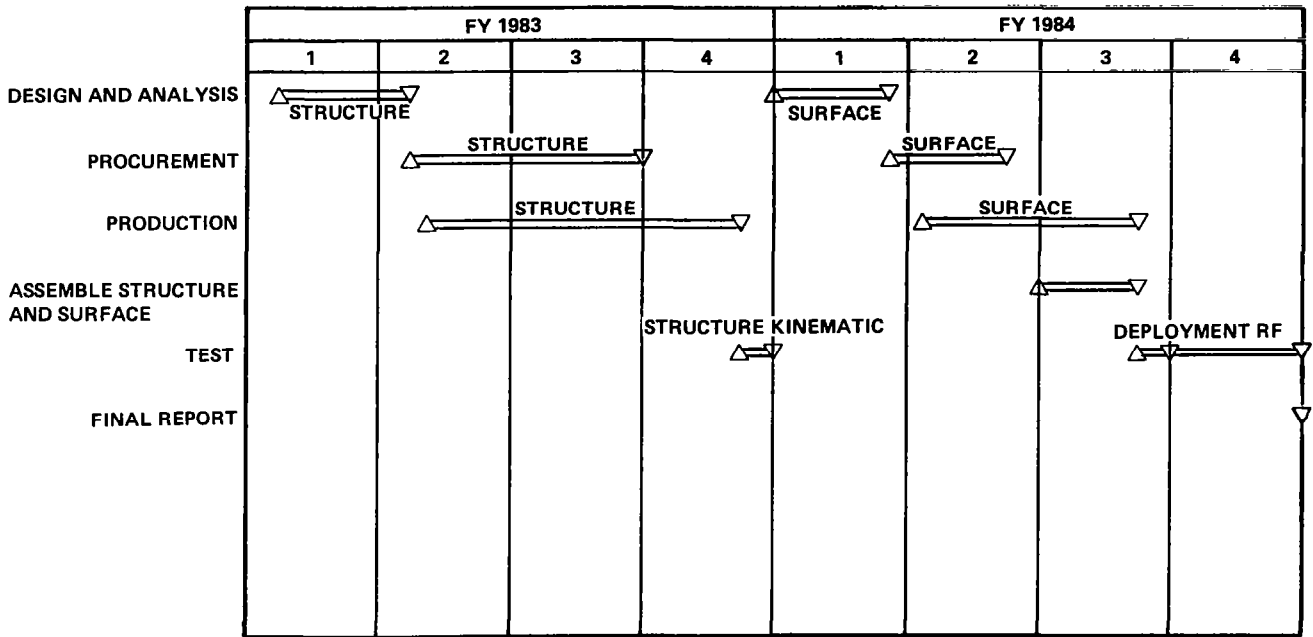
STATUS OF DEPLOYABLE GEO-TRUSS DEVELOPMENT

J. A. Fager
General Dynamics Corporation, Convair Division
San Diego, California

Large Space Antenna Systems Technology – 1982
NASA Langley Research Center
November 30 – December 3, 1982

GEO-TRUSS DESIGN MATURITY

The General Dynamics Convair geo-truss concept is entering its third generation of development. The early aluminum version demonstrated that the mechanism worked, and a viable mesh system could be integrated into the geo-truss substructure.

In the second generation, thermally stable, lightweight, rigid, graphite components enhanced the structure. Graphite grid cable and low CTE moly mesh enabled the mesh to be contoured to an EHF operation level. Refinements and analytical tools, deployment analysis, transient thermal shadowing interaction, and thermal distortion models were made to predict accurately the solar thermal vacuum simulation performance. Distortions were predicted using NASTRAN models and then were evaluated against photogrammetric measurements in the chamber under various space-simulated Sun conditions within a 3.5-mil accuracy. The packaged reflector, with over a 150°F thermal gradient through the pack, was deployed successfully in the vacuum environment.

The third evolving generation of geo-truss concepts to be considered includes large offset reflectors, multireflectors in the common structure, and multibeam systems with secondary antennas mounted to the periphery of the geo-truss. A 500-ft reflector can be accommodated in the STS payload compartment with a Centaur G' booster and a realistic spacecraft.

1ST GENERATION

ALUMINUM
20 MIL RMS
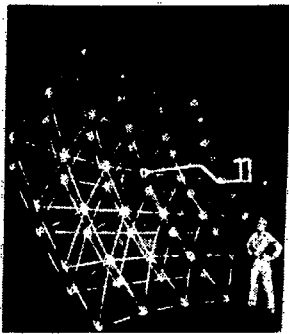
EDGE HELD

2ND GENERATION
THERMALLY STABLE
GRAPHITE/EPOXY

TDRSS
20 MIL
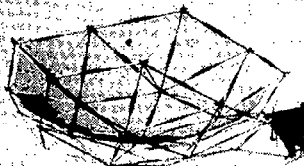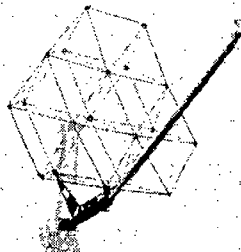
SECTION OF REFLECTOR

MULTI-REFLECTOR IN ONE STRUCTURE

3RD GENERATION

LARGE OFFSET
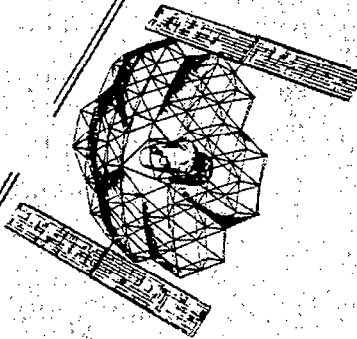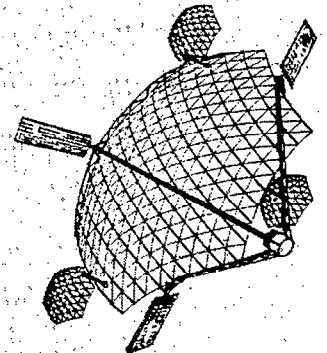
LARGE MULTI-BEAM COMMUNICATION

DEPLOYABLE GEO-TRUSS ANTENNA CHARACTERISTICS

General Dynamics Convair's (GDC) deployable geo-truss concept is basically a packaging system for Buckminister Fuller's three-dimensional isotropic structure. Fuller proved the optimum structure from a weight, strength, and cost basis to enclose a given area in a geodetic truss. The basic building block of the geo-truss is the tetrahedron. GDC integrated a folding carpenter tape into the bottom and top surface members of a tetrahedron to allow all six members to fold under the intersection points (or spider). The depth of the structure determines the stiffness needed for pointing the narrow-beam antenna. Thermal stability is also enhanced by the depth of the structure. GDC has built multiple geo-truss modules with a mesh contoured to 10-mil surface accuracy.

High package natural frequency of the geo-truss is achieved by interlocking spiders that are interlocked with shear connections, with a band around the periphery. The package in most cases is in the 50-Hz natural frequency range. Weight and rigidity vary as the depth of the structure is shown below. A lower number of bays will reduce the weight and cost, and increase stiffness. As the tetrahedron element increases, the ability to adjust the mesh will decrease. The optimum size and weight for a given size reflector are therefore a function of the peak frequency, and the depth of the truss is a function of the pointing accuracy. In a normal system the triangular mesh elements can be broken up into 105 subtriangles to match the paraboloidal surface within each tetrahedron; e.g., an 8-bay 100-ft reflector would have 840 control triangles across a major diagonal.

The carpenter tape deployment mechanism is an integral part of the structure providing optimum weight usage. There are no motor drive systems; only cutting a band is required. Deployment loads are highly predictable since the spring loads are known. While it is more involved, the basic principle is F=MA where F is the known spring energy.

TETRAHEDRON IS BASIC BUILDING BLOCK

PACKAGED   RELEASED   DEPLOYED

6-BAY ANTENNA

FREQ (Hz) / RIGIDITY / WEIGHT / DIAMETER (FT)
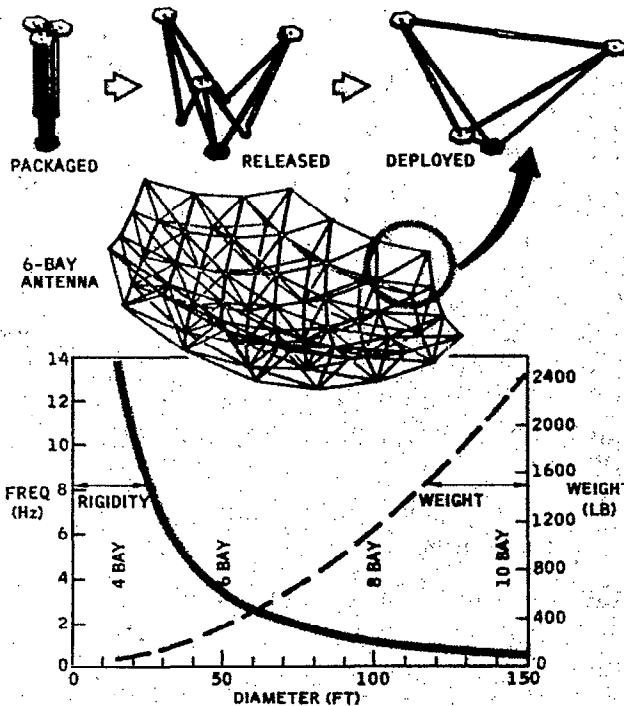
- DEPTH OF STRUCTURE PROVIDES
  - HIGH STIFFNESS NEEDED FOR POINTING
  - THERMAL STABILITY

- MESH CONTOUR ACCURACY
  - PROVEN TO 10-MIL RMS

- HIGH PACKAGED NATURAL FREQUENCY

- DOUBLE FAIL-SAFE DESIGN
  - CARPENTER TAPE WEAKEST LINK
  - REDUNDANT STRUCTURE

- DEPLOYMENT MECHANISM INTEGRAL PART OF STRUCTURE
  - OPTIMUM WEIGHT USAGE
  - NO MOTOR DRIVE

- MODULARITY SIMPLIFIES FABRICATION & TESTING OF LARGE SYSTEMS

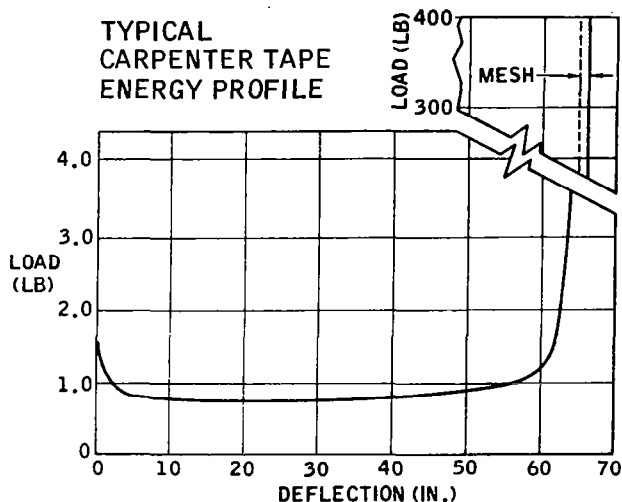- ONE-G DROOP EFFECT MINIMIZED BY LOCAL TRIANGULAR ELEMENTS

515

DEPLOYMENT DRIVE SYSTEM

Deployment is provided by the carpenter tape springs, which are very simple Lufkin-rule-type curved leaf spring elements that provide both the hinge and lock mechanism for the antenna. The concept is simple, reliable, and economical. As seen in the chart below, the spring drive characteristics are ideal. A curved leaf spring is basically a negator spring during the first part of its operation, so that load is uniform over a large range of the sweep of the deploying surface members motion. The curvature comes into the spring at the same time that the mesh cabling system load comes on. The carpenter tapes provide the ample "kick" to pull the mesh grid taut. There is a brief quiver loading on the order of a thousandth of a second when the carpenter tapes lock up. This loading can give you 95 to 100 G's, but, of course, these are low energy (the area under the G-curve is the energy).

In general there is 60% less energy in deployment than the spacecraft has to endure during boost. Fast or slow deployment had very little effect on the reliability of a mechanism, and, as can be seen from the chart, the loads were highly predictable. Our deployment program predicted load was 268 lbs vs. test load of 200 lbs in one case and 296 lbs vs. 278 lbs in another case. The given load is used conservatively as a static load in design. In most cases minimum graphite component gages design the bulk of the geo-truss members.

SPRINGS ARE ⟷ SIMPLE / RELIABLE → / ECONOMICAL ⟶ { HINGE DRIVE LOCK

KNOWN ENERGY LEVEL

TYPICAL CARPENTER TAPE ENERGY PROFILE

MESH

LOAD (LB) vs. DEFLECTION (IN.)
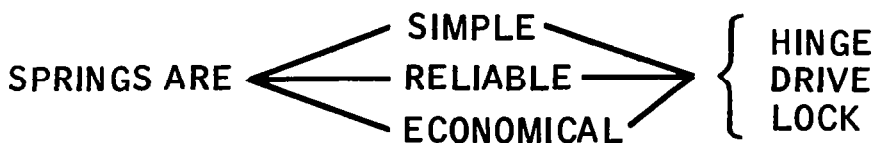
DEPLOYMENTS PREDICTABLE

SOLAR THERMAL VACUUM TEST

PREDICTED	TEST
268 LB	200 LB
-296 LB	-278 LB
1.60 SEC	1.52 SEC

EFFECT OF CARPENTER TAPE CHANGING FROM FLAT TO CURVE

SPIDER 1040

-119 Gs

-95 Gs

0.01 SEC →
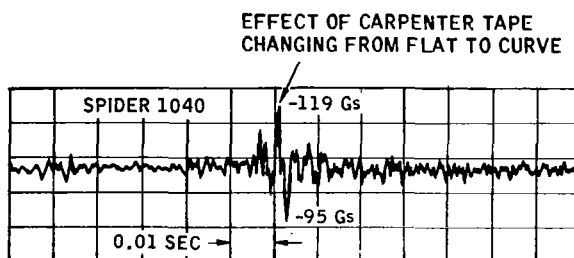
- 60% LESS ENERGY IN DEPLOYMENT AT SPACECRAFT INTERFACE THAN DURING BOOST

- FAST OR SLOW DEPLOYMENT HAS NO EFFECT ON RELIABILITY OF A MECHANISM

WORKING GEO-TRUSS CONCEPTS

Five different geo-truss concepts have been deployed for over 250 successful deployments. The mechanism has been deployed attached only to feed booms, edge-held, center-mounted with two different mount concepts and free deployed. Two-, four-, six-, and eight-bay versions have been deployed successfully.

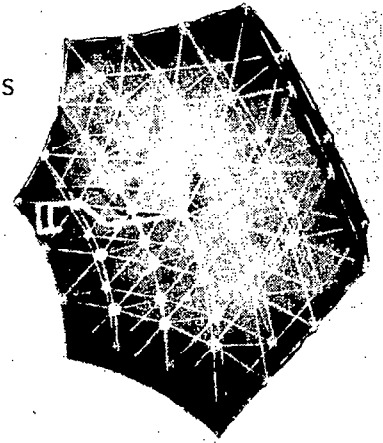There is no doubt that the mechanism and mesh system work based on this number of tests.
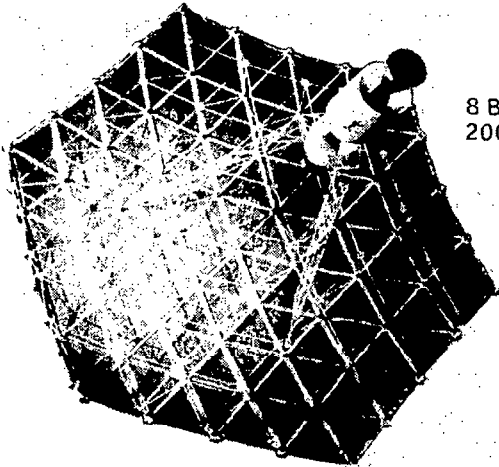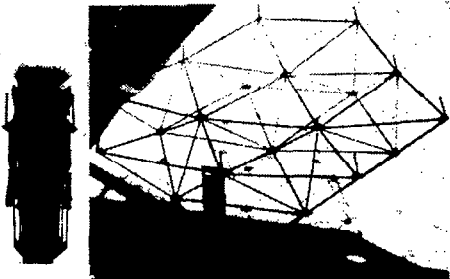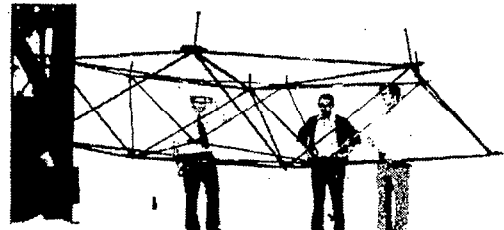
8 BAY
200 + DEPLOYMENTS
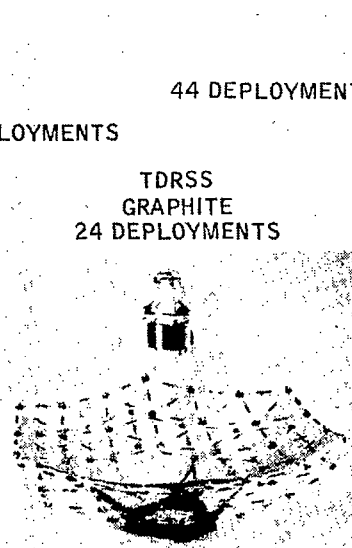
44 DEPLOYMENTS

TDRSS
GRAPHITE
24 DEPLOYMENTS

PROOF-OF-CONCEPT

GRAPHITE
4 DEPLOYMENTS

GRAPHITE
8 DEPLOYMENTS
SOLAR THERMAL
VACUUM CHAMBER

PROOF OF CONCEPT

A 3-bay flight-weight graphite reflector was selected to determine the accuracy to which the mesh system can be adjusted. This edge-held 16.3-ft reflector contained all the aspects of a large system with all the peripheral constraints as well as an interior triangle that simulated the edge effects of other interior triangles on a large system.

The pack was 6.3 feet high with the mesh held in a parachute rigging type of configuration.

The mesh used was gold-plated moly wire with a graphite cord grid system to contour the mesh. An EHF compatible accuracy was achieved on the paraboloidal mesh surface.

The weight of the basic reflector is 40 lbs.
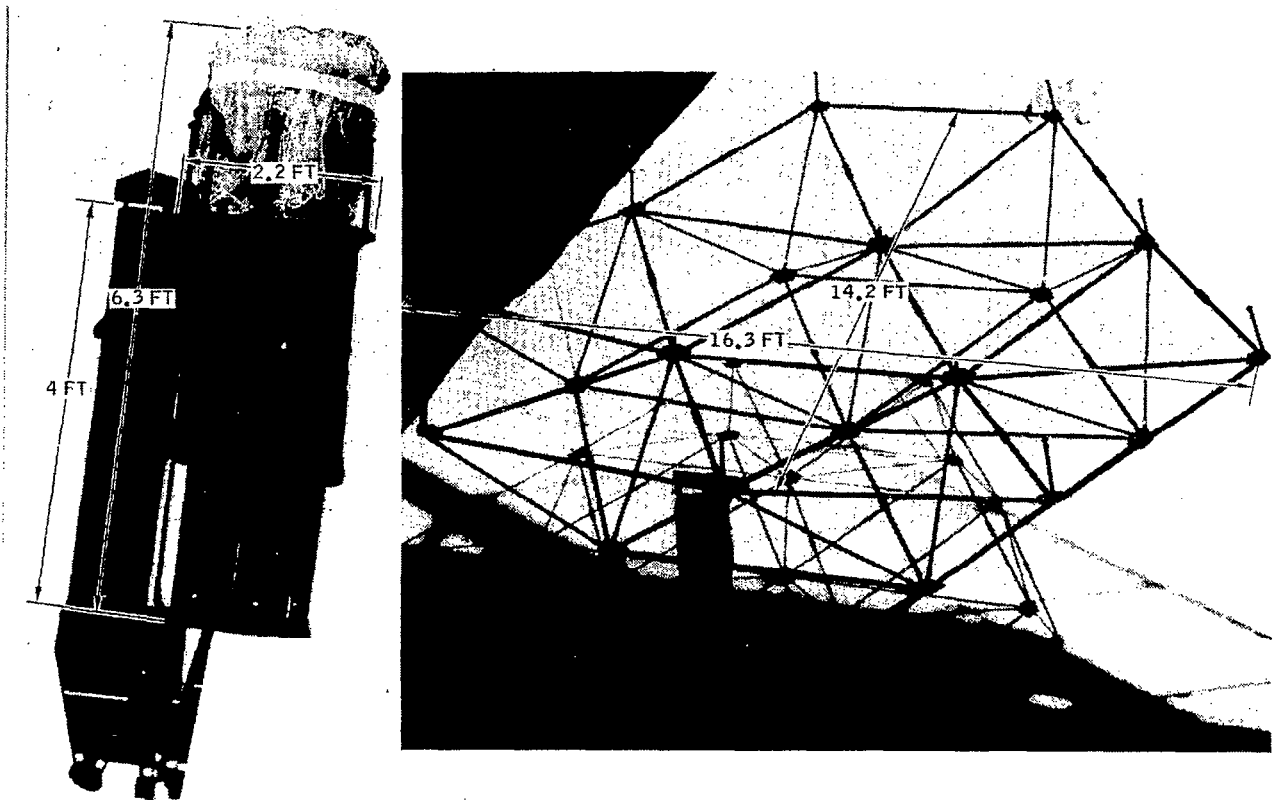
GEO-TRUSS PROOF OF CONCEPTS COMPLETED DEVELOPMENT PROGRAM

A full development program using graphite flight-weight components throughout was developed on the POC antenna. The surface strut tubes were designed to have a near-zero coefficient of thermal expansion. Tubes were in a 20-mil wall thickness category, and the titanium carpenter tapes were in the 8-mil thickness range.

The packaged antenna was thermally cycled from $+230^{\circ}F$ to $-250^{\circ}F$ prior to deploying the geo-truss without the mesh components. This is the worst-case dynamic loading, since the mesh grid system acts as a snubber. After reducing the load in geo-truss members, the mesh was then installed and the antenna deployed again; mesh contours were measured before and after each test.

A 1-G droop effect was evaluated by measuring the antenna face up, face sideways, and face down with and without zero-G constraints. The side-mounted reflector suffered a 1.4-mil change from the 12.7 mils contour to which the mesh was initially set, and cup-down increased distortion 3.5 mil. There is no significant effect from 1-G droop.

Hot and cold soak in a vacuum was performed prior to going to the more expensive large solar thermal vacuum chamber. In-air deployment was again achieved to ensure that the structure would be ready for the solar thermal vacuum chamber, and photogrammetric measurements were made of its surface under various thermal conditions including half-shadowing conditions that might occur from this shadowing by solar cells or other spacecraft elements. Good correlation was obtained between the predicted and the NASTRAN modelling. Final proof of the system was done on the RF range where it was tested into the EHF range.
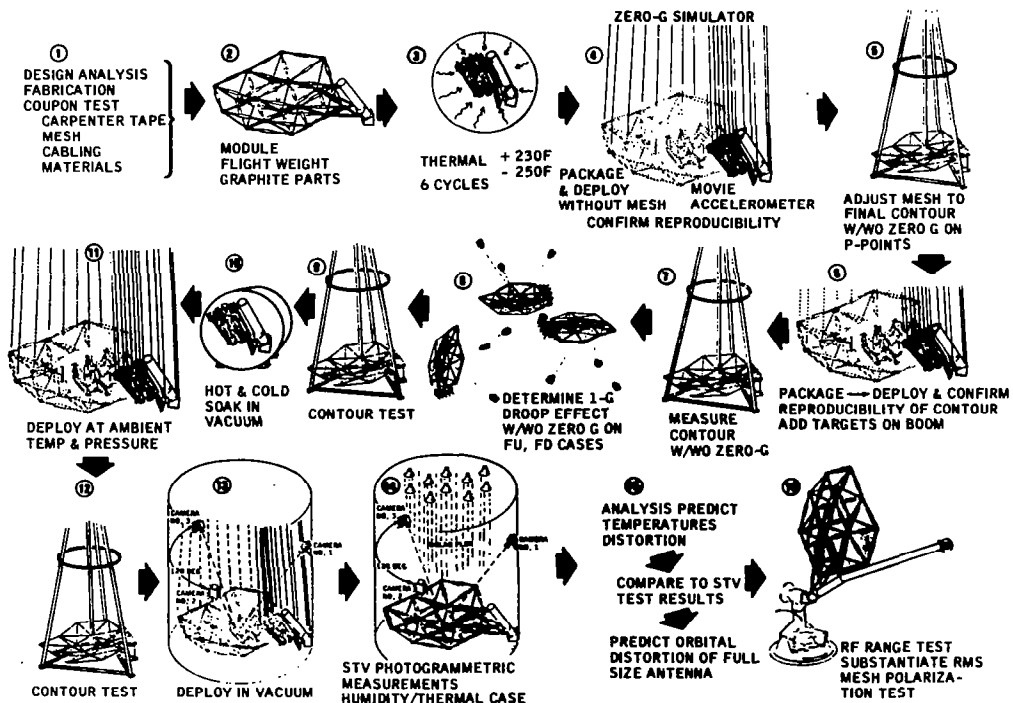
DEPLOYABLE GEO-TRUSS ANALYTICAL TOOL VERIFICATION

From the previous tests we have been able to match the deployment loads and times from our analytical program to the actual antenna deployment conditions. The figure shows the results of our computerized modelling tool sequences for an 8-bay center deployment. The carpenter tapes are modified by using this analytical tool to finally achieve a uniform effective low load deployment. Good correlation was obtained between test and analysis.

Transient temperatures were readily predictable on the tubes. A 100-element model is used on each tube and includes both shadowing effects from one tube to the other and mesh shadowing effects. While the mesh is 80% transparent when looking perpendicular to it, it becomes opaque and forms a shadow at more oblique angles. This full thermal analysis has been correlated against the STV program.

Thermal distortion predictions from a NASTRAN model versus the STS thermal vacuum test results were accurate within the 3.5-mil closure error of the photogrammetric measurement system.

With verified analytical tools, large antennas that will not fit into the available STV chamber can be designed with a high degree of confidence.

DEPLOYMENT PROGRAM
- COMPLETELY COMPUTERIZED
- MATCHES TEST DATA TO 15% (POC)

THERMAL ANALYSIS

STV TEST
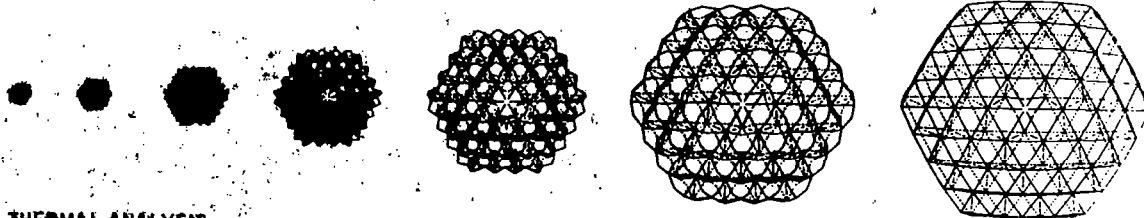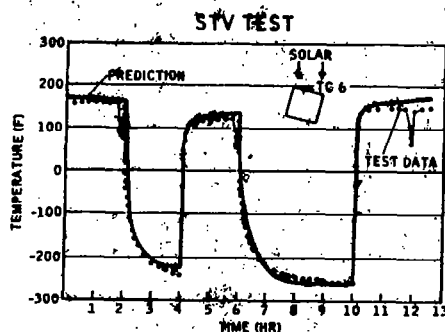
- TEMPERATURE PREDICTIONS CORRELATE WITH TEST DATA
- TRANSIENT OR STEADY STATE TEMPERATURE PREDICTIONS
- INCLUDES SHADOWING OF MESH, TUBE-ON-TUBE, VEHICLE COMPONENTS
- 100 ELEMENTS PER TUBE CONSIDERED FOR SHADOWING

THERMAL DISTORTION

O PREDICTIONS MATCH STV TEST RESULTS WITH PHOTOGRAMMETRIC ACCURACY (± 3.5 MIL)

DEPLOYMENT DYNAMICS CAN BE SIGNIFICANTLY REDUCED

For very large antennas with peripheral equipment, it may be desirable to increase deployment time to reduce terminal loads. Two options have been evaluated; one is spin deployment, which has an added advantage since it reduces the required spring energy. Spin can be obtained in space at a very modest weight penalty. Spin adds energy and maximizes the pull on peripheral elements where it is needed to pull the mesh taut. In the present system the spring drives have ample static margin to pull the mesh taut. With a spin drive system, the static margin would be obtained from the inertia loading. The advantages are potentially lighter weight due to thinner gage titanium carpenter tapes and lighter weight structure throughout. The disadvantage is that despin would be required.

Another concept is the damped deployment, in which viscous dampers, proven for use on solar arrays, could be applied at the spider points controlling the adjacent bent carpenter tapes. These continuously rotating vanes can be set for any deployment time event — one or two hours if desired. The dampers are the size of a quarter and would probably add at the maximum 10 to 15 percent to the weight of the total reflector system. Since the antenna is designed to have ample static margin, it is doubtful that it would be necessary to increase energy requirements.
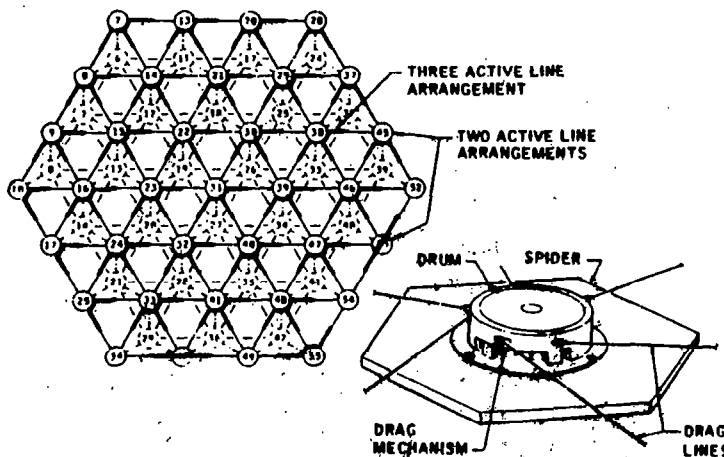
TWO OPTIONS

SPIN DEPLOYED

1/2 RPM
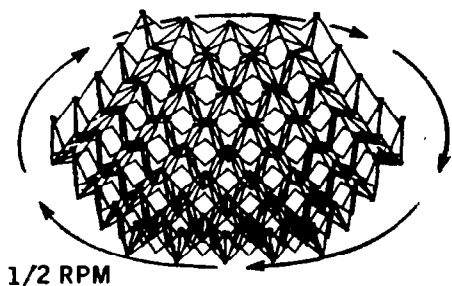
ADVANTAGES

- LIGHT WEIGHT
- SPIN ADDS ENERGY AT MINIMAL WEIGHT

DISADVANTAGE

- SPIN/DESPIN CAPABILITY REQUIREMENT

DAMPED DEPLOYMENT

THREE ACTIVE LINE ARRANGEMENT

TWO ACTIVE LINE ARRANGEMENTS

DRUM   SPIDER

DRAG MECHANISM   DRAG LINES

ADVANTAGES

- VISCOUS DAMPER CONTROLS EACH SET
- 1 TO 2 HR DEPLOYMENT FEASIBLE
- LOADS REDUCED TO STATIC CONDITION
- PROVEN ON SKY LAB

DISADVANTAGES

- MORE ENERGY REQUIRED TO DRIVE DAMPERS
- INCREASED WEIGHT

As the antenna diameter increases, gain increases and beam width diminishes. If 1/10 of the 3-dB beam width is considered a rational beam pointing requirement, pointing stability becomes a significant problem. For instance, the 500-ft reflector would require a pointing accuracy of 7.2 arc seconds. At 12 GHz, which is in the new range of communication frequencies, a 500-ft reflector would need to have a 4.3-arc-seconds pointing capability.

These very rigorous pointing accuracies illustrate the need for rigid structure to control and point these narrow beam systems.

GEO-TRUSS PERFORMANCE/BEAM POINTING REQUIREMENTS

- HIGH STIFFNESS NEEDED FOR NARROW BEAM POINTING

- THERMAL STABILITY ACHIEVED WITH THERMAL COMPENSATED MEMBERS

- DEPTH OF STRUCTURE CAN BE ADJUSTED TO INCREASE STABILITY
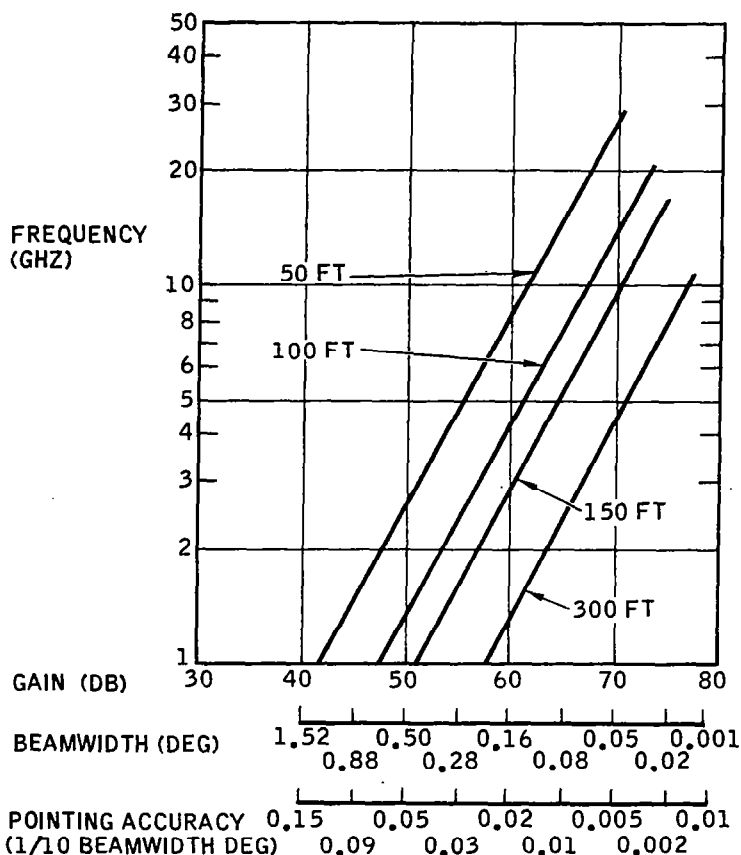
NOTE:
AN APERTURE EFFICIENCY OF 55% & A 10 DB TAPER WERE USED TO COMPUTE GAIN & BEAMWIDTH VALUES

POC ON SHUTTLE

An excellent experiment could be achieved with POC building blocks. It would provide both geo-truss structural experience and needed RF knowledge for future narrow-beam systems.

Some candidate experiments are as follows. (1) EVA support of geo-truss from both a primary and a contingency basis could be evaluated. (2) Secondary hardware and geo-truss elements could be attached to show building block capability. (3) RF alignment can be achieved with astronaut support and STS antenna measurements of gain and surface accuracy. (4) Photogrammetric measurements could be made to evaluate the surface accuracy. (5) World-wide RF noise models could be developed.

Currently, RF noise models are based at looking at the entire Earth or half-hemisphere environment. Large antennas with narrow beams would now see much smaller areas, and therefore noise models must be developed for these narrow beams; otherwise, errors on the order of 3 dB could be made in designing communication systems.
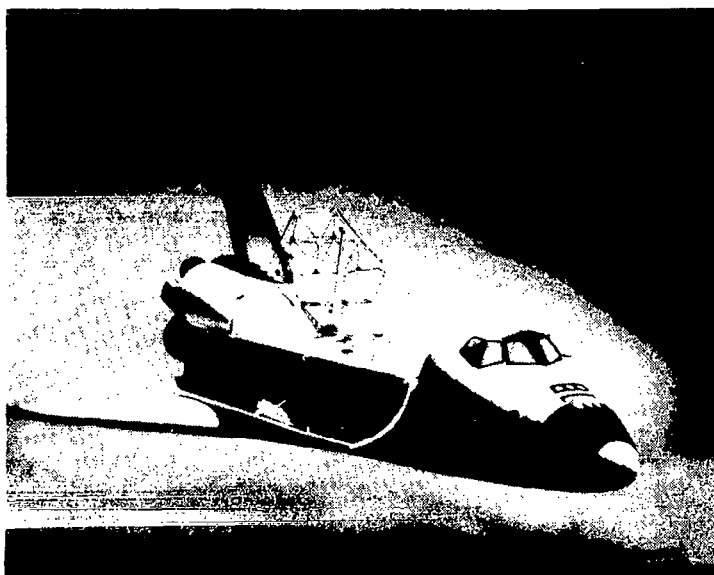

USE OF AVAILABLE POC COULD PROVIDE:

- DEMO OF EVA SUPPORT
- MEASUREMENT OF REFLECTOR IN ORBIT
- RF TESTS ON ANTENNA
- RF NOISE MAP IN KEY COMMUNICATION BANDS

OFFSET REFLECTOR

The geo-truss can be held at any 3 or more points within the structure. Edge support is an ideal geometry for offset reflectors. The semihexagonal mount seen below the mesh illustrates the size of the packaged reflector. Ample room for electronics can be developed around the reflector mount.

Early consideration of the geo-truss packaged/deployed configuration in the spacecraft design phase is the key to achieving the optimum total spacecraft.
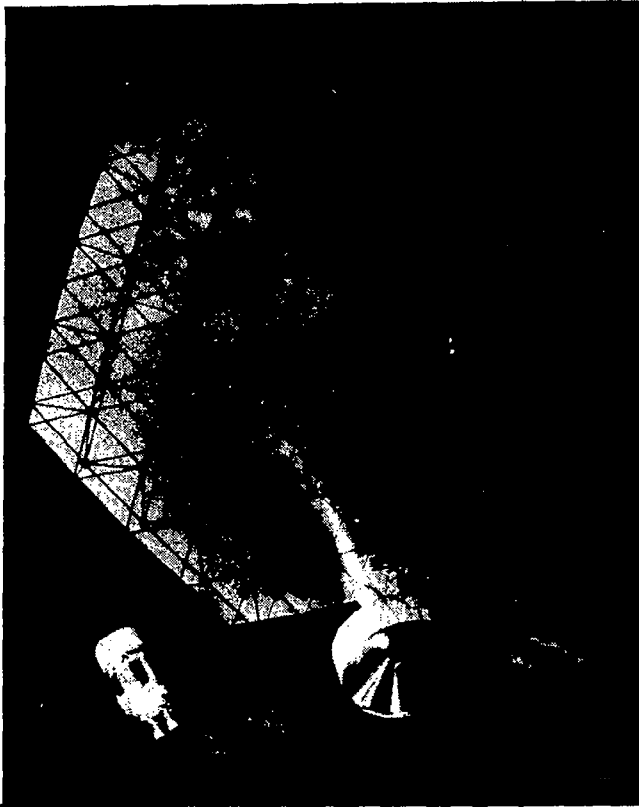
GEO-TRUSS IDEALLY SUITED TO EDGE MOUNT
- NO SECONDARY BOOM NEEDED
- SPACECRAFT INTEGRATED INTO MOUNT
- HIGH STABILITY/RIGIDITY
- UNIFORM SURFACE ACCURACY OVER ENTIRE SURFACE
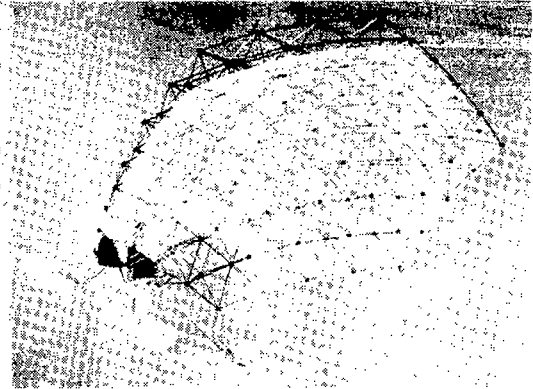
MULTIREFLECTOR LARGE COMMUNICATION ANTENNA

This centered-body pressurized container would contain all the feed/electronic systems and could be docked to the Shuttle initially for checkout and during the startup period. If later synchronous-orbit manned capability is available, docking could be achieved and refurbishment of transmitters and receivers performed.

With six beams, the four time zones could be covered as well as Alaska and Hawaii. The solar cells mounted on the periphery of the antenna eliminate the need for secondary booms.
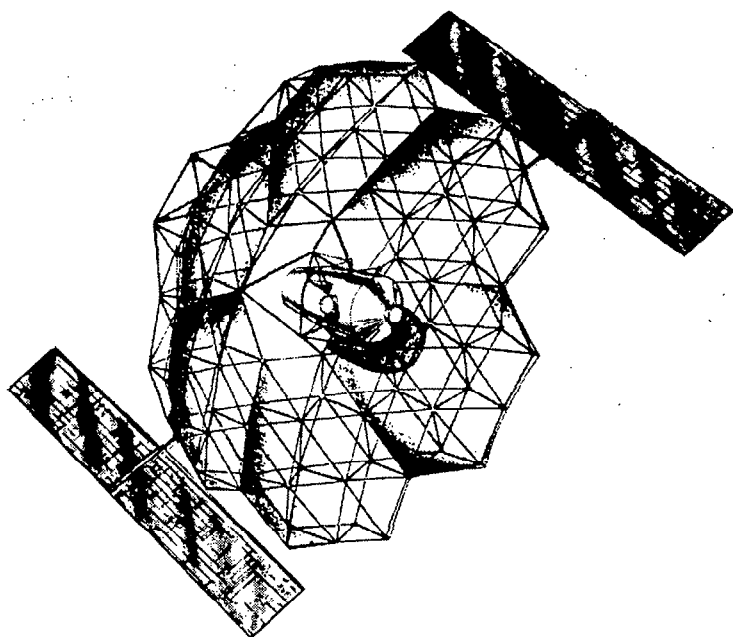
- SIX REFLECTORS IN COMMON STRUCTURE
- PRESSURIZED OFFSET FEED/ ELECTRONICS
- SOLAR POWER INTEGRATED INTO REFLECTOR
- STS DOCK CAPABILITY

525

BOX TRUSS DEVELOPMENT
AND APPLICATIONS

J. V. Coyner, Jr.
Martin Marietta Corporation
Denver Aerospace
Denver, Colorado

Large Space Antenna Systems Technology – 1982
NASA Langley Research Center
November 30 – December 3, 1982

Since 1977, MMDA has aggressively pursued development of deployable structural systems applicable to a wide variety of Shuttle-transportable large space system requirements. This effort has focused on the deployable box truss. Figure 1 illustrates the box truss terminology and shows how the box truss cube is incorporated into LSS structures.

The box truss cube is comprised of a deployable frame consisting of two equal length structural members ("verticals"), two structural members hinged in the middle ("surface tubes") which connect the ends of the verticals and fold inward to stow between the adjoining verticals, and telescoping diagonal braces that lie in, and control the shape of, the deployed frame (figure 1).

The shape of a box truss reflector, platform, or feed mast is controlled by the diagonal tension braces in each frame face. The diagonals are multiple-ply graphite-epoxy tapes that telescope for stowage and deployment. Both diagonal tapes in each frame face lie flat in the plane of the frame, thereby equalizing solar input to the two tapes and minimizing thermal distortions.

Deployable Box Truss

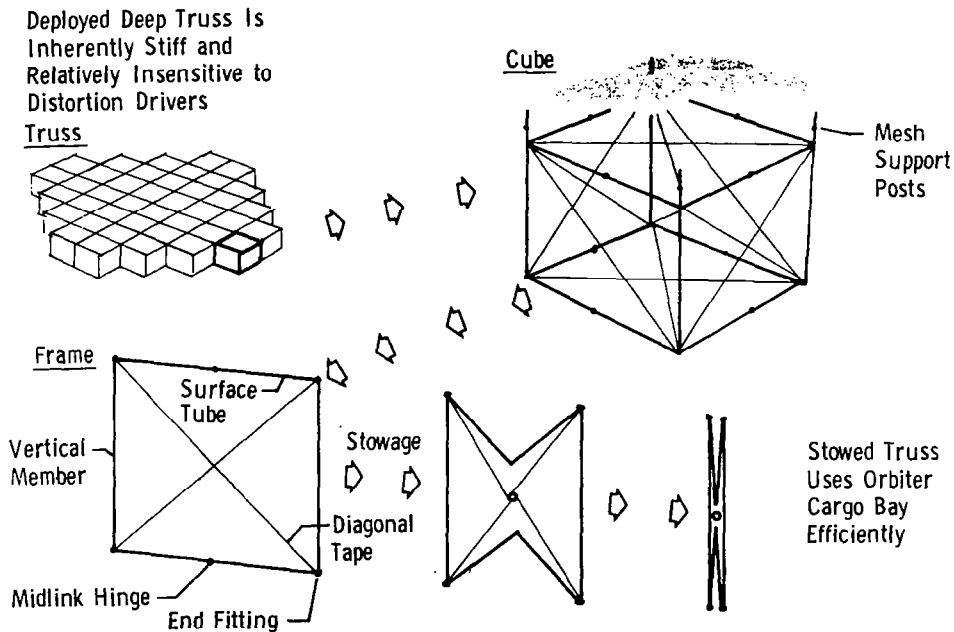
Figure 1

EVOLUTION OF BOX TRUSS STRUCTURES

Each year significant steps were taken in the maturity of the box truss design and the understanding of the supporting analysis. Figure 2 summarizes the evolution of the deployable box truss, including progress to be completed in 1983. During 1977 and 1978, the emphasis was placed on design and analytical verification of the box truss structure performance. During 1979, 1980, and 1981, design refinements and hardware fabrication were directed towards GFRP integration with primary emphasis on low cost. This activity culminated in the fabrication and demonstration of the 4.6-meter cube. During 1982 and 1983, the emphasis has been placed on demonstrating the performance of a multicube truss antenna.

1977   o Box Truss design conceived on IR&D
        o Design developed and analyzed on "On Orbit Assembly" program
        o Single frame demonstration model fabricated

1978   o Design and fabrication of single frame prototype structure
          (GFRP tubes and metallic fitting)

1979   o Design refinement integrating low cost GFRP fittings and members

1980   o Design of GFRP 4.6-meter Box Truss Cube
        o Fabrication of all components

1981   o Assembly and test of 4.6-meter Cube

1982   o Design and fabrication of half-scale MSDA model started

1983   o Assembly and test of MSDA half-scale model

Figure 2

FEATURES OF BOX TRUSS SPACE STRUCTURE

Figure 3 summarizes many of the fine features that are available when using the box truss for LSS structures.

Versatility – The box truss can be used for any configurations needed. By varying the lengths of the diagonal tension braces, the box truss cubes can be used for platforms, parabolic, spherical, and parabolic toric reflectors, and feed masts or beams. Also, by varying the stiffnesses of the various box truss members, required system performance versus weight and stowed package size can be optimized.

Orthogonal-Sequential Deployment – Structures composed of box truss cubes are deployed in a controlled sequence of steps. Feed masts and beams are deployed one cube at a time, and trusses are deployed one row of cubes at a time. In the latter case, the steps are accomplished in a preselected sequence in the two orthogonal deployment directions. This type of deployment is compatible with flat, parabolic, spherical, and parabolic toric trusses, and virtually any beam shape.

Cube Corner Fitting – The cube corner fitting forms the structural ties between the cube's vertical members, surface tubes, and diagonal braces. The cube corner fitting is made of 1.25-cm compression-molded chopped graphite-fiber in an epoxy matrix to give rigidity and thermal stability to the structure.

Efficient Stowage – All structural members stow compactly; the stowage size of a cube is dependent upon vertical member and surface tube diameters. In the stowed condition, the cube corner fittings butt against each other and form a plane at the top and bottom surfaces. The plane formed by the cube corner fittings provides a load path for loads incurred during launch with inplane shearing loads handled by interlocking pins between the fittings.

o VERSATILITY

o ORTHOGONAL-SEQUENTIAL DEPLOYMENT ACCOMPLISHED WITH NO ADDED COST OR COMPLEXITY

o PARABOLIC AND SPHERICAL SURFACES EASILY ACHIEVED WITH MINIMAL ADDED COMPLEXITY
   - PIN HOLE LOCATIONS VARY IN IDENTICAL GENERIC END FITTINGS
   - SURFACE AND DIAGONAL MEMBER LENGTHS ARE GROUPED INTO SETS OF IDENTICAL LENGTH MEMBERS INSTEAD OF ALL IDENTICAL
   - NO OTHER DESIGN IMPACTS

o CUBE CORNER FITTING RIGIDITY AND STABILITY INHERENT IN TRUSS DESIGN

o EFFICIENT STOWED PACKAGING WITH ALL MEMBERS AUTOMATICALLY RESTRAINED DURING LAUNCH

o WHEN BOX TRUSS IS OPTIMIZED AS A TOTAL S/C SYSTEM, PERFORMANCE AND COMPLEXITY FACTORS SWING IN FAVOR OF BOX TRUSS VS TETRAHEDRAL TRUSS AND OTHER ANTENNA SYSTEMS

Figure 3

Before 1979, the box truss concept existed only on paper. It was decided at this point that a first-generation deployable box truss kinematic model incorporating multiple cubes should be produced. To maximize this model's utility, it was decided that it should be a parabolic truss, thereby permitting demonstrations of both basic truss kinematics and its parabolic implementation. The model's surface tubes are hinged in the middle to provide folding for compact stowage. The midlink hinges (modified toggle bolts) contain six-turn coil springs wound on the 0.125-in. hinge pins using 0.035 spring wire. Each hinge pin's axis is perpendicular to the outer edge of its surface tube halves. Accordingly, when a surface tube is deployed straight, it is statically locked straight by the overcenter position of the hinge pin relative to the tube-end hinge pins. This is identical to the flight-hardware design philosophy.

The kinematic model was stowed and deployed by hand repeatedly in a sequence of row and column steps. Full truss deployment could be accomplished in approximately 1 min. The stowed truss (figure 4) is 15 in. long by 5 in. in dia. The deployed truss is 15 in. deep, 58 in. in dia., and has a focal length of 29 in. The relatively simple first-generation kinematic model demonstrated both truss kinematics and compatibility with a stowed, deploying, and deployed reflective mesh surface. The kinematic truss, with mesh, also substantiated a key design requirement for the midlink hinges in dynamic and flight truss systems. The requirement is that the midlink hinge provides an impulse of energy as its surface-tube halves approach full deployment. The impulse is required to tension the flight truss diagonals and stretch the antenna surface.
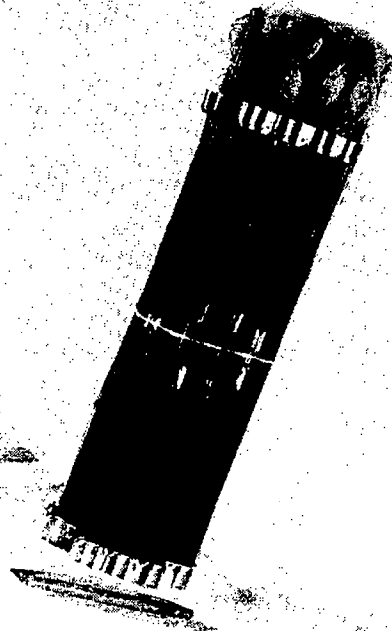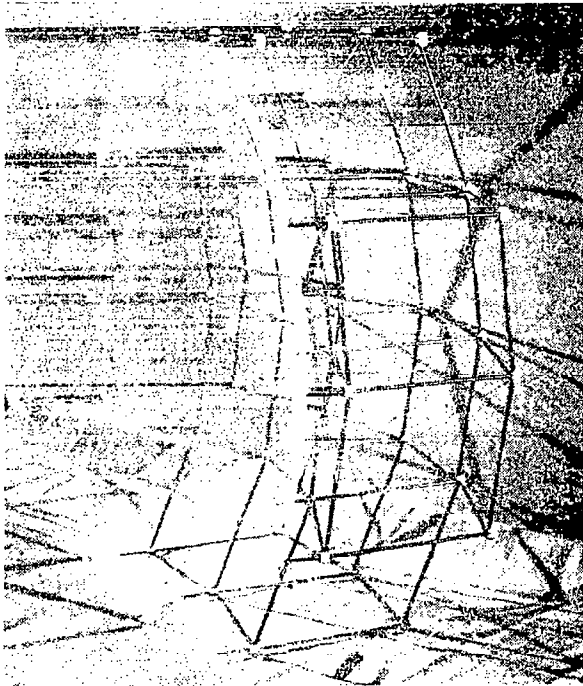

Figure 4

Based on previously known design requirements and insight gained from the kinematic model (figure 4), a 4-ft single-frame dynamic model was built incorporating both graphite/epoxy composite members and a general purpose midlink hinge design (figure 5). The diagonal tapes used in the dynamic model were a first-generation design to meet specific requirements of stowage, deployment, and load capability. The double sliding tapes were a forerunner for the exiting tube and tape telescoping diagonals and were compatible with the stowage and telescoping features of the present design. The over-center design of the aluminum midlink hinge met the deployment requirements, but a thermal analysis on the frame showed the fitting must be made of graphite/epoxy to reduce thermal distortions. Also, the complexity of the fitting made it expensive to machine out of aluminum or to be easily made of graphite. For these reasons, alternate designs that incorporate the overcenter latch were started.
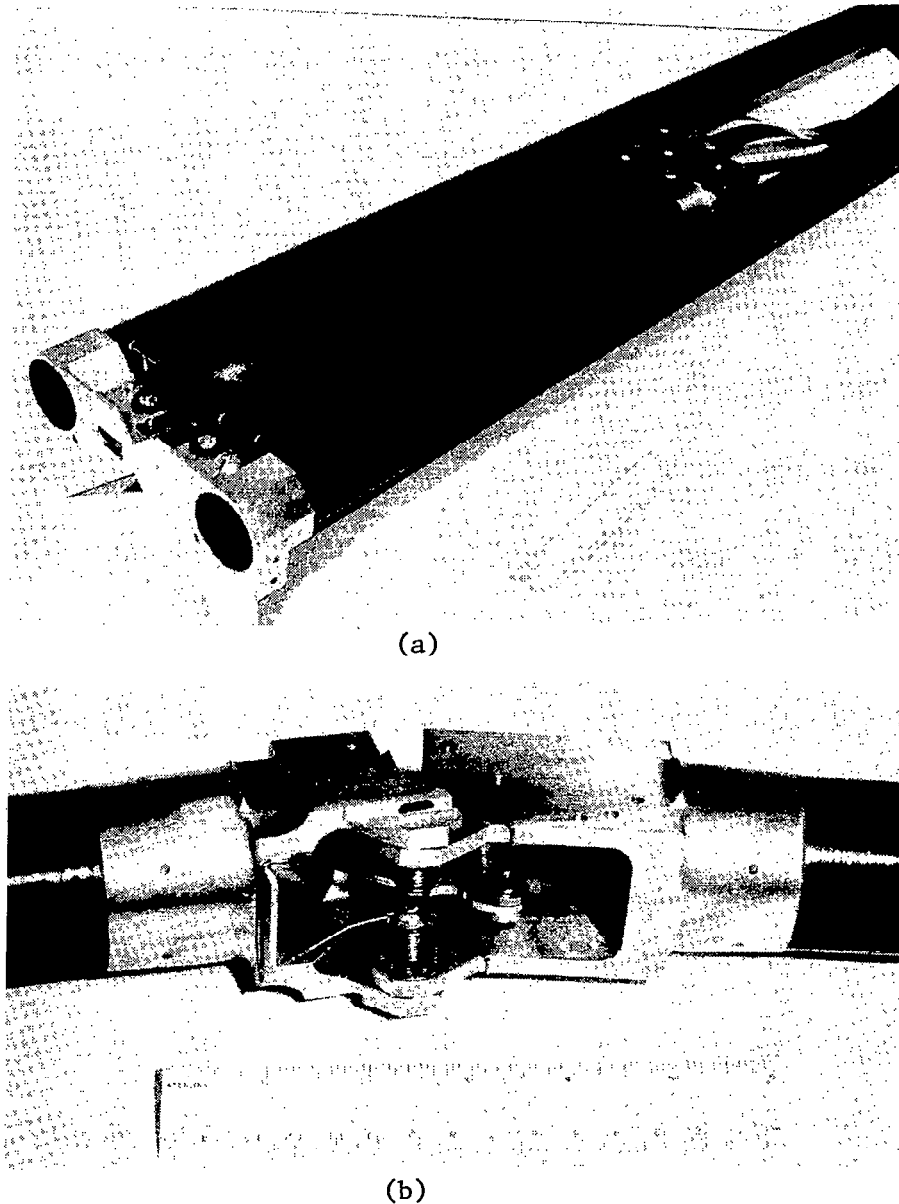

(a)

(b)

Figure 5

FULL-SCALE PROTOTYPE CUBE

During 1980, the design of each of the box truss components was reviewed and redesigned to achieve maximum weight, cost, and thermal stability while meeting the stowed, deploying, and deployed structural requirements. A prototype was made for each component and tested to verify manufacturing methods (feasibility and tolerance manageability) and stiffness, strength, and weight. By the end of 1980, all components for a full-scale prototype 15-ft, deployable box truss cube were completed and assembly had started. Final assembly was completed in 1981. Figure 6 summarizes the design features of the full-scale prototype cube. Figure 7 shows the resulting prototype cube in a deployed and stowed configuration, respectively.

- 4.6 m DEPLOYABLE CUBE

- STOWS IN 0.3 m SQUARE BY 4.6 m LONG (0.15 m PER MODULE)
    -- 36 MODULES (28 m x 28 m DEPLOYED) STOW IN 1 m BY 1 m BY 4.6 m

- ALL GFRP EXCEPT FOR HINGE PINS AND SPRINGS

- HIGH PERFORMANCE (HIGH STIFFNESS, LOW CTE)

- LOW WEIGHT - 27 kg

- HIGH ACCURACY - BETTER THAN 0.1 mm ON ALL AXES

- 50 N DIAGONAL PRETENSION

- EXHIBITS IDEAL TRUSS CHARACTERISTICS FOUND IN ALL BOX TRUSS SYSTEMS
    -- PURITY OF LOAD PATHS, I.E., NO BENDING MOMENTS IN DEPLOYED
       STRUCTURE

- ALL COMPONENTS AND MEMBERS FULLY CONSTRAINED WHEN STOWED

- EVERY CORNER FITTING STABILIZED BY BONDED INTERFACE TO VERTICAL TUBE

Figure 6

STOWED CUBE

All of the structural members of the prototype box truss cube stow compactly,
allowing the antenna to easily meet stowage requirements (figure 7). In stowed
condition, the cube corner fittings butt against each other, forming a plane at the
top and bottom surfaces. The plane formed by the cube corner fittings provides a
load path for loads incurred during launch with inplane shearing loads handled by
interlocking pins between the fittings. The surface tubes are restrained by fold-
ing them into the finned vertical members; the cross-over fitting stows between the
surface tube midlink hinge. When the cube is fully stowed, all components are
restrained.

(a)

(b)

Figure 7

534
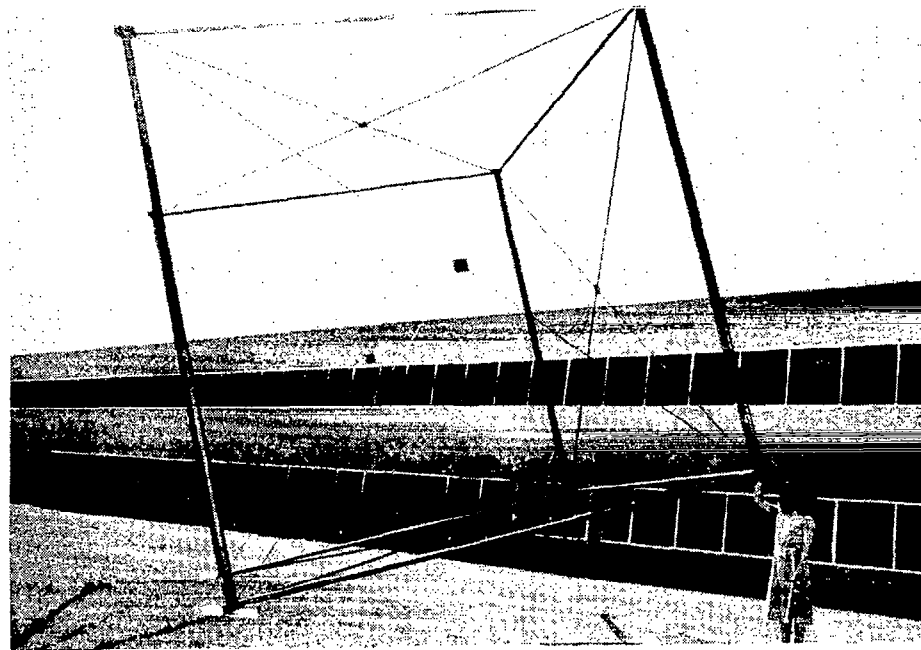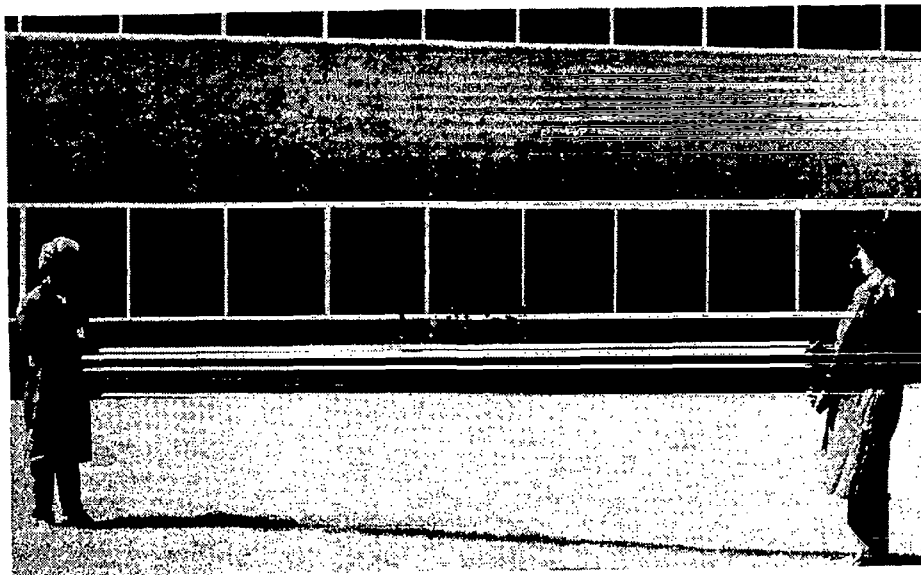
These graphite/epoxy laminated tubes are of conventional construction, molded on an aluminum mandrel. The ply orientation, materials, and number of plies can be varied to optimize stiffness and strength requirements versus weight. A significant improvement was made in the cost of the surface tube end fitting during 1980. In 1979, molded graphite/epoxy laminated end fittings (composed of four parts and requiring several assembly steps) were developed for the 4-ft dynamic model (figure 5). While these met the low coefficient of thermal expansion requirements, they were costly to produce and assemble on the tubes. A design and fabrication effort was initiated to improve this situation. The result is the integrally manufactured end fitting shown on the cutaway sample in figure 8. The design features of the surface tubes are:

> Integrally Molded End Fitting
> > - one part
> > - one manufacturing step
> > - one machining process
> > - no end fitting bonding qualification and inspection
>
> Comparison to Titanium or Aluminum Fittings
> > - lower thermal distortion (factors of 15 and 30)
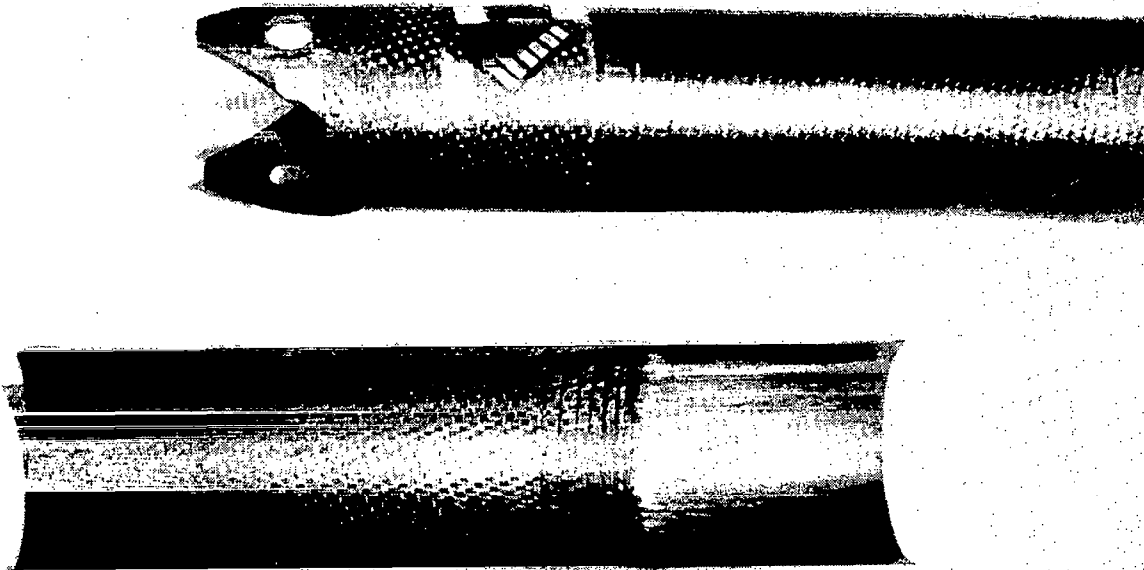> > - lower weight (40% and 60% reductions)
> > - equal or lower cost

Figure 8

FINNED VERTICAL MEMBERS

These graphite/epoxy laminated members, called verticals because they span the front to the rear of a box truss platform or dish, are composed of a square center box section with (as required) fins of varying thicknesses and lengths added at 45° to each corner of the box (figure 9). This design provides more compact stowage than round tubes of equal column load capability since the surface tubes nest inside the fins. Also, the flat sides of the box section act as launch restraints for the stowed interior diagonals. Fabricating the vertical members for the 15 ft cube presented significant problems in cost and dimensional stability. To meet stowed volume constraints, the members must be held to 0.010 in. on end-to-end straightness. The final design and manufacturing processes consistently produce vertical members meeting the dimensional tolerance and load carrying requirements with reasonable cost. The design features of the finned vertical members are:

- Basic member is a molded GFRP box section

- Faces of the box section restrain the stowed surface tubes and telescoping diagonals

- Two or four U-channel fins are used to increase column allowables when necessary without affecting stowage efficiency

- Bonding corner fittings to vertical members provides high moment-carrying capability at each truss node
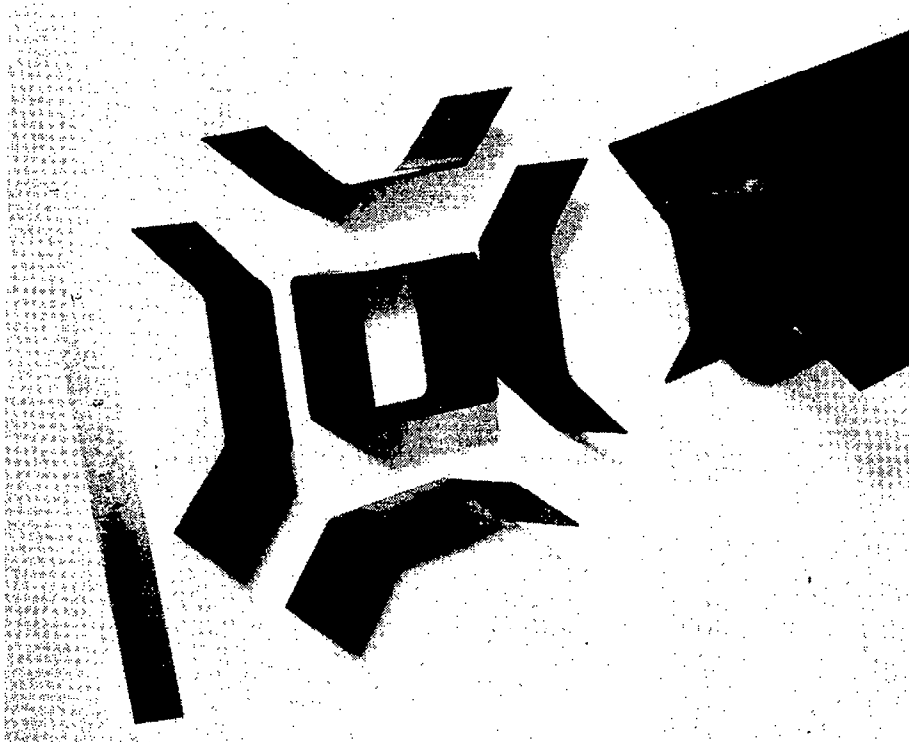

Figure 9

CUBE CORNER FITTING

This fitting forms the structural tie between the cube vertical member, surface tubes, and interior and exterior diagonal braces. Flanges are provided to accommodate the stowage and deployment hinge pins for the surface tube and interior diagonal brace. The fitting-edge faces and top plate provide, respectively, the load-bearing surface and load path for compression loads applied in the stowed configuration. In a multi-cube truss, the fitting-top plate is also the location for deployment release latches that permit sequenced release of truss rows and columns. The square hole in the top plate can accommodate payload attachments such as support posts for antenna mesh.

A compression-molded, chopped-graphite-fiber fitting that uses state-of-the-art techniques was selected (figure 10). The fittings were made using 1/2 in. chopped graphite fiber and two different matrices (15 fittings with each matrix material). The arrangement of flanges on the fitting's lower side accommodates the hinge pins as already described and also forms a cavity matched to the finned vertical member configuration.

During assembly, room-temperature-cure adhesive is injected into the vertical member-to-fitting interface slots, forming a shear bond with strength well in excess of the 500-lb typical maximum vertical-member tension or compression load. The design features of the cube corner fitting are:

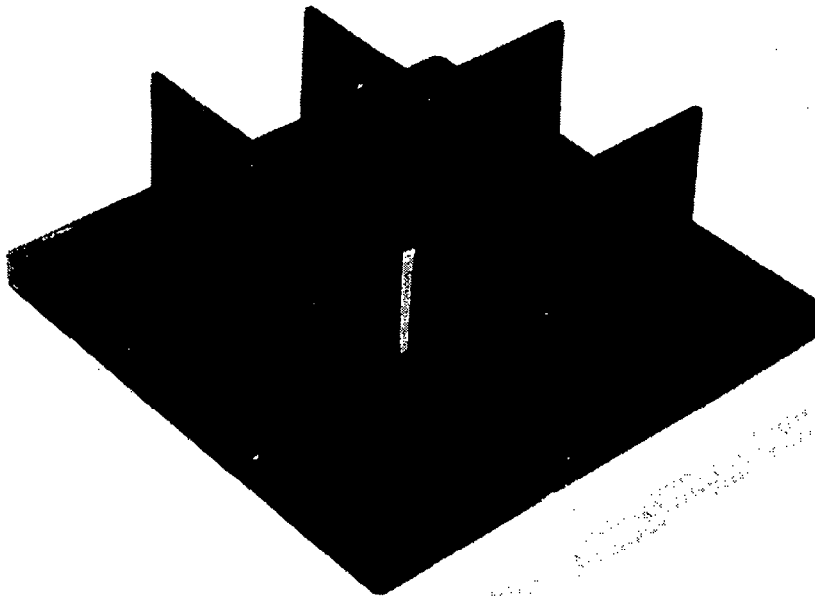|	
Payload Attachment	--- fitting rigidly bonded to vertical member
Low Cost	--- $100 per raw part, minimal final machining
High Thermal Stability	--- 12 times better than aluminum
Low Weight	--- 40% less than aluminum

Figure 10

MIDLINK HINGE AND DEPLOYMENT LINKAGE HARDWARE

These devices form the structural link between the deployed surface tubes and assist in the deployment operation. The design selected and fabricated in 1979 is shown in figure 5. While it met the mechanical function requirements for this device, it was judged to be too complex and costly, and because of its metallic body, it possessed an undesirably high coefficient of thermal expansion. A combined mechanical design and graphite/epoxy component fabrication effort was initiated to improve the device. The basic design approach, which incorporated an internal, spring-driven, overcenter latch, was preserved. This latch meets four design requirements: deployment drive torque; high torque at latchup to add tension to the diagonal braces and reflector surface; positive locking of the deployed surface tube halves; and tension-load path (with the hinge pins) in the deployed surface tube.

The result of this 1980 effort is the dramatically simpler (less than half as many parts) midlink hinge with latch shown in figure 11. Except for the spring and hinge pins, the device is fabricated completely with laminated graphite/epoxy materials. Each of the parts in the new device requires relatively simple machining procedures. The high tolerance (±0.001 in.) on the overcenter latch is achieved by drilling the final hole in the long center link with the deployed hinge and latch assembly in a fixture that aligns the hinge halves. The hinge pin holes are match-drilled in the same fixture. Each hinge assembly is completely fabricated and tested in the sleeves that are later bonded to the inside of the surface tube halves. The new design permits the latch drive spring (average torque of 2.5 in.-lb) to drive the frame deployment, giving the 15-ft frames a deployment time of approximately 7 seconds.
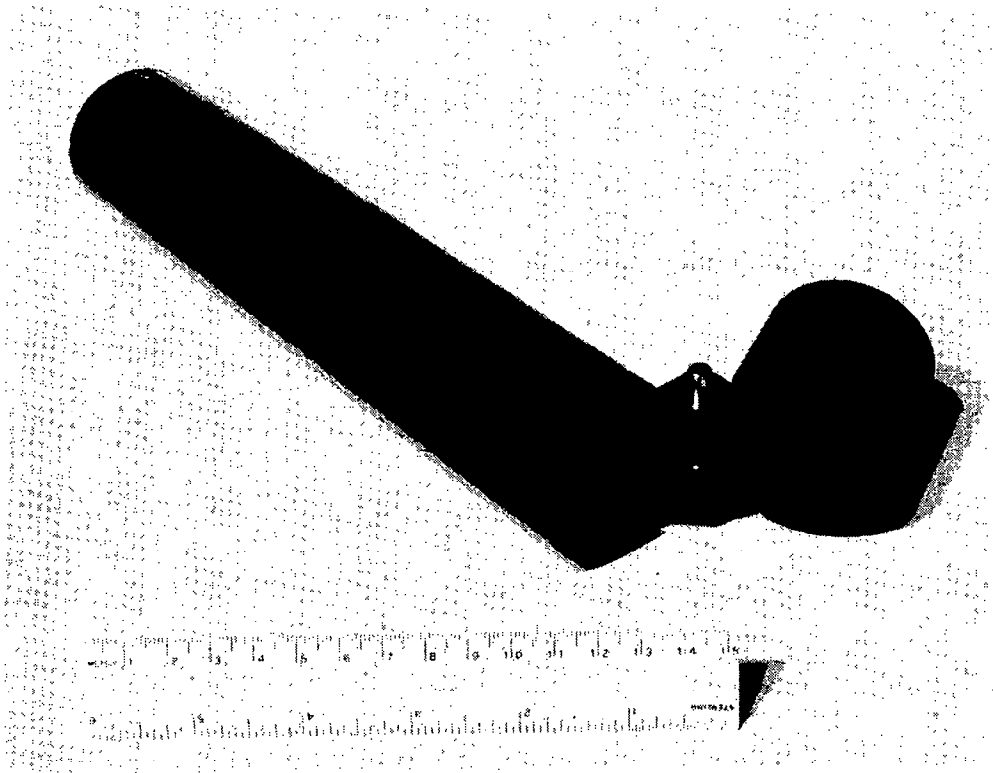

Figure 11

MIDLINK HINGE AND DEPLOYMENT LINKAGE TORQUE PROFILE

Figure 12 summarizes the design features of the midlink hinge and presents a curve showing the mechanical advantage of the midlink hinge drive spring torque.
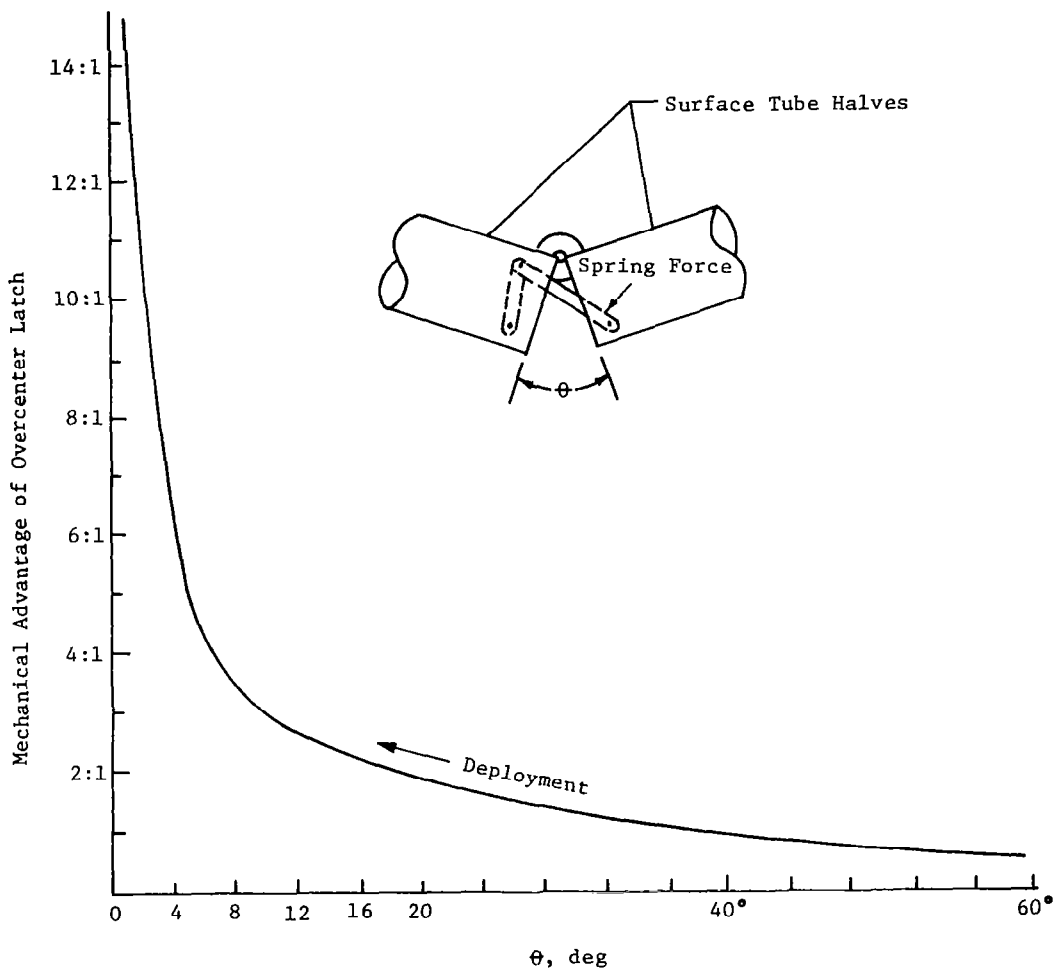

Figure 12

HALF-SCALE MODEL HARDWARE DEVELOPMENT

The next logical step in box truss development is to build a self-deployable scale model that demonstrates the features of step-by-step orthogonal deployment. The prototype model will also demonstrate:

    1) deployed stiffness

    2) repeatability of deployment

    3) multicube manufacturing processes

    4) manufacturing precision

    5) precision requirements for tooling

    6) reflector surface integration

    7) truss antenna performance

Figure 13 describes the activities that have been completed this year and the schedule for completing the prototype model.

o HALF-SCALE MODEL OF MSDA IN PROGRESS

    - DESIGN COMPLETED
    - PIECE PART PROCUREMENT STARTED
    - HARDWARE DESIGN IS FLIGHT-LIKE BUT GFRP REPLACED WITH METALLIC
    - REFLECTOR AND FEED MAST STRUCTURES COMPLETE JUNE 1983
    - DEPLOYMENT AND DYNAMIC TESTING COMPLETE OCT 1983
    - MESH REFLECTOR FABRICATION AND INTEGRATION COMPLETE MARCH 1984

o OBJECTIVE OF TEST HARDWARE

    - DEMONSTRATE ORTHOGONAL-SEQUENTIAL DEPLOYMENT
    - DEMONSTRATE TRUSS ASSEMBLY ACCURACY
    - VALIDATE DEPLOYMENT ANALYSIS (RATE, ACCELERATIONS, AND LOADS)
    - DEMONSTRATE FIXTURING AND TOOLING DESIGN
    - DEMONSTRATE MESH FABRICATION AND INTEGRATION
    - DEMONSTRATE INTEGRATED OFFSET FEED MAST

Figure 13

The illustration shown in figure 14 is of a half-scale model prototype of the 15-meter-dia. mechanically scanned deployable antenna (MSDA). MSDA was designed using the deployable box truss structure to form the parabolic dish and feed mast.

A unique deployable feed mast has been developed for the offset feed space-deployable antenna. The novel feature of this design is that it uses an extension of the reflector truss structure rather than adding appendages. The design features efficient stowage, simple integration to the reflector structure, excellent thermal stability, light weight, and very high stiffness and dynamic stability. These features are achieved by using the efficiency and features of a deep truss structure. Previous offset feed masts were appendages added to the reflector structure and had less efficient packaging, more difficult integration, and substantially lower dynamic stability. Because of the high strength and stiffness, this mast can easily accommodate the more complicated and massive advanced feeds (e.g., line feeds, array feeds, and multifrequency multibeam feeds).

To reduce manufacturing costs, the half-scale model was designed using aluminum for the majority of parts. The full-scale flight article would use graphite composites, but the stiffness and thermal stability of graphite were not required for a kinematic representative system. Also, aluminum is readily available and will not degrade the validity of the test model.

29-FT INTEGRATED OFFSET FEED MAST

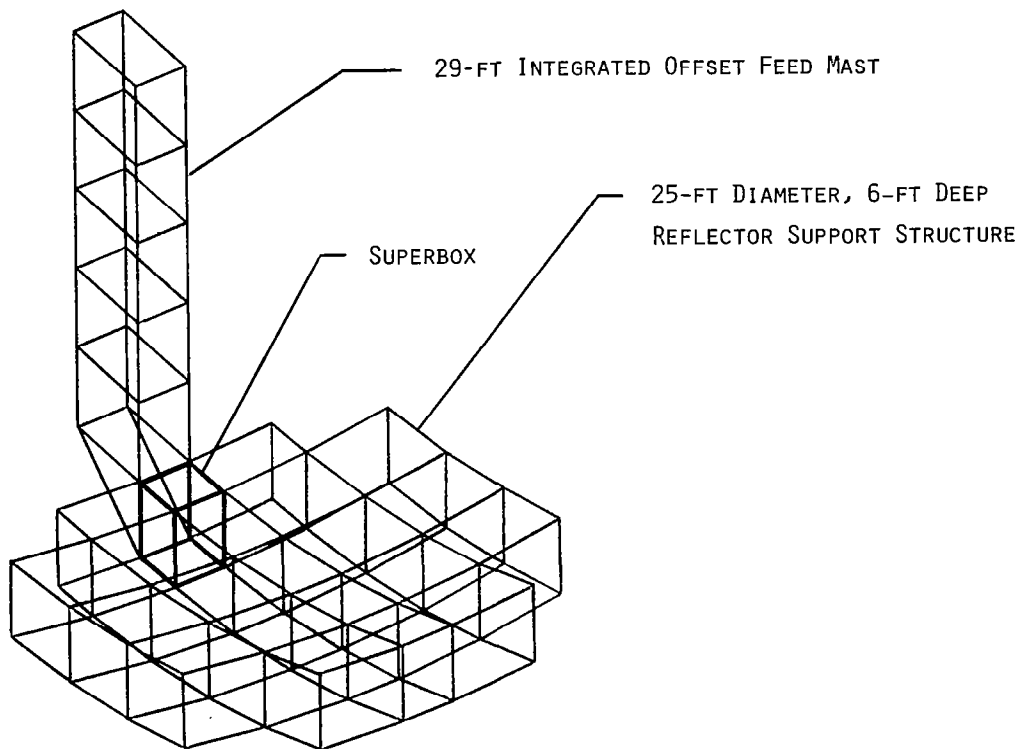25-FT DIAMETER, 6-FT DEEP REFLECTOR SUPPORT STRUCTURE

SUPERBOX

Figure 14

STOWED MSDA ANTENNA

The MSDA stowed configuration is shown in figure 15. All of the structural members compactly stow about the superbox, and this allows the antenna to easily meet the stowage requirement. In the stowed condition, the cube corner fittings butt against each other to form a plane at the top and bottom surfaces. The plane formed by the cube corner fittings provides a load path for loads incurred during launch with inplane shearing loads handled by interlocking pins between the fittings.

The dynamic characteristics of the MSDA in the stowed configuration were analyzed with the NASA Structural Analysis (NASTRAN) Finite Element Program. The model was conservative in the sense that it only contained the superbox stiffness with the rest of the masses lumped at the model's eight nodes. The first fundamental frequency obtained was 17.2 Hz, but this number is extremely conservative considering that the model did not take into account the stiffness added by the members being pinned and supported together during stowage. An additional restraint ring would readily permit attainment of the 25-Hz requirement.
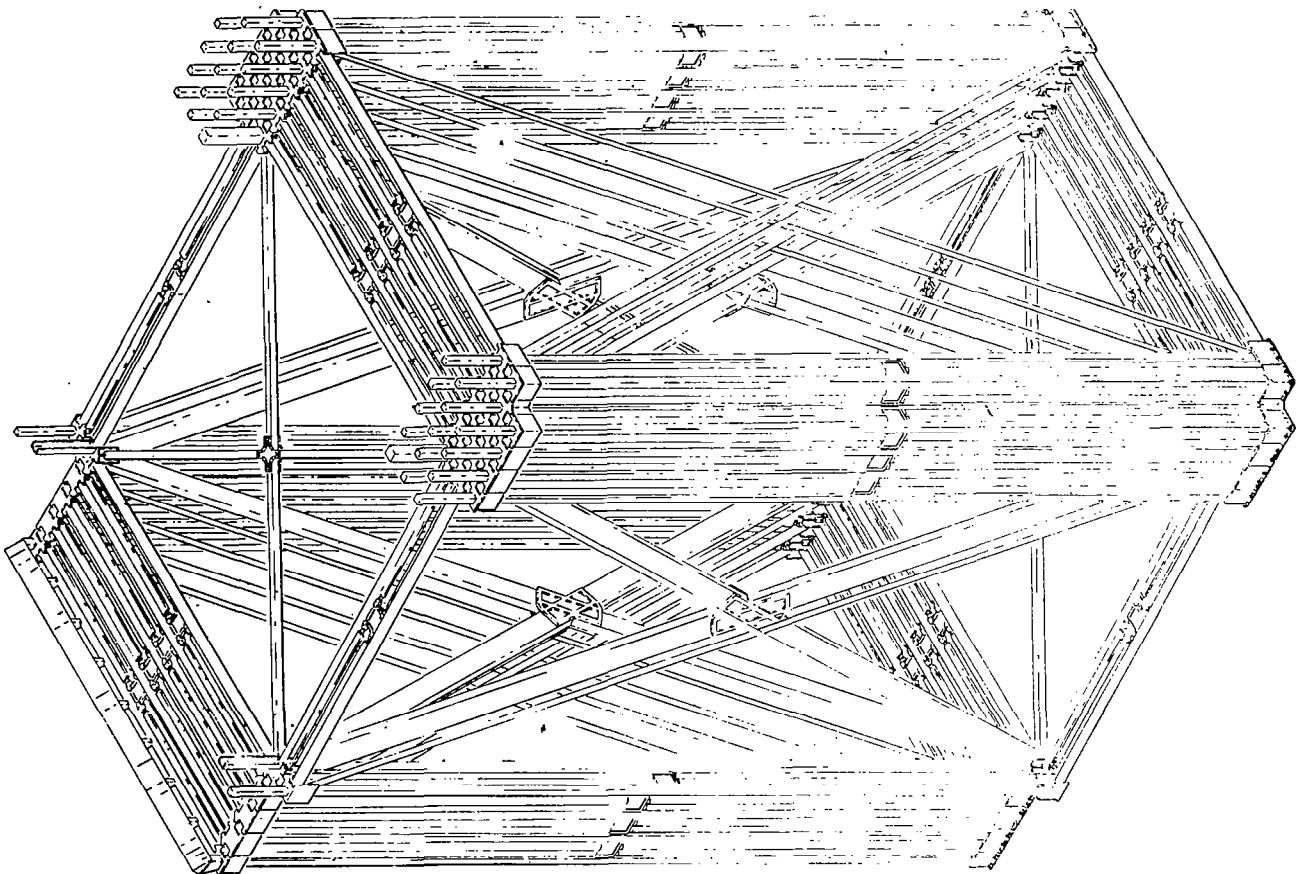

Figure 15

NEXT LOGICAL STEP PAST HALF-SCALE MSDA MODEL

Design has started on a 100-meter deployable box truss mast. The use of a deployable mast from the STS payload bay provides the LSS community with the opportunity to study truss deployment and dynamic behavior (i.e., with joints unloaded). Figure 16 summarizes the requirements and approach we have used to determine the design requirements of the 100-meter mast.

SPACE DEMONSTRATION OF DEPLOYABLE TRUSS STRUCTURE

O REQUIREMENTS:
- DEMONSTRATE COMPONENT DESIGN AND PERFORMANCE
- DEMONSTRATE LINEAR TRUSS DESIGN AND PERFORMANCE
- DEMONSTRATE AREA TRUSS DESIGN AND PERFORMANCE
- DEMONSTRATE DEPLOYMENT AND VALIDATE PERFORMANCE ANALYSIS
- CORRELATE GROUND TEST AND ANALYSIS WITH SPACE TEST
    -- DAMPING
    -- STIFFNESS
    -- DEPLOYMENT RATES, ACCELERATIONS, LOADS
    -- THERMAL RESPONSE
    -- NONLINEARITIES
- RELATIVELY LOW COST EXPERIMENTS
- DEMONSTRATE REFLECTOR AND ARRAY SURFACE INTEGRATION
- DEMONSTRATE SUBSYSTEM AND UTILITY INTEGRATION

O APPROACH: "KILL TWO BIRDS WITH ONE MAST"
- PERFORM LINEAR BEAM EXPERIMENT, BUT USE LINEAR TRUSS APPLICABLE TO AREA STRUCTURES (NOT JUST A LATTICE MAST)
- MAST DEPLOYMENT SHOULD SIMULATE/DEMONSTRATE AREA DEPLOYMENT
- START WITH SIMPLE MAST THAT IS EASILY MODIFIABLE FOR A SEQUENCE OF FLIGHT EXPERIMENTS
- EVOLUTIONARY/REUSABLE MAST EXPERIMENT TO EVENTUALLY DEMONSTRATE 2-DIMENSIONAL AND 3-DIMENSIONAL STRUCTURES, AND SURFACE, SUBSYSTEM, AND UTILITY INTEGRATION

Figure 16

INFLATED ANTENNAS

G. J. Friese and M. Thomas
L'Garde, Inc.
Newport Beach, California

W. F. Hinson
NASA Langley Research Center
Hampton, Virginia

INFLATABLE STRUCTURE HISTORY

The purpose of Figure 1 is to present a general picture of the timespan for basic research, development, and application conducted on inflatable devices for aerospace projects by NASA and industry. The figure shows an extensive amount of work between the late fifties and the early seventies on several innovative structural systems. A cross section of the documentation of the work is presented in references 1 to 13. Applications were in the field of determining atmospheric density, communications, and geodetic measurements. A one-man inflatoplane was built and flight tested.

The latest projects using inflatable technology conducted by NASA in the seventies were a blanket (solar shield) for Skylab and a 3.66-meter-diameter balloon for upper atmospheric density research. The blanket was approximately 2 mils thick and 6.09 meters square and was made from one layer of polyester covered on both sides with a layer of aluminum foil. Inflatable tubes were attached to the upper and lower surfaces of the flat sheet for erection.

The 3.66-meter orbital balloon differed from previous balloon designs in that the surface of the balloon had one percent surface area perforations. A 5-ply laminate, 2 layers of polyester and 3 layers of aluminum foil, was used to construct the balloon. Inflation was by staged mass flow rates of compressed nitrogen gas.

Some inflated reflector antenna work was conducted by NASA in the late fifties and since that time other projects have been considered by industry, including a cone-paraboloid concept by L'Garde in 1982.
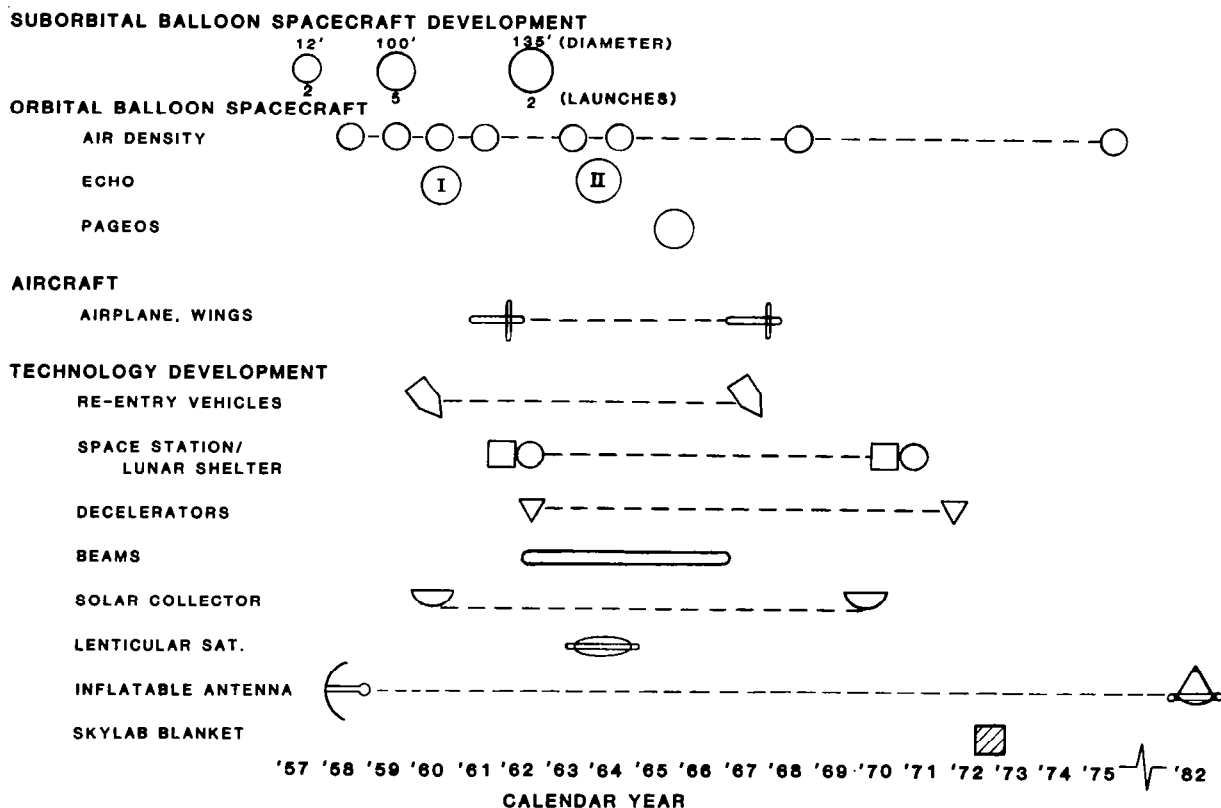

Figure 1

INFLATABLE ANTENNA SYSTEM
(NASA LaRC, 1958)

The purpose of this antenna system was to investigate fabrication techniques in establishing procedures for forming, cutting, sealing, and handling; to evaluate manufacturing procedures by constructing models using flat surfaces or curved mandrels and molds; and to determine number of gores, thickness, and type of laminated materials.

The reflector shown in Figure 2 was approximately 3.66 meters in diameter and was constructed using a polyester and aluminum foil laminate approximately 2 mils thick. The front surface material was 1/2 mil thick plain polyester. Pressure in the antenna and torus was approximately 689 Pa.
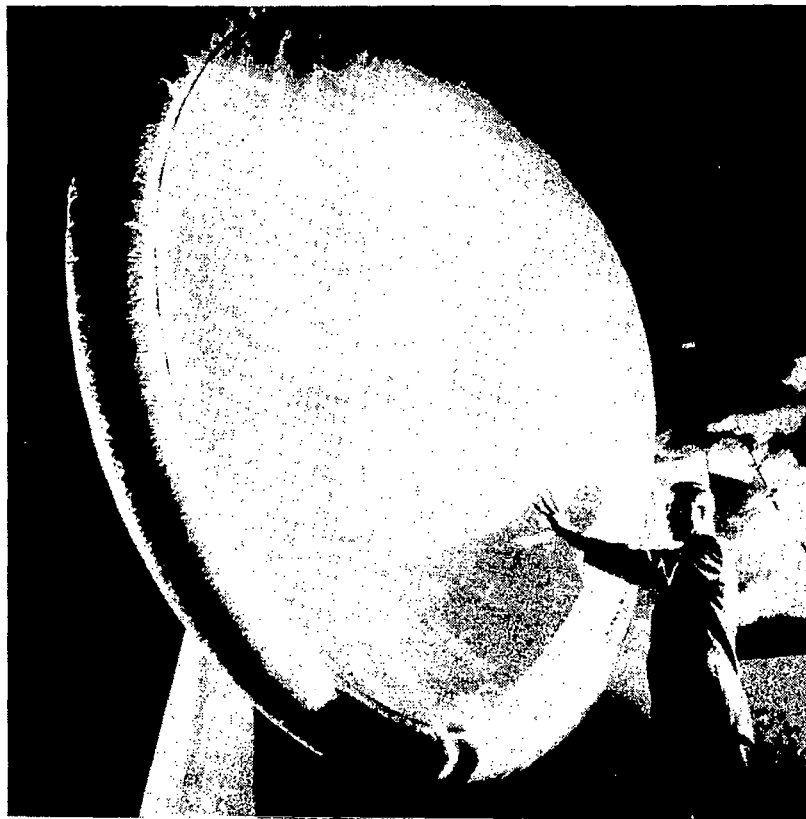

Figure 2

INFLATABLE ANTENNA SYSTEM
(BIRDAIR, 1963)

This antenna system is discussed in detail in reference 13. In general the antenna when inflated measured approximately 3 meters in diameter and could be packaged in a container 25.4 by 25.4 by 17.8 cm. Weight was approximately 3.6 kg. The antenna structure was measured to be within a tolerance of 1.58 mm. Material used was a polyester and aluminum foil laminate (1 mil thick) for the reflector and plain polyester (1/2 mil thick) for the front surface. Inflation was by compressed nitrogen gas at a pressure of 2482 Pa. (See Figure 3.)
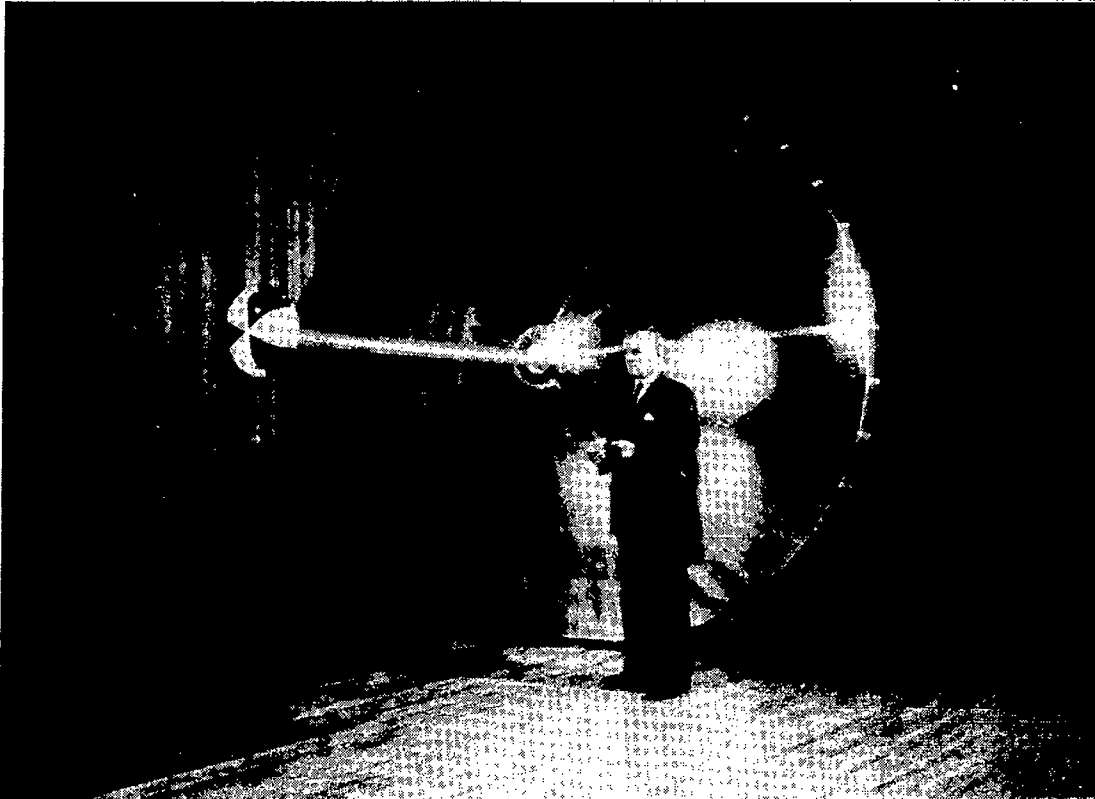

Figure 3

ANTENNA CONFIGURATION

The current antenna configuration, shown in Figure 4(a), consists of a thin film cone and paraboloid held to the proper shape by internal pressure and a self-rigidizing torus. The cone and paraboloid are made from tailored, pie-shaped gores. The paraboloid is coated with vapor deposited aluminum (VDA) to provide reflectivity. The self-rigidizing torus is made of an aluminum-polyester-aluminum composite that, when inflated, erects to a smooth aluminum shell that can take loads without internal pressure. The feed would normally be located at the cone apex. Most other hardware, such as electronics, pressure control, attitude control and power supply, would be located on or in the torus.
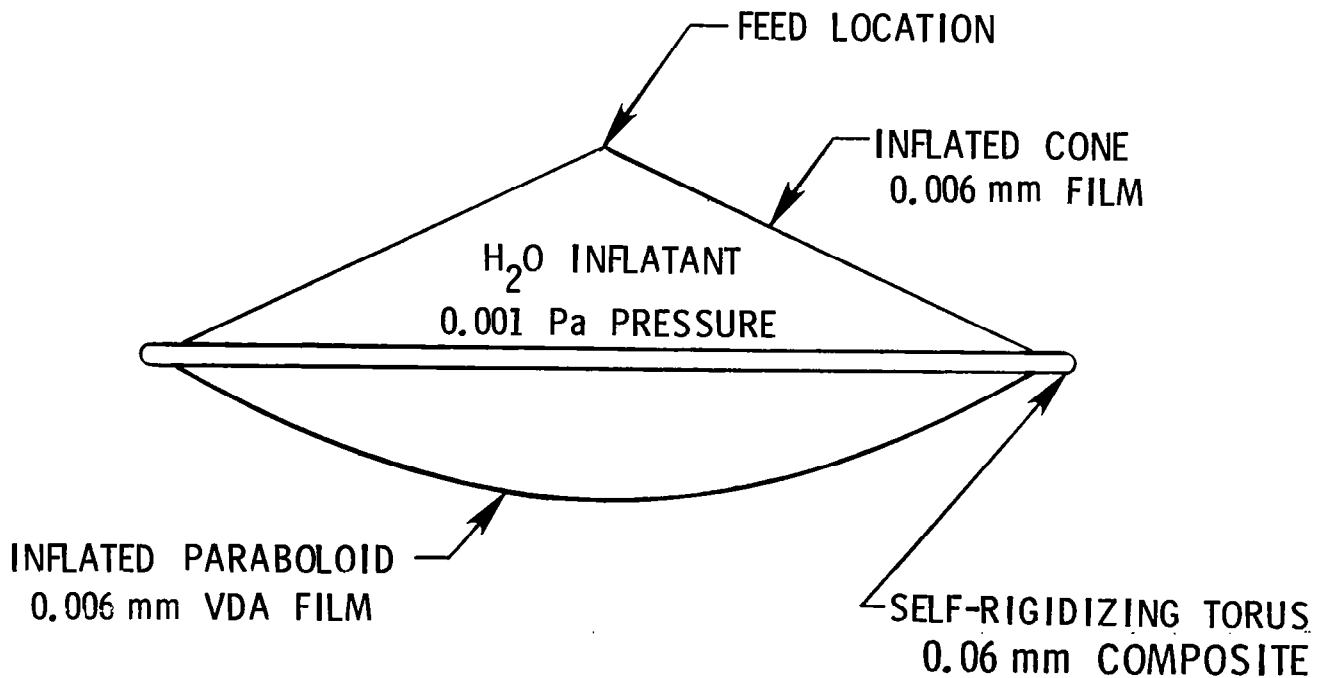
FEED LOCATION

INFLATED CONE
0.006 mm FILM

H_2O INFLATANT
0.001 Pa PRESSURE

INFLATED PARABOLOID
0.006 mm VDA FILM

SELF-RIGIDIZING TORUS
0.06 mm COMPOSITE

Figure 4(a)

INFLATABLE ANTENNA CONCEPT

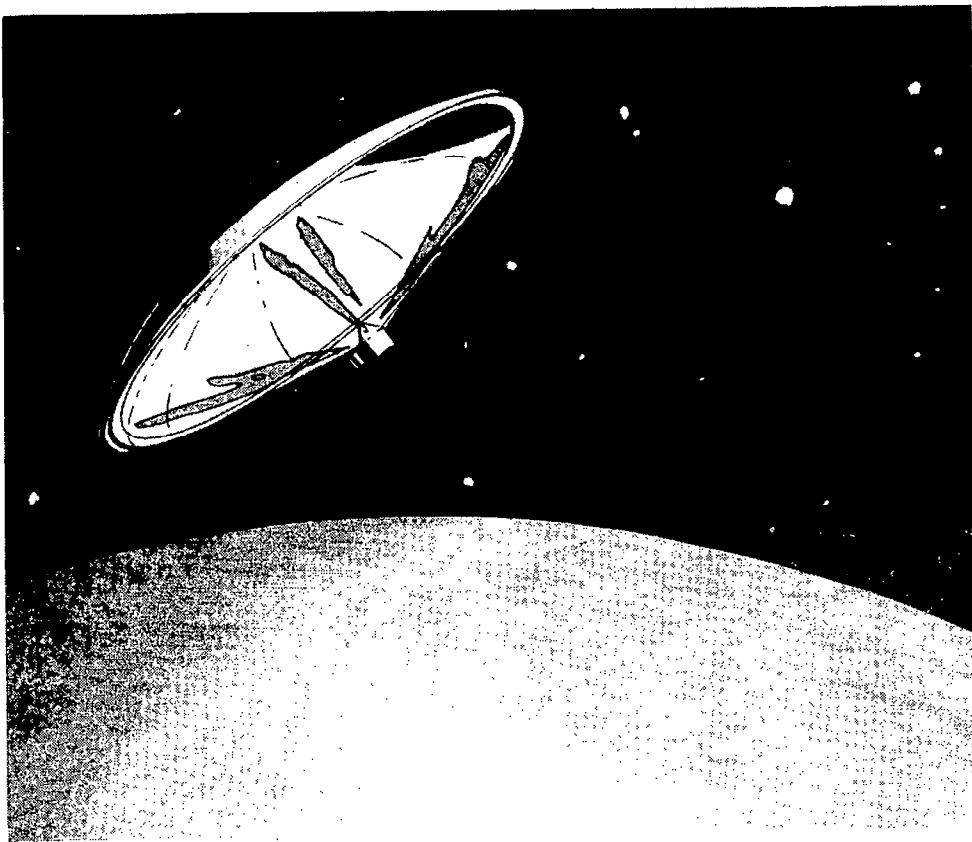Figure 4(b) is an artist's concept of the inflatable antenna configuration discussed herein.

Figure 4(b)

CURRENT APPROACH

The thin film antenna concept just described had not been considered practical a decade ago primarily because of thermal distortions and meteoroid damage. Thermal distortions are minimized by reduced temperature differentials. For instance, use of commercially available dyed polyester for the cone and paraboloid resulted in a maximum differential temperature on the paraboloid of only 30 K (calculated) for the worst solar angle, which would typically cause a gain loss < 1 dB at 10 GHz. Development of custom films for antennas can provide smaller differentials.

The antenna will be punctured by meteoroids during its life. The weight of the replacement gas (W) is proportional to the parameters on Figure 5 where M is the molecular weight of the gas, P is the internal pressure, A is the antenna projected area, and t is time. Replacement gas weight is reduced to an acceptable level by operating at a very low 0.001 Pa pressure -- about 100 times the solar pressure. Water (passive) or the product of hydrazine decomposition (active) is the recommended inflatant, being lowest in molecular weight and inert. For very large antennas, the replacement gas for a 10-year lifetime is only a few percent of the total system weight.

● TAILORED PIE-SHAPED GORES

● TREATED POLYESTER OR POLYIMIDE

       DYED POLYESTER → 30K MAX ΔT

             → SOLAR PROTECTION

● SELF-RIGIDIZING TORUS

● FULLY INFLATED (EXCEPT TORUS) FOR 10 + YEAR LIFE

       WATER (MW = 18)

       HYDRAZINE → $2H_2 + N_2$ (AVERAGE MW = 10.7)

● REPLACEMENT GAS FOR METEOROID HOLES

$$W \ \alpha \ \sqrt{M} \, P \, A \, t^2$$

Figure 5

PROGRAM MAJOR TASKS

NASA Langley funded L'Garde to do development work on inflated antennas. The major areas are listed in Figure 6 and are the subjects for the remainder of this paper.

- PARABOLOID FABRICATION AND TEST

- SELF-RIGIDIZING STRUCTURE FABRICATION AND TEST

- WEIGHT AND PACKAGE VOLUME CALCULATIONS

Figure 6

INFLATED PARABOLOID

The paraboloid shown in Figure 7 is 3 meters in diameter, and was designed to have an f/D of one. It is made from 32 gores of 0.006 mm (¼ mil) VDA polyester. The gores were assembled with 19 mm wide tape made of 0.013 mm polyester and 0.013 mm heat sensitive adhesive. The paraboloid was accuracy tested at 2.5 mm H_2O (0.003 psi) pressure (near optimum) and then at twice that pressure.
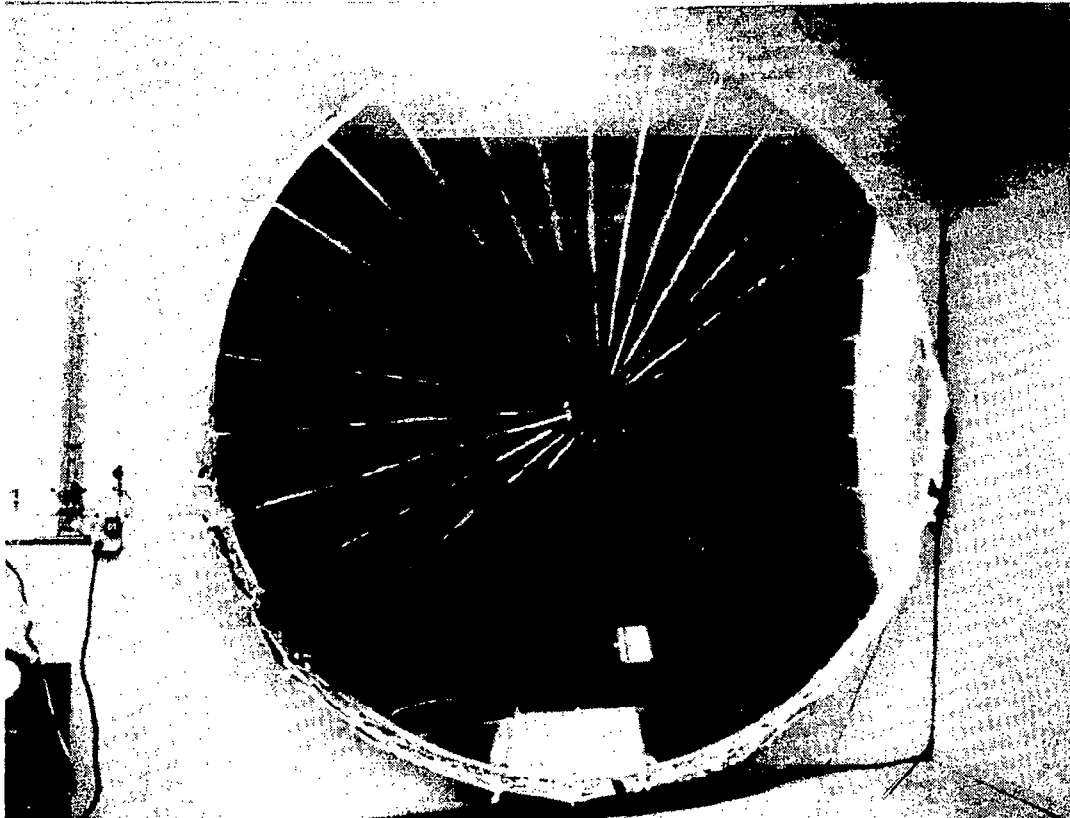

Figure 7

TEST SET-UP

The test set-up is shown in Figure 8. A laser on an optical bench was set up in front of the paraboloid. If the paraboloid were perfect and the laser were normal to the paraboloid axis, the laser's reflected light would always pass through the theoretical focus. The laser was moved horizontally across the paraboloid approximately 680 mm below the paraboloid axis. About every 30 mm, ΔX would be measured and recorded. The value of Z was calculated based on the laser location. The horizontal slope of the paraboloid at the point of measurement was then calculated using ΔX and Z.

TOP VIEW   SIDE VIEW

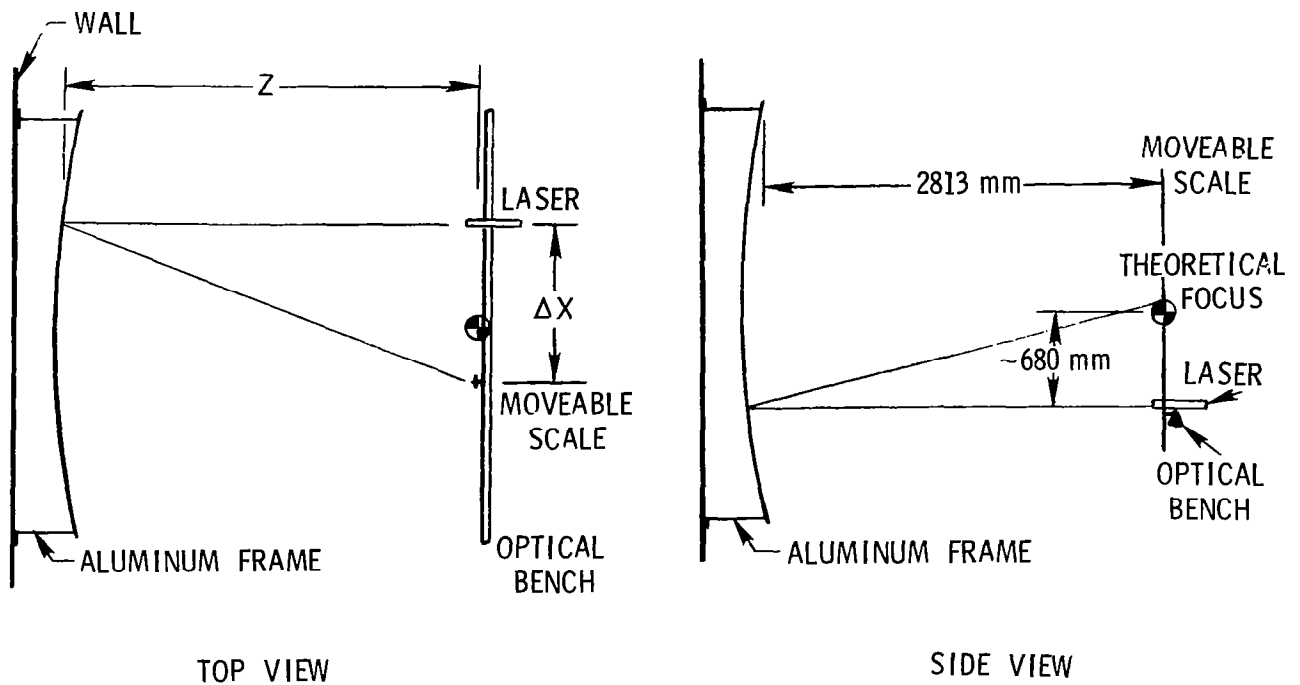Figure 8

SLOPES OF POLYESTER PARABOLOID

The reduced data are shown in Figure 9. The short, straight lines connect the test points from single gores; that the points form a straight, sloping line show that the flat gore has been strained to a parabolic curvature by the pressure. The curve fit is for a perfect paraboloid, and shows that the focal length was 2.96 meters rather than 3.0 meters as designed.
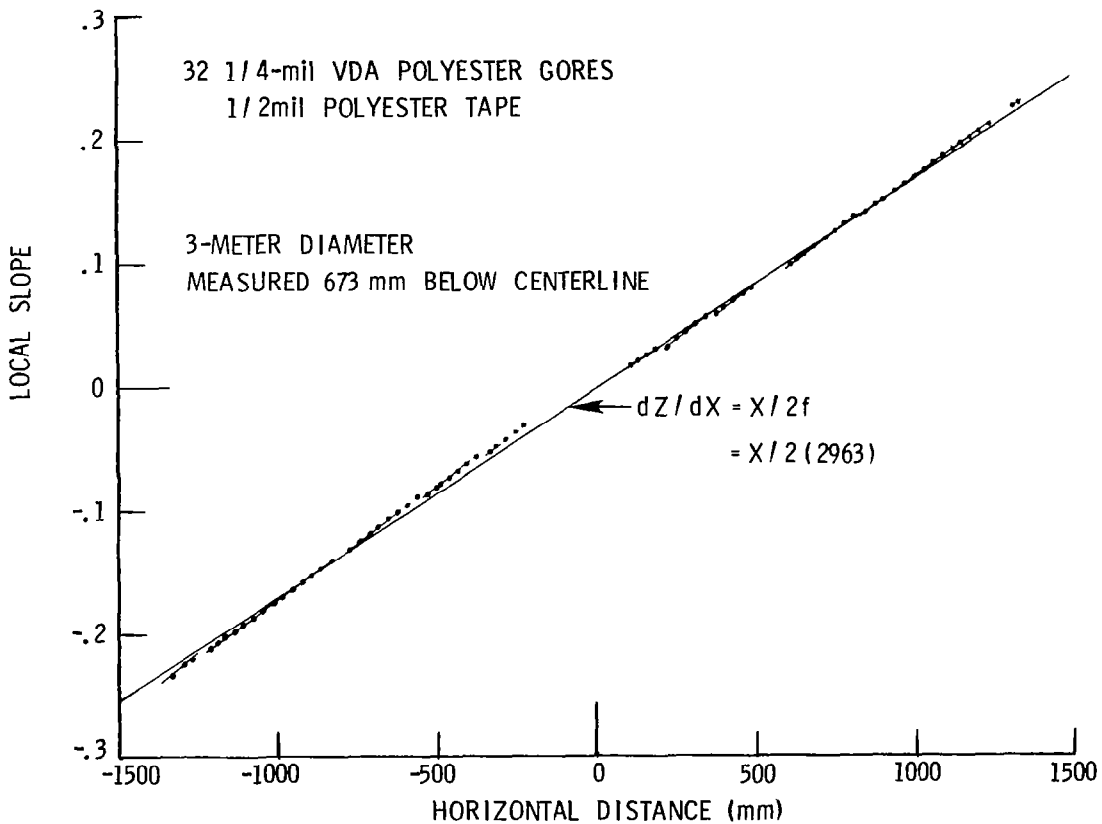
32 1/4-mil VDA POLYESTER GORES
1/2mil POLYESTER TAPE

3-METER DIAMETER
MEASURED 673 mm BELOW CENTERLINE

$dZ/dX = X/2f$

$= X/2(2963)$

LOCAL SLOPE

HORIZONTAL DISTANCE (mm)

Figure 9

CROSS SECTION OF POLYESTER PARABOLOID

The data from Figure 9 were numerically integrated from the rim inward to produce Figure 10. A parabolic curve fit was calculated for the points, and the data points were subtracted from the curve fit to determine the paraboloid accuracy. The inaccuracy was only 0.76 mm rms. This was the first paraboloid that L'Garde built and measured for accuracy.

32 1/4-mil VDA POLYESTER GORES   3 METER DIAMETER
1/2-mil POLYESTER TAPE   MEASURED 673 mm BELOW CENTERLINE

$$Z = \frac{X^2 + Y^2 - (D/2)^2}{4f}$$

$$= \frac{X^2 + (673)^2 - (1500)^2}{4(2963)}$$
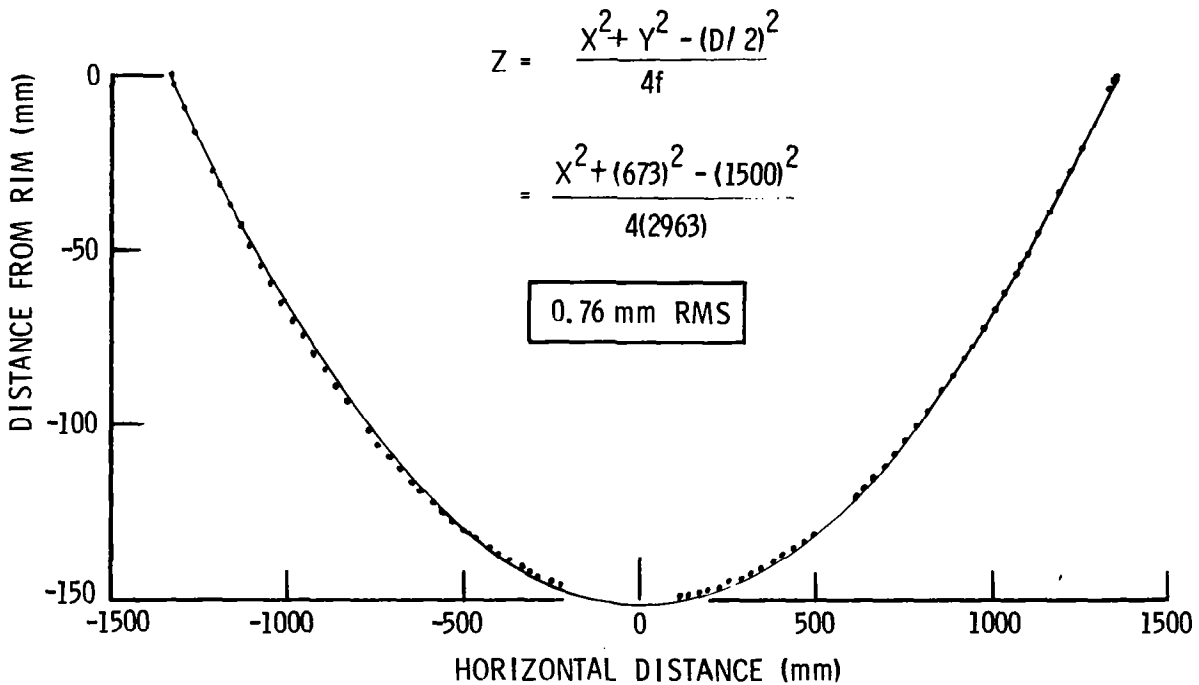
$$\boxed{0.76 \text{ mm RMS}}$$

Figure 10

556

INACCURACY OF POLYESTER PARABOLOID

Figure 11 shows the actual deviations of the data points from the curve fit. All points are within 1½ mm of desired.

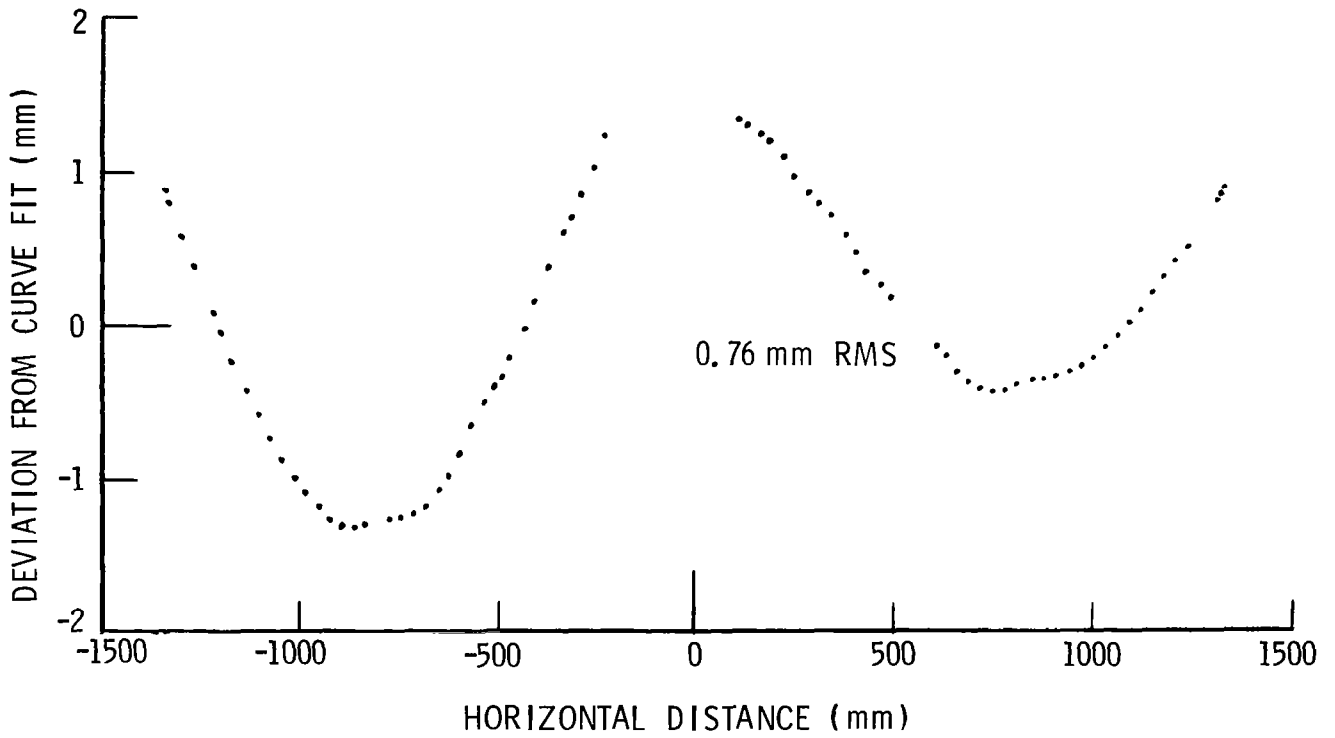
Figure 11

PARABOLOID TEST RESULTS

The polyester paraboloid was also tested at a pressure of 5 mm of water (Figure 12). This overpressurization resulted in a slightly larger inaccuracy (0.94 mm rms) and a shorter focal length (2.82 meters).

For large antennas, the paraboloid can and will be designed for orders of magnitude lower pressure to operate with a low film stress. The pressure just holds the film in place. The paraboloid then is less sensitive to pressure changes (according to calculations).

MEASURED PRESSURE (mm H$_2$O)	CALCULATED FILM STRESS (MPa)	INACCURACY (mm RMS)	FOCAL LENGTH (m)
2.5	13.0	0.76	2.96
5.0	26.0	0.94	2.82

Figure 12

SELF-RIGIDIZING STRUCTURE

The composite was made by bonding aluminum foil to 0.013 mm polyester film (Figure 13). The polyester provides tear resistance and a gas seal. Three different composites were made from three thicknesses of aluminum foil:

Aluminum Thickness (mm)	Total Thickness (mm)
0.050	0.113
0.076	0.139
0.102	0.156

In production, the total adhesive thickness would only be about 0.006 mm thick instead of 0.050 mm.

Structures such as cylinders and tori can be made from such composites and packaged. Gas pressure erects the structure, and removes packaging wrinkles from the aluminum. The gas is no longer needed since the remaining aluminum shell can take loads.

1100-0 ALUMINUM FOIL

0.025 mm
0.038 mm
0.051 mm

POLYESTER FILM
0.013 mm

HEAT ACTIVATED ADHESIVE
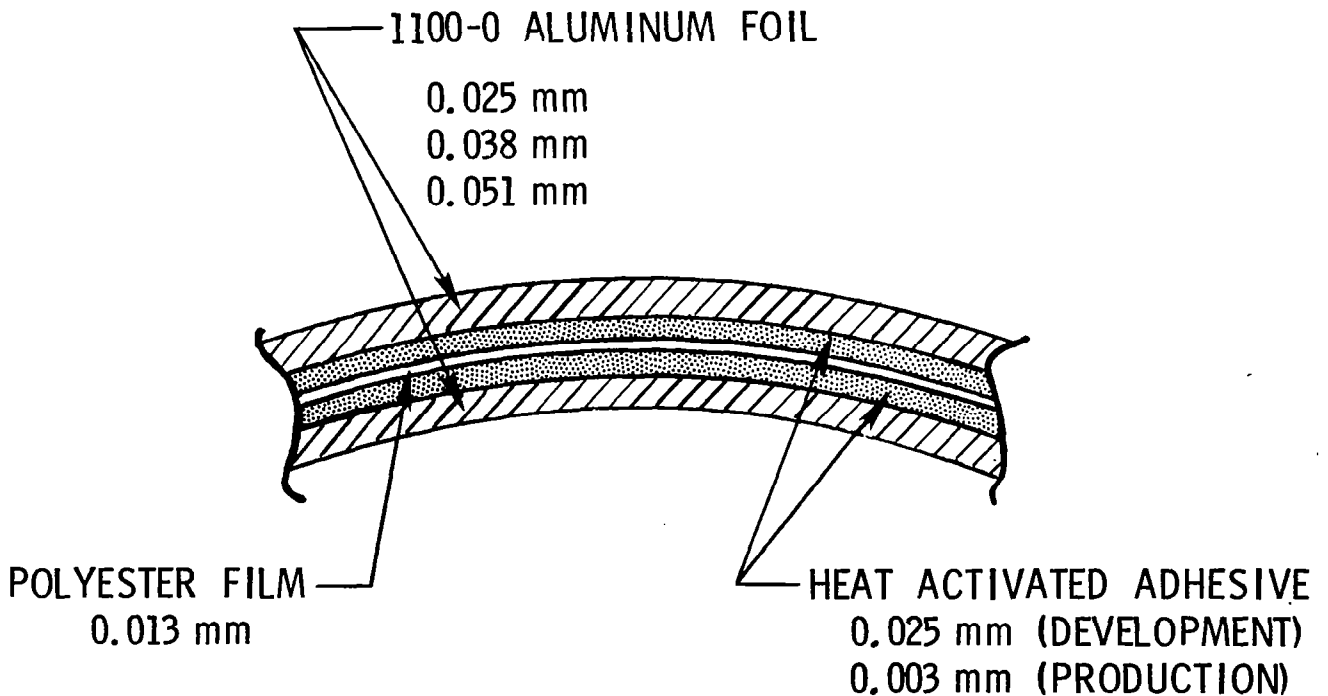0.025 mm (DEVELOPMENT)
0.003 mm (PRODUCTION)

Figure 13

STRESS-STRAIN

The stress-strain curves for the aluminum foil and polyester are shown in Figure 14. The shell is pressurized such that the aluminum is stressed into its plastic region. The packaging wrinkles are thus permanently removed, and the composite can then resist loads without internal pressure. The polyester is elastic at these stresses, so when the pressure is removed, the aluminum is under compression. This pre-compression reduces the allowable buckling load of the shell, and therefore must be minimized by (a) having a high aluminum to polyester thickness ratio, and (b) stressing the aluminum as little as possible beyond its elastic limit.
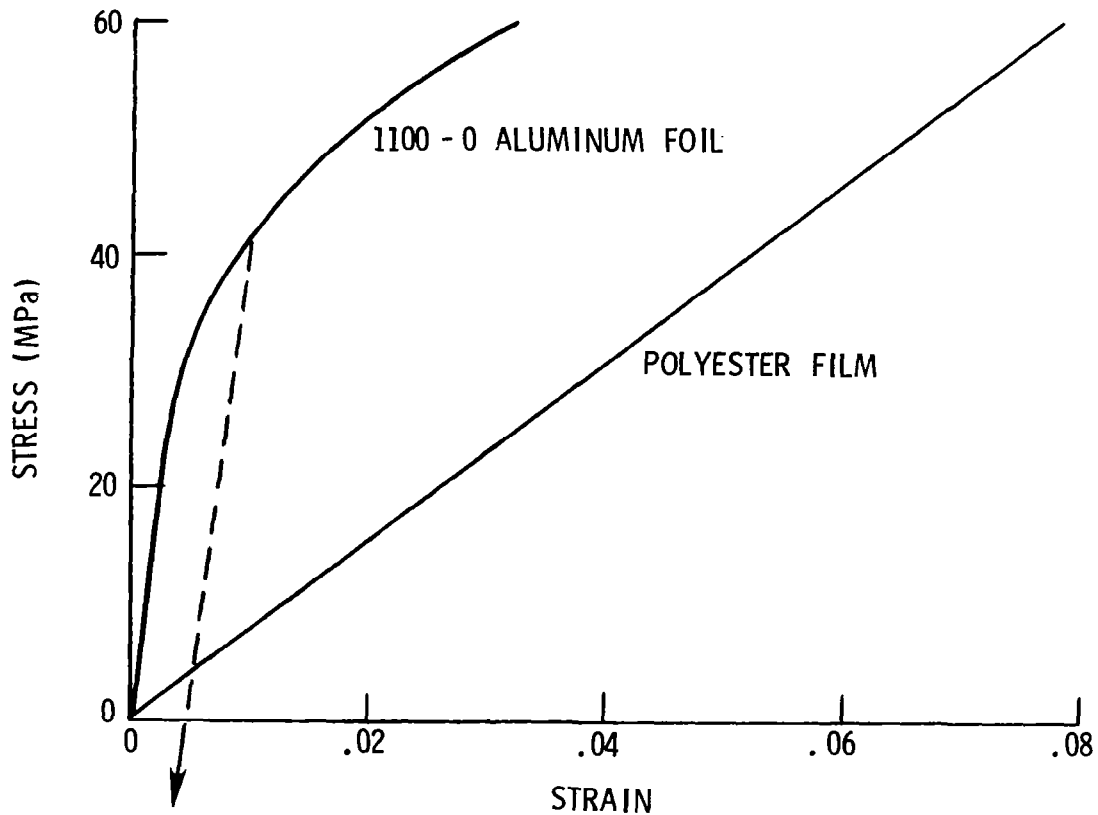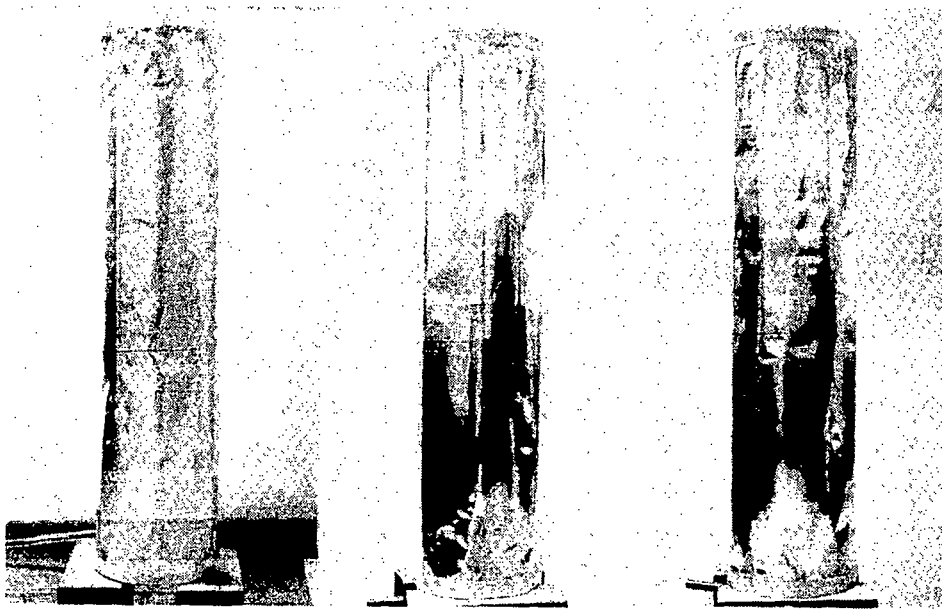
Figure 14

AS-BUILT CYLINDERS

Seven cylinders, 102 mm in diameter by 460 mm long, were built for compression testing. Three of these are shown in Figure 15. Each had two longitudinal seams, and end caps made of rigid plastic.
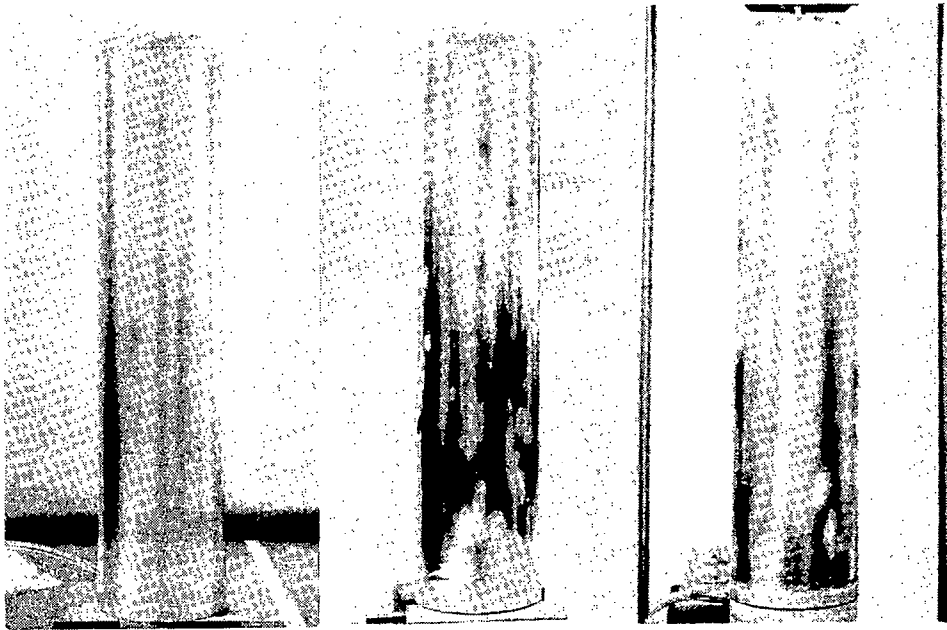

| Thickness of aluminum = 0.050 mm | Thickness of aluminum = 0.076 mm | Thickness of aluminum = 0.102 mm |

Figure 15

POST-PRESSURIZED TEST CYLINDERS

Figure 16 shows three of the cylinders after they were pressurized and deflated. These had been pressurized such that the aluminum was stressed just above the proportional limit. Some wrinkles can still be seen, indicating that perhaps a higher pressure would be beneficial.

Thickness of aluminum = 0.050 mm

Thickness of aluminum = 0.076 mm

Thickness of aluminum = 0.102 mm

Figure 16

CYLINDER LOADING METHODS

   Two cylinders were loaded by weights as shown on the left in Figure 17. However, it appeared that bending moments were being generated so the remaining cylinders were tested in the tester shown on the right.
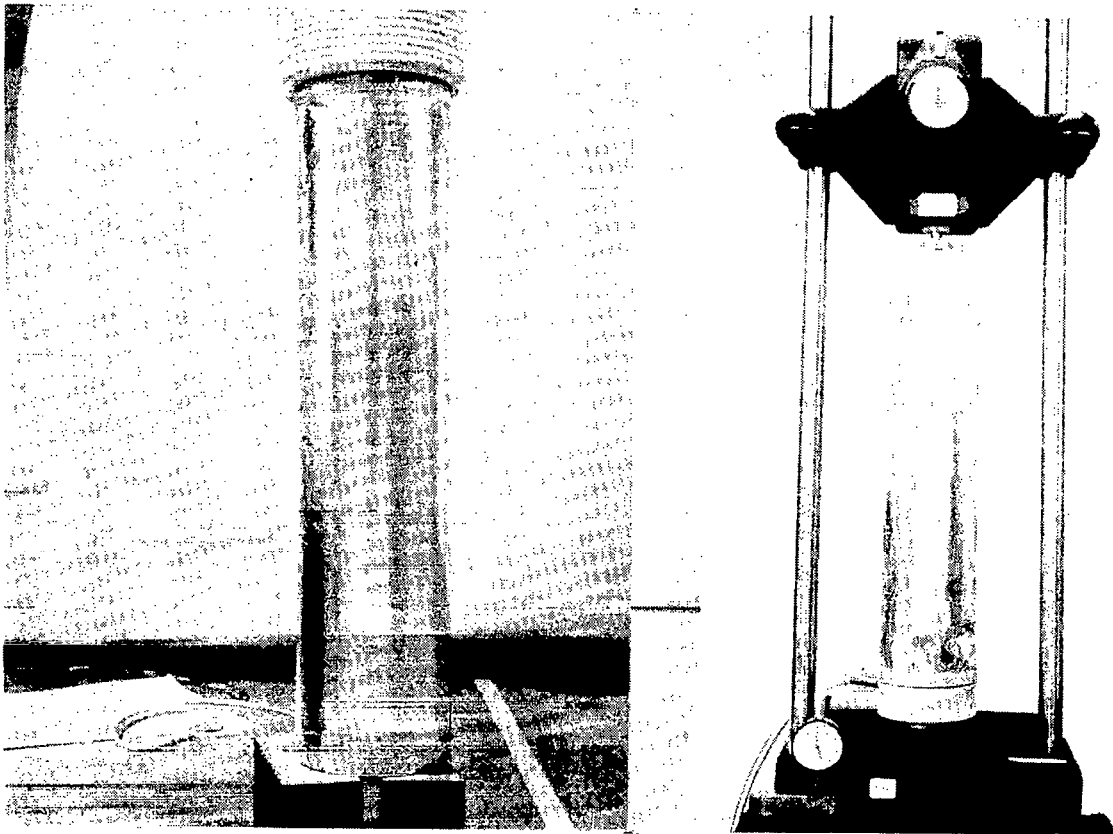

Figure 17

BUCKLING OF CYLINDERS (0.050 mm)

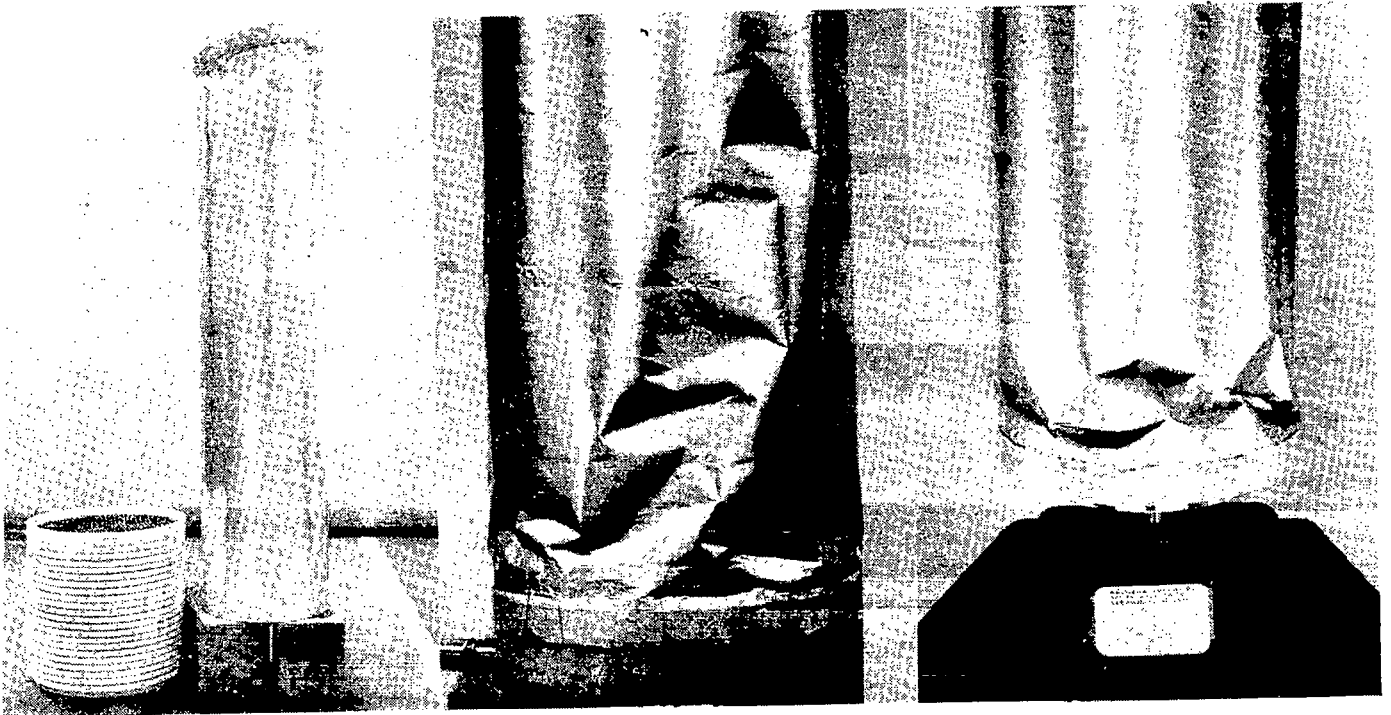All of the 0.050 mm cylinders (Figure 18) buckled near the ends.

Figure 18

BUCKLING OF CYLINDERS (0.076 mm)

The cylinder on the left in Figure 19 buckled in a manner suggesting an applied bending moment. The other two cylinders buckled at the ends.
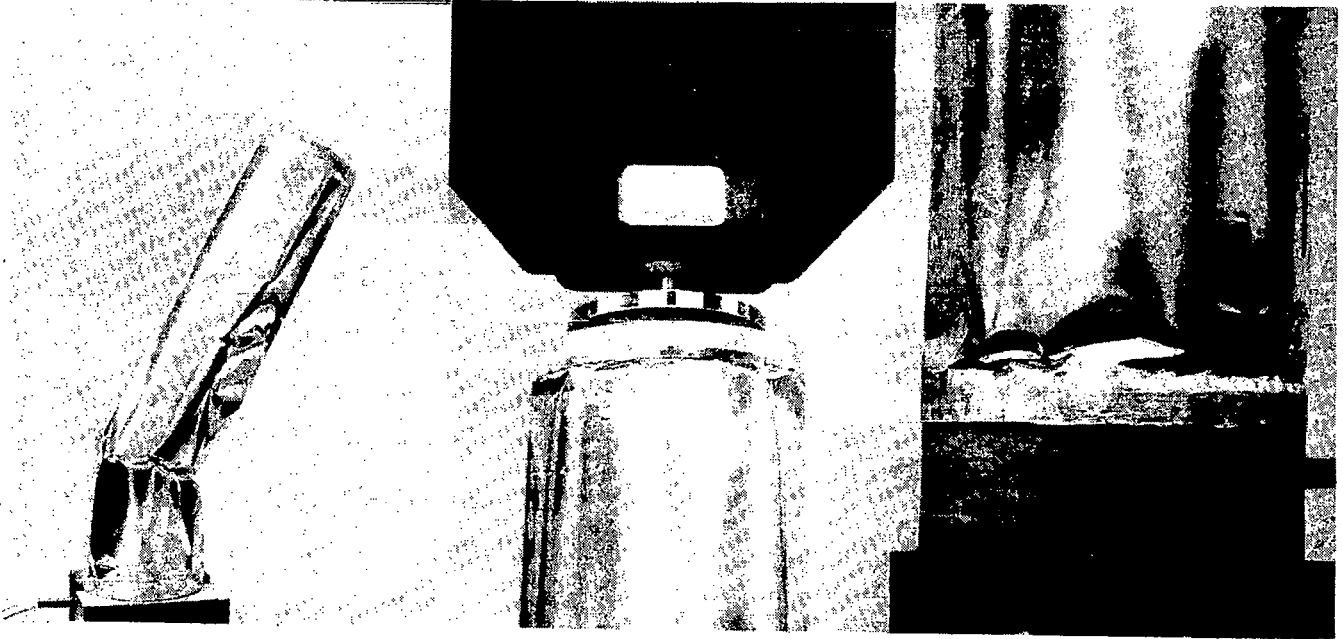

Figure 19

BUCKLING OF CYLINDER (0.102 mm)

The 0.102 mm thick cylinder (Figure 20) buckled near the center. Note the classical buckling diamonds in this photo and some of the previous photos.

Figure 20

CRITICAL COMPRESSIVE FORCE

The critical buckling force is calculated from

(a) classical buckling theory

(b) less the pre-compression stress produced by the polyester

(c) plus the strength produced by the multilayer design

Since the aluminum was stressed just beyond its elastic limit, pre-compression was near zero. The strength increase due to the multilayer composite was also small. Therefore, the buckling strength should follow the equation in Figure 21 where P_{cr} is the critical buckling load, E_a and t_a are the aluminum elastic modulus and thickness, and C is an empirical buckling coefficient used to account for manufacturing imperfections. A relationship published by NASA for conventional cylinders was used (reference 14).

$$P_{cr} \ \alpha \ C \ E_a t_a^2$$

$$C = 1 - 0.901 \left[1 - \exp\left(-\sqrt{r/256t}\right) \right]$$

$$= .22 \text{ for } t = 0.050 \text{ mm}$$

$$= .28 \text{ for } t = 0.076 \text{ mm}$$

$$= .32 \text{ for } t = 0.102 \text{ mm}$$

Figure 21

BUCKLING STRENGTH

The test data are shown in Figure 22 with curves per the analysis just
described for three elastic moduli:

70000 MPa - typical aluminum
17000 MPa - curve fit of the cylinder test data
8300 MPa - test data for 0.025 mm aluminum foil

The aluminum foil modulus was measured at 8300 MPa. Even though this was verified
by a different machine and other personnel, it is suspect because the buckling co-
efficient would be greater than one for the cylinder test data. The cylinder test
data indicate that the foil elastic modulus is less than 70,000 MPa and/or the
empirical buckling coefficient is less than that predicted in Figure 21. It is im-
portant, however, that

   (a) the buckling compressive force is proportional to the
       square of the aluminum thickness

   (b) the cylinders had the strength needed for the antenna
       torus

Optimization of composite characteristics and initial pressurization level are
needed to achieve greater strength. This type of structure would be suitable for
many applications in space because of its high strength to weight ratio and low
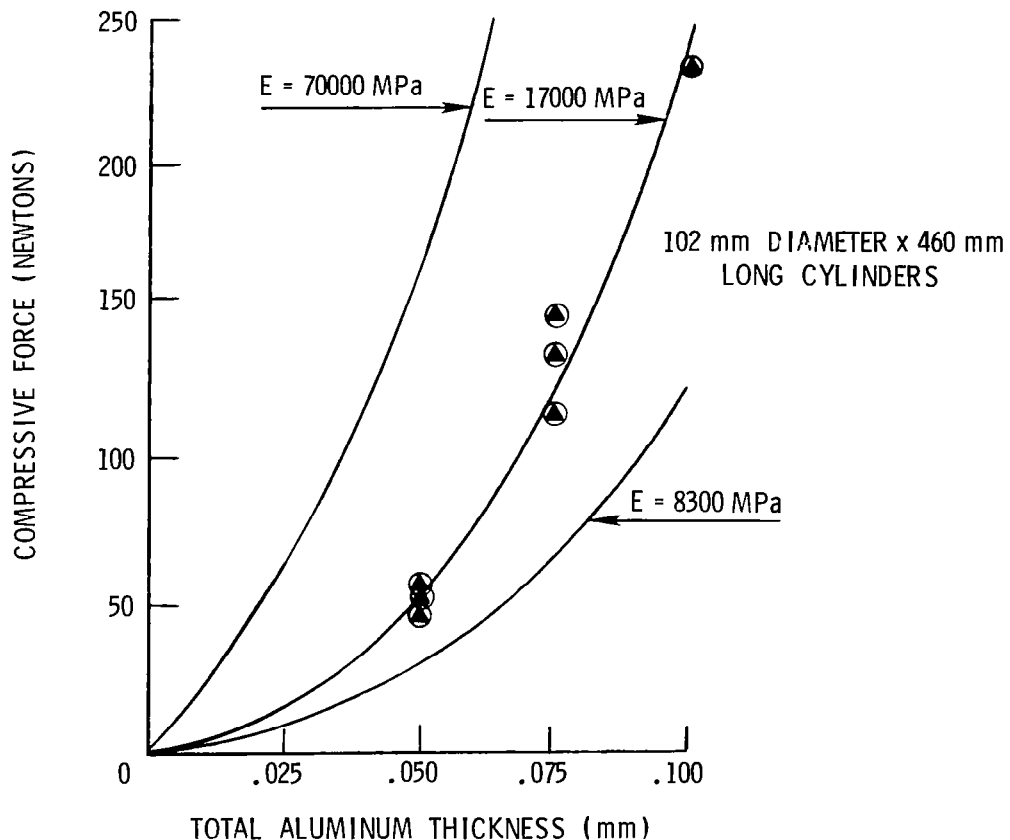package volume.

Figure 22

ANTENNA WEIGHT

The antenna total structure and inflation system weight is shown in Figure 23 as a function of diameter and f/D. Not included are the antenna feed, telemetry, attitude control, propulsion and power supply, which are mission dependent. The weights are competitive with mechanical devices reported in reference 15.

The Orbiter can carry a payload weighing as much as 30,000 kg. Therefore, an inflatable antenna approaching 1000 meters in diameter could be carried on one Orbiter flight. A second flight would deliver the propulsion system to place an antenna of this size into geosynchronous orbit.
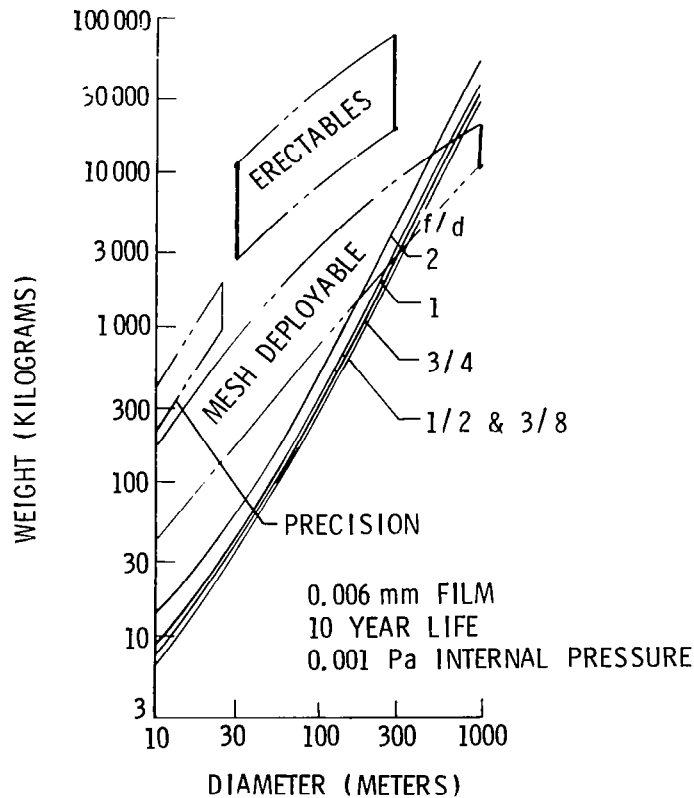

Figure 23

WEIGHT BREAKDOWN FOR 100-METER DIAMETER REFLECTOR

The component weights for a 100-meter diameter antenna are shown in Figure 24 as a function of f/D. Most of the antenna weight is that of the thin film. About 10% of the total weight is for water used to maintain pressure for at least ten years. The carbon dioxide is used at deployment to erect the torus.
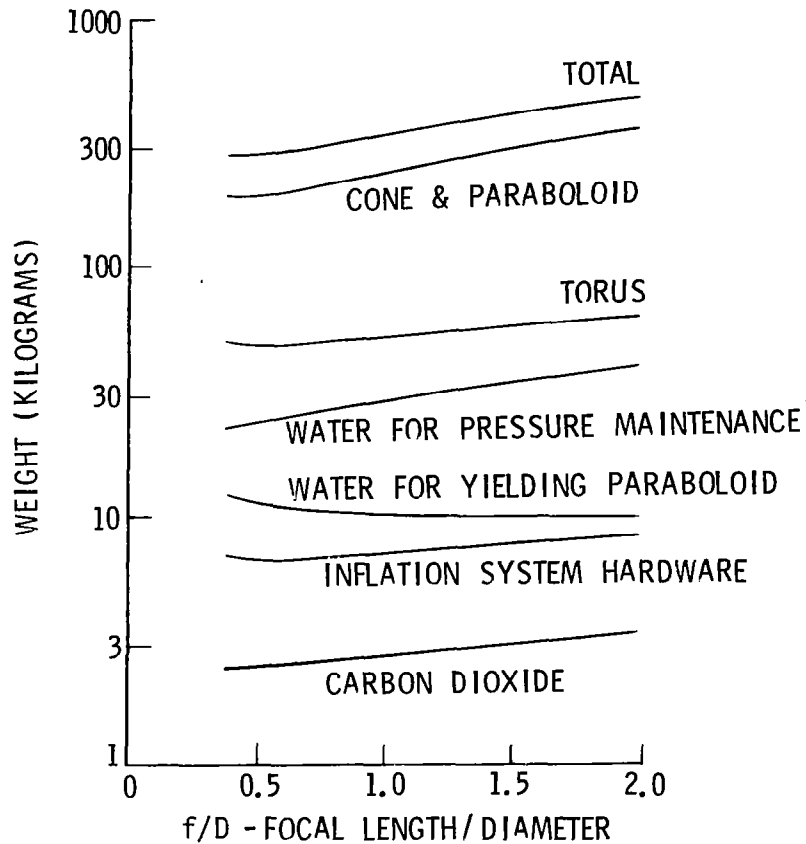
Figure 24

ANTENNA PACKAGE VOLUME

Package volume is shown in Figure 25 as a function of diameter and f/D. Inflatables can be packaged more efficiently than mechanical systems. The high packaging density could be especially advantageous if the packaged antenna were sharing the payload bay with another payload. Most payloads have densities less than the Orbiter's average allowable. Therefore, the inflatable antenna could have a higher density, and the launch cost would still be based upon package volume.

Figure 25

CONCLUSIONS

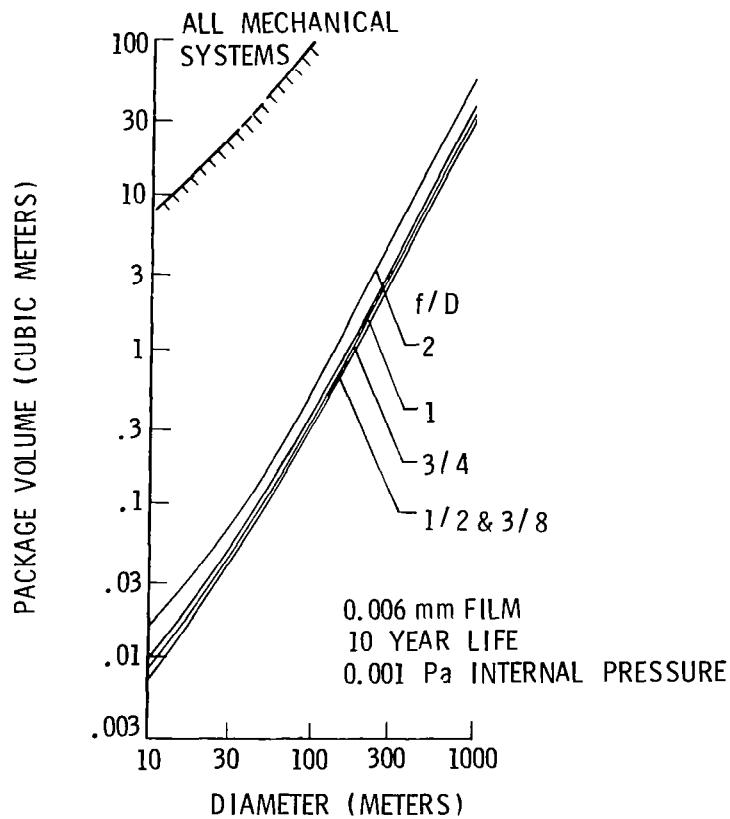The results of the inflated antenna work performed for NASA produced the conclusions of Figure 26. The 3-meter diameter paraboloid built for NASA had a measured inaccuracy of 0.76 mm rms. Since this was the first built and tested, one would expect that improvements are possible.

The self-rigidizing structure is packageable and, after being erected and yielded by pressure, does perform like a thin aluminum shell. This approach, taken from NASA' development of the ECHO II sphere, should be suitable not only for the antenna torus but also for many other space structures.

The weight and package volume of inflated antennas are low relative to mechanical systems. This will reduce the number of Orbiter flights and the amount of on-orbit assembly required. Cost savings are significant.

- INFLATED PARABOLOIDS CAN BE BUILT WITH 0.8 mm RMS ACCURACY

- THE POLYESTER-ALUMINUM FOIL APPEARS PRACTICAL FOR ANTENNAS AND SPACE STRUCTURES

- WEIGHT AND PACKAGE VOLUME OF INFLATED ANTENNAS ARE LOW

Figure 26

RECOMMENDATIONS

The next step per Figure 27 is to build and test a complete ground test unit. About the largest unit that can be ground tested in existing facilities would be one about 15 meters in diameter or less.

The major efforts are to develop the self-rigidizing structure in a torus configuration, and to develop the cone-torus-paraboloid interface. The unit would be used to determine antenna accuracy, and to determine the degree of thermal effects and distortion that occur using state-of-the-art thin films.

DEVELOP A LARGE (~15m) GROUND TEST UNIT.

- SELF-RIGIDIZING TORUS

- INTEGRATION OF TORUS, CONE, AND PARABOLOID

- PARABOLOID ACCURACY

- THERMAL EFFECTS AND DISTORTION

Figure 27

REFERENCES

1. Coffee, Claude W., Jr.; Bressette, Walter E.; and Keating, Gerald M.: Design of the NASA Lightweight Inflatable Satellites for the Determination of Atmospheric Density at Extreme Altitudes. NASA TN D-1243, 1962.

2. Wood, G. P.; and Carter, Arlen F.: Predicted Characteristics of an Inflatable Aluminized-Plastic Spherical Earth Satellite With Regard to Temperature, Visibility, Reflection of Radar Waves, and Protection From Ultraviolet Radiation. NASA TN D-115, 1959.

3. Clemmons, Dewey L., Jr.: The Echo I Inflation System. NASA TN D-2194, 1964.

4. Bowker, David E.: PAGEOS Project, Compilation of Information for Use of Experimenter. NASA TM X-1344, 1967.

5. Inflatable Structures in Space. Hearing Before the Committee of Science and Astronautics, U.S. House of Representatives, 87th Congress, 1st Session, May 19, 1961.

6. Leonard, R. W.; Brooks, G. W.; and McComb, H. G.: Structural Considerations of Inflatable Reentry Vehicles. NASA TN D-457, 1960.

7. Keffer, Clarence O.: Experimental Investigation of Packaging and Deployment Characteristics of an Inflatable Toroidal-Sapce-Station Configuration. NASA TM X-1079, 1965.

8. Keffer, Clarence O.: Investigation of Packaging, Deployment, and Leak-Rate Characteristics of an Inflatable Lunar-Shelter Model. NASA TM X-2393, 1971.

9. Nebiker, F. R.: Expandable Drag Devised for Mach 10 Flight Regime. Aerospace Expandable Structures Conference Transactions, Air Force Aeropropulsion Laboratory, Wright-Patterson Air Force Base, 1963, pp. 501-510.

10. Fichter, W. B.: A Theory for Inflated Thin-Wall Cylindrical Beams. NASA TN D-3466, 1966.

11. Heath, Atwood R., Jr.; and Maxwell, Preston T.: Solar Collector Development. Astronautics and Aerospace Engineering, May 1963.

12. Stimler, F. J.: Design Studies of Advanced Lenticular Passive Communication Satellites From Low to Synchronous Orbit. Report No. GER 12356, Goodyear Aerospace Corporation, Akron, Ohio, 1965.

13. Reitmeier, G. F.: Inflatable Space Antenna System. Aerospace Expandable Structures Conference Transactions, Air Force Aeropropulsion Laboratories, Wright-Patterson Air Force Base, 1963, pp. 605-612.

14. Buckling of Thin-Walled Circular Cylinders. NASA Space Vehicle Design Criteria, NASA SP-8007, Aug. 1968.

15. Freeland, R. E.: Industry Capability for Large Space Antenna Structures. Jet Propulsion Laboratory Report No. 710-12, May 1978.

ELECTROSTATICALLY FIGURED MEMBRANE REFLECTORS:
AN OVERVIEW

J. H. Lang
Research Laboratory of Electronics
Massachusetts Institute of Technology
Cambridge, Massachusetts

ELECTROSTATICALLY FIGURED MEMBRANE REFLECTOR OPERATION

A schematic diagram of the electrostatically figured membrane reflector (EFMR) is presented in Figure 1 [1]. Here, active reflector figure control is exercised via electrostatic stresses which operate between the reflector and a second surface called the command surface. The command surface is located a short distance behind the reflector and is pulled firmly into an approximate paraboloid by a network of guy wires or comparable structure. This same surface supports insulated conducting segments which are individually addressable by dedicated control voltages. The control voltages are, in turn, collectively biased with respect to the reflector. The reflector, tensioned by a rigid rim at the perimeter, is distended toward the command surface by the bias. The resulting command surface potential distribution, and hence the electrostatic stress distribution acting on the reflector, is continuously and rapidly refined via the control voltages so as to produce and maintain a precise parabolic reflector figure. Optical reflector figure measurements provide the data necessary for computer-supervised figure control. Finally, in order to prevent command surface discharging by photons and charged particles, the command surface is completely enclosed by a conducting shroud of which the reflector serves as the front side. Guy wires to the back-side shroud can be used to figure the command surface. The complete shroud is not pictured in Figure 1.
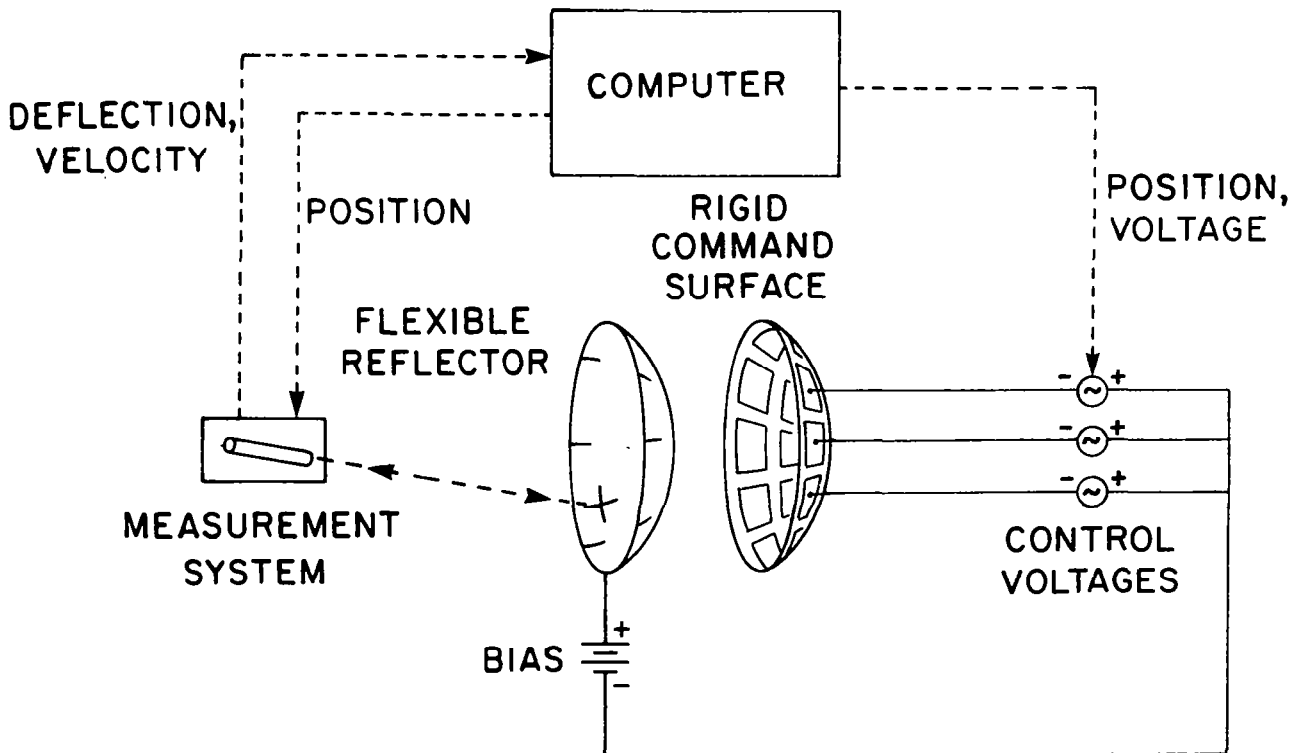
EFMR FUNCTIONAL SCHEMATIC

Figure 1. A schematic diagram of the EFMR.

EFMR MOTIVATIONS

Several characteristics of the EFMR serve to motivate its development. First, the complete antenna is characterized by a low mass. The major contributors to antenna mass are the reflector, command surface, back-side shroud, and support structure. The three surfaces could each be constructed from a thin metalized plastic with a mass density of approximately 0.01 kg/m^2; the support structure is estimated to require a comparable mass. In this case, a 100-m antenna, for example, would exhibit a mass of approximately 310 kg. A second favorable characteristic of the EFMR is its potentially high precision continuous reflecting surface [2]. It is estimated that the EFMR could achieve a ratio of diameter-to-surface tolerance, D/ε, of 10^5 to 10^6 over the range 10 m $\lesssim$ D $\lesssim$ 300 m. Further, this precision is achieved with relatively few electrostatic actuators [3]. Figure 2 presents N, the number of actuators (and hence points of reflector figure measurement) necessary to achieve a given D/ε for various combinations of D and ratio of focal length to diameter, δ. A final advantageous characteristic of the EFMR is the low construction tolerance requirements of the command surface and the support structure. This, combined with the low mass, appears to make the EFMR relatively inexpensive.
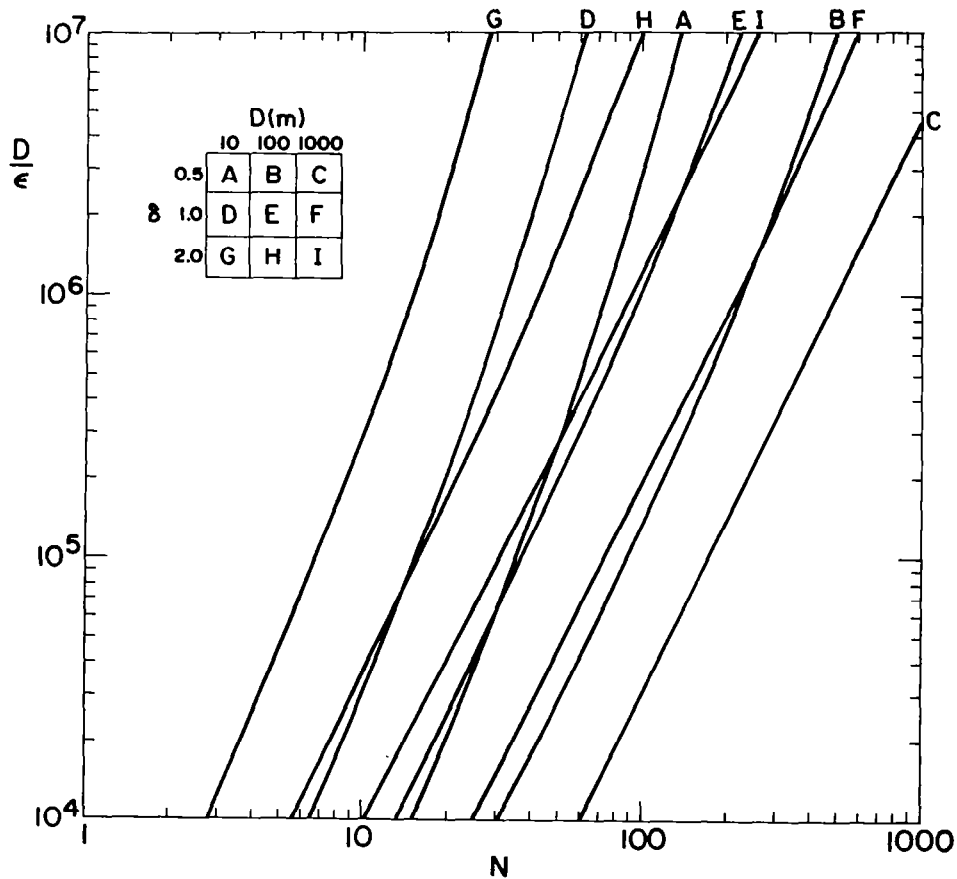

Figure 2. EFMR actuator and sensor requirements.

SCIENTIFIC AND ENGINEERING CHALLENGES

The successful development of the EFMR requires scientific and/or developmental advancements in at least the following areas:

1) reflector figure electromechanical dynamics
2) reflector disturbances
3) reflector figure control systems
4) reflector materials
5) reflector support structures
6) optical reflector figure sensors
7) reflector figure actuator amplifiers

The advancements required in these areas are discussed below.

Two natural phenomena work against the maintenance of a smooth EFMR figure. Figure disturbances, both static and dynamic, are the first. Static disturbances result from nonuniformities in the command surface figure, reflector elasticity, and the support structure geometry [2,3]. Dynamic disturbances result from thermally driven vibrations in the support structure, command surface discharging due primarily to charged particles, and momentum transfer to the reflector from impinging particles. The second phenomenon is figure instability [1-4]. In certain geometries, particularly those with low δ, the equilibrium EFMR figure can exhibit Rayleigh-Taylor modal deflection instabilities. The number of unstable modes is approximately $D/\delta H\pi^2$ where H is the reflector-to-command-surface separation. This is typically several meters. As a consequence of these two phenomena, it is necessary to actively control the EFMR figure as indicated in Figure 1. In order to successfully design the control system, models of the EFMR dynamics and disturbances must be developed [1,2,3]. Further, the control system must be built upon new control theories and implementations. This is necessary as a consequence of the distributed nature of the EFMR, the large number of actuators and sensors involved relative to more standard control problems, the phenomenon of actuator and sensor spillover, and the on-line control computation requirements [1-5]. Successful EFMR development also requires advancements in the areas of reflector materials and support structures. The metalized reflector must exhibit an elasticity sufficient to permit the electrostatic actuators to pull out reflector wrinkles and nonuniformities. Tensions of 1 N/m are typically available [1,3]. Further, the reflector and shroud must prevent significant penetration by charged particles. The support structure must provide safe storage for the reflector during launch, be deployable, and support the reflector with a minimum of vibration during antenna operation. Finally, high-voltage actuator amplifiers and an optical sensing system must be developed [1,3]. The amplifiers must approximately provide a 20-kV dynamic range, exclusive of the bias, and a 100-Hz bandwidth. The sensing must make 10^3 to 10^4 measurements per second with an accuracy somewhat finer than ϵ.

The promise of successful scientific and/or developmental advancement within the areas described above appeared, at the start of the MIT EFMR Program, to be most uncertain with respect to the control-related areas. Consequently, the MIT EFMR Program has concentrated on research in the control-related areas.

EARLY CONTROL-RELATED EFMR DEVELOPMENT

The MIT EFMR Program has developed both static and dynamic models of EFMR electromechanics [1-4]. These models have been used for the purpose of EFMR control system design [1,2,4] and performance evaluation [3]. The primary control-related goal of this effort was to demonstrate the stabilization of EFMR instabilities with a control system that could additionally provide EFMR disturbance rejection, thereby eliminating the instabilities as an argument against operation of the EFMR in its most advantageous and competitive configurations. This goal was achieved using the experiment pictured in Figure 3 [2-4]. Here, a 1-m-square mesh membrane, suspended vertically in tension with rigid boundaries and biased by a high-voltage source, served to simulate the electromechanical dynamics of the EFMR. An array of conducting plates, located to one side of the membrane and addressable via low-voltage amplifiers, simulated the EFMR command surface by providing electrostatic membrane deflection actuation. A similar set of plates equally spaced to the opposite side of the membrane served as capacitive membrane deflection sensors. A computer connected the sensor measurements to the actuator commands so as to support closed-loop membrane deflection control. The electrostatic attraction of the membrane to both sets of plates cancelled so as to produce a grounded-actuator equilibrium in which all three surfaces were parallel. With increasing bias, mesh deflection modes could be successively destabilized in a manner identical to that of the EFMR. LQG (linear quadratic Gaussian) control systems based upon truncated modal EFMR dynamic models were implemented in the computer. These control systems successfully stabilized three open-loop unstable membrane deflection modes limiting deflections to approximately 10^{-5} m rms [2-4]. The results of these experiments indicated that EFMR's with $10 \text{ m} \leq D \leq 300 \text{ m}$, $\delta \approx 1$, and $10^5 \leq D/\varepsilon \leq 10^6$ could be achieved. Equally important, these experiments demonstrated actuator and sensor spillover to be a predictable cause of control system destabilization and disturbance rejection degradation [4].
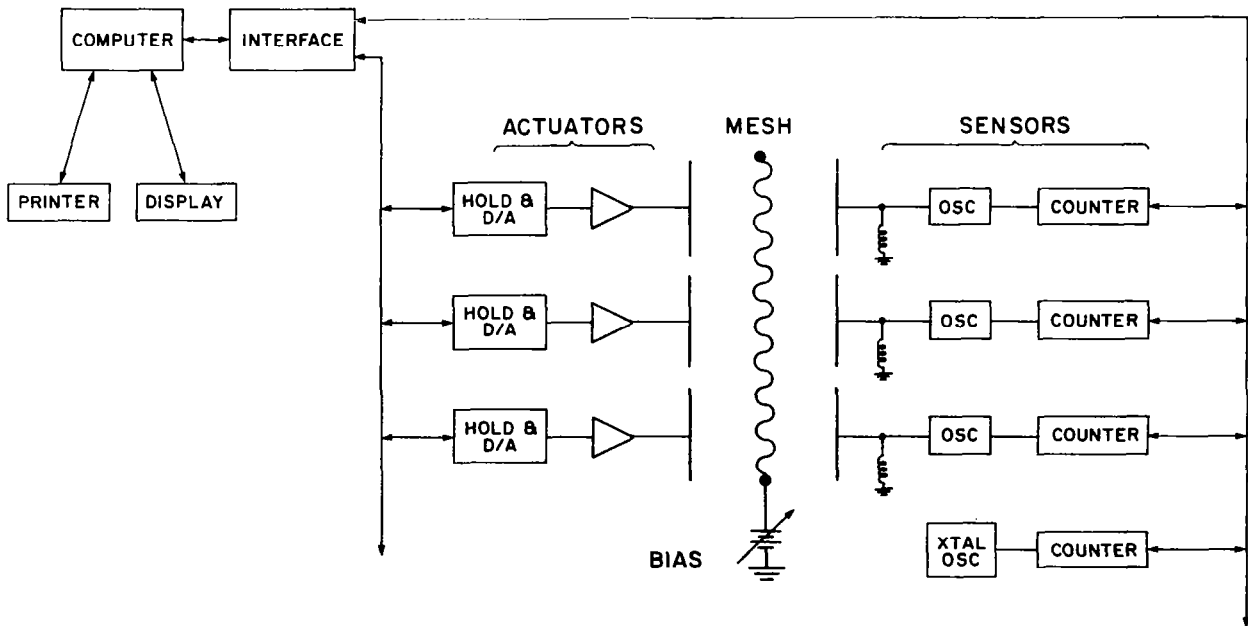

Figure 3. The early MIT EFMR control experiment.

PRESENT CONTROL-RELATED EFMR DEVELOPMENT

The early EFMR control experiments illuminated several control system deficiencies [4]. The LQG control systems were computationally demanding on line and often included open-loop unstable filters. Further, spillover often worked against the control system functions of EFMR stabilization and disturbance rejection. Consequently, the MIT EFMR Program undertook to develop an alternative EFMR control system [5]. The new control system is derived from an EFMR model reduction based upon actuator and sensor influence functions. This model reduction pays close attention to spillover and allows a perturbational analysis of closed-loop system dynamics which can be made arbitrarily accurate through proper control system design. More important, the perturbations can be used to develop control system design constraints that guarantee, to within the validity of the perturbations, that spillover is a stabilizing phenomenon. Currently, these theories are being tested on the EFMR experiment pictured in Figure 4. The left side of the figure shows the 2-meter reflector, while the right side of the figure shows the command surface that has been dropped down and slid out from under the reflector. This new experiment functions identically to the EFMR of Figure 1 with the exception that the command surface electrodes double as capacitive reflector deflection sensors, replacing the optical system of Figure 1. In addition to serving as a control system test facility, the experiment is expected to serve as an EFMR proof of concept. The actuators and sensors are sufficiently accurate to permit the achievement of $D/\varepsilon \approx 10^6$, exclusive of membrane fabrication irregularities.
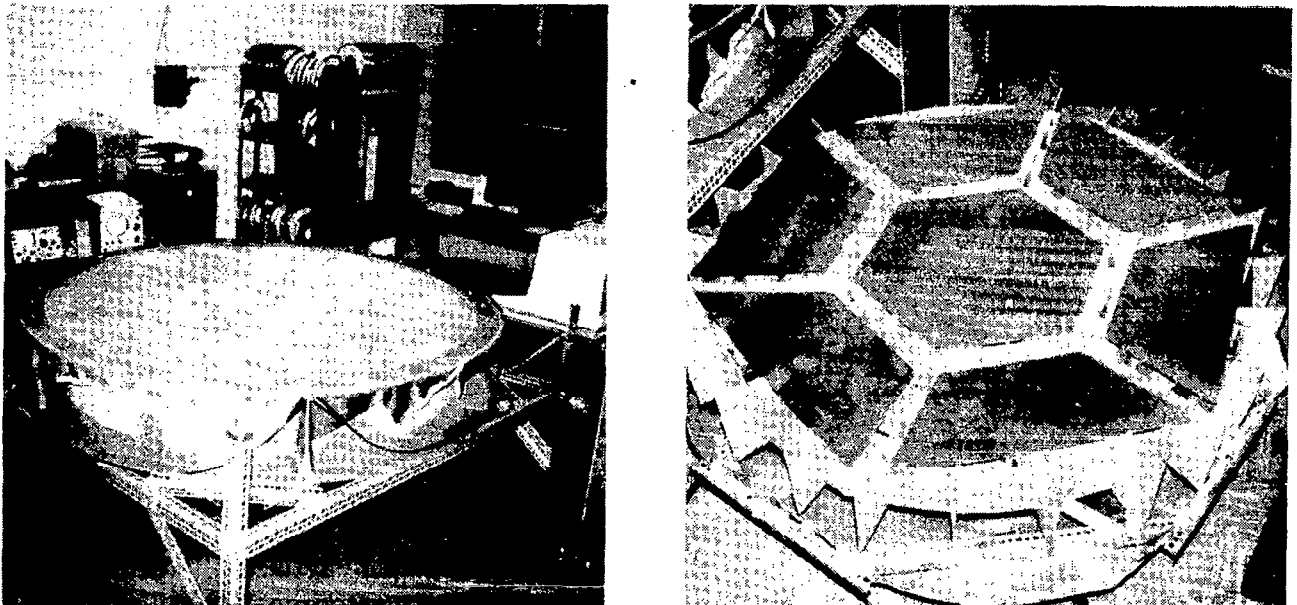

Figure 4. The present MIT EFMR control experiment.

SUMMARY

In summary, the EFMR concept has been described, and those areas of the concept which require development have been identified. In the control-related areas, the MIT EFMR Program has developed and experimentally verified both static and dynamic EFMR electromechanical models. Further, these models have been used to develop control systems capable of stabilizing EFMR instabilities and providing EFMR disturbance rejection. Based upon these results, it appears that the EFMR could be expected to achieve a reflector figure diameter-to-surface-tolerance ratio of $10^5 \leq D/\varepsilon \leq 10^6$ over the diameter range of 10 m $\leq$ D $\leq$ 300 m with a modest number of actuators [3]. This operating regime is summarized in Figure 5 and is compared to the operating regimes of alternative ground-based and space-based technologies [3]. In the figure, Ω and G are the diffraction-limited beamwidth and gain, respectively, which correspond to D/ε. Additionally, a scale is presented which relates D/ε, Ω, and G to the product δN where N is now the number of pointwise actuators necessary to mechanically figure a membrane reflector so as to achieve a given reflector performance. A comparison of N in Figures 2 and 5 shows that electrostatic reflector figure actuation requires far fewer actuators to achieve a given reflector performance than does mechanical actuation.
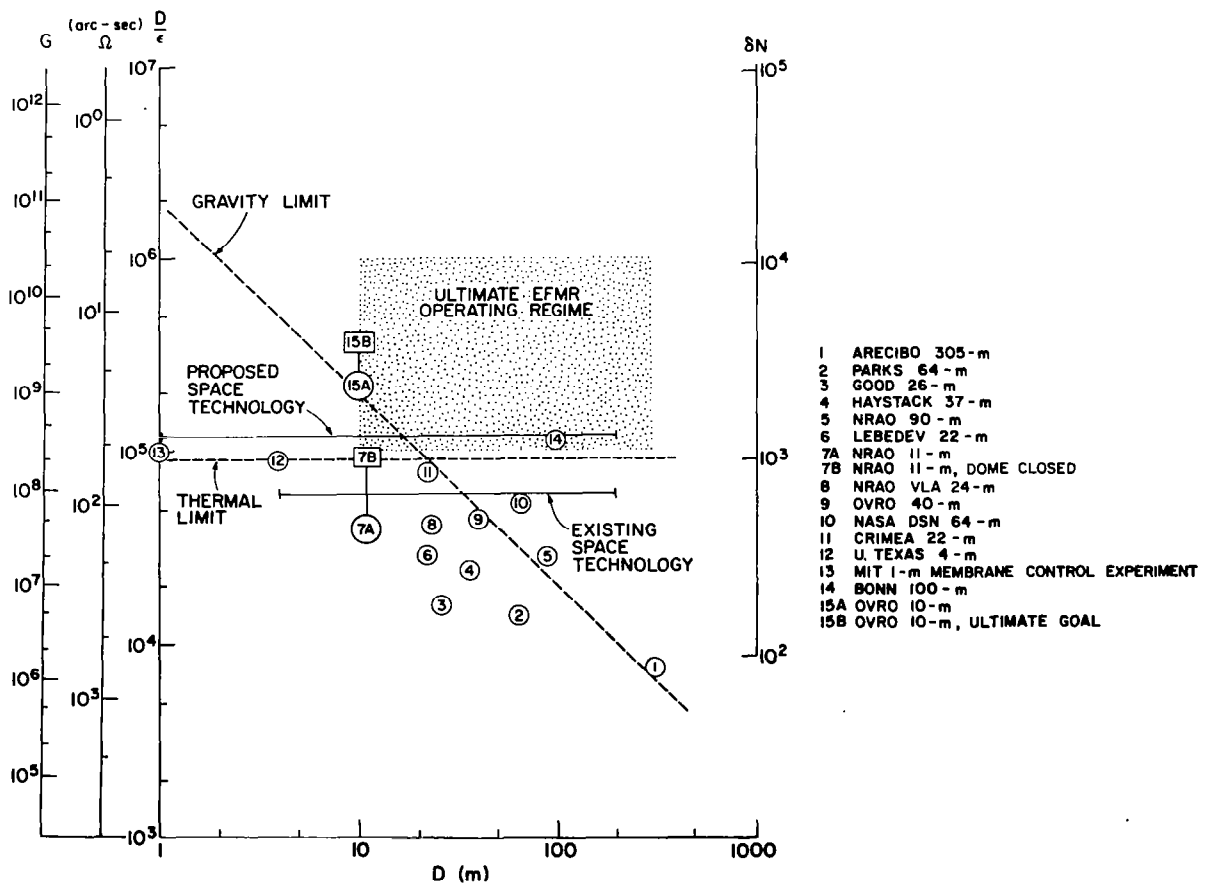
Figure 5. A comparison of reflector technologies.

REFERENCES

[1] J. H. Lang, J. R. Gersh, and D. H. Staelin, "Electrostatically-controlled wire mesh antenna," Electronics Letters, Vol. 14, No. 20, September 1978, pp. 665-666.

[2] J. H. Lang, "Experiments on the electrostatic control of a flexible membrane and their relation to membrane-antenna figure control," Proceedings of the AIAA Guidance and Control Conference, 1981, pp.187-191.

[3] J. H. Lang and D. H. Staelin, "Electrostatically figured reflecting membrane antennas for satellites," IEEE Transactions on Automatic Control, Vol. 27, No. 3, June 1982, pp. 666-670.

[4] J. H. Lang and D. H. Staelin, "The computer-controlled stabilization of a noisy two-dimensional hyperbolic system," IEEE Transactions on Automatic Control, Vol. 27, No. 5, October 1982, pp. 1033-1043.

[5] Y. Yam, J. H. Lang, T. L. Johnson, S. Shih, and D. H. Staelin, "Large space structure model reduction and control system design based upon actuator and sensor influence functions," presented at NASA/JPL Workshop on Applications of Distributed System Theory to the Control of Large Space Structures (Pasadena, CA), July 14-16, 1982.

1. Report No.	2. Government Accession No.	3. Recipient's Catalog No.
NASA CP-2269, Part 1		

4. Title and Subtitle	5. Report Date
LARGE SPACE ANTENNA SYSTEMS TECHNOLOGY - 1982	May 1983
	6. Performing Organization Code
	506-62-23-01

7. Author(s)	8. Performing Organization Report No.
E. Burton Lightner, compiler	L-15614
	10. Work Unit No.

9. Performing Organization Name and Address	
NASA Langley Research Center	11. Contract or Grant No.
Hampton, VA 23665	
	13. Type of Report and Period Covered

12. Sponsoring Agency Name and Address	Conference Publication
National Aeronautics and Space Administration	
Washington, DC 20564	14. Sponsoring Agency Code

15. Supplementary Notes

16. Abstract

This publication is a compilation of the unclassified papers presented at the NASA Conference on Large Space Antenna Systems Technology, which was held at the Langley Research Center, Hampton, Virginia, November 30 – December 3, 1982. The conference, which was sponsored jointly by the NASA Office of Aeronautics and Space Technology (OAST) and the NASA Langley Research Center, was organized into five sessions: Systems, Structures Technology, Control Technology, Electromagnetics, and Space Flight Test and Evaluation. All speakers and topics were selected by the session cochairmen and included representation from industry, universities, and government. The program was organized to provide a comprehensive review of space missions requiring large antenna systems and of the status of key technologies required to enable these missions.

17. Key Words (Suggested by Author(s))	18. Distribution Statement
Large space systems Large antenna systems Structures, materials, and analyses Flight technology experiments	Unclassified – Unlimited Subject Category 15

19. Security Classif. (of this report)	20. Security Classif. (of this page)	21. No. of Pages	22. Price
Unclassified	Unclassified	596	A25

N-305

National Aeronautics and
Space Administration

Washington, D.C.
20546

SPECIAL FOURTH CLASS MAIL
BOOK

Postage and Fees Paid
National Aeronautics and
Space Administration
NASA-451

U.S.MAIL

6   1 SP-7046,   830508 F933760U
DEPT OF THE AIR FORCE
AFWAL/ARAA
ATTN: D WASHBURN
KIRTLAND AFB NM 87115

NASA

POSTMASTER: